P-08-104

Analysis of uncertainty in orientation of fractures coupled to PFL anomalies

Site descriptive modelling SDM-Site Laxemar

Martin Stigsson, Reinertsen Sverige AB

April 2008

Svensk Kärnbränslehantering AB
Swedish Nuclear Fuel
and Waste Management Co

Box 250, SE-101 24 Stockholm
Phone +46 8 459 84 00

ISSN 1651-4416
SKB P-08-104

Analysis of uncertainty in orientation of fractures coupled to PFL anomalies

Site descriptive modelling SDM-Site Laxemar

Martin Stigsson, Reinertsen Sverige AB

April 2008

Keywords: Laxemar, Fracture, Orientation, PFL, Sample space, Uncertainty.

Abstract

This report concerns the orientation uncertainty of fractures that are identified to be flowing by using the Posiva Flow Log in 43 cored boreholes in Laxemar sub-area.

The maximum orientation uncertainty, Ω, is calculated for 1957 PFL fractures and the corresponding 90th percentile sample space for each fracture is shown on an equal area lower hemisphere stereogram.

Of the 1957 studied fractures 566 have a maximum uncertainty, Ω, larger than 10° and 156 of them a maximum uncertainty larger than 30°.

Sammanfattning

Denna rapport berör osäkerhet i orientering hos sprickor förknippade med flöden mätta med Posiva Flow Log i 43 kärnborrhål i Laxemarområdet.

Den maximala orienteringsosäkerheten, Ω, är beräknad för 1957 PFL-sprickor och 90-percentilsutfallsrummet visas projicerad på ett Schmidt-steronät för var spricka.

Av de 1957 studerade sprickorna har 566 en maximal orienteringsosäkerhet som är större än 10° och 156 av dem har maximal osäkerhet större än 30°.

Contents

1 Introduction

SKB has, during the period September 2006 to October 2007, carried out an extensive work to quality assure the orientation of mapped objects in boreholes. The result of the work is that fracture orientation measurements have been altered and that it is now possible to calculate a sample space for the uncertainty of the fracture orientation, see /Munier and Stigsson 2007 in prep./

The database Sicada contains information about the best estimate orientation together with the uncertainty values of each fracture. If the uncertainty is large there is a large possibility that a fracture might have another orientation than the best estimated in the Sicada database tables. For disciplines that use single fractures, e.g. hydrogeology, this sample space can be used to see how accurate the measurements are and might explain orientations that do not fit into conceptual models.

The work reported here shows a stereogram with the 90th percentile sample space of each fracture pole of fractures connected to PFL-f features in the KLX boreholes at Laxemar.

1.1 Scope of work

The data used in the analyses comes from the KLX holes listed in Table 1-1. Three KLX boreholes are missing in the analysis due to different reasons. KLX01 and KLX02 are boreholes that were drilled before the site investigations started and hence are not exact comparable with the holes drilled during the site investigations. The borehole KLX27A was, on the other hand, drilled so late in the investigations that the data was not available when the anaysis, presented in this report, started. The location of the boreholes are shown in Figure 1-1 together with the rock domains /SKB 2008/ and in Figure 1-2 together with fracture domains /La Pointe et al. 2008/ based on the model dated February 2008.

There are, in total, 1987 PFL-f features coupled to fractures in the boreholes listed in Table 1-1 and reported in /Teurneau et al. 2007, Wikström et al. 2007abc and, Forsmark et al. 2007/.

Table 1-1. Boreholes from which data is used in the current analysis.

KLX03	KLX09C	KLX11B	KLX16A	KLX23B
KLX04	KLX09D	KLX11C	KLX17A	KLX24A
KLX05	KLX09E	KLX11D	KLX18A	KLX25A
KLX06	KLX09F	KLX11E	KLX19A	KLX26A
KLX07A	KLX09G	KLX11F	KLX20A	KLX26b
KLX07B	KLX10	KLX12A	KLX21B	KLX28A
KLX08	KLX10B	KLX13A	KLX22A	KLX29A
KLX09	KLX10C	KLX14A	KLX22B	
KLX09B	KLX11A	KLX15A	KLX23A	

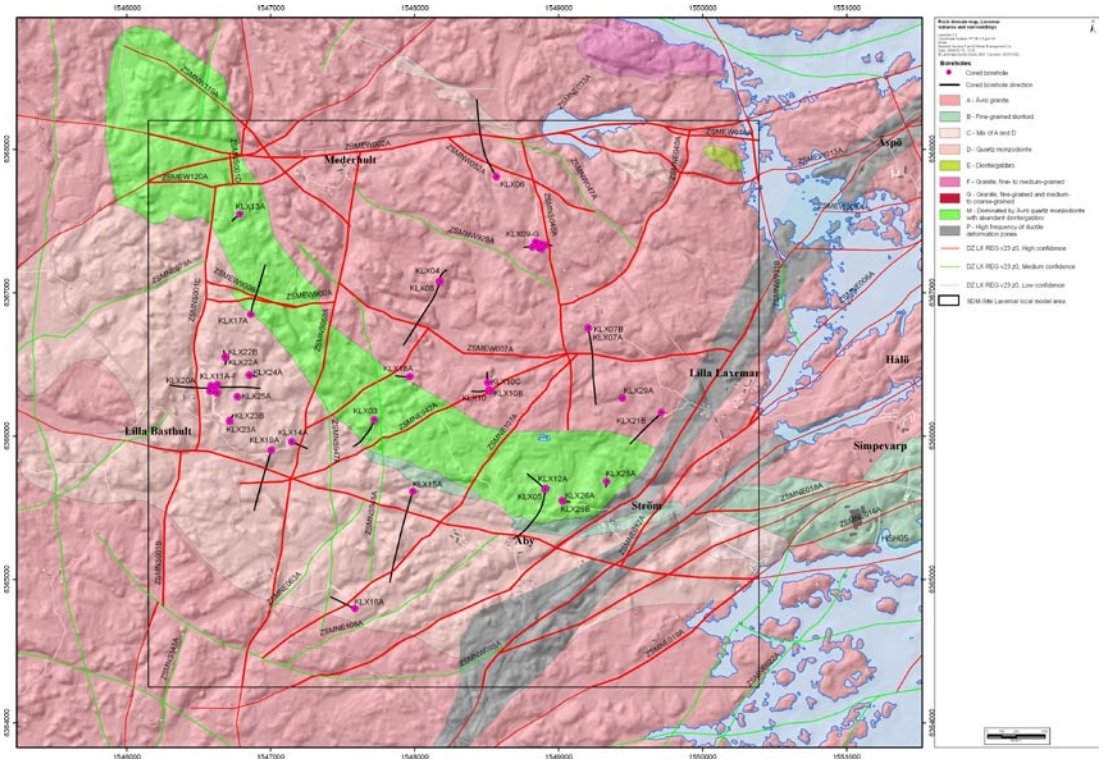

Figure 1-1. *Definition of rock domains, RSM, in Laxemar, as defined on the surface, together with the interpreted deformation zones and location and direction of the boreholes studied in this report.*

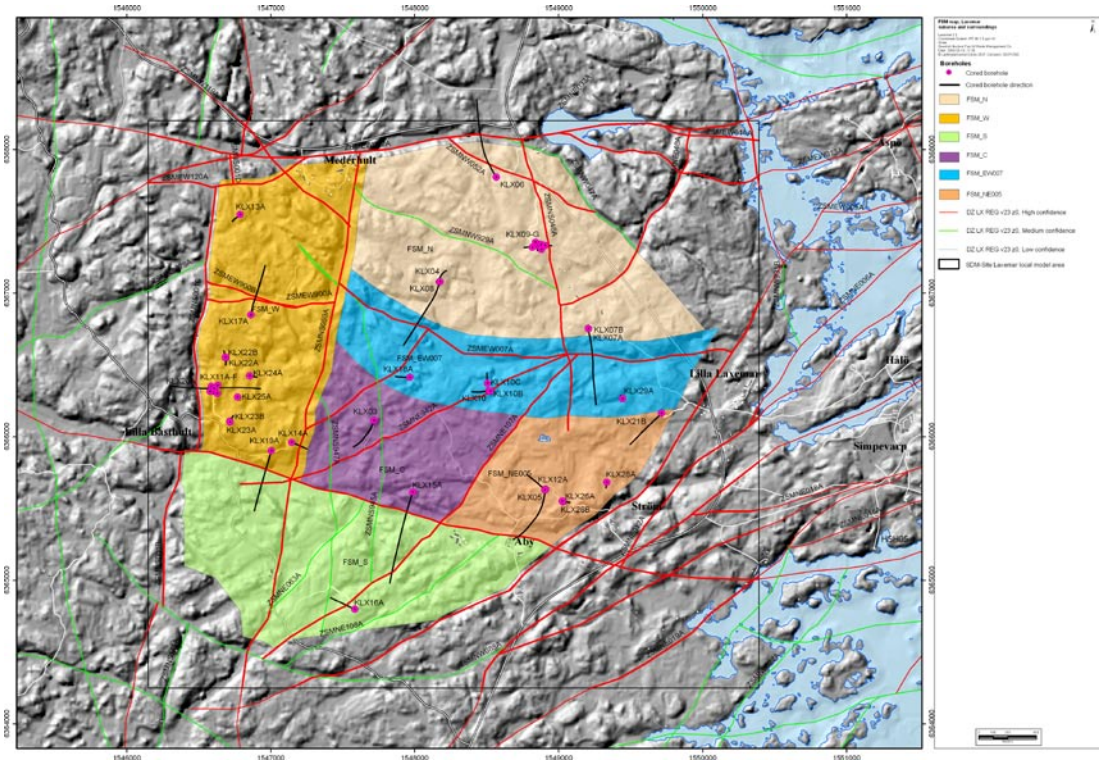

Figure 1-2. *Definition of fracture domains, FSM, in Laxemar, as defined on the surface (based on the February 2008 model) together with the interpreted deformation zones and location and direction of the boreholes studied in this report.*

Of these fractures eleven is missing orientation, see Table 1-2 and consequently omitted from this report. It is though highly recommended that it is further investigated why the fractures are missing orientation, and, if possible, calculate orientations for the fractures.

Another 19 PFL-f features are coupled to fractures that are already coupled to other PFL-f features. The transmissivities of these flow measurements have been summed to each fracture according to Table 1-3 and afterwards treated as one PFL-f feature each. In Appendix B is shown alternate couplings and the corresponding sample spaces.

There are 14 PFL-f features, seen as flow anomalies along the borehole, that have been identified to position in the borehole and hence been coupled to individual fractures, but transmissivity calculations are missing. The reason is that it was not possible to perform the measurements in such a way (two flow rates with different heads as driving force) that it was possible to calculate the transmissivity, see the reports for the PFL-measurements /Kristiansson et al. 2006 and Pöllänen 2007/.

Table 1-2. Fractures missing orientation information and thus excluded from the report.

Borehole	Adj Secup (m)	PFL no	Transmissivity (m2/s)	Feature ID
KLX04	576.79	93	$1.95 \cdot 10^{-8}$	CF54438B2B18C0F4
KLX04	586.15	96	$2.11 \cdot 10^{-7}$	6594438B2B18E566
KLX05	188.89	36	$4.68 \cdot 10^{-9}$	30D5438B2B12E1BD
KLX06	736.35	175	$1.23 \cdot 10^{-9}$	DF96438B2B1B307C
KLX07B	51.70	14	$3.05 \cdot 10^{-9}$	6597438B0910C920
KLX07B	186.49	79	$1.90 \cdot 10^{-8}$	2717438B0912D508
KLX09	755.75	68	$7.73 \cdot 10^{-6}$	5C59438B2B1B7E32
KLX14A	49.36	11	$7.23 \cdot 10^{-8}$	7BD4478B0A10C009
KLX19A	105.09	5	$2.55 \cdot 10^{-6}$	0099478B0A119AFC
KLX20A	276.81	46	$1.65 \cdot 10^{-9}$	20904B8B0A1436CE
KLX23A	94.04	17	$3.91 \cdot 10^{-9}$	40934B8B0A216EBD

Table 1-3. PFL-f features coupled to the same fracture.

Borehole	PFL no	Transmissivity (m2/s)	Fracture Feature ID
KLX05	7, 8	$4.51 \cdot 10^{-9}$	1315438B2B11CF52
KLX06	11, 12	$3.78 \cdot 10^{-8}$	40D6438B2B11C98A
KLX06	30, 31	$1.07 \cdot 10^{-6}$	BF96438B2B12B7E1
KLX07A	51, 52	$2.43 \cdot 10^{-8}$	2F57438B0A1312AD
KLX07A	91, 92	$6.37 \cdot 10^{-8}$	2117438B0A14B8E1
KLX07B	40, 41	$2.04 \cdot 10^{-6}$	08D7438B09117C7A
KLX07B	45, 46, 47, 48, 49, 50	$1.60 \cdot 10^{-5}$	FFD7438B09119A6F
KLX11A	33, 34	$3.33 \cdot 10^{-8}$	E051478B0A16BB78
KLX11F	16, 17	$4.59 \cdot 10^{-5}$	6091478B0D11138B
KLX12A	5, 6	$1.62 \cdot 10^{-7}$	2A52478B0A119AC1
KLX12A	57, 58	$3.56 \cdot 10^{-8}$	FC12478B0A13FA68
KLX15A	5, 6	$6.27 \cdot 10^{-8}$	13D5478B0A116226
KLX18A	149, 150	$3.24 \cdot 10^{-8}$	4098478B0A190D65
KLX19A	11, 12	$1.02 \cdot 10^{-6}$	8099478B0A11AE35
KLX19A	27, 28	$8.70 \cdot 10^{-5}$	4099478B0A14913E

Table 1-4. PFL anomalies without transmissivity value.

Borehole	Adj Secup (m)	PFL no	Feature ID
KLX22A	18.768	1	C0924B8B0A10496F
KLX22A	22.115	2	A0924B8B0A105689
KLX22A	25.187	3	C0924B8B0A10628F
KLX22B	16.87	1	C0924B8B091041C4
KLX22B	17.899	2	00924B8B091045C6
KLX23A	22.511	1	A0934B8B0A2057D6
KLX23B	18.803	1	80934B8B09204923
KLX23B	25.979	2	A0934B8B09206504
KLX24A	20.529	1	60944B8B0A10501A
KLX24A	23.641	2	20944B8B0A105C3E
KLX24A	28.276	3	60944B8B0A106E52
KLX25A	17.101	1	80954B8B0A104286
KLX29A	7.339	1	00994B8B0A101CAB
KLX29A	13.088	2	00994B8B0A103320

From the 1987 fractures reported in /Teurneau et al. 2007, Wikström et al. 2007abc and, Forsmark et al. 2007/ there remain 1957 that is run through all uncertainty calculations and shown in chapter 2. However the cross plots of transmissivity versus uncertainty only consists of 1943 fractures because the lack of transmissivity data.

The report does not go through the mathematics to calculate the orientation uncertainty in the boreholes, instead the reader is encouraged to read /Munier and Stigsson 2007, in prep/ in which the theories are elaborated. However, the implementation of the algorithms using Microsoft Excel VBA code is shown in Appendix C.

1.2 Disposition

Section 2.1 shows the cumulative density function, CDF, of the maximum uncertainty for each borehole to provide an oversight of which boreholes having PFL fractures with large uncertainty together with fracture pole diagrams of all PFL fractures and, where applicable, PFL fractures with maximum orientation uncertainty greater than 30°. Section 2.2 shows cross plots of maximum uncertainty versus transmissivity is shown. This section can be used as a guidance of which boreholes having fractures with large uncertainty together with large flow. Section 2.3 shows a stereogram with the uncertainty sample space for each individual fracture so that details of each fracture can be studied.

Chapter 3 shows a few graphs where the data has been divided on rock and fracture domains instead of boreholes.

During the current work SKB discovered an error in the orientation uncertainty values in Sicada. Instead of waiting until the error is corrected and a new delivery can be sent, the corrections were made in this work to the table p_fract_core_eshi /Sicada 2008/. The algorithm used is shown in Appendix A. In Appendix B is the sample space for some alternative couplings shown and Appendix C show the Microsoft Excel VBA code used in the work.

1.3 Nomenclature and definitions

Alpha angle is the angle between the fracture plane and the axis of the borehole, i.e. a fracture parallel to the borehole has alpha = 0° and a fracture perpendicular to the borehole has alpha = 90°.

Beta angle is the angle between the reference line in the Bips image and the lower extreme in the direction of the borehole. It is measured from 0° to 360° clockwise.

CDF is the cumulative density function, i.e. the probability that an arbitrary value, following the distribution, is less than a given value.

Dihedral angle is the angle between two vectors in 3D space, see e.g. /Munier and Stigsson 2007 in prep/.

Large uncertainty, fractures where the maximum uncertainty is greater than 30°.

Low uncertainty, fractures where the maximum uncertainty is less than 10°.

Maximum uncertainty, Ω, the maximum dihedral angle from the best estimate of the fracture orientation to the point in the 90^{th} percentile sample space that is furthest away. Maximum possible value is 90º, see /Munier and Stigsson 2007 in prep/ for details.

PFL fractures are flowing fractures as determined with the Posiva Flow Log. The geometrical interpretations, location and orientation, of the PFL fractures are reported in /Teurneau et al. 2007, Wikström et al. 2007abc and, Forsmark et al. 2007/.

2 Uncertainty of orientation per borehole

2.1 Maximum uncertainty, Ω

This section shows one graph for each borehole of the maximum uncertainty to give an overview of boreholes with high orientation uncertainty that might need to be paid further attention. Each section also shows fracture pole diagrams for all PFL fractures and, where applicable, a second fracture pole diagram for PFL fractures with maximum orientation uncertainty greater than 30°. Finally, in Section 2.1.44, all PFL fractures are merged into one set and plotted in a graph that can be used as a benchmark to the results for individual boreholes.

2.1.1 KLX03

The CDF (Cumulative Density Function) of the maximum uncertainty is shown in Figure 2-1. About 20% of the fractures have a maximum uncertainty less than 10°. 90% of the data have maximum uncertainty less than 16°. The two fractures with Ω greater than 30° fall within the horizontal and NW striking sets of PFL fractures, see Figure 2-2.

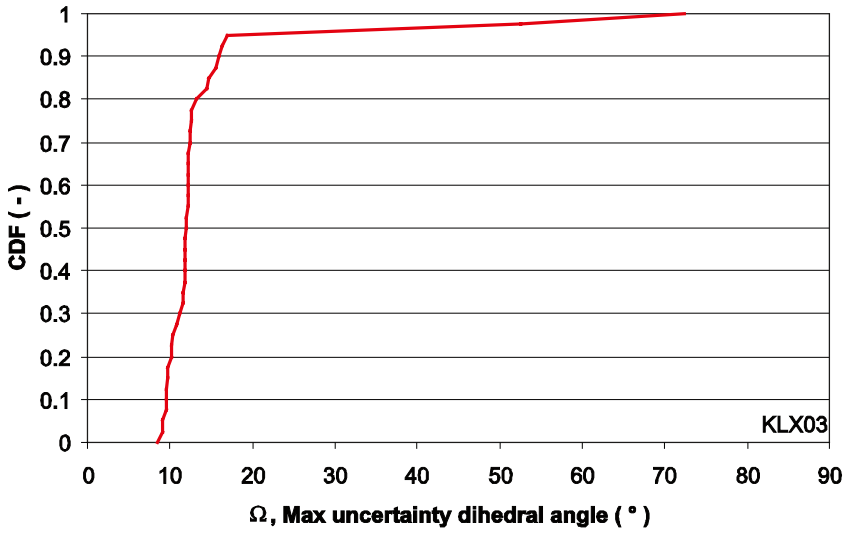

Figure 2-1. *The cumulative density function of the largest orientation uncertainties of PFL fractures in KLX03.*

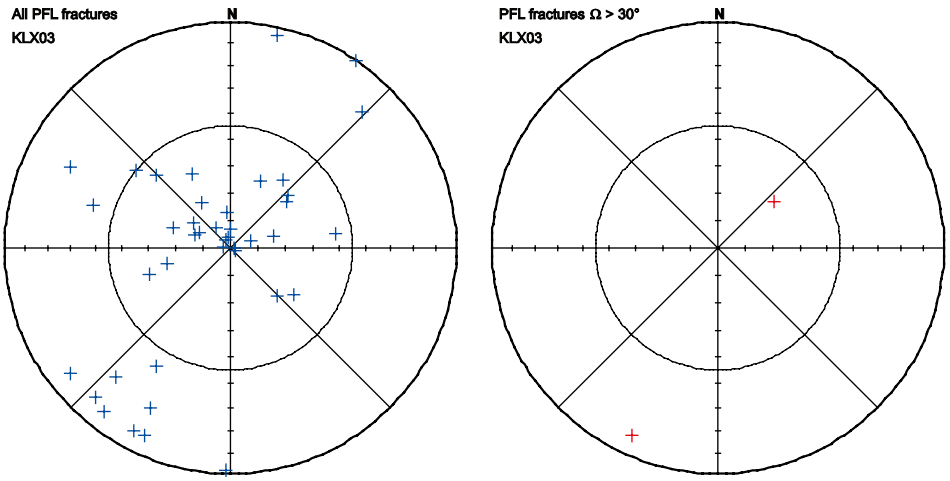

Figure 2-2. *To the left the poles of all PFL fractures in KLX03 and to the right the poles of the PFL fractures that have Ω greater than 30°.*

2.1.2 KLX04

Two fractures associated with flow in KLX04 did not have any information about orientation or uncertainty of orientation in the table p_fract_core_eshi /Sicada 2008/. Thus these two fractures can not be part of the uncertainty analysis. The CDF of the maximum uncertainty of the remaining fractures is shown in Figure 2-3. The maximum uncertainty is less than 10° for only 13% of the fractures whilst 90% of the data have maximum uncertainty less than 17°.

The three PFL fractures with Ω larger than 30° are all within the sub horizontal fractures. They are all within the band of NE-SW striking fractures that is the main orientation of all PFL fractures in KLX04, see Figure 2-4. A look at the sample spaces, Section 2.3.2 show that the SW striking fracture, D854438B2B15A1BF, has such large uncertainty that it may be between SE to NW. The north striking fracture, F114438B2B1982BE, also has such large uncertainty that it might be between west to east striking.

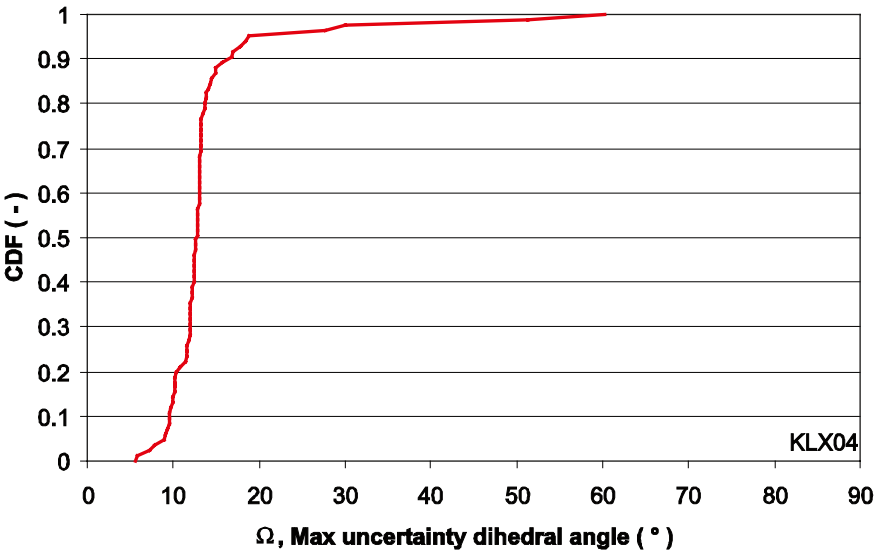

Figure 2-3. *The cumulative density function of the largest orientation uncertainties of PFL fractures in KLX04.*

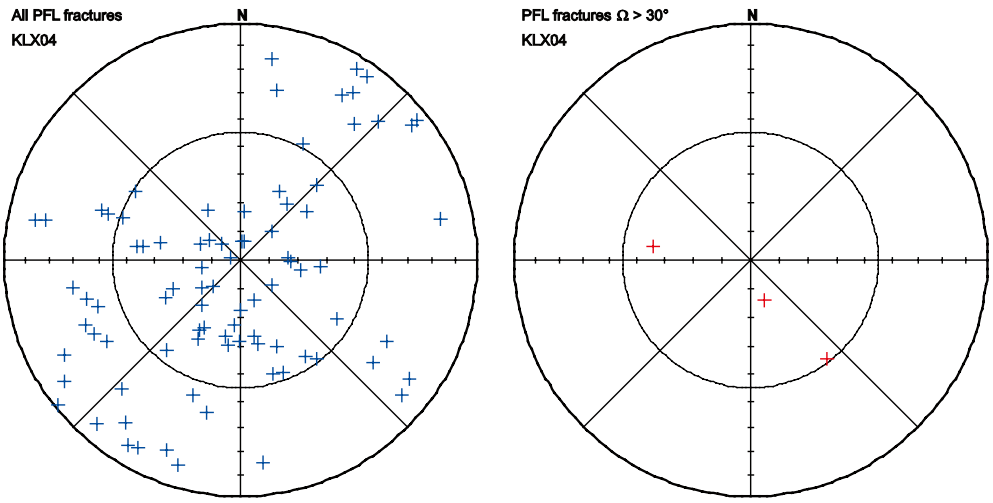

Figure 2-4. *To the left the poles of all PFL fractures in KLX04 and to the right the poles of the PFL fractures that have Ω greater than 30°.*

2.1.3 KLX05

There is missing information about orientation for one PFL fracture in KLX05 and thus this fracture has been omitted from the analysis of the maximum uncertainty shown in Figure 2-5. Most of the fractures in KLX05 have a low uncertainty, 47% of the fractures have maximum uncertainty less than 10°, and 80% less than 12°. But on the other hand there is a relatively large portion of data with high uncertainty, 10% of the data have maximum uncertainty greater than 50°.

The PFL fractures with uncertainty larger than 30° follow the same pattern as all PFL fractures in KLX05, see Figure 2-6. The SE striking fracture, A955438B2B164300, might be a little bit of the pattern, but looking at Section 2.3.3 the fracture has such uncertainty that it is steep and can have any orientation but SW.

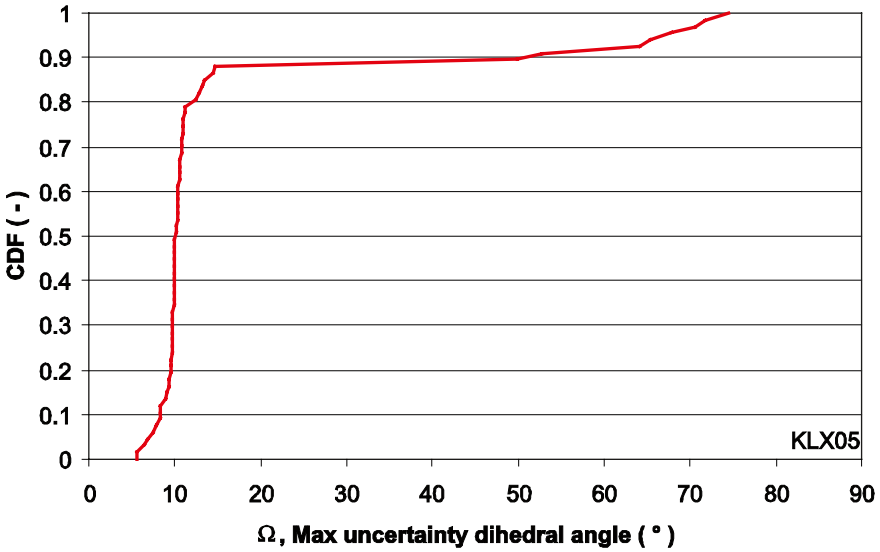

Figure 2-5. *The cumulative density function of the largest orientation uncertainties of PFL fractures in KLX05.*

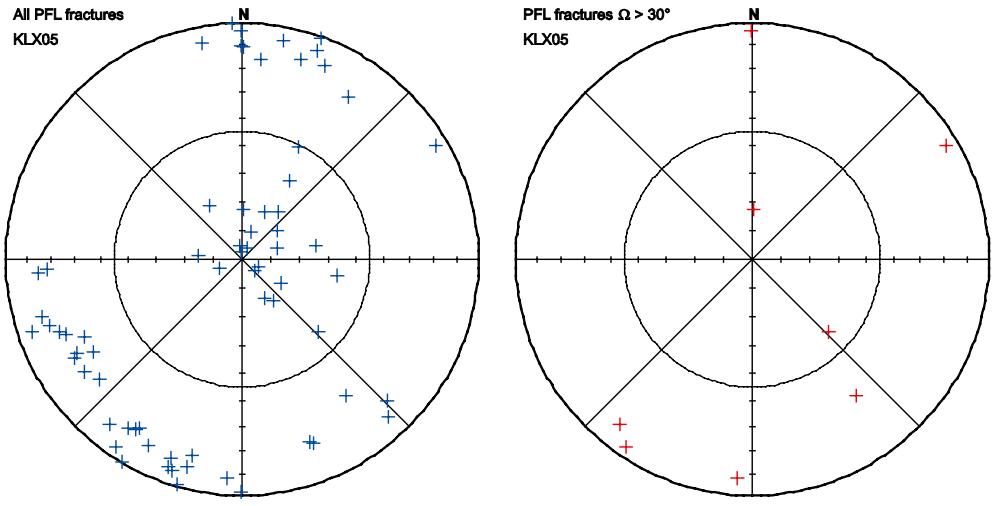

Figure 2-6. *To the left the poles of all PFL fractures in KLX05 and to the right the poles of the PFL fractures that have* Ω *greater than 30°.*

2.1.4 KLX06

The orientation information is missing for one fracture, that is associated with flow, in table p_fract_core_eshi /Sicada 2008/ and hence this fracture is excluded from orientation analysis. The CDF of maximum uncertainty of the remaining fractures is shown in Figure 2-7. The uncertainty is low for most fractures in KLX06, 70% of the fractures have maximum uncertainty less than 10° and 90% less than 16°.

All but three of the PFL fractures follow the orientation pattern of all the PFL fractures, see Figure 2-8. The south striking fracture, 3C56438B2B17B5EA, has maximum uncertainty 75° and could hence be part of the SE striking fractures, see 2.3.4. The NE striking PFL fractures, 7BD6438B2B1DDEE8 and 1CD6438B2B1CBE16, have both maximum uncertainty less than 10° and thus has a deviant orientation to the other fractures.

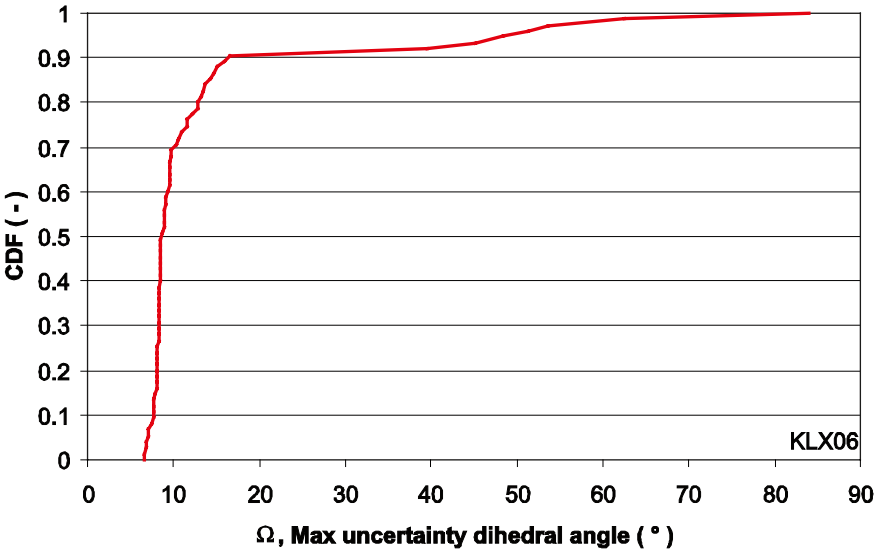

Figure 2-7. The cumulative density function of the largest orientation uncertainties of PFL fractures in KLX06.

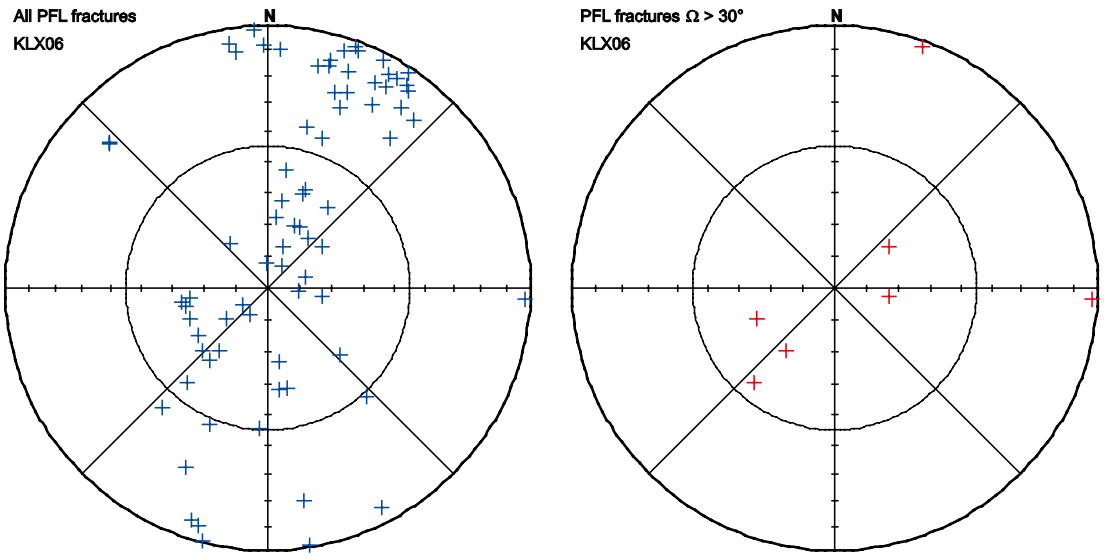

Figure 2-8. To the left the poles of all PFL fractures in KLX06 and to the right the poles of the PFL fractures that have Ω greater than 30°.

2.1.5 KLX07A

The maximum uncertainty is low for most fractures associated with flow in KLX07A, see Figure 2-9. About 86% of the PFL fractures have maximum uncertainty less than 10° and 90% of them have maximum uncertainty less than 13°.

There are no orientations that deviates from the main orientation pattern in KLX07A, see Figure 2-10.

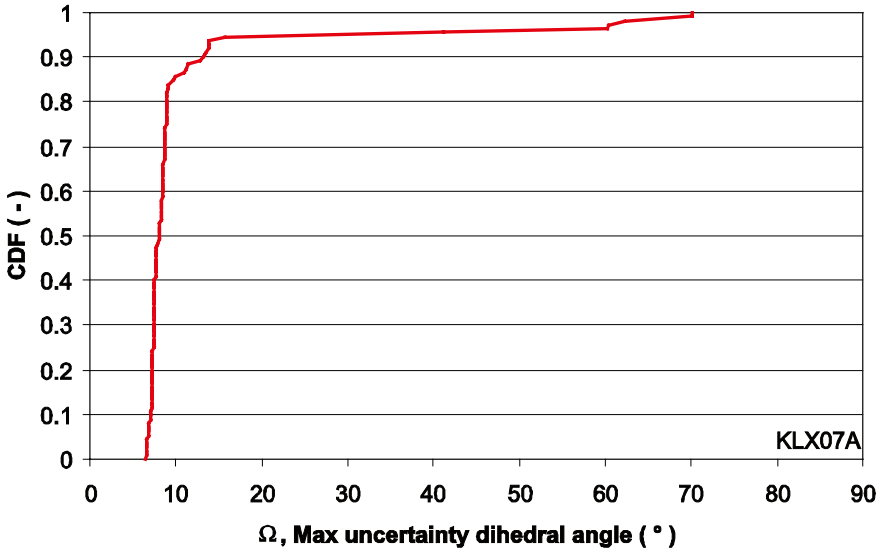

Figure 2-9. *The cumulative density function of the largest orientation uncertainties of PFL fractures in KLX07A*

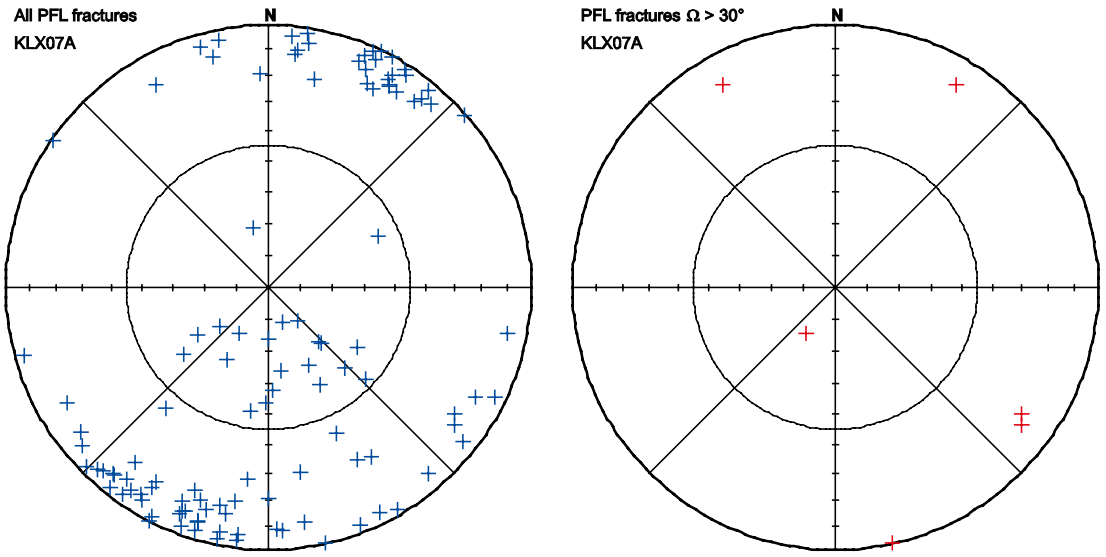

Figure 2-10. *To the left the poles of all PFL fractures in KLX07A and to the right the poles of the PFL fractures that have Ω greater than 30°.*

2.1.6 KLX07B

The table p_fract_core_eshi /Sicada 2008/ is missing orientation information of two PFL fractures in KLX07B and thus these are omitted from the orientation analysis. The CDF of the remaining fractures is shown in Figure 2-11. About 24% of the PFL fractures have maximum uncertainty less than 10° and 90% less than 20°.

There are no PFL fractures that deviate from the general orientation pattern in KLX07B, see Figure 2-12. The steep north striking fracture, 1C17438B0910D6E4, though has such large uncertainty that it might be part of either the ESE striking set or the W striking set. The sub horizontal SE striking fracture, 2397438B09113C9B, could as well be SW striking and hence be closer to the mean pole of the sub horizontal set.

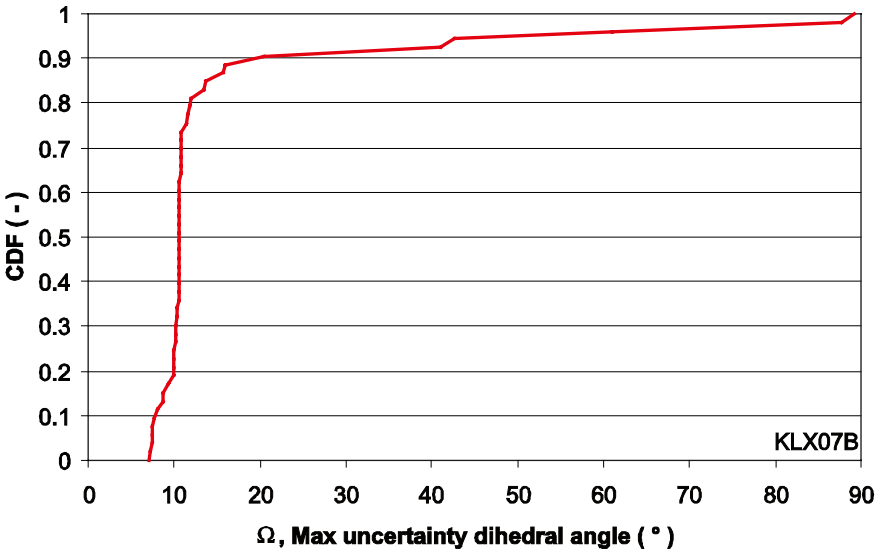

Figure 2-11. The cumulative density function of the largest orientation uncertainties of PFL fractures in KLX07B.

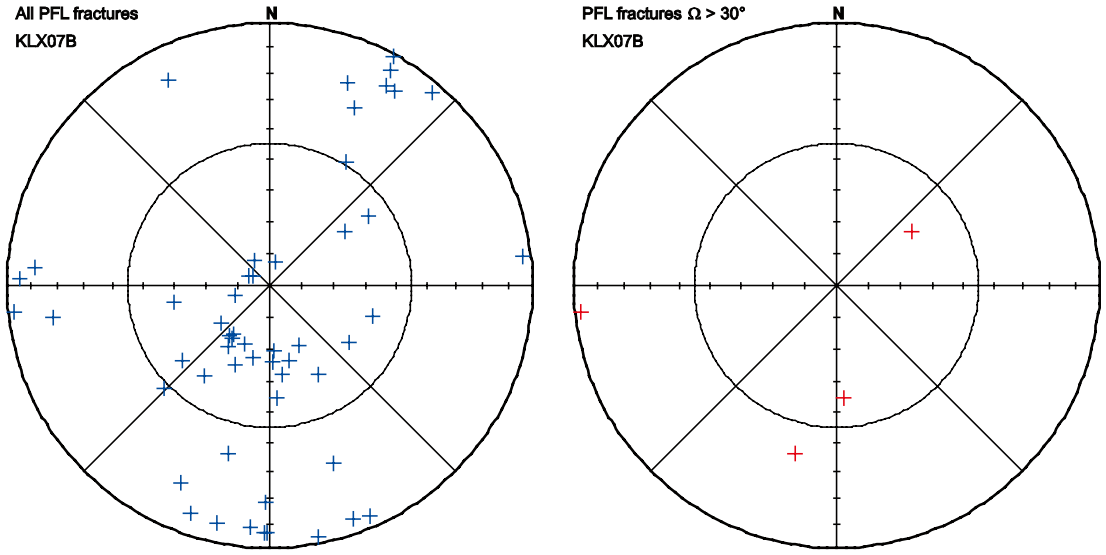

Figure 2-12. To the left the poles of all PFL fractures in KLX07B and to the right the poles of the PFL fractures that have Ω greater than 30°.

2.1.7 KLX08

The uncertainty of the fractures associated with flow in KLX08 is mostly low. The maximum uncertainty is less than 10° for 77% of the fractures, 90% have maximum uncertainty less than 13° and the largest uncertainty is 33°.

There are no fractures that deviate much from the general pattern, though the north striking set is a bit indistinct, see Figure 2-14.

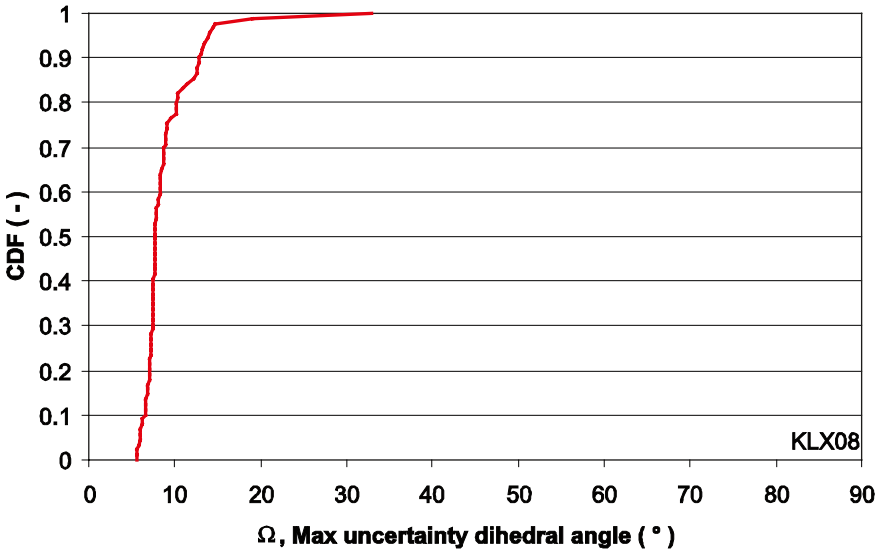

Figure 2-13. *The cumulative density function of the largest orientation uncertainties of PFL fractures in KLX08.*

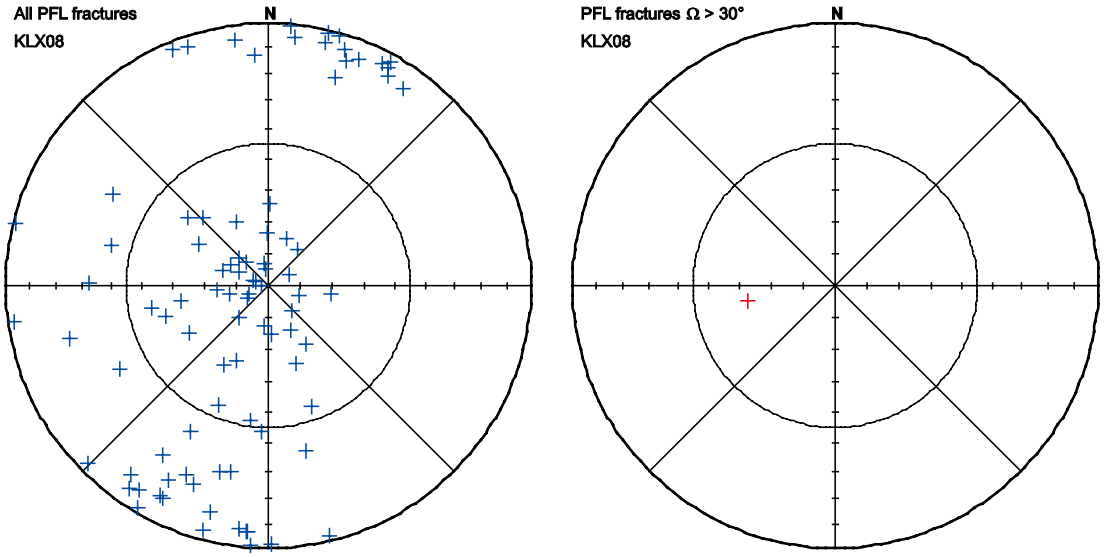

Figure 2-14. *To the left the poles of all PFL fractures in KLX08 and to the right the poles of the PFL fractures that have Ω greater than 30°.*

2.1.8 KLX09

There is one fracture associated with flow that is missing orientation data in p_fract_core_eshi / Sicada 2008/. This fracture is omitted from the orientation analysis. The CDF of the remaining fractures is shown in Figure 2-15. The analysed PFL fractures show low uncertainty, 78% have maximum uncertainty less than 10°, 90% less than 13° and the most uncertain fracture has a maximum uncertainty of 21°.

The poles of the PFL fractures are shown in Figure 2-16. The two fractures that deviates about 20° from the NW/SE striking set have uncertainty about 9° and could hence be a little bit closer to the mean pole. Since no fracture has $\Omega > 30°$ the stereogram of fractures with large uncertainty is omitted.

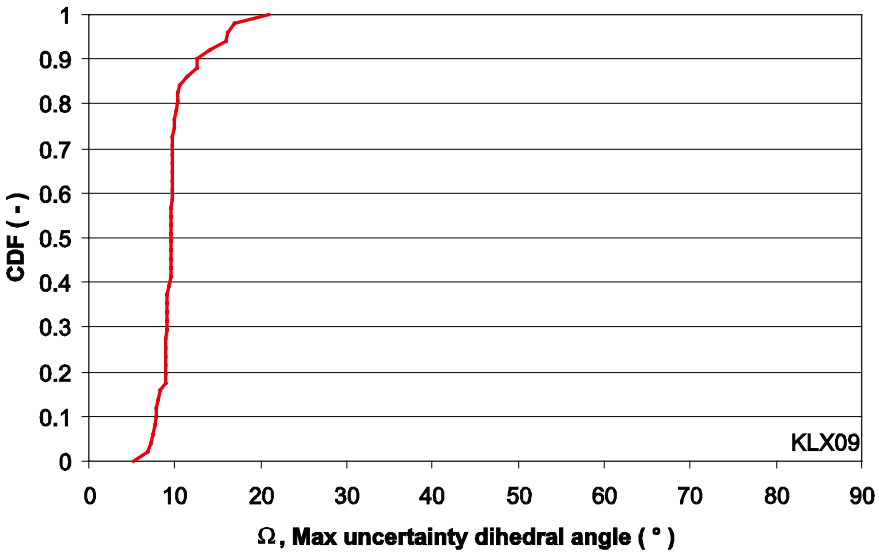

Figure 2-15. The cumulative density function of the largest orientation uncertainties of PFL fractures in KLX09.

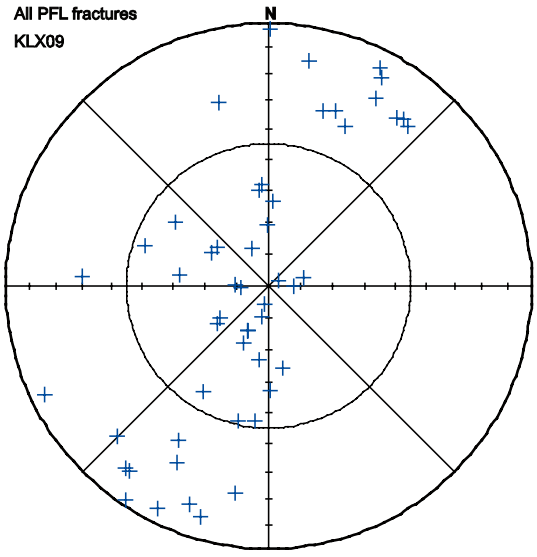

Figure 2-16. The poles of all PFL fractures in KLX09.

2.1.9 KLX09B

The borehole with the largest uncertainties is KLX09B. This is due to the large bearing uncertainty, 133°, which, together with the beta uncertainty, will result in a nearly full beta range uncertainty, see further Section 2.3.9, for many fractures. The borehole has inclination steeper than –89° and thus is the steepest of the KLX holes, together with KLX11B. This makes them harder to measure accurate, see e.g. /Munier and Stigsson 2007 in prep/. Only one PFL fracture has maximum uncertainty less than 10° and 42% have maximum uncertainty close to 90°, which is the maximum possible, see Figure 2-17.

The uncertainties in KLX09B are large and most of the PFL fractures can have an almost random strike, see Figure 2-18 and Section 2.3.9. The orientation of the surrounding KLX09x with low uncertainty might be used as guidance for the orientation of the PFL fractures in KLX09B. However the uncertainties in alpha angles are small and the borehole is almost vertical resulting in low uncertainty in dip.

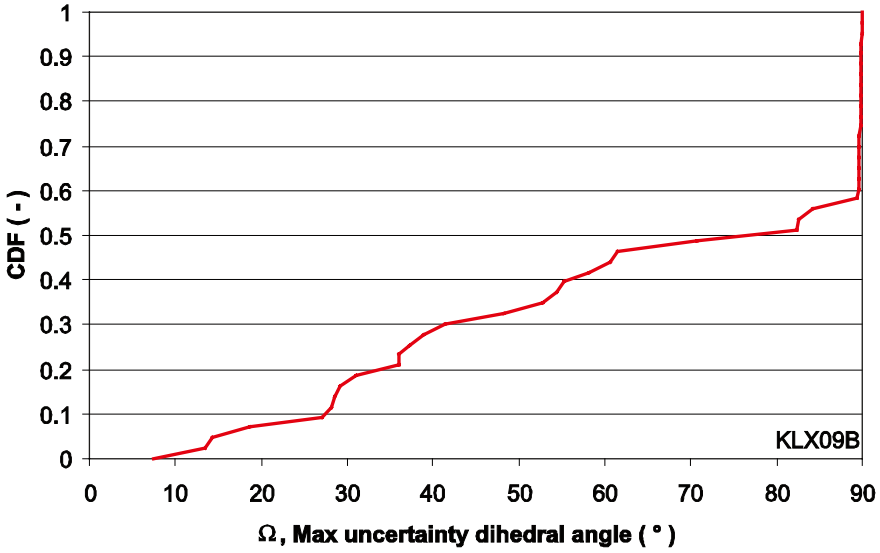

Figure 2-17. The cumulative density function of the largest orientation uncertainties of PFL fractures in KLX09B.

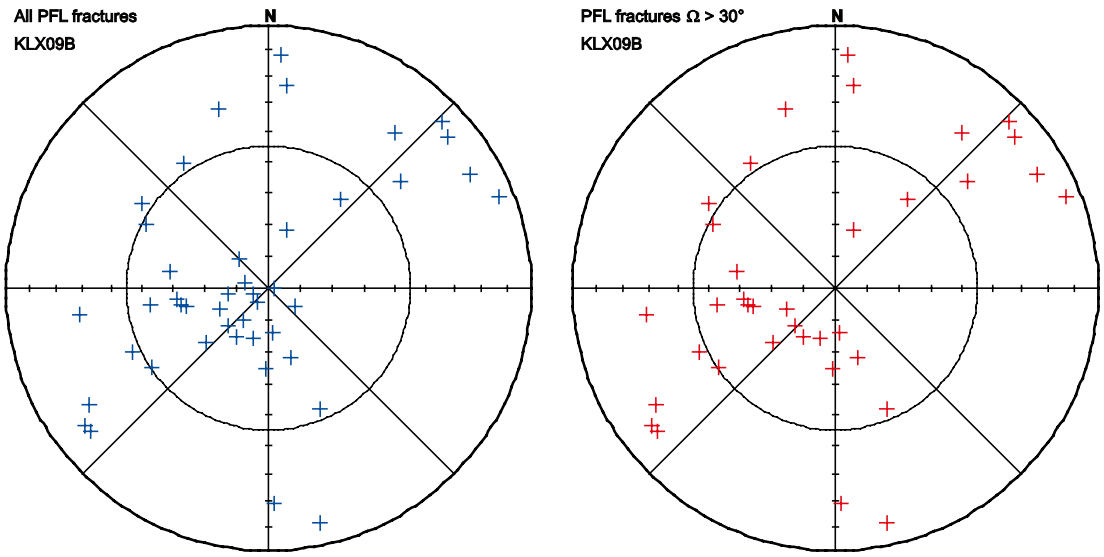

Figure 2-18. To the left the poles of all PFL fractures in KLX09B and to the right the poles of the PFL fractures that have Ω greater than 30°.

2.1.10 KLX09C

KLX09C is a borehole where the PFL fractures have low uncertainty, see Figure 2-19. About 90% of the fractures have maximum uncertainty less than 10° and the greatest uncertainty of any fracture associated with flow is 15°.

The poles of the PFL fractures in KLX09C show a sub horizontal fracture set and a sparsely distributed west striking fracture set, see Figure 2-20. Using the information of the sample space in Section 2.3.10, still keep the poles spread for the PFL fractures. The two south striking fractures might be part of a set, but due to the small amount of data it is hard to draw any conclusions. However, there are south striking PFL fractures present in KLX09D, -09F and -09G.

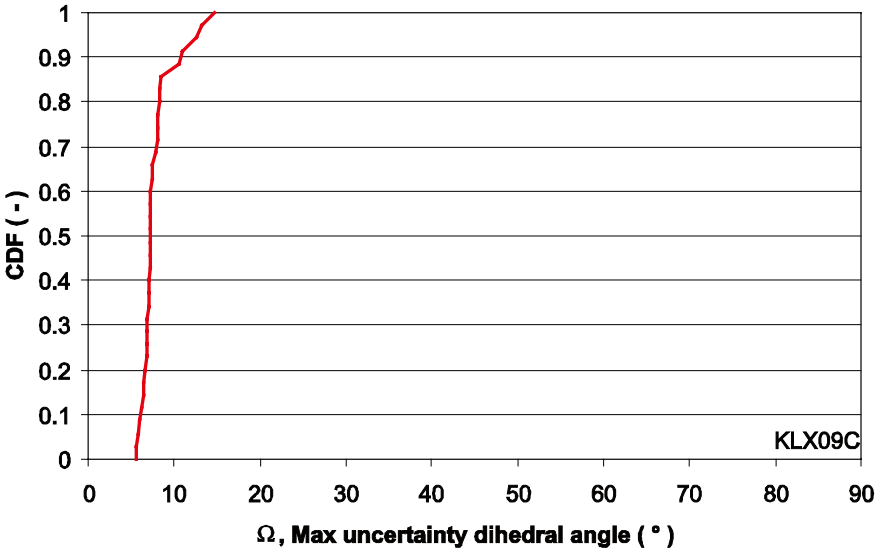

Figure 2-19. *The cumulative density function of the largest orientation uncertainties of PFL fractures in KLX09C.*

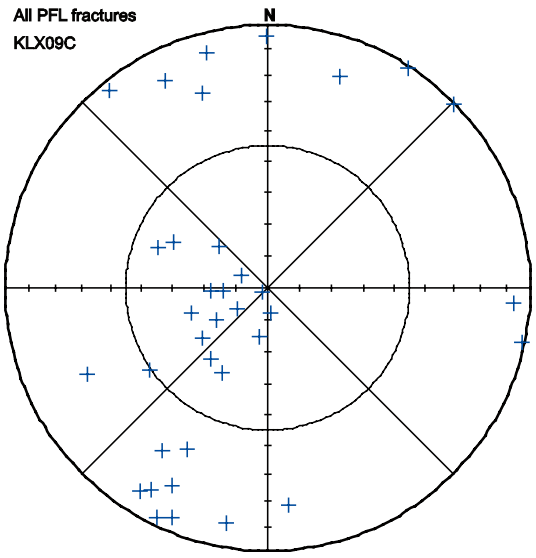

Figure 2-20. *The poles of all PFL fractures in KLX09C.*

2.1.11 KLX09D

The CDF of the maximum uncertainty for fractures associated with flow in KLX09D is shown in Figure 2-21. The maximum uncertainty is less than 10° for 65% of the fractures and 90% of the fractures have maximum uncertainty less than 24°.

The poles of the PFL fractures are sparsely distributed over the hemisphere and hence no distinct sets are seen, see Figure 2-22. The NE striking fracture, 3499438B0F114CC1, has such large uncertainty that it might be part of the steep NW striking fractures or the gently dipping SE striking fractures. Another fracture with large uncertainty is the sub horizontal fracture, 42D9438B0F114618, striking SW. This fracture might also be part of a steep NW striking fracture set, see Section 2.3.11.

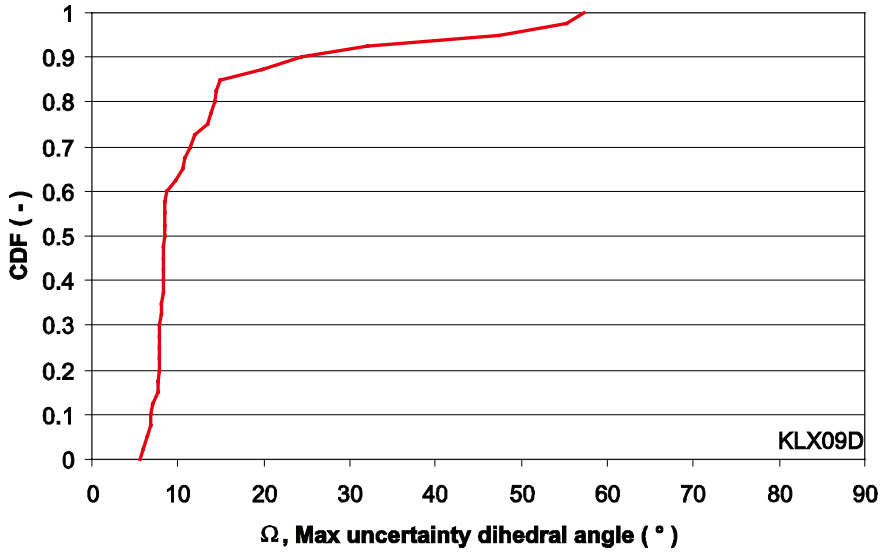

Figure 2-21. The cumulative density function of the largest orientation uncertainties of PFL fractures in KLX09D.

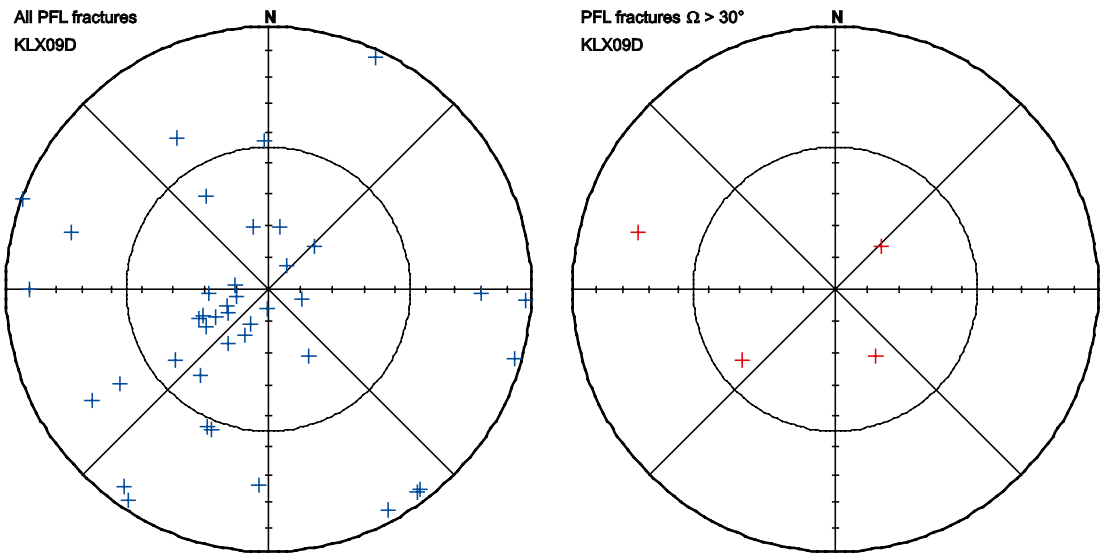

Figure 2-22. To the left the poles of all PFL fractures in KLX09D and to the right the poles of the PFL fractures that have Ω greater than 30°.

2.1.12 KLX09E

The CDF of the maximum uncertainty for PFL fractures is shown in Figure 2-23. The maximum uncertainty is low and less than 10° for about 82% of the data. For 90% of the data the maximum uncertainty is less than 13°.

All the poles of the PFL fractures shown in Figure 2-24 fall within a sub horizontal set or a ESE striking steep set. The fracture, B3D9438B0E11B368, with high orientation uncertainty may well fit into any of these two set due to the large uncertainty, see Section 2.3.12.

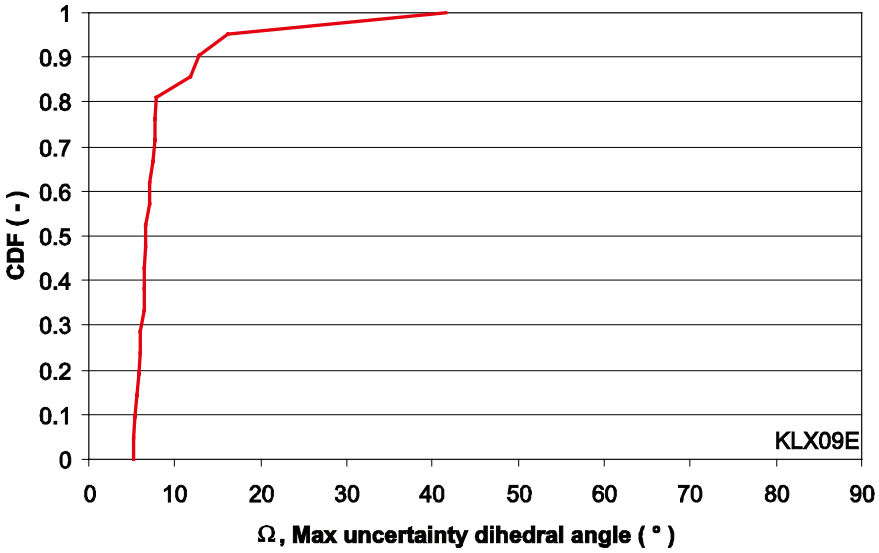

Figure 2-23. The cumulative density function of the largest orientation uncertainties of PFL fractures in KLX09E.

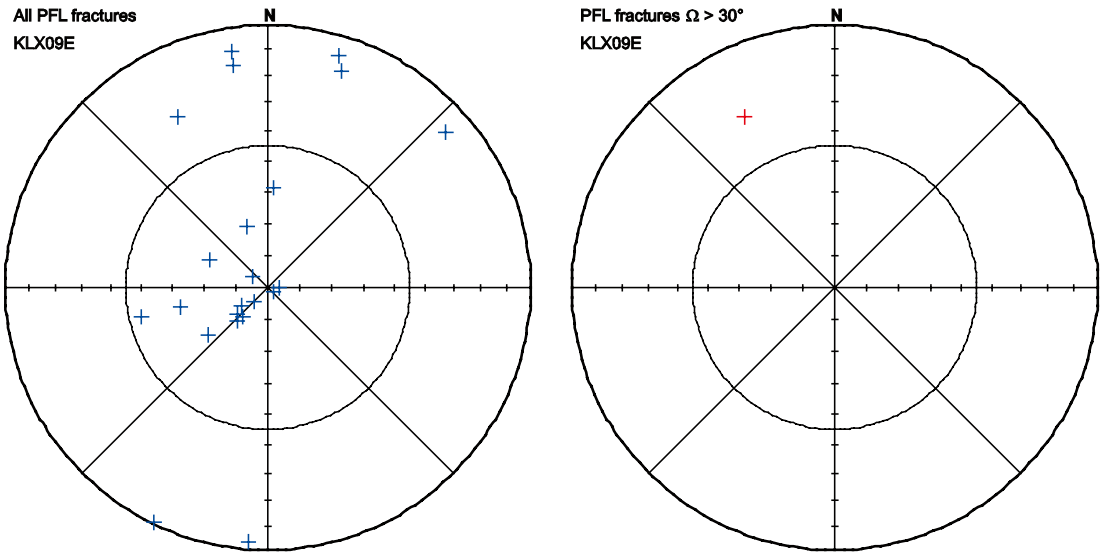

Figure 2-24. To the left the poles of all PFL fractures in KLX09E and to the right the poles of the PFL fractures that have Ω greater than 30°.

2.1.13 KLX09F

In KLX09F the vast majority of the fractures associated with flow have a low uncertainty but there are a couple of PFL fractures where the orientation uncertain is high, see Figure 2-25. About 92% of the fractures have uncertainty less than 10°.

Four different PFL fracture sets can, by visual inspection, be identified in KLX09F, according to Figure 2-26. One of the two fractures with large uncertainty, ID 9599438B0D108369, that is sub horizontal can, as well, be interpreted as belonging to the SE striking fractures, see Section 2.3.13.

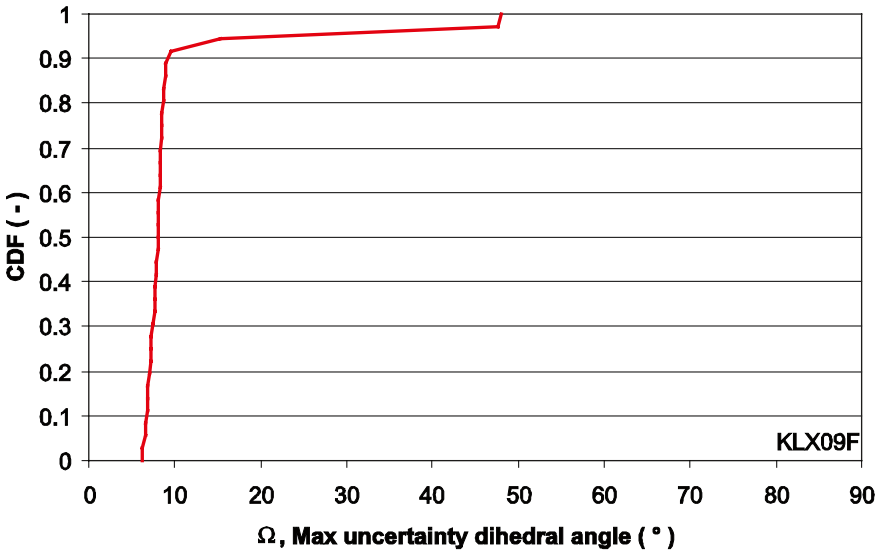

Figure 2-25. *The cumulative density function of the largest orientation uncertainties of PFL fractures in KLX09F.*

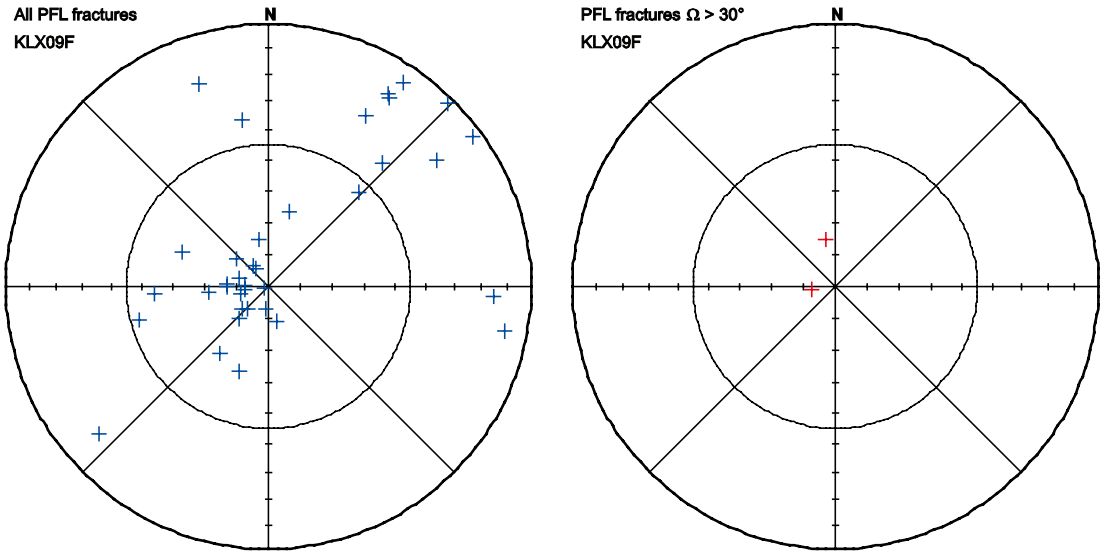

Figure 2-26. *To the left the poles of all PFL fractures in KLX09F and to the right the poles of the PFL fractures that have Ω greater than 30°.*

2.1.14 KLX09G

The majority of the PFL fractures in KLX09G have low uncertainty. Figure 2-27 shows that about 90% of the fractures, associated with flow, have maximum uncertainty less than 10°.

The PFL fractures in KLX09G are sparsely and almost evenly distributed over the hemisphere and hence no distinct sets can be recognized among the few data. Almost all of the sample space of the sub horizontal fracture CF99438B0C106216 is within the 45° dip circle and hence should be interpreted as a slightly dipping to horizontal fracture.

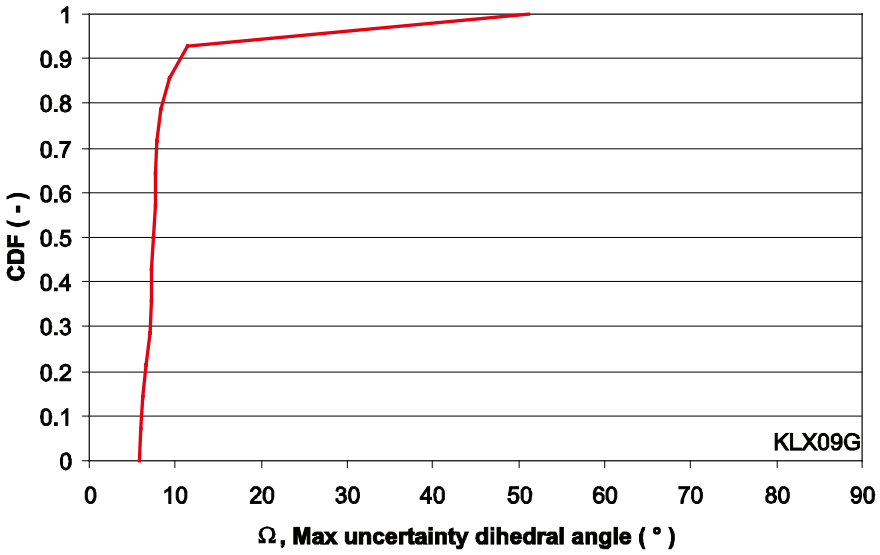

Figure 2-27. The cumulative density function of the largest orientation uncertainties of PFL fractures in KLX09G.

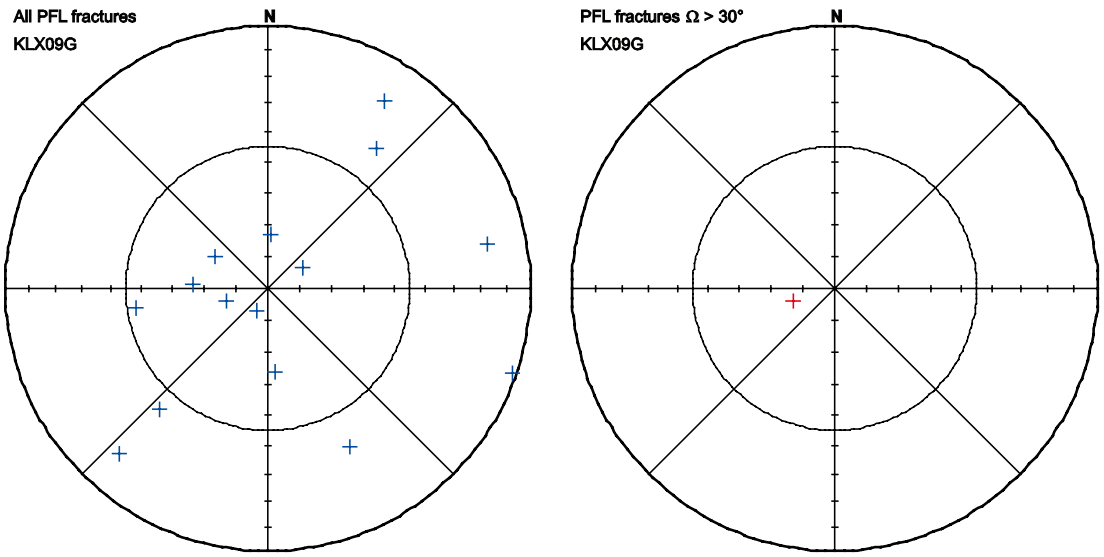

Figure 2-28. To the left the poles of all PFL fractures in KLX09G and to the right the poles of the PFL fractures that have Ω greater than 30°.

2.1.15 KLX10

The fractures associated with flow in KLX10 show high uncertainty, see Figure 2-29. Only 4% of the PFL fractures have maximum uncertainty less than 10° whilst 90% of the fractures have uncertainty less than 17°. There are 5 PFL fractures that have maximum uncertainty larger than 66°.

There are three PFL fractures that deviates from the general pattern of orientations in KLX10, see Figure 2-30. Of these three only the NE striking fracture, 4910478B2B156B74, has large uncertainty and it can be interpreted to be among the WNW striking fractures. None of the other two have sample space that makes it possible to interpret them as members of any fracture set. The steep eastly striking fracture, FF50478B2B164782, has it sample space stretching almost along the whole perimeter of the hemisphere.

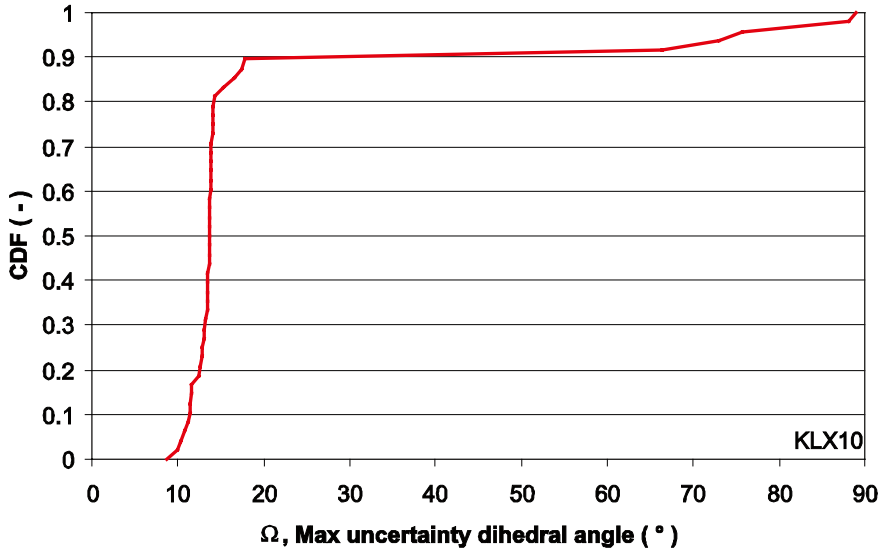

Figure 2-29. The cumulative density function of the largest orientation uncertainties of PFL fractures in KLX10.

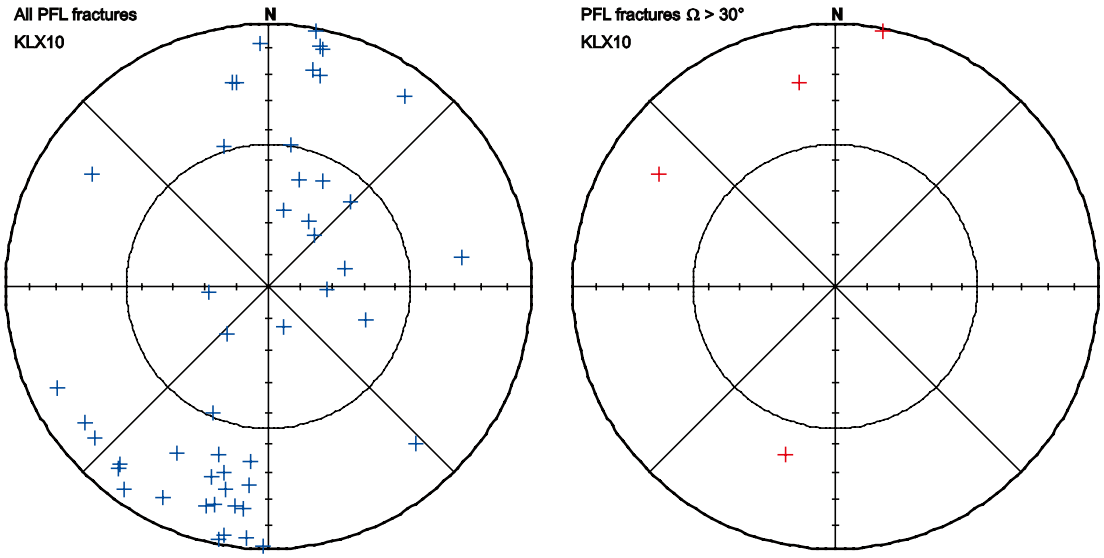

Figure 2-30. To the left the poles of all PFL fractures in KLX10 and to the right the poles of the PFL fractures that have Ω greater than 30°.

2.1.16 KLX10B

The maximum uncertainty for PFL fractures are small in KLX10B, see Figure 2-31. About 77% of the fractures associated with flow have maximum uncertainty less than 10° whilst 90% of the fractures have maximum uncertainty less than 14°. The largest maximum uncertainty of the PFL fractures is 16°.

The few PFL fractures in KLX10B show a tendency to group into four fracture sets, see Figure 2-32.

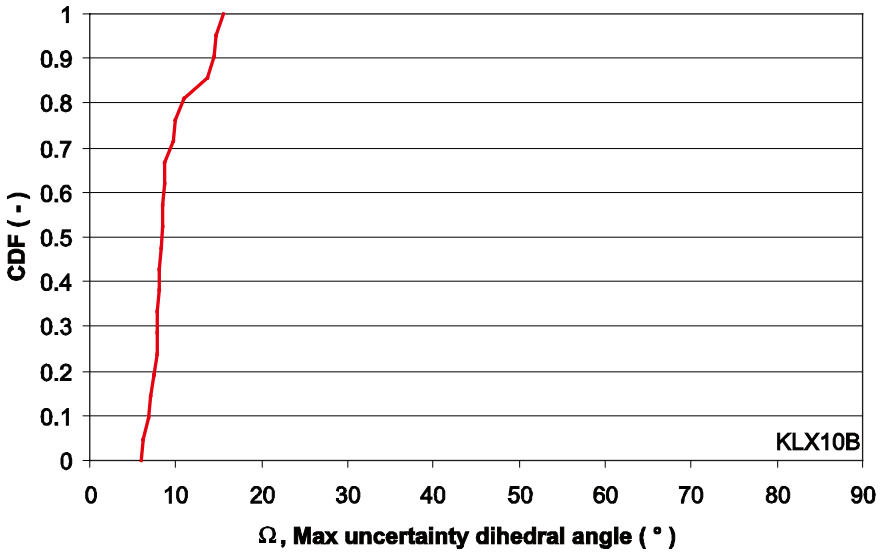

Figure 2-31. The cumulative density function of the largest orientation uncertainties of PFL fractures in KLX10B.

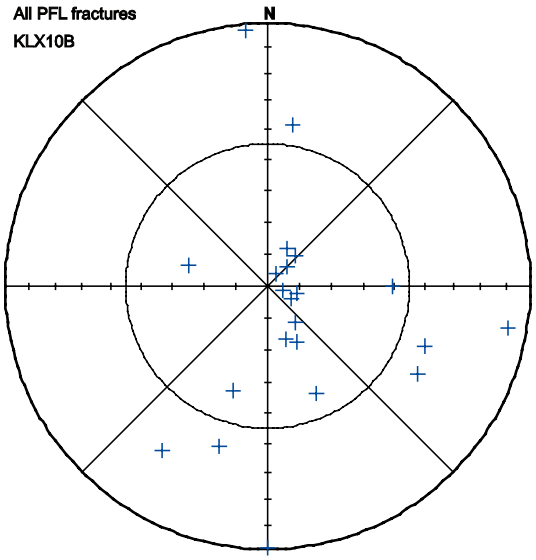

Figure 2-32. The poles of all PFL fractures in KLX10B.

2.1.17 KLX10C

The CDF of maximum uncertainty of PFL fractures in KLX10C is shown in Figure 2-33. No PFL fracture show any maximum uncertainty larger than 14°, 90% is less than 12° and about 82% is less than 10°.

The PFL fracture poles plotted in Figure 2-34 show a relatively well clustered NE striking set together with a sparse sub horizontal set.

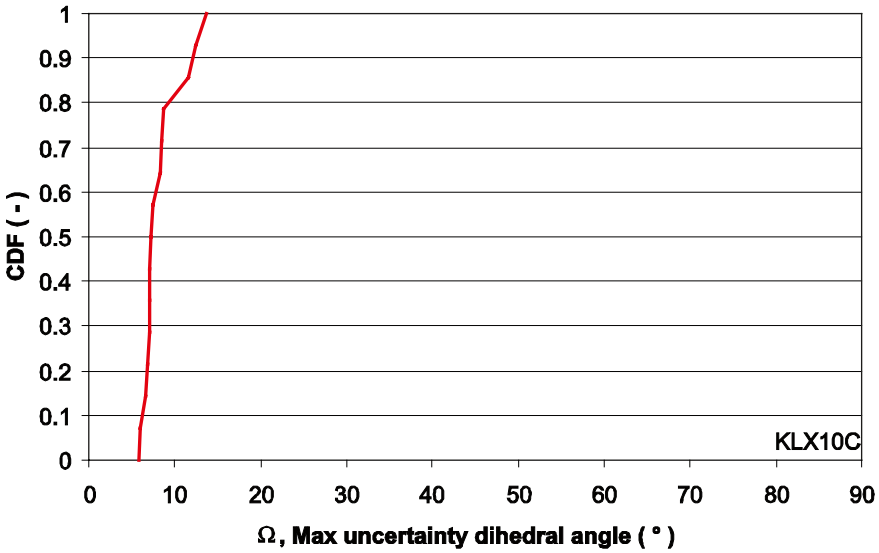

Figure 2-33. The cumulative density function of the largest orientation uncertainties of PFL fractures in KLX10C.

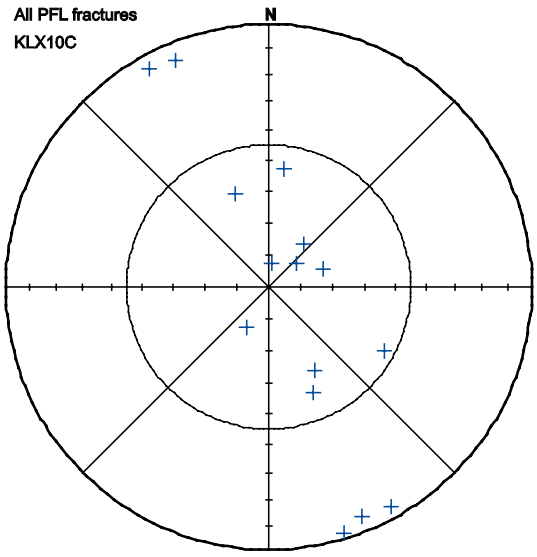

Figure 2-34. The poles of all PFL fractures in KLX10C.

2.1.18 KLX11A

The CDF of the maximum uncertainty for PFL fractures in KLX11A is shown in Figure 2-35. About 72% of the fractures associated with flow have maximum uncertainty less than 10° and 90% have maximum uncertainty less than 15°.

The PFL fractures in KLX11A show a relatively large spread, but a visual inspection of the poles in Figure 2-36 show four fracture sets. The north striking fracture, 4B91478B0A1800A9, with large uncertainty can be interpreted as belonging to the small cluster of west striking fractures, see Section 2.3.18.

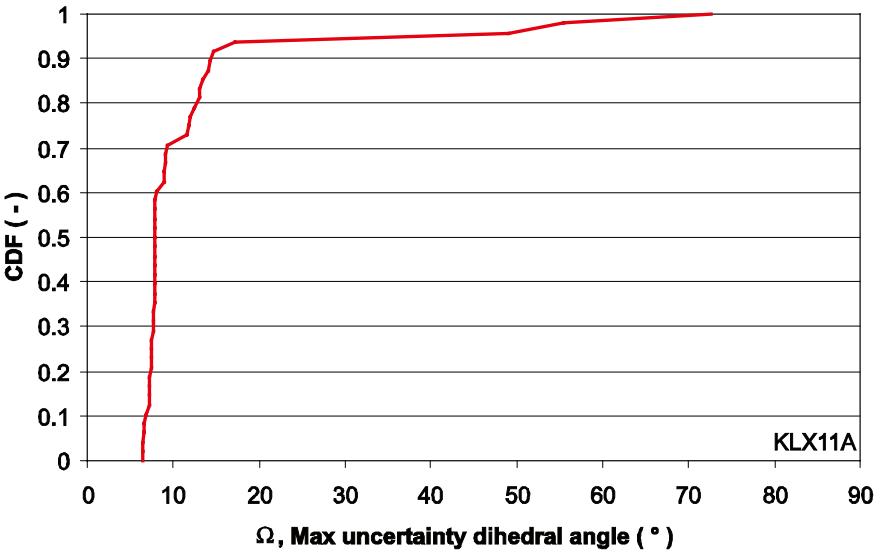

Figure 2-35. The cumulative density function of the largest orientation uncertainties of PFL fractures in KLX11A.

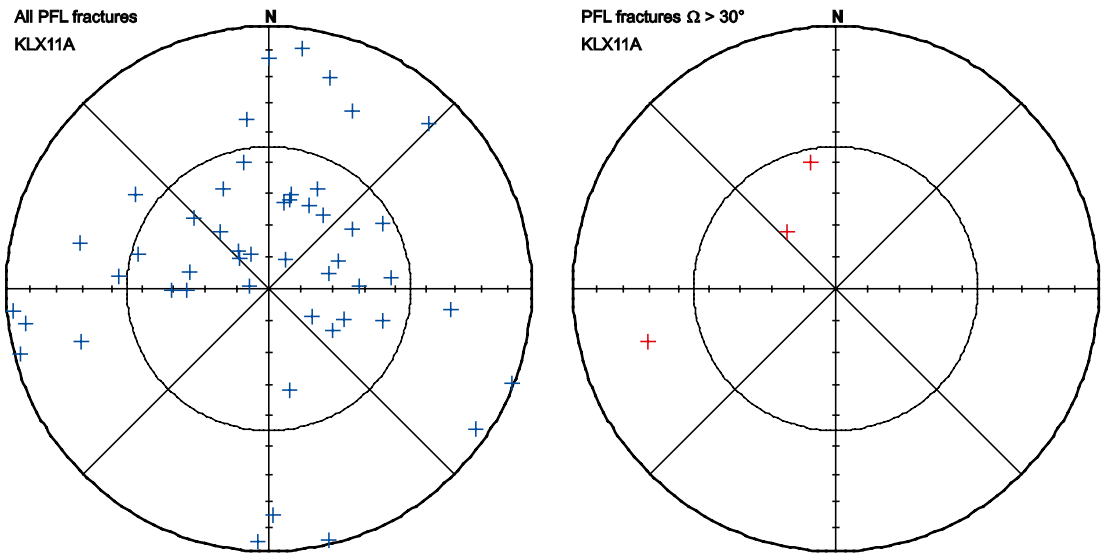

Figure 2-36. To the left the poles of all PFL fractures in KLX11A and to the right the poles of the PFL fractures that have Ω greater than 30°.

2.1.19 KLX11B

The maximum uncertainty for the PFL fractures is large for KLX11B, but not as extreme as KLX09B, see Section 2.1.9. The steep inclination, steeper than –89°, and large bearing uncertainty, 15°, together with a large beta uncertainty for a steep fracture result in maximum uncertainties close to 90°. No PFL fracture has maximum uncertainty less than 10°, and 10% have maximum uncertainty greater than 37°.

There are too few steep fractures in KLX11B to be able to see any clusters and furthermore all the five steep fractures have orientation uncertainty larger than 20° resulting in the possibility that they might cluster or spread evenly along the perimeter of the hemisphere.

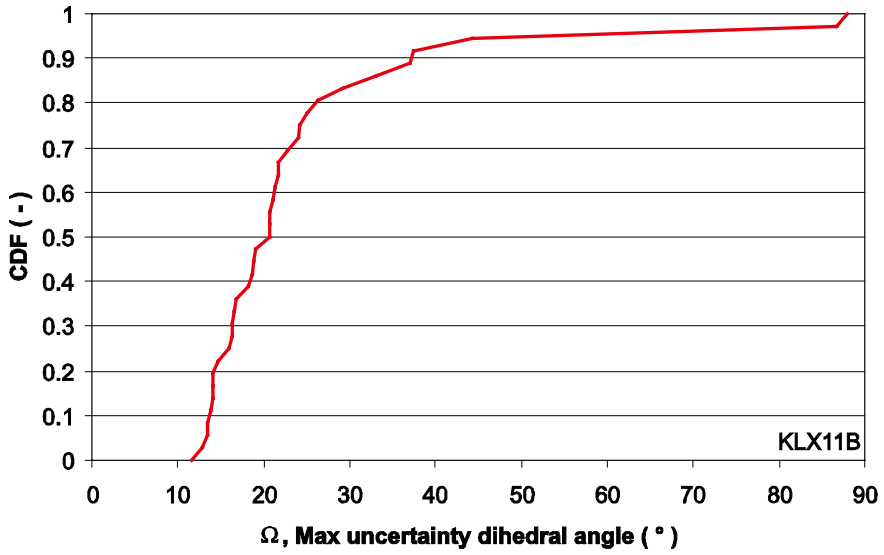

Figure 2-37. The cumulative density function of the largest orientation uncertainties of PFL fractures in KLX11B.

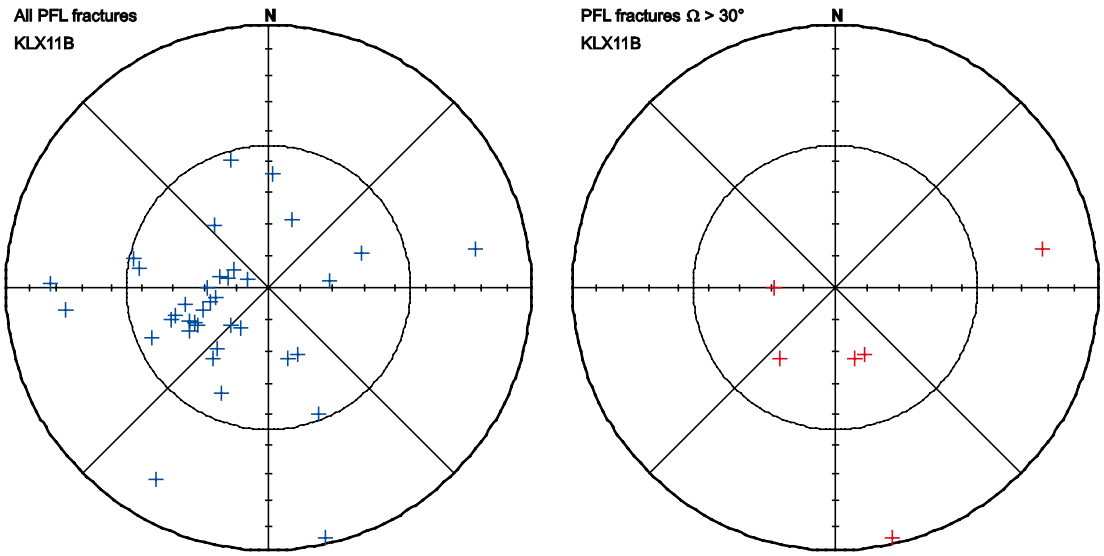

Figure 2-38. To the left the poles of all PFL fractures in KLX11B and to the right the poles of the PFL fractures that have Ω greater than 30°.

2.1.20 KLX11C

The CDF of the maximum uncertainty for PFL fractures in KLX11C is shown in Figure 2-39. About 69% of the fractures associated with flow have maximum uncertainty less than 10° and the 15% most uncertain fractures have a maximum uncertainty exceeding 24°.

The orientation of the PFL fractures cluster into one sparse sub horizontal set and, maybe, one very sparse EW set, see Figure 2-40. Both the NW striking PFL fracture, 2091478B081080D7, and the WNW fracture, 2091478B0810CE05, with large orientation uncertainties has sample spaces so large that it can belong to the sub horizontal fractures as well as the EW fractures, see Section 2.3.20.

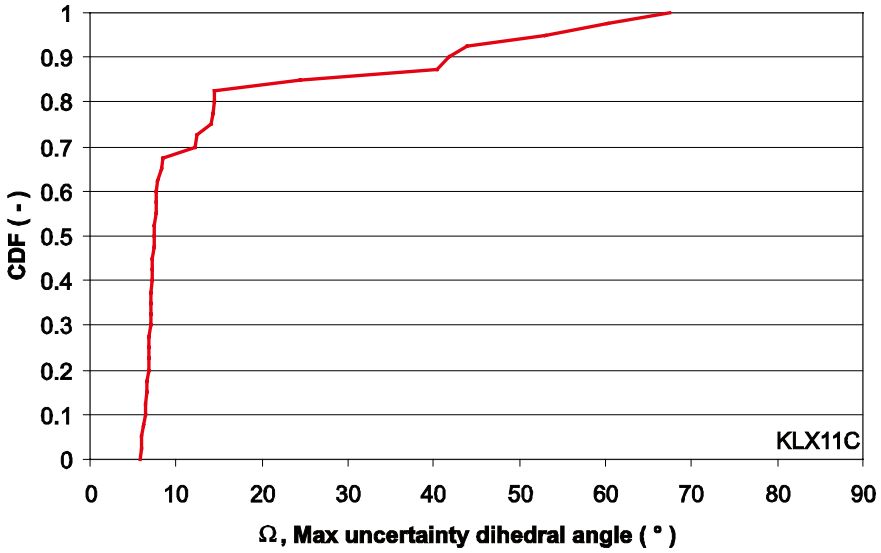

Figure 2-39. *The cumulative density function of the largest orientation uncertainties of PFL fractures in KLX11C.*

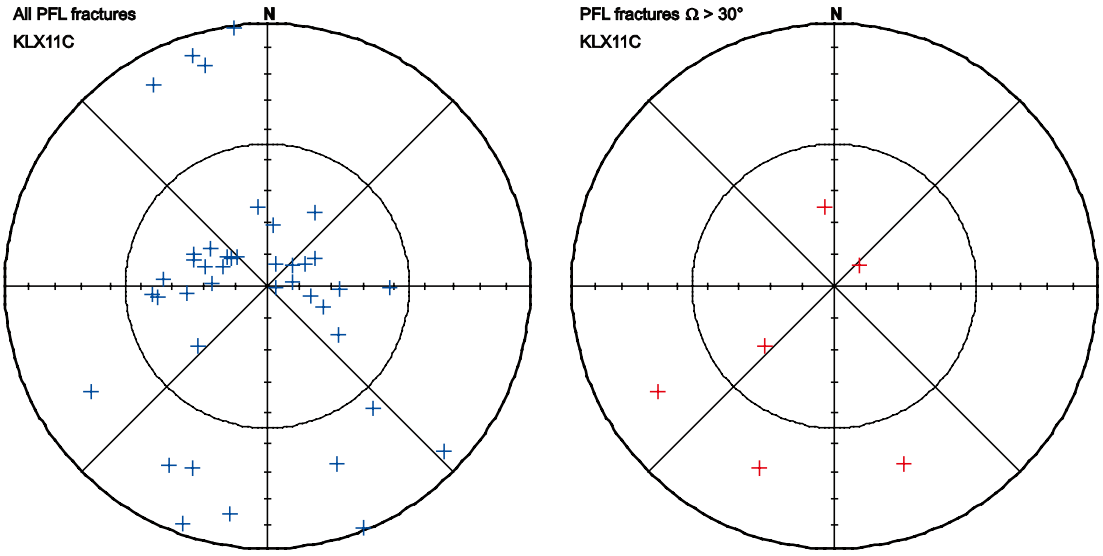

Figure 2-40. *To the left the poles of all PFL fractures in KLX11C and to the right the poles of the PFL fractures that have Ω greater than 30°.*

2.1.21 KLX11D

The CDF of the maximum uncertainty for the PFL fractures in KLX11D is shown in Figure 2-41. About 2/3 of the fractures have maximum uncertainty less than 10° whilst 90% of the fractures have maximum uncertainty less than 13°.

The PFL fractures in KLX11D show three clusters of fractures and none of the fractures with large uncertainty is outside the general pattern or have such large uncertainty that it can belong to any other cluster, see Figure 2-42 and Section 2.3.21.

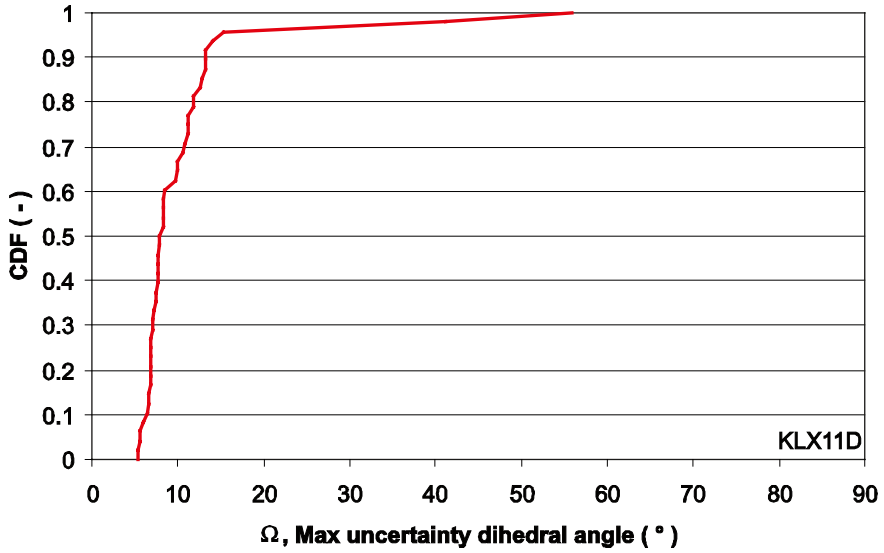

Figure 2-41. The cumulative density function of the largest orientation uncertainties of PFL fractures in KLX11D.

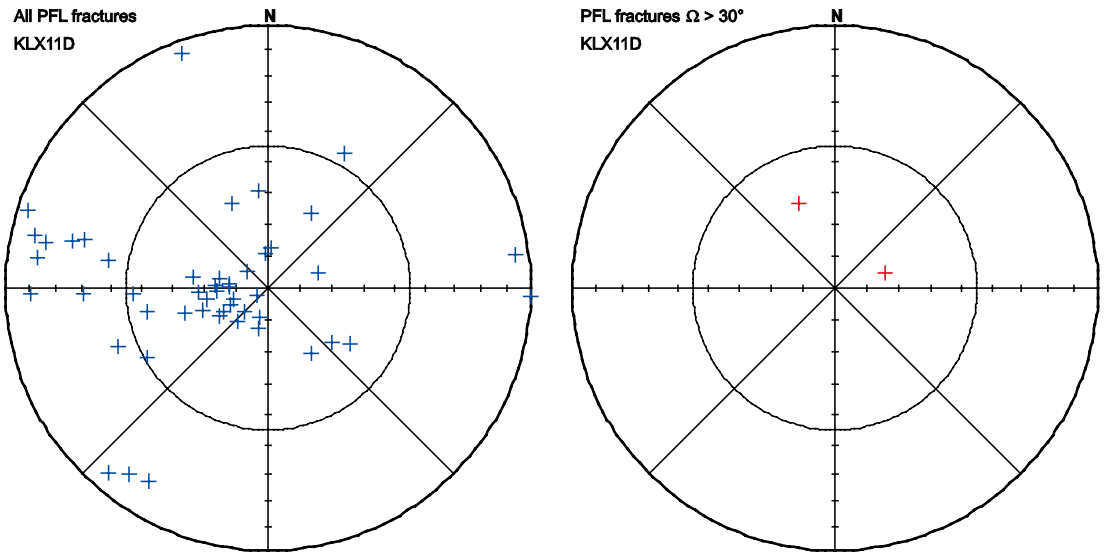

Figure 2-42. To the left the poles of all PFL fractures in KLX11D and to the right the poles of the PFL fractures that have Ω greater than 30°.

2.1.22 KLX11E

The maximum uncertainties for the PFL fractures in KLX11E are shown in Figure 2-43. Most fractures associated with flow, 87%, have maximum uncertainty below 10° and 90% of the fractures have maximum uncertainty less than 14°.

One can interpret the poles in the stereogram in Figure 2-44 to cluster into four fracture sets. The two fractures with large uncertainty can, as an alternative, be interpreted as belonging to the north striking fractures, see 2.3.22.

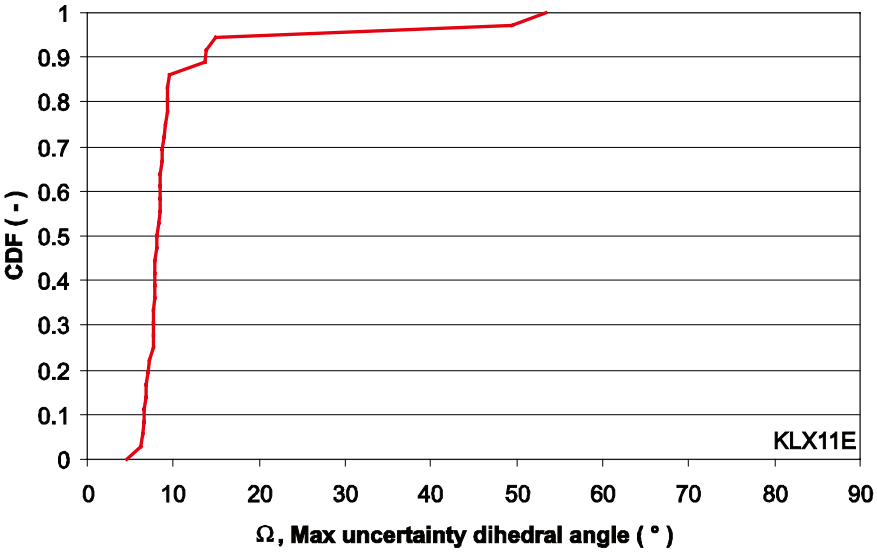

Figure 2-43. The cumulative density function of the largest orientation uncertainties of PFL fractures in KLX11E.

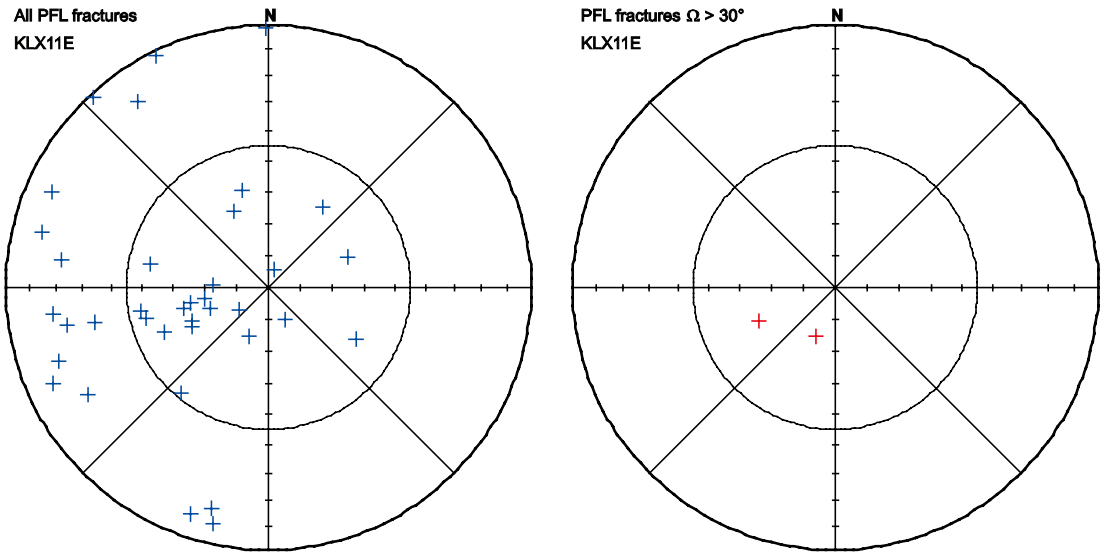

Figure 2-44. To the left the poles of all PFL fractures in KLX11E and to the right the poles of the PFL fractures that have Ω greater than 30°.

2.1.23 KLX11F

The maximum uncertainty values for PFL fractures in KLX11F are low. About 80% of the fractures have maximum uncertainty less than 10° and 90% less than 13°. The largest uncertainty is 26°.

There are few and sparsely distributed PFL fractures in KLX11F making it hard to, by visual inspection, draw any conclusions about any clustering into different fracture sets.

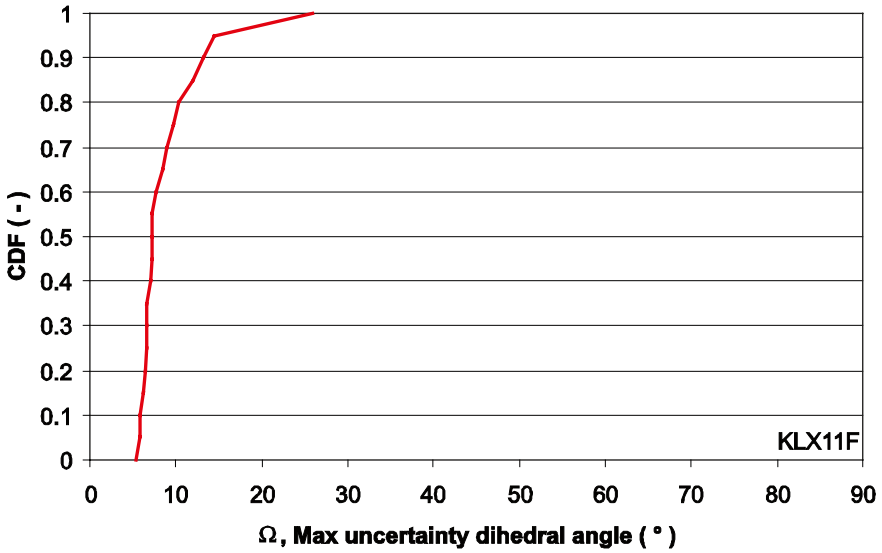

Figure 2-45. *The cumulative density function of the largest orientation uncertainties of PFL fractures in KLX11F.*

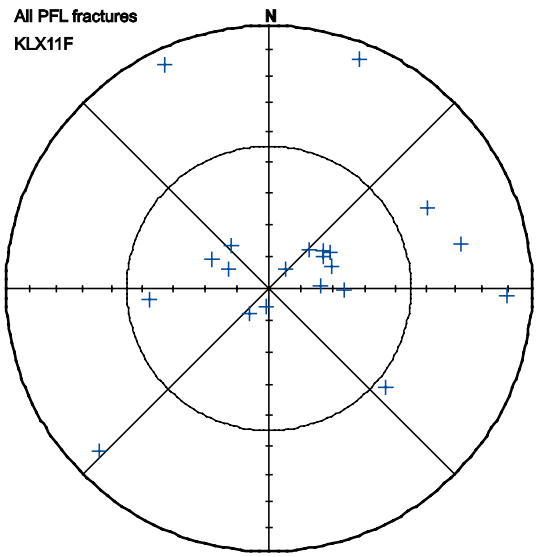

Figure 2-46. *The poles of all PFL fractures in KLX11F.*

2.1.24 KLX12A

Just a little bit more than half, 54%, of the PFL fractures in KLX12A have a maximum uncertainty below 10°. There is also a large portion of fractures with highly uncertain orientation, see Figure 2-47, 13% of the fractures associated with flow exceed 30° maximum uncertainty.

Especially the south striking and the two WNW striking fractures, to the right in Figure 2-48, have such large uncertainty that they may be interpreted as belonging to other clusters of fractures, see further Section 2.3.24.

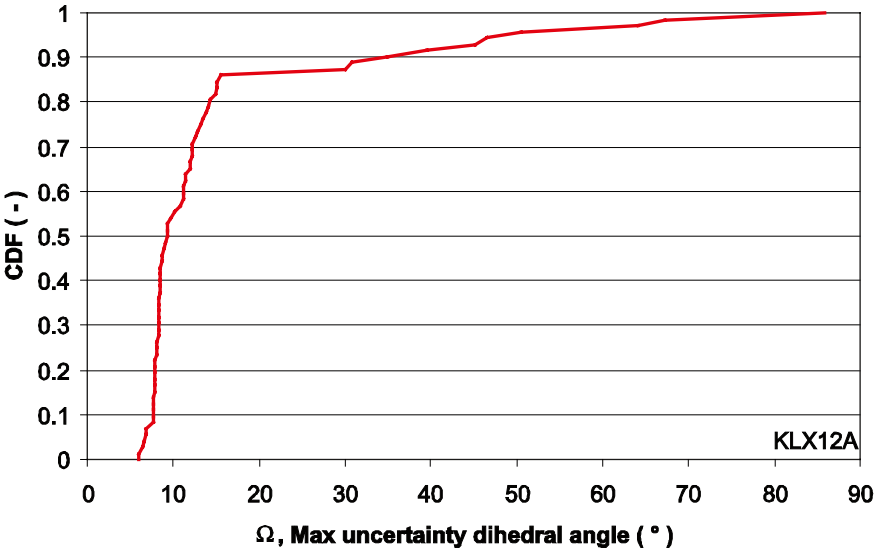

Figure 2-47. *The cumulative density function of the largest orientation uncertainties of PFL fractures in KLX12A.*

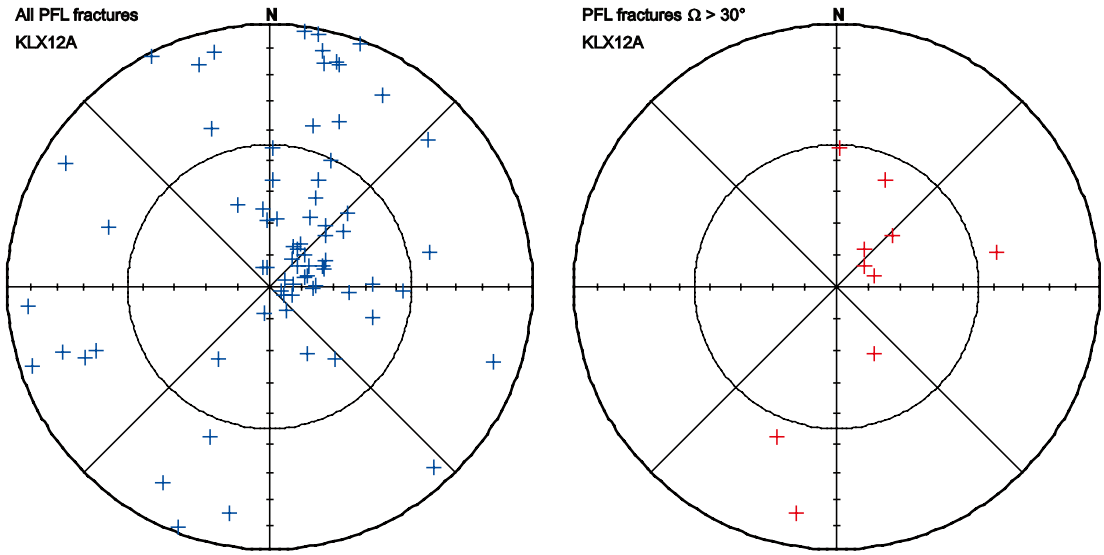

Figure 2-48. *To the left the poles of all PFL fractures in KLX12A and to the right the poles of the PFL fractures that have Ω greater than 30°.*

2.1.25 KLX13A

The CDF of maximum uncertainty of PFL fractures in KLX13A is shown in Figure 2-49. The maximum uncertainty is less than 10° for 58% of the fractures associated with flow and 90% is less than 15°.

The main orientation of the hydraulic active fractures in KLX13A is NW striking and it is not possible to, by visual inspection, divide the fractures into different sets, see Figure 2-50. Most of the highly orientation uncertain fractures have orientations that follow the general pattern. The exception is the south striking fracture A093478B0A15BBBB, but the uncertainty is so large that it might be closer to other fracture orientations.

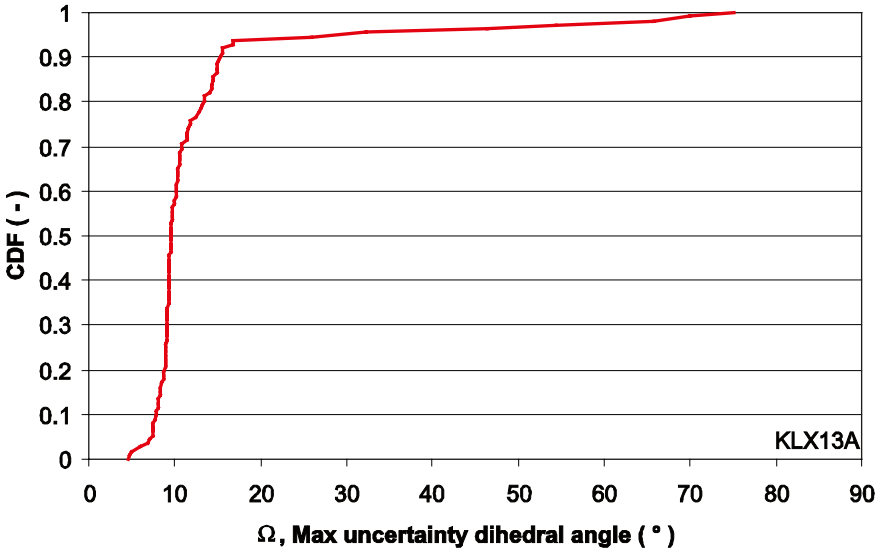

Figure 2-49. The cumulative density function of the largest orientation uncertainties of PFL fractures in KLX13A.

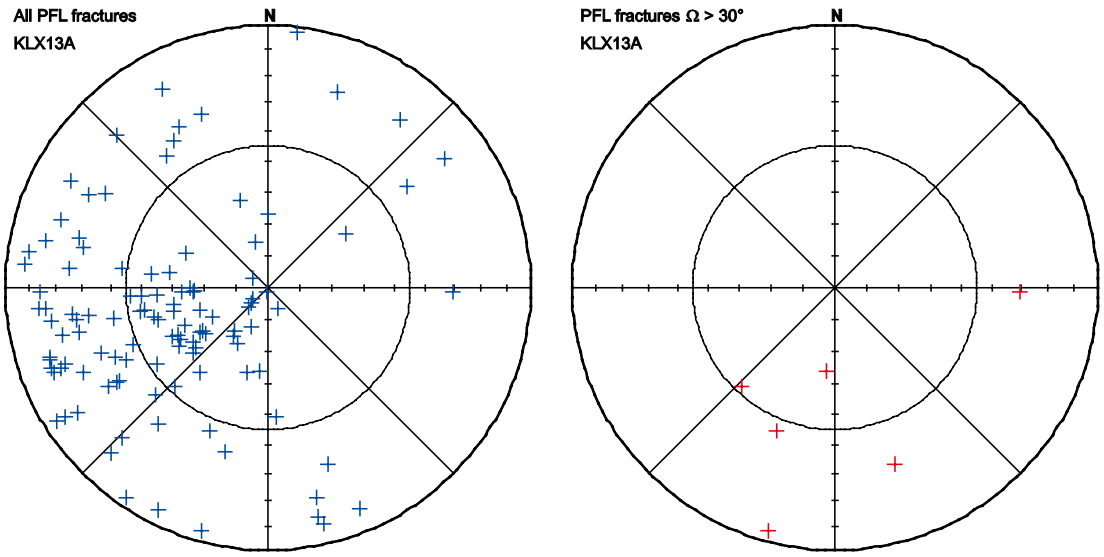

Figure 2-50. To the left the poles of all PFL fractures in KLX13A and to the right the poles of the PFL fractures that have Ω greater than 30°.

2.1.26 KLX14A

There is missing information about orientation for one PFL fracture in KLX14A in the table p_fract_core_eshi /Sicada 2008/ and thus this fracture has been omitted from the analysis of the maximum uncertainty shown in Figure 2-51. All but one PFL fracture have maximum uncertainty less than 10°, but the orientation of that fracture is highly uncertain, 88°, of possible 90°.

The clustering is, by visual inspection, weak in KLX14A, see Figure 2-52, which might be an effect of the few data for steeply dipping PFL fractures. However three sets seem to be present and the fracture with large orientation uncertainty does not deviate from the pattern, but has such sample space that it might be part of the SE striking PFL fractures.

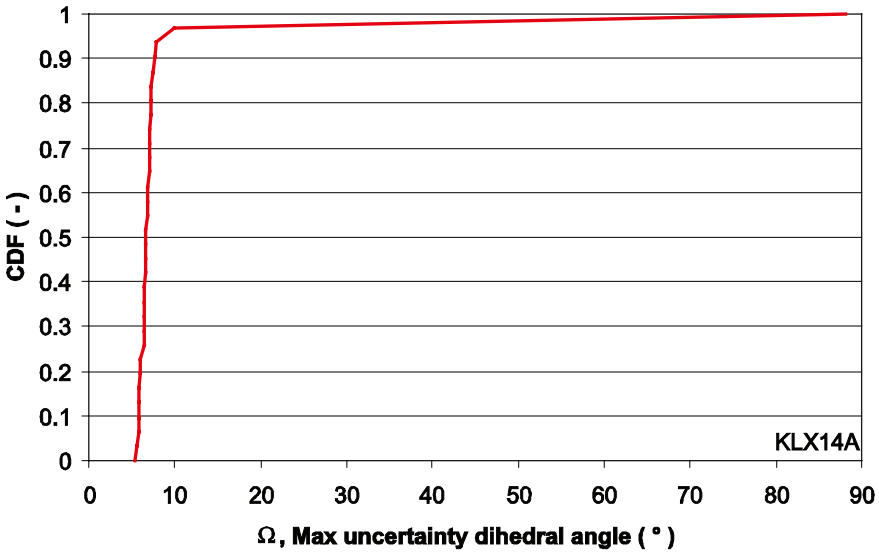

Figure 2-51. The cumulative density function of the largest orientation uncertainties of PFL fractures in KLX14A.

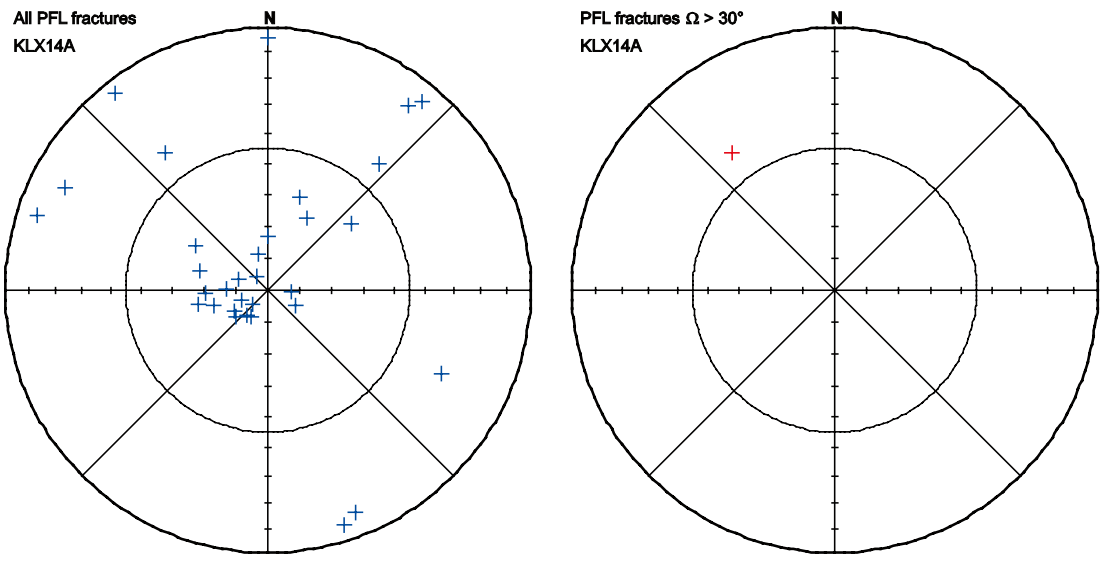

Figure 2-52. To the left the poles of all PFL fractures in KLX14A and to the right the poles of the PFL fractures that have Ω greater than 30°.

2.1.27 KLX15A

The CDF of maximum uncertainty of PFL fractures in KLX15A is shown in Figure 2-53. The maximum uncertainty is less than 10° for 72% of the fractures associated with flow and 90% have maximum uncertainty less than 14°.

Most PFL fractures in KLX15A are SW to NW striking or sub horizontal, see Figure 2-54. The PFL fractures with large uncertainty follow the general pattern for the rest of the PFL fractures in KLX15A.

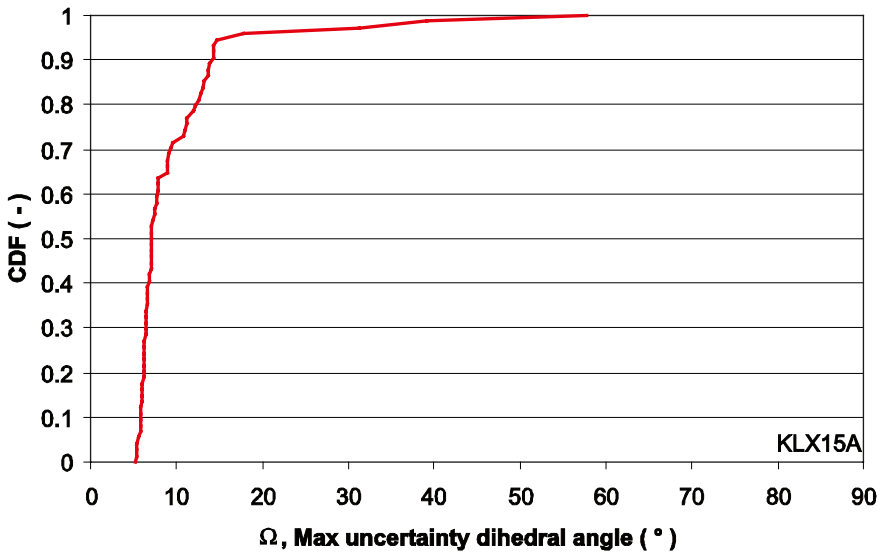

Figure 2-53. The cumulative density function of the largest orientation uncertainties of PFL fractures in KLX15A.

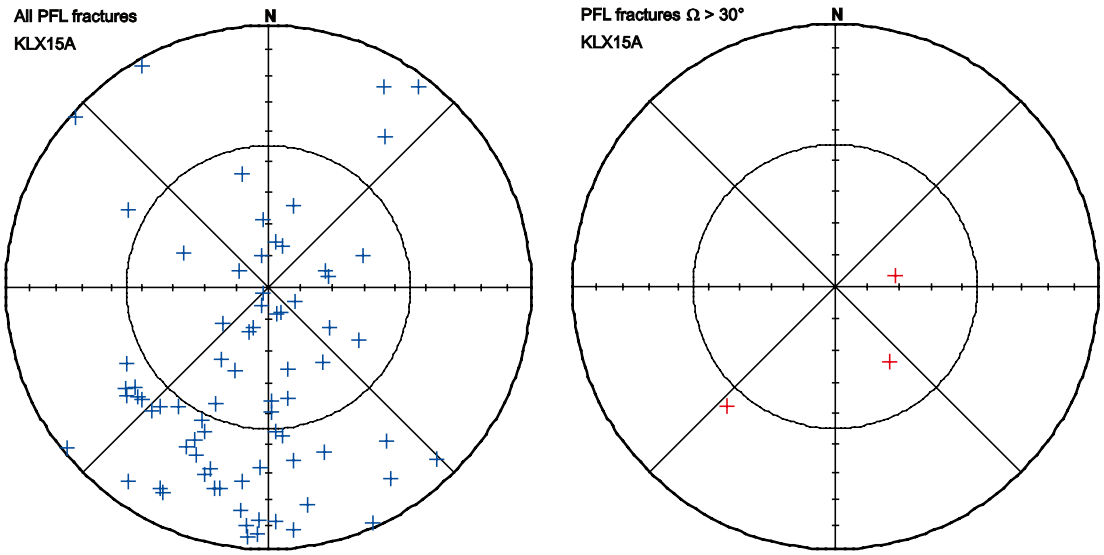

Figure 2-54. To the left the poles of all PFL fractures in KLX15A and to the right the poles of the PFL fractures that have Ω greater than 30°.

2.1.28 KLX16A

The uncertainty in orientation is low for the vast majority of the PFL fractures in KLX16A, see Figure 2-55. About 90% of the fractures associated with flow have maximum uncertainty less than 10° and only one PFL fracture have uncertainty larger than 17°.

There is only one fracture with large orientation uncertainty in KLX16A, see Figure 2-56. This fracture can be part of the small SW striking cluster as well as the west striking set that the best estimate orientation suggests.

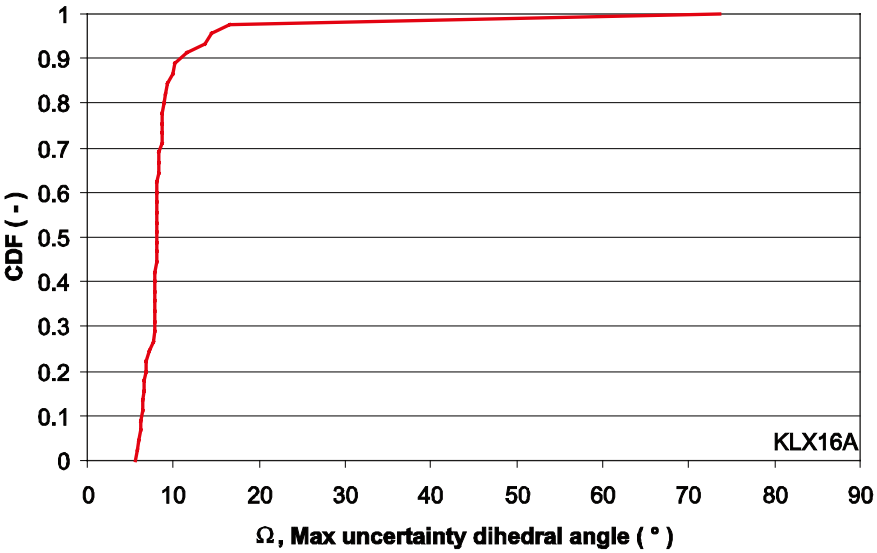

Figure 2-55. The cumulative density function of the largest orientation uncertainties of PFL fractures in KLX16A.

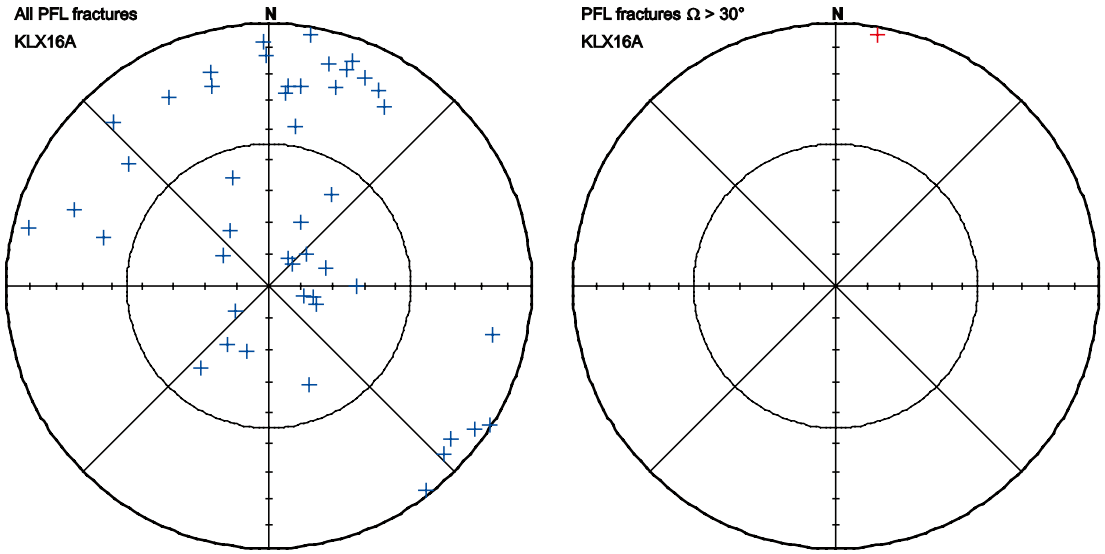

Figure 2-56. To the left the poles of all PFL fractures in KLX16A and to the right the poles of the PFL fractures that have Ω greater than 30°.

2.1.29 KLX17A

The CDF of maximum uncertainty for PFL fractures in KLX17A is shown in Figure 2-55. The maximum uncertainty is less than 10° only for 25% of the fractures associated with flow and 90% of the fractures have maximum uncertainty less than 17°.

The PFL fractures in KLX17A follow a band with NW-SE striking features over the hemisphere and the two PFL fractures with large orientation uncertainty are as well within this pattern, see Figure 2-58.

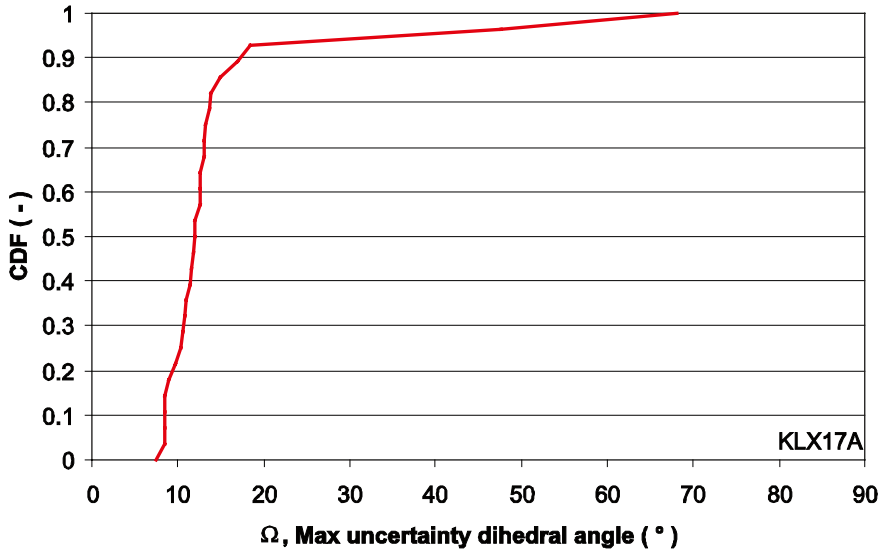

Figure 2-57. The cumulative density function of the largest orientation uncertainties of PFL fractures in KLX17A.

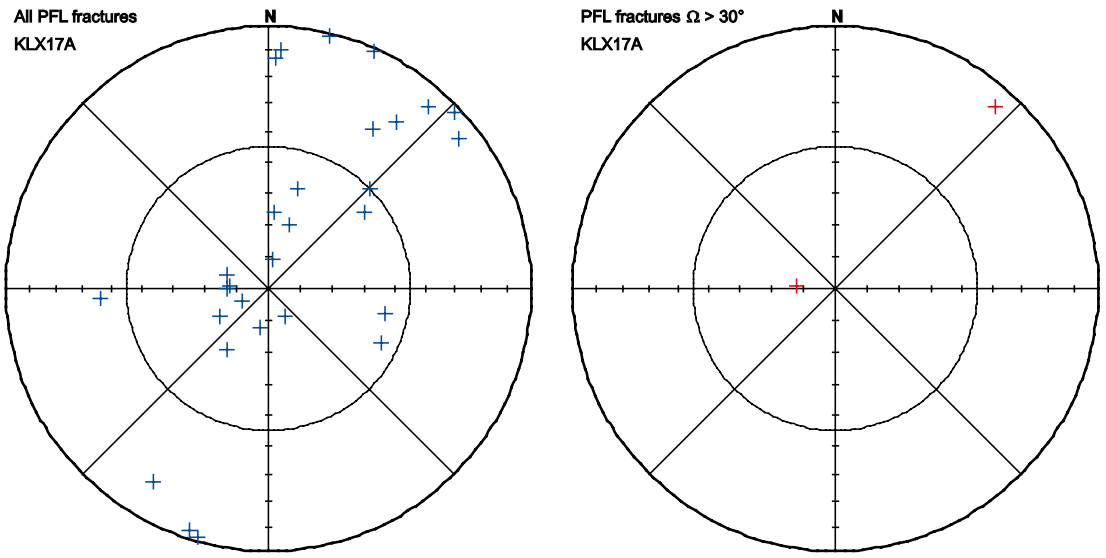

Figure 2-58. To the left the poles of all PFL fractures in KLX17A and to the right the poles of the PFL fractures that have Ω greater than 30°.

2.1.30 KLX18A

The uncertainty in orientation is low for the vast majority of the PFL fractures in KLX18A, 90% of the PFL fractures have uncertainty less than 10°, see Figure 2-59. The remaining fractures show high uncertainty. There are 12 fractures, associated with flow, exceeding 30° maximum uncertainty.

Most of the PFL fractures in KLX18A have orientations that follow a band of fractures striking NW-SE. The fractures with large orientation uncertainty follow this pattern as well, see Figure 2-60.

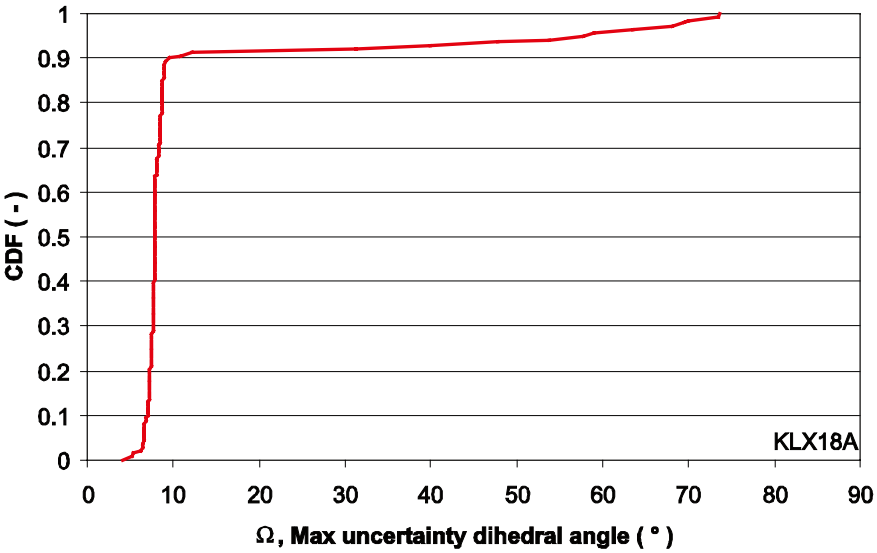

Figure 2-59. *The cumulative density function of the largest orientation uncertainties of PFL fractures in KLX18A.*

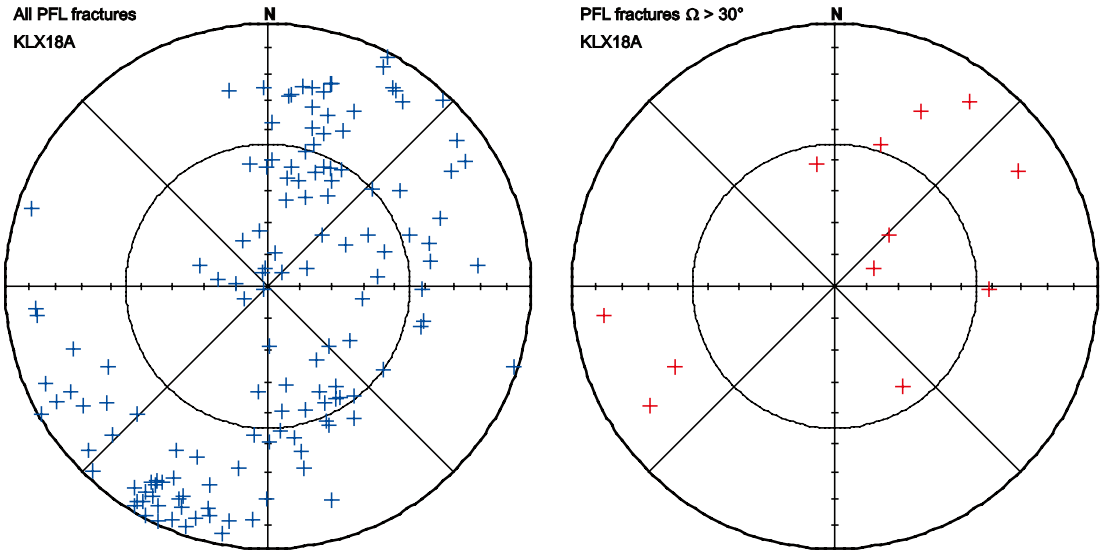

Figure 2-60. *To the left the poles of all PFL fractures in KLX18A and to the right the poles of the PFL fractures that have Ω greater than 30°.*

2.1.31 KLX19A

The orientation information is missing for one fracture, which is associated with flow, in KLX19A and thus is omitted from orientation analysis. The CDF of maximum uncertainty of the remaining fractures is shown in Figure. The PFL fractures in KLX19A have relatively many fractures with large uncertainty. The maximum uncertainty is less than 10° for 70% and 86% of the fractures have maximum uncertainty below 14°. However, the remaining 5 fractures have uncertainties exceeding 38°.

The PFL fracture poles in KLX19A are sparsely distributed over the hemisphere, see Figure 2-62. The PFL fractures with large orientation uncertainty follow the pattern of the rest of the PFL fracture orientations.

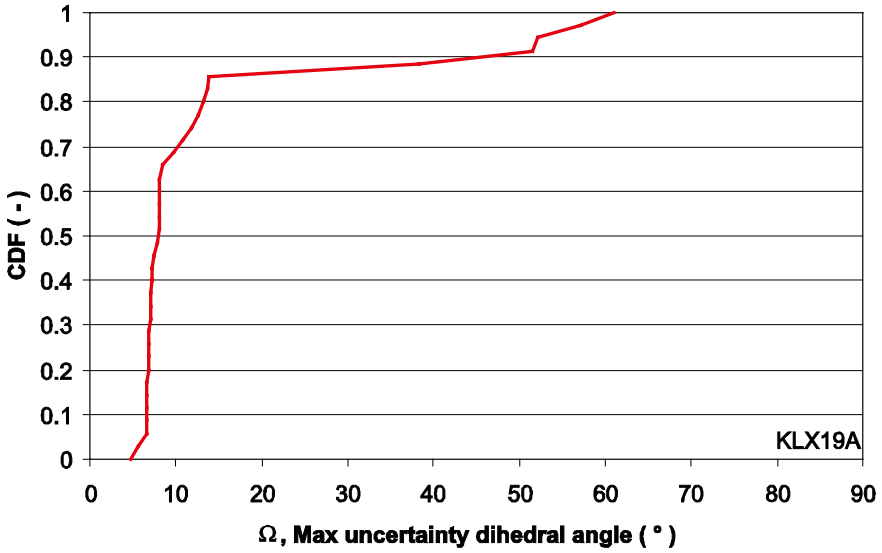

Figure 2-61. *The cumulative density function of the largest orientation uncertainties of PFL fractures in KLX19A.*

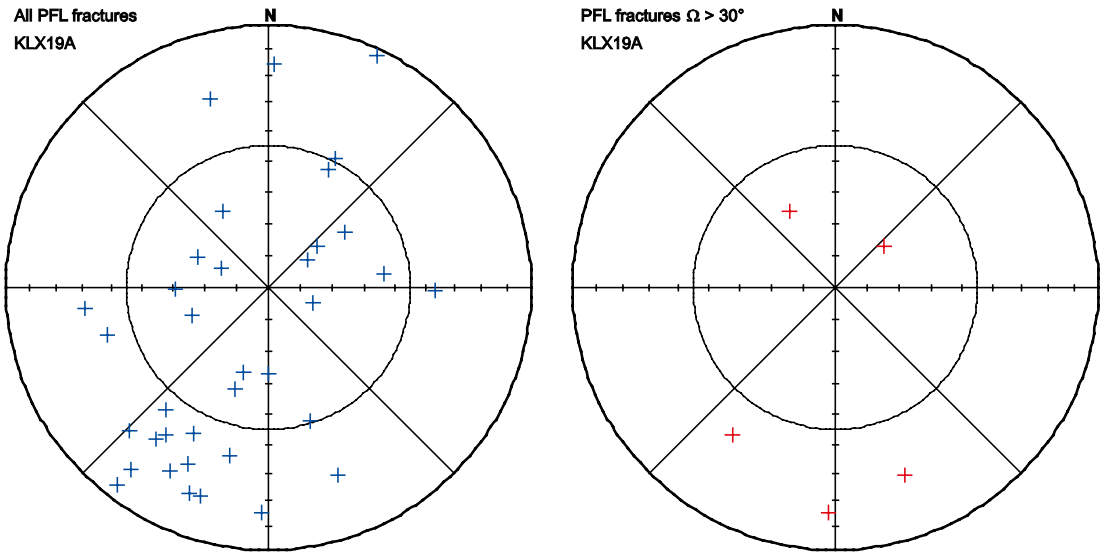

Figure 2-62. *To the left the poles of all PFL fractures in KLX19A and to the right the poles of the PFL fractures that have Ω greater than 30°.*

2.1.32 KLX20A

There is missing information about orientation for one PFL fracture in KLX20A in the table p_fract_core_eshi /Sicada 2008/ and thus this fracture has been omitted from the analysis of the maximum uncertainty shown in Figure 2-63. The uncertainties are relatively large for the fractures associated with flow, only a little bit more than half, 52%, of the PFL fractures has maximum uncertainty less than 10°. The uncertainty exceeds 25° for 20% of the PFL fractures.

The PFL fractures with large orientation uncertainty follow about the same pattern as the rest of the PFL fractures in KLX20A, see Figure 2-64.

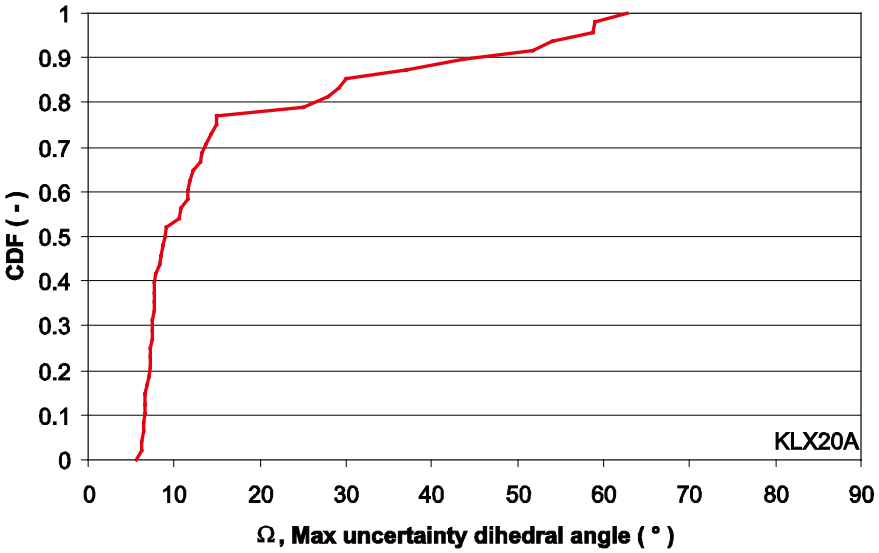

Figure 2-63. *The cumulative density function of the largest orientation uncertainties of PFL fractures in KLX20A.*

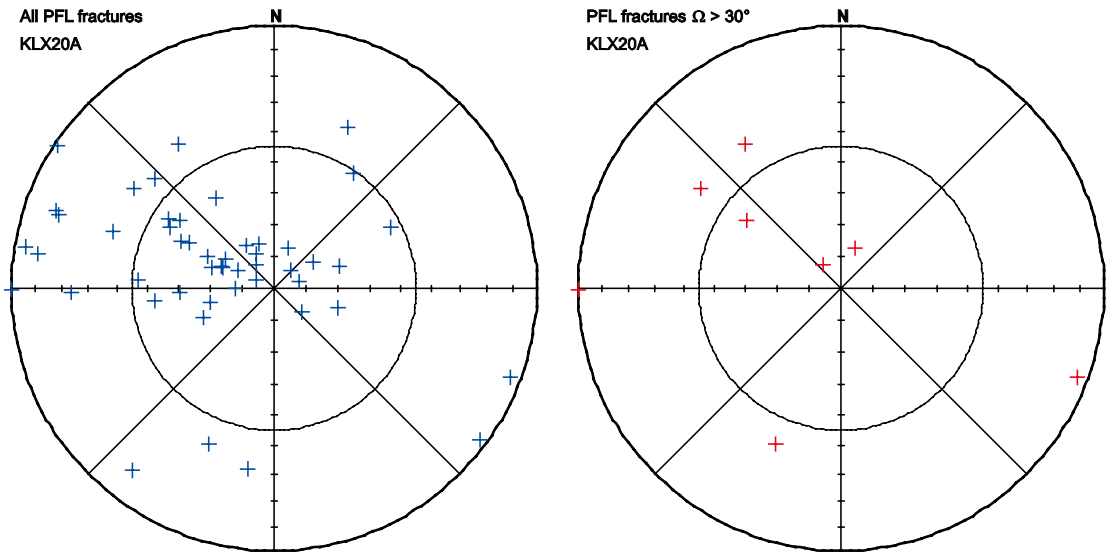

Figure 2-64. *To the left the poles of all PFL fractures in KLX20A and to the right the poles of the PFL fractures that have Ω greater than 30°.*

2.1.33 KLX21B

The CDF of maximum uncertainty of PFL fractures in KLX21B is shown in Figure 2-65. No PFL fracture show any maximum uncertainty larger than 17°, 90% is less than 13° and 60% is less than 10°.

There are relatively few and sparsely distributed PFL fractures in KLX21B making it hard to draw any conclusions about fracture clusters or outliers, see Figure 2-66.

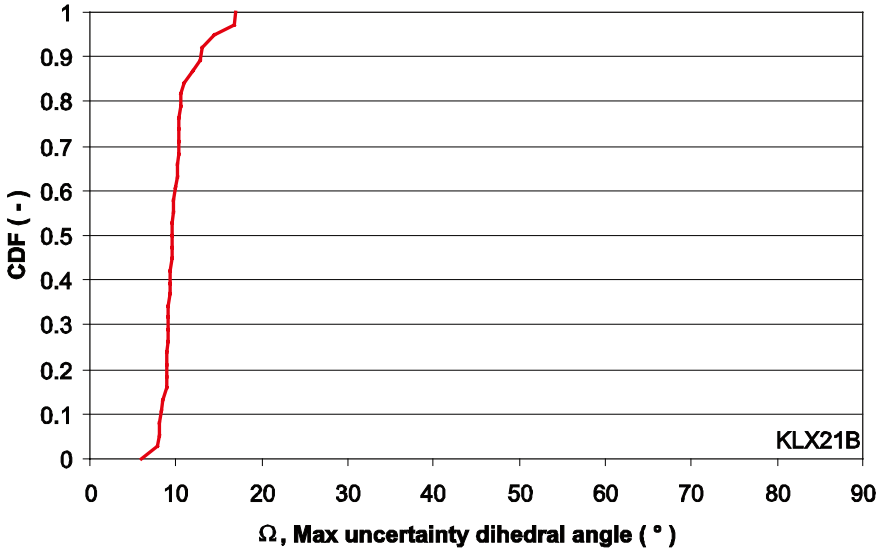

Figure 2-65. The cumulative density function of the largest orientation uncertainties of PFL fractures in KLX21B.

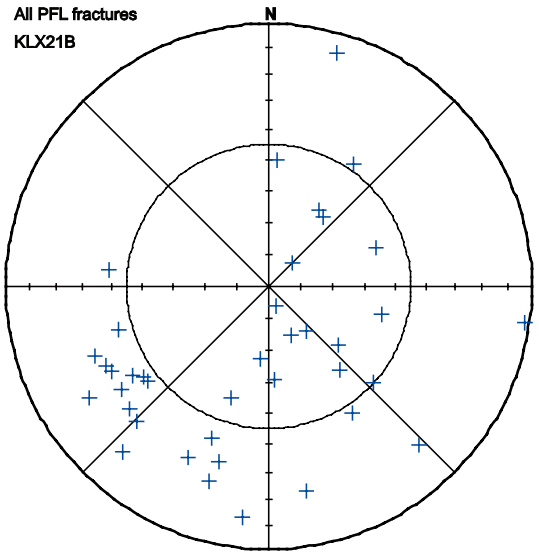

Figure 2-66. The poles of all PFL fractures in KLX21B.

2.1.34 KLX22A

There is no PFL fractures in KLX22A with large orientation uncertainty, see Figure 2-67. The maximum uncertainty is less than 10° for 77% of the fractures associated with flow and 90% have maximum uncertainty less than 13°. The largest uncertainty for the PFL fractures in KLX22A is 16°.

The PFL fractures in KLX22A group into two or maybe three sets by visual inspection, see Figure 2-68. There is one outlier, the north striking fracture 20924B8B0A107447, that might be a single fracture in a larger fracture set, but due to the limited number of poles it is not possible to judge.

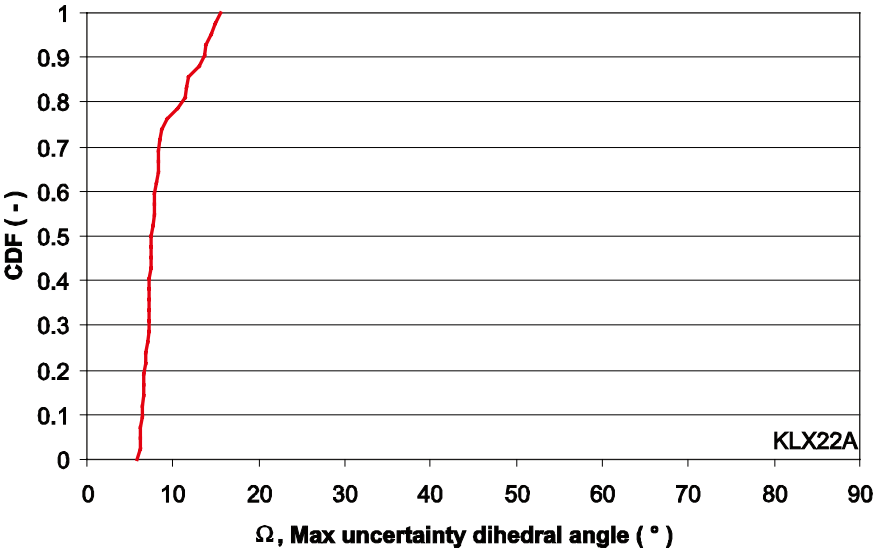

Figure 2-67. *The cumulative density function of the largest orientation uncertainties of PFL fractures in KLX22A.*

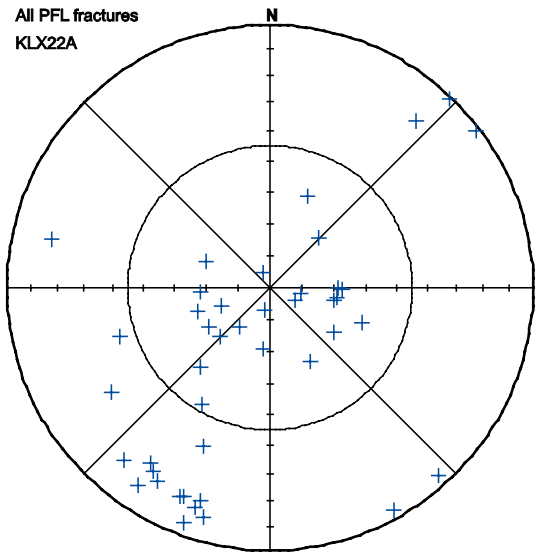

Figure 2-68. *The poles of all PFL fractures in KLX22A.*

2.1.35 KLX22B

About 2/3 of the PFL fractures in KLX22B have maximum uncertainty below 10°, see Figure 2-69. Of the 27 fractures associated with flow 4 exceed a maximum uncertainty of 23°.

The fracture poles in KLX22B spread more or less evenly over the hemisphere and hence it is hard to judge if the two fractures having large orientation uncertainty should have an alternative orientation to the best estimated shown in Figure 2-70.

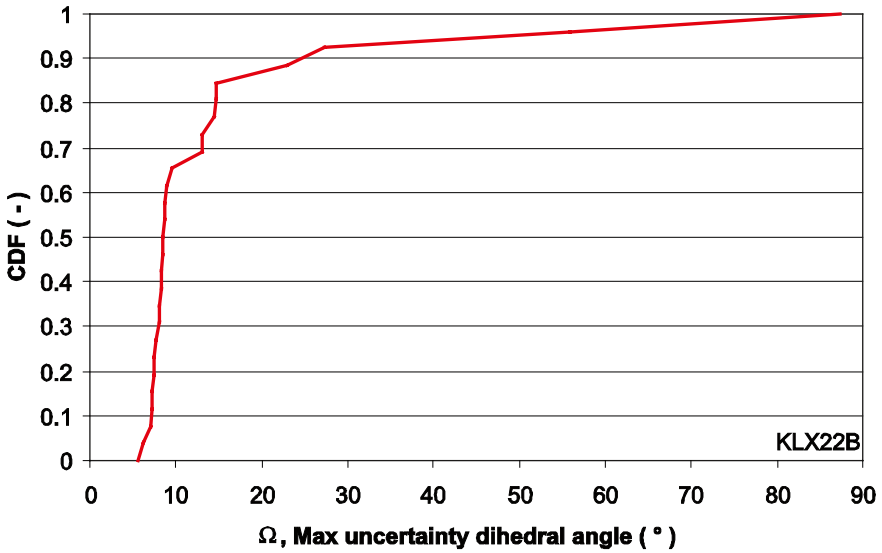

Figure 2-69. The cumulative density function of the largest orientation uncertainties of PFL fractures in KLX22B.

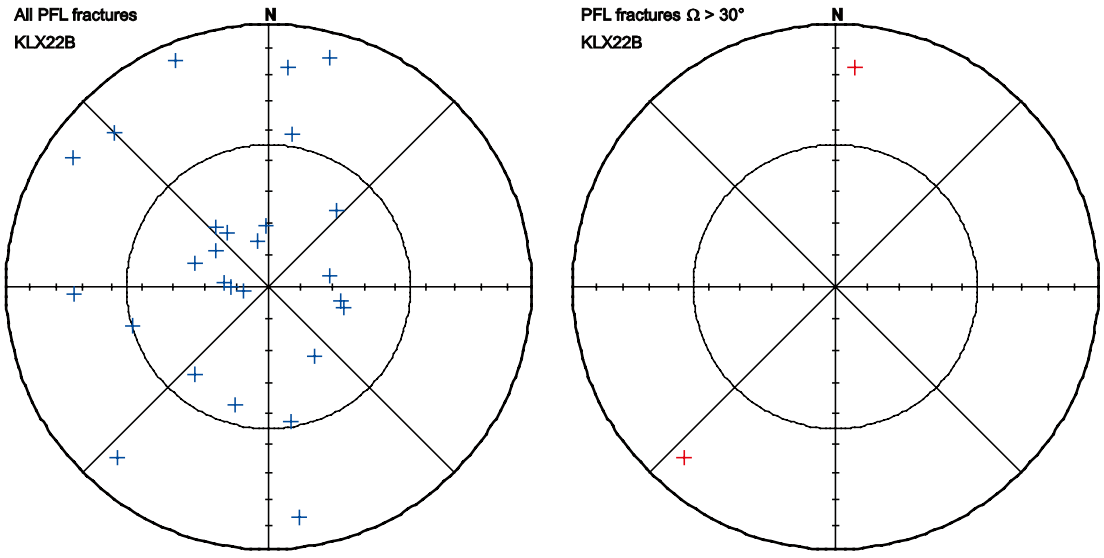

Figure 2-70. To the left the poles of all PFL fractures in KLX22B and to the right the poles of the PFL fractures that have Ω greater than 30°.

2.1.36 KLX23A

In KLX23A orientation information is missing for one fracture, that is associated with flow, in table p_fract_core_eshi /Sicada 2008/ and consequently this fracture is omitted from orientation analysis. The CDF of maximum uncertainty of the remaining 16 fractures is shown in Figure 2-71. The PFL fractures in KLX23A have relatively low uncertainty; about 90% of the fractures have maximum uncertainty below 10° and all but one fracture has uncertainty less than 11°.

The few PFL fractures in KLX23A spread evenly over the hemisphere and it is hard to find any sets by visual inspection, see Figure 2-72.

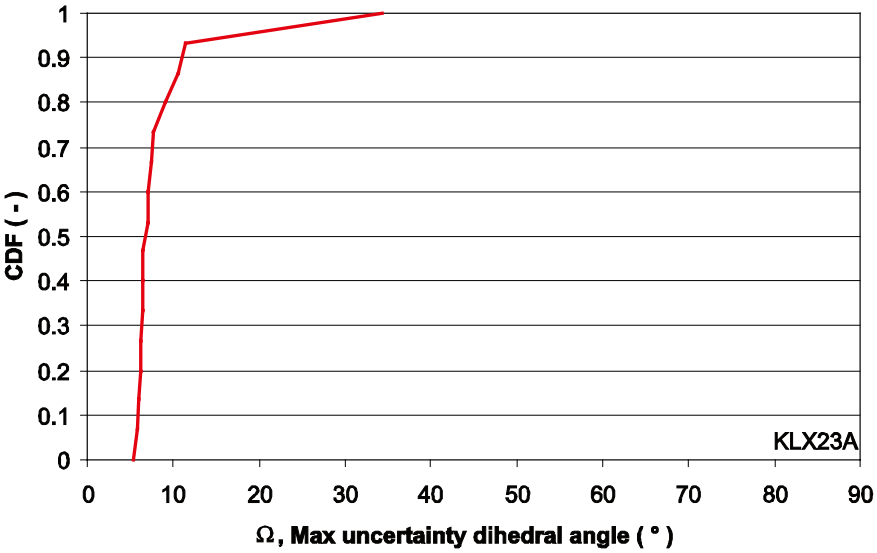

Figure 2-71. The cumulative density function of the largest orientation uncertainties of PFL fractures in KLX23A.

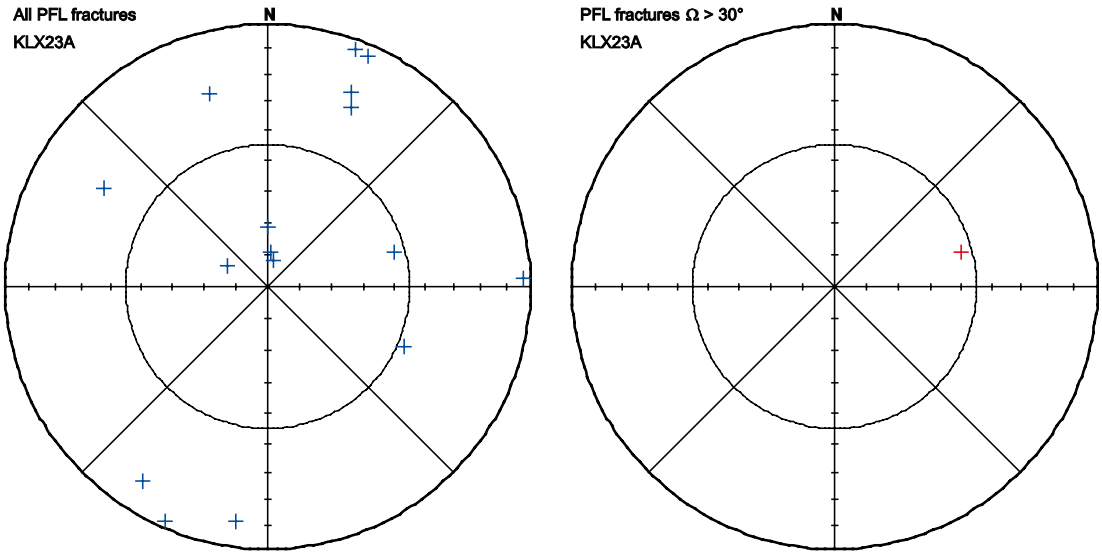

Figure 2-72. To the left the poles of all PFL fractures in KLX23A and to the right the poles of the PFL fractures that have Ω greater than 30°.

2.1.37 KLX23B

There is only four PFL fractures in KLX23B, see Figure 2-73. Three of them have maximum uncertainty less than 10° and the fourth has maximum uncertainty 41°.

The only conclusion possible to draw, regarding the orientation, from the four fracture poles is that there probably is a sub horizontal water conductive fracture set in KLX23B and hence the best estimate orientation of the PFL fracture with large orientation uncertainty, see Figure 2-74, is relatively correct.

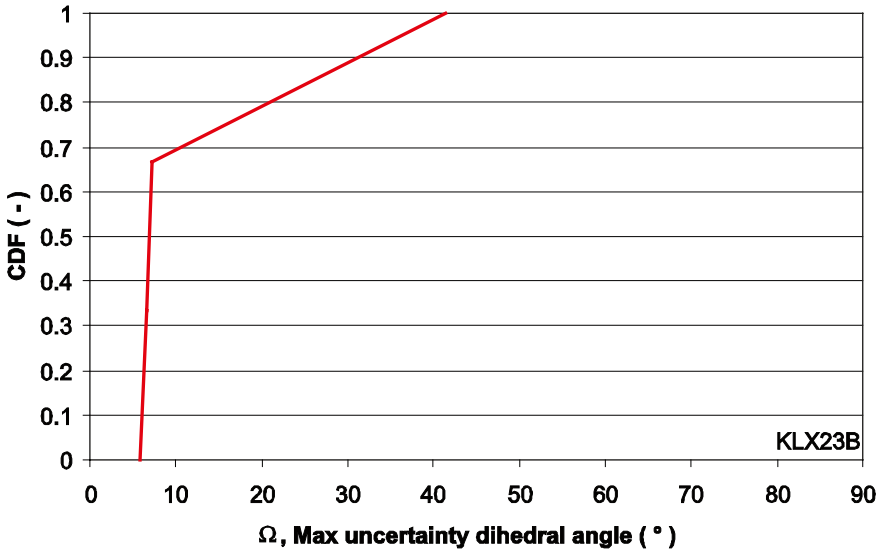

Figure 2-73. The cumulative density function of the largest orientation uncertainties of PFL fractures in KLX23B.

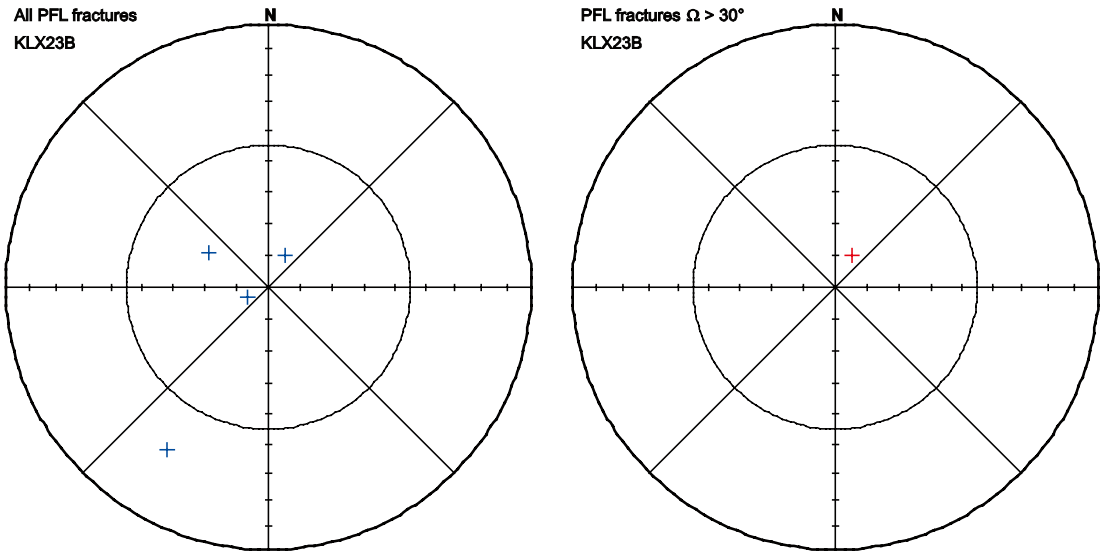

Figure 2-74. To the left the poles of all PFL fractures in KLX23B and to the right the poles of the PFL fractures that have Ω greater than 30°.

2.1.38 KLX24A

The CDF of the maximum uncertainty for PFL fractures in KLX24A is shown in Figure 2-75. The maximum uncertainty is less than 10° for 72% of the fractures and 90% have maximum uncertainty less than 14°.

The only PFL fracture with large orientation uncertainty in KLX24A is within the SSW striking fracture set, but could as well be part of the SE striking fractures, see Figure 2-76 and Section 2.3.38.

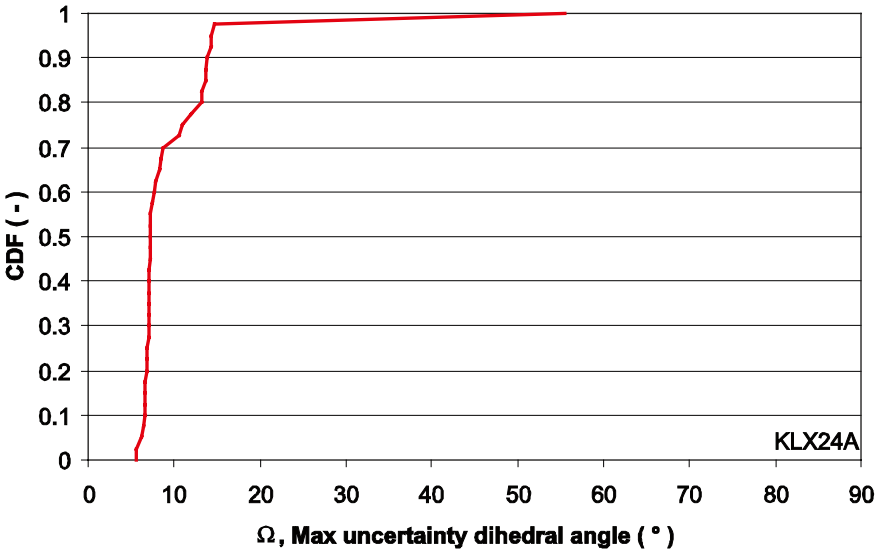

Figure 2-75. The cumulative density function of the largest orientation uncertainties of PFL fractures in KLX24A.

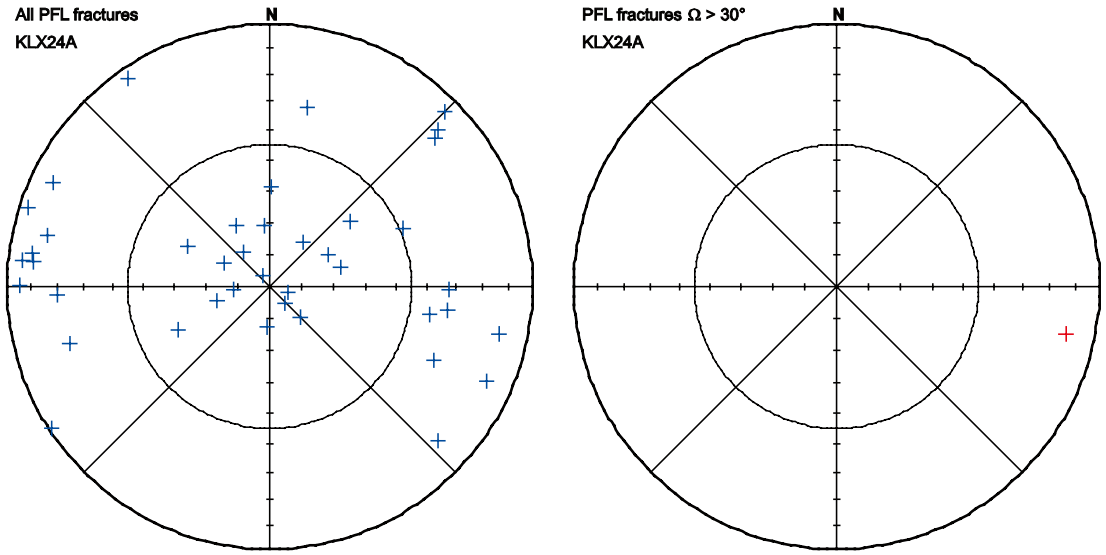

Figure 2-76. To the left the poles of all PFL fractures in KLX24A and to the right the poles of the PFL fractures that have Ω greater than 30°.

2.1.39 KLX25A

There are eight PFL fractures in KLX25A of which four have maximum uncertainty less than 10°, see Figure 2-77. Of the remaining four all but one has maximum uncertainty below 14°.

There are few PFL fractures in KLX25A and hence hard to draw any conclusions about orientation of the water conductive fractures, see Figure 2-78. There is a west striking set and two outliers. The fracture with large orientation uncertainty does not have uncertainty large enough to interpret it as a member of the west striking fractures, see Figure 2-78 and Section 2.3.39.

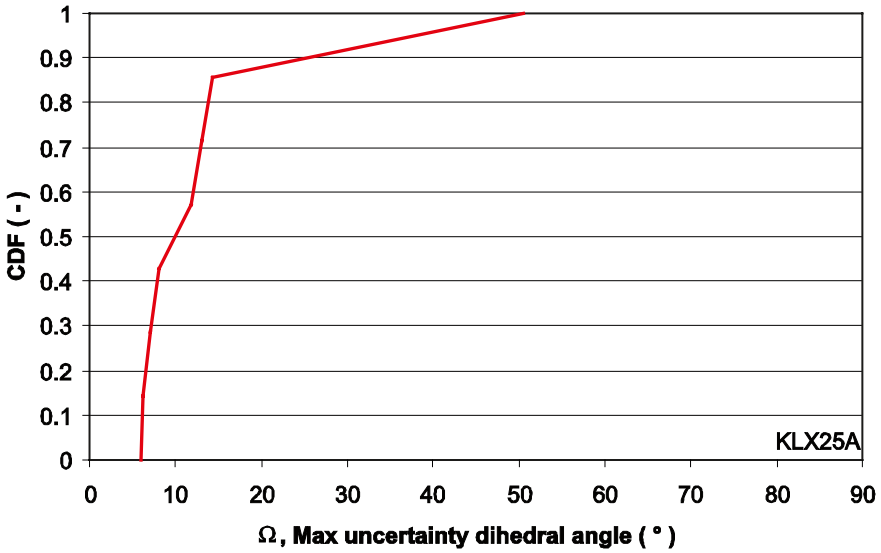

Figure 2-77. The cumulative density function of the largest orientation uncertainties of PFL fractures in KLX25A.

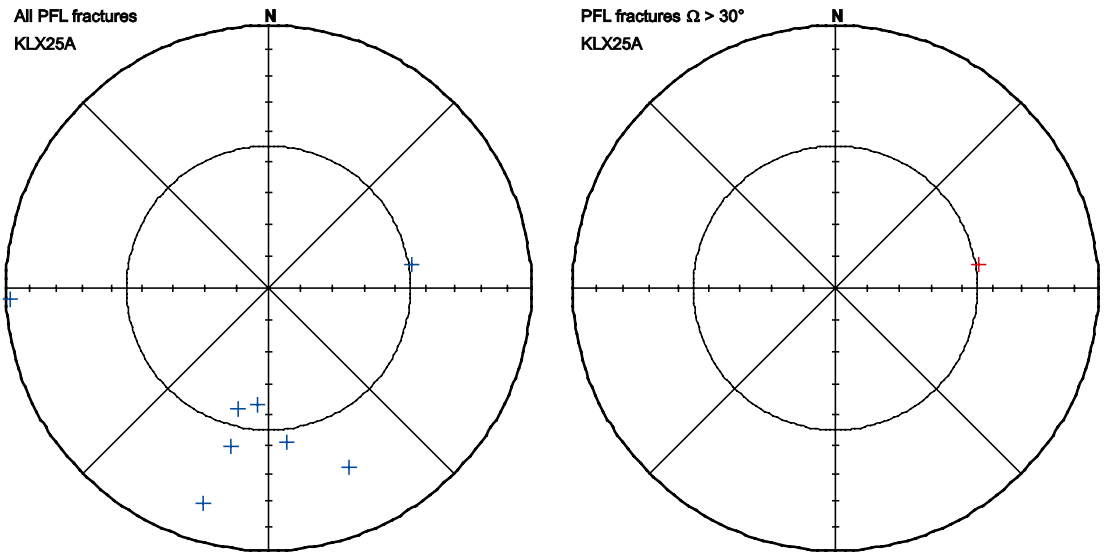

Figure 2-78. To the left the poles of all PFL fractures in KLX25A and to the right the poles of the PFL fractures that have Ω greater than 30°.

2.1.40 KLX26A

The CDF of the maximum uncertainty for PFL fractures in KLX26A is shown in Figure 2-79. The maximum uncertainty is less than 10° for 86% of the fractures and 90% have maximum uncertainty less than 14°.

The few PFL fractures in KLX26A can, by visual inspection, be divided into three sparse fracture sets, see Figure 2-80. The PFL fracture with large orientation uncertainty, C0964B8B0A1096D9, has such uncertainty that it might be ESE striking, and group with the other two PFL fractures, instead of the sub horizontal orientation as is the best estimated, see Figure 2-80 and Section 2.3.40.

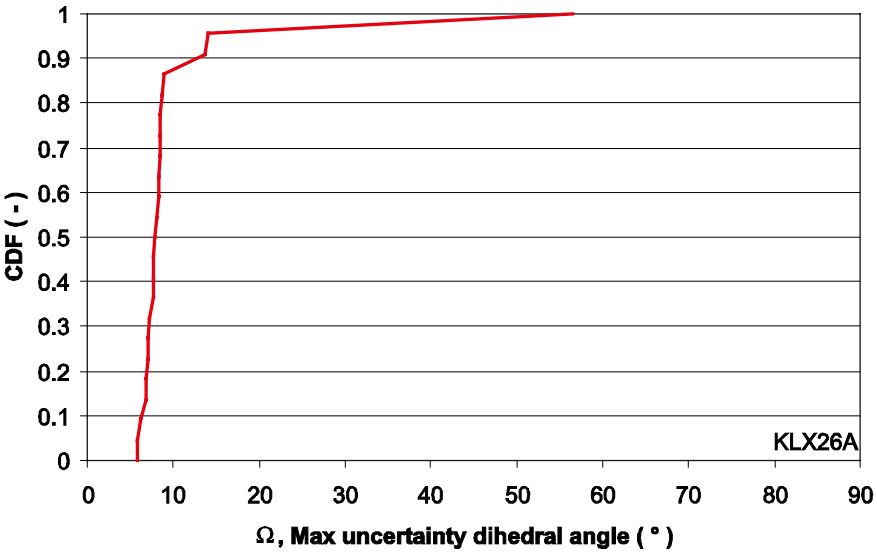

Figure 2-79. *The cumulative density function of the largest orientation uncertainties of PFL fractures in KLX26A.*

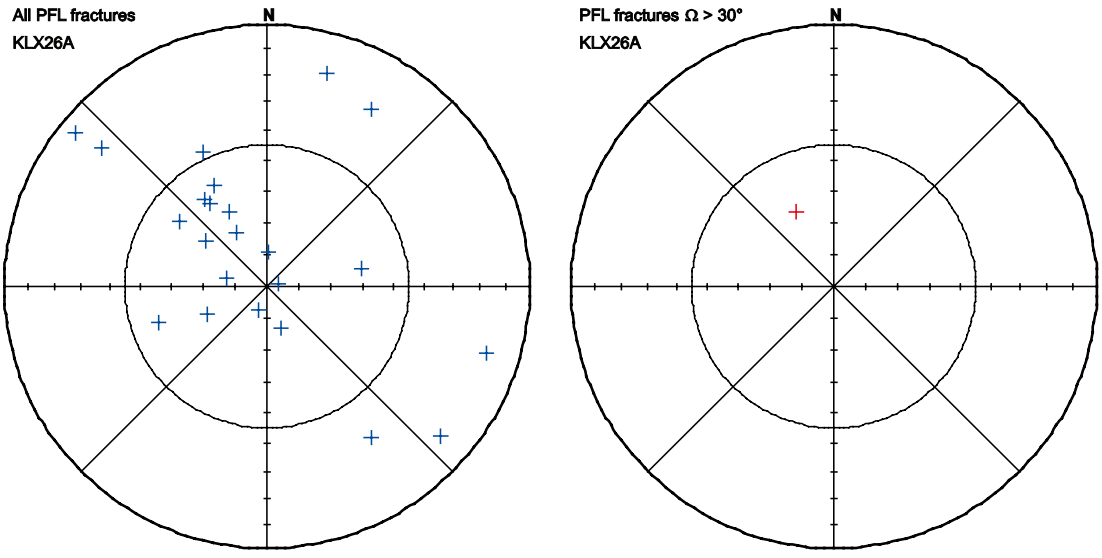

Figure 2-80. *To the left the poles of all PFL fractures in KLX26A and to the right the poles of the PFL fractures that have Ω greater than 30°.*

2.1.41 KLX26B

All PFL fractures in KLX26B have maximum uncertainty less than 12°, see Figure 2-81, and thus KLX26B is the borehole with least uncertainties for the fractures associated with flow.

Despite the few PFL fractures in KLX26B the fractures seem to cluster in three sparse fracture sets and one NW striking outlier, see Figure 2-82. It is not possible to judge whether the NW striking fracture belong to a fracture set or not.

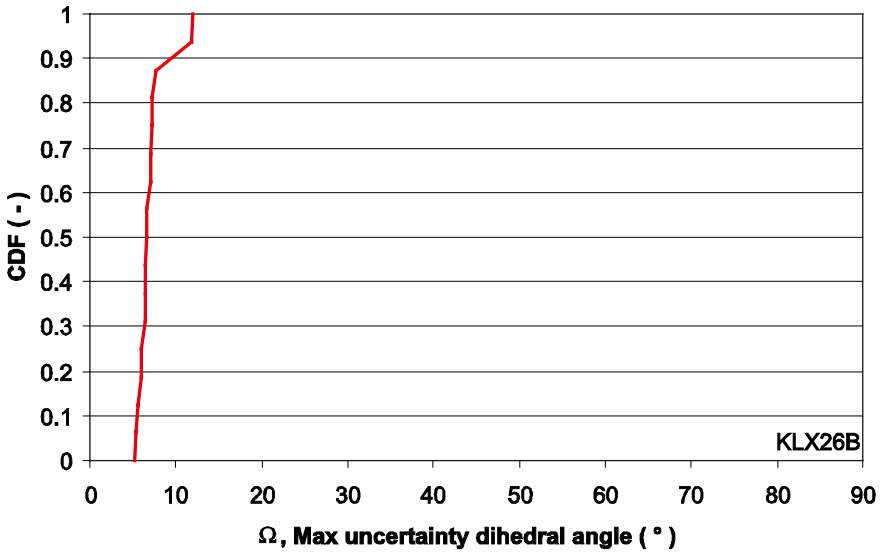

Figure 2-81. The cumulative density function of the largest orientation uncertainties of PFL fractures in KLX26B.

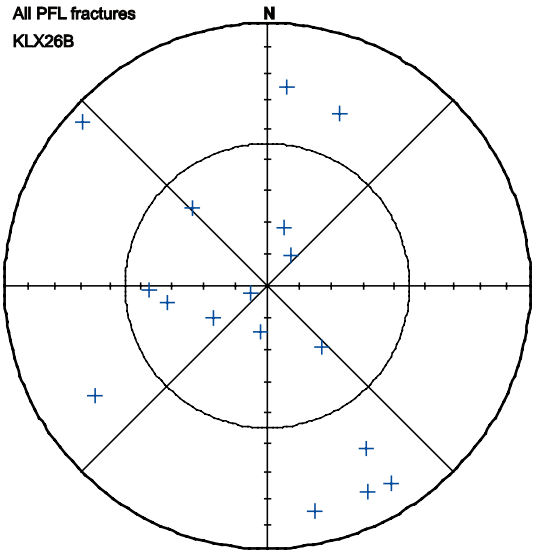

Figure 2-82. The poles of all PFL fractures in KLX26B.

2.1.42 KLX28A

The CDF of maximum uncertainty for PFL fractures in KLX28A is shown in Figure 2-83. The maximum uncertainty is less than 10° for 80% of the fractures associated with flow and 90% have maximum uncertainty less than 12°. Largest uncertainty is 15°.

The PFL fractures in KLX28A cluster along a band of sparsely distributed NW/SE striking fractures, see Figure 2-84.

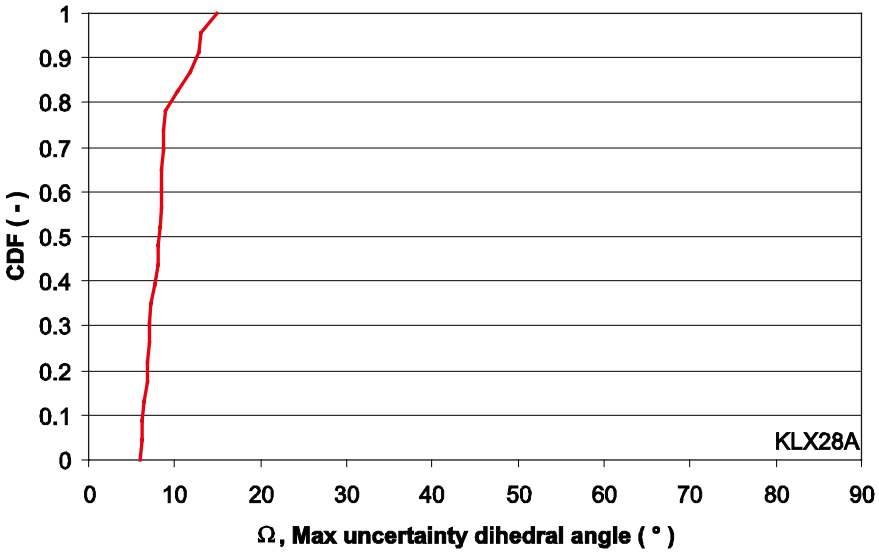

Figure 2-83. *The cumulative density function of the largest orientation uncertainties of PFL fractures in KLX28A.*

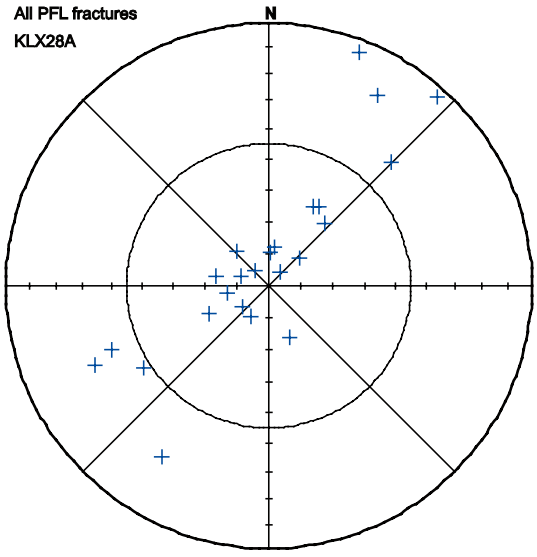

Figure 2-84. *The poles of all PFL fractures in KLX28A.*

2.1.43 KLX29A

The orientation uncertainty for the PFL fractures in KLX29A is low, see Figure 2-85, no fracture associated with flow exceeds 15° uncertainty. The maximum uncertainty is less than10° for 80% of the PFL fractures and less than 13° for 90% of the fractures.

The few steeply dipping fractures in KLX29A do not cluster into fracture sets, but spread along the perimeter of the hemisphere, see Figure 2-86. Hence, no conclusion can be drawn regarding orientation sets by visual inspection.

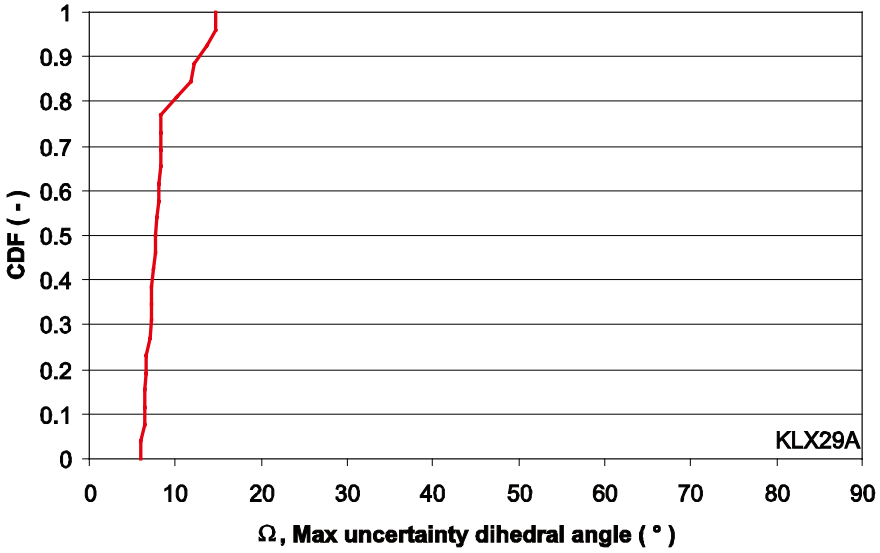

Figure 2-85. The cumulative density function of the largest orientation uncertainties of PFL fractures in KLX29A.

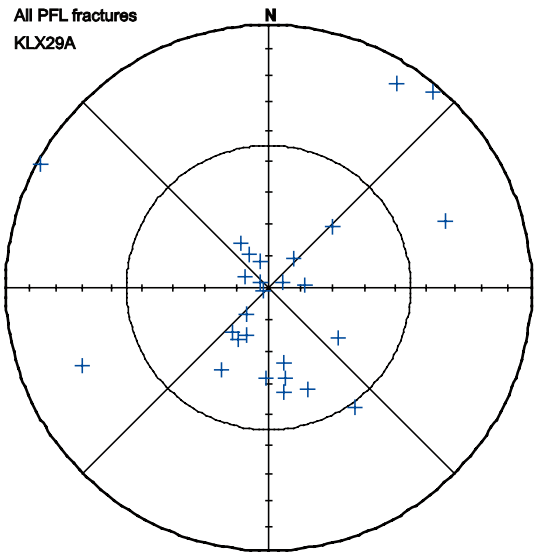

Figure 2-86. The poles of all PFL fractures in KLX29A.

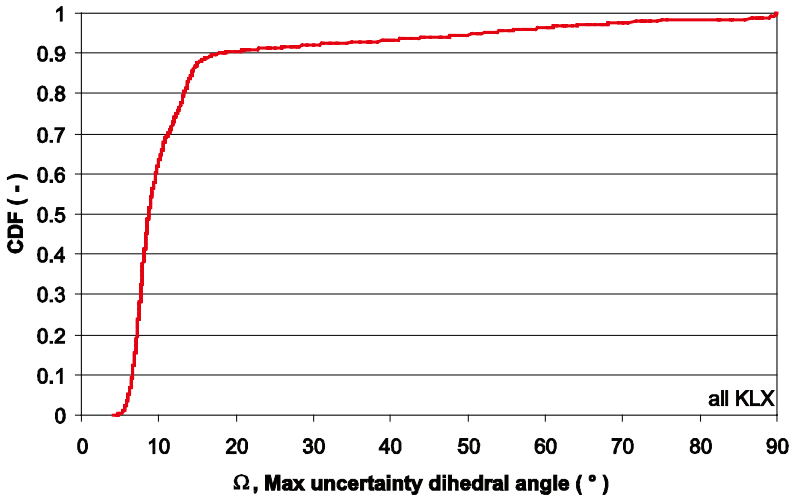

Figure 2-87. *The cumulative density function for the largest orientation uncertainties of all PFL fracture in all KLX boreholes.*

2.1.44 All Combined

The CDF of maximum uncertainty for all 1957 PFL fractures with orientation information is shown in Figure 2-87. The graph shows that 63%, 1235, fractures associated with flow have maximum uncertainty less than 10° and thus can be regarded as certain. However, there are 156 PFL fractures with maximum orientation uncertainty larger than 30° and it is highly recommended that any user of orientation information for flowing fractures give extra attention to these fractures. The remaining 566 PFL fractures should be paid attention if they are important explaining or are overturning conceptual models.

2.2 Maximum uncertainty versus transmissivity

This section shows one cross plot of uncertainty versus transmissivity of each borehole to get a grasp picture of which PFL fractures that have high uncertainty and at the same time are important for any hydrogeological modelling. Further details on the sample space for each fracture are shown in Section 2.3.

2.2.1 KLX03

Figure 2-88 shows that the two fractures with the highest uncertainties, FE53438B2B1206B4 and F653438B2B1216AF, are among the ten fractures with the lowest transmissivity values.

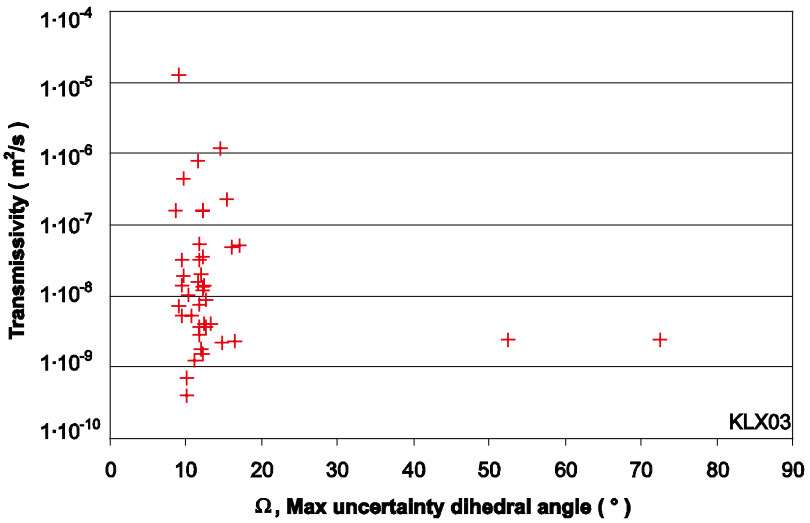

Figure 2-88. *The transmissivity versus the uncertainty of the PFL fractures in KLX03.*

2.2.2 KLX04

The three PFL fractures with the highest uncertainty, 4554438B2B14C370, D854438B2B15A1BF and F114438B2B1982BE, are all on the lower half of the transmissivity scale, see Figure 2-89. Though they are relatively low they should be paid attention if important for any hydrogeological modelling.

The Figure 2-89 lacks two PFL fractures, CF54438B2B18C0F4 (PFL no 93) and 6594438B2B18E566 (PFL no 96), that do not have any orientation information, see Section 2.1.2, and thus no uncertainty value. The transmissivity values of these fractures are $1.95 \cdot 10^{-8}$ and $2.11 \cdot 10^{-7}$ m^2/s and hence in the mid of the transmissivity values in KLX04. It is recommended that the reason for the lack of orientation data is further investigated and, if possible, the orientation together with the uncertainty is calculated.

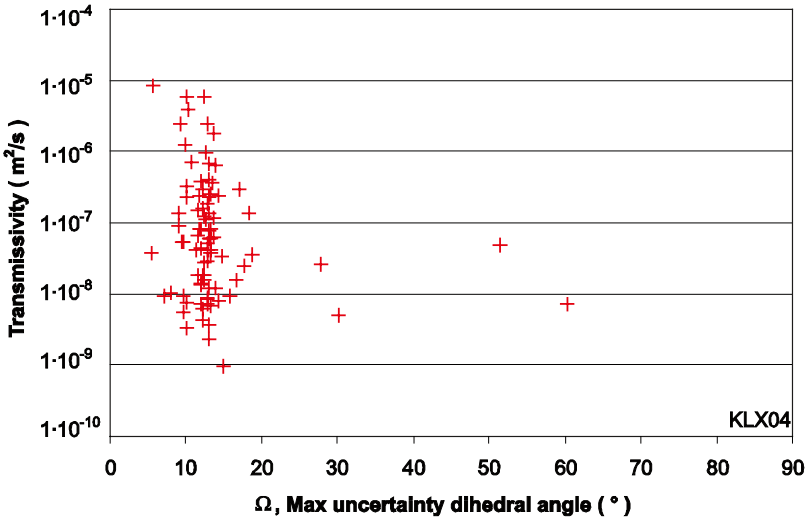

Figure 2-89. *The transmissivity versus the uncertainty of the PFL fractures in KLX04.*

2.2.3 KLX05

There is eight fractures with high uncertainty in KLX05, 31D5438B2B125BFA, 5515438B2B12E3B7, 4C15438B2B1339F7, 01D5438B2B13C92E, A955438B2B164300, 0A55438B2B167E07, 8F95438B2B17886A and 4555438B2B1DA76F, see Figure 2-90. Fortunately most of them have transmissivity below $1 \cdot 10^{-9}$ m^2/s and no one have larger transmissivity than $4.63 \cdot 10^{-9}$ m^2/s.

One PFL fracture, 30D5438B2B12E1BD (PFL no 36), is missing orientation information and thus excluded from Figure 2-90. The transmissivity value is relatively low $4.68 \cdot 10^{-9}$ m^2/s. It is yet recommended that the reason for the lack of data is investigated.

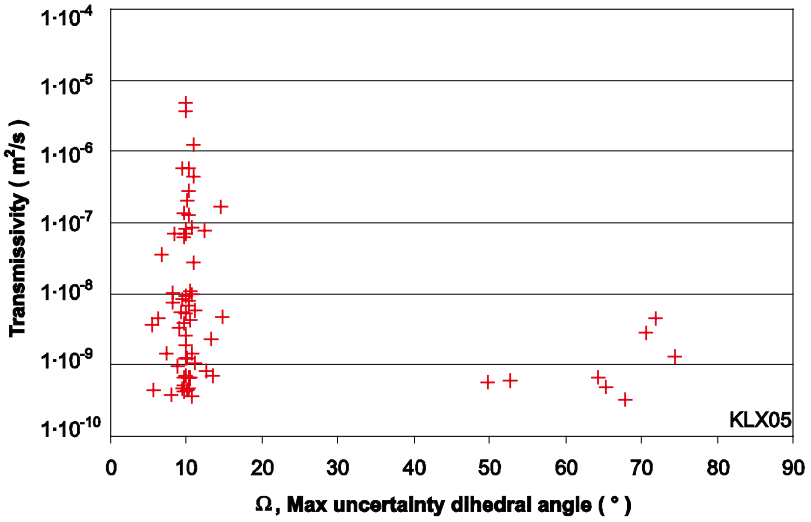

Figure 2-90. *The transmissivity versus the uncertainty of the PFL fractures in KLX05.*

2.2.4 KLX06

The seven most uncertain PFL fracture in KLX06, 0496438B2B118D03, E216438B2B127ADF, F596438B2B127B43, FE96438B2B129E5A, 3796438B2B14053F, 3C56438B2B17B5EA and 8CD6438B2B1E42B8, span over the whole range of transmissivity values, see Figure 2-91, and should be given attention before used in modelling.

There is one PFL fracture, DF96438B2B1B307C (PFL no 175), missing in Figure 2-91. The low transmissivity value $1.23 \cdot 10^{-9}$ m^2/s might make it unnecessary to find the reason for the missing orientation information unless important for the hydrogeological modelling.

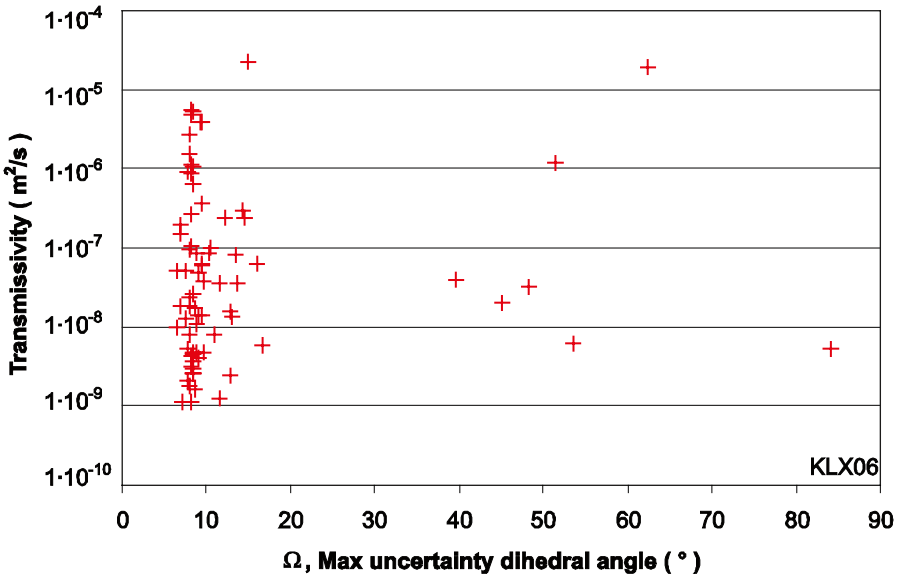

Figure 2-91. *The transmissivity versus the uncertainty of the PFL fractures in KLX06.*

2.2.5 KLX07A

All the six PFL fractures, 7117438B0A12B79A, F717438B0A13CF3C, 1957438B0A169432, 2517438B0A1824C3, 4BD7438B0A18BCEA and 9A97438B0A1A28E0, with high uncertainty have relatively low transmissivity values, see Figure 2-92. All is below $5.18 \cdot 10^{-8}$ m^2/s that is just above the median transmissivity of KLX07A, $2.17 \cdot 10^{-8}$ m^2/s, and of all boreholes treated in this report, $3.12 \cdot 10^{-8}$ m^2/s.

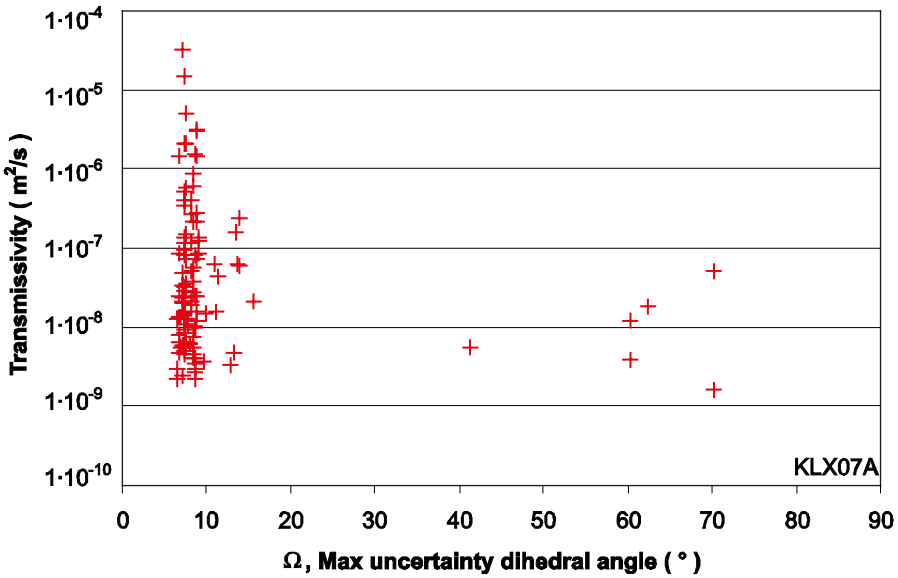

Figure 2-92. *The transmissivity versus the uncertainty of the PFL fractures in KLX07A.*

2.2.6 KLX07B

The two most uncertain PFL fractures, 1C17438B0910D6E4 and FFD7438B09119A6F, is among the four most transmissive fractures in KLX07B and it is highly recommended that these PFL fractures should be investigated further before used in modelling, see Figure 2-93. The other three PFL fractures, 2397438B09113C9B, 5257438B09116B70 and E6D7438B0912B35E, have relatively high transmissivity values as well and should also be paid attention.

The Figure 2-93 lacks two PFL fractures, 6597438B0910C920 (PFL no 14) and 2717438B0912D508 (PFL no 79), that do not have any orientation information and thus no uncertainty value. The transmissivity values of these fractures are $3.05 \cdot 10^{-9}$ and $1.9 \cdot 10^{-8}$ m^2/s and hence in the lower scale of the transmissivity values in KLX07B. It is tough recommended that the reason for the lack of orientation data is investigated and, if possible, the orientation together with the uncertainty is calculated.

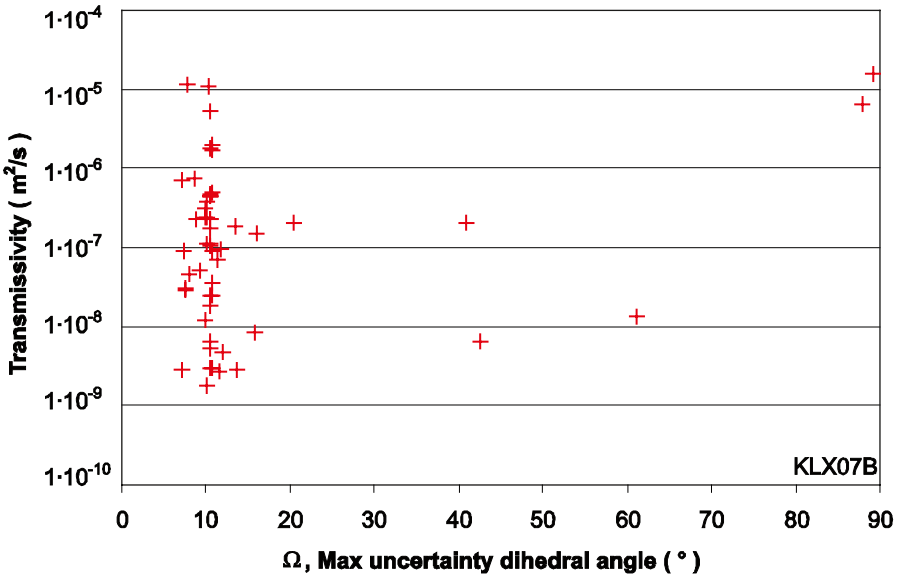

Figure 2-93. *The transmissivity versus the uncertainty of the PFL fractures in KLX07B.*

2.2.7 KLX08

Only one PFL fracture, 4058438B2B1A3C36, has uncertainty larger than 30°. The transmissivity is intermediate and the orientation sample space should be evaluated for this fracture, see Figure 2-94.

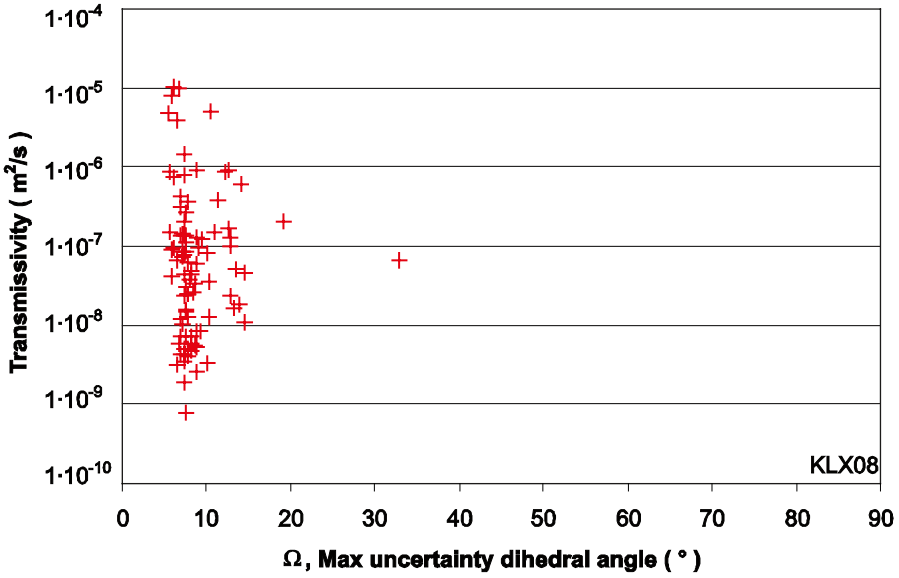

Figure 2-94. *The transmissivity versus the uncertainty of the PFL fractures in KLX08.*

2.2.8 KLX09

No PFL fracture has large uncertainty in KLX09, see Figure 2-95. The most uncertain fracture is well beneath the median transmissivity of the bore hole and maximum uncertainty just above 20°.

The PFL fracture 5C59438B2B1B7E32 (PFL no 68) lacks orientation information and thus is excluded from Figure 2-95. The transmissivity is high, $7.73 \cdot 10^{-6}$ m^2/s and it is highly recommended that the reason for the missing orientation data is investigated and, if possible, calculate the orientation together with the uncertainty values.

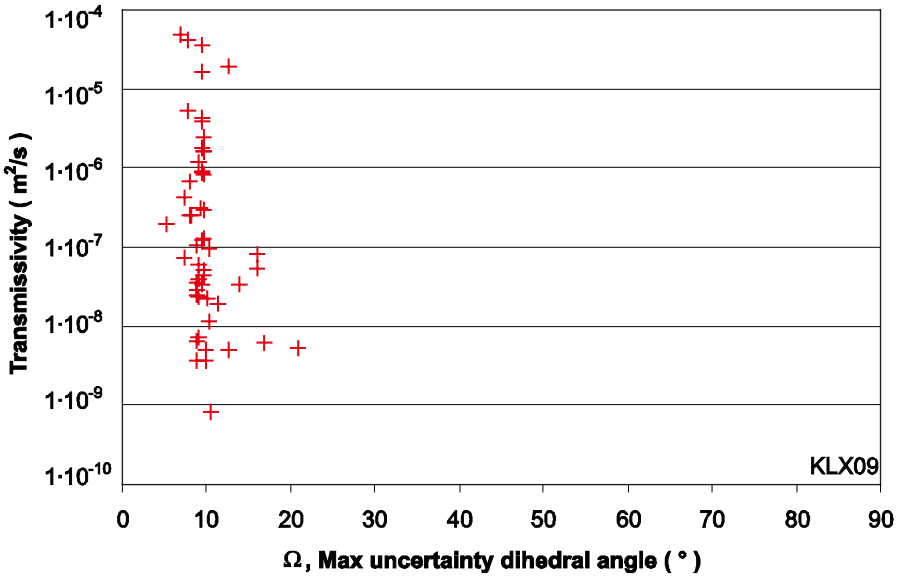

Figure 2-95. The transmissivity versus the uncertainty of the PFL fractures in KLX09.

2.2.9 KLX09B

The orientation uncertainty is large in KLX09B, see Figure 2-96 and Section 2.1.9. It is questionable if it is possible at all to use any orientation information on steep fractures from this borehole, see further in Section 2.3.9.

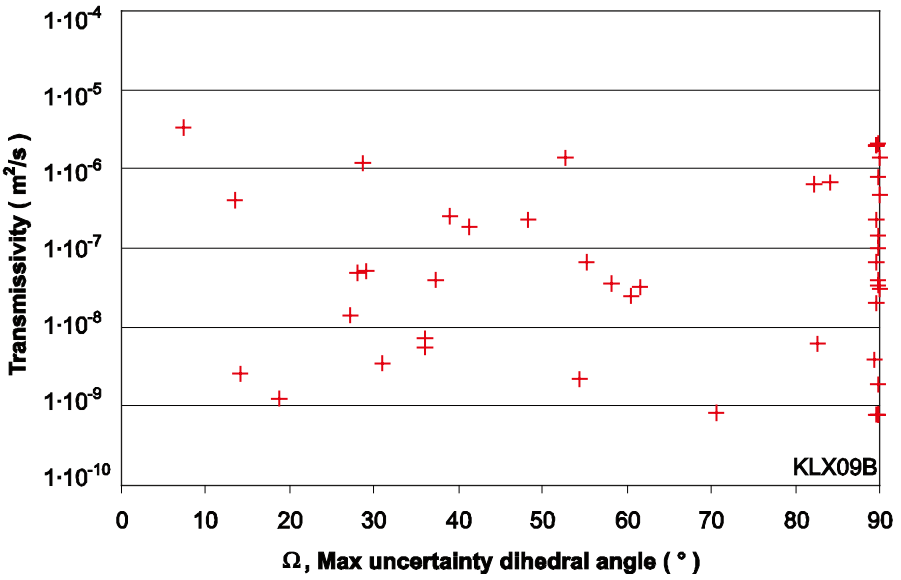

Figure 2-96. The transmissivity versus the uncertainty of the PFL fractures in KLX09B.

2.2.10 KLX09C

The orientation uncertainty in borehole KLX09 is low, only a few PFL fractures have maximum uncertainty greater than 10°. Although the transmissivity values for these fractures are intermediate they are still low compared to other transmissivity values measured in the borehole, see Figure 2-97.

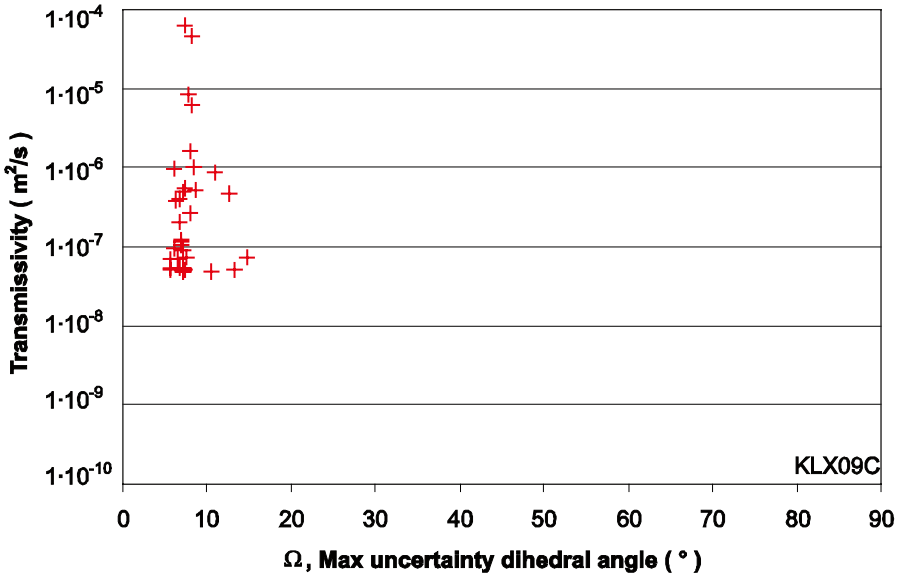

Figure 2-97. The transmissivity versus the uncertainty of the PFL fractures in KLX09C.

2.2.11 KLX09D

There are four PFL fractures in KLX09D, CE19438B0F10D9BF, A0D9438B0F113E65, 42D9438B0F114618 and 3499438B0F114CC1, with large uncertainty, see Figure 2-98. The three most uncertain of these fractures have intermediate transmissivity and should be paid attention.

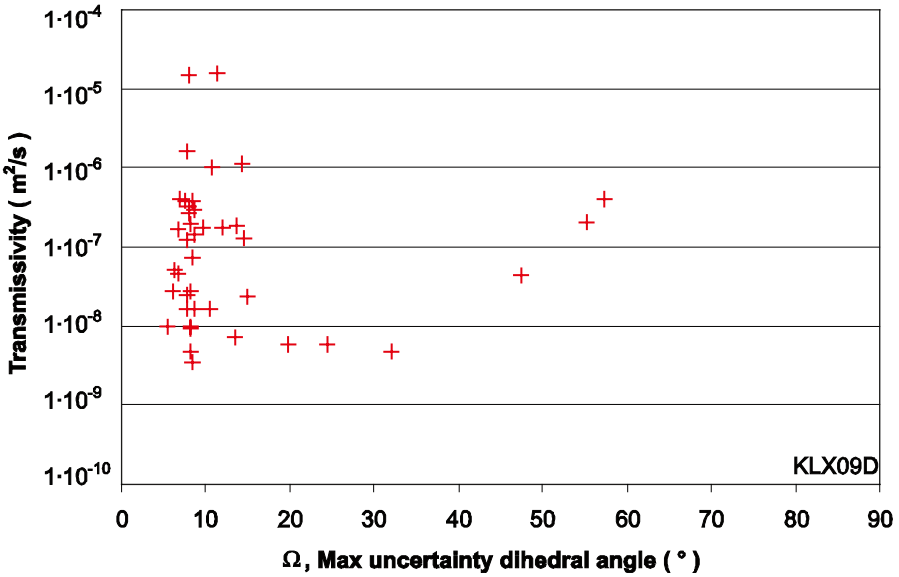

Figure 2-98. The transmissivity versus the uncertainty of the PFL fractures in KLX09D.

2.2.12 KLX09E

Most PFL fractures in KLX09E have intermediate transmissivity and relatively low uncertainty, see Figure 2-99. However, there is one exception, B3D9438B0E11B368, that has both high orientation uncertainty and high transmissivity. This fracture should be investigated further before any hydraulic modelling that is dependent on orientation.

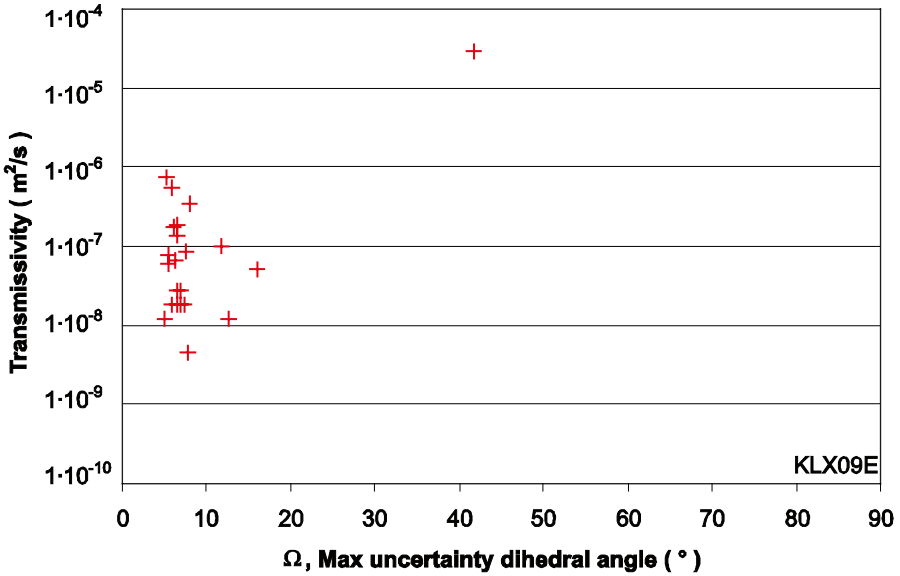

Figure 2-99. *The transmissivity versus the uncertainty of the PFL fractures in KLX09E*

2.2.13 KLX09F

Only two PFL fractures, 9599438B0D108369 and 3499438B0D109634, have high uncertainty but have relatively low transmissivity compared to other PFL fractures in KLX09F, see Figure 2-100.

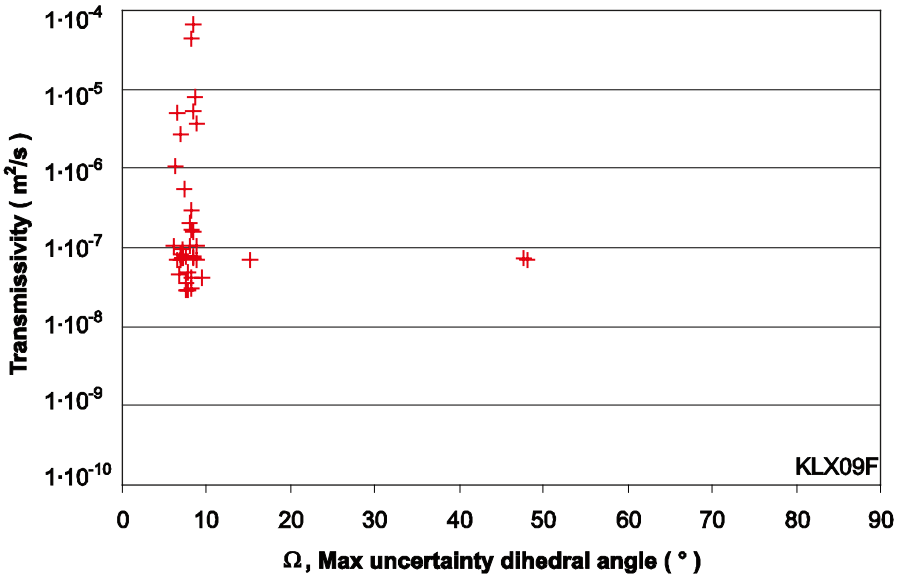

Figure 2-100. *The transmissivity versus the uncertainty of the PFL fractures in KLX09F.*

2.2.14 KLX09G

Compared to other KLX09 boreholes the transmissivity values are low in KLX09G, see Figure 2-101. There is one fracture with high orientation uncertainty, CF99438B0C106216, but the transmissivity is among the three lowest values, so the fracture might not be crucial for further hydrogeological modelling.

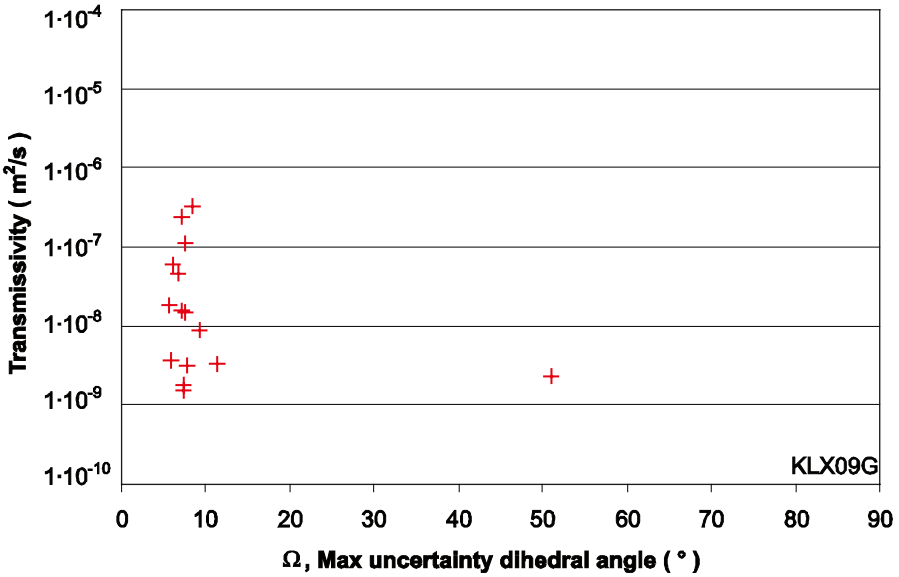

Figure 2-101. The transmissivity versus the uncertainty of the PFL fractures in KLX09G.

2.2.15 KLX10

There is a distinct difference in orientation uncertainty between the five fractures, 4910478B2B156B74, 8690478B2B157E33, DC90478B2B16107C, FF50478B2B164782 and F1D0478B2B165B27, with high uncertainty and the rest with intermediate uncertainty, see Figure 2-102. Three of the fractures with high orientation uncertainty have relatively low transmissivity, but two of them is among the ten with highest transmissivities and thus should be paid attention.

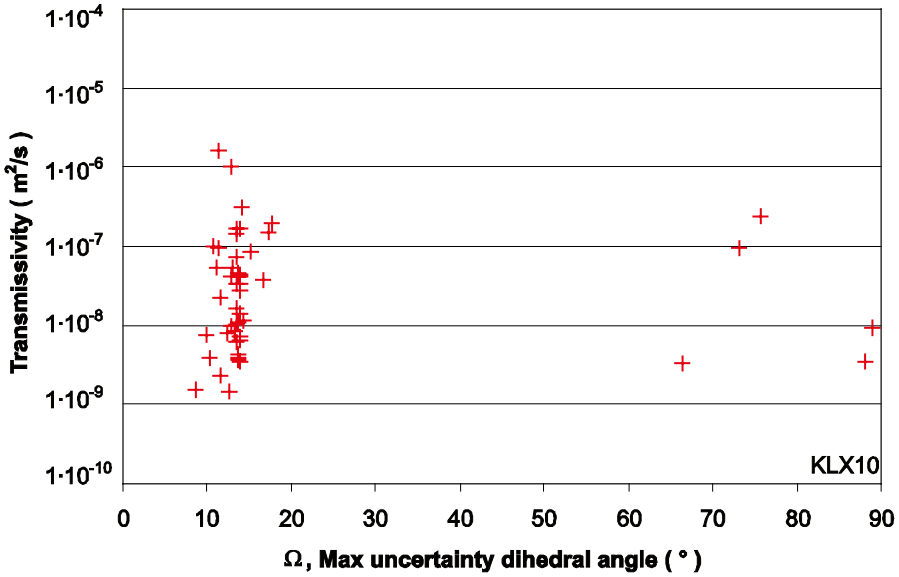

Figure 2-102. The transmissivity versus the uncertainty of the PFL fractures in KLX10

2.2.16 KLX10B

The transmissivity values are relatively high in KLX10B but no PFL fracture has any large uncertainty, see Figure 2-103, and thus no extra work regarding orientation need to be done, unless important to a hydrogeological orientation model.

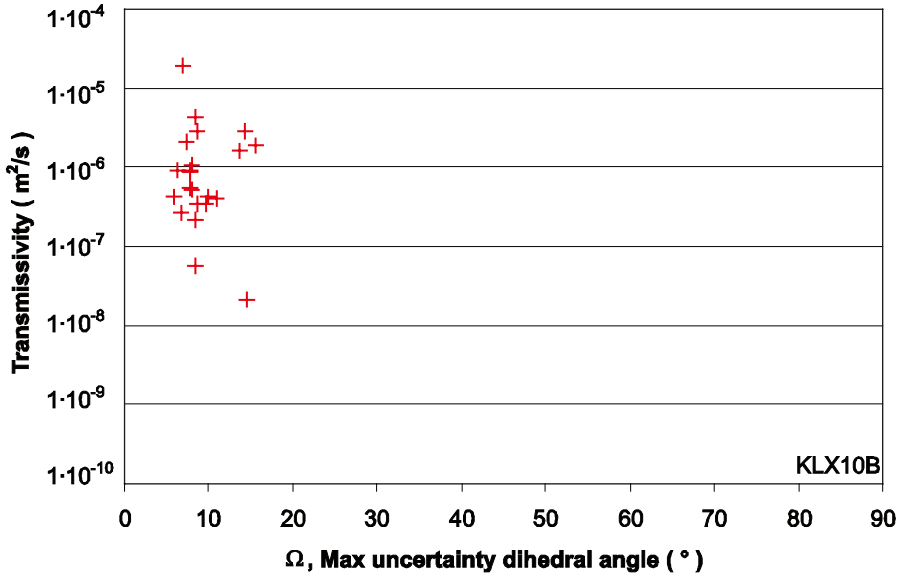

Figure 2-103. The transmissivity versus the uncertainty of the PFL fractures in KLX10B.

2.2.17 KLX10C

Neither the transmissivities nor the orientation uncertainties are high in KLX10C, see Figure 2-104, and no extra work regarding orientation should be needed for further orientation analysis.

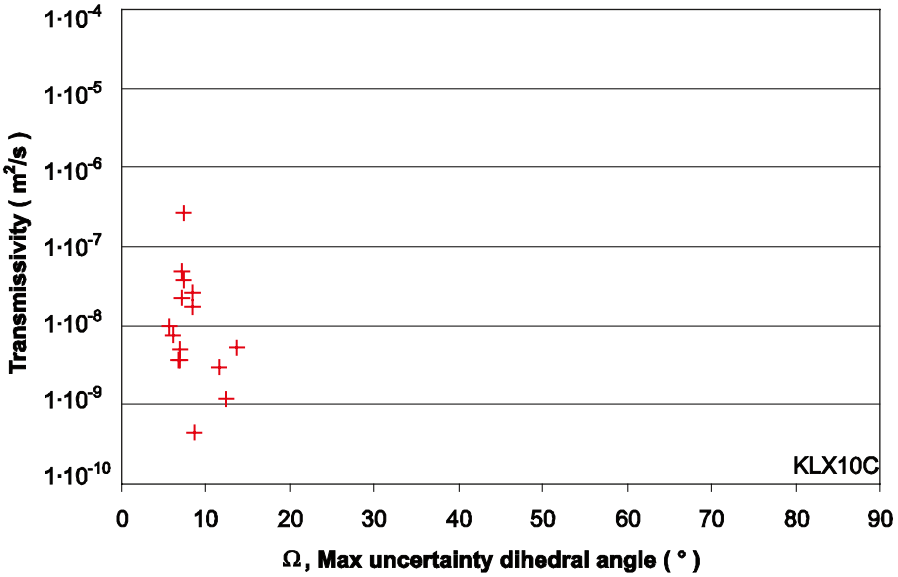

Figure 2-104. The transmissivity versus the uncertainty of the PFL fractures in KLX10C.

2.2.18 KLX11A

Three fractures in KLX11A, D211478B0A11E388, 4B91478B0A1800A9 and 5C91478B0A1AD343, have high orientation uncertainty, see Figure 2-105. Two of them have relatively low transmissivity values whilst the third is among the highest values in the borehole and therefore needs further attention.

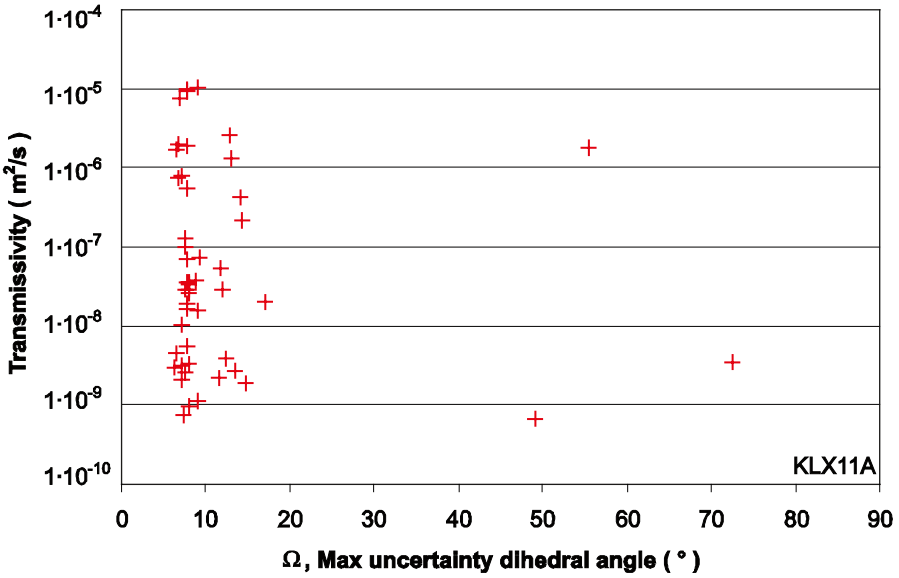

Figure 2-105. The transmissivity versus the uncertainty of the PFL fractures in KLX11A.

2.2.19 KLX11B

Although not as extreme as the other almost vertical borehole, KLX09B, all of the PFL fractures in KLX11B have maximum uncertainty greater than 10°, see Figure 2-106, and thus the orientation information from this borehole should be used with caution.

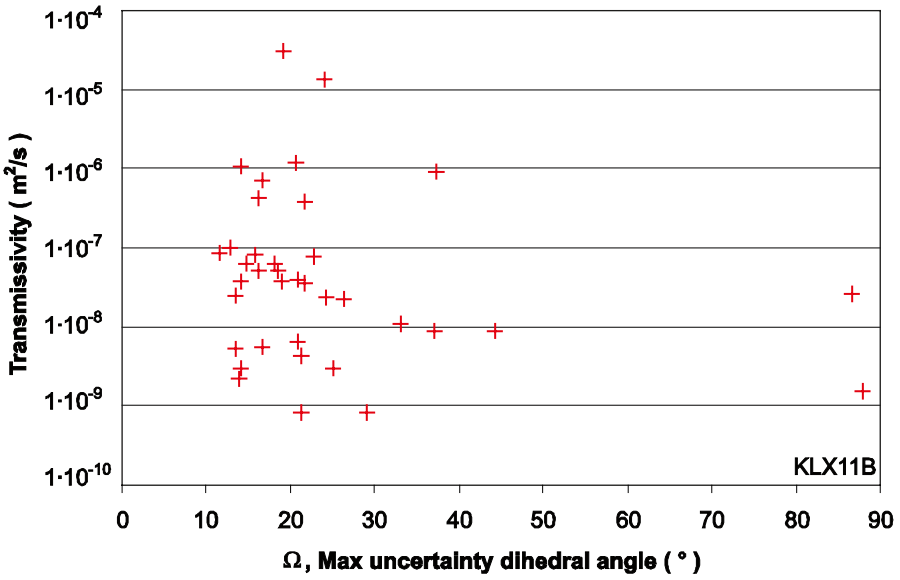

Figure 2-106. The transmissivity versus the uncertainty of the PFL fractures in KLX11B.

2.2.20 KLX11C

About 15% of the PFL fractures in KLX11C have high orientation uncertainty, but they have low to intermediate transmissivity values, see Figure 2-107. The six fractures, C091478B0810799F, 2091478B081080D7, E091478B08108665, 2091478B0810CE05, 4091478B0810FB33 and E091478B081125E4, have the greatest orientation uncertainties and should thus be given attention if important for any hydrogeological modelling.

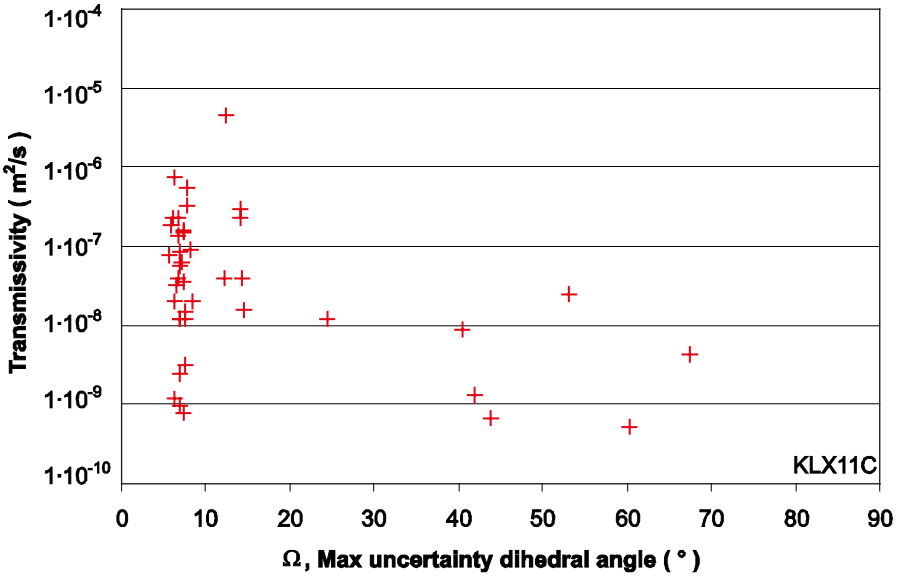

Figure 2-107. *The transmissivity versus the uncertainty of the PFL fractures in KLX11C.*

2.2.21 KLX11D

Only two PFL fractures in KLX11D have large orientation uncertainty, 4091478B0F10AEDA and 4091478B0F10E9DD, see Figure 2-108. Compared to other PFL fractures in KLX11D the two fractures have transmissivity values below the median.

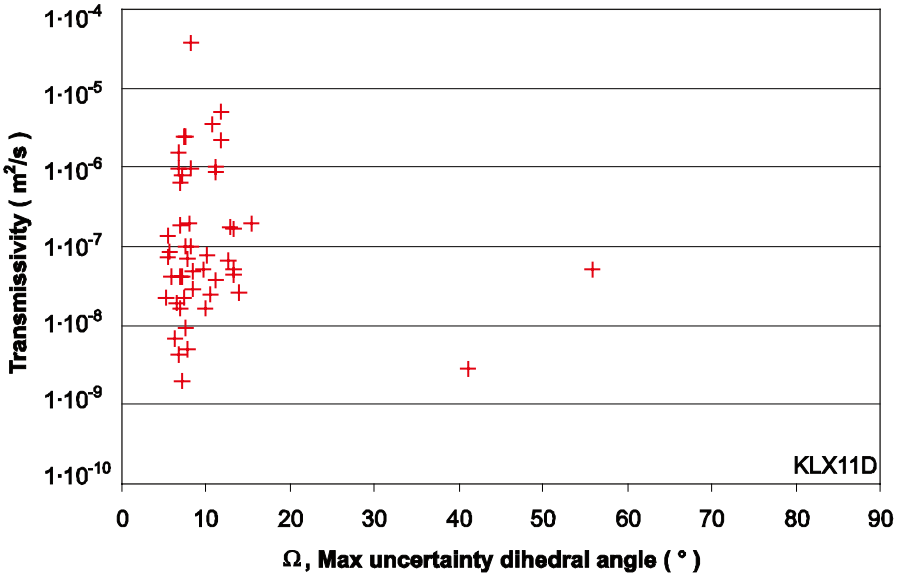

Figure 2-108. *The transmissivity versus the uncertainty of the PFL fractures in KLX11D.*

2.2.22 KLX11E

Also in KLX11E two fractures, 0091478B0E10BA7B and 6091478B0E111005, have large orientation uncertainty, see Figure 2-109. Though both fractures have intermediate transmissivity values they are close to or above the median of the transmissivities in KLX11E and hence need attention regarding their orientation if important for any hydrogeological modelling.

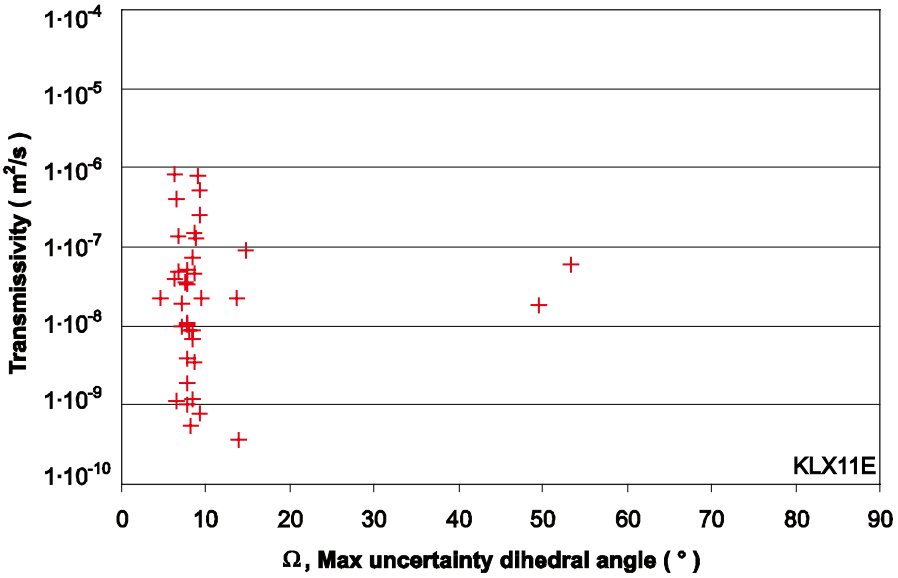

Figure 2-109. The transmissivity versus the uncertainty of the PFL fractures in KLX11E.

2.2.23 KLX11F

All PFL fractures in KLX11F have maximum uncertainty less than 30°, see Figure 2-110. The most uncertain fracture, E091478B0D10AB54, has maximum uncertainty 26° and is below the median transmissivity of the borehole, thus it might not need any further attention regarding orientation unless important for any model.

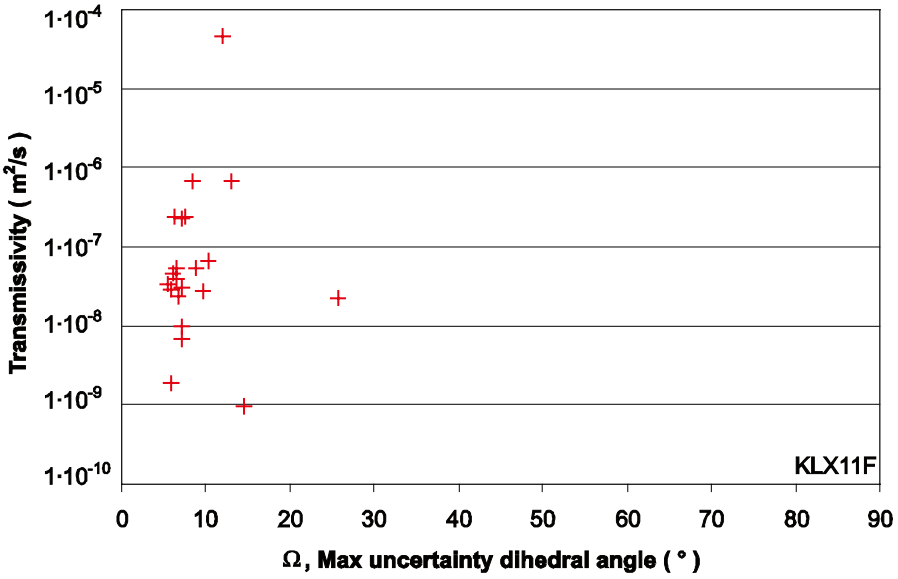

Figure 2-110. The transmissivity versus the uncertainty of the PFL fractures in KLX11F.

2.2.24 KLX12A

In KLX12A there are ten fractures having large orientation uncertainty, but most of them have relatively low transmissivity values compared to other PFL fractures in the same borehole, see Figure 2-111. Further information about the sample space is shown in Section 2.3.24 and it is recommended that the PFL fractures with highest orientation uncertainties are paid attention before any further hydrogeological modelling using orientation data is accomplished.

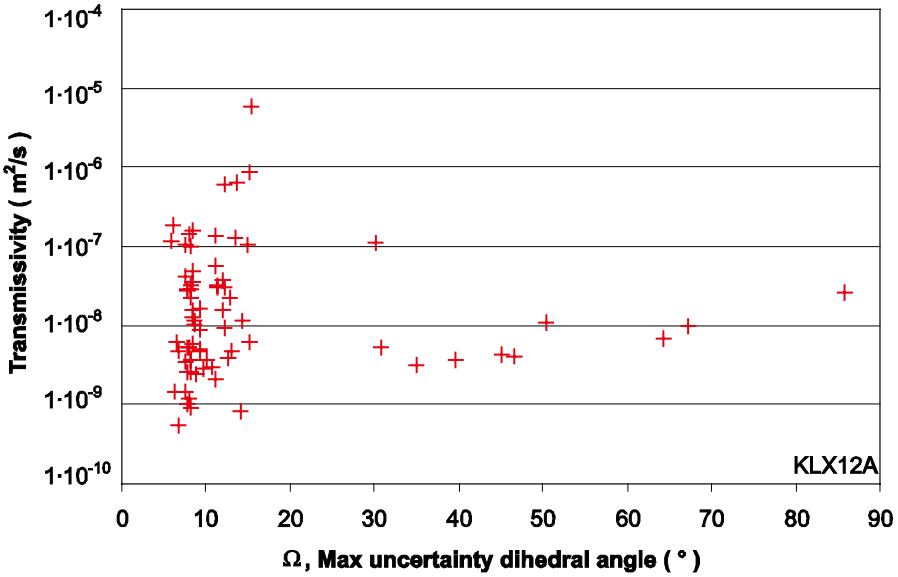

Figure 2-111. The transmissivity versus the uncertainty of the PFL fractures in KLX12A.

2.2.25 KLX13A

In KLX13A there are six PFL fractures, A093478B0A1190AE, 2093478B0A12A889, 8093478B0A133A80, 2093478B0A13DBB8, A093478B0A15BBBB and 4093478B0A175336, having orientation uncertainty greater than 30°, see Figure 2-112. These 5% of the total number of PFL fractures in KLX13A should be investigated further if important for any hydrogeological modelling.

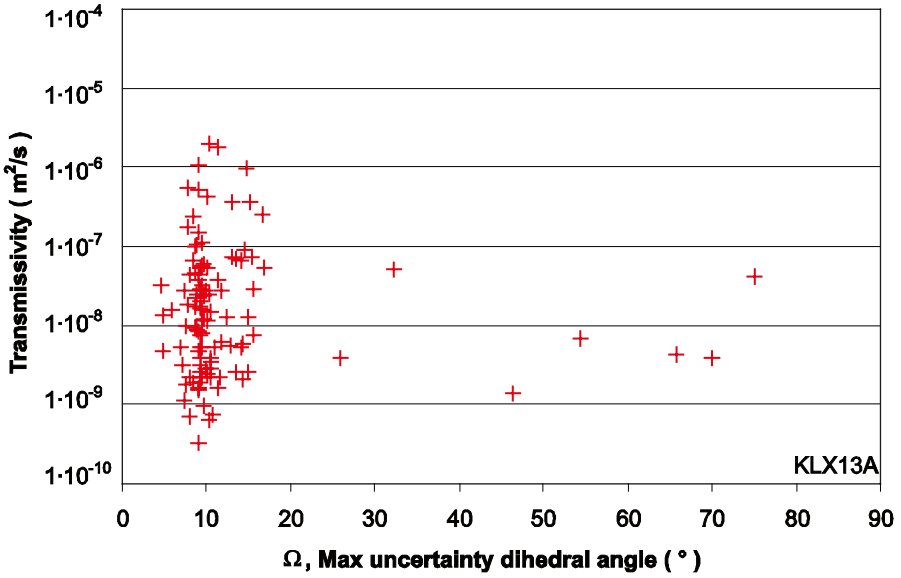

Figure 2-112. The transmissivity versus the uncertainty of the PFL fractures in KLX13A.

2.2.26 KLX14A

Only one fracture, C0D4478B0A10AB07, has large orientation uncertainty, see Figure 2-113. Unfortunately the maximum uncertainty is close to 90° and the transmissivity is the fourth largest in the borehole; hence the fracture needs to be paid attention in any hydrogeological modelling.

There is also one PFL fracture, 7BD4478B0A10C009 (PFL no 11), that is excluded from Figure 2-113 due to lack of orientation data. The transmissivity value, $7.23 \cdot 10^{-8}$ m^2/s is in the mid range of transmissivity values and it is thus recommended that the reason for the lack of data is investigated and that, if possible, orientation and uncertainty values are calculated.

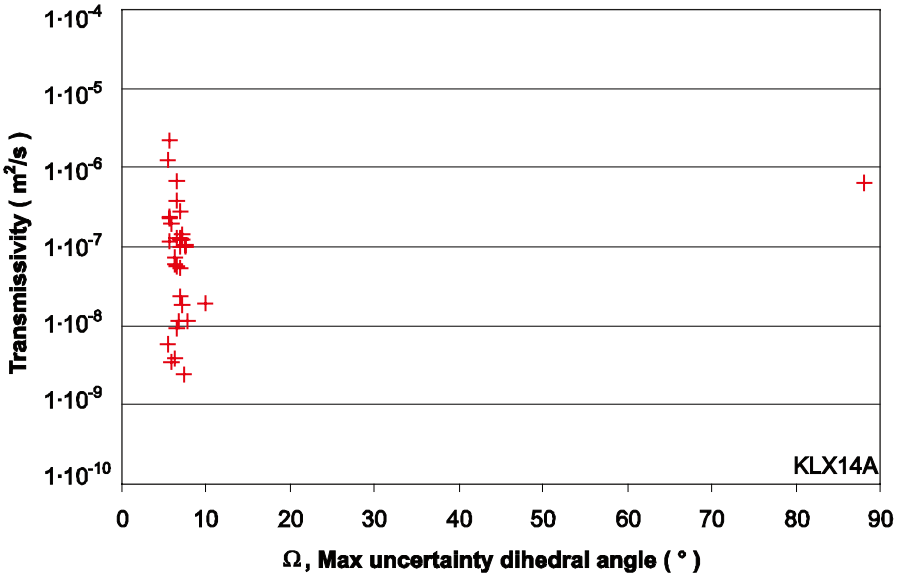

Figure 2-113. *The transmissivity versus the uncertainty of the PFL fractures in KLX14A.*

2.2.27 KLX15A

Three fractures, BDD5478B0A130515, C095478B0A15E87F and F895478B0A15EE3E, have large orientation uncertainty, see Figure 2-114. The two latter have relatively low transmissivity values whilst the first have intermediate transmissivity value and hence should be paid attention when used in hydrogeological modelling using orientation information.

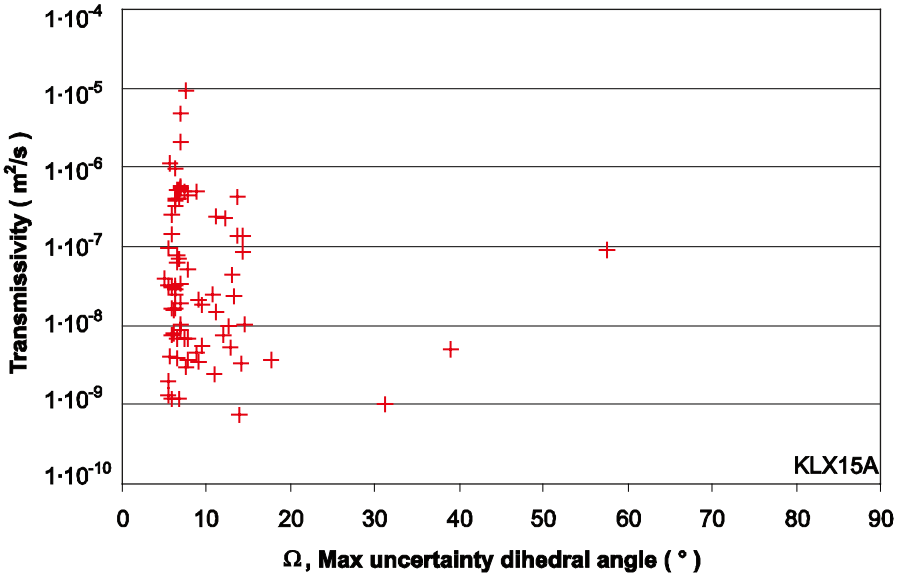

Figure 2-114. *The transmissivity versus the uncertainty of the PFL fractures in KLX15A.*

2.2.28 KLX16A

Most PFL fractures in KLX16A have relatively low maximum uncertainty, see Figure 2-115. The only PFL fracture with large uncertainty, E8D6478B0A23A756, has the third lowest transmissivity value and, though high uncertainty, should not need any extra attention unless important for conceptual hydrogeological modelling.

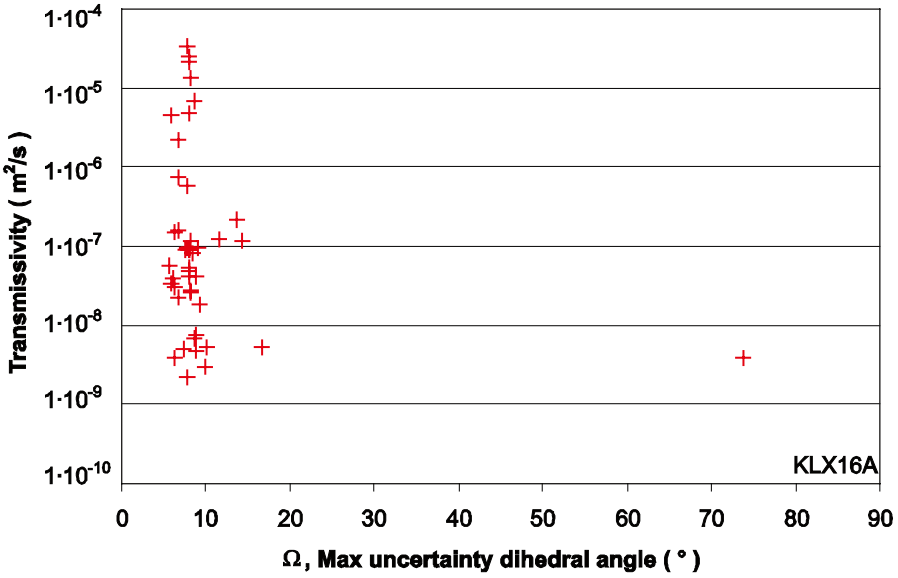

Figure 2-115. The transmissivity versus the uncertainty of the PFL fractures in KLX16A.

2.2.29 KLX17A

The two fractures, BBD7478B0A33BFB4 and EE17478B0A367F28, having the largest orientation uncertainty are among the six fractures with the lowest transmissivity values, see Figure 2-116. Unless important to the hydrogeological modelling there should not be a major incitement to investigate those two fractures further.

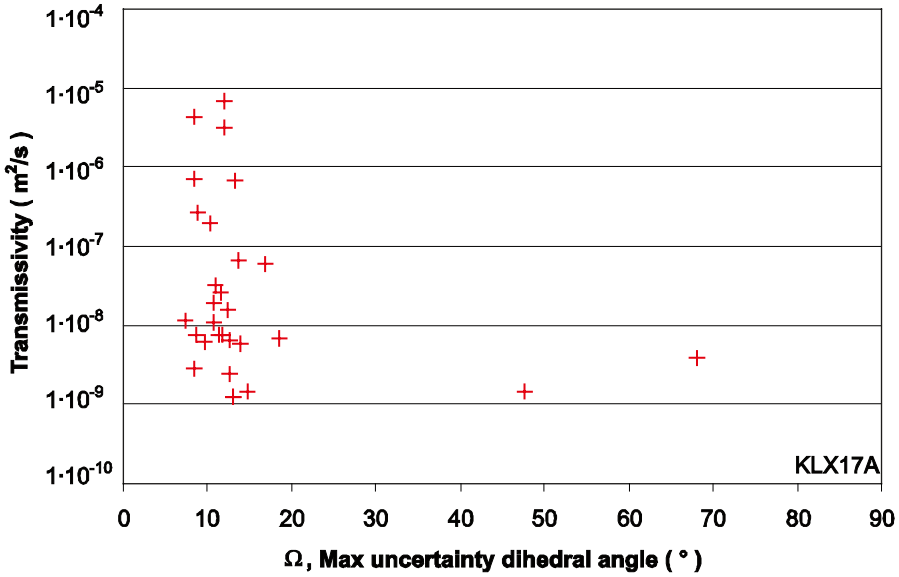

Figure 2-116. The transmissivity versus the uncertainty of the PFL fractures in KLX17A.

2.2.30 KLX18A

The vast majority of the PFL fractures in KLX18A have low maximum uncertainty, see Figure 2-117. However, the 13 PFL fractures with maximum uncertainty greater than 30° have transmissivity values that spread almost as much as the rest in KLX18A and thus these fractures need attention before further hydrogeological modelling, see e.g. Section 2.3.30.

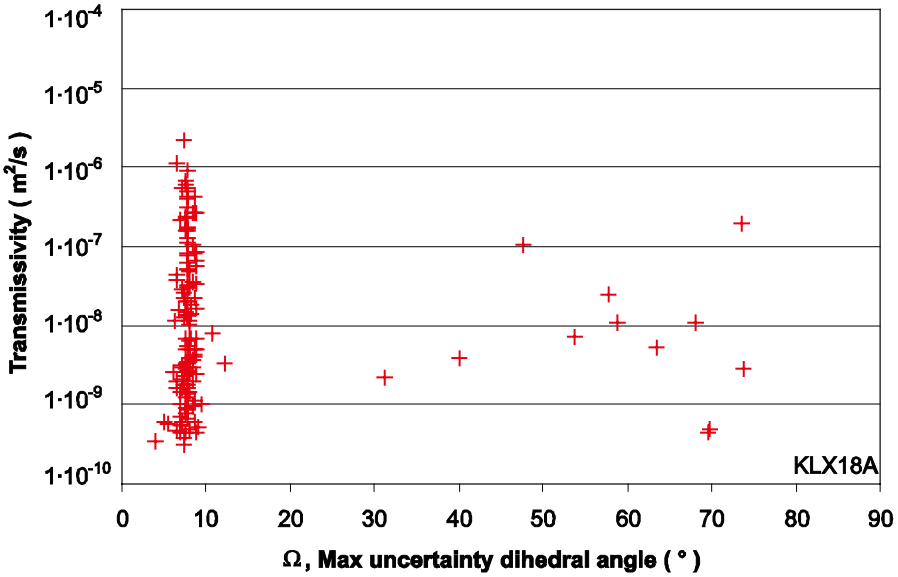

Figure 2-117. The transmissivity versus the uncertainty of the PFL fractures in KLX18A.

2.2.31 KLX19A

There are five PFL fractures, 0099478B0A119244, 6099478B0A11979B, 2099478B0A123FBC, 0099478B0A1A2F1C and 4099478B0A1A3230, having orientation uncertainty greater than 30° in KLX19A, see Figure 2-118. The transmissivity values of the PFL fractures are high in KLX19A and despite that all but one of the fractures with high uncertainty is below the median transmissivity of the borehole these fractures should be paid attention before any further hydrogeological modelling.

One of the most transmissive fractures, $2.55 \cdot 10^{-6}$ m²/s, in KLX19A, 0099478B0A119AFC (PFL no 5), is omitted from Figure 2-118 due to lack of orientation information. It is highly recommended that the reason for the missing orientation data is investigated and, if possible, calculate the orientation together with the uncertainty values.

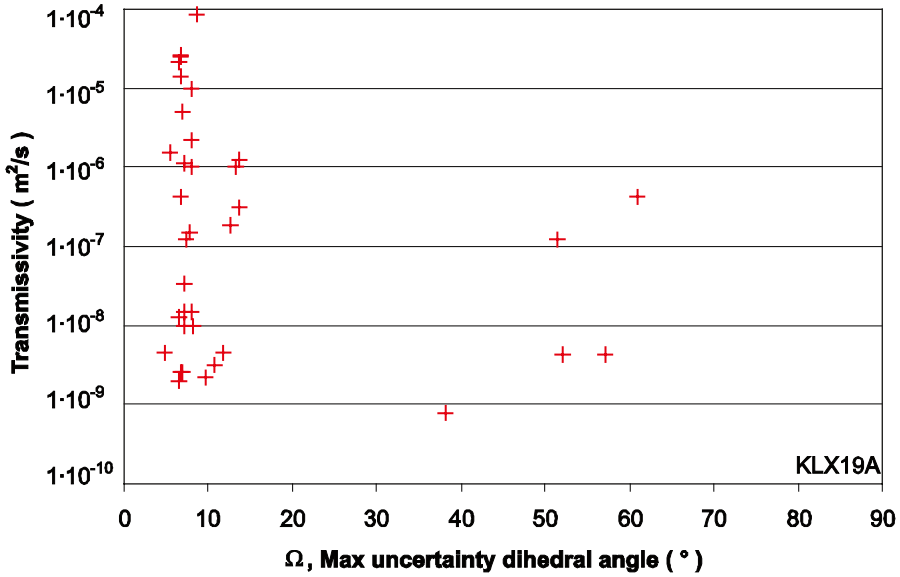

Figure 2-118. The transmissivity versus the uncertainty of the PFL fractures in KLX19A.

2.2.32 KLX20A

There is a large spread of the orientation uncertainties in KLX20A, see Figure 2-119. The transmissivity values, for the eight fractures with orientation uncertainty greater than 30°, spread as much as the transmissivity values for all PFL fractures and thus the fractures need to be investigated further, see e.g. Section 2.3.32.

One PFL fracture, 20904B8B0A1436CE (PFL no 46), is excluded from Figure 2-119 due to missing information about orientation. Though the transmissivity value is among the lowest, $1.65 \cdot 10^{-9}$ m^2/s, in KLX20A it is anyhow recommended that the reason for lack of data is investigated if important to any hydrogeological model and, if possible, orientation data and uncertainty is calculated.

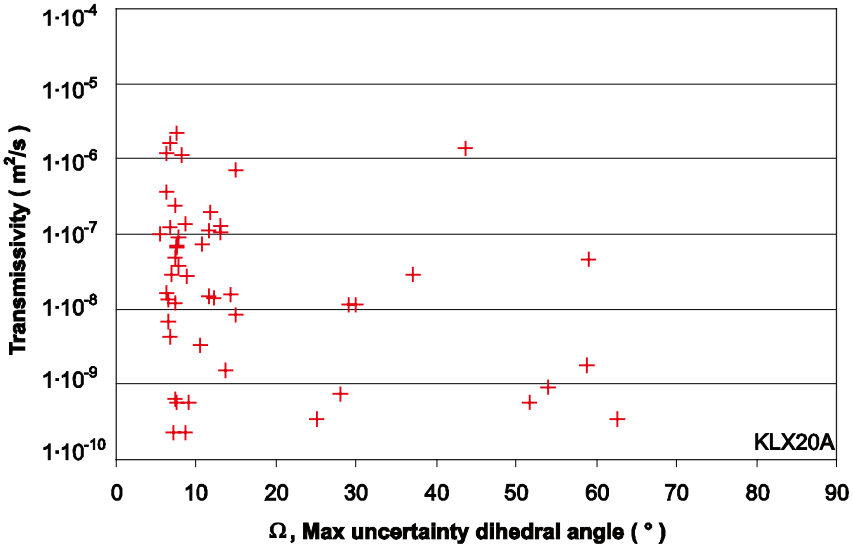

Figure 2-119. The transmissivity versus the uncertainty of the PFL fractures in KLX20A.

2.2.33 KLX21B

No PFL fractures in KLX21B have large orientation uncertainty, see Figure 2-120, and thus no further analyses regarding orientation should be needed for the PFL fractures, unless important for the hydrogeological model.

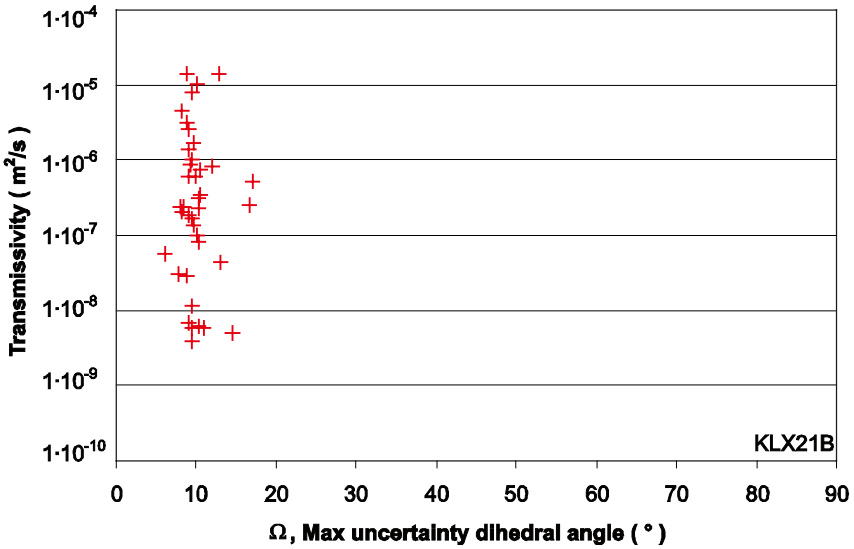

Figure 2-120. The transmissivity versus the uncertainty of the PFL fractures in KLX21B.

2.2.34 KLX22A

There is no large orientation uncertainty for the PFL fractures in KLX22A and, unless important for the hydrogeological model, no further analyses regarding orientation should be needed for the PFL fractures, see Figure 2-121.

Three PFL fractures, C0924B8B0A10496F (PFL no 1), A0924B8B0A105689 (PFL no 2) and C0924B8B0A10628F (PFL no 3), are omitted from Figure 2-121 due to lack of transmissivity information, see Section 1.1. The maximum uncertainty of the three fractures is all below 16°.

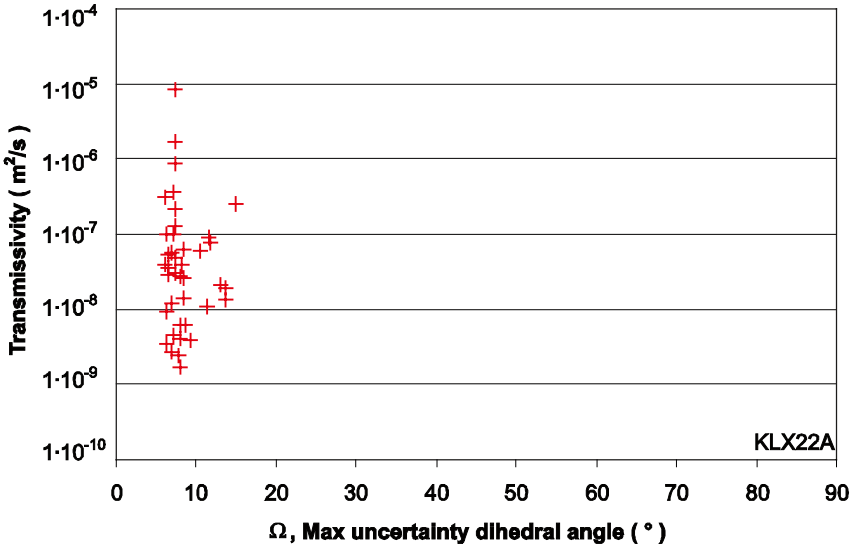

Figure 2-121. *The transmissivity versus the uncertainty of the PFL fractures in KLX22A.*

2.2.35 KLX22B

There are two PFL fractures, C0924B8B0910781F and 00924B8B09109F3B, in KLX22B having large orientation uncertainty, see Figure 2-122. Though having as low transmissivity values as in the $1 \cdot 10^{-8}$ m²/s range, they are in the mid range of transmissivity values in KLX22B and thus it is recommended that the fractures are paid attention when doing hydrogeological work that take orientation into account.

Two PFL fractures, C0924B8B091041C4 PFL no 1) and 00924B8B091045C6 (PFL no 2), in KLX22B are missing transmissivity values and hence excluded from Figure 2-122. The maximum orientation uncertainty of these two fractures is less than 15°.

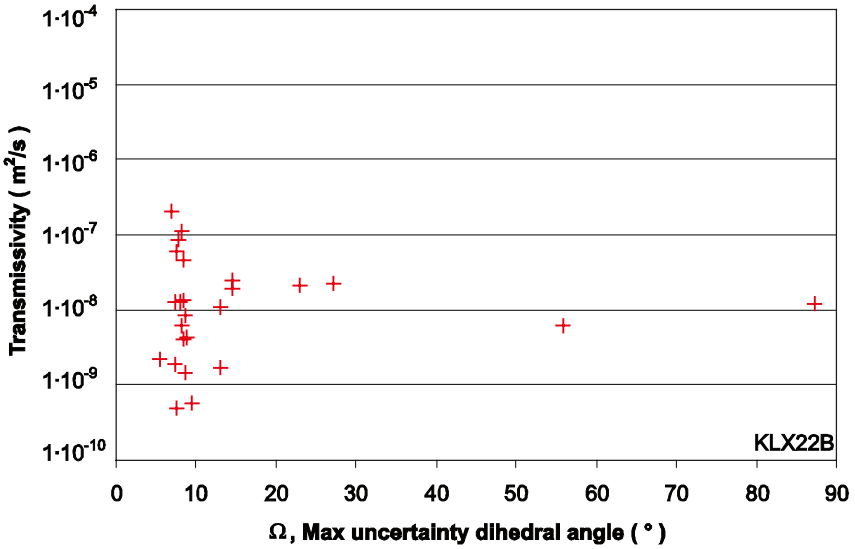

Figure 2-122. *The transmissivity versus the uncertainty of the PFL fractures in KLX22B.*

2.2.36 KLX23A

Only one PFL fracture, A0D34B8B0A216B13, has orientation uncertainty greater than 30°, see Figure 2-123.The transmissivity values is in the mid range of the values in KLX23A and thus should be paid attention when used in hydrogeological modelling using orientation information.

KLX23A is missing orientation information for one fracture, 40934B8B0A216EBD (PFL no 17), and transmissivity data for one fracture, A0934B8B0A2057D6 (PFL no 1). These two fractures are consequently omitted from Figure 2-123.

The fracture missing orientation data have a transmissivity value of $3.91 \cdot 10^{-9}$ m^2/s and hence in the lower range of transmissivity values in KLX23A. Despite the relatively low transmissivity it is recommended that the reason for the lack of orientation information is investigated and, if possible, calculate orientation and uncertainty values. The fracture that is missing transmissivity information has maximum uncertainty 11°.

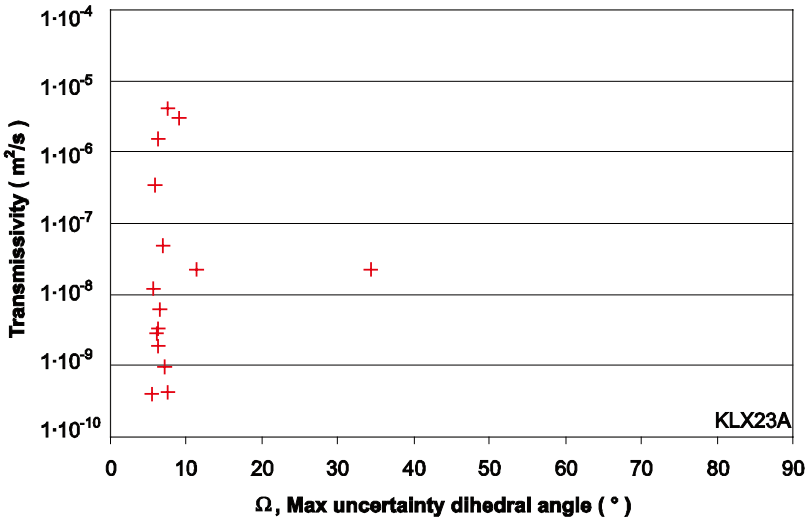

Figure 2-123. *The transmissivity versus the uncertainty of the PFL fractures in KLX23A.*

2.2.37 KLX23B

There are only four PFL fractures in KLX23B and two of them, 80934B8B09204923 (PFL no 1) and A0934B8B09206504 (PFL no 2), are missing information about transmissivity and thus omitted from Figure 2-124. The remaining two fractures have low orientation uncertainty and do not need any further attention regarding the orientation.

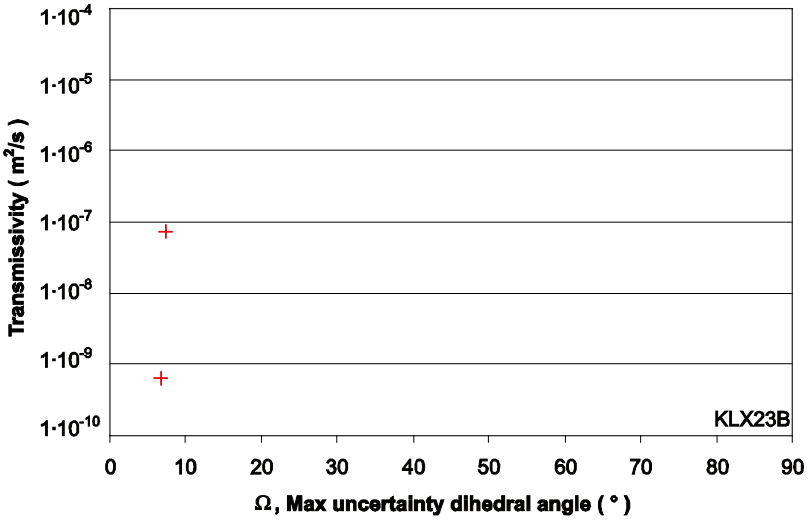

Figure 2-124. *The transmissivity versus the uncertainty of the PFL fractures in KLX23B.*

2.2.38 KLX24A

There is one PFL fracture, 00944B8B0A107BC2, in KLX24A that has orientation uncertainty greater than 30°, see Figure 2-125.The transmissivity value is among the largest in the borehole and thus should be paid attention when used in hydrogeological modelling using orientation information.

Three fractures, 60944B8B0A10501A (PFL no 1), 20944B8B0A105C3E (PFL no 2) and 60944B8B0A106E52 (PFL no 3), that are missing transmissivity values are consequently omitted from Figure 2-125. The maximum uncertainty for these fractures is less than 11°.

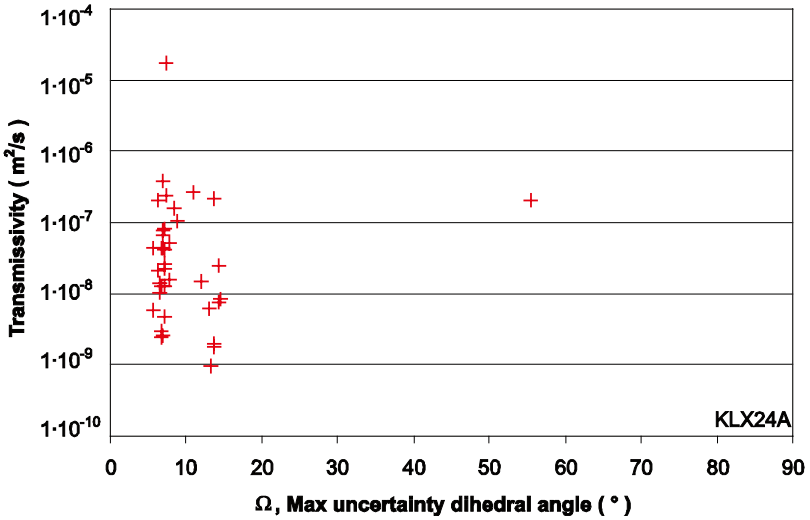

Figure 2-125. The transmissivity versus the uncertainty of the PFL fractures in KLX24A.

2.2.39 KLX25A

There are few PFL fractures in KLX25A, see Figure 2-126. One of them, 20954B8B0A10840C, has a large orientation uncertainty but has the lowest transmissivity in the borehole. This fracture might not need further attention unless important for the hydrogeological orientation model.

One fracture, 80954B8B0A104286, with maximum orientation uncertainty 8° is missing transmissivity information and thus excluded from Figure 2-126.

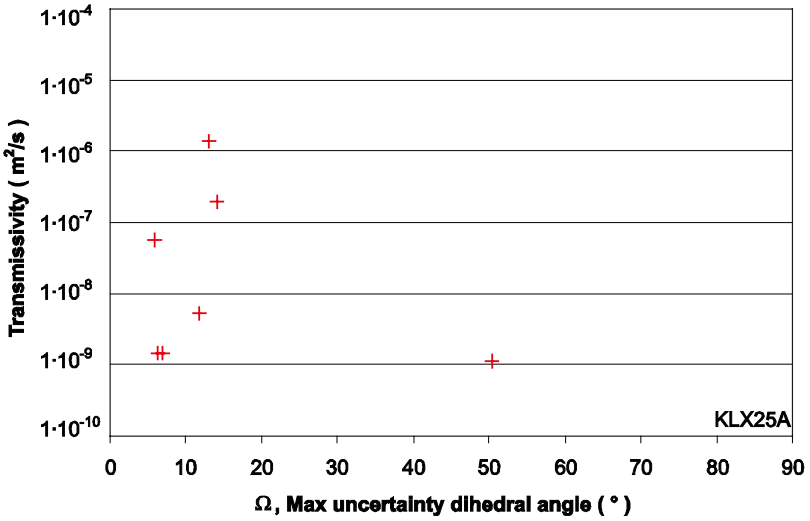

Figure 2-126. The transmissivity versus the uncertainty of the PFL fractures in KLX25A.

2.2.40 KLX26A

Only one PFL fracture, C0964B8B0A1096D9, has large orientation uncertainty in KLX26A, see Figure 2-128. The fracture is among the most transmissive and consequently need attention when used in hydrogeological modelling using orientation information.

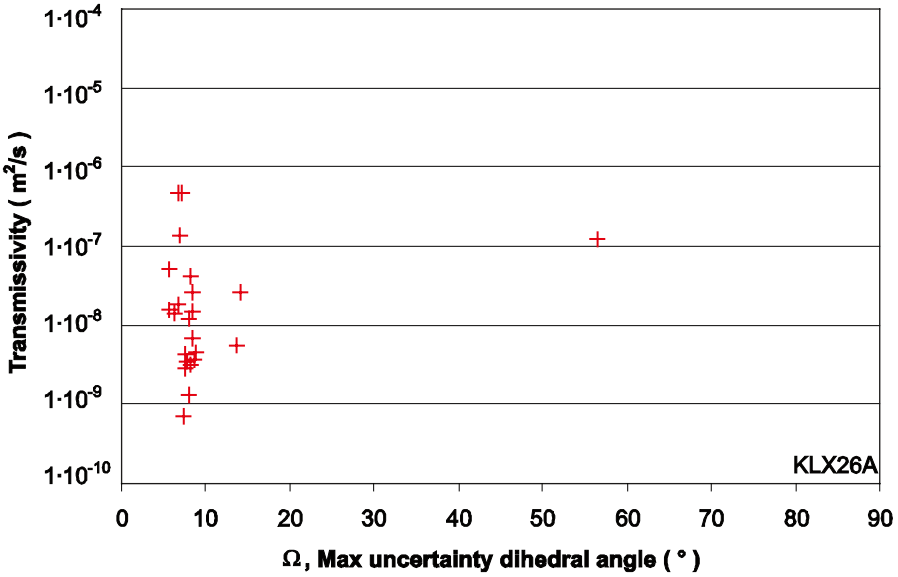

Figure 2-127. The transmissivity versus the uncertainty of the PFL fractures in KLX26A.

2.2.41 KLX26B

No PFL fracture has large maximum orientation uncertainty in KLX26B, see Figure 2-128. The maximum uncertainty is less than 12° and thus no further investigation should be needed when using the data in hydrogeological modelling.

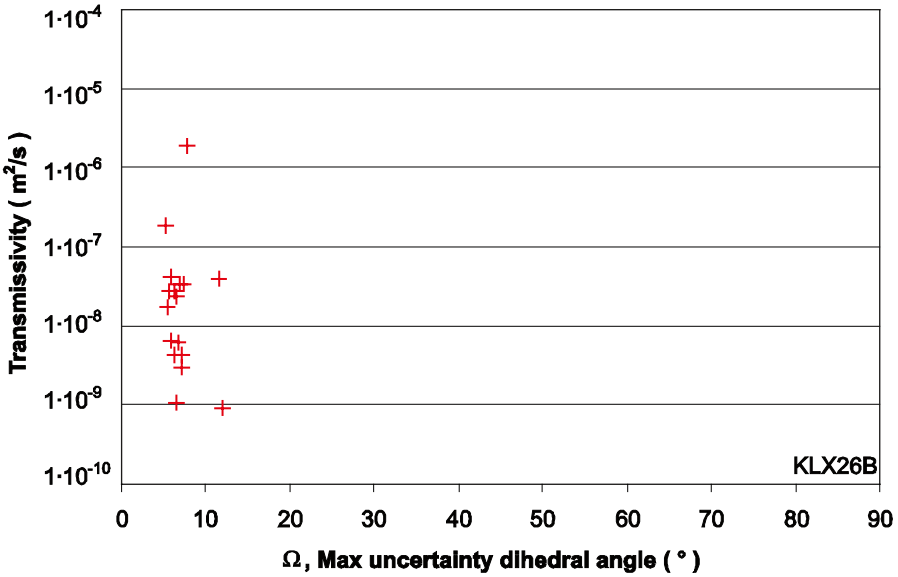

Figure 2-128. The transmissivity versus the uncertainty of the PFL fractures in KLX26B.

2.2.42 KLX28A

There is no large orientation uncertainty for the PFL fractures in KLX28A and, unless important for the hydrogeological model, no further analyses regarding orientation should be needed for the PFL fractures, see Figure 2-129.

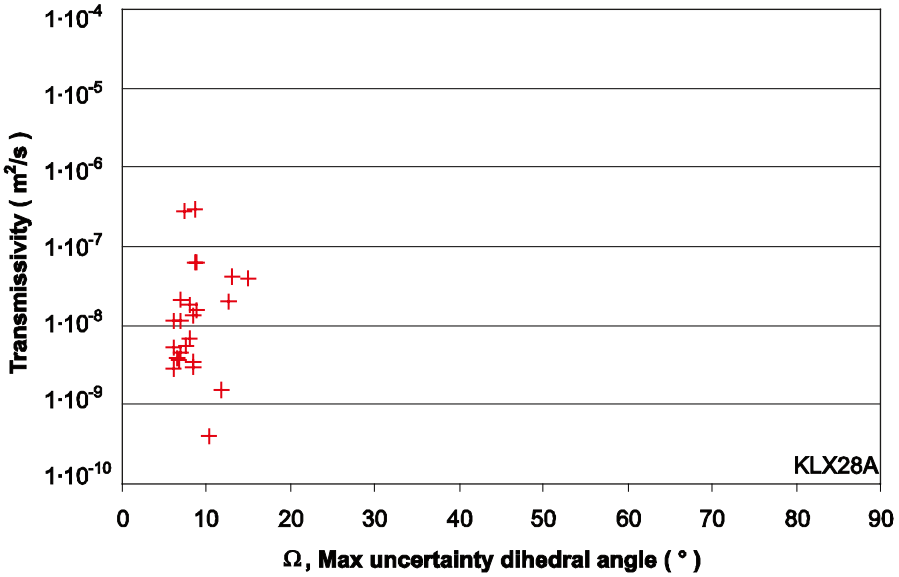

Figure 2-129. *The transmissivity versus the uncertainty of the PFL fractures in KLX28A.*

2.2.43 KLX29A

There is no PFL fracture with large orientation uncertainty in KLX29A, see Figure 2-130. Unless important for the hydrogeological model, there should be no need for further analyses regarding the orientation.

Two PFL fractures, 00994B8B0A101CAB (PFL no 1) and 00994B8B0A103320 (PFL no 2), are missing transmissivity values and hence omitted from Figure 2-130. Both fractures have low maximum uncertainty, less than 7°.

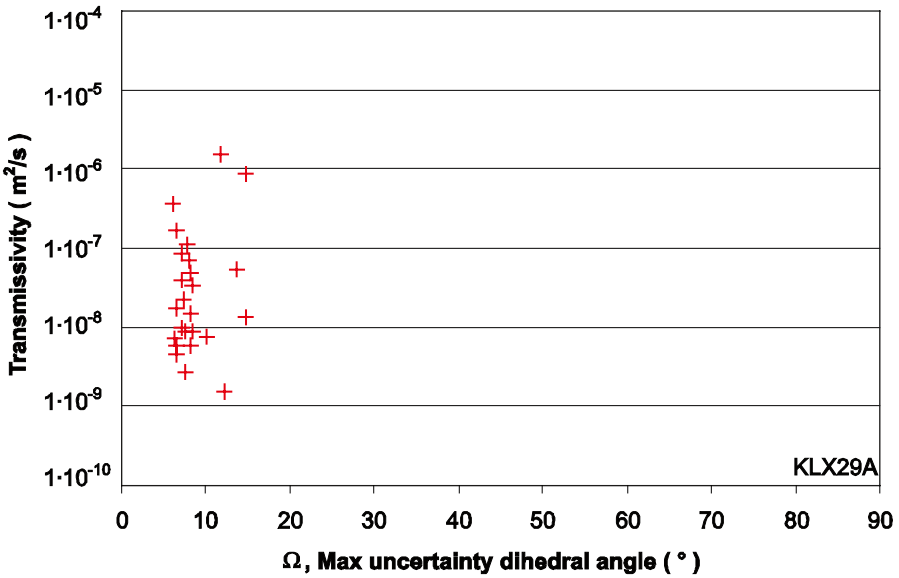

Figure 2-130. *The transmissivity versus the uncertainty of the PFL fractures in KLX29A.*

2.2.44 All Combined

All the 1943 PFL fractures, with both orientation and transmissivity information, in the studied KLX holes are shown in Figure 2-131. There are 716 fractures that have an orientation uncertainty larger than 10° and 155 fractures with orientation uncertainty larger than 30°, the latter are listed in Table 2-2. As expected there does not seem to be any major difference in transmissivity values due to orientation uncertainty; the median transmissivity of all PFL fractures is $3.1 \cdot 10^{-8}$ m²/s whilst the median transmissivity for the fractures with orientation uncertainty larger than 30° is $1.1 \cdot 10^{-8}$ m²/s.

Table 2-1 shows the number of PFL fractures in each borehole that have maximum orientation uncertainty larger than 10° and 30°, respectively. There are nine boreholes having more than 10% PFL fractures with maximum uncertainty larger than 30° with KLX09B standing out with more than 80% of the fractures having maximum uncertainty larger than 30°. Eleven of the boreholes have no fractures with maximum uncertainty above 30°.

To give more details about the PFL fractures with most uncertain orientation the 155 PFL fractures with maximum uncertainty larger than 30° and having a transmissivity value are listed in Table 2-2. Further details of the shape of the sample space are shown in Section 2.3.

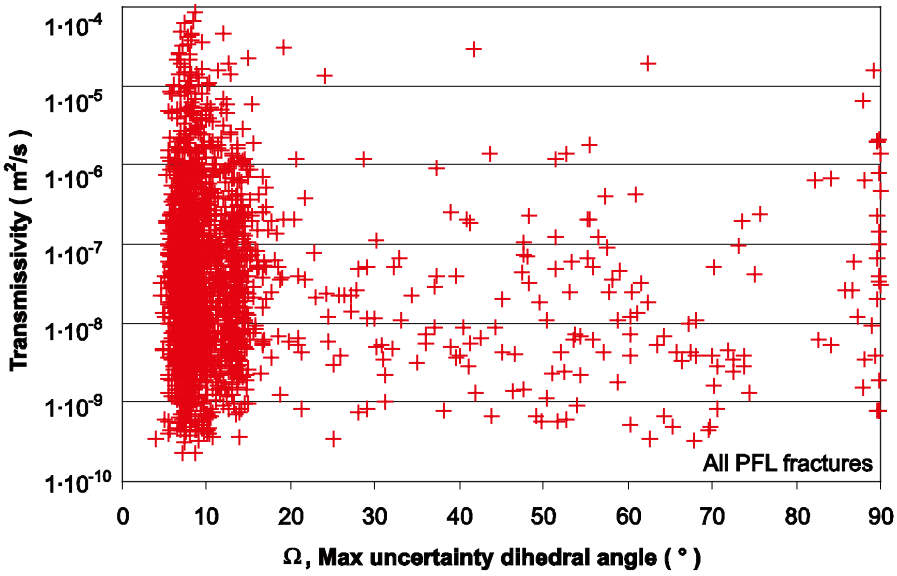

Figure 2-131. *The transmissivity versus the uncertainty of the PFL fractures in all KLX holes.*

Table 2-1. Compilation of PFL fractures with transmissivity value having maximum orientation uncertainty larger than 10° and 30°, respectively, compared to all PFL fractures.

Borehole	Total # of PFL fractures	PFL fractures Ω>10°		PFL fractures Ω>30°	
		number	%	number	%
KLX03	41	33	80.5	2	4.9
KLX04	86	74	86.0	4	4.7
KLX05	68	36	52.9	8	11.8
KLX06	76	23	30.3	7	9.2
KLX07A	113	16	14.2	6	5.3
KLX07B	54	41	75.9	5	9.3
KLX08	90	21	23.3	1	1.1
KLX09	52	12	23.1	0	0.0
KLX09B	44	43	97.7	36	81.8
KLX09C	36	5	13.9	0	0.0
KLX09D	41	15	36.6	4	9.8
KLX09E	22	4	18.2	1	4.5
KLX09F	37	3	8.1	2	5.4
KLX09G	15	2	13.3	1	6.7
KLX10	49	47	95.9	5	10.2
KLX10B	22	5	22.7	0	0.0
KLX10C	15	3	20.0	0	0.0
KLX11A	49	14	28.6	3	6.1
KLX11B	37	37	100.0	6	16.2
KLX11C	41	13	31.7	6	14.6
KLX11D	49	17	34.7	2	4.1
KLX11E	37	5	13.5	2	5.4
KLX11F	21	5	23.8	0	0.0
KLX12A	73	33	45.2	10	13.7
KLX13A	113	47	41.6	6	5.3
KLX14A	32	1	3.1	1	3.1
KLX15A	75	21	28.0	3	4.0
KLX16A	46	6	13.0	1	2.2
KLX17A	29	22	75.9	2	6.9
KLX18A	140	14	10.0	12	8.6
KLX19A	36	11	30.6	5	13.9
KLX20A	49	23	46.9	8	16.3
KLX21B	39	15	38.5	0	0.0
KLX22A	40	8	20.0	0	0.0
KLX22B	25	8	32.0	2	8.0
KLX23A	15	2	13.3	1	6.7
KLX23B	2	0	0.0	0	0.0
KLX24A	38	11	28.9	1	2.6
KLX25A	7	4	57.1	1	14.3
KLX26A	23	3	13.0	1	4.3
KLX26B	17	2	11.8	0	0.0
KLX28A	24	5	20.8	0	0.0
KLX29A	25	6	24.0	0	0.0
All	1,943	716	36.9	155	8.0

Table 2-2. The 155 PFL fractures with transmissivity value and having maximum orientation uncertainty larger than 30°.

Borehole	PFL-f no	Adjusted Secup (m)	Feature Id	Ω (°)	T (m^2/s)
KLX03	4	132.98	FE53438B2B1206B4	72.4	$2.41 \cdot 10^{-9}$
KLX03	5	137.09	F653438B2B1216AF	52.6	$2.49 \cdot 10^{-9}$
KLX04	51	314.18	4554438B2B14C370	30.0	$5.10 \cdot 10^{-9}$
KLX04	74	371.34	D854438B2B15A1BF	60.2	$7.04 \cdot 10^{-9}$
KLX04	90	568.95	E414438B2B18A26A	86.8	$6.11 \cdot 10^{-8}$
KLX04	108	626.59	F114438B2B1982BE	51.4	$4.97 \cdot 10^{-8}$
KLX05	26	154.56	31D5438B2B125BFA	71.8	$4.63 \cdot 10^{-9}$
KLX05	37	189.40	5515438B2B12E3B7	52.8	$6.07 \cdot 10^{-10}$
KLX05	42	211.52	4C15438B2B1339F7	65.3	$5.00 \cdot 10^{-10}$
KLX05	53	248.25	01D5438B2B13C92E	64.2	$6.79 \cdot 10^{-10}$
KLX05	62	411.16	A955438B2B164300	74.4	$1.32 \cdot 10^{-9}$
KLX05	64	426.33	0A55438B2B167E07	49.8	$5.78 \cdot 10^{-10}$
KLX05	66	494.76	8F95438B2B17886A	67.9	$3.30 \cdot 10^{-10}$
KLX05	71	897.64	4555438B2B1DA76F	70.6	$2.81 \cdot 10^{-9}$
KLX06	1	101.70	0496438B2B118D03	51.3	$1.21 \cdot 10^{-6}$
KLX06	19	163.12	E216438B2B127ADF	39.6	$3.97 \cdot 10^{-8}$
KLX06	20	163.22	F596438B2B127B43	45.1	$1.99 \cdot 10^{-8}$
KLX06	28	172.25	FE96438B2B129E5A	48.4	$3.18 \cdot 10^{-8}$
KLX06	72	264.55	3796438B2B14053F	62.4	$1.89 \cdot 10^{-5}$
KLX06	162	507.40	3C56438B2B17B5EA	84.0	$5.39 \cdot 10^{-9}$
KLX06	186	938.81	8CD6438B2B1E42B8	53.6	$6.03 \cdot 10^{-9}$
KLX07A	41	178.35	7117438B0A12B79A	70.1	$5.18 \cdot 10^{-8}$
KLX07A	63	250.28	F717438B0A13CF3C	60.4	$1.21 \cdot 10^{-8}$
KLX07A	159	432.38	1957438B0A169432	41.2	$5.54 \cdot 10^{-9}$
KLX07A	182	535.36	2517438B0A1824C3	60.2	$3.98 \cdot 10^{-9}$
KLX07A	187	574.49	4BD7438B0A18BCEA	70.2	$1.66 \cdot 10^{-9}$
KLX07A	204	668.08	9A97438B0A1A28E0	62.4	$1.79 \cdot 10^{-8}$
KLX07B	15	55.24	1C17438B0910D6E4	87.8	$6.36 \cdot 10^{-6}$
KLX07B	30	81.41	2397438B09113C9B	42.6	$6.40 \cdot 10^{-9}$
KLX07B	39	93.46	5257438B09116B70	61.1	$1.31 \cdot 10^{-8}$
KLX07B	50	105.55	FFD7438B09119A6F	89.1	$1.60 \cdot 10^{-5}$
KLX07B	78	177.83	E6D7438B0912B35E	40.9	$2.01 \cdot 10^{-7}$
KLX08	135	673.44	4058438B2B1A3C36	32.9	$6.65 \cdot 10^{-8}$
KLX09B	1	15.23	7459438B09103B78	55.2	$6.63 \cdot 10^{-8}$
KLX09B	2	16.40	4599438B09104003	89.6	$8.03 \cdot 10^{-10}$
KLX09B	3	17.55	5999438B09104488	36.1	$7.38 \cdot 10^{-9}$
KLX09B	5	23.83	19D9438B09105D06	82.6	$6.13 \cdot 10^{-9}$
KLX09B	6	24.13	FE99438B09105E31	31.0	$3.46 \cdot 10^{-9}$
KLX09B	9	27.99	FAD9438B09106D40	89.9	$1.92 \cdot 10^{-9}$
KLX09B	10	31.03	4699438B0910791A	36.0	$5.59 \cdot 10^{-9}$
KLX09B	11	31.82	8C19438B09107C32	61.5	$3.15 \cdot 10^{-8}$
KLX09B	12	32.60	8D99438B09107F3A	82.3	$6.27 \cdot 10^{-7}$
KLX09B	13	39.58	CF99438B09109A76	39.0	$2.50 \cdot 10^{-7}$
KLX09B	14	39.98	9B99438B09109BFF	89.6	$2.34 \cdot 10^{-7}$
KLX09B	15	42.87	2559438B0910A743	54.4	$2.22 \cdot 10^{-9}$
KLX09B	16	45.03	6D99438B0910AFB8	48.3	$2.24 \cdot 10^{-7}$
KLX09B	17	46.57	E559438B0910B5B8	60.5	$2.55 \cdot 10^{-8}$
KLX09B	18	48.53	7719438B0910BD57	58.1	$3.52 \cdot 10^{-8}$
KLX09B	19	49.30	0259438B0910C059	52.8	$1.36 \cdot 10^{-6}$
KLX09B	20	59.33	E299438B0910E777	89.9	$2.08 \cdot 10^{-6}$
KLX09B	21	59.96	CC59438B0910E9F6	89.6	$2.03 \cdot 10^{-6}$
KLX09B	22	61.32	94D9438B0910EF3B	90.0	$1.36 \cdot 10^{-6}$
KLX09B	23	61.73	2159438B0910F0D9	90.0	$4.74 \cdot 10^{-7}$
KLX09B	25	63.62	AC59438B0910F836	89.7	$1.01 \cdot 10^{-7}$
KLX09B	26	65.37	8559438B0910FF0D	84.1	$6.77 \cdot 10^{-7}$
KLX09B	27	67.80	2819438B09110889	89.8	$4.04 \cdot 10^{-8}$

Borehole	PFL-f no	Adjusted Secup (m)	Feature Id	Ω (°)	T (m^2/s)
KLX09B	29	69.36	E659438B09110E98	89.5	$6.47 \cdot 10^{-8}$
KLX09B	31	76.60	D299438B09112AD5	89.4	$3.88 \cdot 10^{-9}$
KLX09B	32	77.90	5BD9438B09112FE8	37.3	$3.89 \cdot 10^{-8}$
KLX09B	33	78.83	A519438B09113387	89.8	$1.44 \cdot 10^{-7}$
KLX09B	34	79.61	F119438B09113699	89.8	$7.75 \cdot 10^{-7}$
KLX09B	35	80.83	0A99438B09113B5C	89.7	$1.95 \cdot 10^{-6}$
KLX09B	36	81.37	BE99438B09113D75	41.4	$1.82 \cdot 10^{-7}$
KLX09B	38	82.81	0C59438B0911430E	89.6	$1.99 \cdot 10^{-8}$
KLX09B	39	82.99	7899438B091143C9	89.7	$3.31 \cdot 10^{-8}$
KLX09B	40	86.19	CC19438B0911503E	89.9	$7.74 \cdot 10^{-10}$
KLX09B	41	91.44	4319438B091164BB	70.7	$8.36 \cdot 10^{-10}$
KLX09B	42	91.86	DD19438B0911665E	89.8	$7.80 \cdot 10^{-10}$
KLX09B	44	97.29	B2D9438B09117B8B	90.0	$2.99 \cdot 10^{-8}$
KLX09D	18	56.17	CE19438B0F10D9BF	55.3	$2.10 \cdot 10^{-7}$
KLX09D	26	82.17	A0D9438B0F113E65	32.1	$4.73 \cdot 10^{-9}$
KLX09D	29	84.16	42D9438B0F114618	57.3	$4.11 \cdot 10^{-7}$
KLX09D	32	85.88	3499438B0F114CC1	47.3	$4.40 \cdot 10^{-8}$
KLX09E	33	111.67	B3D9438B0E11B368	41.7	$2.85 \cdot 10^{-5}$
KLX09F	11	33.79	9599438B0D108369	47.6	$7.33 \cdot 10^{-8}$
KLX09F	13	38.63	3499438B0D109634	48.1	$7.08 \cdot 10^{-8}$
KLX09G	2	25.11	CF99438B0C106216	51.1	$2.37 \cdot 10^{-9}$
KLX10	140	356.99	4910478B2B156B74	73.1	$9.57 \cdot 10^{-8}$
KLX10	143	361.80	8690478B2B157E33	88.1	$3.56 \cdot 10^{-9}$
KLX10	151	399.36	DC90478B2B16107C	75.6	$2.43 \cdot 10^{-7}$
KLX10	162	413.51	FF50478B2B164782	89.0	$9.23 \cdot 10^{-9}$
KLX10	163	418.56	F1D0478B2B165B27	66.4	$3.25 \cdot 10^{-9}$
KLX11A	8	123.61	D211478B0A11E388	55.5	$1.75 \cdot 10^{-6}$
KLX11A	48	524.35	4B91478B0A1800A9	72.6	$3.54 \cdot 10^{-9}$
KLX11A	64	709.84	5C91478B0A1AD343	49.1	$6.70 \cdot 10^{-10}$
KLX11B	10	29.53	2091478B09107313	37.0	$8.92 \cdot 10^{-9}$
KLX11B	14	35.25	A091478B0910895B	86.7	$2.62 \cdot 10^{-8}$
KLX11B	21	49.94	C091478B0910C294	33.1	$1.10 \cdot 10^{-8}$
KLX11B	29	70.09	E091478B09111107	44.3	$8.98 \cdot 10^{-9}$
KLX11B	34	76.28	E091478B09112922	37.4	$9.28 \cdot 10^{-7}$
KLX11B	35	85.01	A091478B09114B18	87.9	$1.51 \cdot 10^{-9}$
KLX11C	14	31.13	C091478B0810799F	60.3	$5.25 \cdot 10^{-10}$
KLX11C	15	32.98	2091478B081080D7	67.4	$4.34 \cdot 10^{-9}$
KLX11C	16	34.40	E091478B08108665	41.9	$1.32 \cdot 10^{-9}$
KLX11C	24	52.73	2091478B0810CE05	53.1	$2.45 \cdot 10^{-8}$
KLX11C	27	64.28	4091478B0810FB33	40.4	$8.92 \cdot 10^{-9}$
KLX11C	34	75.19	E091478B081125E4	43.8	$6.63 \cdot 10^{-10}$
KLX11D	17	44.65	4091478B0F10AEDA	55.8	$5.04 \cdot 10^{-8}$
KLX11D	26	59.75	4091478B0F10E9DD	41.1	$2.91 \cdot 10^{-9}$
KLX11E	16	47.90	0091478B0E10BA7B	49.5	$1.83 \cdot 10^{-8}$
KLX11E	26	69.68	6091478B0E111005	53.3	$5.94 \cdot 10^{-8}$
KLX12A	3	103.28	9DD2478B0A11935E	85.8	$2.60 \cdot 10^{-8}$
KLX12A	18	121.25	A052478B0A11D925	30.8	$5.39 \cdot 10^{-9}$
KLX12A	21	123.83	D312478B0A11E32D	35.1	$3.09 \cdot 10^{-9}$
KLX12A	23	126.35	B292478B0A11ED06	39.6	$3.69 \cdot 10^{-9}$
KLX12A	24	128.27	A952478B0A11F47D	45.1	$4.32 \cdot 10^{-9}$
KLX12A	48	182.82	CB92478B0A12C8DD	30.0	$1.13 \cdot 10^{-7}$
KLX12A	53	236.38	6392478B0A139959	50.4	$1.08 \cdot 10^{-8}$
KLX12A	67	396.60	F8D2478B0A1608CE	46.5	$3.99 \cdot 10^{-9}$
KLX12A	71	407.67	7992478B0A1633D1	64.2	$7.01 \cdot 10^{-9}$
KLX12A	76	542.91	E1D2478B0A184269	67.2	$9.73 \cdot 10^{-9}$
KLX13A	1	102.52	A093478B0A1190AE	32.2	$5.07 \cdot 10^{-8}$
KLX13A	13	173.26	2093478B0A12A889	65.9	$4.27 \cdot 10^{-9}$
KLX13A	20	210.63	8093478B0A133A80	46.3	$1.40 \cdot 10^{-9}$

Borehole	PFL-f no	Adjusted Secup (m)	Feature Id	Ω (°)	T (m^2/s)
KLX13A	35	251.98	2093478B0A13DBB8	54.4	$6.76 \cdot 10^{-9}$
KLX13A	58	374.75	A093478B0A15BBBB	70.0	$3.82 \cdot 10^{-9}$
KLX13A	111	479.07	4093478B0A175336	75.1	$4.13 \cdot 10^{-8}$
KLX14A	9	43.96	C0D4478B0A10AB07	88.2	$6.55 \cdot 10^{-7}$
KLX15A	43	198.14	BDD5478B0A130515	57.6	$9.09 \cdot 10^{-8}$
KLX15A	59	387.75	C095478B0A15E87F	31.2	$1.03 \cdot 10^{-9}$
KLX15A	61	389.23	F895478B0A15EE3E	39.0	$5.08 \cdot 10^{-9}$
KLX16A	41	239.94	E8D6478B0A23A756	73.7	$3.82 \cdot 10^{-9}$
KLX17A	28	245.98	BBD7478B0A33BFB4	68.0	$3.92 \cdot 10^{-9}$
KLX17A	42	425.94	EE17478B0A367F28	47.6	$1.43 \cdot 10^{-9}$
KLX18A	10	111.09	E098478B0A11B1EB	58.9	$1.10 \cdot 10^{-8}$
KLX18A	26	141.82	A098478B0A1229B0	31.3	$2.21 \cdot 10^{-9}$
KLX18A	28	146.31	2098478B0A123B2C	39.9	$3.81 \cdot 10^{-9}$
KLX18A	59	347.65	A098478B0A154B54	53.8	$7.38 \cdot 10^{-9}$
KLX18A	61	348.51	6098478B0A154EB2	73.5	$1.96 \cdot 10^{-7}$
KLX18A	62	350.06	C098478B0A1554BC	63.5	$5.25 \cdot 10^{-9}$
KLX18A	71	375.29	2098478B0A15B6DC	68.2	$1.11 \cdot 10^{-8}$
KLX18A	76	379.14	6098478B0A15C5D6	73.7	$2.90 \cdot 10^{-9}$
KLX18A	86	402.51	4098478B0A1620B2	47.7	$1.03 \cdot 10^{-7}$
KLX18A	106	431.62	C098478B0A1691EE	57.8	$2.47 \cdot 10^{-8}$
KLX18A	114	460.71	6098478B0A17032C	69.6	$4.46 \cdot 10^{-10}$
KLX18A	134	538.01	C098478B0A18301A	69.9	$4.84 \cdot 10^{-10}$
KLX19A	3	102.92	0099478B0A119244	51.5	$1.21 \cdot 10^{-7}$
KLX19A	4	104.25	6099478B0A11979B	61.0	$4.16 \cdot 10^{-7}$
KLX19A	19	147.25	2099478B0A123FBC	57.1	$4.34 \cdot 10^{-9}$
KLX19A	53	668.18	0099478B0A1A2F1C	38.2	$7.81 \cdot 10^{-10}$
KLX19A	54	668.96	4099478B0A1A3230	52.1	$4.26 \cdot 10^{-9}$
KLX20A	4	106.94	A0904B8B0A11A169	43.6	$1.41 \cdot 10^{-6}$
KLX20A	5	110.02	40904B8B0A11AD40	58.8	$1.77 \cdot 10^{-9}$
KLX20A	12	125.84	80904B8B0A11EAEB	54.0	$9.28 \cdot 10^{-10}$
KLX20A	15	127.77	80904B8B0A11F27A	58.9	$4.58 \cdot 10^{-8}$
KLX20A	29	165.54	80904B8B0A128593	62.6	$3.50 \cdot 10^{-10}$
KLX20A	30	167.64	00904B8B0A128DC1	51.6	$5.83 \cdot 10^{-10}$
KLX20A	47	278.01	A0904B8B0A143B7A	37.1	$2.94 \cdot 10^{-8}$
KLX20A	49	280.44	00904B8B0A1444E7	30.0	$1.16 \cdot 10^{-8}$
KLX22B	9	30.82	C0924B8B0910781F	87.3	$1.18 \cdot 10^{-8}$
KLX22B	14	40.86	00924B8B09109F3B	55.9	$6.22 \cdot 10^{-9}$
KLX23A	16	93.10	A0D34B8B0A216B13	34.4	$2.19 \cdot 10^{-8}$
KLX24A	4	31.72	00944B8B0A107BC2	55.5	$2.03 \cdot 10^{-7}$
KLX25A	6	33.97	20954B8B0A10840C	50.4	$1.12 \cdot 10^{-9}$
KLX26A	15	38.63	C0964B8B0A1096D9	56.4	$1.21 \cdot 10^{-7}$

2.3 Sample space

To give a detailed picture of the uncertainty of the orientation for all PFL fractures the 90th percentile sample space is shown for each of the 1957 PFL fracture having orientation information. The figures are equal area lower hemisphere stereograms and tagged with; Borehole name, Adjusted secUp, Rock Domain, Fracture Domain, Transmissivity, Maximum uncertainty and Feature Id, see Figure 2-132. To further facilitate the border of the stereogram is coloured with respect to the rock domain whilst the plot area is coloured with respect to the fracture domain. The colour scheme used is identical to the one used in GIS and RVS, see Figure 1-1, Figure 1-2 and Figure 2-133.

To facilitate the search for PFL fractures with large orientation uncertainty each Section begins with a table where all PFL fractures having maximum uncertainty larger than 30° is listed in the order of appearance in the borehole.

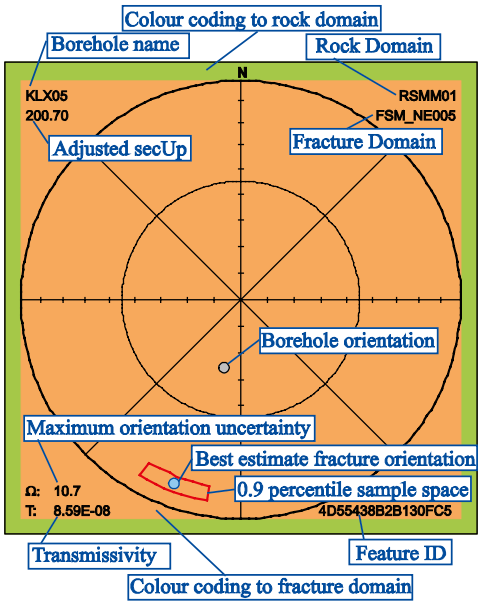

Figure 2-232. Guide to the information in the stereograms.

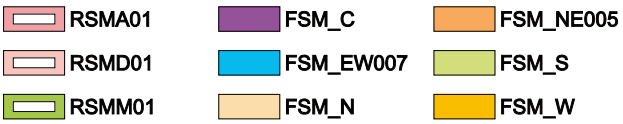

Figure 2-233. The colour coding used for the stereograms. To the left; the colours of the borders correspond to the rock domains /SKB 2008/. Middle and right; the colours of the plot area correspond to the fracture domains /La Pointe et al. 2008/.

2.3.1 KLX03

Below follow the 90th percentile sample space of uncertainty for the 41 PFL fractures in KLX03. Attention should be paid to the two fractures listed in Table 2-3. These fractures have a maximum uncertainty, on the 90th percentile, larger than 30°. Fractures having large uncertainty can have an alternative interpretation of orientation compared to the best estimate orientation that is found in the table p_fract_core in /Sicada 2008/.

Table 2-3. Fractures in KLX03 with uncertainty, Ω, larger than 30°.

FeatureId	PFL-f no	Adjusted Secup	Ω
FE53438B2B1206B4	4	132.98	72.4
F653438B2B1216AF	5	137.09	52.6

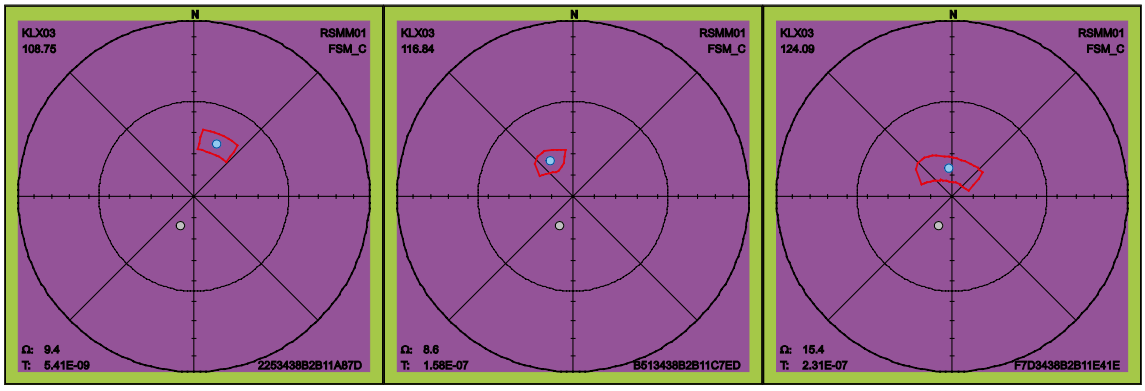

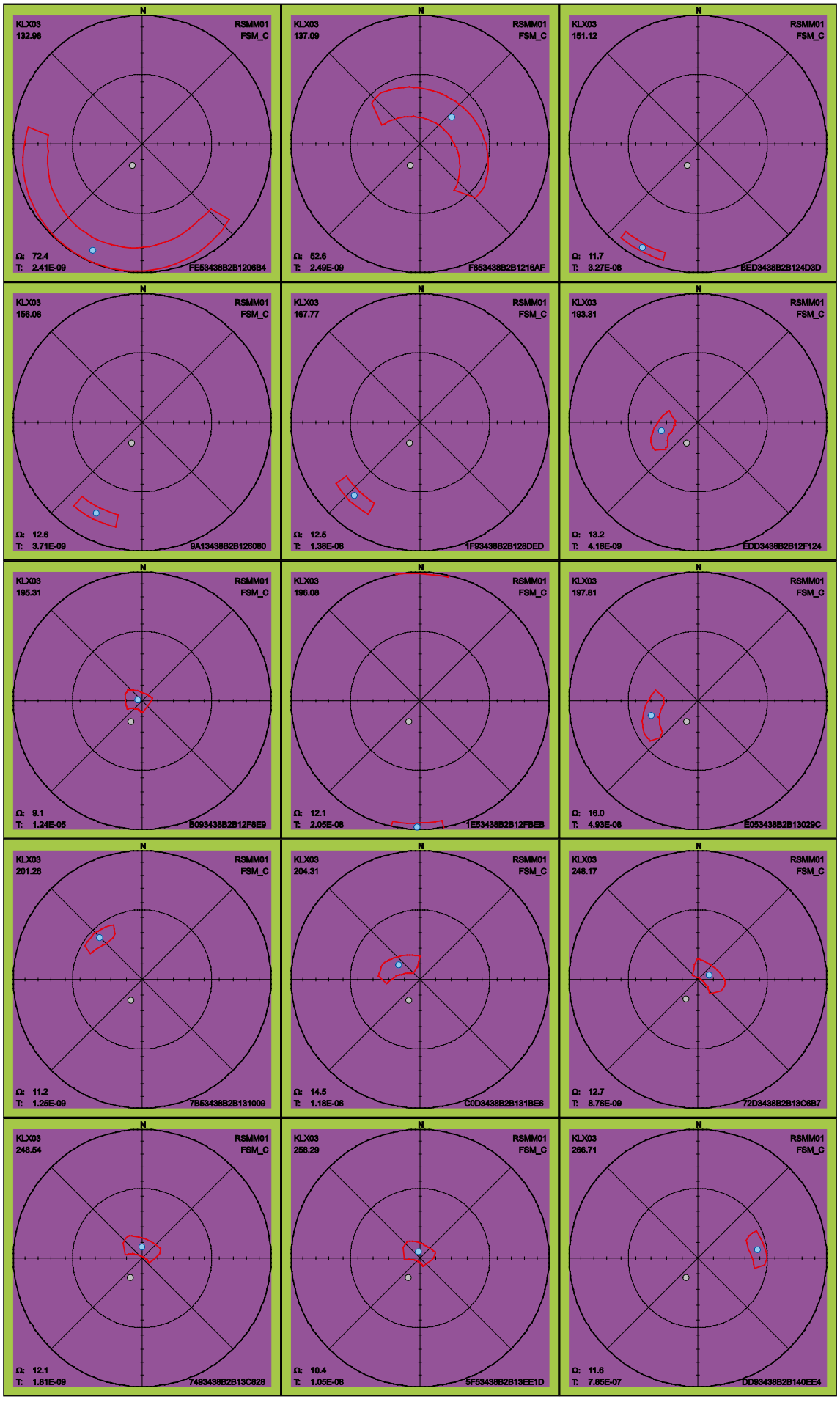
KLX03
132.98
RSMM01
FSM_C
N
Ω: 72.4
T: 2.41E-09
FE53438B2B1206B4
KLX03
137.09
RSMM01
FSM_C
N
Ω: 52.6
T: 2.49E-09
F653438B2B1216AF
KLX03
151.12
RSMM01
FSM_C
N
Ω: 11.7
T: 3.27E-06
BED3438B2B124D3D
KLX03
156.08
RSMM01
FSM_C
N
Ω: 12.6
T: 3.71E-09
9A13438B2B126080
KLX03
167.77
RSMM01
FSM_C
N
Ω: 12.5
T: 1.38E-08
1F93438B2B128DED
KLX03
193.31
RSMM01
FSM_C
N
Ω: 13.2
T: 4.18E-09
EDD3438B2B12F124
KLX03
195.31
RSMM01
FSM_C
N
Ω: 9.1
T: 1.24E-05
B093438B2B12F8E9
KLX03
196.08
RSMM01
FSM_C
N
Ω: 12.1
T: 2.05E-08
1E53438B2B12FBEB
KLX03
197.81
RSMM01
FSM_C
N
Ω: 16.0
T: 4.93E-08
E053438B2B13029C
KLX03
201.26
RSMM01
FSM_C
N
Ω: 11.2
T: 1.25E-09
7B53438B2B131009
KLX03
204.31
RSMM01
FSM_C
N
Ω: 14.5
T: 1.18E-06
C0D3438B2B131BE6
KLX03
248.17
RSMM01
FSM_C
N
Ω: 12.7
T: 8.76E-09
72D3438B2B13C6B7
KLX03
248.54
RSMM01
FSM_C
N
Ω: 12.1
T: 1.81E-09
7493438B2B13C828
KLX03
258.29
RSMM01
FSM_C
N
Ω: 10.4
T: 1.05E-08
5F53438B2B13EE1D
KLX03
266.71
RSMM01
FSM_C
N
Ω: 11.6
T: 7.85E-07
DD83438B2B140EE4

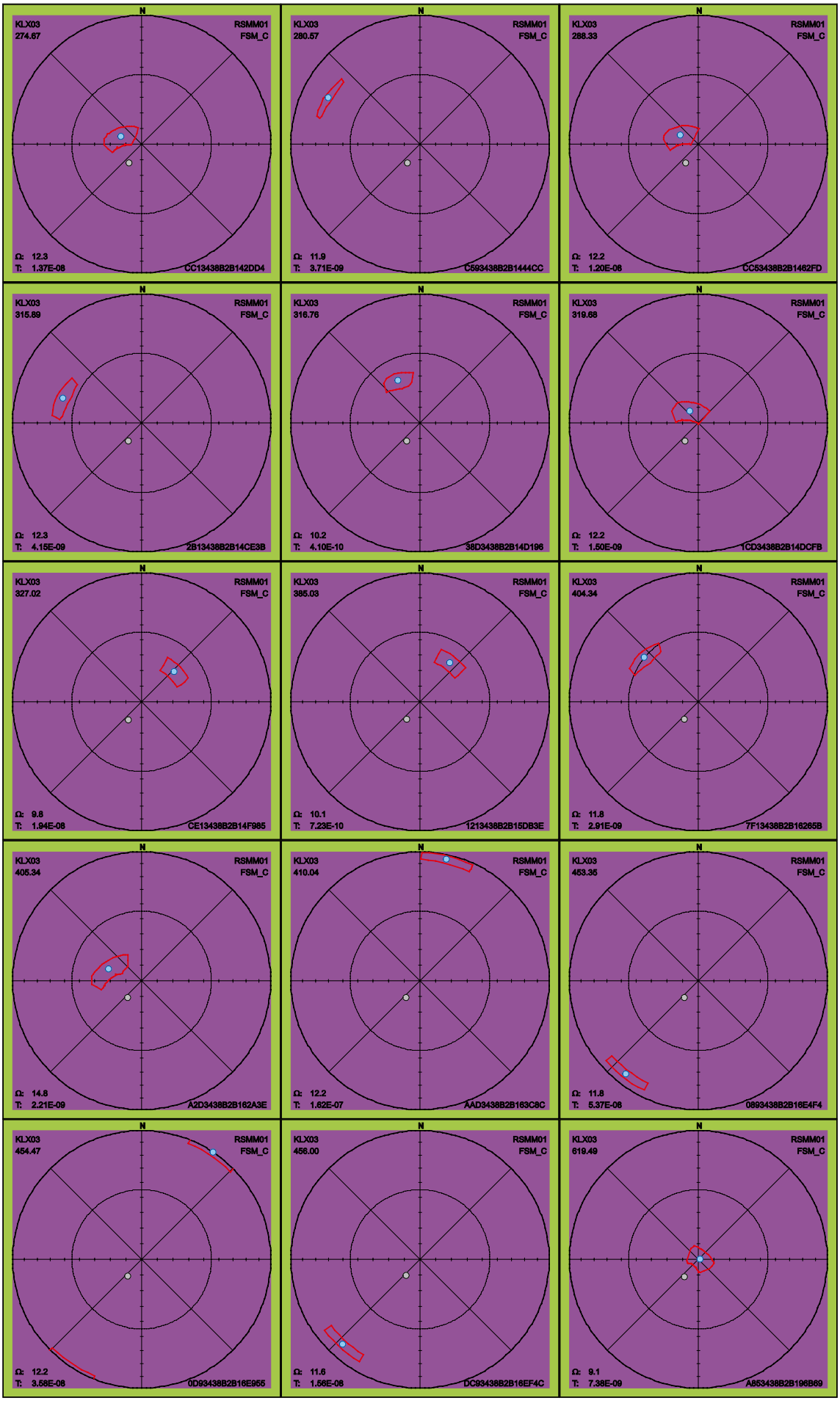
N
KLX03
274.67
RSMM01
FSM_C
Ω: 12.3
T: 1.37E-08
CC13438B2B142DD4
KLX03
280.57
RSMM01
FSM_C
Ω: 11.9
T: 3.71E-09
C693438B2B1444CC
KLX03
288.33
RSMM01
FSM_C
Ω: 12.2
T: 1.20E-08
CC53438B2B1462FD
KLX03
315.89
RSMM01
FSM_C
Ω: 12.3
T: 4.15E-09
2B13438B2B14CE3B
KLX03
316.76
RSMM01
FSM_C
Ω: 10.2
T: 4.10E-10
38D3438B2B14D196
KLX03
319.68
RSMM01
FSM_C
Ω: 12.2
T: 1.50E-09
1CD3438B2B14DCFB
KLX03
327.02
RSMM01
FSM_C
Ω: 9.8
T: 1.94E-08
CE13438B2B14F985
KLX03
385.03
RSMM01
FSM_C
Ω: 10.1
T: 7.23E-10
1213438B2B15DB3E
KLX03
404.34
RSMM01
FSM_C
Ω: 11.8
T: 2.91E-09
7F13438B2B16265B
KLX03
405.34
RSMM01
FSM_C
Ω: 14.8
T: 2.21E-09
A2D3438B2B162A3E
KLX03
410.04
RSMM01
FSM_C
Ω: 12.2
T: 1.62E-07
AAD3438B2B163C8C
KLX03
453.35
RSMM01
FSM_C
Ω: 11.8
T: 5.37E-08
0893438B2B16E4F4
KLX03
454.47
RSMM01
FSM_C
Ω: 12.2
T: 3.58E-08
0D93438B2B16E955
KLX03
456.00
RSMM01
FSM_C
Ω: 11.6
T: 1.56E-08
DC93438B2B16EF4C
KLX03
619.49
RSMM01
FSM_C
Ω: 9.1
T: 7.38E-09
A853438B2B196B69

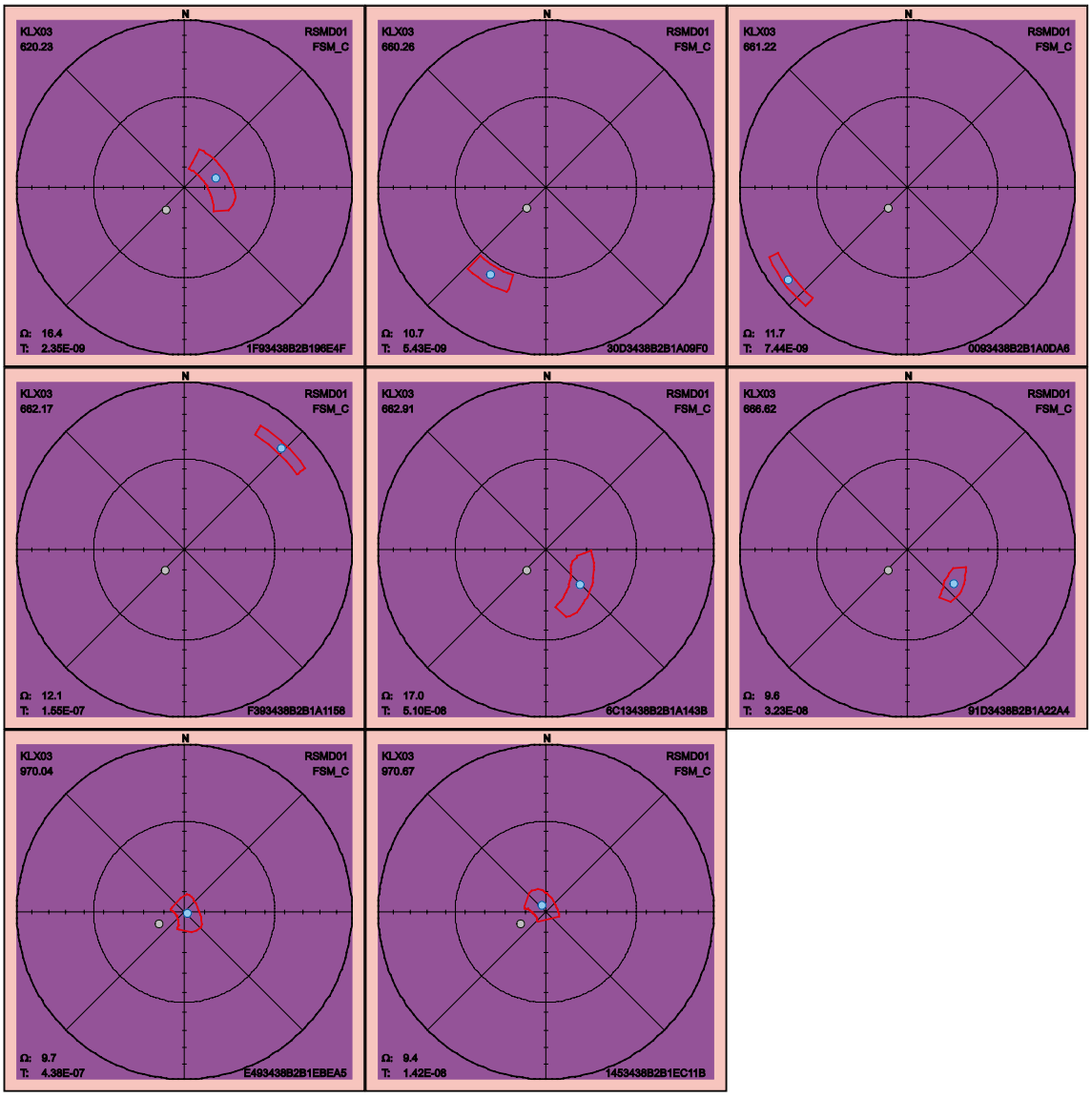

2.3.2 KLX04

There are two PFL fractures in KLX04 missing orientation information. Below follow the 90th percentile sample space of uncertainty for the remaining 86 PFL fractures. Attention should be paid to the fractures have a maximum uncertainty larger than 30°, on the 90th percentile, since these may have an alternative interpretation of orientation compared to the best estimate stored in /Sicada 2008/. There are three such PFL fractures in KLX04 listed in Table 2-4.

Table 2-4. Fractures in KLX04 with uncertainty, Ω, larger than 30°.

FeatureId	PFL-f no	Adjusted Secup	Ω
4554438B2B14C370	51	314.18	30.0
D854438B2B15A1BF	74	371.34	60.2
F114438B2B1982BE	108	626.59	51.4

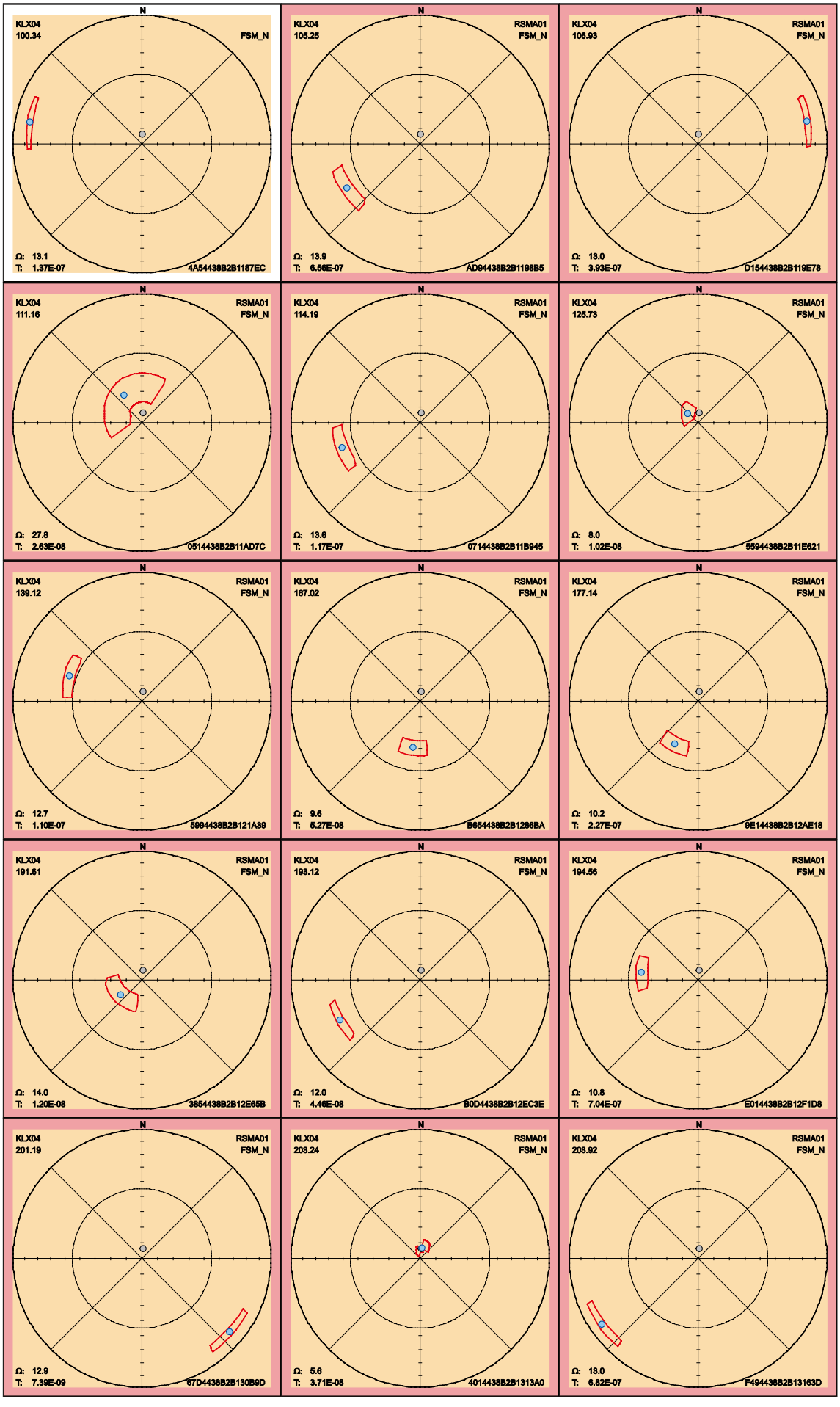
KLX04
100.34
FSM_N
Ω: 13.1
T: 1.37E-07
4A54438B2B1187EC
KLX04
105.25
RSMA01
FSM_N
Ω: 13.9
T: 6.56E-07
AD94438B2B1198B5
KLX04
106.93
RSMA01
FSM_N
Ω: 13.0
T: 3.93E-07
D154438B2B119E78
KLX04
111.16
RSMA01
FSM_N
Ω: 27.8
T: 2.63E-08
0514438B2B11AD7C
KLX04
114.19
RSMA01
FSM_N
Ω: 13.6
T: 1.17E-07
0714438B2B11B945
KLX04
125.73
RSMA01
FSM_N
Ω: 8.0
T: 1.02E-08
5594438B2B11E621
KLX04
139.12
RSMA01
FSM_N
Ω: 12.7
T: 1.10E-07
5994438B2B121A39
KLX04
167.02
RSMA01
FSM_N
Ω: 9.6
T: 5.27E-08
B654438B2B1286BA
KLX04
177.14
RSMA01
FSM_N
Ω: 10.2
T: 2.27E-07
9E14438B2B12AE18
KLX04
191.61
RSMA01
FSM_N
Ω: 14.0
T: 1.20E-08
3854438B2B12E65B
KLX04
193.12
RSMA01
FSM_N
Ω: 12.0
T: 4.46E-08
B0D4438B2B12EC3E
KLX04
194.56
RSMA01
FSM_N
Ω: 10.8
T: 7.04E-07
E014438B2B12F1D8
KLX04
201.19
RSMA01
FSM_N
Ω: 12.9
T: 7.39E-09
67D4438B2B130B9D
KLX04
203.24
RSMA01
FSM_N
Ω: 5.6
T: 3.71E-08
4014438B2B1313A0
KLX04
203.92
RSMA01
FSM_N
Ω: 13.0
T: 6.82E-07
F494438B2B13163D

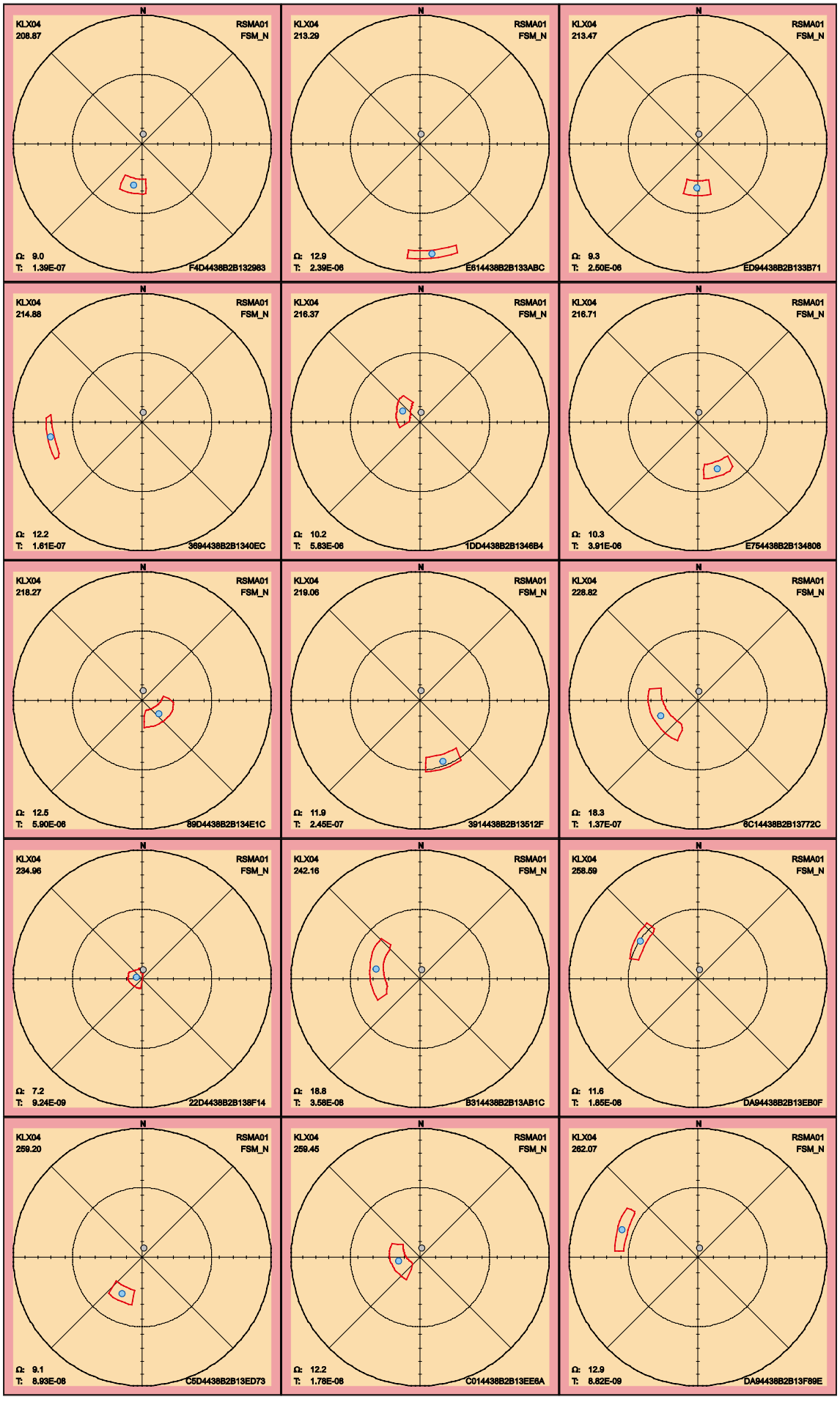
KLX04
208.87
RSMA01
FSM_N
N
Ω: 9.0
T: 1.39E-07
F4D4438B2B132983
KLX04
213.29
RSMA01
FSM_N
N
Ω: 12.9
T: 2.39E-06
E614438B2B133ABC
KLX04
213.47
RSMA01
FSM_N
N
Ω: 9.3
T: 2.50E-06
ED94438B2B133B71
KLX04
214.88
RSMA01
FSM_N
N
Ω: 12.2
T: 1.61E-07
3694438B2B1340EC
KLX04
216.37
RSMA01
FSM_N
N
Ω: 10.2
T: 5.83E-06
1DD4438B2B1346B4
KLX04
216.71
RSMA01
FSM_N
N
Ω: 10.3
T: 3.91E-06
E754438B2B134806
KLX04
218.27
RSMA01
FSM_N
N
Ω: 12.5
T: 5.90E-06
89D4438B2B134E1C
KLX04
219.06
RSMA01
FSM_N
N
Ω: 11.9
T: 2.45E-07
3914438B2B13512F
KLX04
228.82
RSMA01
FSM_N
N
Ω: 18.3
T: 1.37E-07
6C14438B2B13772C
KLX04
234.96
RSMA01
FSM_N
N
Ω: 7.2
T: 9.24E-09
22D4438B2B138F14
KLX04
242.16
RSMA01
FSM_N
N
Ω: 18.8
T: 3.58E-08
B314438B2B13AB1C
KLX04
258.59
RSMA01
FSM_N
N
Ω: 11.6
T: 1.85E-08
DA94438B2B13EB0F
KLX04
259.20
RSMA01
FSM_N
N
Ω: 9.1
T: 8.93E-08
C5D4438B2B13ED73
KLX04
259.45
RSMA01
FSM_N
N
Ω: 12.2
T: 1.78E-08
C014438B2B13EE6A
KLX04
262.07
RSMA01
FSM_N
N
Ω: 12.9
T: 8.82E-09
DA94438B2B13F89E

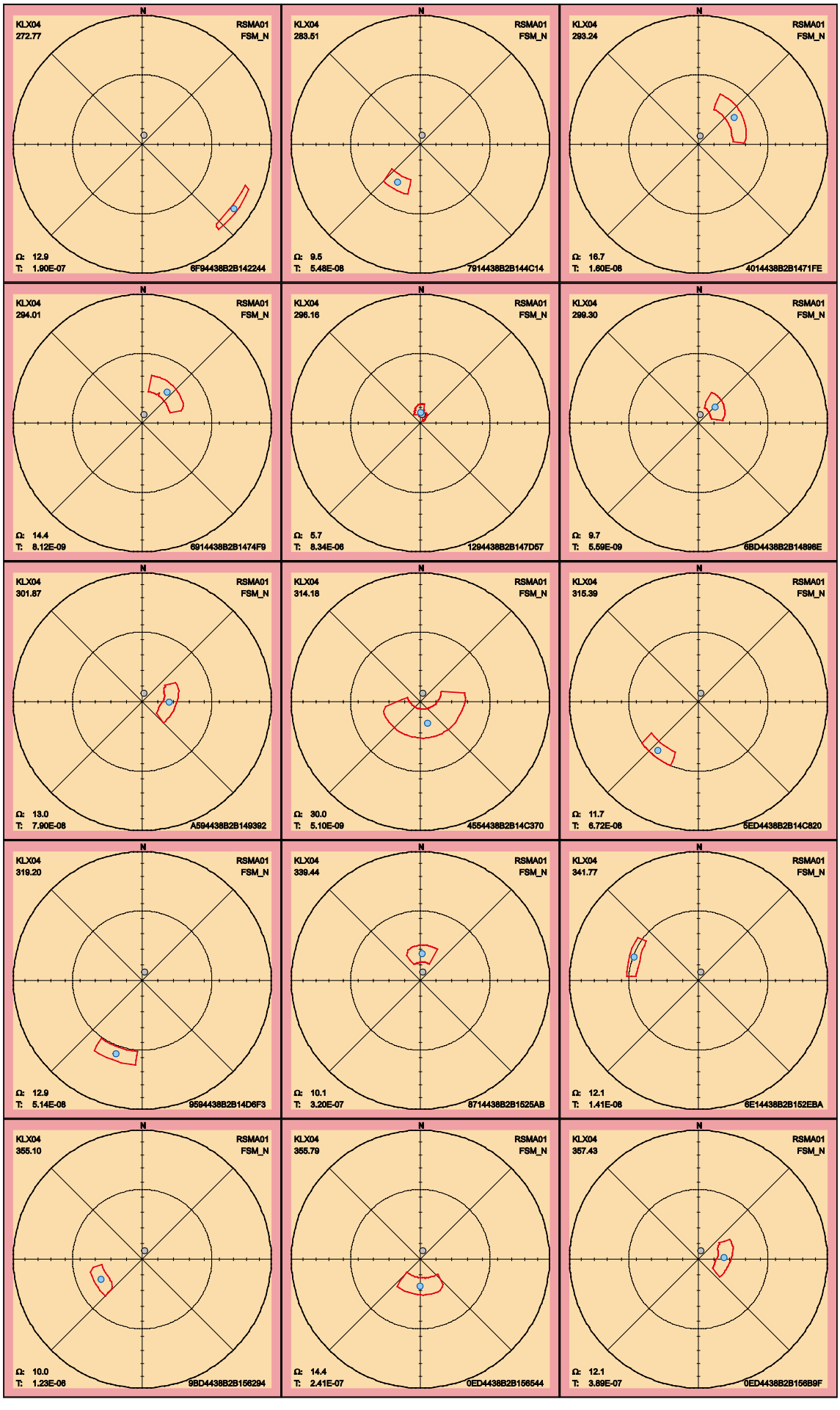
KLX04
272.77
RSMA01
FSM_N
Ω: 12.9
T: 1.90E-07
6F94438B2B142244
KLX04
283.51
RSMA01
FSM_N
Ω: 9.5
T: 5.48E-08
7914438B2B144C14
KLX04
293.24
RSMA01
FSM_N
Ω: 16.7
T: 1.60E-08
4014438B2B1471FE
KLX04
294.01
RSMA01
FSM_N
Ω: 14.4
T: 8.12E-09
6914438B2B1474F9
KLX04
296.16
RSMA01
FSM_N
Ω: 5.7
T: 8.34E-06
1294438B2B147D57
KLX04
299.30
RSMA01
FSM_N
Ω: 9.7
T: 5.59E-09
6BD4438B2B14896E
KLX04
301.87
RSMA01
FSM_N
Ω: 13.0
T: 7.90E-08
A594438B2B149392
KLX04
314.18
RSMA01
FSM_N
Ω: 30.0
T: 5.10E-09
4554438B2B14C370
KLX04
315.39
RSMA01
FSM_N
Ω: 11.7
T: 6.72E-08
5ED4438B2B14C820
KLX04
319.20
RSMA01
FSM_N
Ω: 12.9
T: 5.14E-08
9594438B2B14D6F3
KLX04
339.44
RSMA01
FSM_N
Ω: 10.1
T: 3.20E-07
8714438B2B1525AB
KLX04
341.77
RSMA01
FSM_N
Ω: 12.1
T: 1.41E-08
6E14438B2B152EBA
KLX04
355.10
RSMA01
FSM_N
Ω: 10.0
T: 1.23E-08
9BD4438B2B156294
KLX04
355.79
RSMA01
FSM_N
Ω: 14.4
T: 2.41E-07
0ED4438B2B156544
KLX04
357.43
RSMA01
FSM_N
Ω: 12.1
T: 3.89E-07
0ED4438B2B156B9F

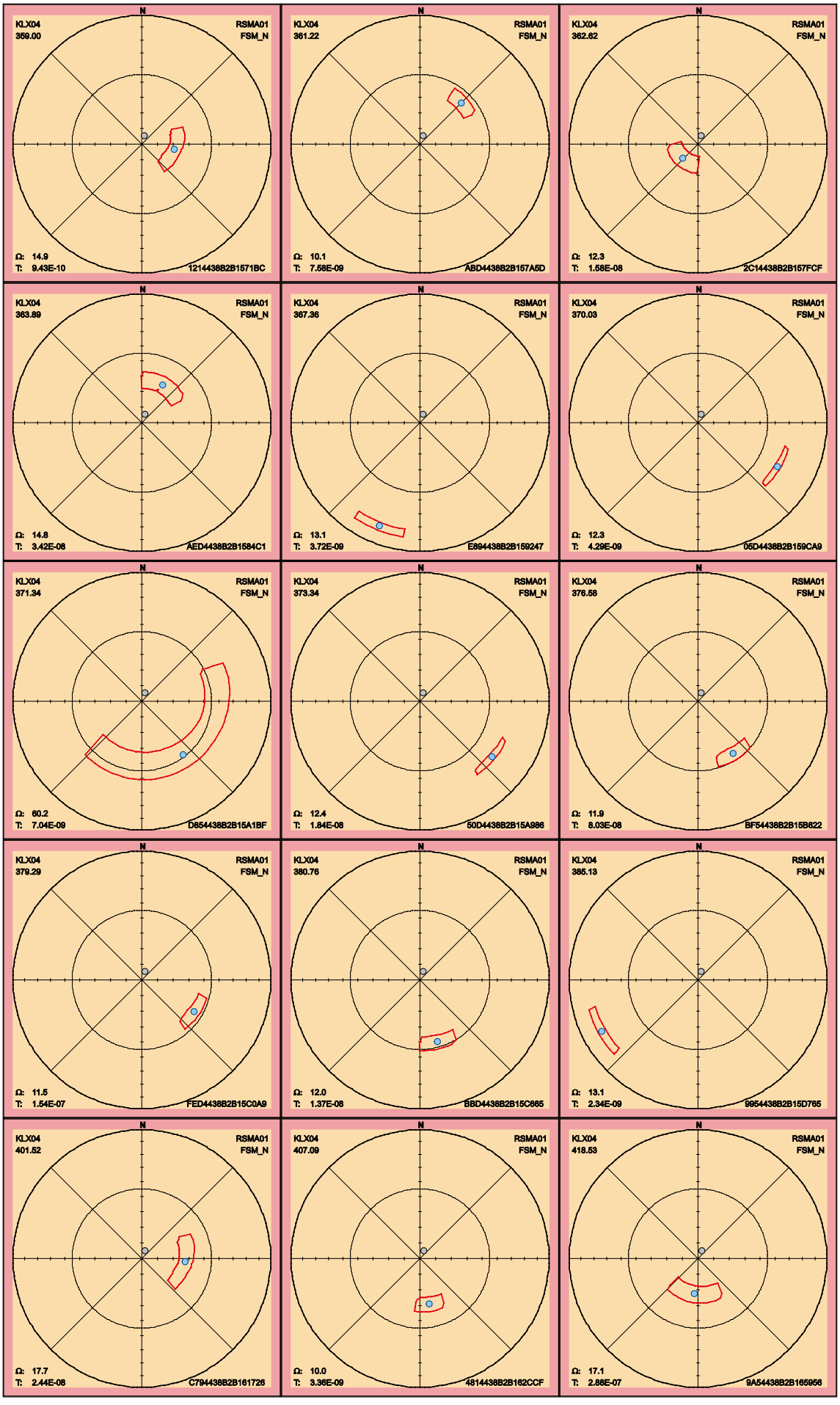
KLX04
359.00
RSMA01
FSM_N
N
Ω: 14.9
T: 9.43E-10
1214438B2B1571BC
KLX04
361.22
RSMA01
FSM_N
N
Ω: 10.1
T: 7.58E-09
ABD4438B2B157A5D
KLX04
362.62
RSMA01
FSM_N
N
Ω: 12.3
T: 1.58E-08
2C14438B2B157FCF
KLX04
363.89
RSMA01
FSM_N
N
Ω: 14.8
T: 3.42E-08
AED4438B2B1584C1
KLX04
367.36
RSMA01
FSM_N
N
Ω: 13.1
T: 3.72E-09
E894438B2B159247
KLX04
370.03
RSMA01
FSM_N
N
Ω: 12.3
T: 4.29E-09
05D4438B2B159CA9
KLX04
371.34
RSMA01
FSM_N
N
Ω: 60.2
T: 7.04E-09
D854438B2B15A1BF
KLX04
373.34
RSMA01
FSM_N
N
Ω: 12.4
T: 1.84E-08
50D4438B2B15A986
KLX04
376.58
RSMA01
FSM_N
N
Ω: 11.9
T: 8.03E-08
BF54438B2B15B622
KLX04
379.29
RSMA01
FSM_N
N
Ω: 11.5
T: 1.54E-07
FED4438B2B15C0A9
KLX04
380.76
RSMA01
FSM_N
N
Ω: 12.0
T: 1.37E-08
BBD4438B2B15C865
KLX04
385.13
RSMA01
FSM_N
N
Ω: 13.1
T: 2.34E-09
9954438B2B15D765
KLX04
401.52
RSMA01
FSM_N
N
Ω: 17.7
T: 2.44E-08
C794438B2B161726
KLX04
407.09
RSMA01
FSM_N
N
Ω: 10.0
T: 3.36E-09
4814438B2B162CCF
KLX04
418.53
RSMA01
FSM_N
N
Ω: 17.1
T: 2.88E-07
9A54438B2B165956

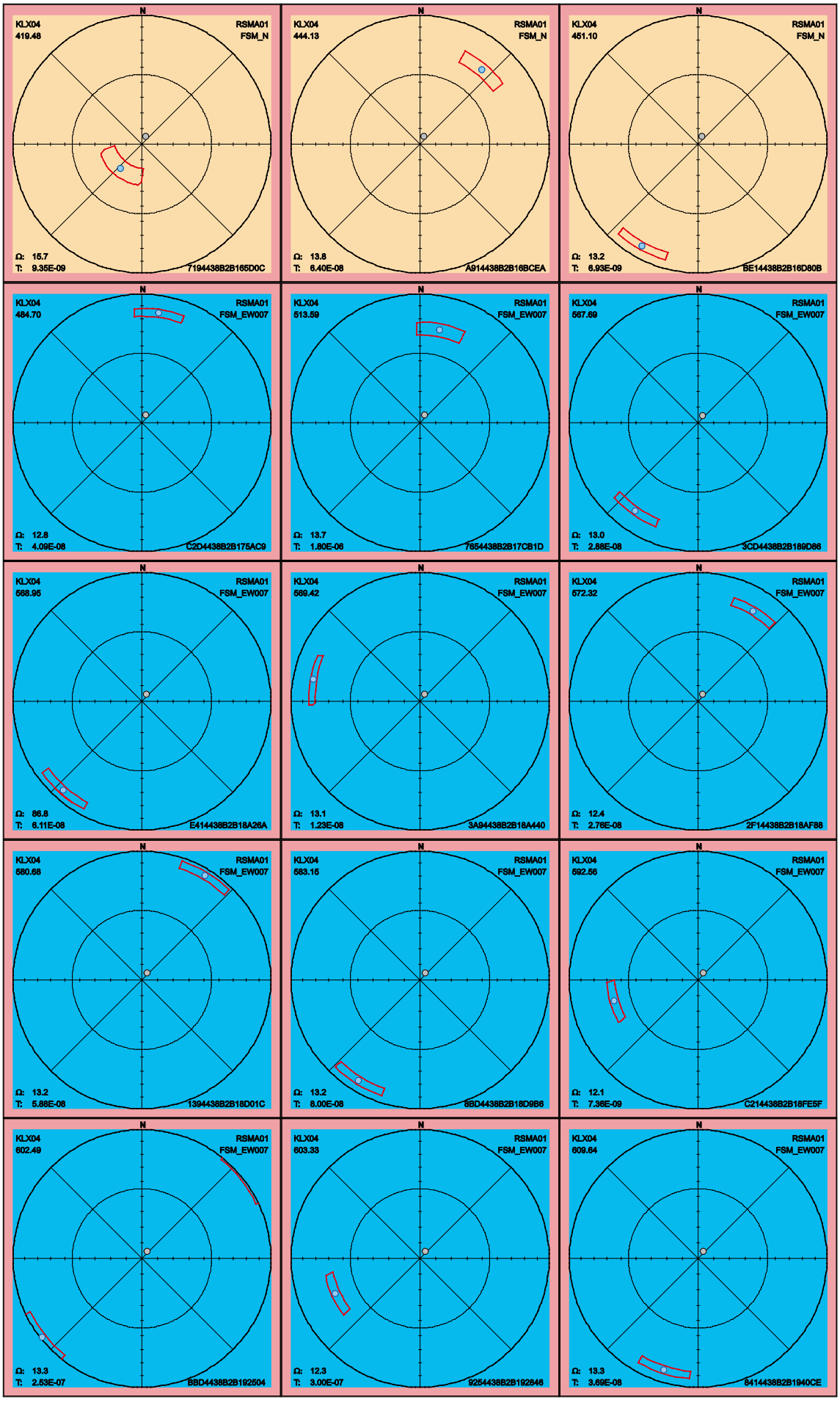
KLX04
419.48
RSMA01
FSM_N
Ω: 15.7
T: 9.35E-09
7194438B2B165D0C
KLX04
444.13
RSMA01
FSM_N
Ω: 13.8
T: 6.40E-08
A914438B2B16BCEA
KLX04
451.10
RSMA01
FSM_N
Ω: 13.2
T: 6.93E-09
BE14438B2B16D80B
KLX04
484.70
RSMA01
FSM_EW007
Ω: 12.8
T: 4.09E-08
C2D4438B2B175AC9
KLX04
513.59
RSMA01
FSM_EW007
Ω: 13.7
T: 1.80E-06
7854438B2B17CB1D
KLX04
567.69
RSMA01
FSM_EW007
Ω: 13.0
T: 2.88E-08
3CD4438B2B189D66
KLX04
568.95
RSMA01
FSM_EW007
Ω: 86.8
T: 6.11E-08
E414438B2B18A26A
KLX04
569.42
RSMA01
FSM_EW007
Ω: 13.1
T: 1.23E-08
3A94438B2B18A440
KLX04
572.32
RSMA01
FSM_EW007
Ω: 12.4
T: 2.76E-08
2F14438B2B18AF88
KLX04
580.68
RSMA01
FSM_EW007
Ω: 13.2
T: 5.88E-08
1394438B2B18D01C
KLX04
583.15
RSMA01
FSM_EW007
Ω: 13.2
T: 8.00E-08
8BD4438B2B18D9B6
KLX04
592.56
RSMA01
FSM_EW007
Ω: 12.1
T: 7.36E-09
C214438B2B18FE5F
KLX04
602.49
RSMA01
FSM_EW007
Ω: 13.3
T: 2.53E-07
BBD4438B2B192504
KLX04
603.33
RSMA01
FSM_EW007
Ω: 12.3
T: 3.00E-07
9254438B2B192846
KLX04
609.64
RSMA01
FSM_EW007
Ω: 13.3
T: 3.69E-08
8414438B2B1940CE

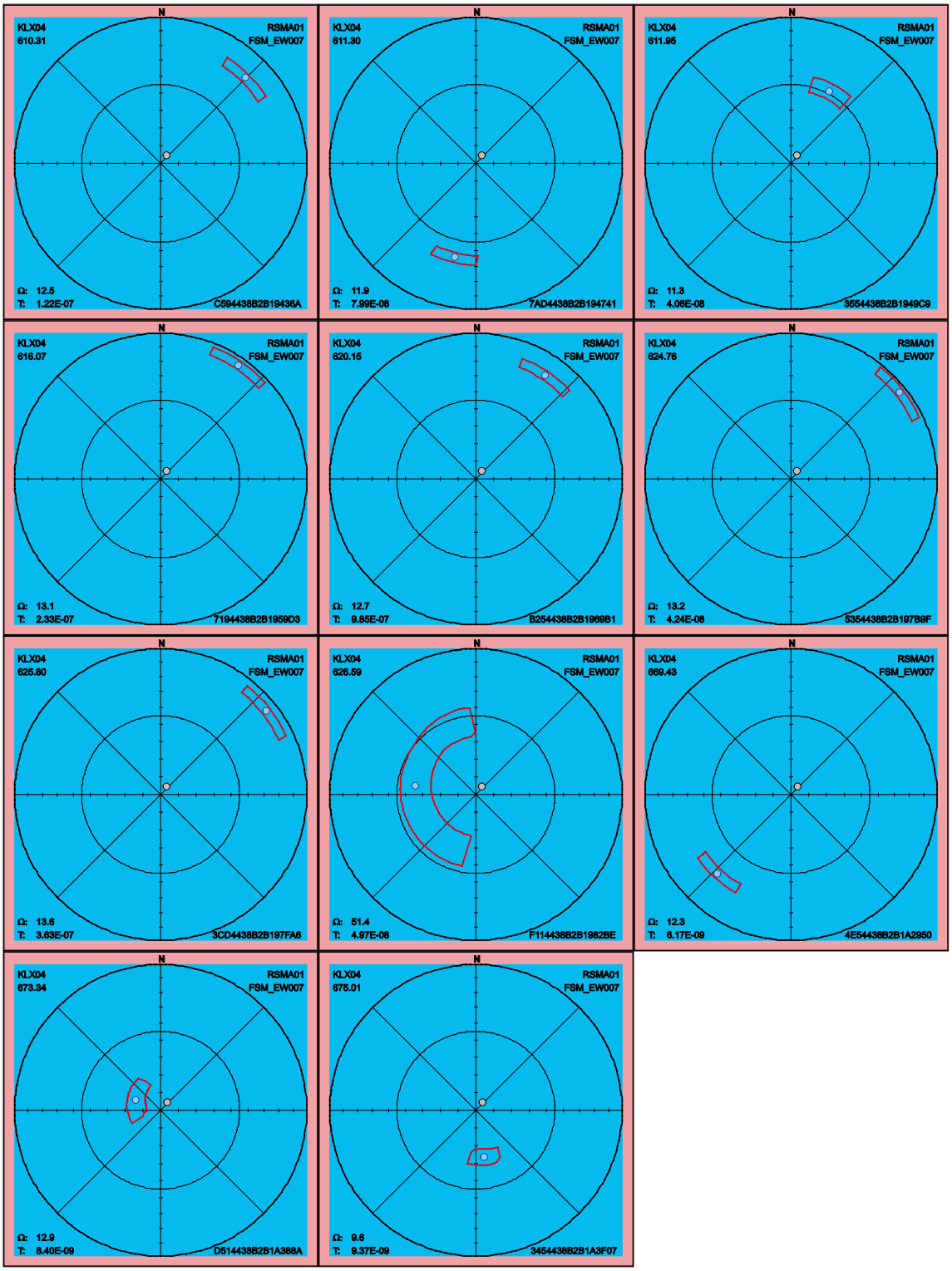
KLX04
610.31
RSMA01
FSM_EW007
N
Ω: 12.5
T: 1.22E-07
C594438B2B19436A
KLX04
611.30
RSMA01
FSM_EW007
N
Ω: 11.9
T: 7.99E-08
7AD4438B2B194741
KLX04
611.95
RSMA01
FSM_EW007
N
Ω: 11.3
T: 4.06E-08
3554438B2B1949C9
KLX04
616.07
RSMA01
FSM_EW007
N
Ω: 13.1
T: 2.33E-07
7194438B2B1959D3
KLX04
620.15
RSMA01
FSM_EW007
N
Ω: 12.7
T: 9.85E-07
B254438B2B1969B1
KLX04
624.76
RSMA01
FSM_EW007
N
Ω: 13.2
T: 4.24E-08
5354438B2B197B9F
KLX04
625.80
RSMA01
FSM_EW007
N
Ω: 13.6
T: 3.63E-07
3CD4438B2B197FA8
KLX04
626.59
RSMA01
FSM_EW007
N
Ω: 51.4
T: 4.97E-08
F114438B2B1982BE
KLX04
669.43
RSMA01
FSM_EW007
N
Ω: 12.3
T: 6.17E-09
4E54438B2B1A2950
KLX04
673.34
RSMA01
FSM_EW007
N
Ω: 12.9
T: 8.40E-09
D514438B2B1A388A
KLX04
675.01
RSMA01
FSM_EW007
N
Ω: 9.6
T: 9.37E-09
3454438B2B1A3F07

2.3.3 KLX05

In KLX05 one PFL fracture is missing orientation and thus omitted from this section. Below follow the 90th percentile sample space of uncertainty for the remaining 68 PFL fractures. Attention should be paid to the eight fractures listed in Table 2-5. These fractures have a maximum uncertainty, on the 90th percentile, larger than 30° and hence there can be an alternative interpretation of orientation compared to the best estimate orientation found in the table p_fract_core in /Sicada 2008/.

Table 2-5. Fractures in KLX05 with uncertainty, Ω, larger than 30°.

FeatureId	PFL-f no	Adjusted Secup	Ω
31D5438B2B125BFA	26	154.56	71.8
5515438B2B12E3B7	37	189.40	52.8
4C15438B2B1339F7	42	211.52	65.3
01D5438B2B13C92E	53	248.25	64.2
A955438B2B164300	62	411.16	74.4
0A55438B2B167E07	64	426.33	49.8
8F95438B2B17886A	66	494.76	67.9
4555438B2B1DA76F	71	897.64	70.6

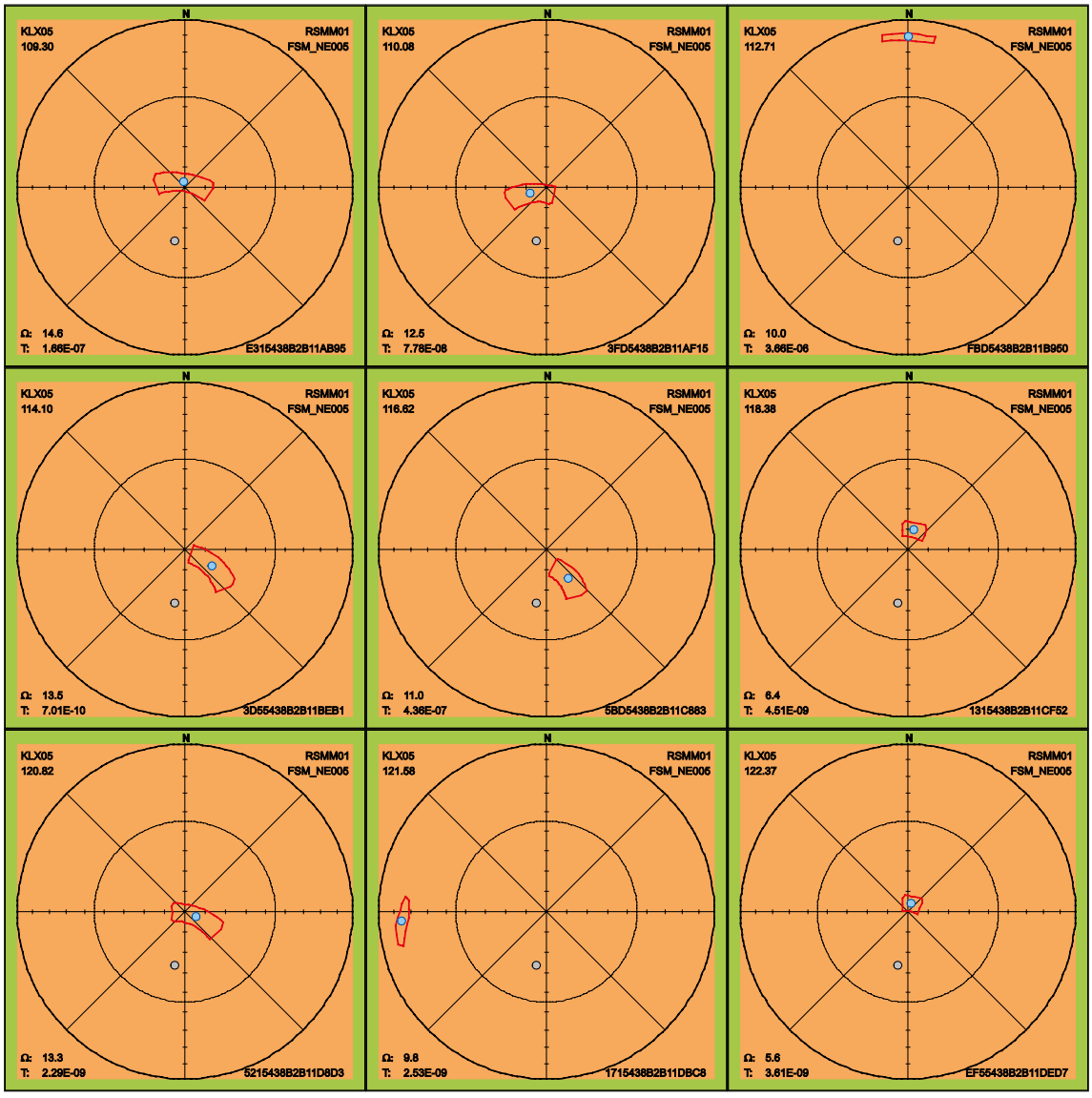

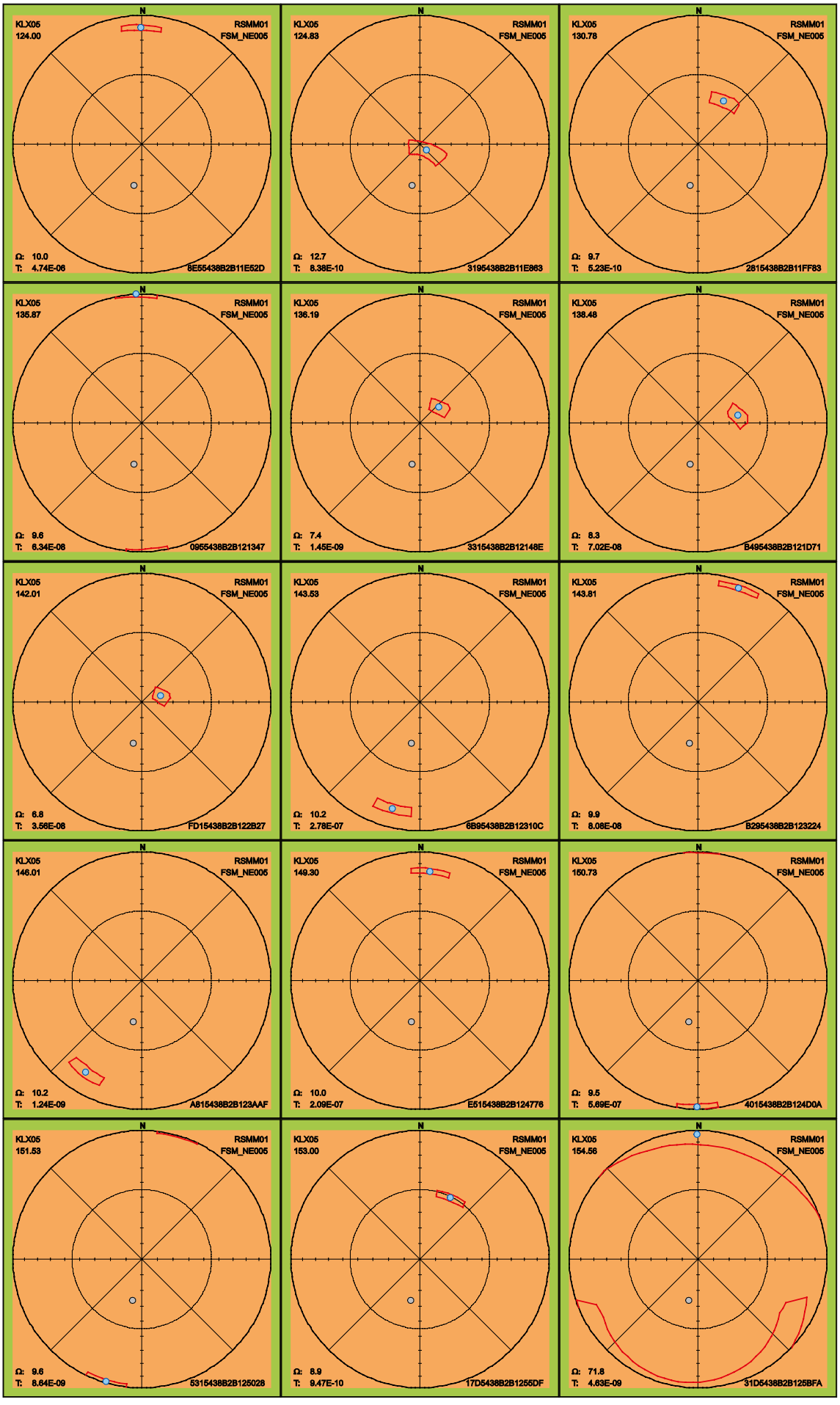
KLX05
124.00
RSMM01
FSM_NE005
N
Ω: 10.0
T: 4.74E-06
8E55438B2B11E52D
KLX05
124.83
RSMM01
FSM_NE005
N
Ω: 12.7
T: 8.38E-10
3195438B2B11E863
KLX05
130.78
RSMM01
FSM_NE005
N
Ω: 9.7
T: 5.23E-10
2815438B2B11FF83
KLX05
135.87
RSMM01
FSM_NE005
N
Ω: 9.6
T: 6.34E-06
0955438B2B121347
KLX05
136.19
RSMM01
FSM_NE005
N
Ω: 7.4
T: 1.45E-09
3315438B2B12148E
KLX05
138.48
RSMM01
FSM_NE005
N
Ω: 8.3
T: 7.02E-08
B495438B2B121D71
KLX05
142.01
RSMM01
FSM_NE005
N
Ω: 6.8
T: 3.56E-06
FD15438B2B122B27
KLX05
143.53
RSMM01
FSM_NE005
N
Ω: 10.2
T: 2.78E-07
6B95438B2B12310C
KLX05
143.81
RSMM01
FSM_NE005
N
Ω: 9.9
T: 8.08E-08
B295438B2B123224
KLX05
146.01
RSMM01
FSM_NE005
N
Ω: 10.2
T: 1.24E-09
A815438B2B123AAF
KLX05
149.30
RSMM01
FSM_NE005
N
Ω: 10.0
T: 2.09E-07
E515438B2B124776
KLX05
150.73
RSMM01
FSM_NE005
N
Ω: 9.5
T: 5.69E-07
4015438B2B124D0A
KLX05
151.53
RSMM01
FSM_NE005
N
Ω: 9.6
T: 8.64E-09
5315438B2B125028
KLX05
153.00
RSMM01
FSM_NE005
N
Ω: 8.9
T: 9.47E-10
17D5438B2B1255DF
KLX05
154.56
RSMM01
FSM_NE005
N
Ω: 71.8
T: 4.63E-09
31D5438B2B125BFA

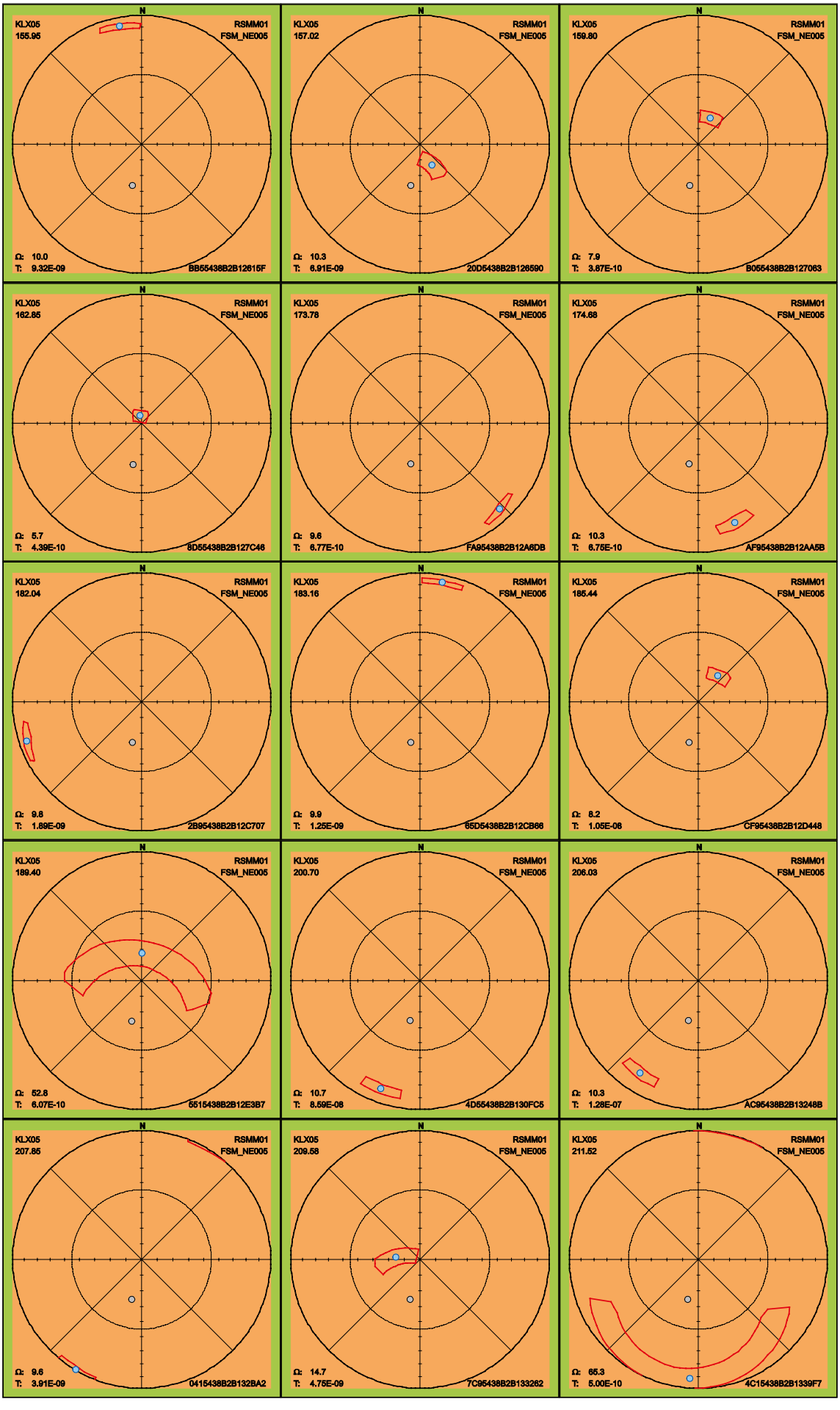
KLX05
155.95
RSMM01
FSM_NE005
Ω: 10.0
T: 9.32E-09
BB55438B2B12615F
KLX05
157.02
RSMM01
FSM_NE005
Ω: 10.3
T: 6.91E-09
20D5438B2B126590
KLX05
159.80
RSMM01
FSM_NE005
Ω: 7.9
T: 3.87E-10
B055438B2B127063
KLX05
162.85
RSMM01
FSM_NE005
Ω: 5.7
T: 4.39E-10
8D55438B2B127C46
KLX05
173.78
RSMM01
FSM_NE005
Ω: 9.6
T: 6.77E-10
FA95438B2B12A6DB
KLX05
174.68
RSMM01
FSM_NE005
Ω: 10.3
T: 6.75E-10
AF95438B2B12AA5B
KLX05
182.04
RSMM01
FSM_NE005
Ω: 9.8
T: 1.89E-09
2B95438B2B12C707
KLX05
183.16
RSMM01
FSM_NE005
Ω: 9.9
T: 1.25E-09
85D5438B2B12CB66
KLX05
185.44
RSMM01
FSM_NE005
Ω: 8.2
T: 1.05E-08
CF95438B2B12D448
KLX05
189.40
RSMM01
FSM_NE005
Ω: 52.8
T: 6.07E-10
5515438B2B12E3B7
KLX05
200.70
RSMM01
FSM_NE005
Ω: 10.7
T: 8.59E-08
4D55438B2B130FC5
KLX05
206.03
RSMM01
FSM_NE005
Ω: 10.3
T: 1.28E-07
AC95438B2B13248B
KLX05
207.85
RSMM01
FSM_NE005
Ω: 9.6
T: 3.91E-09
0415438B2B132BA2
KLX05
209.58
RSMM01
FSM_NE005
Ω: 14.7
T: 4.75E-09
7C95438B2B133262
KLX05
211.52
RSMM01
FSM_NE005
Ω: 65.3
T: 5.00E-10
4C15438B2B1339F7

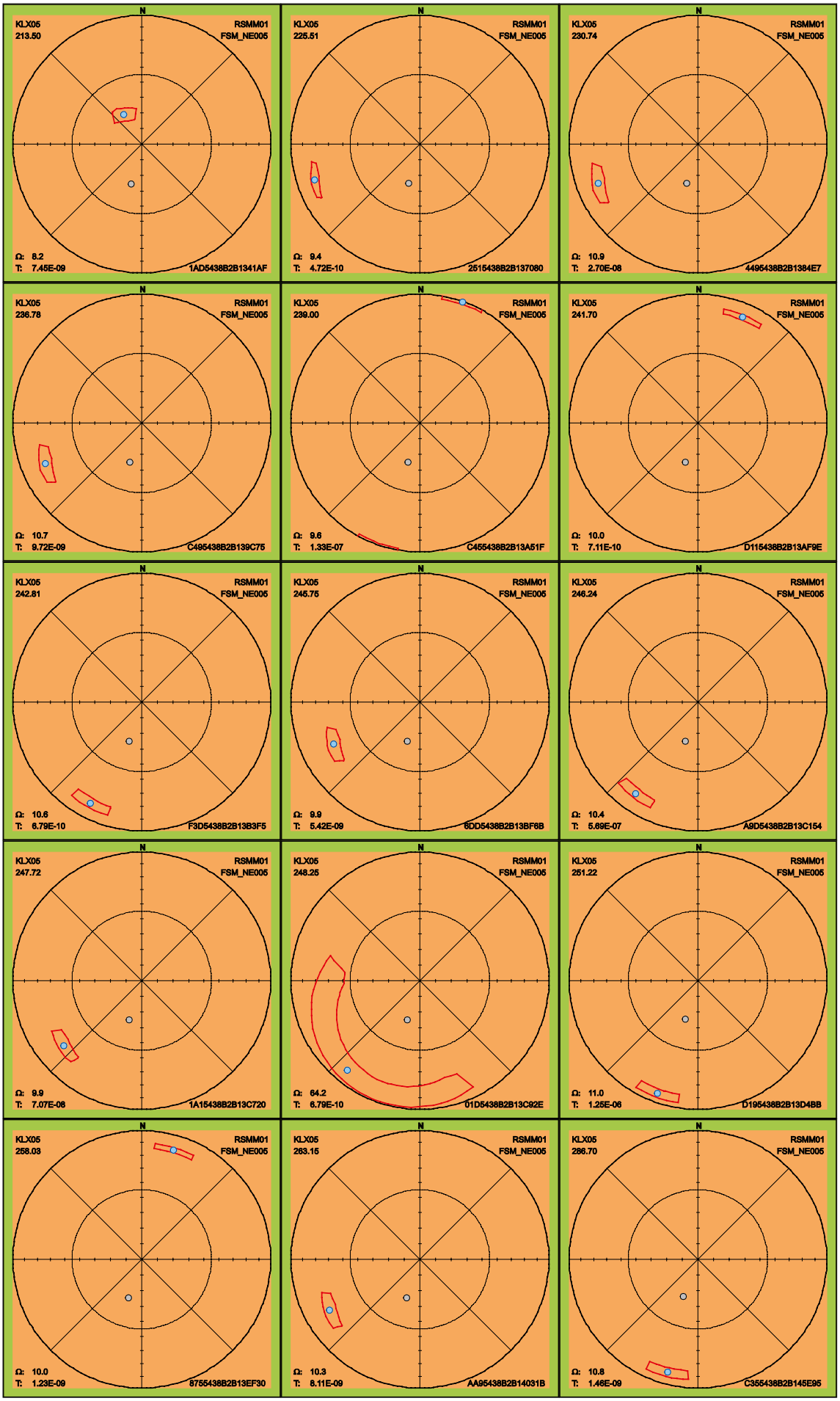
KLX05
213.50
RSMM01
FSM_NE005
N
Ω: 8.2
T: 7.45E-09
1AD5438B2B1341AF
KLX05
225.51
RSMM01
FSM_NE005
N
Ω: 9.4
T: 4.72E-10
2515438B2B137080
KLX05
230.74
RSMM01
FSM_NE005
N
Ω: 10.9
T: 2.70E-08
4495438B2B1384E7
KLX05
236.78
RSMM01
FSM_NE005
N
Ω: 10.7
T: 9.72E-09
C495438B2B139C75
KLX05
239.00
RSMM01
FSM_NE005
N
Ω: 9.6
T: 1.33E-07
C455438B2B13A51F
KLX05
241.70
RSMM01
FSM_NE005
N
Ω: 10.0
T: 7.11E-10
D115438B2B13AF9E
KLX05
242.81
RSMM01
FSM_NE005
N
Ω: 10.6
T: 6.79E-10
F3D5438B2B13B3F5
KLX05
245.75
RSMM01
FSM_NE005
N
Ω: 9.9
T: 5.42E-09
6DD5438B2B13BF6B
KLX05
246.24
RSMM01
FSM_NE005
N
Ω: 10.4
T: 5.69E-07
A9D5438B2B13C154
KLX05
247.72
RSMM01
FSM_NE005
N
Ω: 9.9
T: 7.07E-08
1A15438B2B13C720
KLX05
248.25
RSMM01
FSM_NE005
N
Ω: 64.2
T: 6.79E-10
01D5438B2B13C92E
KLX05
251.22
RSMM01
FSM_NE005
N
Ω: 11.0
T: 1.25E-06
D195438B2B13D4BB
KLX05
258.03
RSMM01
FSM_NE005
N
Ω: 10.0
T: 1.23E-09
8755438B2B13EF30
KLX05
263.15
RSMM01
FSM_NE005
N
Ω: 10.3
T: 8.11E-09
AA95438B2B14031B
KLX05
286.70
RSMM01
FSM_NE005
N
Ω: 10.8
T: 1.46E-09
C355438B2B145E95

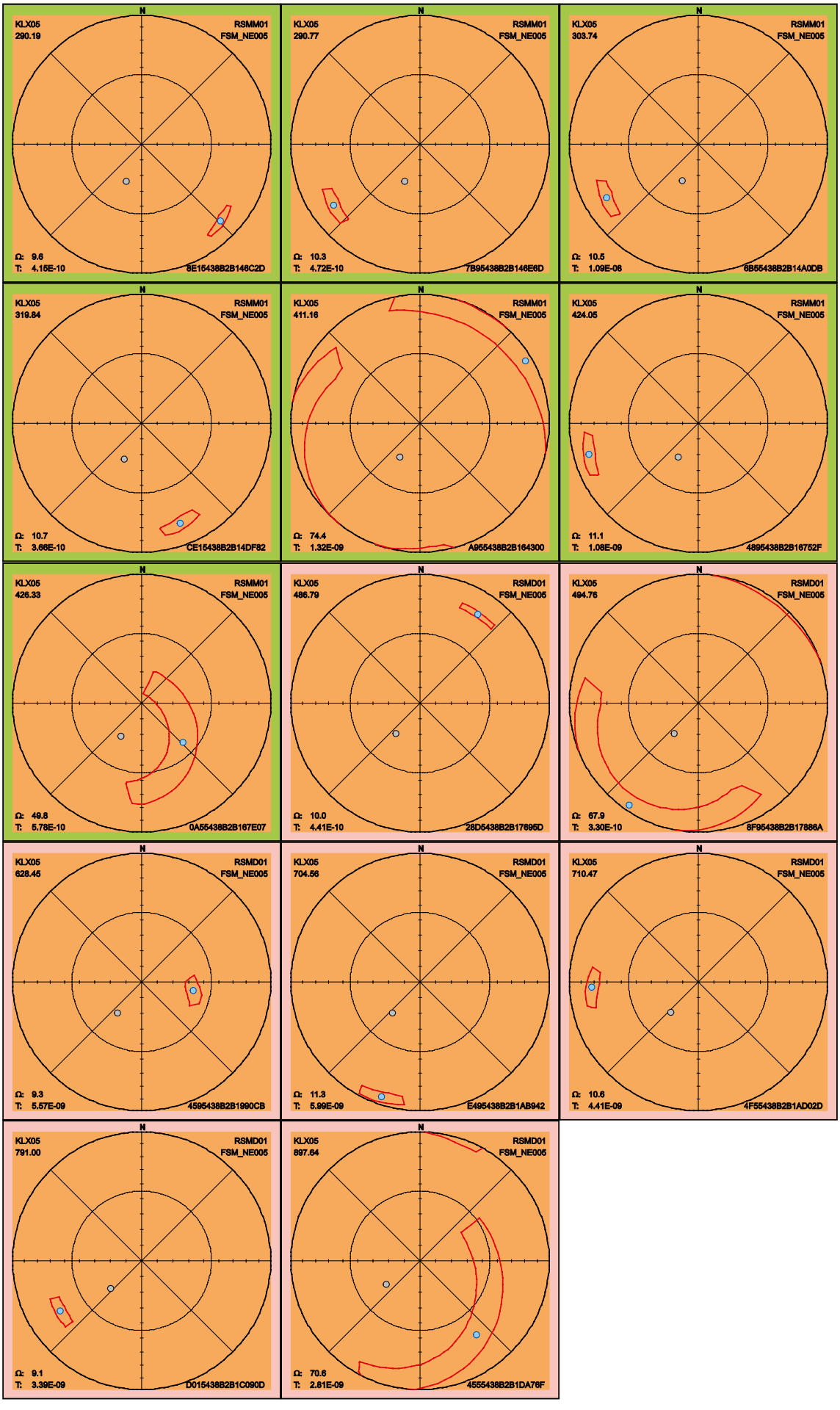
KLX05
290.19
RSMM01
FSM_NE005
Ω: 9.6
T: 4.15E-10
8E15438B2B146C2D
KLX05
290.77
RSMM01
FSM_NE005
Ω: 10.3
T: 4.72E-10
7B95438B2B146E6D
KLX05
303.74
RSMM01
FSM_NE005
Ω: 10.5
T: 1.09E-08
6B55438B2B14A0DB
KLX05
319.84
RSMM01
FSM_NE005
Ω: 10.7
T: 3.66E-10
CE15438B2B14DF82
KLX05
411.16
RSMM01
FSM_NE005
Ω: 74.4
T: 1.32E-09
A955438B2B164300
KLX05
424.05
RSMM01
FSM_NE005
Ω: 11.1
T: 1.08E-09
4895438B2B16752F
KLX05
426.33
RSMM01
FSM_NE005
Ω: 49.8
T: 5.78E-10
0A55438B2B167E07
KLX05
486.79
RSMD01
FSM_NE005
Ω: 10.0
T: 4.41E-10
28D5438B2B17695D
KLX05
494.76
RSMD01
FSM_NE005
Ω: 67.9
T: 3.30E-10
8F95438B2B17886A
KLX05
628.45
RSMD01
FSM_NE005
Ω: 9.3
T: 5.57E-09
4595438B2B1990CB
KLX05
704.56
RSMD01
FSM_NE005
Ω: 11.3
T: 5.99E-09
E495438B2B1AB942
KLX05
710.47
RSMD01
FSM_NE005
Ω: 10.6
T: 4.41E-09
4F55438B2B1AD02D
KLX05
791.00
RSMD01
FSM_NE005
Ω: 9.1
T: 3.39E-09
D015438B2B1C090D
KLX05
897.64
RSMD01
FSM_NE005
Ω: 70.6
T: 2.61E-09
4555438B2B1DA78F

2.3.4 KLX06

Yet another PFL fracture is missing orientation in KLX06. The 90th percentile sample space of uncertainty for the remaining 76 PFL fractures in KLX06 follow below. Attention should be paid to the seven fractures listed in Table 2-6. These fractures have a maximum uncertainty on the 90th percentile larger than 30°. The fractures having large uncertainty can have an alternative interpretation of orientation compared to the best estimate orientation that is found in the table p_fract_core in /Sicada 2008/.

Table 2-6. Fractures in KLX06 with uncertainty, Ω, larger than 30°.

FeatureId	PFL-f no	Adjusted Secup	Ω
0496438B2B118D03	1	101.70	51.3
E216438B2B127ADF	19	163.12	39.6
F596438B2B127B43	20	163.22	45.1
FE96438B2B129E5A	28	172.25	48.4
3796438B2B14053F	72	264.55	62.4
3C56438B2B17B5EA	162	507.40	75.6
8CD6438B2B1E42B8	186	938.81	53.6

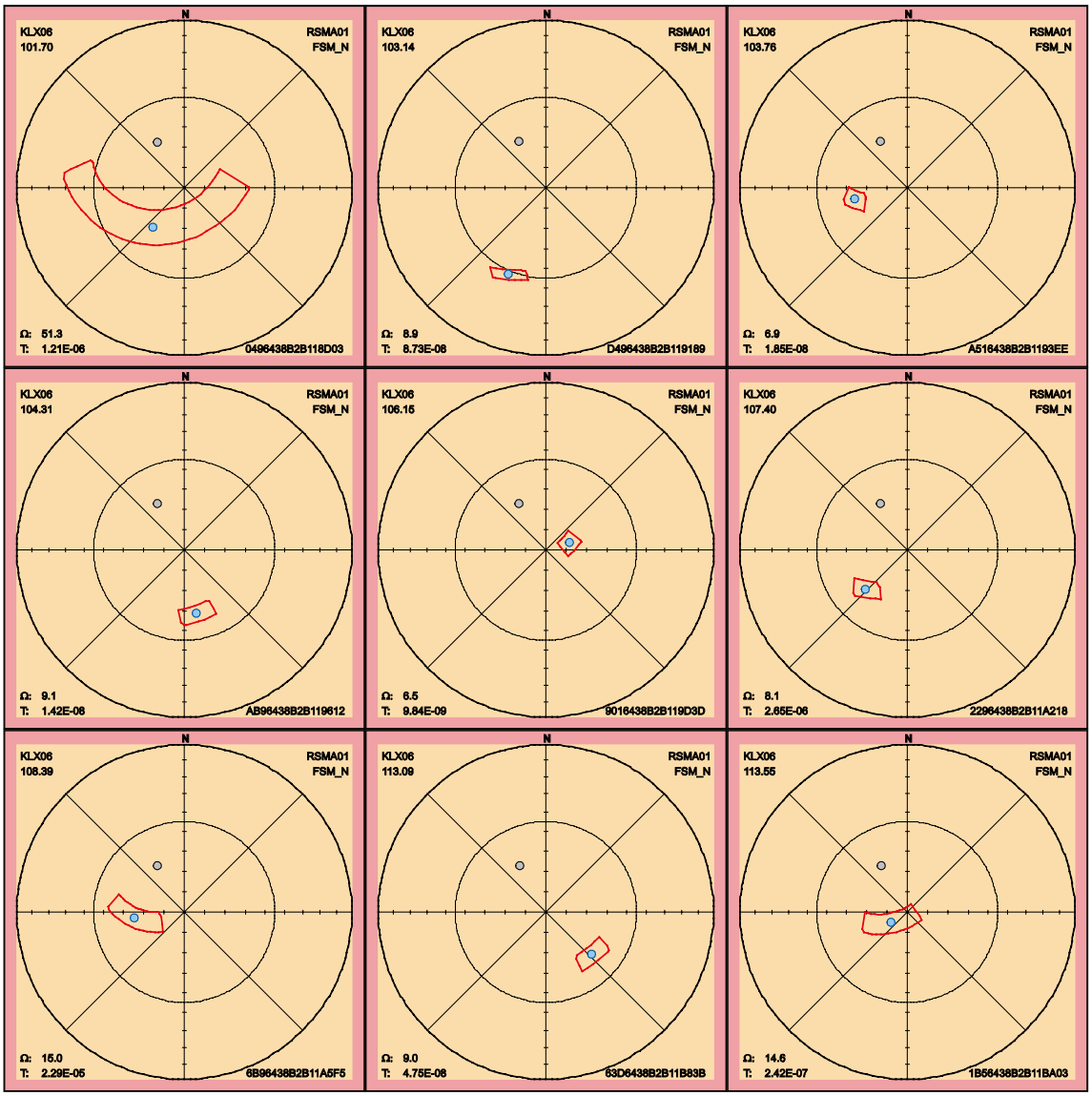

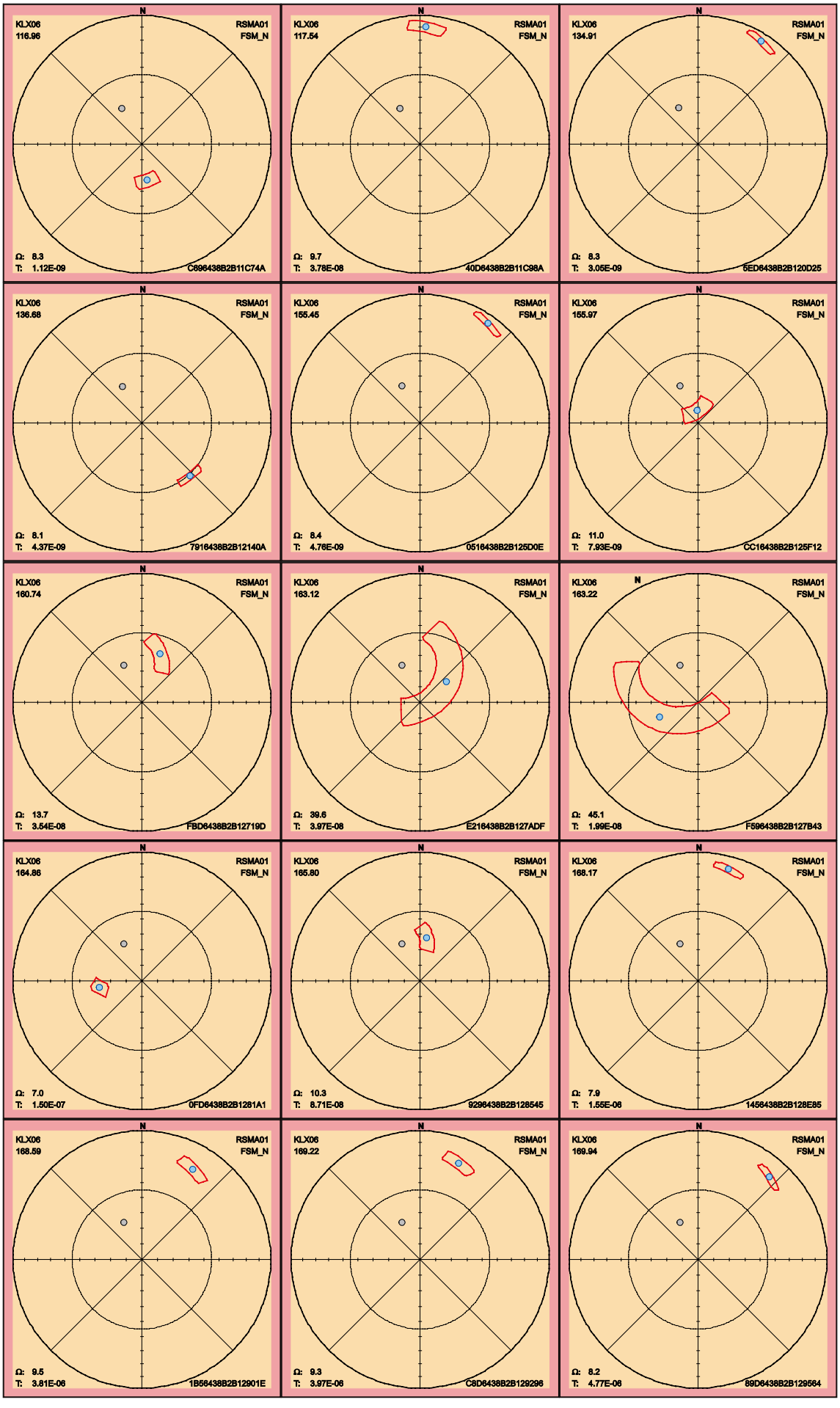
KLX06
116.96
RSMA01
FSM_N
Ω: 8.3
T: 1.12E-09
C896438B2B11C74A
KLX06
117.54
RSMA01
FSM_N
Ω: 9.7
T: 3.78E-08
40D6438B2B11C98A
KLX06
134.91
RSMA01
FSM_N
Ω: 8.3
T: 3.05E-09
5ED6438B2B120D25
KLX06
136.68
RSMA01
FSM_N
Ω: 8.1
T: 4.37E-09
7916438B2B12140A
KLX06
155.45
RSMA01
FSM_N
Ω: 8.4
T: 4.76E-09
0516438B2B125D0E
KLX06
155.97
RSMA01
FSM_N
Ω: 11.0
T: 7.93E-09
CC16438B2B125F12
KLX06
160.74
RSMA01
FSM_N
Ω: 13.7
T: 3.54E-08
FBD6438B2B12719D
KLX06
163.12
RSMA01
FSM_N
Ω: 39.6
T: 3.97E-08
E216438B2B127ADF
KLX06
163.22
RSMA01
FSM_N
Ω: 45.1
T: 1.99E-08
F596438B2B127B43
KLX06
164.86
RSMA01
FSM_N
Ω: 7.0
T: 1.50E-07
0FD6438B2B1281A1
KLX06
165.80
RSMA01
FSM_N
Ω: 10.3
T: 8.71E-08
9296438B2B128545
KLX06
168.17
RSMA01
FSM_N
Ω: 7.9
T: 1.55E-06
1456438B2B128E85
KLX06
168.59
RSMA01
FSM_N
Ω: 9.5
T: 3.81E-06
1B56438B2B12901E
KLX06
169.22
RSMA01
FSM_N
Ω: 9.3
T: 3.97E-06
C8D6438B2B129296
KLX06
169.94
RSMA01
FSM_N
Ω: 8.2
T: 4.77E-06
89D6438B2B129564

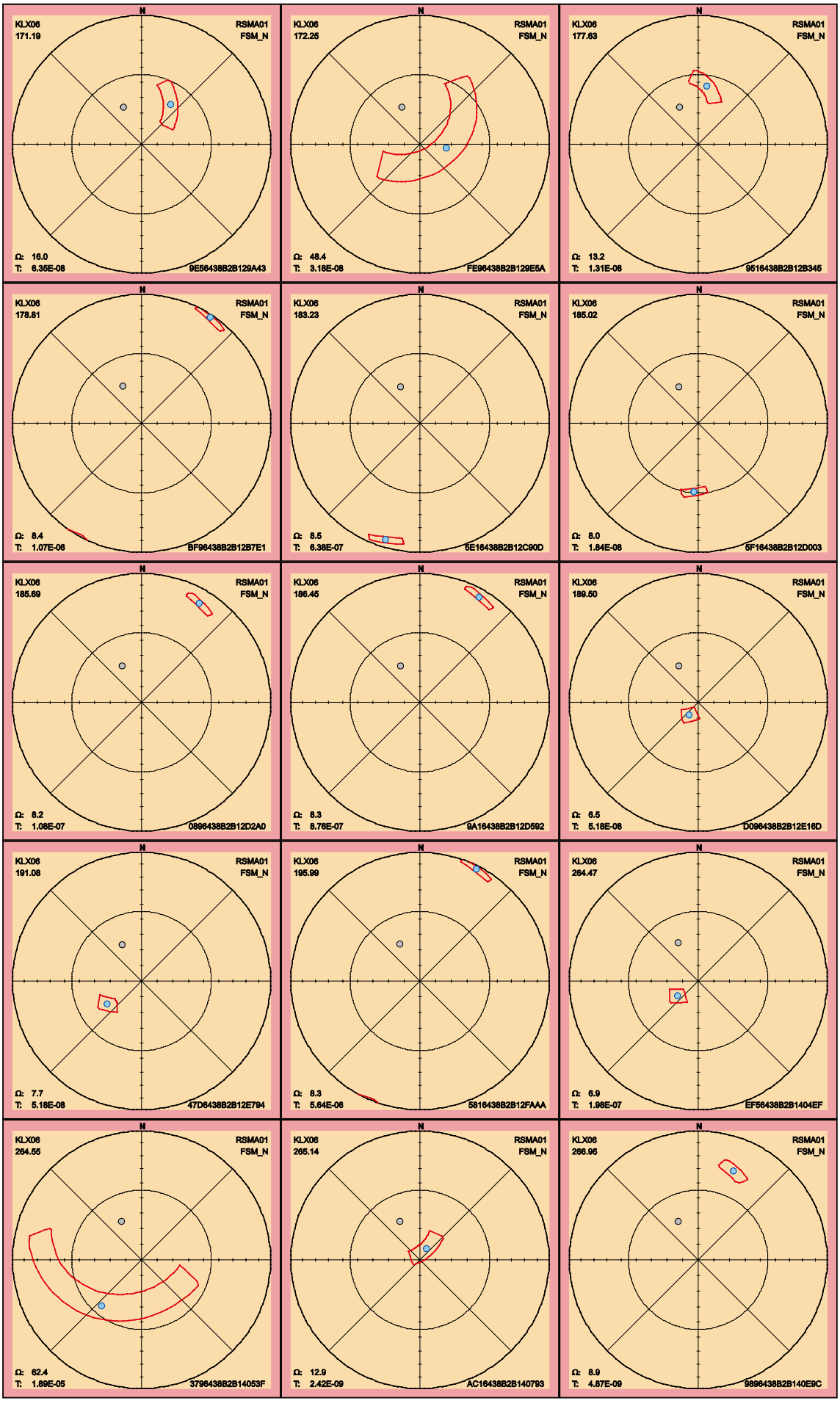
KLX06
171.19
RSMA01
FSM_N
Ω: 16.0
T: 6.35E-08
9E56438B2B129A43
KLX06
172.25
RSMA01
FSM_N
Ω: 48.4
T: 3.18E-08
FE96438B2B129E5A
KLX06
177.63
RSMA01
FSM_N
Ω: 13.2
T: 1.31E-08
9516438B2B12B345
KLX06
178.81
RSMA01
FSM_N
Ω: 8.4
T: 1.07E-08
BF96438B2B12B7E1
KLX06
183.23
RSMA01
FSM_N
Ω: 8.5
T: 6.38E-07
5E16438B2B12C90D
KLX06
185.02
RSMA01
FSM_N
Ω: 8.0
T: 1.84E-08
5F16438B2B12D003
KLX06
185.69
RSMA01
FSM_N
Ω: 8.2
T: 1.08E-07
0896438B2B12D2A0
KLX06
186.45
RSMA01
FSM_N
Ω: 8.3
T: 8.76E-07
9A16438B2B12D592
KLX06
189.50
RSMA01
FSM_N
Ω: 6.5
T: 5.18E-08
D096438B2B12E16D
KLX06
191.08
RSMA01
FSM_N
Ω: 7.7
T: 5.18E-08
47D6438B2B12E794
KLX06
195.99
RSMA01
FSM_N
Ω: 8.3
T: 5.64E-06
5816438B2B12FAAA
KLX06
264.47
RSMA01
FSM_N
Ω: 6.9
T: 1.98E-07
EF56438B2B1404EF
KLX06
264.55
RSMA01
FSM_N
Ω: 62.4
T: 1.89E-05
3796438B2B14053F
KLX06
265.14
RSMA01
FSM_N
Ω: 12.9
T: 2.42E-09
AC16438B2B140793
KLX06
266.95
RSMA01
FSM_N
Ω: 8.9
T: 4.67E-09
9896438B2B140E9C

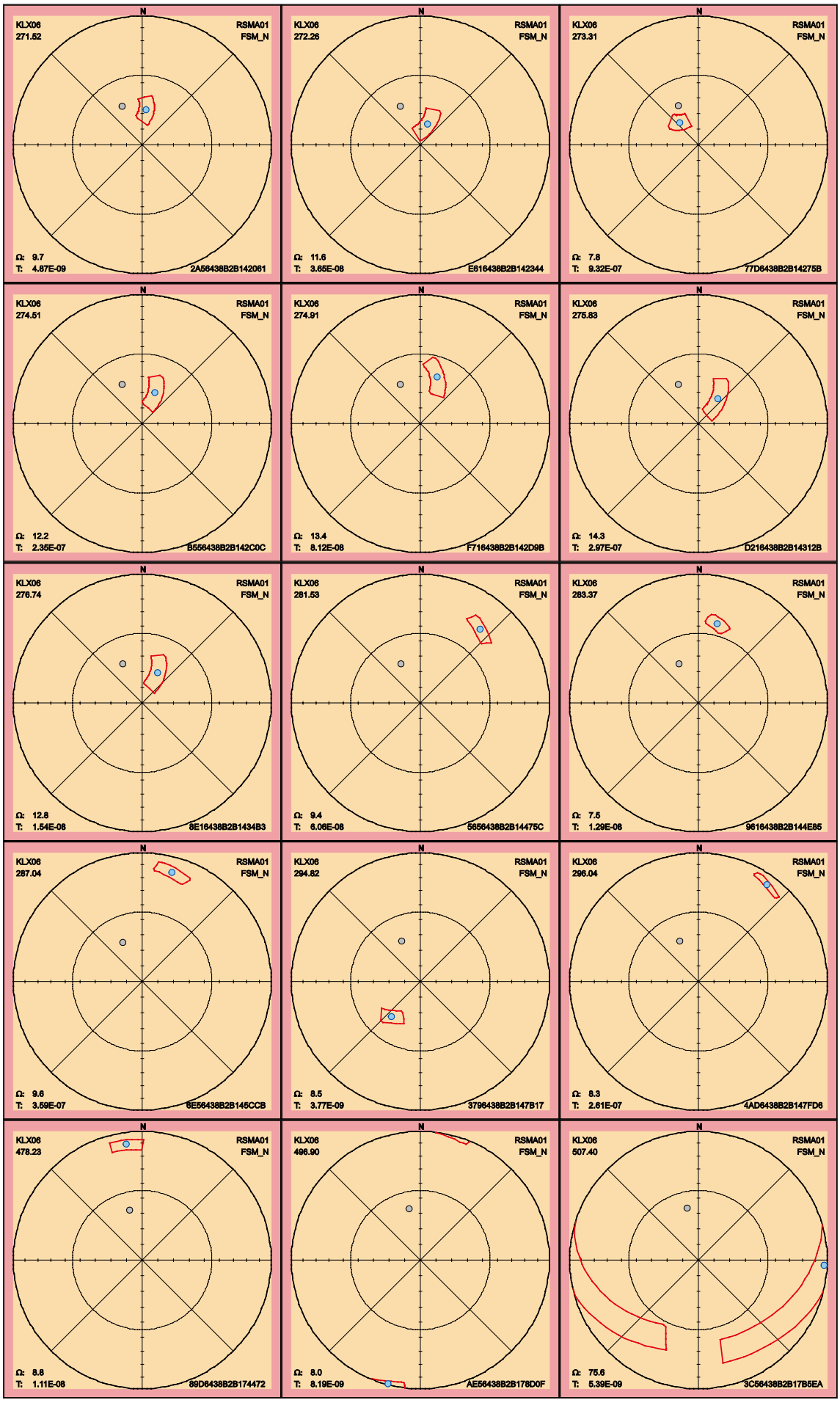
KLX06
271.52
RSMA01
FSM_N
Ω: 9.7
T: 4.87E-09
2A56438B2B142061
KLX06
272.26
RSMA01
FSM_N
Ω: 11.6
T: 3.65E-08
E616438B2B142344
KLX06
273.31
RSMA01
FSM_N
Ω: 7.8
T: 9.32E-07
77D6438B2B14275B
KLX06
274.51
RSMA01
FSM_N
Ω: 12.2
T: 2.35E-07
B556438B2B142C0C
KLX06
274.91
RSMA01
FSM_N
Ω: 13.4
T: 8.12E-08
F716438B2B142D9B
KLX06
275.83
RSMA01
FSM_N
Ω: 14.3
T: 2.97E-07
D216438B2B14312B
KLX06
276.74
RSMA01
FSM_N
Ω: 12.8
T: 1.54E-08
8E16438B2B1434B3
KLX06
281.53
RSMA01
FSM_N
Ω: 9.4
T: 6.06E-08
5856438B2B14475C
KLX06
283.37
RSMA01
FSM_N
Ω: 7.5
T: 1.29E-06
9616438B2B144E85
KLX06
287.04
RSMA01
FSM_N
Ω: 9.6
T: 3.59E-07
6E56438B2B145CCB
KLX06
294.82
RSMA01
FSM_N
Ω: 8.5
T: 3.77E-09
3796438B2B147B17
KLX06
296.04
RSMA01
FSM_N
Ω: 8.3
T: 2.61E-07
4AD6438B2B147FD6
KLX06
478.23
RSMA01
FSM_N
Ω: 8.8
T: 1.11E-08
89D6438B2B174472
KLX06
496.90
RSMA01
FSM_N
Ω: 8.0
T: 8.19E-09
AE56438B2B178D0F
KLX06
507.40
RSMA01
FSM_N
Ω: 75.6
T: 5.39E-09
3C56438B2B17B5EA

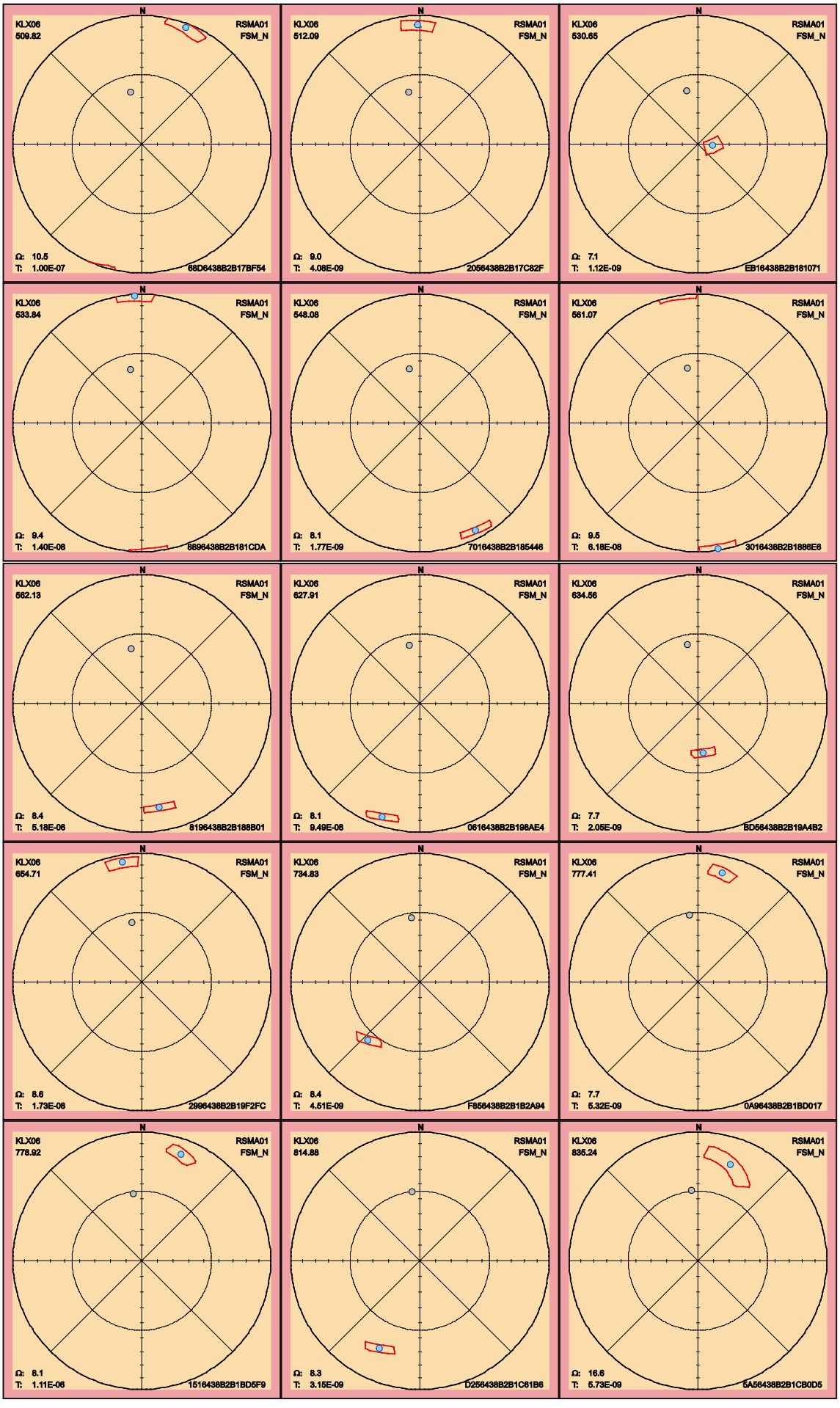
KLX06
509.82
RSMA01
FSM_N
N
Ω: 10.5
T: 1.00E-07
68D6438B2B17BF54
KLX06
512.09
RSMA01
FSM_N
N
Ω: 9.0
T: 4.08E-09
2056438B2B17C82F
KLX06
530.65
RSMA01
FSM_N
N
Ω: 7.1
T: 1.12E-09
EB16438B2B181071
KLX06
533.84
RSMA01
FSM_N
N
Ω: 9.4
T: 1.40E-06
8896438B2B181CDA
KLX06
548.08
RSMA01
FSM_N
N
Ω: 8.1
T: 1.77E-09
7016438B2B185446
KLX06
561.07
RSMA01
FSM_N
N
Ω: 9.5
T: 6.18E-08
3016438B2B1886E6
KLX06
562.13
RSMA01
FSM_N
N
Ω: 8.4
T: 5.18E-06
8196438B2B188B01
KLX06
627.91
RSMA01
FSM_N
N
Ω: 8.1
T: 9.49E-08
0616438B2B198AE4
KLX06
634.56
RSMA01
FSM_N
N
Ω: 7.7
T: 2.05E-09
BD56438B2B19A4B2
KLX06
654.71
RSMA01
FSM_N
N
Ω: 8.6
T: 1.73E-08
2996438B2B19F2FC
KLX06
734.83
RSMA01
FSM_N
N
Ω: 8.4
T: 4.51E-09
F856438B2B1B2A94
KLX06
777.41
RSMA01
FSM_N
N
Ω: 7.7
T: 5.32E-09
0A96438B2B1BD017
KLX06
778.92
RSMA01
FSM_N
N
Ω: 8.1
T: 1.11E-06
1516438B2B1BD5F9
KLX06
814.88
RSMA01
FSM_N
N
Ω: 8.3
T: 3.15E-09
D256438B2B1C61B6
KLX06
835.24
RSMA01
FSM_N
N
Ω: 16.6
T: 5.73E-09
6A56438B2B1CB0D5

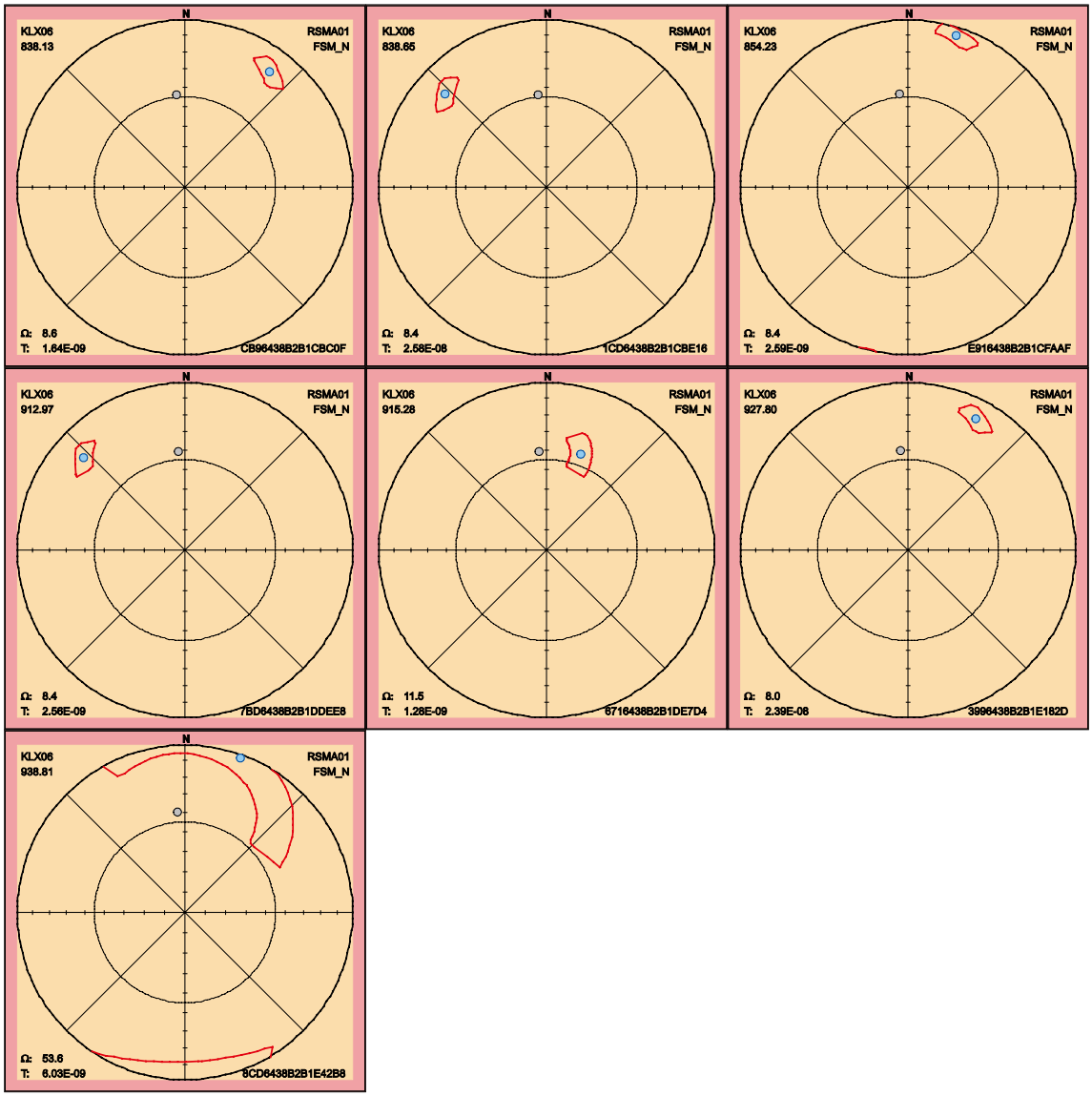

2.3.5 KLX07A

Below follow the 90th percentile sample space of uncertainty for the 113 PFL fractures in KLX07A. There are seven fractures listed in Table 2-7 having maximum uncertainty, on the 90th percentile, larger than 30°. The fractures having large uncertainty can have an alternative interpretation of orientation compared to the best estimate orientation that is found in the table p_fract_core in /Sicada 2008/.

Table 2-7. Fractures in KLX07A with uncertainty, Ω, larger than 30°.

FeatureId	PFL-f no	Adjusted Secup	Ω
7117438B0A12B79A	41	178.35	70.1
F717438B0A13CF3C	63	250.28	60.4
1957438B0A169432	159	432.38	41.2
2517438B0A1824C3	182	535.36	60.2
4BD7438B0A18BCEA	187	574.49	70.2
9A97438B0A1A28E0	204	668.08	62.4
7117438B0A12B79A	41	178.35	70.1

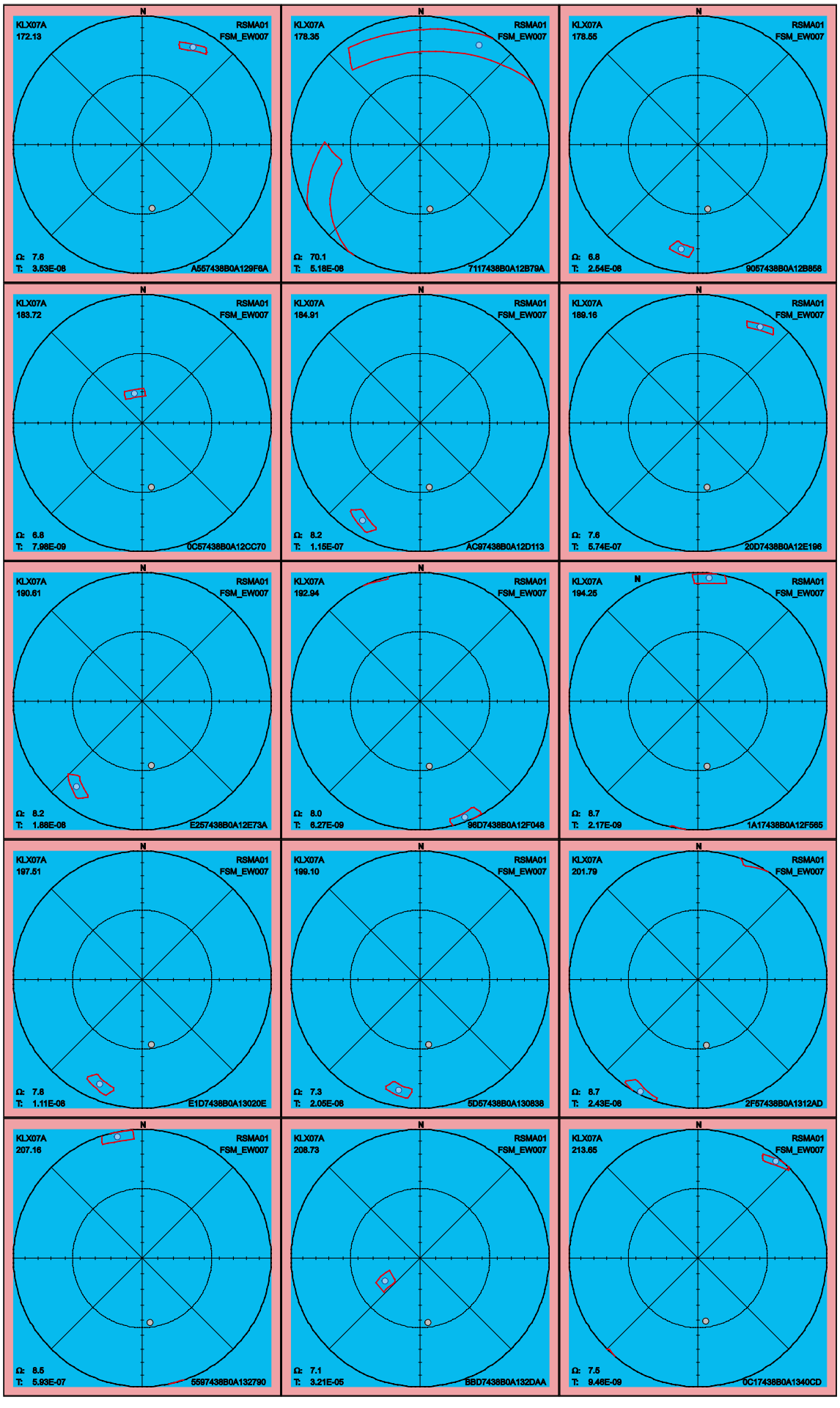
KLX07A
172.13
RSMA01
FSM_EW007
Ω: 7.6
T: 3.53E-08
A557438B0A129F6A
KLX07A
178.35
RSMA01
FSM_EW007
Ω: 70.1
T: 5.18E-08
7117438B0A12B79A
KLX07A
178.55
RSMA01
FSM_EW007
Ω: 6.8
T: 2.54E-08
9057438B0A12B858
KLX07A
183.72
RSMA01
FSM_EW007
Ω: 6.8
T: 7.98E-09
0C57438B0A12CC70
KLX07A
184.91
RSMA01
FSM_EW007
Ω: 8.2
T: 1.15E-07
AC97438B0A12D113
KLX07A
189.16
RSMA01
FSM_EW007
Ω: 7.6
T: 5.74E-07
20D7438B0A12E196
KLX07A
190.61
RSMA01
FSM_EW007
Ω: 8.2
T: 1.88E-08
E257438B0A12E73A
KLX07A
192.94
RSMA01
FSM_EW007
Ω: 8.0
T: 6.27E-09
98D7438B0A12F048
KLX07A
194.25
RSMA01
FSM_EW007
Ω: 8.7
T: 2.17E-09
1A17438B0A12F565
KLX07A
197.51
RSMA01
FSM_EW007
Ω: 7.8
T: 1.11E-08
E1D7438B0A13020E
KLX07A
199.10
RSMA01
FSM_EW007
Ω: 7.3
T: 2.05E-08
5D57438B0A130838
KLX07A
201.79
RSMA01
FSM_EW007
Ω: 8.7
T: 2.43E-08
2F57438B0A1312AD
KLX07A
207.16
RSMA01
FSM_EW007
Ω: 8.5
T: 5.93E-07
5597438B0A132790
KLX07A
208.73
RSMA01
FSM_EW007
Ω: 7.1
T: 3.21E-05
BBD7438B0A132DAA
KLX07A
213.65
RSMA01
FSM_EW007
Ω: 7.5
T: 9.46E-09
0C17438B0A1340CD

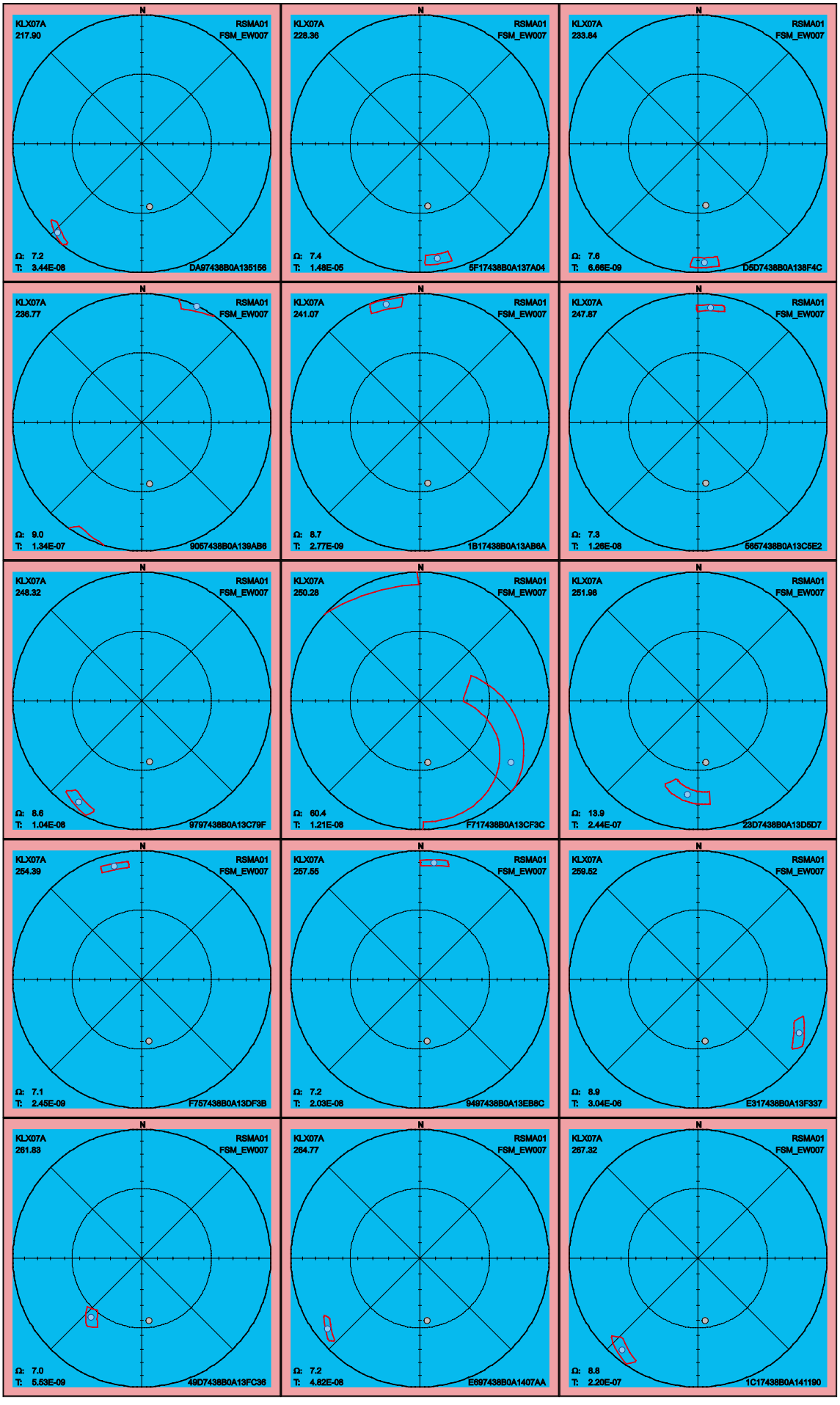
KLX07A
217.90
RSMA01
FSM_EW007
Ω: 7.2
T: 3.44E-08
DA97438B0A135158
KLX07A
228.36
RSMA01
FSM_EW007
Ω: 7.4
T: 1.48E-05
5F17438B0A137A04
KLX07A
233.84
RSMA01
FSM_EW007
Ω: 7.6
T: 6.66E-09
D5D7438B0A138F4C
KLX07A
236.77
RSMA01
FSM_EW007
Ω: 9.0
T: 1.34E-07
9057438B0A139AB6
KLX07A
241.07
RSMA01
FSM_EW007
Ω: 8.7
T: 2.77E-09
1B17438B0A13AB6A
KLX07A
247.87
RSMA01
FSM_EW007
Ω: 7.3
T: 1.26E-08
5657438B0A13C5E2
KLX07A
248.32
RSMA01
FSM_EW007
Ω: 8.6
T: 1.04E-08
9797438B0A13C79F
KLX07A
250.28
RSMA01
FSM_EW007
Ω: 60.4
T: 1.21E-08
F717438B0A13CF3C
KLX07A
251.98
RSMA01
FSM_EW007
Ω: 13.9
T: 2.44E-07
23D7438B0A13D5D7
KLX07A
254.39
RSMA01
FSM_EW007
Ω: 7.1
T: 2.45E-09
F757438B0A13DF3B
KLX07A
257.55
RSMA01
FSM_EW007
Ω: 7.2
T: 2.03E-08
9497438B0A13EB8C
KLX07A
259.52
RSMA01
FSM_EW007
Ω: 8.9
T: 3.04E-06
E317438B0A13F337
KLX07A
261.83
RSMA01
FSM_EW007
Ω: 7.0
T: 5.53E-09
49D7438B0A13FC36
KLX07A
264.77
RSMA01
FSM_EW007
Ω: 7.2
T: 4.82E-08
E697438B0A1407AA
KLX07A
267.32
RSMA01
FSM_EW007
Ω: 8.8
T: 2.20E-07
1C17438B0A141190

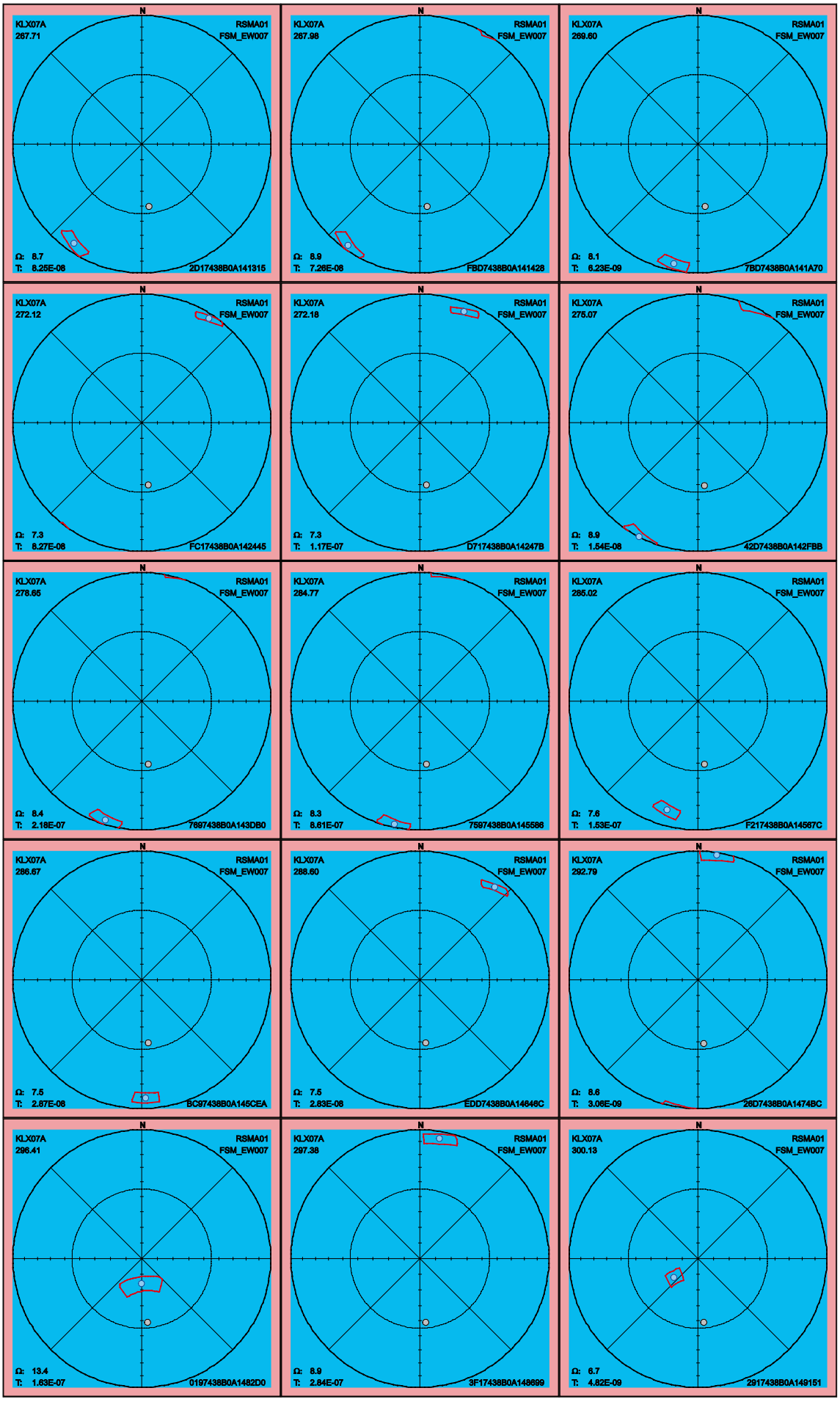
KLX07A
267.71
RSMA01
FSM_EW007
N
Ω: 8.7
T: 8.25E-08
2D17438B0A141315
KLX07A
267.98
RSMA01
FSM_EW007
N
Ω: 8.9
T: 7.26E-08
FBD7438B0A141428
KLX07A
269.60
RSMA01
FSM_EW007
N
Ω: 8.1
T: 6.23E-09
7BD7438B0A141A70
KLX07A
272.12
RSMA01
FSM_EW007
N
Ω: 7.3
T: 8.27E-08
FC17438B0A142445
KLX07A
272.18
RSMA01
FSM_EW007
N
Ω: 7.3
T: 1.17E-07
D717438B0A14247B
KLX07A
275.07
RSMA01
FSM_EW007
N
Ω: 8.9
T: 1.54E-08
42D7438B0A142FBB
KLX07A
278.65
RSMA01
FSM_EW007
N
Ω: 8.4
T: 2.18E-07
7897438B0A143DB0
KLX07A
284.77
RSMA01
FSM_EW007
N
Ω: 8.3
T: 8.61E-07
7597438B0A145588
KLX07A
285.02
RSMA01
FSM_EW007
N
Ω: 7.6
T: 1.53E-07
F217438B0A14567C
KLX07A
286.67
RSMA01
FSM_EW007
N
Ω: 7.5
T: 2.67E-08
BC97438B0A145CEA
KLX07A
288.60
RSMA01
FSM_EW007
N
Ω: 7.5
T: 2.83E-08
EDD7438B0A14646C
KLX07A
292.79
RSMA01
FSM_EW007
N
Ω: 8.6
T: 3.06E-09
26D7438B0A1474BC
KLX07A
296.41
RSMA01
FSM_EW007
N
Ω: 13.4
T: 1.63E-07
0197438B0A1482D0
KLX07A
297.38
RSMA01
FSM_EW007
N
Ω: 8.9
T: 2.84E-07
3F17438B0A148899
KLX07A
300.13
RSMA01
FSM_EW007
N
Ω: 6.7
T: 4.82E-09
2917438B0A149151

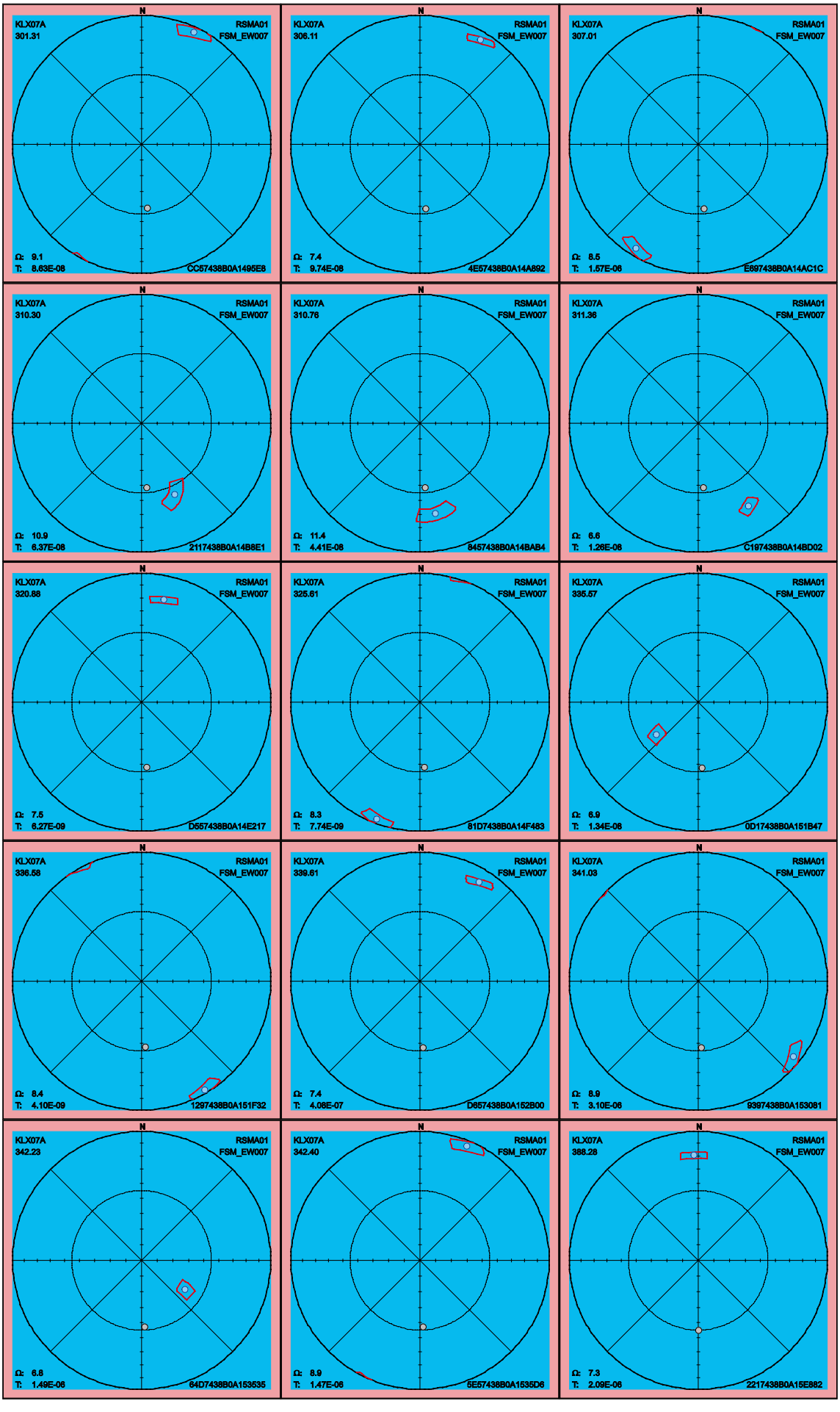
KLX07A
301.31
RSMA01
FSM_EW007
Ω: 9.1
T: 8.63E-08
CC57438B0A1495E8
KLX07A
306.11
RSMA01
FSM_EW007
Ω: 7.4
T: 9.74E-08
4E57438B0A14A892
KLX07A
307.01
RSMA01
FSM_EW007
Ω: 8.5
T: 1.57E-06
E697438B0A14AC1C
KLX07A
310.30
RSMA01
FSM_EW007
Ω: 10.9
T: 6.37E-08
2117438B0A14B8E1
KLX07A
310.76
RSMA01
FSM_EW007
Ω: 11.4
T: 4.41E-08
8457438B0A14BAB4
KLX07A
311.36
RSMA01
FSM_EW007
Ω: 6.6
T: 1.26E-06
C197438B0A14BD02
KLX07A
320.88
RSMA01
FSM_EW007
Ω: 7.5
T: 6.27E-09
D557438B0A14E217
KLX07A
325.61
RSMA01
FSM_EW007
Ω: 8.3
T: 7.74E-09
81D7438B0A14F483
KLX07A
335.57
RSMA01
FSM_EW007
Ω: 6.9
T: 1.34E-06
0D17438B0A151B47
KLX07A
336.58
RSMA01
FSM_EW007
Ω: 8.4
T: 4.10E-09
1297438B0A151F32
KLX07A
339.61
RSMA01
FSM_EW007
Ω: 7.4
T: 4.08E-07
D857438B0A152B00
KLX07A
341.03
RSMA01
FSM_EW007
Ω: 8.9
T: 3.10E-06
9397438B0A153081
KLX07A
342.23
RSMA01
FSM_EW007
Ω: 6.8
T: 1.49E-08
64D7438B0A153535
KLX07A
342.40
RSMA01
FSM_EW007
Ω: 8.9
T: 1.47E-06
5E57438B0A1535D6
KLX07A
388.28
RSMA01
FSM_EW007
Ω: 7.3
T: 2.09E-06
2217438B0A15E882

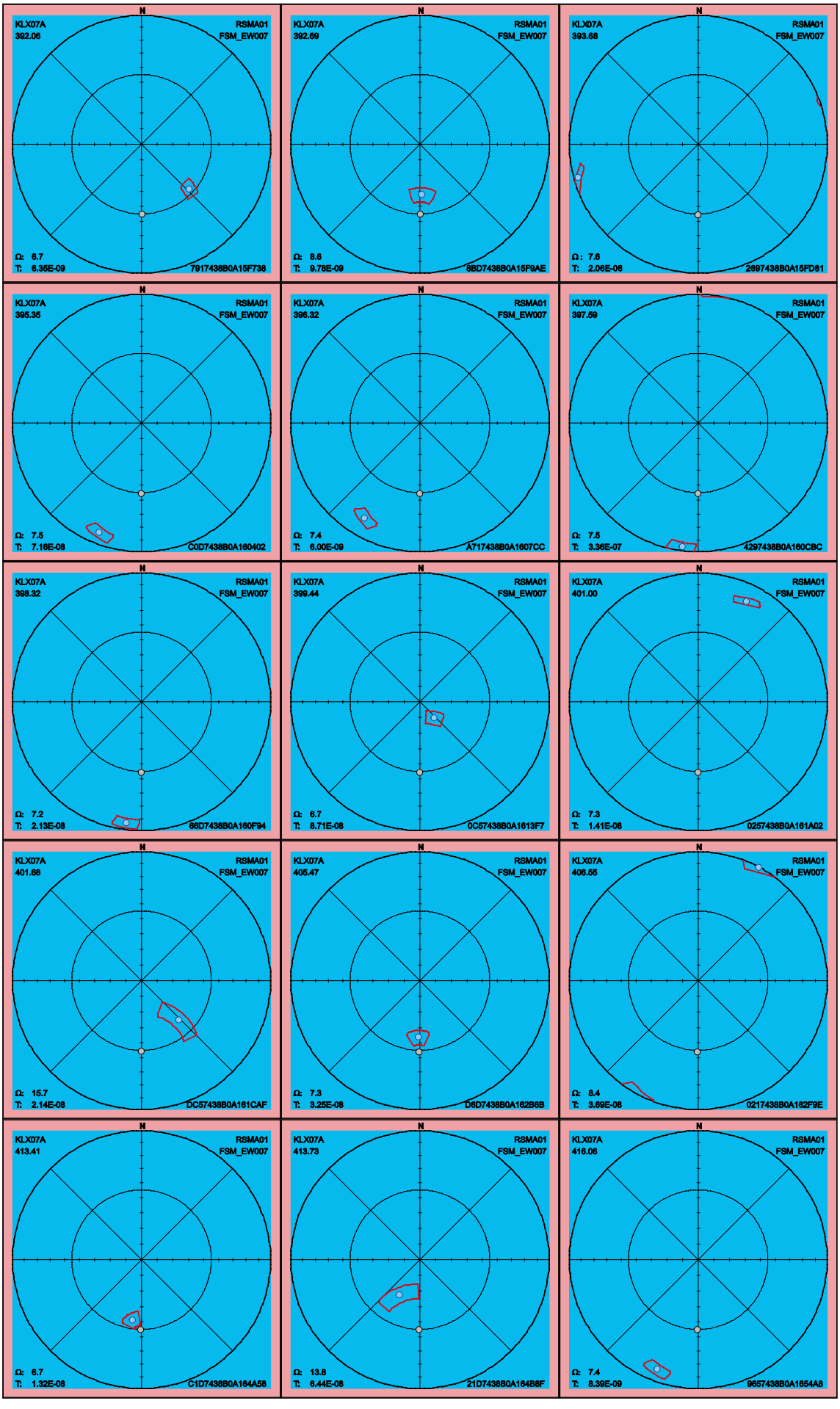
KLX07A
392.06
RSMA01
FSM_EW007
N
Ω: 6.7
T: 6.35E-09
7917438B0A15F738
KLX07A
392.69
RSMA01
FSM_EW007
N
Ω: 8.6
T: 9.78E-09
8BD7438B0A15F9AE
KLX07A
393.68
RSMA01
FSM_EW007
N
Ω: 7.6
T: 2.06E-06
2697438B0A15FD81
KLX07A
395.35
RSMA01
FSM_EW007
N
Ω: 7.5
T: 7.16E-08
C0D7438B0A160402
KLX07A
396.32
RSMA01
FSM_EW007
N
Ω: 7.4
T: 6.00E-09
A717438B0A1607CC
KLX07A
397.59
RSMA01
FSM_EW007
N
Ω: 7.5
T: 3.36E-07
4297438B0A160CBC
KLX07A
398.32
RSMA01
FSM_EW007
N
Ω: 7.2
T: 2.13E-08
68D7438B0A160F94
KLX07A
399.44
RSMA01
FSM_EW007
N
Ω: 6.7
T: 8.71E-08
0C57438B0A1613F7
KLX07A
401.00
RSMA01
FSM_EW007
N
Ω: 7.3
T: 1.41E-08
0257438B0A161A02
KLX07A
401.68
RSMA01
FSM_EW007
N
Ω: 15.7
T: 2.14E-08
DC57438B0A161CAF
KLX07A
405.47
RSMA01
FSM_EW007
N
Ω: 7.3
T: 3.25E-08
D6D7438B0A162B6B
KLX07A
406.55
RSMA01
FSM_EW007
N
Ω: 8.4
T: 3.69E-08
0217438B0A162F9E
KLX07A
413.41
RSMA01
FSM_EW007
N
Ω: 6.7
T: 1.32E-08
C1D7438B0A164A58
KLX07A
413.73
RSMA01
FSM_EW007
N
Ω: 13.8
T: 6.44E-08
21D7438B0A164B8F
KLX07A
416.06
RSMA01
FSM_EW007
N
Ω: 7.4
T: 8.39E-09
9857438B0A1654A8

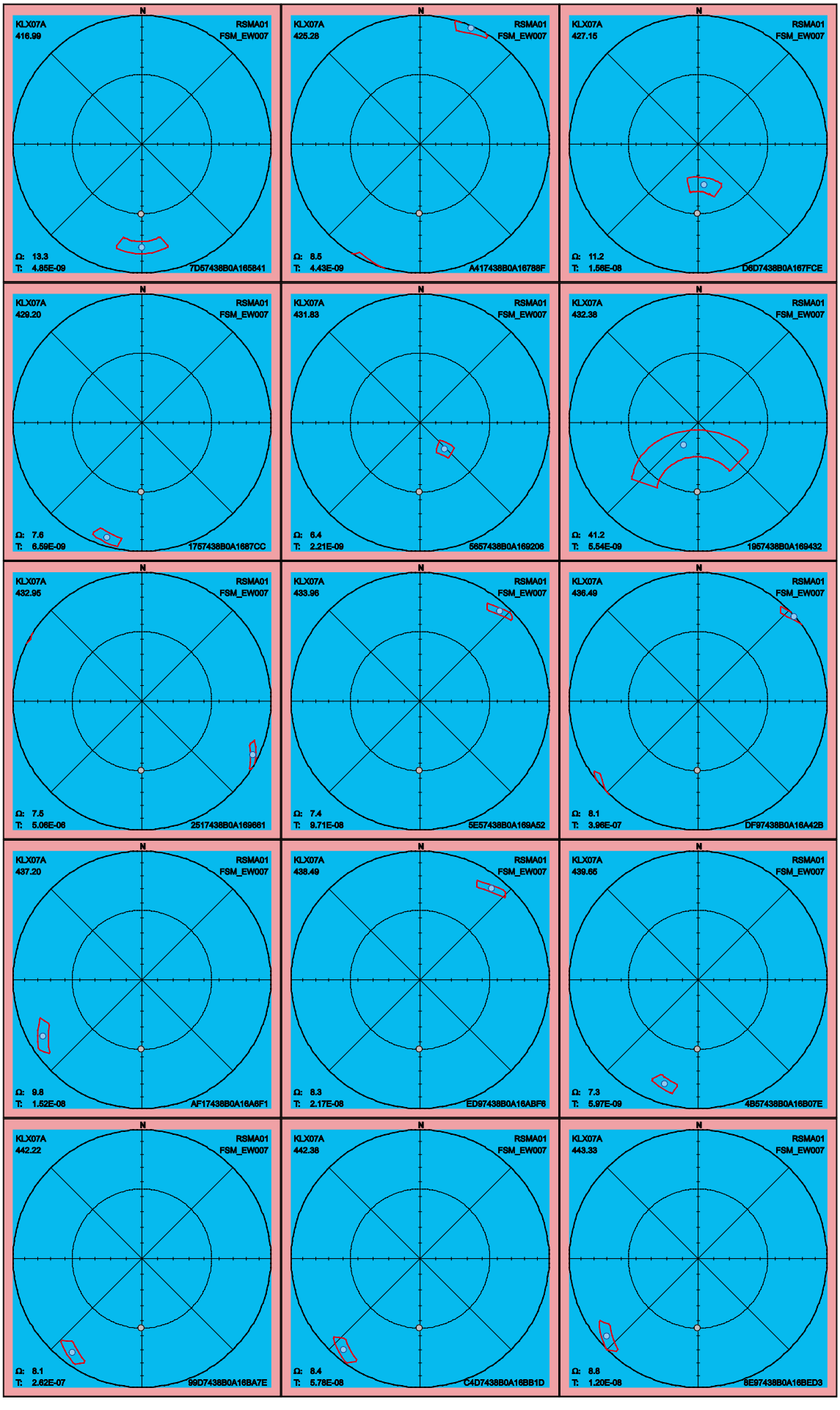
KLX07A
416.99
RSMA01
FSM_EW007
Ω: 13.3
T: 4.85E-09
7D57438B0A165841
KLX07A
425.28
RSMA01
FSM_EW007
Ω: 8.5
T: 4.43E-09
A417438B0A16788F
KLX07A
427.15
RSMA01
FSM_EW007
Ω: 11.2
T: 1.56E-08
D6D7438B0A167FCE
KLX07A
429.20
RSMA01
FSM_EW007
Ω: 7.6
T: 6.59E-09
1757438B0A1687CC
KLX07A
431.83
RSMA01
FSM_EW007
Ω: 6.4
T: 2.21E-09
5657438B0A169206
KLX07A
432.38
RSMA01
FSM_EW007
Ω: 41.2
T: 5.54E-09
1957438B0A169432
KLX07A
432.95
RSMA01
FSM_EW007
Ω: 7.5
T: 5.06E-06
2517438B0A169661
KLX07A
433.96
RSMA01
FSM_EW007
Ω: 7.4
T: 9.71E-08
5E57438B0A169A52
KLX07A
436.49
RSMA01
FSM_EW007
Ω: 8.1
T: 3.96E-07
DF97438B0A16A42B
KLX07A
437.20
RSMA01
FSM_EW007
Ω: 9.8
T: 1.52E-08
AF17438B0A16A6F1
KLX07A
438.49
RSMA01
FSM_EW007
Ω: 8.3
T: 2.17E-08
ED97438B0A16ABF8
KLX07A
439.65
RSMA01
FSM_EW007
Ω: 7.3
T: 5.97E-09
4B57438B0A16B07E
KLX07A
442.22
RSMA01
FSM_EW007
Ω: 8.1
T: 2.62E-07
99D7438B0A16BA7E
KLX07A
442.38
RSMA01
FSM_EW007
Ω: 8.4
T: 5.78E-08
C4D7438B0A16BB1D
KLX07A
443.33
RSMA01
FSM_EW007
Ω: 8.8
T: 1.20E-08
8E97438B0A16BED3

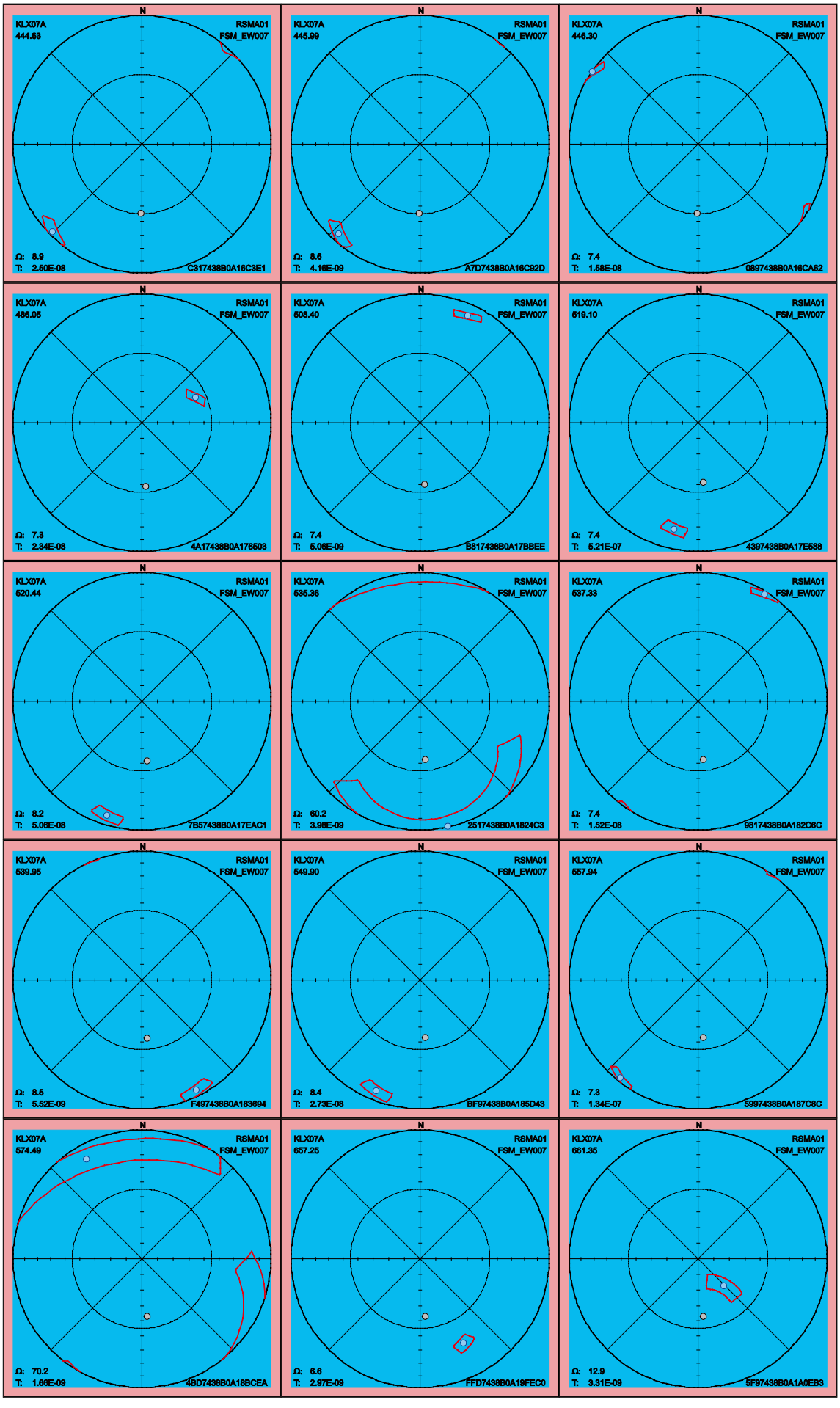
KLX07A
444.63
RSMA01
FSM_EW007
N
Ω: 8.9
T: 2.50E-08
C317438B0A16C3E1
KLX07A
445.99
RSMA01
FSM_EW007
N
Ω: 8.6
T: 4.16E-09
A7D7438B0A16C92D
KLX07A
446.30
RSMA01
FSM_EW007
N
Ω: 7.4
T: 1.58E-08
0897438B0A16CA62
KLX07A
486.05
RSMA01
FSM_EW007
N
Ω: 7.3
T: 2.34E-08
4A17438B0A176503
KLX07A
508.40
RSMA01
FSM_EW007
N
Ω: 7.4
T: 5.06E-09
B817438B0A17BBEE
KLX07A
519.10
RSMA01
FSM_EW007
N
Ω: 7.4
T: 5.21E-07
4397438B0A17E588
KLX07A
520.44
RSMA01
FSM_EW007
N
Ω: 8.2
T: 5.06E-08
7B57438B0A17EAC1
KLX07A
535.36
RSMA01
FSM_EW007
N
Ω: 60.2
T: 3.98E-09
2517438B0A1824C3
KLX07A
537.33
RSMA01
FSM_EW007
N
Ω: 7.4
T: 1.52E-08
9817438B0A182C8C
KLX07A
539.95
RSMA01
FSM_EW007
N
Ω: 8.5
T: 5.52E-09
F497438B0A183694
KLX07A
549.90
RSMA01
FSM_EW007
N
Ω: 8.4
T: 2.73E-08
BF97438B0A185D43
KLX07A
557.94
RSMA01
FSM_EW007
N
Ω: 7.3
T: 1.34E-07
5997438B0A187C8C
KLX07A
574.49
RSMA01
FSM_EW007
N
Ω: 70.2
T: 1.66E-09
4BD7438B0A18BCEA
KLX07A
657.25
RSMA01
FSM_EW007
N
Ω: 6.6
T: 2.97E-09
FFD7438B0A19FEC0
KLX07A
661.35
RSMA01
FSM_EW007
N
Ω: 12.9
T: 3.31E-09
5F97438B0A1A0EB3

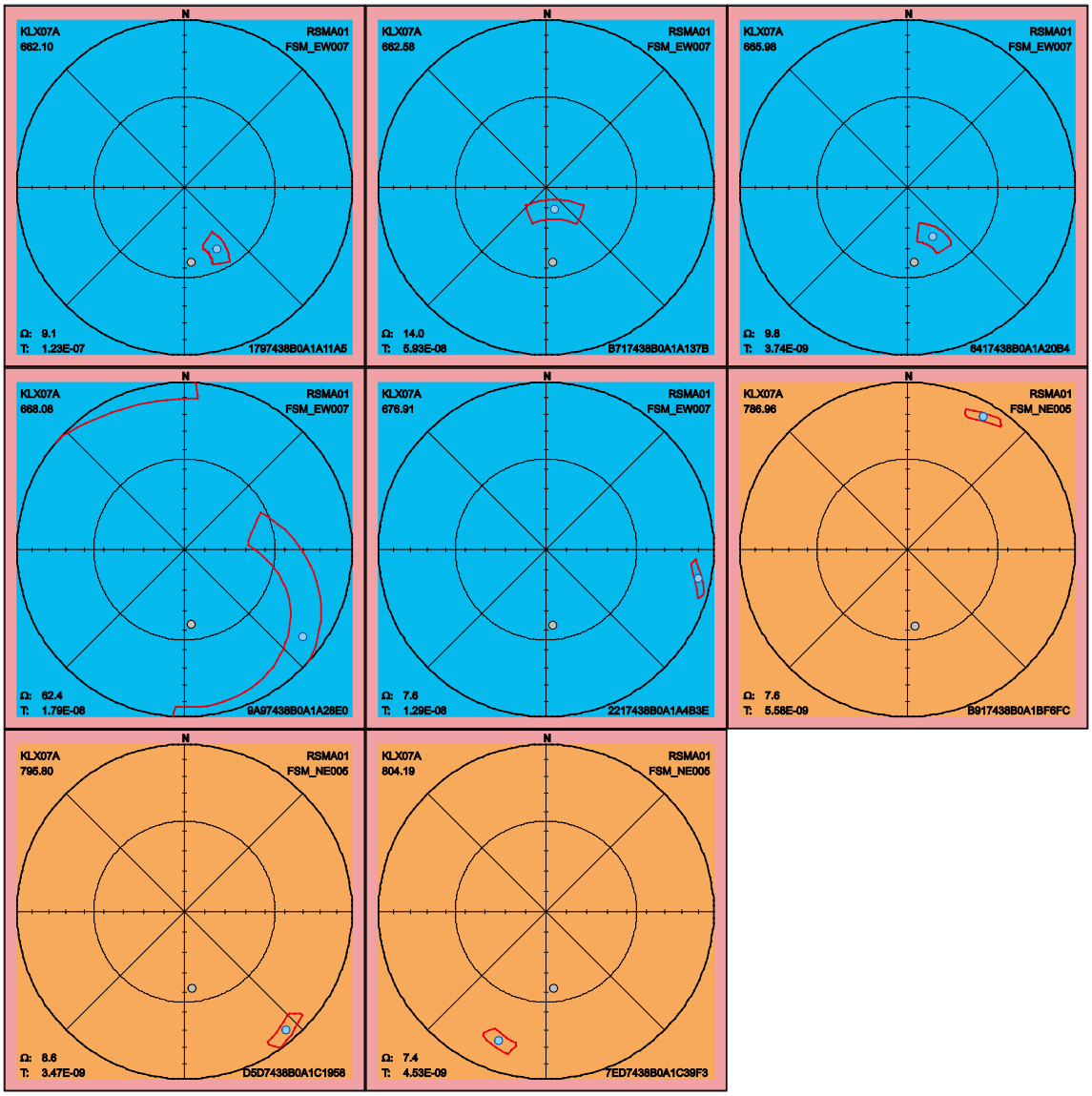

2.3.6 KLX07B

There are two PFL fractures in KLX07B missing orientation information and thus excluded from this section. Below follow the 90th percentile sample space of uncertainty for the remaining 54 PFL fractures. The four fractures listed in Table 2-8 need to be investigated further since they have maximum uncertainty, on the 90th percentile, larger than 30° and hence can have an alternative interpretation of orientation compared to the best estimate orientation that is found in the table p_fract_core in / Sicada 2008/.

Table 2-8. Fractures in KLX07B with uncertainty, Ω, larger than 30°.

FeatureId	PFL-f no	Adjusted Secup	Ω
1C17438B0910D6E4	15	55.24	76.9
2397438B09113C9B	30	81.41	42.6
5257438B09116B70	39	93.46	61.1
E6D7438B0912B35E	78	177.83	40.9

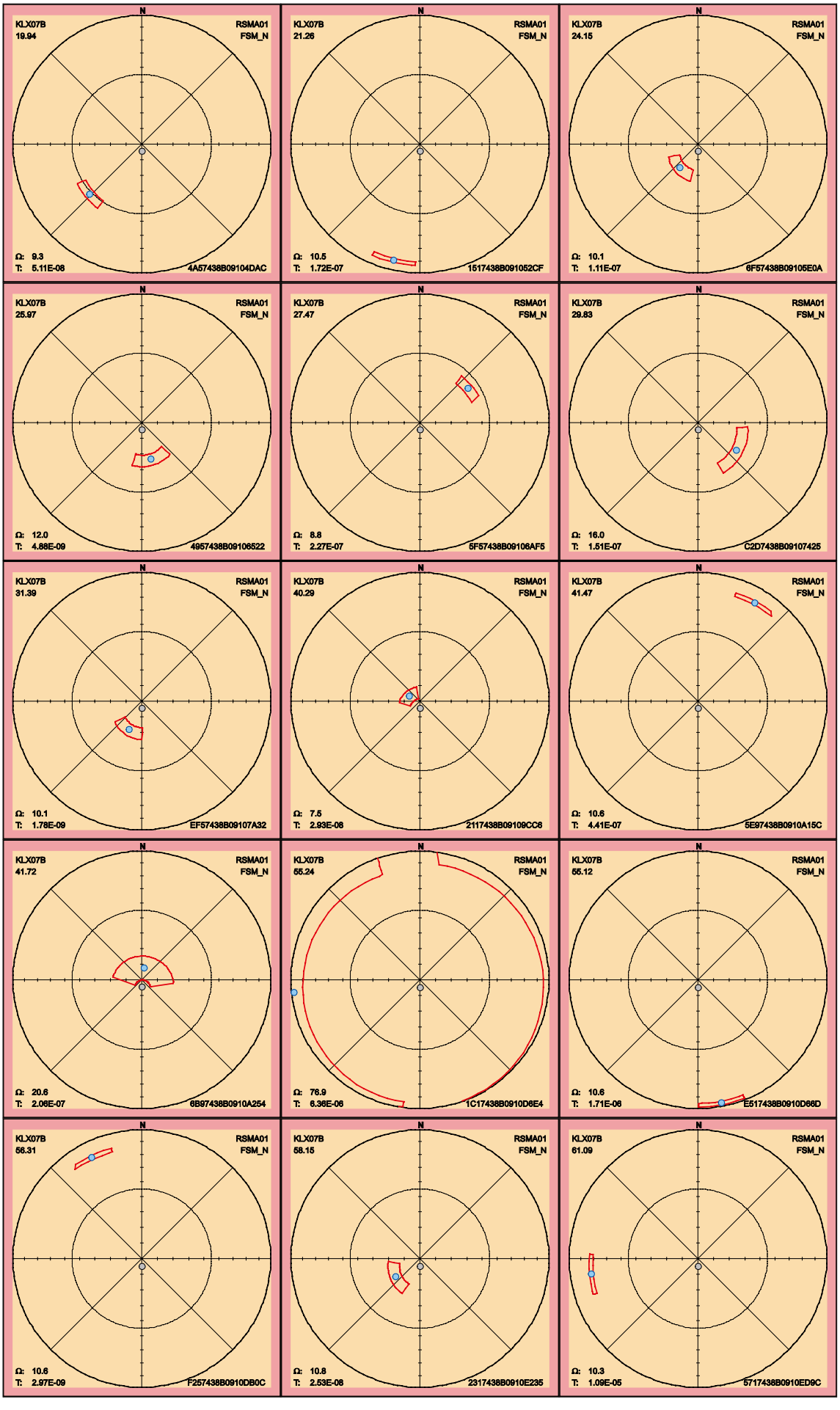
KLX07B
19.94
RSMA01
FSM_N
N
Ω: 9.3
T: 5.11E-08
4A57438B09104DAC
KLX07B
21.26
RSMA01
FSM_N
N
Ω: 10.5
T: 1.72E-07
1517438B091052CF
KLX07B
24.15
RSMA01
FSM_N
N
Ω: 10.1
T: 1.11E-07
6F57438B09105E0A
KLX07B
25.97
RSMA01
FSM_N
N
Ω: 12.0
T: 4.88E-09
4957438B09106522
KLX07B
27.47
RSMA01
FSM_N
N
Ω: 8.8
T: 2.27E-07
5F57438B09106AF5
KLX07B
29.83
RSMA01
FSM_N
N
Ω: 16.0
T: 1.51E-07
C2D7438B09107425
KLX07B
31.39
RSMA01
FSM_N
N
Ω: 10.1
T: 1.78E-09
EF57438B09107A32
KLX07B
40.29
RSMA01
FSM_N
N
Ω: 7.5
T: 2.93E-08
2117438B09109CC6
KLX07B
41.47
RSMA01
FSM_N
N
Ω: 10.6
T: 4.41E-07
5E97438B0910A15C
KLX07B
41.72
RSMA01
FSM_N
N
Ω: 20.6
T: 2.06E-07
6B97438B0910A254
KLX07B
55.24
RSMA01
FSM_N
N
Ω: 76.9
T: 6.36E-06
1C17438B0910D6E4
KLX07B
55.12
RSMA01
FSM_N
N
Ω: 10.6
T: 1.71E-06
E517438B0910D66D
KLX07B
56.31
RSMA01
FSM_N
N
Ω: 10.6
T: 2.97E-09
F257438B0910DB0C
KLX07B
58.15
RSMA01
FSM_N
N
Ω: 10.8
T: 2.53E-08
2317438B0910E235
KLX07B
61.09
RSMA01
FSM_N
N
Ω: 10.3
T: 1.09E-05
5717438B0910ED9C

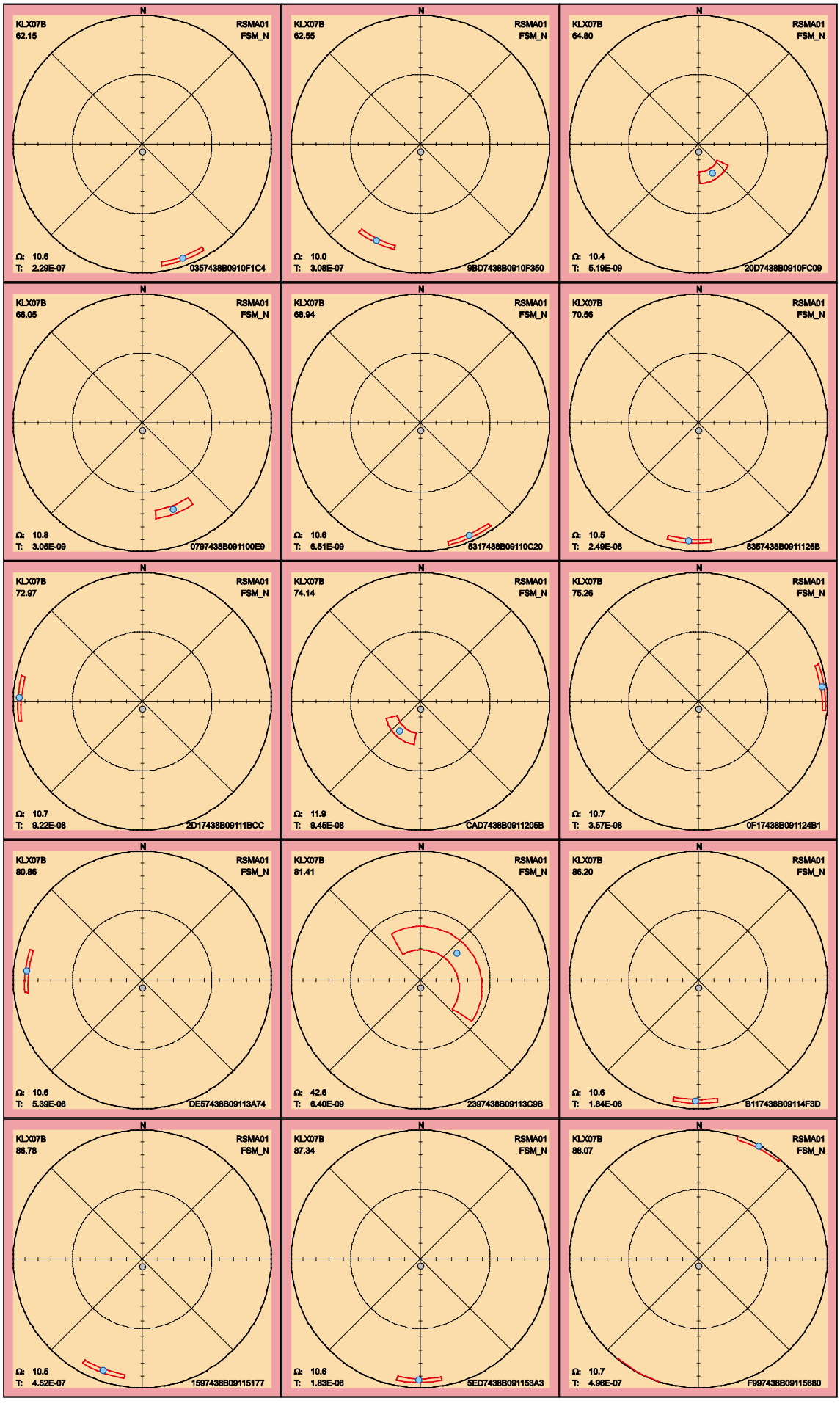
KLX07B
62.15
RSMA01
FSM_N
N
Ω: 10.6
T: 2.29E-07
0357438B0910F1C4
KLX07B
62.55
RSMA01
FSM_N
N
Ω: 10.0
T: 3.08E-07
9BD7438B0910F350
KLX07B
64.80
RSMA01
FSM_N
N
Ω: 10.4
T: 5.19E-09
20D7438B0910FC09
KLX07B
66.05
RSMA01
FSM_N
N
Ω: 10.8
T: 3.05E-09
0797438B091100E9
KLX07B
68.94
RSMA01
FSM_N
N
Ω: 10.6
T: 6.51E-09
5317438B09110C20
KLX07B
70.56
RSMA01
FSM_N
N
Ω: 10.5
T: 2.49E-08
8357438B0911126B
KLX07B
72.97
RSMA01
FSM_N
N
Ω: 10.7
T: 9.22E-08
2D17438B09111BCC
KLX07B
74.14
RSMA01
FSM_N
N
Ω: 11.9
T: 9.45E-08
CAD7438B0911205B
KLX07B
75.26
RSMA01
FSM_N
N
Ω: 10.7
T: 3.57E-08
0F17438B091124B1
KLX07B
80.86
RSMA01
FSM_N
N
Ω: 10.6
T: 5.39E-08
DE57438B09113A74
KLX07B
81.41
RSMA01
FSM_N
N
Ω: 42.6
T: 6.40E-09
2397438B09113C9B
KLX07B
86.20
RSMA01
FSM_N
N
Ω: 10.6
T: 1.84E-08
B117438B09114F3D
KLX07B
86.78
RSMA01
FSM_N
N
Ω: 10.5
T: 4.52E-07
1597438B09115177
KLX07B
87.34
RSMA01
FSM_N
N
Ω: 10.6
T: 1.83E-08
5ED7438B091153A3
KLX07B
88.07
RSMA01
FSM_N
N
Ω: 10.7
T: 4.96E-07
F997438B09115680

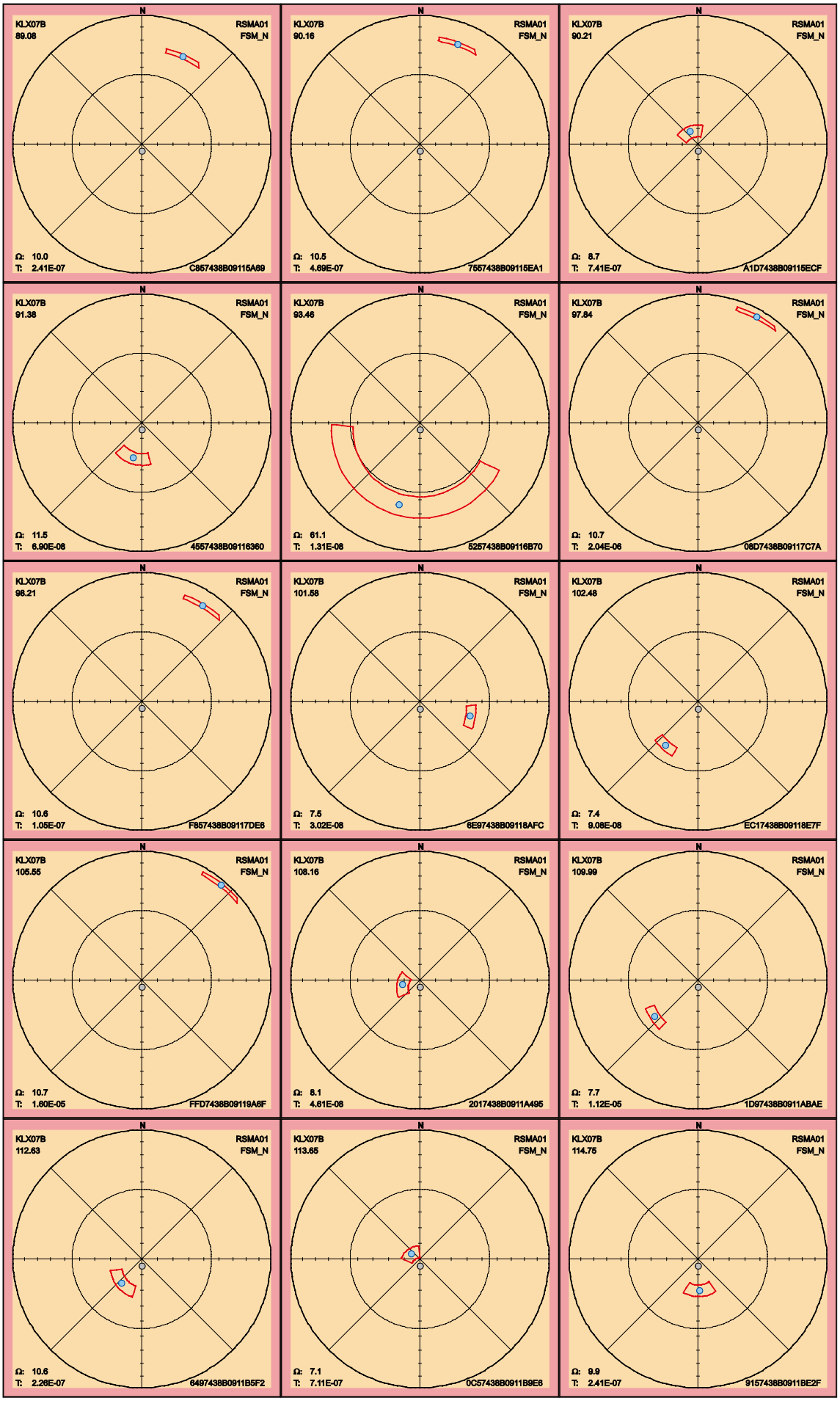
KLX07B
89.08
RSMA01
FSM_N
N
Ω: 10.0
T: 2.41E-07
C857438B09116A69
KLX07B
90.16
RSMA01
FSM_N
N
Ω: 10.5
T: 4.69E-07
7557438B09115EA1
KLX07B
90.21
RSMA01
FSM_N
N
Ω: 8.7
T: 7.41E-07
A1D7438B09115ECF
KLX07B
91.38
RSMA01
FSM_N
N
Ω: 11.5
T: 6.90E-06
4557438B09116360
KLX07B
93.46
RSMA01
FSM_N
N
Ω: 61.1
T: 1.31E-06
5257438B09116B70
KLX07B
97.84
RSMA01
FSM_N
N
Ω: 10.7
T: 2.04E-06
08D7438B09117C7A
KLX07B
98.21
RSMA01
FSM_N
N
Ω: 10.6
T: 1.05E-07
F857438B09117DE8
KLX07B
101.58
RSMA01
FSM_N
N
Ω: 7.5
T: 3.02E-08
6E97438B09118AFC
KLX07B
102.48
RSMA01
FSM_N
N
Ω: 7.4
T: 9.08E-08
EC17438B09118E7F
KLX07B
105.55
RSMA01
FSM_N
N
Ω: 10.7
T: 1.60E-05
FFD7438B09119A6F
KLX07B
108.16
RSMA01
FSM_N
N
Ω: 8.1
T: 4.61E-08
2017438B0911A495
KLX07B
109.99
RSMA01
FSM_N
N
Ω: 7.7
T: 1.12E-05
1D97438B0911ABAE
KLX07B
112.63
RSMA01
FSM_N
N
Ω: 10.6
T: 2.26E-07
6497438B0911B5F2
KLX07B
113.65
RSMA01
FSM_N
N
Ω: 7.1
T: 7.11E-07
0C57438B0911B9E6
KLX07B
114.75
RSMA01
FSM_N
N
Ω: 9.9
T: 2.41E-07
9157438B0911BE2F

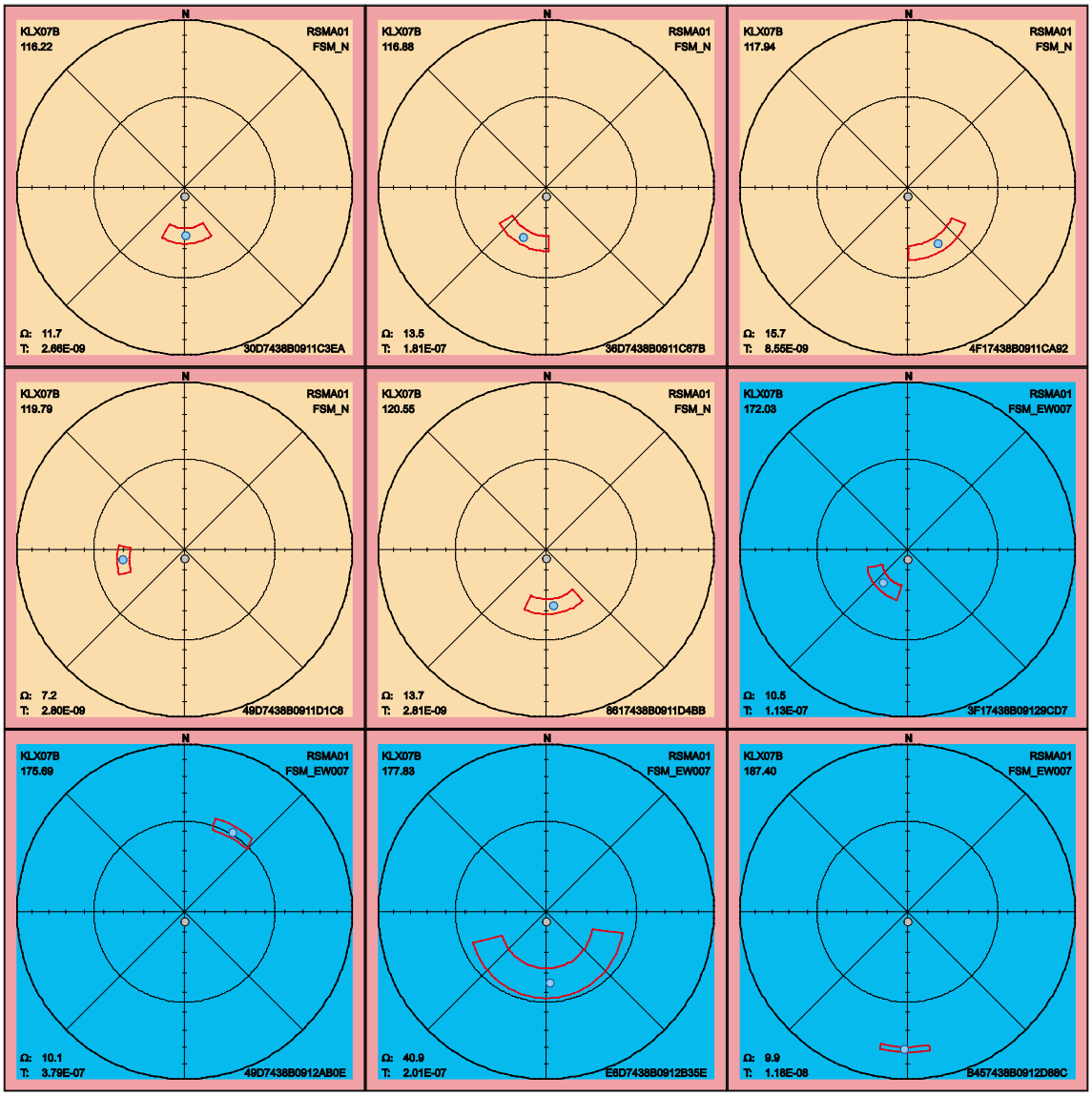

2.3.7 KLX08

Below follow the 90th percentile sample space of uncertainty for the 90 PFL fractures in KLX08. There is only one PFL fracture having maximum uncertainty, on the 90th percentile, larger than 30°, see Table 2-9. A fracture having large uncertainty can have an alternative interpretation of orientation compared to the best estimate orientation that is found in the table p_fract_core in /Sicada 2008/.

Table 2-9. Fractures in KLX08 with uncertainty, Ω, larger than 30°.

FeatureId	PFL-f no	Adjusted Secup	Ω
4058438B2B1A3C36	135	673.44	32.9

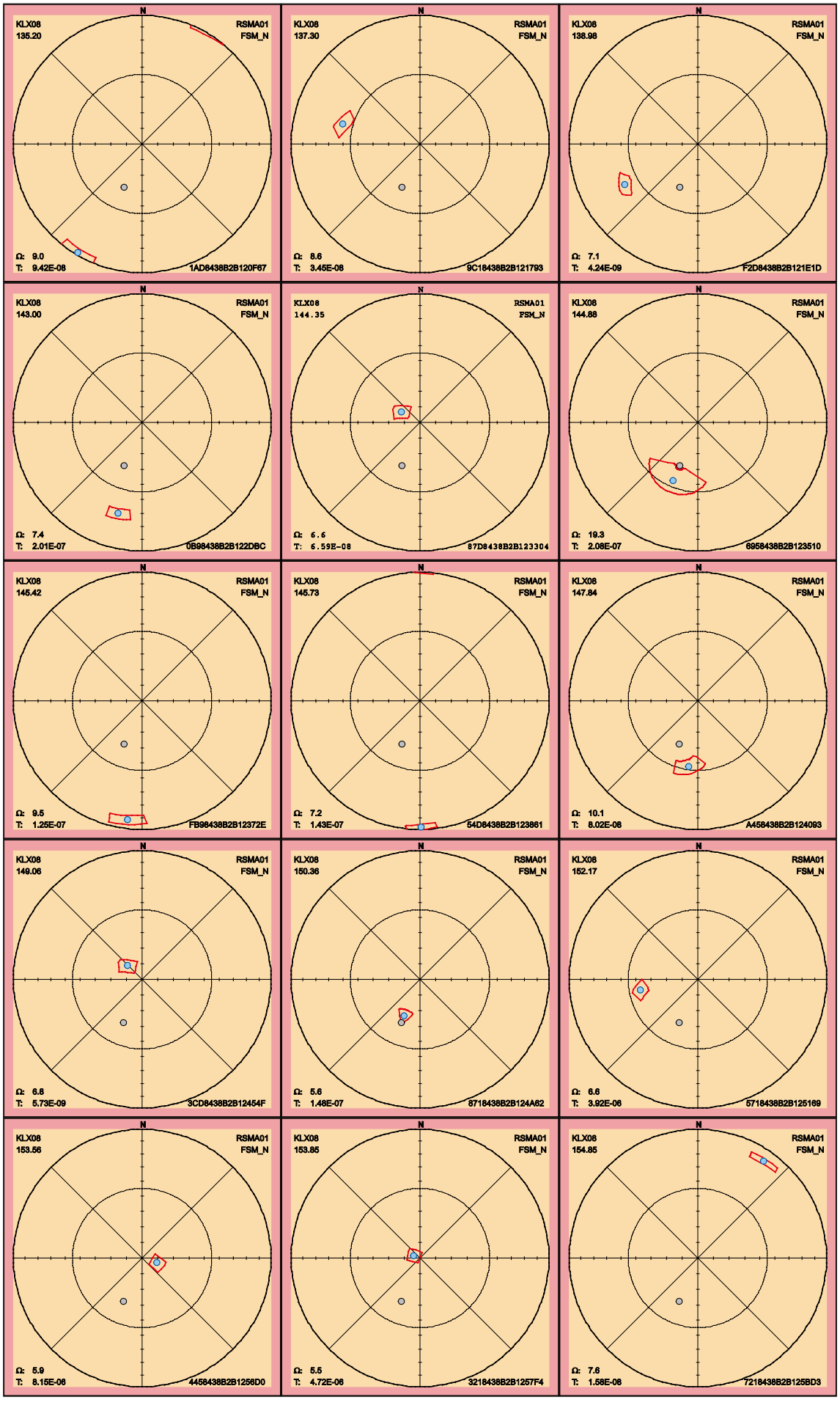
KLX08
135.20
RSMA01
FSM_N
N
Ω: 9.0
T: 9.42E-08
1AD8438B2B120F67
KLX08
137.30
RSMA01
FSM_N
N
Ω: 8.6
T: 3.45E-08
9C18438B2B121793
KLX08
138.98
RSMA01
FSM_N
N
Ω: 7.1
T: 4.24E-09
F2D8438B2B121E1D
KLX08
143.00
RSMA01
FSM_N
N
Ω: 7.4
T: 2.01E-07
0B98438B2B122DBC
KLX08
144.35
RSMA01
FSM_N
N
Ω: 6.6
T: 6.59E-08
87D8438B2B123304
KLX08
144.88
RSMA01
FSM_N
N
Ω: 19.3
T: 2.08E-07
6958438B2B123510
KLX08
145.42
RSMA01
FSM_N
N
Ω: 9.5
T: 1.25E-07
FB98438B2B12372E
KLX08
145.73
RSMA01
FSM_N
N
Ω: 7.2
T: 1.43E-07
54D8438B2B123861
KLX08
147.84
RSMA01
FSM_N
N
Ω: 10.1
T: 8.02E-08
A458438B2B124083
KLX08
149.06
RSMA01
FSM_N
N
Ω: 6.8
T: 5.73E-09
3CD8438B2B12454F
KLX08
150.36
RSMA01
FSM_N
N
Ω: 5.6
T: 1.48E-07
8718438B2B124A62
KLX08
152.17
RSMA01
FSM_N
N
Ω: 6.6
T: 3.92E-06
5718438B2B125169
KLX08
153.56
RSMA01
FSM_N
N
Ω: 5.9
T: 8.15E-06
4458438B2B1256D0
KLX08
153.85
RSMA01
FSM_N
N
Ω: 5.5
T: 4.72E-06
3218438B2B1257F4
KLX08
154.85
RSMA01
FSM_N
N
Ω: 7.6
T: 1.58E-08
7218438B2B125BD3

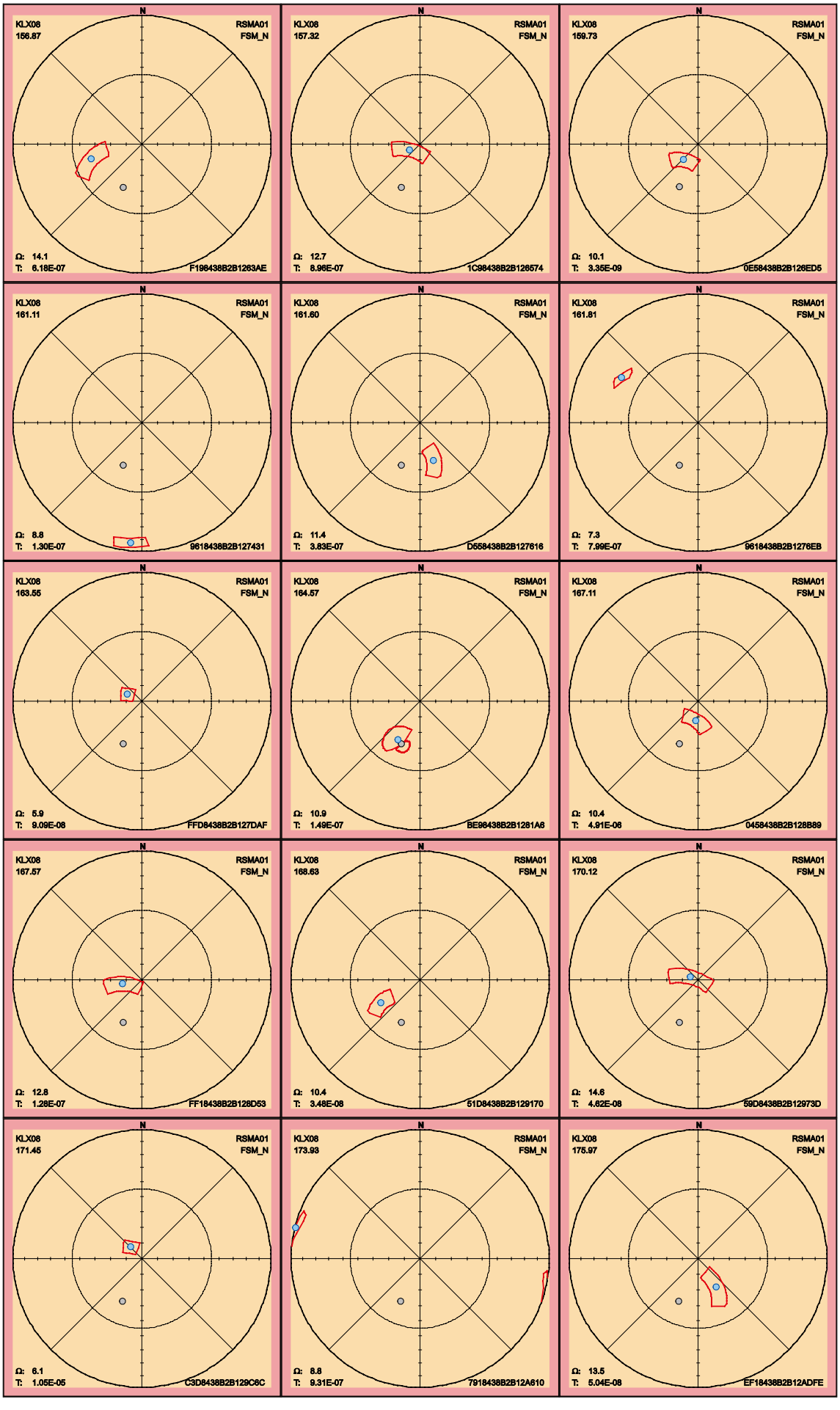
KLX08
156.87
RSMA01
FSM_N
Ω: 14.1
T: 6.18E-07
F198438B2B1263AE
KLX08
157.32
RSMA01
FSM_N
Ω: 12.7
T: 8.96E-07
1C98438B2B126574
KLX08
159.73
RSMA01
FSM_N
Ω: 10.1
T: 3.35E-09
0E58438B2B126ED5
KLX08
161.11
RSMA01
FSM_N
Ω: 8.8
T: 1.30E-07
9618438B2B127431
KLX08
161.60
RSMA01
FSM_N
Ω: 11.4
T: 3.83E-07
D558438B2B127616
KLX08
161.81
RSMA01
FSM_N
Ω: 7.3
T: 7.99E-07
9618438B2B1276EB
KLX08
163.55
RSMA01
FSM_N
Ω: 5.9
T: 9.09E-08
FFD8438B2B127DAF
KLX08
164.57
RSMA01
FSM_N
Ω: 10.9
T: 1.49E-07
BE98438B2B1281A6
KLX08
167.11
RSMA01
FSM_N
Ω: 10.4
T: 4.91E-06
0458438B2B128B89
KLX08
167.57
RSMA01
FSM_N
Ω: 12.8
T: 1.28E-07
FF18438B2B128D53
KLX08
168.63
RSMA01
FSM_N
Ω: 10.4
T: 3.48E-08
51D8438B2B129170
KLX08
170.12
RSMA01
FSM_N
Ω: 14.6
T: 4.62E-08
59D8438B2B12973D
KLX08
171.45
RSMA01
FSM_N
Ω: 6.1
T: 1.05E-05
C3D8438B2B129C8C
KLX08
173.93
RSMA01
FSM_N
Ω: 8.8
T: 9.31E-07
7918438B2B12A610
KLX08
175.97
RSMA01
FSM_N
Ω: 13.5
T: 5.04E-08
EF18438B2B12ADFE

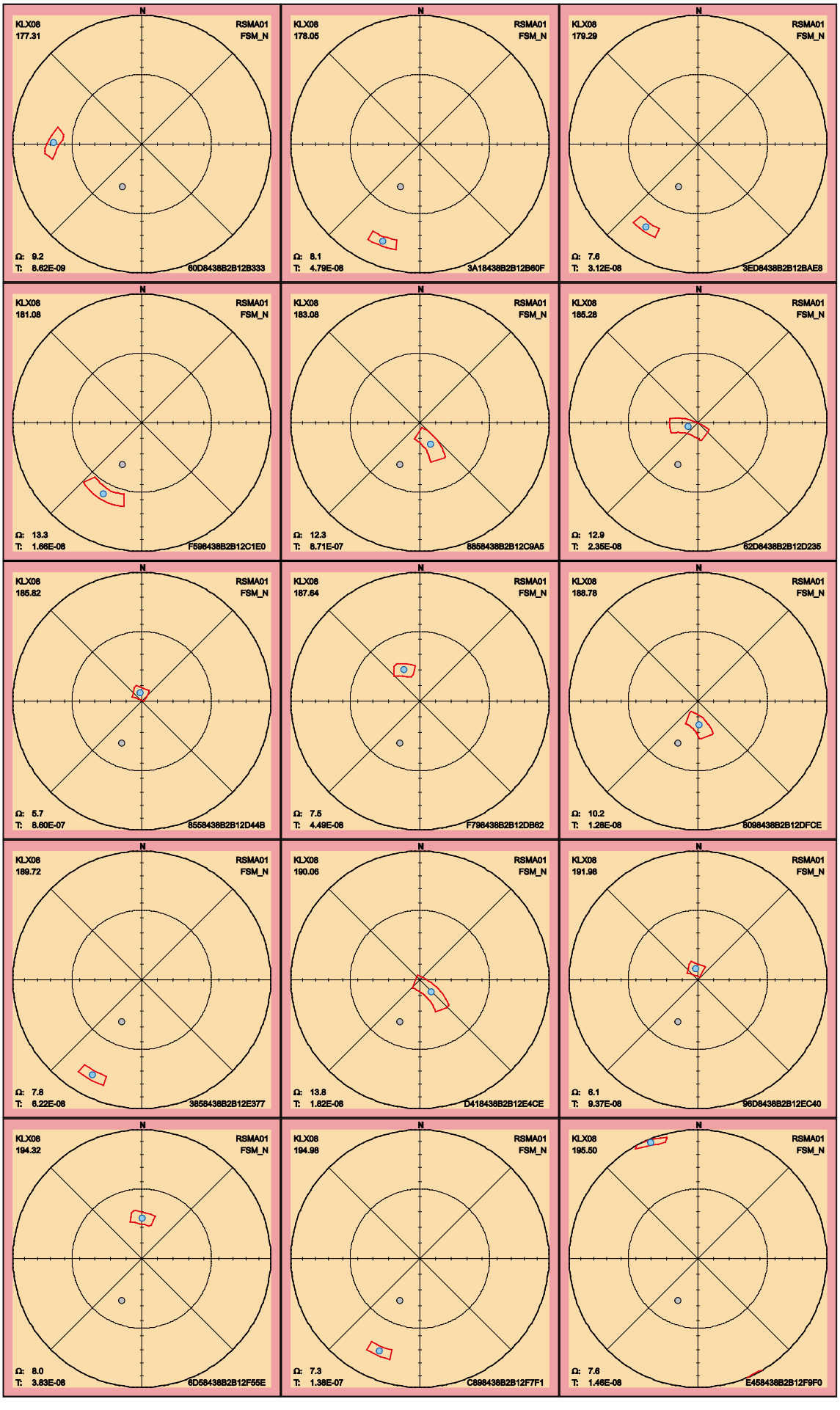
KLX06
177.31
RSMA01
FSM_N
N
Ω: 9.2
T: 8.62E-09
60D8438B2B12B333
KLX06
178.05
RSMA01
FSM_N
N
Ω: 8.1
T: 4.79E-08
3A18438B2B12B60F
KLX06
179.29
RSMA01
FSM_N
N
Ω: 7.6
T: 3.12E-08
3ED8438B2B12BAE8
KLX06
181.08
RSMA01
FSM_N
N
Ω: 13.3
T: 1.66E-08
F598438B2B12C1E0
KLX06
183.08
RSMA01
FSM_N
N
Ω: 12.3
T: 8.71E-07
8858438B2B12C9A5
KLX06
185.28
RSMA01
FSM_N
N
Ω: 12.9
T: 2.35E-08
62D8438B2B12D235
KLX06
185.82
RSMA01
FSM_N
N
Ω: 5.7
T: 8.60E-07
8558438B2B12D44B
KLX06
187.64
RSMA01
FSM_N
N
Ω: 7.5
T: 4.49E-08
F798438B2B12DB62
KLX06
188.78
RSMA01
FSM_N
N
Ω: 10.2
T: 1.28E-08
8098438B2B12DFCE
KLX06
189.72
RSMA01
FSM_N
N
Ω: 7.8
T: 6.22E-08
3858438B2B12E377
KLX06
190.06
RSMA01
FSM_N
N
Ω: 13.8
T: 1.82E-08
D418438B2B12E4CE
KLX06
191.98
RSMA01
FSM_N
N
Ω: 6.1
T: 9.37E-08
96D8438B2B12EC40
KLX06
194.32
RSMA01
FSM_N
N
Ω: 8.0
T: 3.83E-08
6D58438B2B12F55E
KLX06
194.98
RSMA01
FSM_N
N
Ω: 7.3
T: 1.38E-07
C898438B2B12F7F1
KLX06
195.50
RSMA01
FSM_N
N
Ω: 7.6
T: 1.46E-08
E458438B2B12F9F0

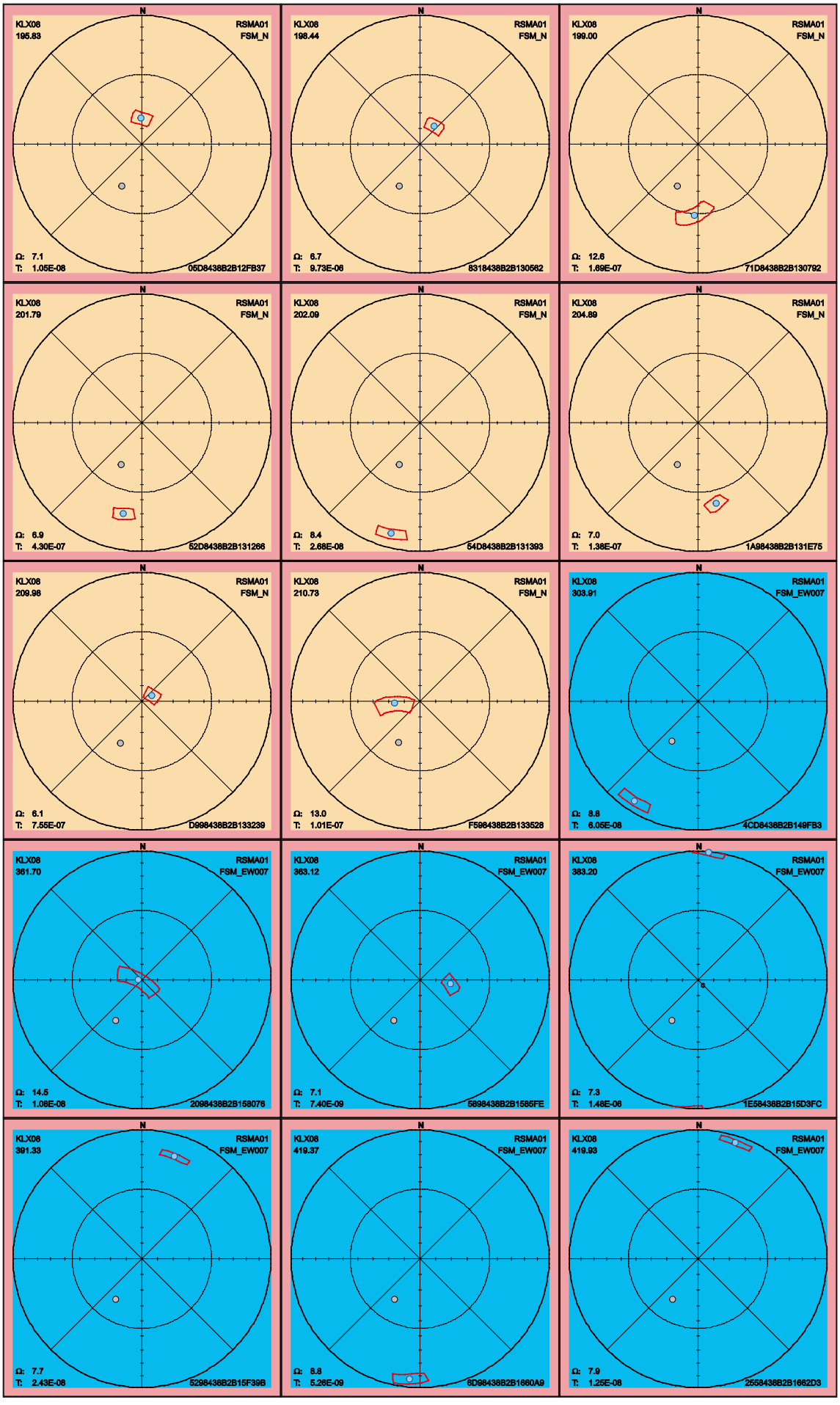
KLX08
195.83
RSMA01
FSM_N
Ω: 7.1
T: 1.05E-08
05D8438B2B12FB37
KLX08
198.44
RSMA01
FSM_N
Ω: 6.7
T: 9.73E-06
8318438B2B130562
KLX08
199.00
RSMA01
FSM_N
Ω: 12.6
T: 1.69E-07
71D8438B2B130792
KLX08
201.79
RSMA01
FSM_N
Ω: 6.9
T: 4.30E-07
52D8438B2B131266
KLX08
202.09
RSMA01
FSM_N
Ω: 8.4
T: 2.68E-08
54D8438B2B131393
KLX08
204.89
RSMA01
FSM_N
Ω: 7.0
T: 1.38E-07
1A98438B2B131E75
KLX08
209.98
RSMA01
FSM_N
Ω: 6.1
T: 7.55E-07
D998438B2B133239
KLX08
210.73
RSMA01
FSM_N
Ω: 13.0
T: 1.01E-07
F598438B2B133528
KLX08
303.91
RSMA01
FSM_EW007
Ω: 8.8
T: 6.05E-08
4CD8438B2B149FB3
KLX08
361.70
RSMA01
FSM_EW007
Ω: 14.5
T: 1.08E-08
2098438B2B158076
KLX08
363.12
RSMA01
FSM_EW007
Ω: 7.1
T: 7.40E-09
5898438B2B1585FE
KLX08
383.20
RSMA01
FSM_EW007
Ω: 7.3
T: 1.48E-08
1E58438B2B15D3FC
KLX08
391.33
RSMA01
FSM_EW007
Ω: 7.7
T: 2.43E-08
5298438B2B15F39B
KLX08
419.37
RSMA01
FSM_EW007
Ω: 8.8
T: 5.26E-09
6D98438B2B1660A9
KLX08
419.93
RSMA01
FSM_EW007
Ω: 7.9
T: 1.25E-08
2558438B2B1662D3

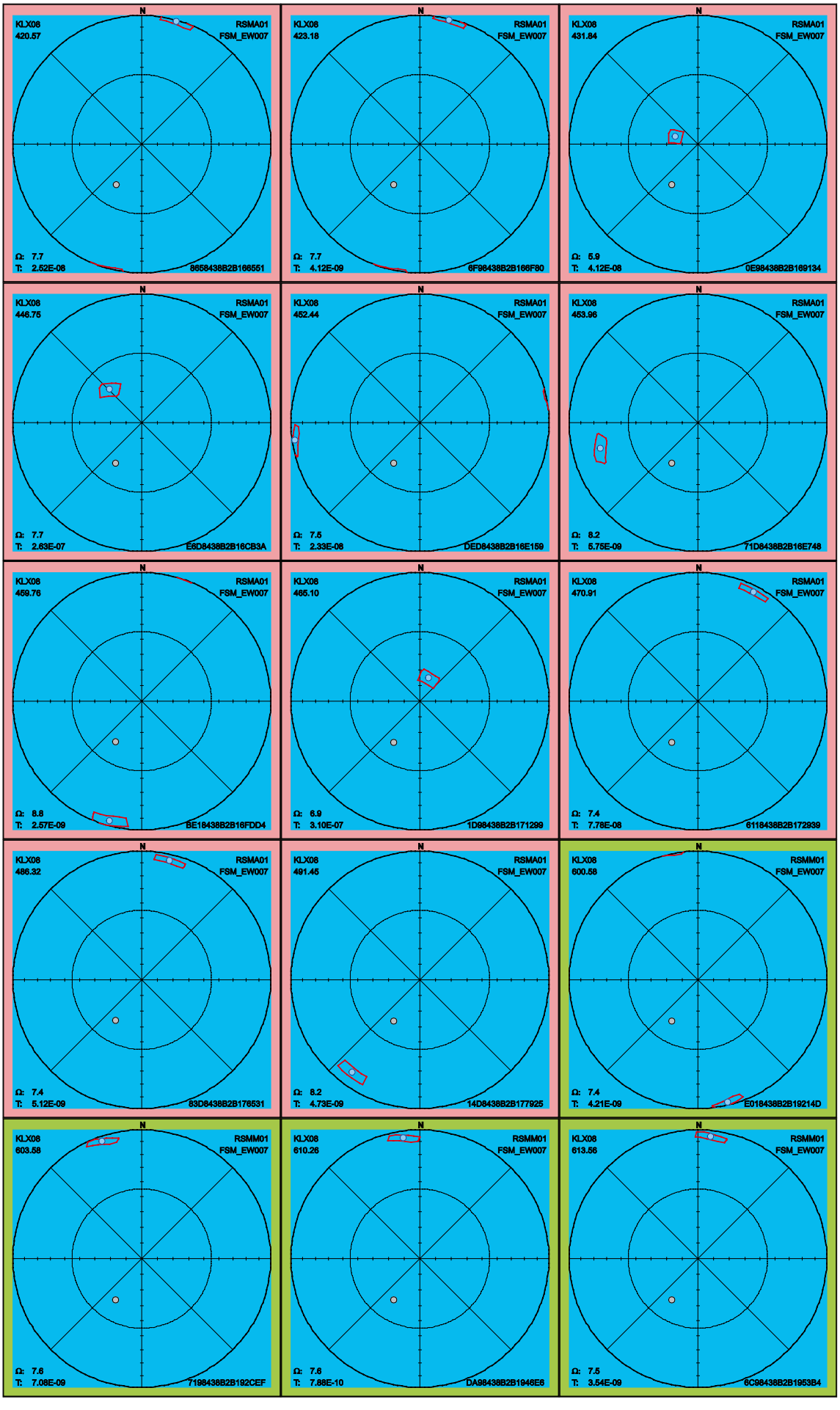
KLX06
420.57
RSMA01
FSM_EW007
Ω: 7.7
T: 2.52E-08
8658438B2B166551
KLX06
423.18
RSMA01
FSM_EW007
Ω: 7.7
T: 4.12E-09
6F98438B2B166F80
KLX06
431.84
RSMA01
FSM_EW007
Ω: 5.9
T: 4.12E-08
0E98438B2B169134
KLX06
446.75
RSMA01
FSM_EW007
Ω: 7.7
T: 2.63E-07
E6D8438B2B16CB3A
KLX06
452.44
RSMA01
FSM_EW007
Ω: 7.5
T: 2.33E-08
DED8438B2B16E159
KLX06
453.96
RSMA01
FSM_EW007
Ω: 8.2
T: 5.75E-09
71D8438B2B16E748
KLX06
459.76
RSMA01
FSM_EW007
Ω: 8.8
T: 2.57E-09
BE18438B2B16FDD4
KLX06
465.10
RSMA01
FSM_EW007
Ω: 6.9
T: 3.10E-07
1D98438B2B171299
KLX06
470.91
RSMA01
FSM_EW007
Ω: 7.4
T: 7.78E-08
6118438B2B172939
KLX06
486.32
RSMA01
FSM_EW007
Ω: 7.4
T: 5.12E-09
83D8438B2B176531
KLX06
491.45
RSMA01
FSM_EW007
Ω: 8.2
T: 4.73E-09
14D8438B2B177925
KLX06
600.58
RSMM01
FSM_EW007
Ω: 7.4
T: 4.21E-09
E018438B2B19214D
KLX06
603.58
RSMM01
FSM_EW007
Ω: 7.6
T: 7.08E-09
7198438B2B192CEF
KLX06
610.26
RSMM01
FSM_EW007
Ω: 7.6
T: 7.88E-10
DA98438B2B1946E8
KLX06
613.56
RSMM01
FSM_EW007
Ω: 7.5
T: 3.54E-09
6C98438B2B1953B4

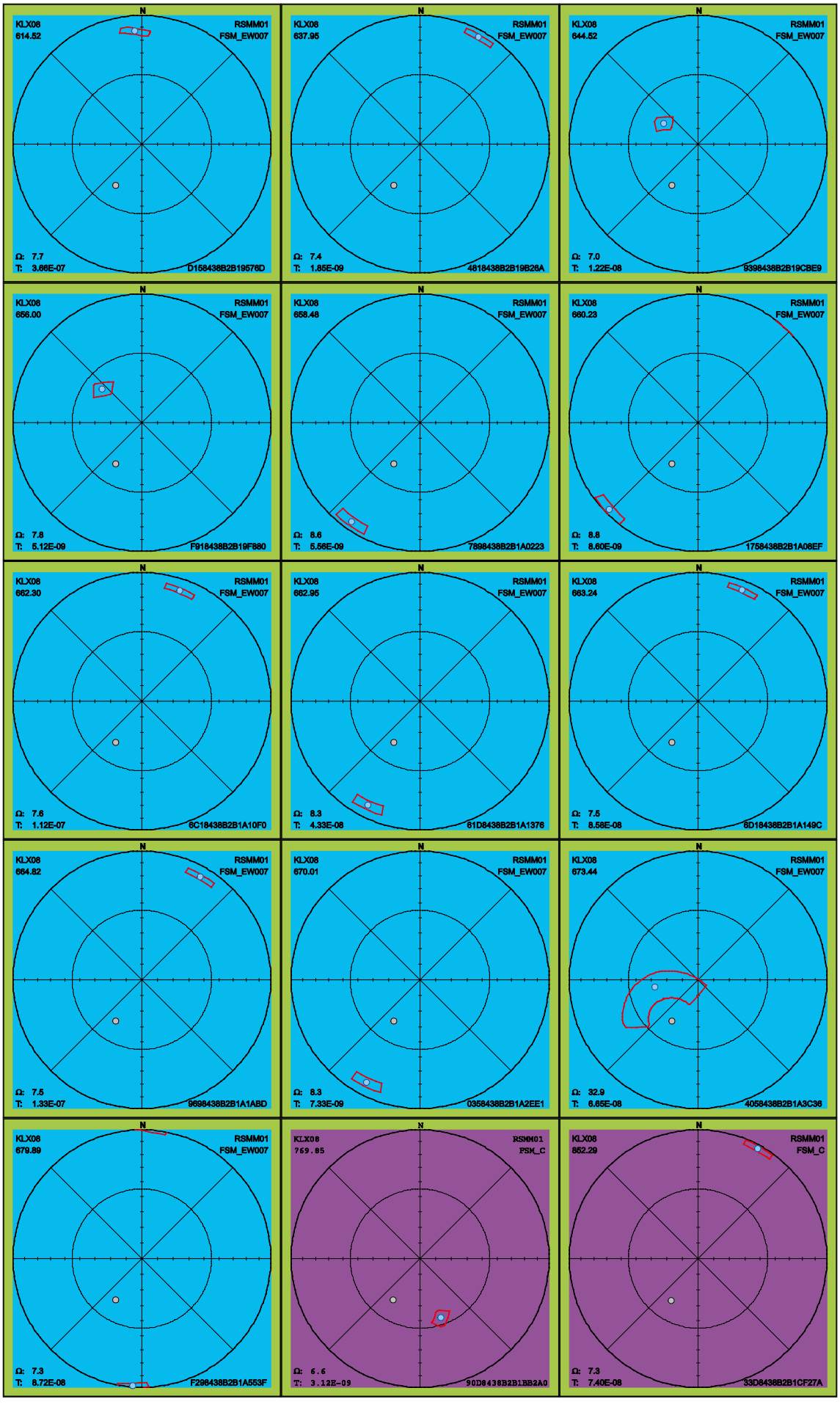
KLX08
614.52
RSMM01
FSM_EW007
Ω: 7.7
T: 3.66E-07
D158438B2B19576D
KLX08
637.95
RSMM01
FSM_EW007
Ω: 7.4
T: 1.85E-09
4818438B2B19B26A
KLX08
644.52
RSMM01
FSM_EW007
Ω: 7.0
T: 1.22E-08
9398438B2B19CBE9
KLX08
656.00
RSMM01
FSM_EW007
Ω: 7.8
T: 5.12E-09
F918438B2B19F880
KLX08
658.48
RSMM01
FSM_EW007
Ω: 8.6
T: 5.56E-09
7898438B2B1A0223
KLX08
660.23
RSMM01
FSM_EW007
Ω: 8.8
T: 8.60E-09
1758438B2B1A08EF
KLX08
662.30
RSMM01
FSM_EW007
Ω: 7.6
T: 1.12E-07
6C18438B2B1A10F0
KLX08
662.95
RSMM01
FSM_EW007
Ω: 8.3
T: 4.33E-08
61D8438B2B1A1376
KLX08
663.24
RSMM01
FSM_EW007
Ω: 7.5
T: 8.58E-08
6D18438B2B1A149C
KLX08
664.82
RSMM01
FSM_EW007
Ω: 7.5
T: 1.33E-07
9698438B2B1A1ABD
KLX08
670.01
RSMM01
FSM_EW007
Ω: 8.3
T: 7.33E-09
0358438B2B1A2EE1
KLX08
673.44
RSMM01
FSM_EW007
Ω: 32.9
T: 6.65E-08
4058438B2B1A3C36
KLX08
679.89
RSMM01
FSM_EW007
Ω: 7.3
T: 8.72E-08
F298438B2B1A553F
KLX08
769.85
RSMM01
FSM_C
Ω: 6.6
T: 3.12E-09
90D8438B2B1BB2A0
KLX08
852.29
RSMM01
FSM_C
Ω: 7.3
T: 7.40E-08
33D8438B2B1CF27A

2.3.8 KLX09

In KLX09 there is one PFL fracture missing orientation information and thus omitted from this section of sample space stereograms. Below follow the 90th percentile sample space of uncertainty for the remaining 52 PFL fractures. No PFL fractures have maximum uncertainty larger than 30°.

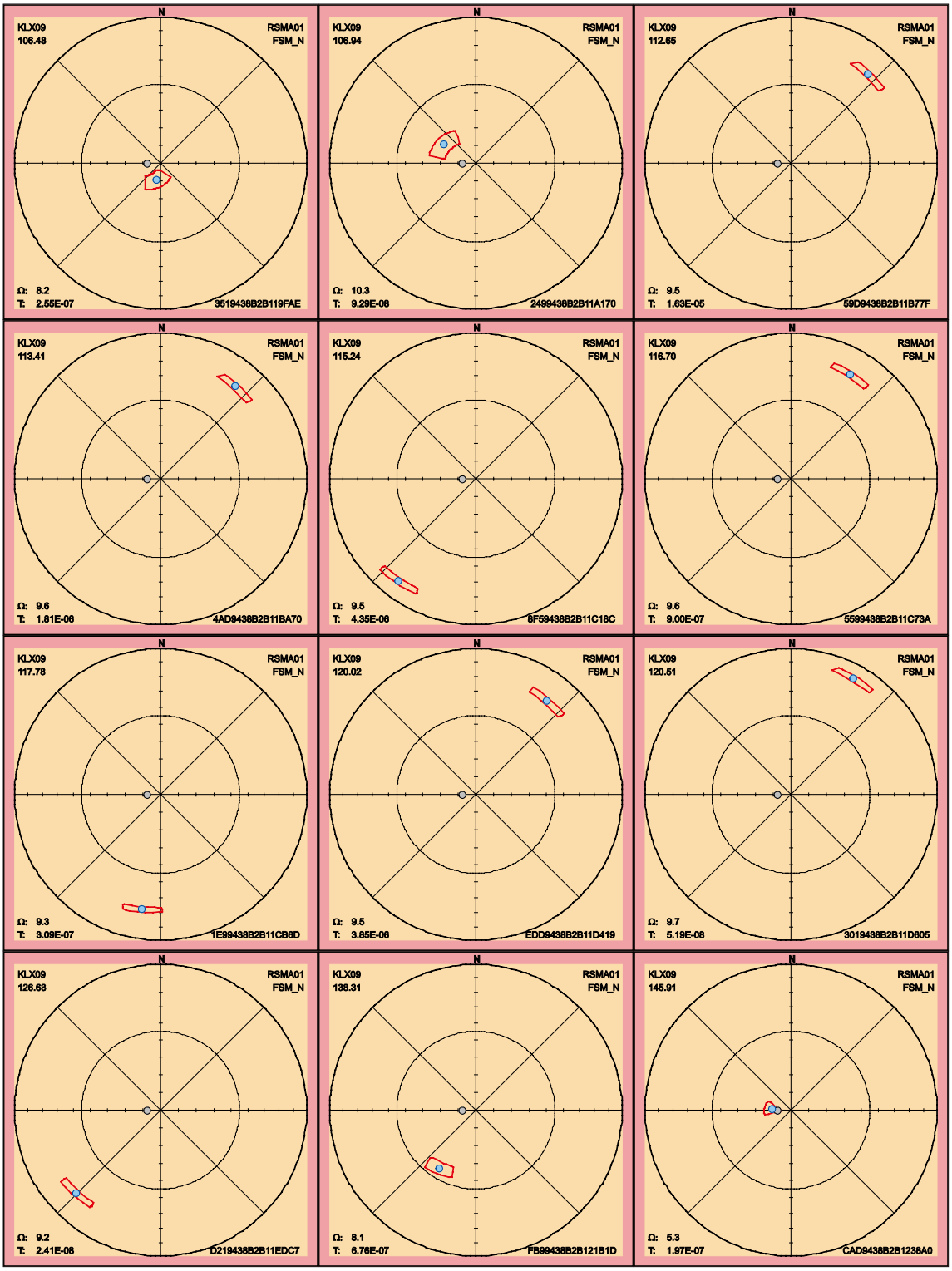

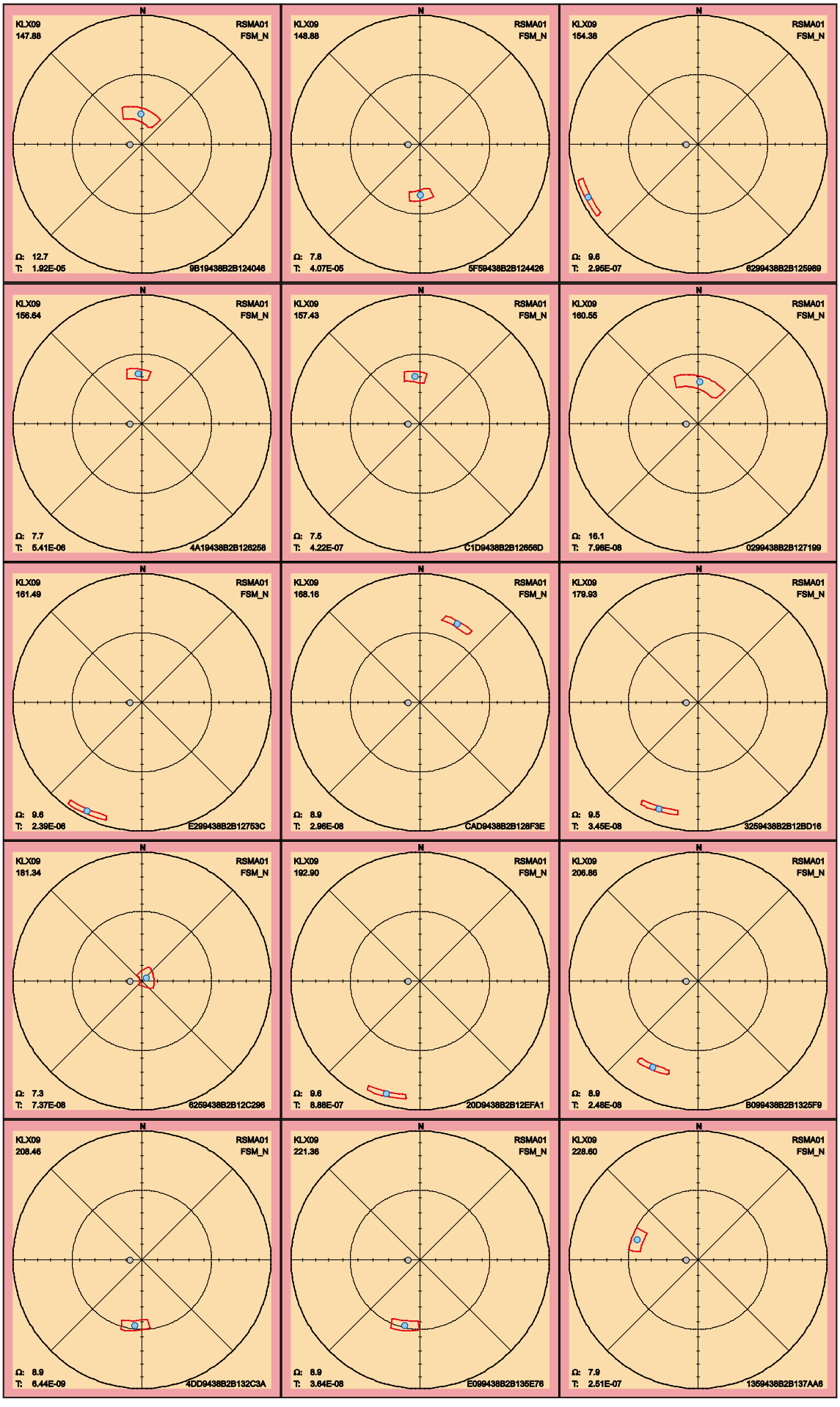
KLX09
147.88
RSMA01
FSM_N
N
Ω: 12.7
T: 1.92E-05
9B19438B2B124046
KLX09
148.88
RSMA01
FSM_N
N
Ω: 7.8
T: 4.07E-05
5F59438B2B124426
KLX09
154.38
RSMA01
FSM_N
N
Ω: 9.6
T: 2.95E-07
6299438B2B125989
KLX09
156.64
RSMA01
FSM_N
N
Ω: 7.7
T: 5.41E-06
4A19438B2B126258
KLX09
157.43
RSMA01
FSM_N
N
Ω: 7.5
T: 4.22E-07
C1D9438B2B12656D
KLX09
160.55
RSMA01
FSM_N
N
Ω: 16.1
T: 7.98E-08
0299438B2B127199
KLX09
161.49
RSMA01
FSM_N
N
Ω: 9.6
T: 2.39E-06
E299438B2B12753C
KLX09
168.16
RSMA01
FSM_N
N
Ω: 8.9
T: 2.96E-08
CAD9438B2B128F3E
KLX09
179.93
RSMA01
FSM_N
N
Ω: 9.5
T: 3.45E-08
3259438B2B12BD16
KLX09
181.34
RSMA01
FSM_N
N
Ω: 7.3
T: 7.37E-08
6259438B2B12C296
KLX09
192.90
RSMA01
FSM_N
N
Ω: 9.6
T: 8.88E-07
20D9438B2B12EFA1
KLX09
206.86
RSMA01
FSM_N
N
Ω: 8.9
T: 2.48E-08
B099438B2B1325F9
KLX09
208.46
RSMA01
FSM_N
N
Ω: 8.9
T: 6.44E-09
4DD9438B2B132C3A
KLX09
221.36
RSMA01
FSM_N
N
Ω: 8.9
T: 3.64E-08
E099438B2B135E76
KLX09
228.60
RSMA01
FSM_N
N
Ω: 7.9
T: 2.51E-07
1359438B2B137AA6

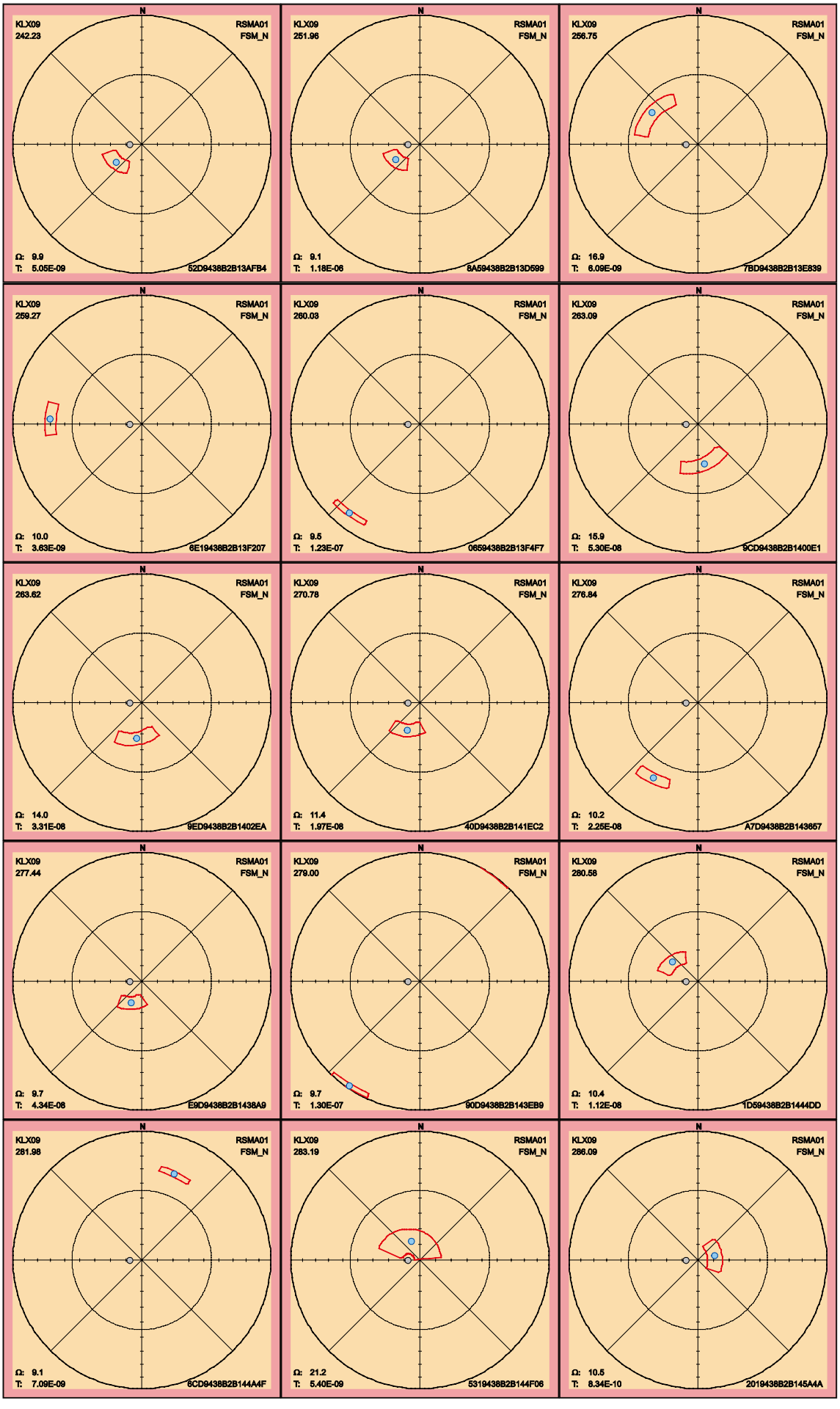
KLX09
242.23
RSMA01
FSM_N
N
Ω: 9.9
T: 5.05E-09
52D9438B2B13AFB4
KLX09
251.96
RSMA01
FSM_N
N
Ω: 9.1
T: 1.18E-06
8A59438B2B13D599
KLX09
256.75
RSMA01
FSM_N
N
Ω: 16.9
T: 6.09E-09
7BD9438B2B13E839
KLX09
259.27
RSMA01
FSM_N
N
Ω: 10.0
T: 3.63E-09
6E19438B2B13F207
KLX09
260.03
RSMA01
FSM_N
N
Ω: 9.5
T: 1.23E-07
0659438B2B13F4F7
KLX09
263.09
RSMA01
FSM_N
N
Ω: 15.9
T: 5.30E-08
9CD9438B2B1400E1
KLX09
263.62
RSMA01
FSM_N
N
Ω: 14.0
T: 3.31E-08
9ED9438B2B1402EA
KLX09
270.78
RSMA01
FSM_N
N
Ω: 11.4
T: 1.97E-08
40D9438B2B141EC2
KLX09
276.84
RSMA01
FSM_N
N
Ω: 10.2
T: 2.25E-08
A7D9438B2B143657
KLX09
277.44
RSMA01
FSM_N
N
Ω: 9.7
T: 4.34E-08
E9D9438B2B1438A9
KLX09
279.00
RSMA01
FSM_N
N
Ω: 9.7
T: 1.30E-07
90D9438B2B143EB9
KLX09
280.58
RSMA01
FSM_N
N
Ω: 10.4
T: 1.12E-08
1D59438B2B1444DD
KLX09
281.98
RSMA01
FSM_N
N
Ω: 9.1
T: 7.09E-09
6CD9438B2B144A4F
KLX09
283.19
RSMA01
FSM_N
N
Ω: 21.2
T: 5.40E-09
5319438B2B144F06
KLX09
286.09
RSMA01
FSM_N
N
Ω: 10.5
T: 8.34E-10
2019438B2B145A4A

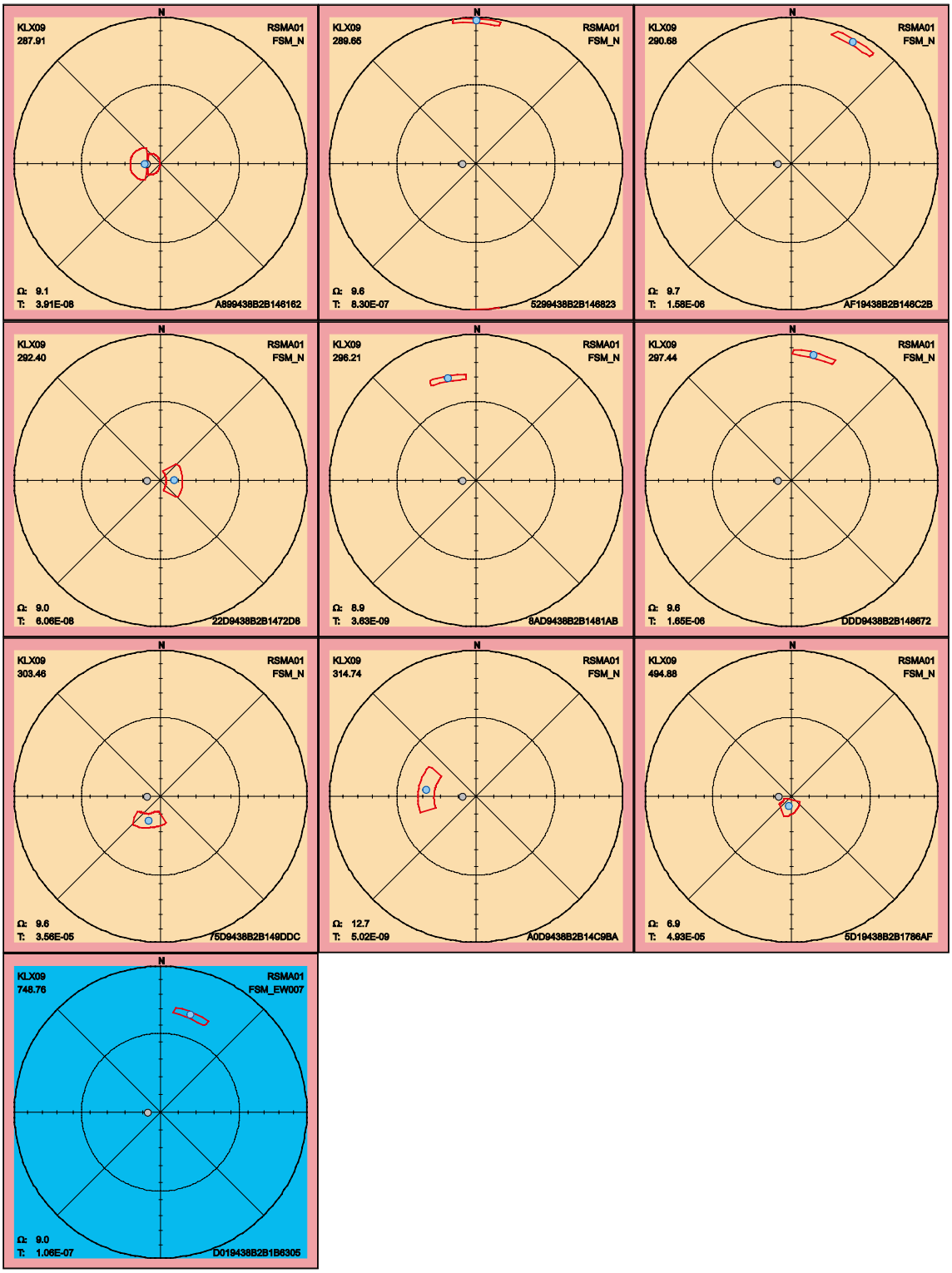
KLX09
287.91
RSMA01
FSM_N
Ω: 9.1
T: 3.91E-08
A899438B2B146162
KLX09
289.65
RSMA01
FSM_N
Ω: 9.6
T: 8.30E-07
5299438B2B146823
KLX09
290.68
RSMA01
FSM_N
Ω: 9.7
T: 1.58E-06
AF19438B2B146C2B
KLX09
292.40
RSMA01
FSM_N
Ω: 9.0
T: 6.06E-08
22D9438B2B1472D8
KLX09
296.21
RSMA01
FSM_N
Ω: 8.9
T: 3.63E-09
8AD9438B2B1481AB
KLX09
297.44
RSMA01
FSM_N
Ω: 9.6
T: 1.65E-06
DDD9438B2B148672
KLX09
303.46
RSMA01
FSM_N
Ω: 9.6
T: 3.56E-05
75D9438B2B149DDC
KLX09
314.74
RSMA01
FSM_N
Ω: 12.7
T: 5.02E-09
A0D9438B2B14C9BA
KLX09
494.88
RSMA01
FSM_N
Ω: 6.9
T: 4.93E-05
5D19438B2B1786AF
KLX09
748.76
RSMA01
FSM_EW007
Ω: 9.0
T: 1.06E-07
D019438B2B1B6305

2.3.9 KLX09B

Of the 44 PFL fractures in KLX09B 36 have maximum uncertainty larger than 30°, see Table 2-10. The 90th percentile sample space of uncertainty for the PFL fractures in KLX09B is shown below and almost all fractures need attention since the fractures having large uncertainty can have an alternative interpretation of orientation compared to the best estimate orientation that is found in the table p_fract_core in /Sicada 2008/.

Table 2-10. Fractures in KLX09B with uncertainty, Ω, larger than 30°.

FeatureId	PFL-f no	Adjusted Secup	Ω
7459438B09103B78	1	15.23	55.2
4599438B09104003	2	16.40	89.6
5999438B09104488	3	17.55	36.1
19D9438B09105D06	5	23.83	82.6
FE99438B09105E31	6	24.13	31.0
FAD9438B09106D40	9	27.99	89.9
4699438B0910791A	10	31.03	36.0
8C19438B09107C32	11	31.82	61.5
8D99438B09107F3A	12	32.60	82.3
CF99438B09109A76	13	39.58	39.0
9B99438B09109BFF	14	39.98	89.6
2559438B0910A743	15	42.87	54.4
6D99438B0910AFB8	16	45.03	48.3
E559438B0910B5B8	17	46.57	60.5
7719438B0910BD57	18	48.53	58.1
0259438B0910C059	19	49.30	52.8
E299438B0910E777	20	59.33	89.9
CC59438B0910E9F6	21	59.96	89.6
94D9438B0910EF3B	22	61.32	90.0
2159438B0910F0D9	23	61.73	90.0
AC59438B0910F836	25	63.62	89.7
8559438B0910FF0D	26	65.37	84.1
2819438B09110889	27	67.80	89.8
E659438B09110E98	29	69.36	89.5
D299438B09112AD5	31	76.60	89.4
5BD9438B09112FE8	32	77.90	37.3
A519438B09113387	33	78.83	89.8
F119438B09113699	34	79.61	89.8
0A99438B09113B5C	35	80.83	89.7
BE99438B09113D75	36	81.37	41.4
0C59438B0911430E	38	82.81	89.6
7899438B091143C9	39	82.99	89.7
CC19438B0911503E	40	86.19	89.9
4319438B091164BB	41	91.44	70.7
DD19438B0911665E	42	91.86	89.8
B2D9438B09117B8B	44	97.29	90.0

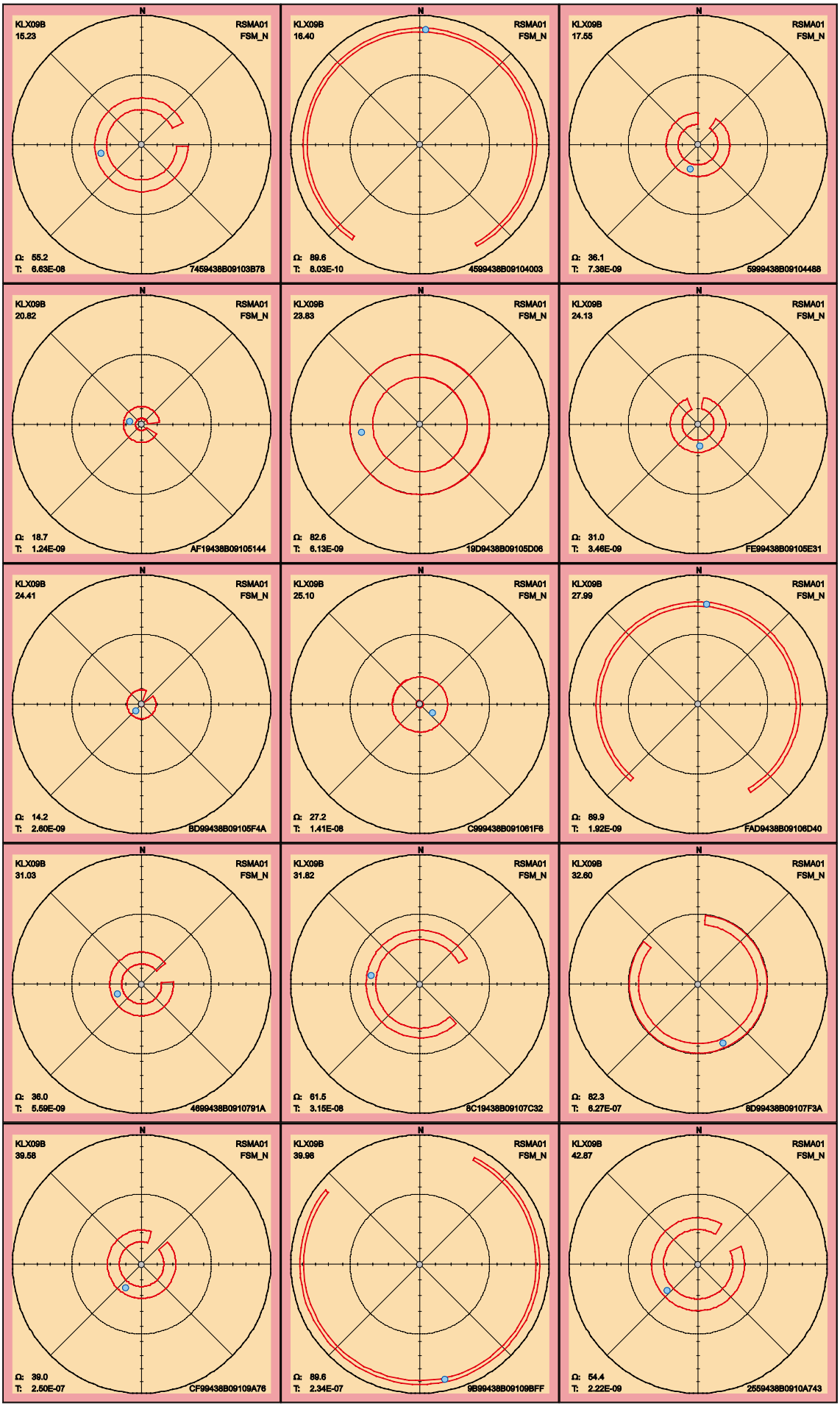
KLX09B
15.23
RSMA01
FSM_N
Ω: 55.2
T: 6.63E-08
7459438B09103B78
KLX09B
16.40
RSMA01
FSM_N
Ω: 89.6
T: 8.03E-10
4599438B09104003
KLX09B
17.55
RSMA01
FSM_N
Ω: 36.1
T: 7.38E-09
5999438B09104488
KLX09B
20.82
RSMA01
FSM_N
Ω: 18.7
T: 1.24E-09
AF19438B09105144
KLX09B
23.83
RSMA01
FSM_N
Ω: 82.6
T: 6.13E-09
19D9438B09105D06
KLX09B
24.13
RSMA01
FSM_N
Ω: 31.0
T: 3.46E-09
FE99438B09105E31
KLX09B
24.41
RSMA01
FSM_N
Ω: 14.2
T: 2.60E-09
BD99438B09105F4A
KLX09B
25.10
RSMA01
FSM_N
Ω: 27.2
T: 1.41E-08
C999438B091061F6
KLX09B
27.99
RSMA01
FSM_N
Ω: 89.9
T: 1.92E-09
FAD9438B09106D40
KLX09B
31.03
RSMA01
FSM_N
Ω: 36.0
T: 5.59E-09
4699438B0910791A
KLX09B
31.82
RSMA01
FSM_N
Ω: 61.5
T: 3.15E-08
6C19438B09107C32
KLX09B
32.60
RSMA01
FSM_N
Ω: 82.3
T: 6.27E-07
8D99438B09107F3A
KLX09B
39.58
RSMA01
FSM_N
Ω: 39.0
T: 2.50E-07
CF99438B09109A76
KLX09B
39.98
RSMA01
FSM_N
Ω: 89.6
T: 2.34E-07
9B99438B09109BFF
KLX09B
42.87
RSMA01
FSM_N
Ω: 54.4
T: 2.22E-09
2559438B0910A743

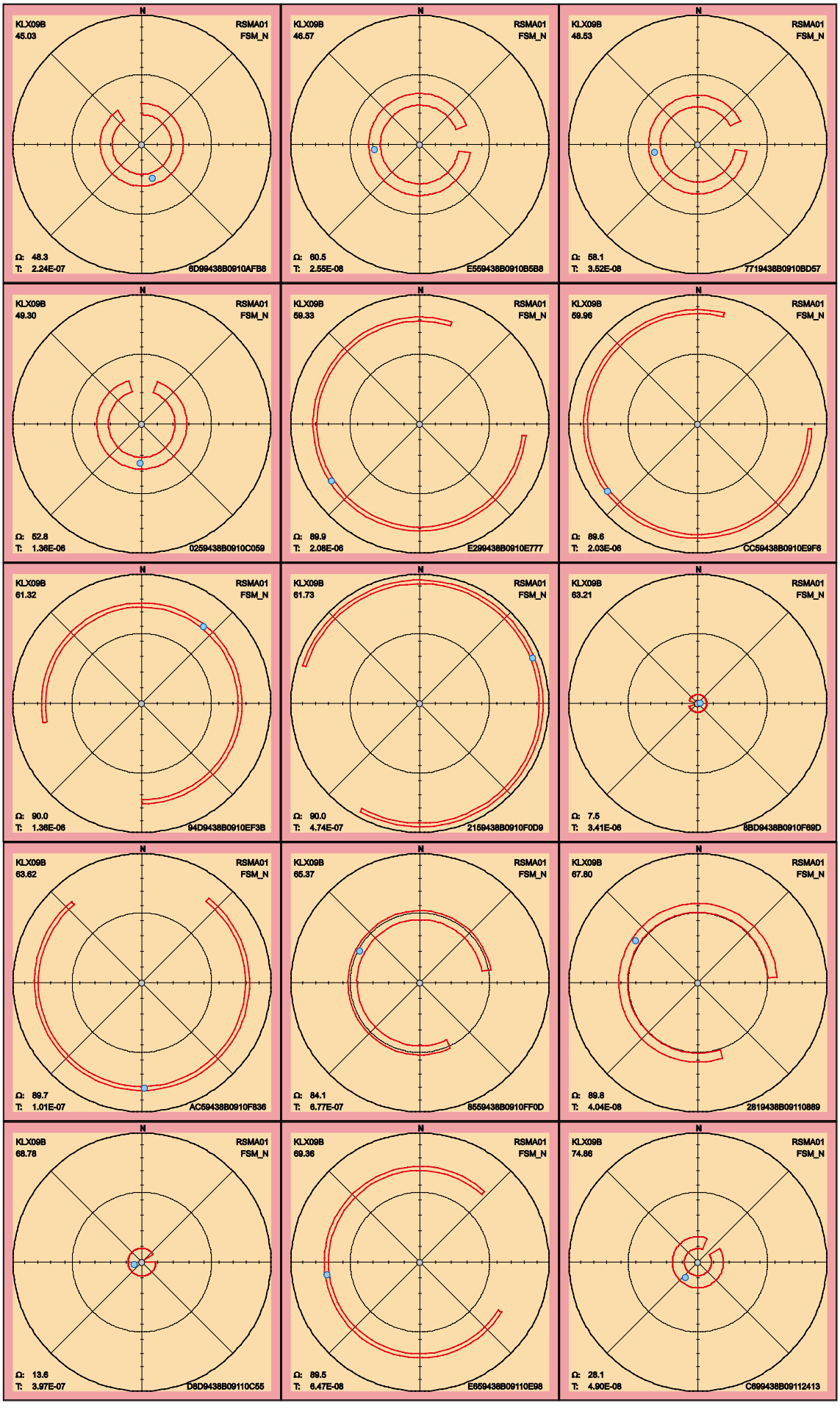
KLX09B
45.03
RSMA01
FSM_N
N
Ω: 48.3
T: 2.24E-07
6D99438B0910AFB8
KLX09B
46.57
RSMA01
FSM_N
N
Ω: 60.5
T: 2.55E-06
E559438B0910B5B8
KLX09B
48.53
RSMA01
FSM_N
N
Ω: 58.1
T: 3.52E-08
7719438B0910BD57
KLX09B
49.30
RSMA01
FSM_N
N
Ω: 52.8
T: 1.36E-06
0259438B0910C059
KLX09B
59.33
RSMA01
FSM_N
N
Ω: 89.9
T: 2.08E-06
E299438B0910E777
KLX09B
59.96
RSMA01
FSM_N
N
Ω: 89.6
T: 2.03E-06
CC59438B0910E9F6
KLX09B
61.32
RSMA01
FSM_N
N
Ω: 90.0
T: 1.36E-06
94D9438B0910EF3B
KLX09B
61.73
RSMA01
FSM_N
N
Ω: 90.0
T: 4.74E-07
2159438B0910F0D9
KLX09B
63.21
RSMA01
FSM_N
N
Ω: 7.5
T: 3.41E-06
8BD9438B0910F69D
KLX09B
63.62
RSMA01
FSM_N
N
Ω: 89.7
T: 1.01E-07
AC59438B0910F836
KLX09B
65.37
RSMA01
FSM_N
N
Ω: 84.1
T: 6.77E-07
8559438B0910FF0D
KLX09B
67.80
RSMA01
FSM_N
N
Ω: 89.8
T: 4.04E-08
2819438B09110889
KLX09B
68.78
RSMA01
FSM_N
N
Ω: 13.6
T: 3.97E-07
D8D9438B09110C55
KLX09B
69.36
RSMA01
FSM_N
N
Ω: 89.5
T: 6.47E-08
E659438B09110E98
KLX09B
74.86
RSMA01
FSM_N
N
Ω: 28.1
T: 4.90E-08
C899438B09112413

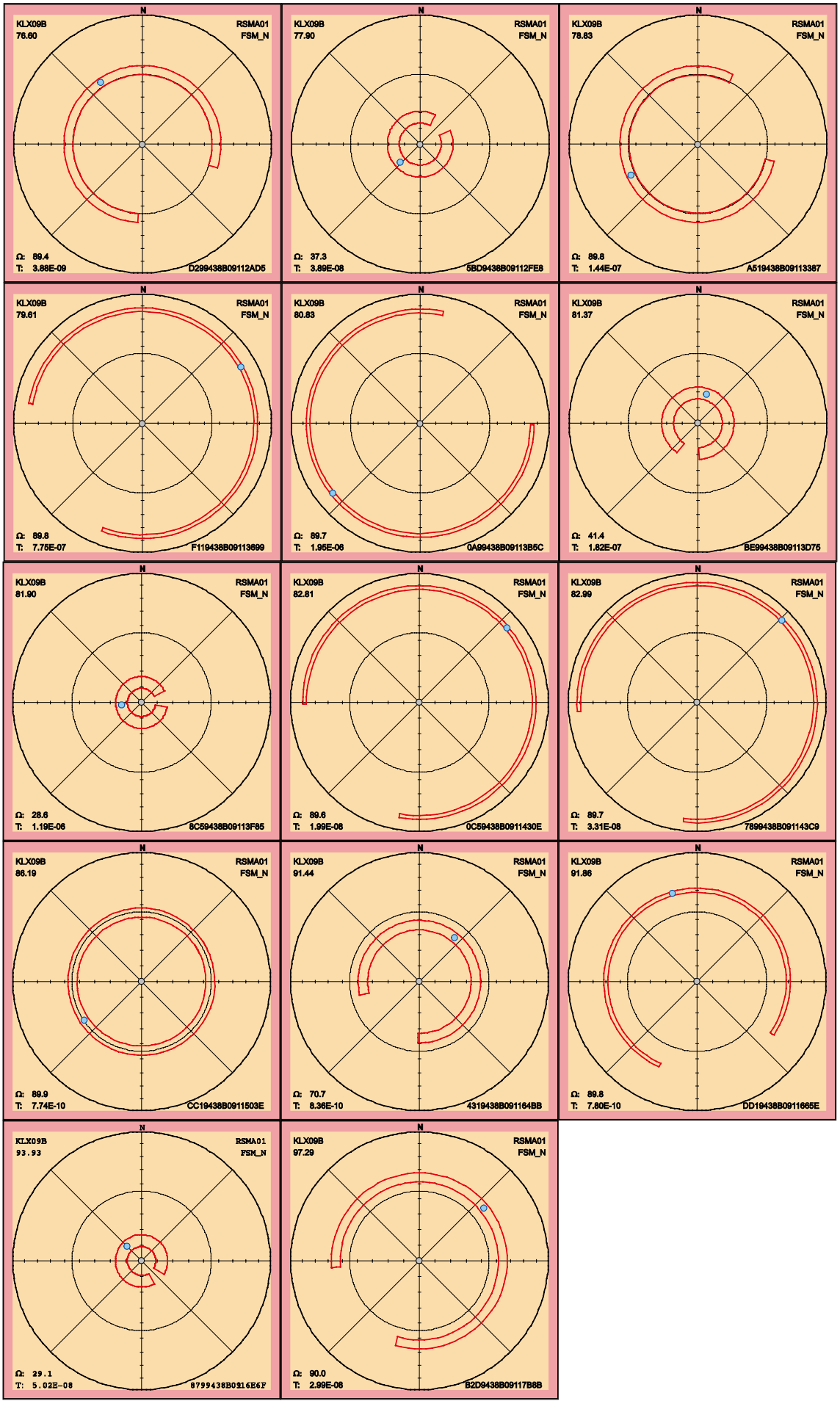
KLX09B
76.60
RSMA01
FSM_N
Ω: 89.4
T: 3.88E-09
D299438B09112AD5
KLX09B
77.90
RSMA01
FSM_N
Ω: 37.3
T: 3.89E-08
5BD9438B09112FE8
KLX09B
78.83
RSMA01
FSM_N
Ω: 89.8
T: 1.44E-07
A519438B09113387
KLX09B
79.61
RSMA01
FSM_N
Ω: 89.8
T: 7.75E-07
F119438B09113699
KLX09B
80.83
RSMA01
FSM_N
Ω: 89.7
T: 1.95E-06
0A99438B09113B5C
KLX09B
81.37
RSMA01
FSM_N
Ω: 41.4
T: 1.82E-07
BE99438B09113D75
KLX09B
81.90
RSMA01
FSM_N
Ω: 28.6
T: 1.19E-06
8C59438B09113F85
KLX09B
82.81
RSMA01
FSM_N
Ω: 89.6
T: 1.99E-08
0C59438B0911430E
KLX09B
82.99
RSMA01
FSM_N
Ω: 89.7
T: 3.31E-08
7899438B091143C9
KLX09B
86.19
RSMA01
FSM_N
Ω: 89.9
T: 7.74E-10
CC19438B0911503E
KLX09B
91.44
RSMA01
FSM_N
Ω: 70.7
T: 8.36E-10
4319438B091164BB
KLX09B
91.86
RSMA01
FSM_N
Ω: 89.8
T: 7.80E-10
DD19438B0911685E
KLX09B
93.93
RSMA01
FSM_N
Ω: 29.1
T: 5.02E-08
8799438B0916E6F
KLX09B
97.29
RSMA01
FSM_N
Ω: 90.0
T: 2.99E-08
B2D9438B09117B8B

2.3.10 KLX09C

No one of the 36 PFL fractures in KLX09C have Maximum uncertainty larger than 30°. The 90th percentile sample space of uncertainty follows below.

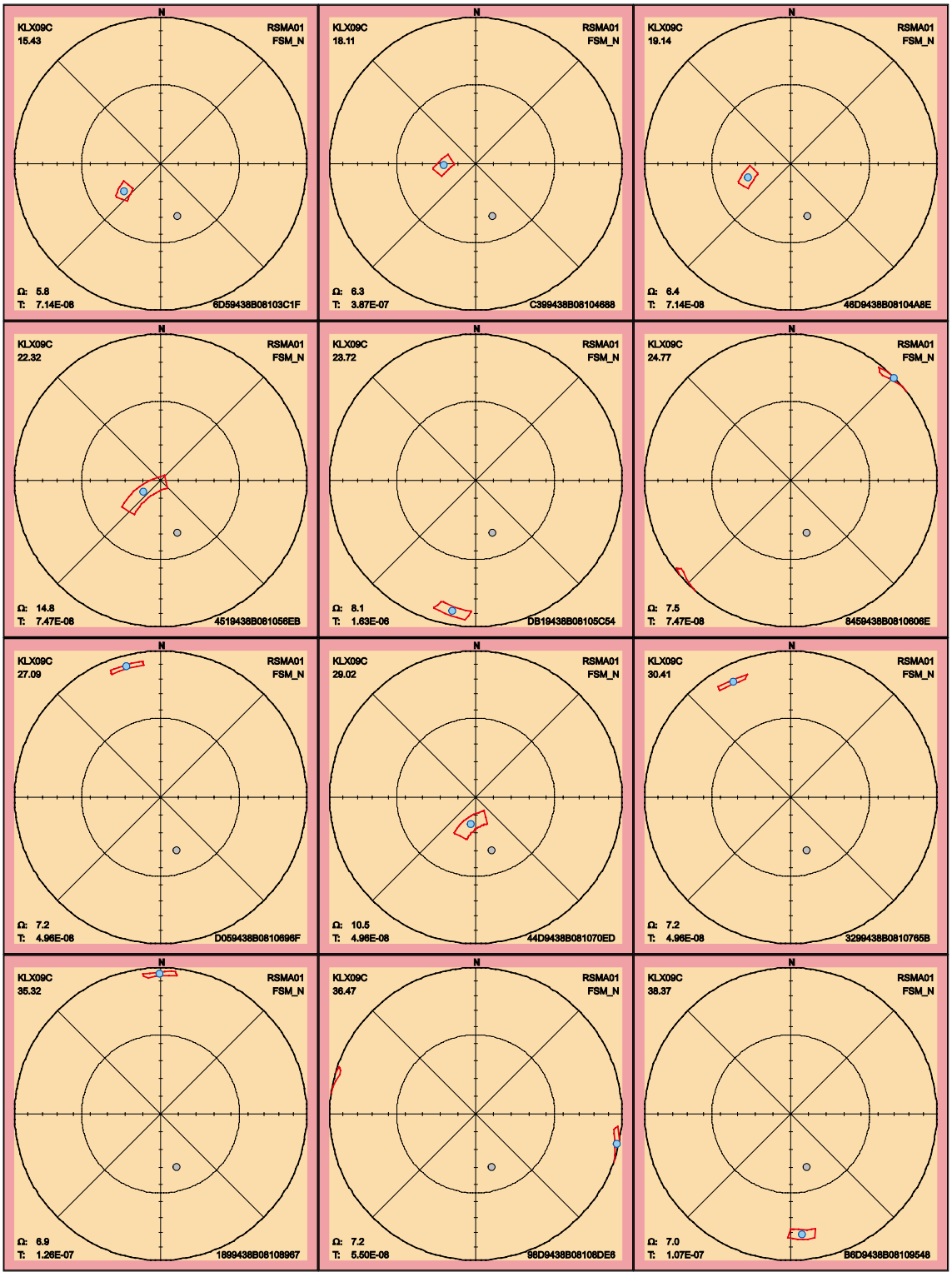

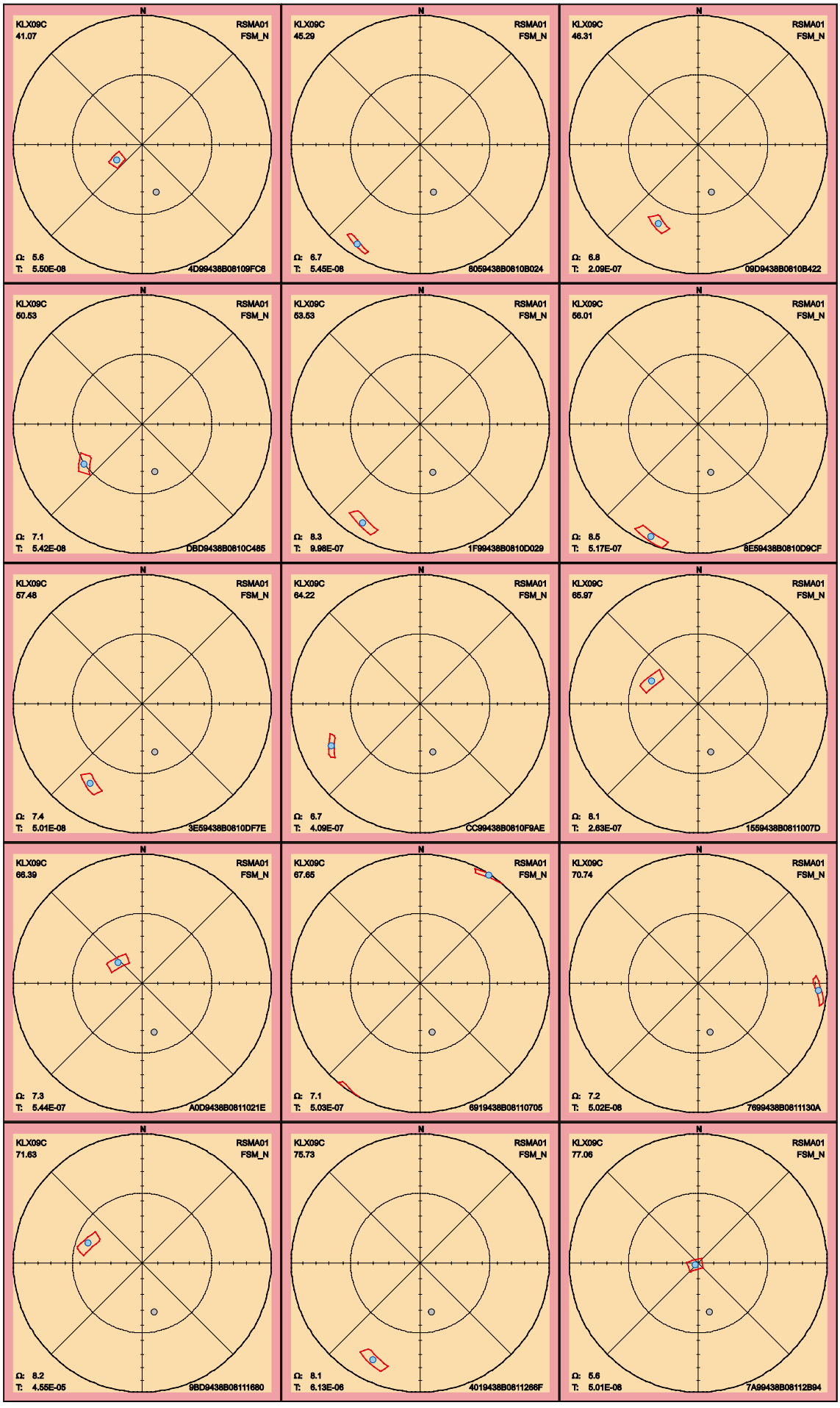
KLX09C
41.07
RSMA01
FSM_N
Ω: 5.6
T: 5.50E-08
4D99438B08109FC6
KLX09C
45.29
RSMA01
FSM_N
Ω: 6.7
T: 5.45E-08
8059438B0810B024
KLX09C
46.31
RSMA01
FSM_N
Ω: 6.8
T: 2.09E-07
09D9438B0810B422
KLX09C
50.53
RSMA01
FSM_N
Ω: 7.1
T: 5.42E-08
DBD9438B0810C485
KLX09C
53.53
RSMA01
FSM_N
Ω: 8.3
T: 9.98E-07
1F99438B0810D029
KLX09C
56.01
RSMA01
FSM_N
Ω: 8.5
T: 5.17E-07
8E59438B0810D9CF
KLX09C
57.48
RSMA01
FSM_N
Ω: 7.4
T: 5.01E-08
3E59438B0810DF7E
KLX09C
64.22
RSMA01
FSM_N
Ω: 6.7
T: 4.09E-07
CC99438B0810F9AE
KLX09C
65.97
RSMA01
FSM_N
Ω: 8.1
T: 2.63E-07
1559438B0811007D
KLX09C
66.39
RSMA01
FSM_N
Ω: 7.3
T: 5.44E-07
A0D9438B0811021E
KLX09C
67.65
RSMA01
FSM_N
Ω: 7.1
T: 5.03E-07
6919438B08110705
KLX09C
70.74
RSMA01
FSM_N
Ω: 7.2
T: 5.02E-08
7699438B0811130A
KLX09C
71.63
RSMA01
FSM_N
Ω: 8.2
T: 4.55E-05
9BD9438B08111680
KLX09C
75.73
RSMA01
FSM_N
Ω: 8.1
T: 6.13E-06
4019438B0811266F
KLX09C
77.06
RSMA01
FSM_N
Ω: 5.6
T: 5.01E-08
7A99438B08112B94

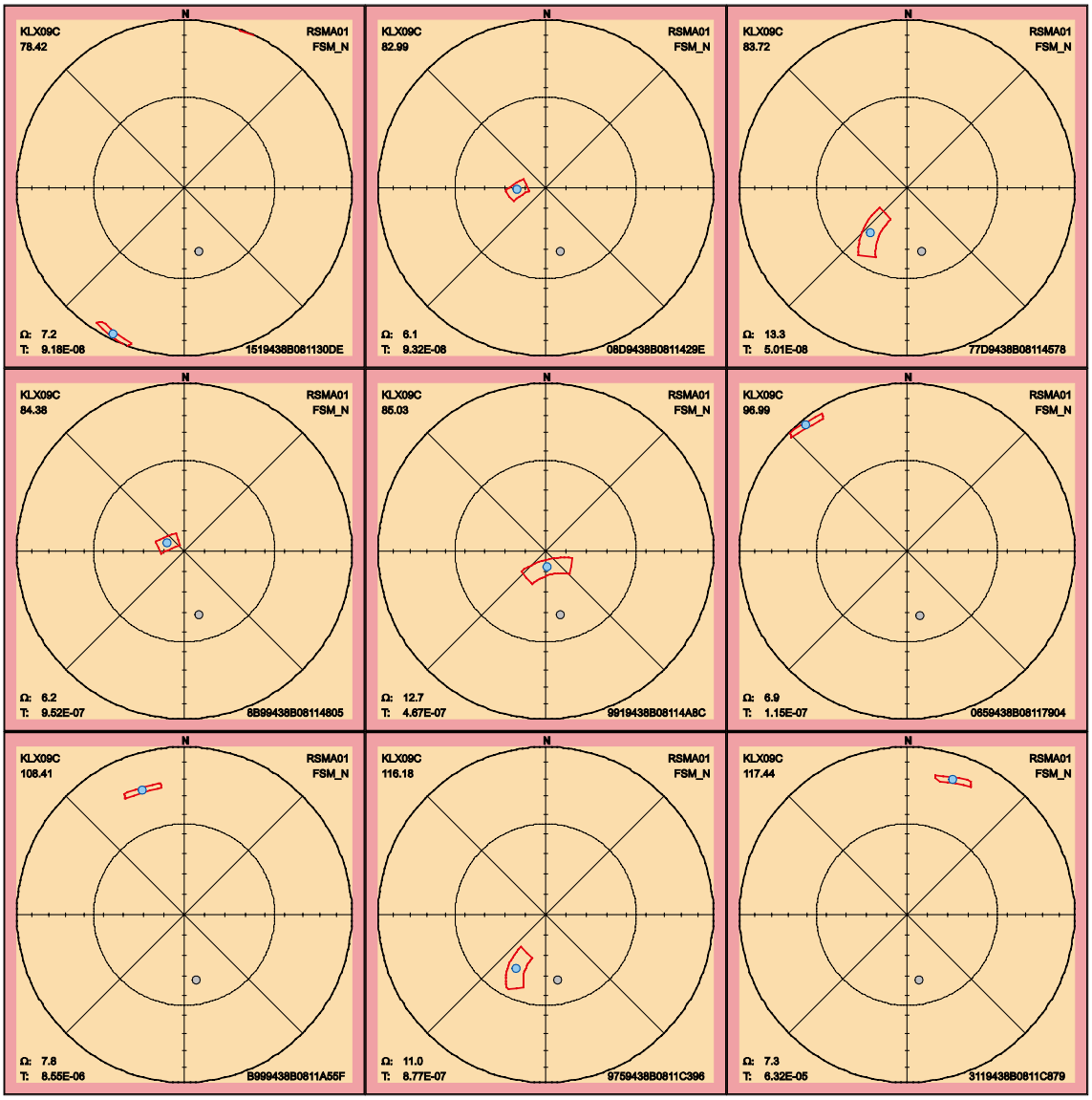

2.3.11 KLX09D

Below follow the 90th percentile sample space of uncertainty for the 41 PFL fractures in KLX09D. Attention should be paid to the four fractures listed in Table 2-11. These fractures have a maximum uncertainty, on the 90th percentile, larger than 30° and thus having uncertainty that can be interpreted differently compared to the best estimate orientation that is found in the table p_fract_core in /Sicada 2008/.

Table 2-11. Fractures in KLX09D with uncertainty, Ω, larger than 30°.

FeatureId	PFL-f no	Adjusted Secup	Ω
CE19438B0F10D9BF	18	56.17	55.3
A0D9438B0F113E65	26	82.17	32.1
42D9438B0F114618	29	84.16	57.3
3499438B0F114CC1	32	85.88	47.3

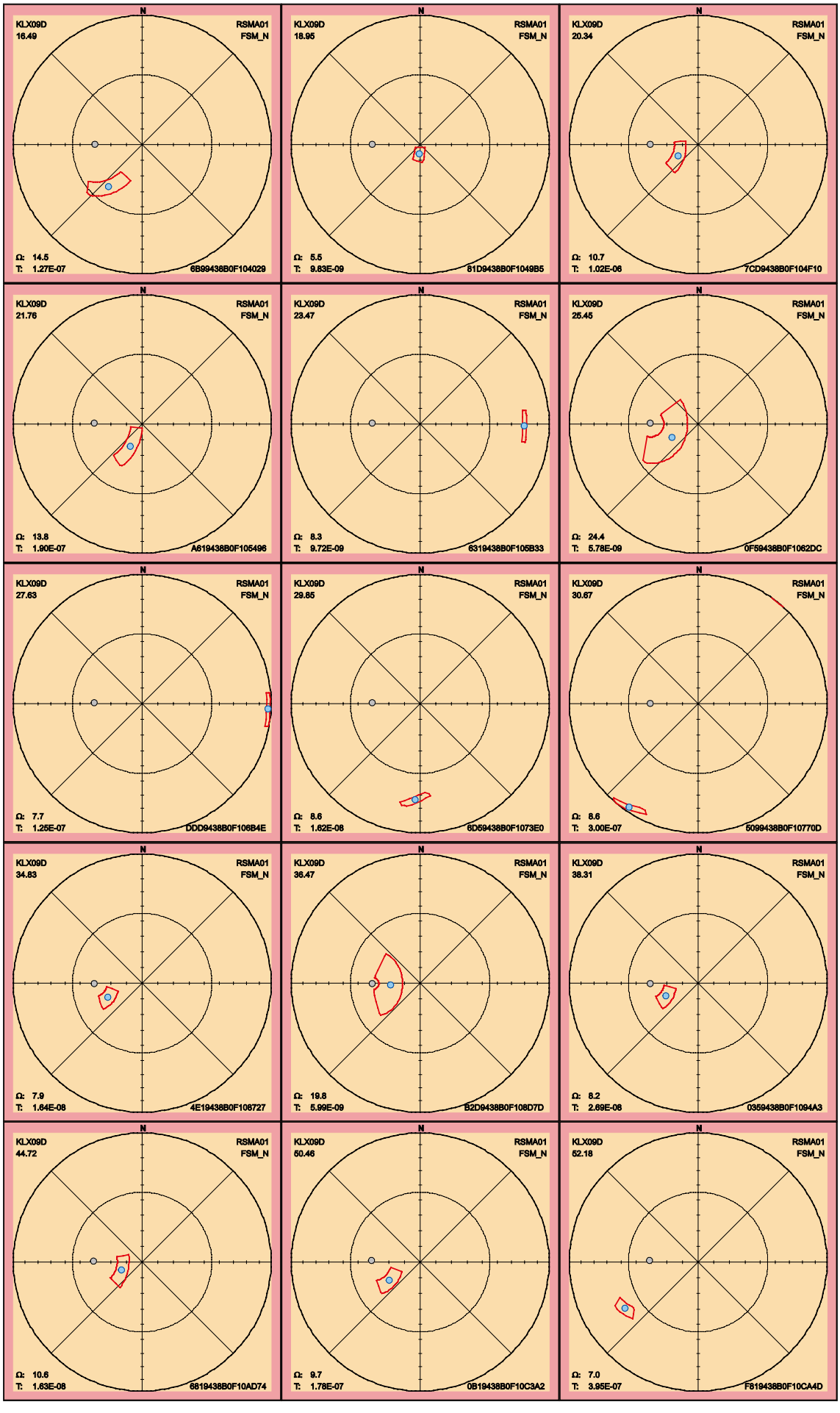
KLX09D
16.49
RSMA01
FSM_N
Ω: 14.5
T: 1.27E-07
6B99438B0F104029
KLX09D
18.95
RSMA01
FSM_N
Ω: 5.5
T: 9.83E-09
81D9438B0F1049B5
KLX09D
20.34
RSMA01
FSM_N
Ω: 10.7
T: 1.02E-06
7CD9438B0F104F10
KLX09D
21.76
RSMA01
FSM_N
Ω: 13.8
T: 1.90E-07
A619438B0F105496
KLX09D
23.47
RSMA01
FSM_N
Ω: 8.3
T: 9.72E-09
6319438B0F105B33
KLX09D
25.45
RSMA01
FSM_N
Ω: 24.4
T: 5.78E-09
0F59438B0F1062DC
KLX09D
27.63
RSMA01
FSM_N
Ω: 7.7
T: 1.25E-07
DDD9438B0F106B4E
KLX09D
29.85
RSMA01
FSM_N
Ω: 8.6
T: 1.62E-08
6D59438B0F1073E0
KLX09D
30.67
RSMA01
FSM_N
Ω: 8.6
T: 3.00E-07
5099438B0F10770D
KLX09D
34.83
RSMA01
FSM_N
Ω: 7.9
T: 1.64E-08
4E19438B0F106727
KLX09D
36.47
RSMA01
FSM_N
Ω: 19.8
T: 5.99E-09
B2D9438B0F108D7D
KLX09D
38.31
RSMA01
FSM_N
Ω: 8.2
T: 2.69E-08
0359438B0F1094A3
KLX09D
44.72
RSMA01
FSM_N
Ω: 10.6
T: 1.63E-08
6819438B0F10AD74
KLX09D
50.46
RSMA01
FSM_N
Ω: 9.7
T: 1.78E-07
0B19438B0F10C3A2
KLX09D
52.18
RSMA01
FSM_N
Ω: 7.0
T: 3.95E-07
F819438B0F10CA4D

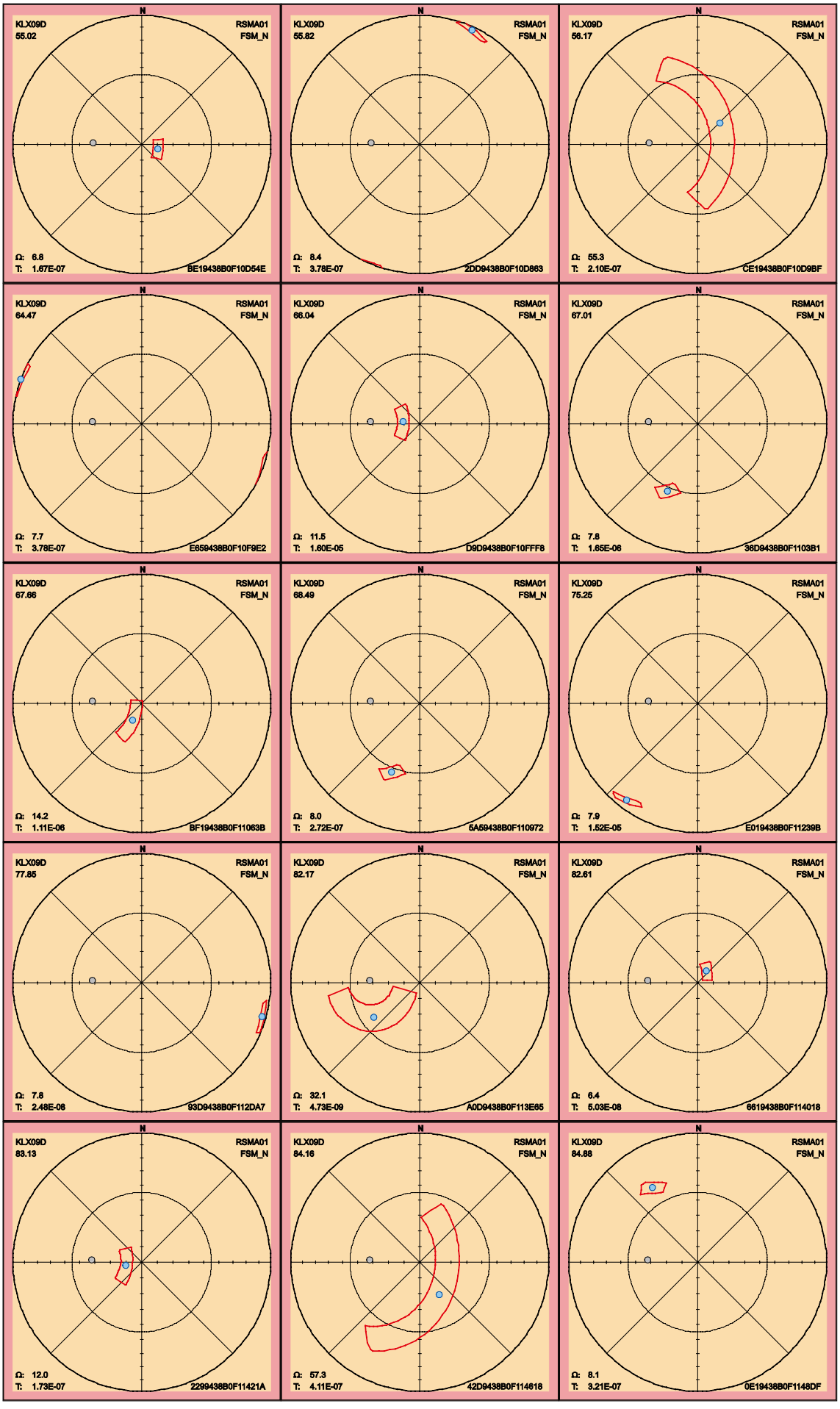
KLX09D
55.02
RSMA01
FSM_N
N
Ω: 6.8
T: 1.67E-07
BE19438B0F10D54E
KLX09D
55.82
RSMA01
FSM_N
N
Ω: 8.4
T: 3.78E-07
2DD9438B0F10D863
KLX09D
56.17
RSMA01
FSM_N
N
Ω: 55.3
T: 2.10E-07
CE19438B0F10D9BF
KLX09D
64.47
RSMA01
FSM_N
N
Ω: 7.7
T: 3.78E-07
E659438B0F10F9E2
KLX09D
66.04
RSMA01
FSM_N
N
Ω: 11.5
T: 1.60E-05
D9D9438B0F10FFF8
KLX09D
67.01
RSMA01
FSM_N
N
Ω: 7.8
T: 1.65E-06
38D9438B0F1103B1
KLX09D
67.66
RSMA01
FSM_N
N
Ω: 14.2
T: 1.11E-06
BF19438B0F11063B
KLX09D
68.49
RSMA01
FSM_N
N
Ω: 8.0
T: 2.72E-07
5A59438B0F110972
KLX09D
75.25
RSMA01
FSM_N
N
Ω: 7.9
T: 1.52E-05
E019438B0F11239B
KLX09D
77.85
RSMA01
FSM_N
N
Ω: 7.8
T: 2.48E-06
93D9438B0F112DA7
KLX09D
82.17
RSMA01
FSM_N
N
Ω: 32.1
T: 4.73E-09
A0D9438B0F113E65
KLX09D
82.61
RSMA01
FSM_N
N
Ω: 6.4
T: 5.03E-08
6619438B0F114018
KLX09D
83.13
RSMA01
FSM_N
N
Ω: 12.0
T: 1.73E-07
2299438B0F11421A
KLX09D
84.16
RSMA01
FSM_N
N
Ω: 57.3
T: 4.11E-07
42D9438B0F114618
KLX09D
84.88
RSMA01
FSM_N
N
Ω: 8.1
T: 3.21E-07
0E19438B0F1148DF

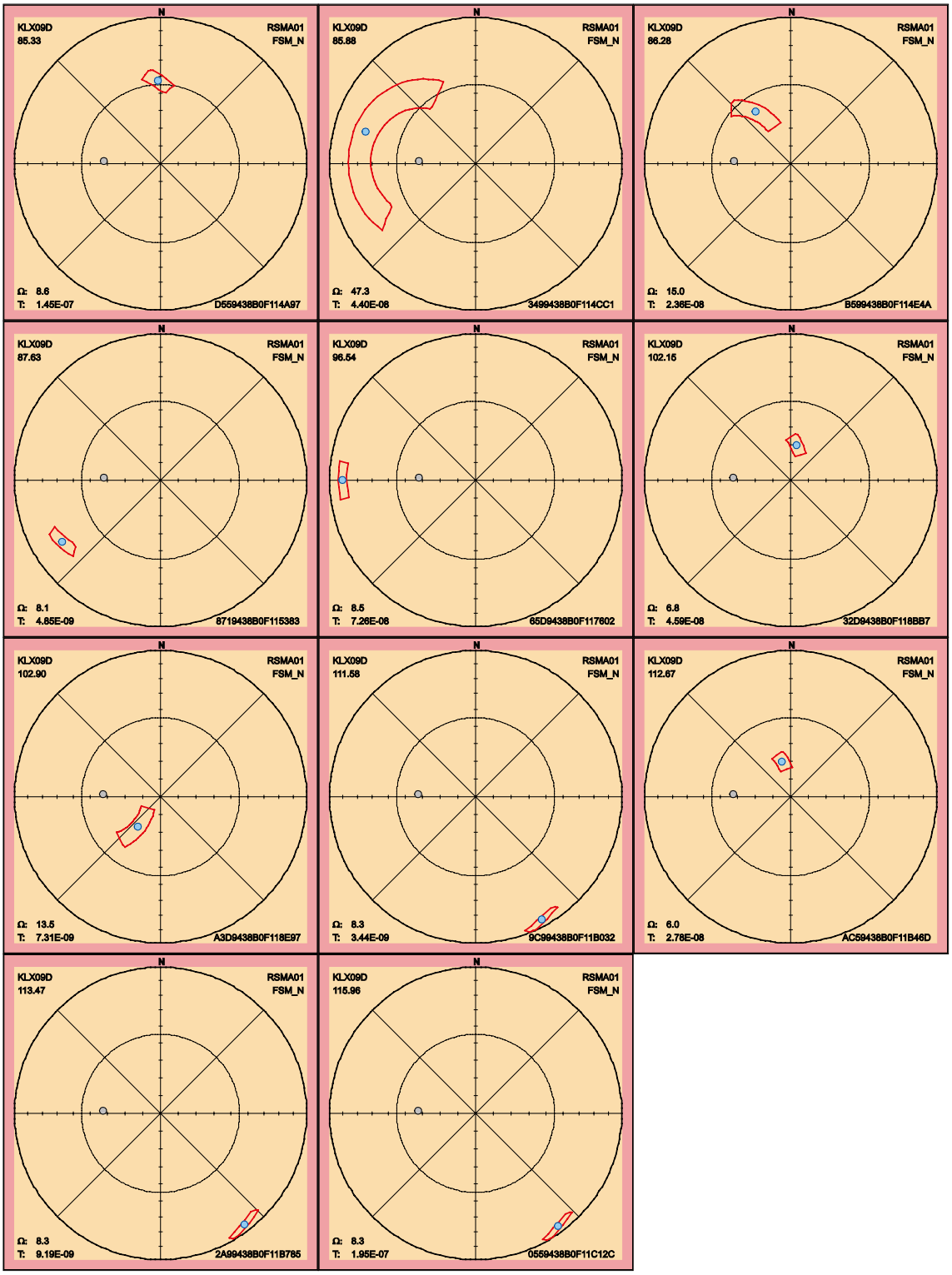
KLX09D
85.33
RSMA01
FSM_N
N
Ω: 8.6
T: 1.45E-07
D559438B0F114A97
KLX09D
85.88
RSMA01
FSM_N
N
Ω: 47.3
T: 4.40E-08
3499438B0F114CC1
KLX09D
86.28
RSMA01
FSM_N
N
Ω: 15.0
T: 2.36E-08
B599438B0F114E4A
KLX09D
87.63
RSMA01
FSM_N
N
Ω: 8.1
T: 4.85E-09
8719438B0F115383
KLX09D
96.54
RSMA01
FSM_N
N
Ω: 8.5
T: 7.26E-08
65D9438B0F117602
KLX09D
102.15
RSMA01
FSM_N
N
Ω: 6.8
T: 4.59E-08
32D9438B0F118BB7
KLX09D
102.90
RSMA01
FSM_N
N
Ω: 13.5
T: 7.31E-09
A3D9438B0F118E97
KLX09D
111.58
RSMA01
FSM_N
N
Ω: 8.3
T: 3.44E-09
9C99438B0F11B032
KLX09D
112.67
RSMA01
FSM_N
N
Ω: 6.0
T: 2.78E-08
AC59438B0F11B46D
KLX09D
113.47
RSMA01
FSM_N
N
Ω: 8.3
T: 9.19E-09
2A99438B0F11B785
KLX09D
115.96
RSMA01
FSM_N
N
Ω: 8.3
T: 1.95E-07
0559438B0F11C12C

2.3.12 KLX09E

Below follow the 90th percentile sample space of uncertainty for the 22 PFL fractures in KLX09E. There is only one fracture having maximum uncertainty, on the 90th percentile, larger than 30°, see Table 2-12, that may be interpreted to have different orientation compared to p_fract_core_eshi / Sicada 2008/

Table 2-12. Fractures in KLX09E with uncertainty, Ω, larger than 30°.

FeatureId	PFL-f no	Adjusted Secup	Ω
B3D9438B0E11B368	33	111.67	41.7

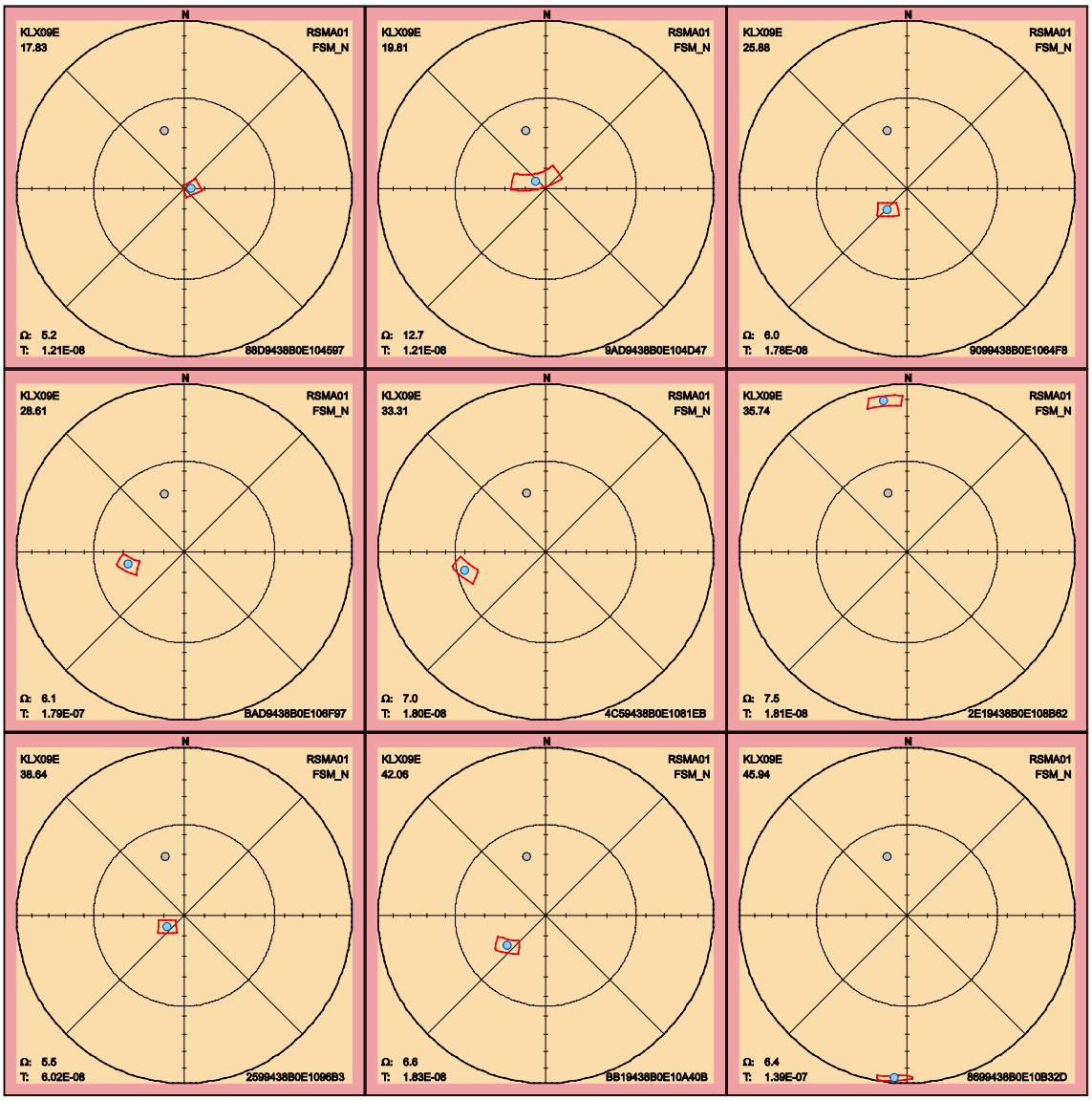

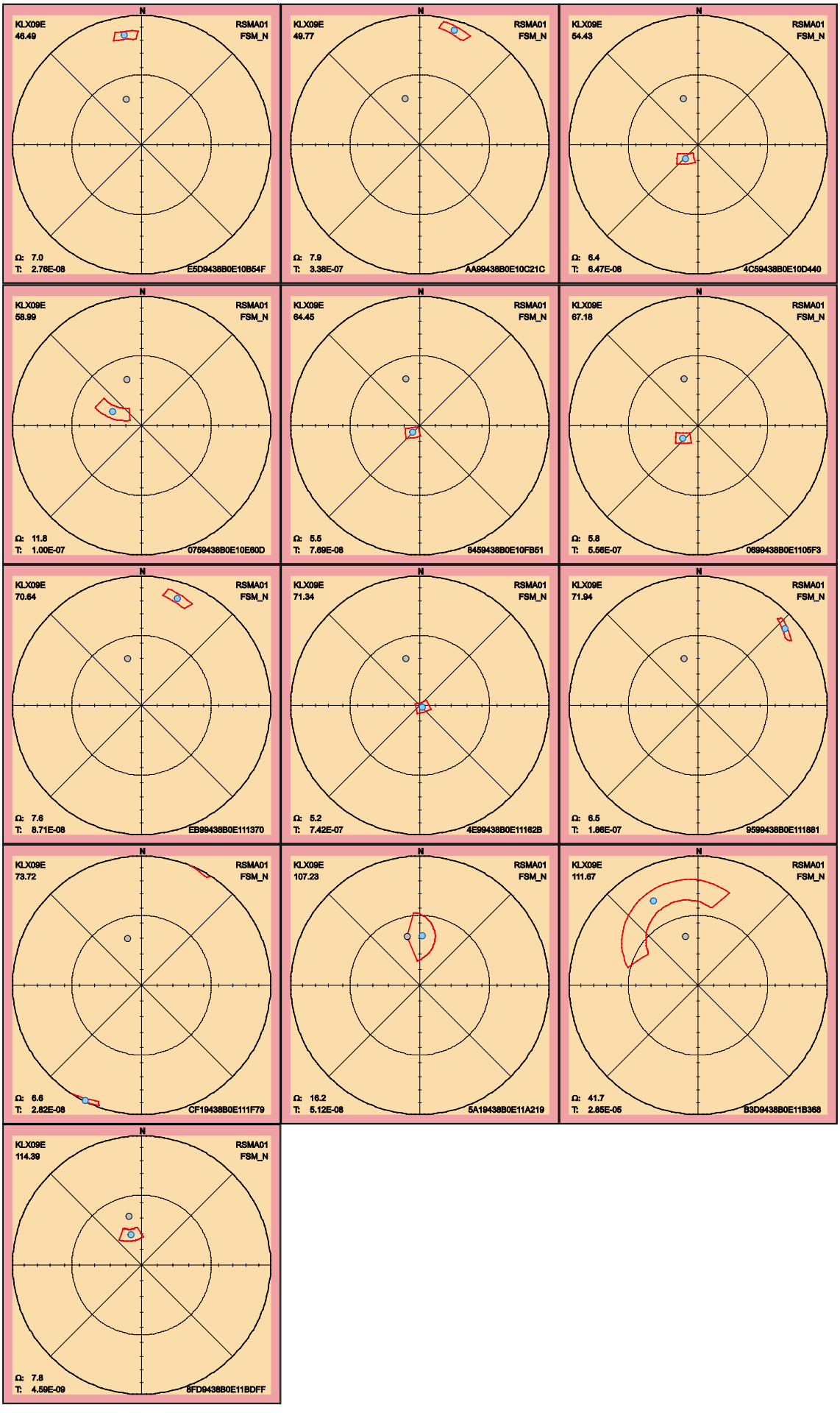
KLX09E
46.49
RSMA01
FSM_N
Ω: 7.0
T: 2.76E-08
E5D9438B0E10B54F
KLX09E
49.77
RSMA01
FSM_N
Ω: 7.9
T: 3.38E-07
AA89438B0E10C21C
KLX09E
54.43
RSMA01
FSM_N
Ω: 6.4
T: 6.47E-08
4C59438B0E10D440
KLX09E
58.99
RSMA01
FSM_N
Ω: 11.8
T: 1.00E-07
0759438B0E10E60D
KLX09E
64.45
RSMA01
FSM_N
Ω: 5.5
T: 7.69E-08
8459438B0E10FB51
KLX09E
67.18
RSMA01
FSM_N
Ω: 5.8
T: 5.56E-07
0699438B0E1105F3
KLX09E
70.64
RSMA01
FSM_N
Ω: 7.6
T: 8.71E-08
EB99438B0E111370
KLX09E
71.34
RSMA01
FSM_N
Ω: 5.2
T: 7.42E-07
4E99438B0E11162B
KLX09E
71.94
RSMA01
FSM_N
Ω: 6.5
T: 1.86E-07
9599438B0E111881
KLX09E
73.72
RSMA01
FSM_N
Ω: 6.6
T: 2.82E-08
CF19438B0E111F79
KLX09E
107.23
RSMA01
FSM_N
Ω: 16.2
T: 5.12E-08
5A19438B0E11A219
KLX09E
111.67
RSMA01
FSM_N
Ω: 41.7
T: 2.85E-05
B3D9438B0E11B368
KLX09E
114.39
RSMA01
FSM_N
Ω: 7.8
T: 4.59E-09
8FD9438B0E11BDFF

2.3.13 KLX09F

Two PFL fractures of the 37, in KLX09F, have maximum uncertainty larger than 30°, see Table 2-13. Attention should be put to these fractures since they can have different interpretation of orientation compared to the best estimated in p_fract_core_eshi /Sicada 2008/.

Table 2-13. Fractures in KLX09F with uncertainty, Ω, larger than 30°.

FeatureId	PFL-f no	Adjusted Secup	Ω
9599438B0D108369	11	33.79	47.6
3499438B0D109634	13	38.63	48.1

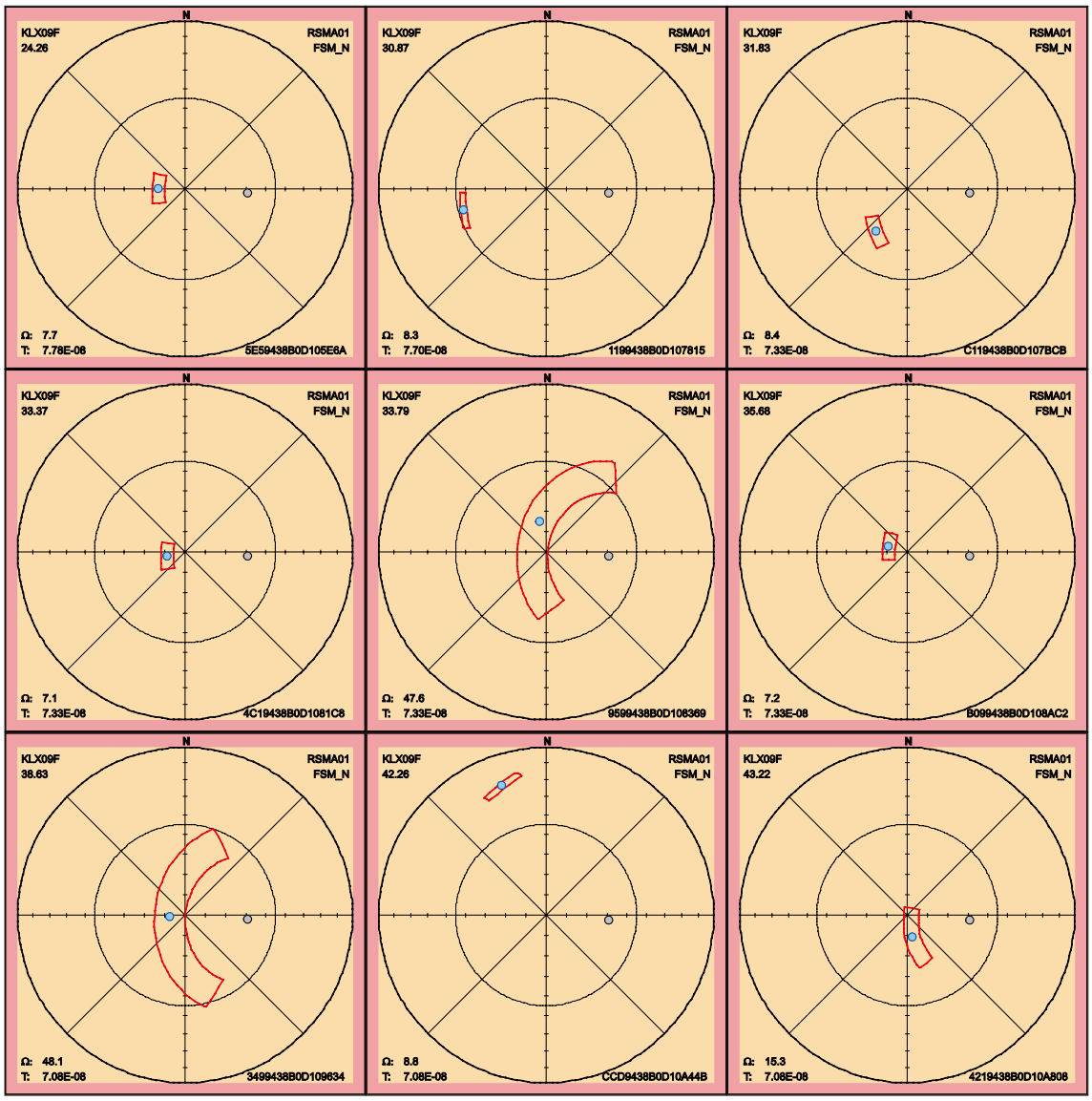

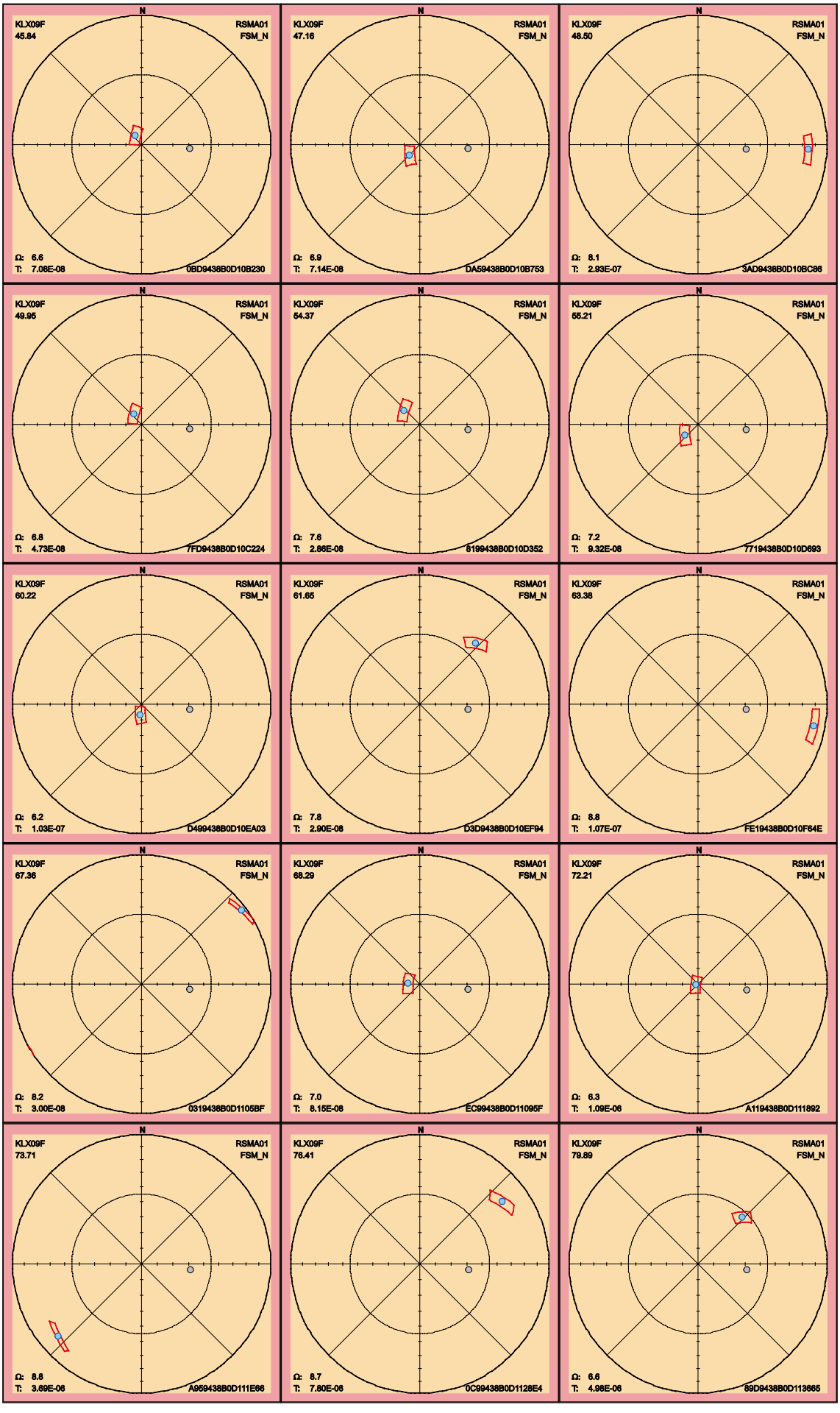
KLX09F
45.84
RSMA01
FSM_N
Ω: 6.6
T: 7.08E-08
0BD9438B0D10B230
KLX09F
47.16
RSMA01
FSM_N
Ω: 6.9
T: 7.14E-08
DA59438B0D10B753
KLX09F
48.50
RSMA01
FSM_N
Ω: 8.1
T: 2.93E-07
3AD9438B0D10BC86
KLX09F
49.95
RSMA01
FSM_N
Ω: 6.8
T: 4.73E-08
7FD9438B0D10C224
KLX09F
54.37
RSMA01
FSM_N
Ω: 7.6
T: 2.86E-08
6199438B0D10D352
KLX09F
55.21
RSMA01
FSM_N
Ω: 7.2
T: 9.32E-08
7719438B0D10D693
KLX09F
60.22
RSMA01
FSM_N
Ω: 6.2
T: 1.03E-07
D499438B0D10EA03
KLX09F
61.65
RSMA01
FSM_N
Ω: 7.8
T: 2.90E-08
D3D9438B0D10EF94
KLX09F
63.38
RSMA01
FSM_N
Ω: 8.8
T: 1.07E-07
FE19438B0D10F64E
KLX09F
67.36
RSMA01
FSM_N
Ω: 8.2
T: 3.00E-08
0319438B0D1105BF
KLX09F
68.29
RSMA01
FSM_N
Ω: 7.0
T: 8.15E-08
EC99438B0D11095F
KLX09F
72.21
RSMA01
FSM_N
Ω: 6.3
T: 1.09E-06
A119438B0D111892
KLX09F
73.71
RSMA01
FSM_N
Ω: 8.8
T: 3.69E-06
A959438B0D111E66
KLX09F
76.41
RSMA01
FSM_N
Ω: 8.7
T: 7.80E-06
0C99438B0D1128E4
KLX09F
79.89
RSMA01
FSM_N
Ω: 6.6
T: 4.98E-06
89D9438B0D113665

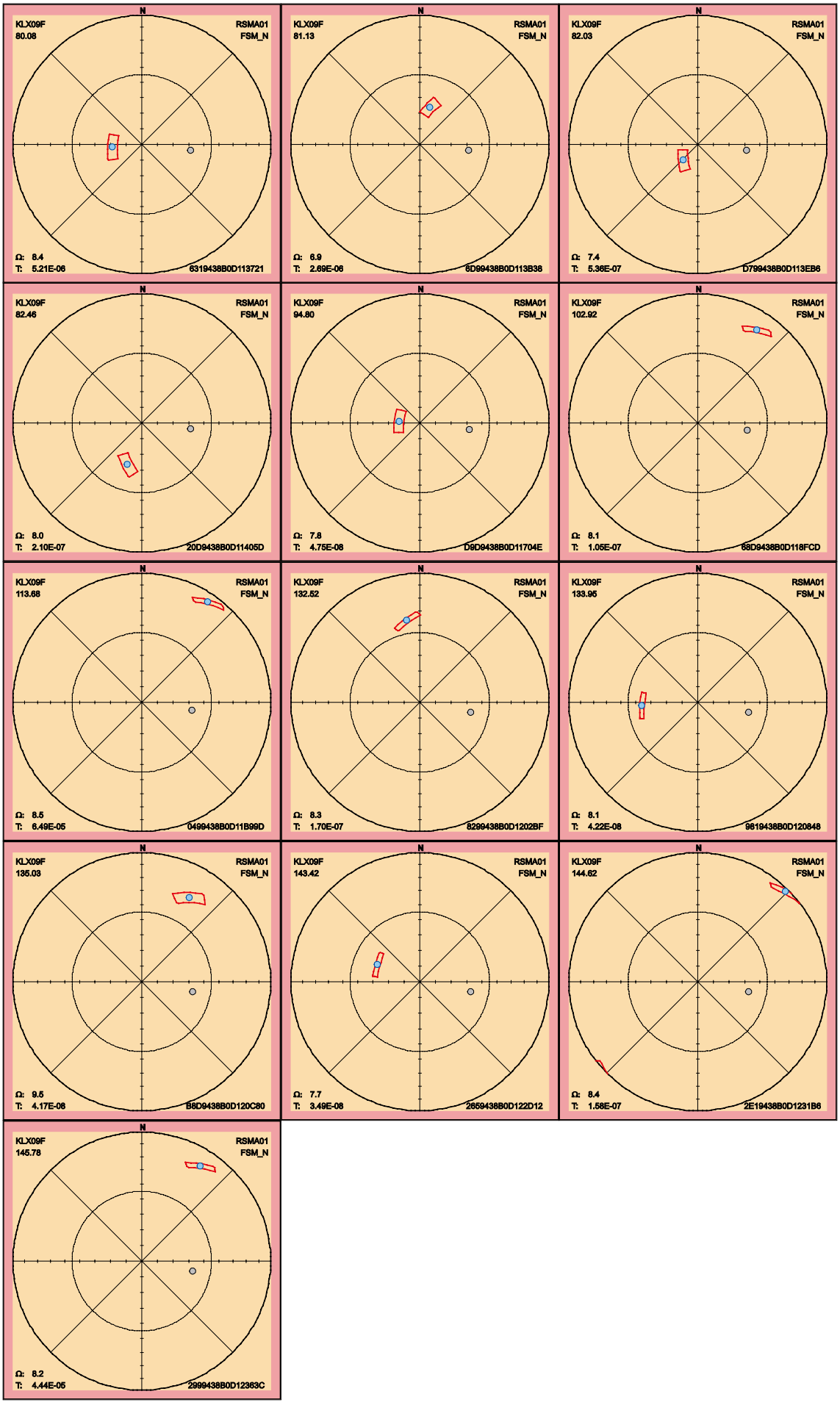
KLX09F
80.08
RSMA01
FSM_N
N
Ω: 8.4
T: 5.21E-06
6319438B0D113721
KLX09F
81.13
RSMA01
FSM_N
N
Ω: 6.9
T: 2.69E-06
6D99438B0D113B38
KLX09F
82.03
RSMA01
FSM_N
N
Ω: 7.4
T: 5.36E-07
D799438B0D113EB6
KLX09F
82.46
RSMA01
FSM_N
N
Ω: 8.0
T: 2.10E-07
20D9438B0D11405D
KLX09F
94.80
RSMA01
FSM_N
N
Ω: 7.8
T: 4.75E-08
D9D9438B0D11704E
KLX09F
102.92
RSMA01
FSM_N
N
Ω: 8.1
T: 1.05E-07
68D9438B0D118FCD
KLX09F
113.68
RSMA01
FSM_N
N
Ω: 8.5
T: 6.49E-05
0499438B0D11B99D
KLX09F
132.52
RSMA01
FSM_N
N
Ω: 8.3
T: 1.70E-07
8299438B0D1202BF
KLX09F
133.95
RSMA01
FSM_N
N
Ω: 8.1
T: 4.22E-08
9619438B0D120848
KLX09F
135.03
RSMA01
FSM_N
N
Ω: 9.5
T: 4.17E-08
B8D9438B0D120C80
KLX09F
143.42
RSMA01
FSM_N
N
Ω: 7.7
T: 3.49E-08
2659438B0D122D12
KLX09F
144.62
RSMA01
FSM_N
N
Ω: 8.4
T: 1.58E-07
2E19438B0D1231B6
KLX09F
145.78
RSMA01
FSM_N
N
Ω: 8.2
T: 4.44E-05
2999438B0D12363C

2.3.14 KLX09G

Below follow the 90th percentile sample space of uncertainty for the 15 PFL fractures in KLX09G. There is only one fracture having larger maximum uncertainty than 30°, see Table 2-14. This fracture can have an alternative interpretation of orientation compared to the best estimate orientation that is found in the table p_fract_core in /Sicada 2008/.

Table 2-14. Fractures in KLX09G with uncertainty, Ω, larger than 30°.

FeatureId	PFL-f no	Adjusted Secup	Ω
CF99438B0C106216	2	25.11	51.1

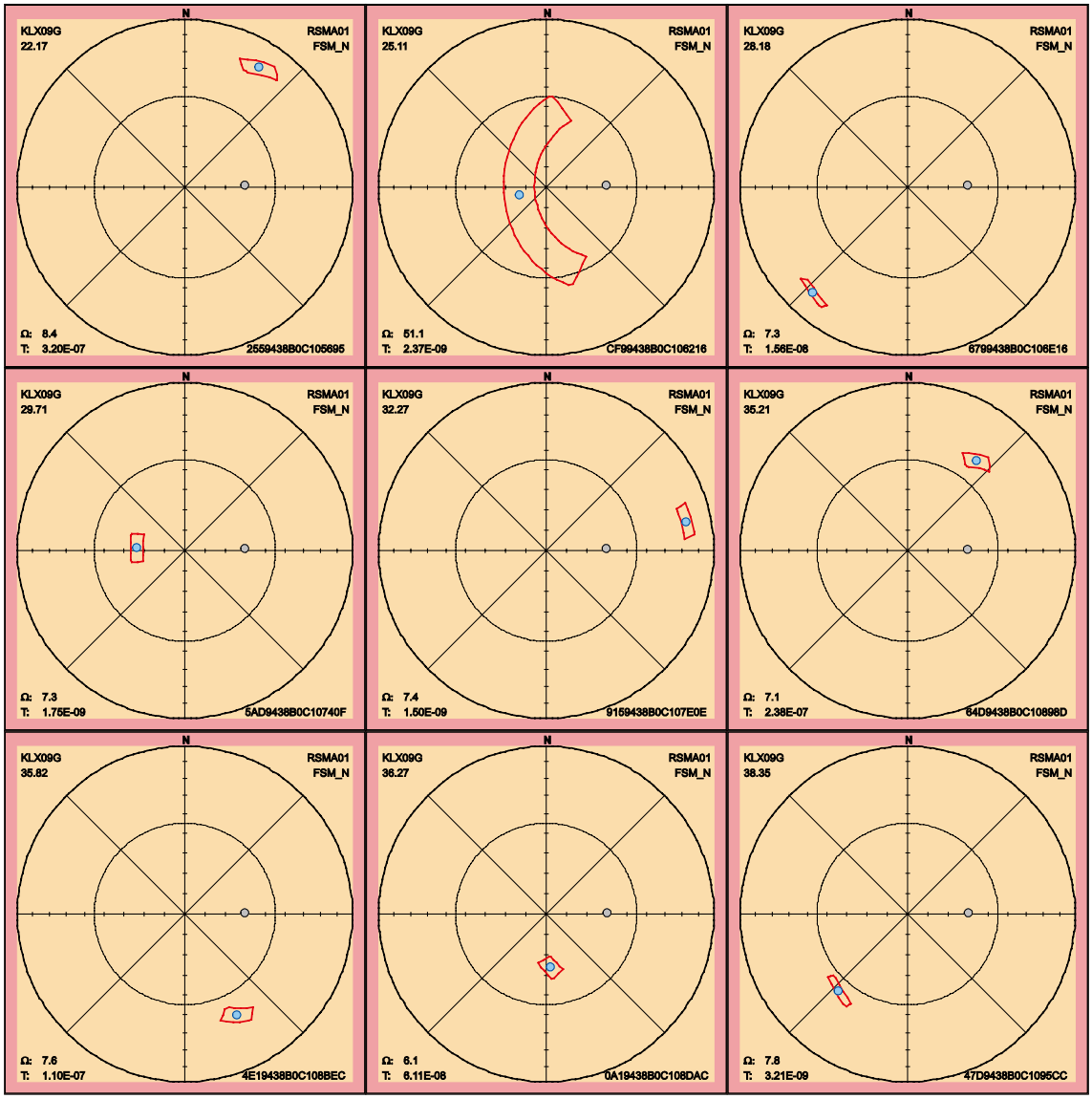

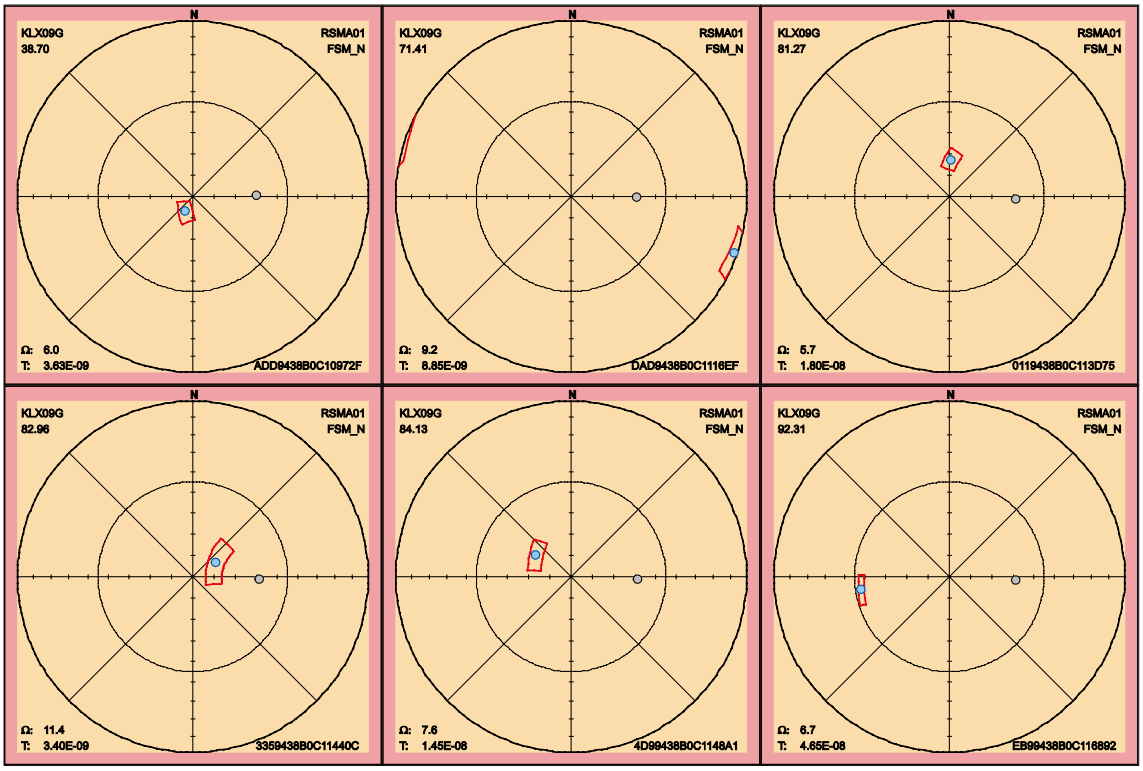

2.3.15 KLX10

Below follow the 90th percentile sample space of uncertainty for the 49 PFL fractures in KLX10. Attention should be paid to the five fractures listed in Table 2-15. These fractures have a maximum uncertainty on the 90th percentile larger than 30° and thus can have an alternative interpretation of orientation compared to the best estimate orientation that is found in the table p_fract_core in /Sicada 2008/.

Table 2-15. Fractures in KLX10 with uncertainty, Ω, larger than 30°.

FeatureId	PFL-f no	Adjusted Secup	Ω
4910478B2B156B74	140	356.99	73.1
8690478B2B157E33	143	361.80	88.1
DC90478B2B16107C	151	399.36	75.6
FF50478B2B164782	162	413.51	89.0
F1D0478B2B165B27	163	418.56	66.4

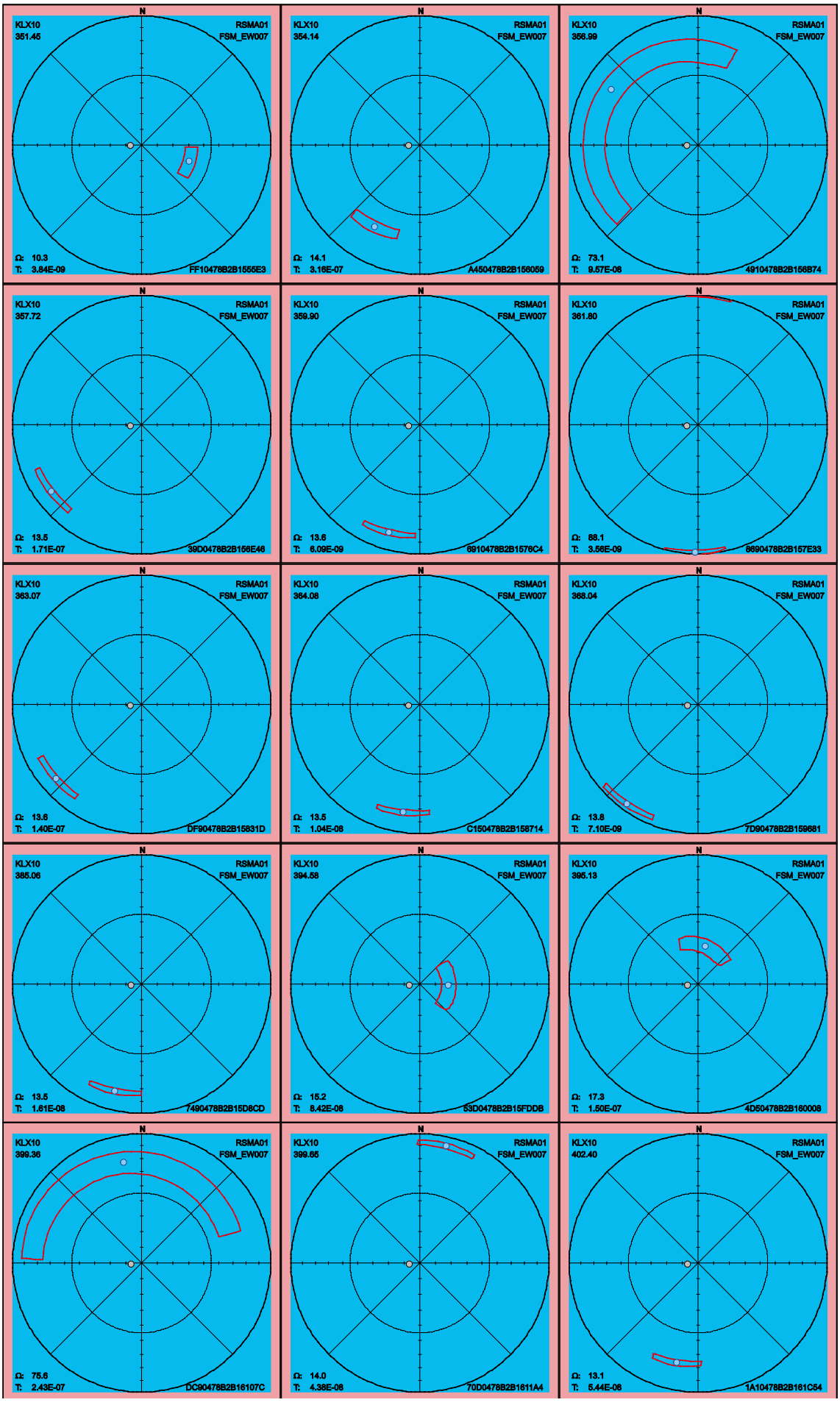
KLX10
351.45
RSMA01
FSM_EW007
Ω: 10.3
T: 3.84E-09
FF10478B2B1555E3
KLX10
354.14
RSMA01
FSM_EW007
Ω: 14.1
T: 3.16E-07
A450478B2B156059
KLX10
356.99
RSMA01
FSM_EW007
Ω: 73.1
T: 9.57E-08
4910478B2B156B74
KLX10
357.72
RSMA01
FSM_EW007
Ω: 13.5
T: 1.71E-07
39D0478B2B156E46
KLX10
359.90
RSMA01
FSM_EW007
Ω: 13.6
T: 6.09E-09
6910478B2B1576C4
KLX10
361.80
RSMA01
FSM_EW007
Ω: 88.1
T: 3.56E-09
8690478B2B157E33
KLX10
363.07
RSMA01
FSM_EW007
Ω: 13.6
T: 1.40E-07
DF90478B2B15831D
KLX10
364.08
RSMA01
FSM_EW007
Ω: 13.5
T: 1.04E-08
C150478B2B158714
KLX10
368.04
RSMA01
FSM_EW007
Ω: 13.8
T: 7.10E-09
7D90478B2B159681
KLX10
385.06
RSMA01
FSM_EW007
Ω: 13.5
T: 1.61E-08
7490478B2B15D8CD
KLX10
394.58
RSMA01
FSM_EW007
Ω: 15.2
T: 8.42E-08
53D0478B2B15FDDB
KLX10
395.13
RSMA01
FSM_EW007
Ω: 17.3
T: 1.50E-07
4D50478B2B160008
KLX10
399.36
RSMA01
FSM_EW007
Ω: 75.6
T: 2.43E-07
DC90478B2B16107C
KLX10
399.65
RSMA01
FSM_EW007
Ω: 14.0
T: 4.38E-08
70D0478B2B1611A4
KLX10
402.40
RSMA01
FSM_EW007
Ω: 13.1
T: 5.44E-08
1A10478B2B161C54

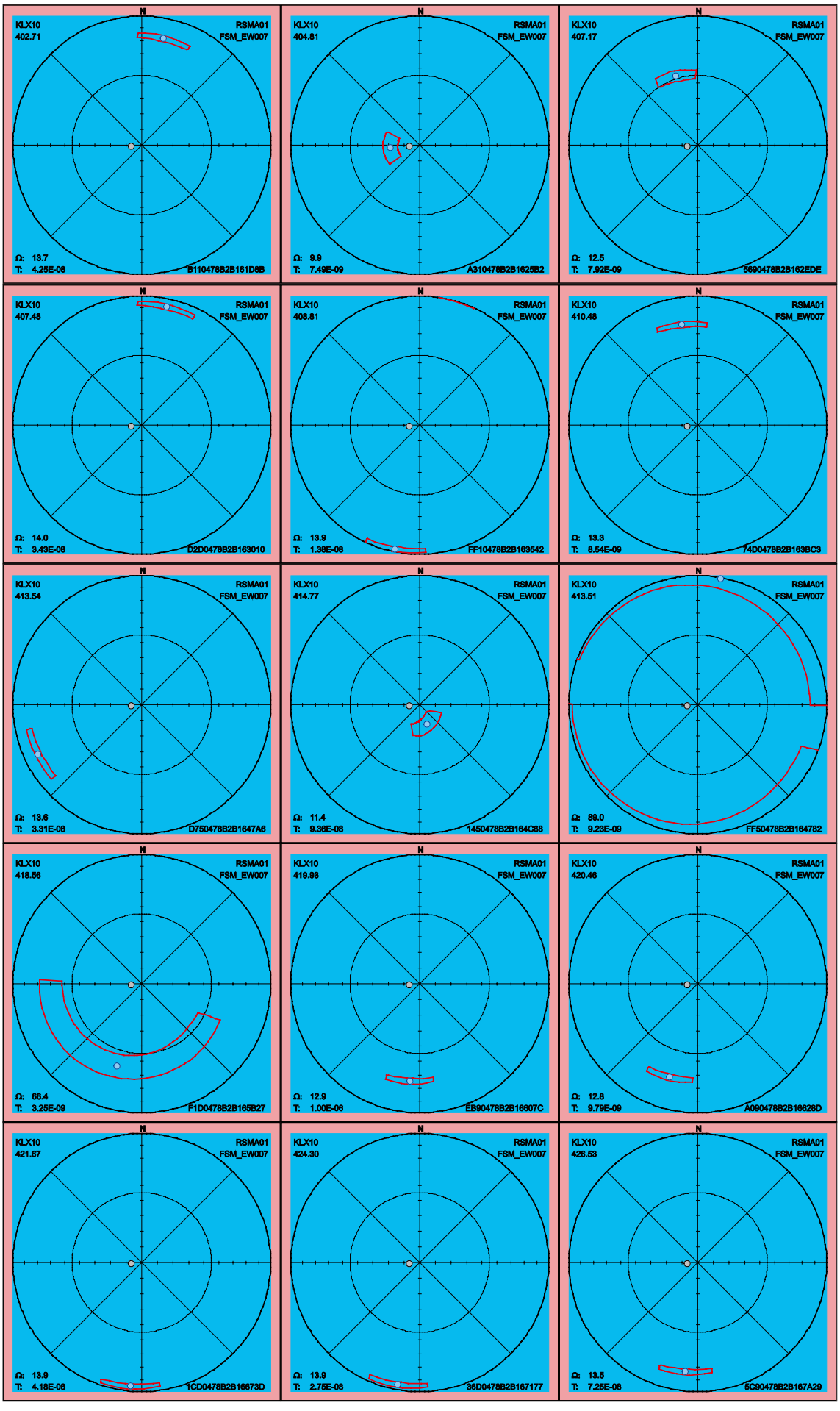
KLX10
402.71
RSMA01
FSM_EW007
Ω: 13.7
T: 4.25E-08
B110478B2B161D8B
KLX10
404.81
RSMA01
FSM_EW007
Ω: 9.9
T: 7.49E-09
A310478B2B1625B2
KLX10
407.17
RSMA01
FSM_EW007
Ω: 12.5
T: 7.92E-09
5690478B2B162EDE
KLX10
407.48
RSMA01
FSM_EW007
Ω: 14.0
T: 3.43E-08
D2D0478B2B163010
KLX10
408.81
RSMA01
FSM_EW007
Ω: 13.9
T: 1.38E-08
FF10478B2B163542
KLX10
410.48
RSMA01
FSM_EW007
Ω: 13.3
T: 8.54E-09
74D0478B2B163BC3
KLX10
413.54
RSMA01
FSM_EW007
Ω: 13.6
T: 3.31E-08
D750478B2B1647A6
KLX10
414.77
RSMA01
FSM_EW007
Ω: 11.4
T: 9.36E-08
1450478B2B164C68
KLX10
413.51
RSMA01
FSM_EW007
Ω: 89.0
T: 9.23E-09
FF50478B2B164782
KLX10
418.56
RSMA01
FSM_EW007
Ω: 66.4
T: 3.25E-09
F1D0478B2B165B27
KLX10
419.93
RSMA01
FSM_EW007
Ω: 12.9
T: 1.00E-06
EB90478B2B16607C
KLX10
420.46
RSMA01
FSM_EW007
Ω: 12.8
T: 9.79E-09
A090478B2B16628D
KLX10
421.67
RSMA01
FSM_EW007
Ω: 13.9
T: 4.18E-08
1CD0478B2B16673D
KLX10
424.30
RSMA01
FSM_EW007
Ω: 13.9
T: 2.75E-08
36D0478B2B167177
KLX10
426.53
RSMA01
FSM_EW007
Ω: 13.5
T: 7.25E-08
5C90478B2B167A29

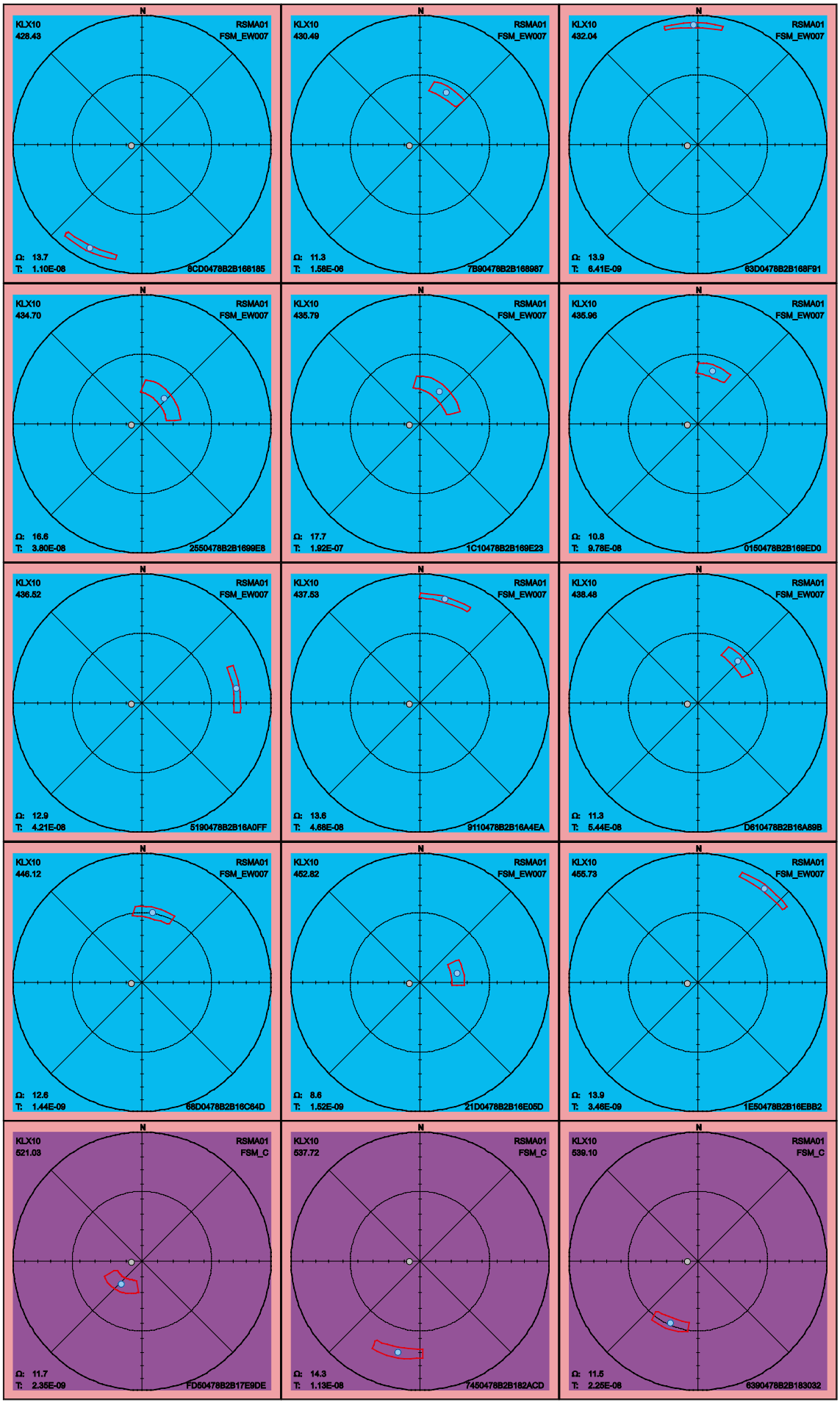
KLX10
428.43
RSMA01
FSM_EW007
Ω: 13.7
T: 1.10E-08
8CD0478B2B168185
KLX10
430.49
RSMA01
FSM_EW007
Ω: 11.3
T: 1.58E-08
7B90478B2B168987
KLX10
432.04
RSMA01
FSM_EW007
Ω: 13.9
T: 6.41E-09
63D0478B2B168F91
KLX10
434.70
RSMA01
FSM_EW007
Ω: 16.6
T: 3.80E-08
2550478B2B1699E8
KLX10
435.79
RSMA01
FSM_EW007
Ω: 17.7
T: 1.92E-07
1C10478B2B169E23
KLX10
435.96
RSMA01
FSM_EW007
Ω: 10.8
T: 9.78E-08
0150478B2B169ED0
KLX10
436.52
RSMA01
FSM_EW007
Ω: 12.9
T: 4.21E-08
5190478B2B16A0FF
KLX10
437.53
RSMA01
FSM_EW007
Ω: 13.6
T: 4.68E-08
9110478B2B16A4EA
KLX10
438.48
RSMA01
FSM_EW007
Ω: 11.3
T: 5.44E-08
D610478B2B16A89B
KLX10
446.12
RSMA01
FSM_EW007
Ω: 12.6
T: 1.44E-09
68D0478B2B16C84D
KLX10
452.82
RSMA01
FSM_EW007
Ω: 8.6
T: 1.52E-09
21D0478B2B16E05D
KLX10
455.73
RSMA01
FSM_EW007
Ω: 13.9
T: 3.46E-09
1E50478B2B16EBB2
KLX10
521.03
RSMA01
FSM_C
Ω: 11.7
T: 2.35E-09
FD50478B2B17E9DE
KLX10
537.72
RSMA01
FSM_C
Ω: 14.3
T: 1.13E-08
7450478B2B182ACD
KLX10
539.10
RSMA01
FSM_C
Ω: 11.5
T: 2.25E-08
6390478B2B183032

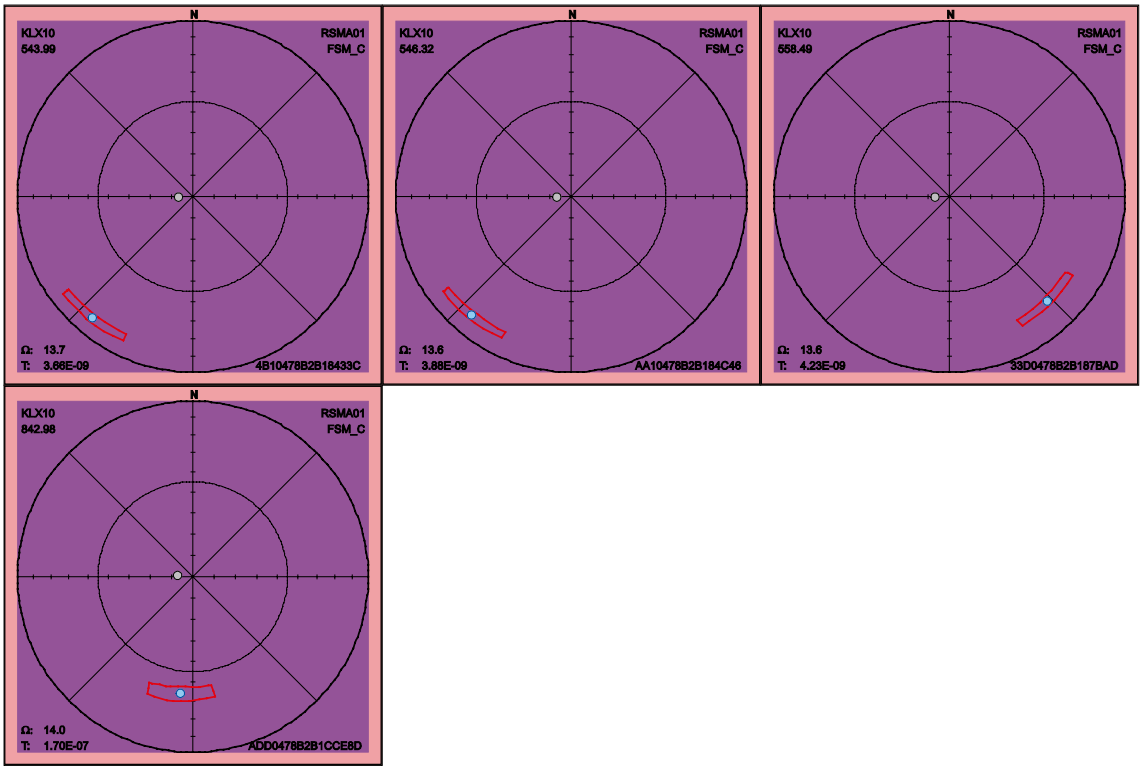

2.3.16 KLX10B

Below follow the 90th percentile sample space of uncertainty for the 22 PFL fractures in KLX10B. No PFL fracture has maximum uncertainty greater than 30°.

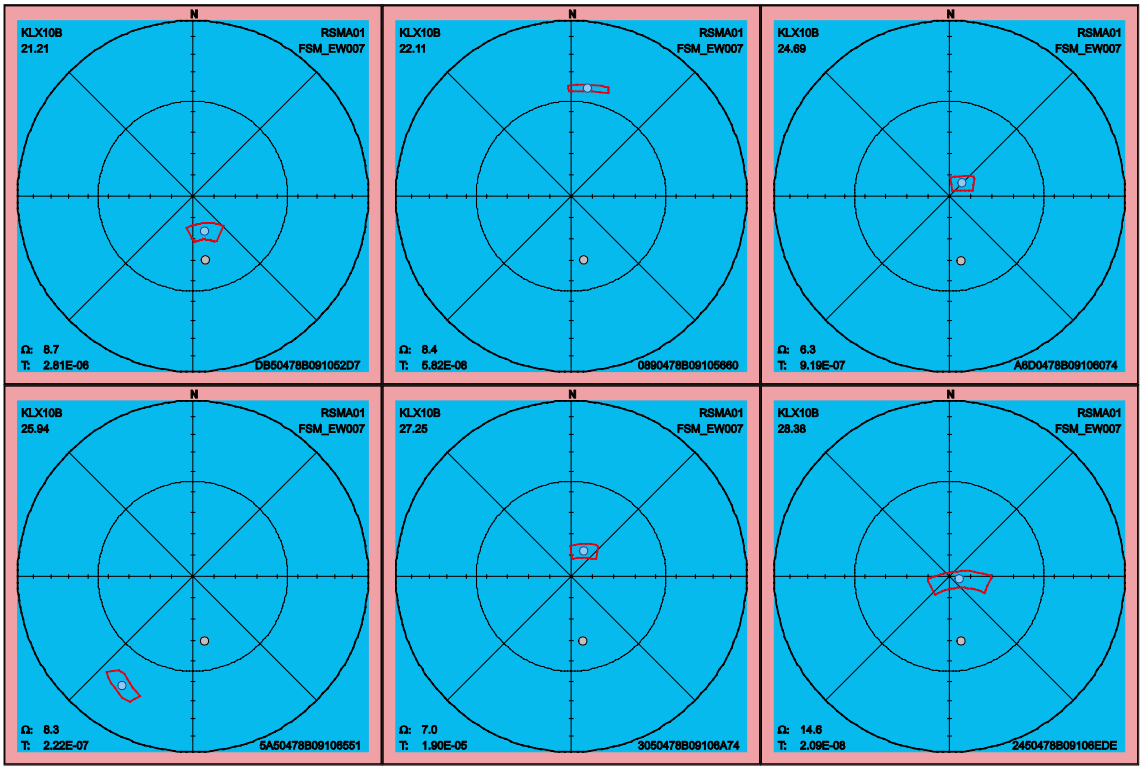

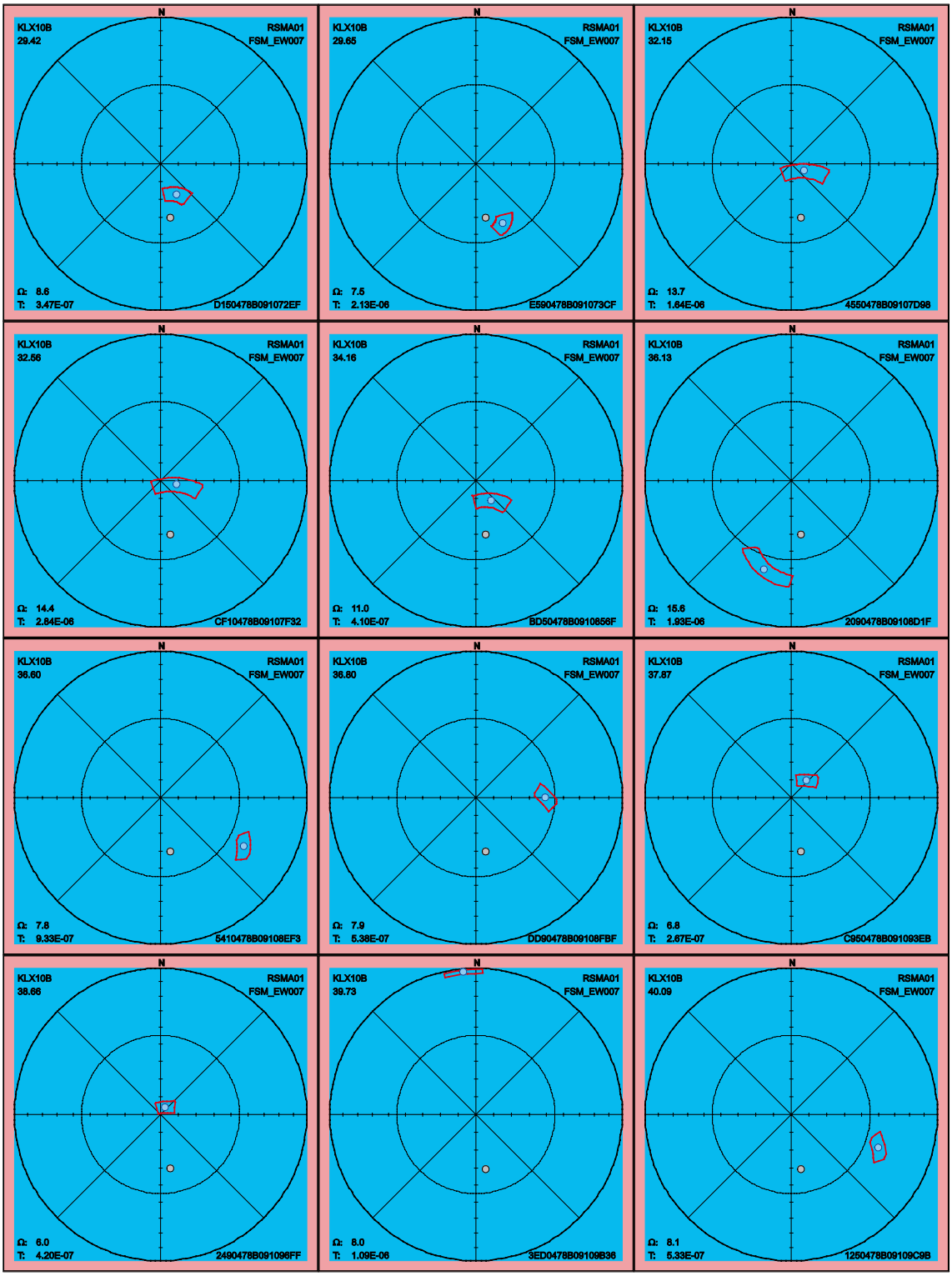
KLX10B
29.42
RSMA01
FSM_EW007
Ω: 8.6
T: 3.47E-07
D150478B091072EF
KLX10B
29.65
RSMA01
FSM_EW007
Ω: 7.5
T: 2.13E-06
E590478B091073CF
KLX10B
32.15
RSMA01
FSM_EW007
Ω: 13.7
T: 1.64E-06
4550478B09107D98
KLX10B
32.56
RSMA01
FSM_EW007
Ω: 14.4
T: 2.84E-06
CF10478B09107F32
KLX10B
34.16
RSMA01
FSM_EW007
Ω: 11.0
T: 4.10E-07
BD50478B0910856F
KLX10B
36.13
RSMA01
FSM_EW007
Ω: 15.6
T: 1.93E-06
2090478B09108D1F
KLX10B
36.60
RSMA01
FSM_EW007
Ω: 7.8
T: 9.33E-07
5410478B09108EF3
KLX10B
36.80
RSMA01
FSM_EW007
Ω: 7.9
T: 5.38E-07
DD90478B09108FBF
KLX10B
37.87
RSMA01
FSM_EW007
Ω: 6.8
T: 2.67E-07
C950478B091093EB
KLX10B
38.66
RSMA01
FSM_EW007
Ω: 6.0
T: 4.20E-07
2490478B091096FF
KLX10B
39.73
RSMA01
FSM_EW007
Ω: 8.0
T: 1.09E-06
3ED0478B09109B36
KLX10B
40.09
RSMA01
FSM_EW007
Ω: 8.1
T: 5.33E-07
1250478B09109C9B

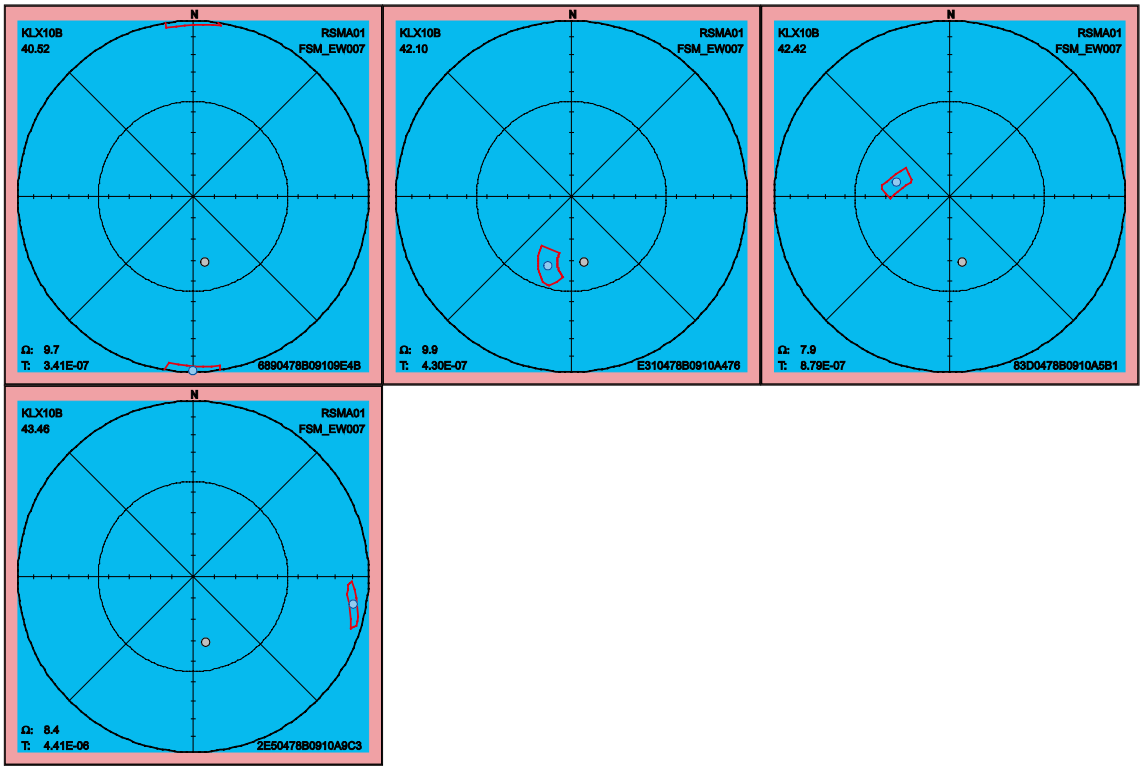

2.3.17 KLX10C

No one of the 15 PFL fractures in KLX10C have maximum uncertainty larger than 30°. The sample space, on 90th percentile level, is shown for all PFL fractures below.

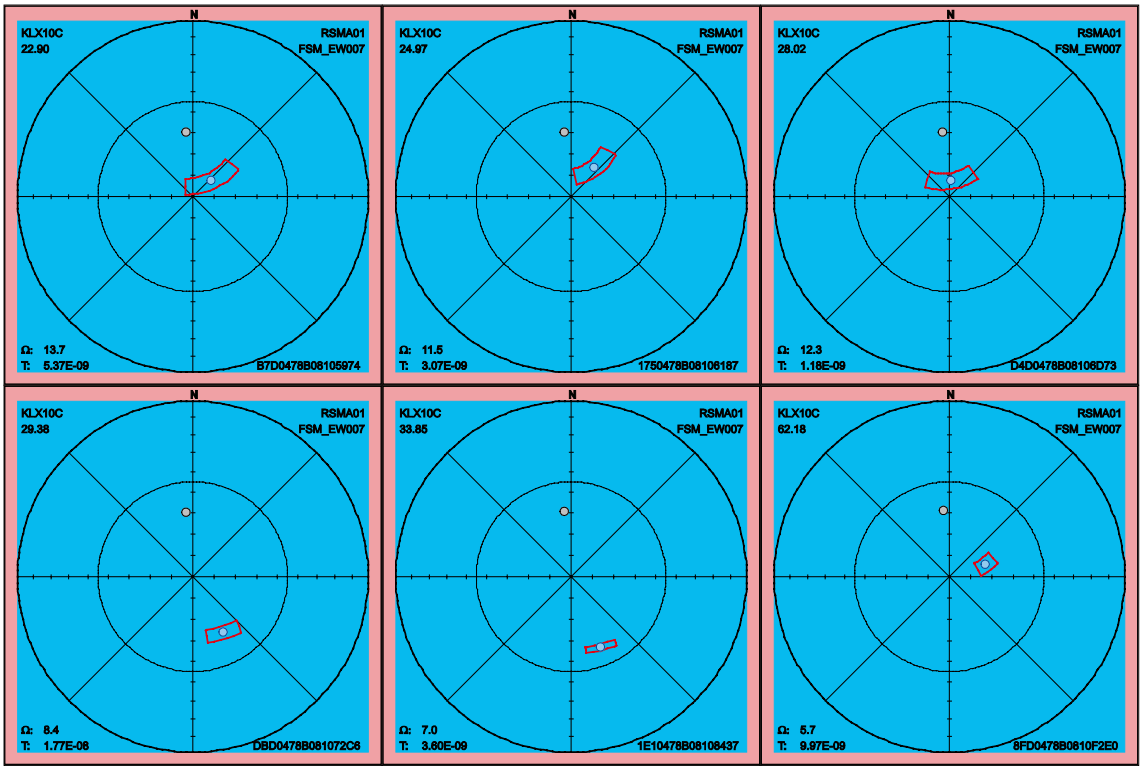

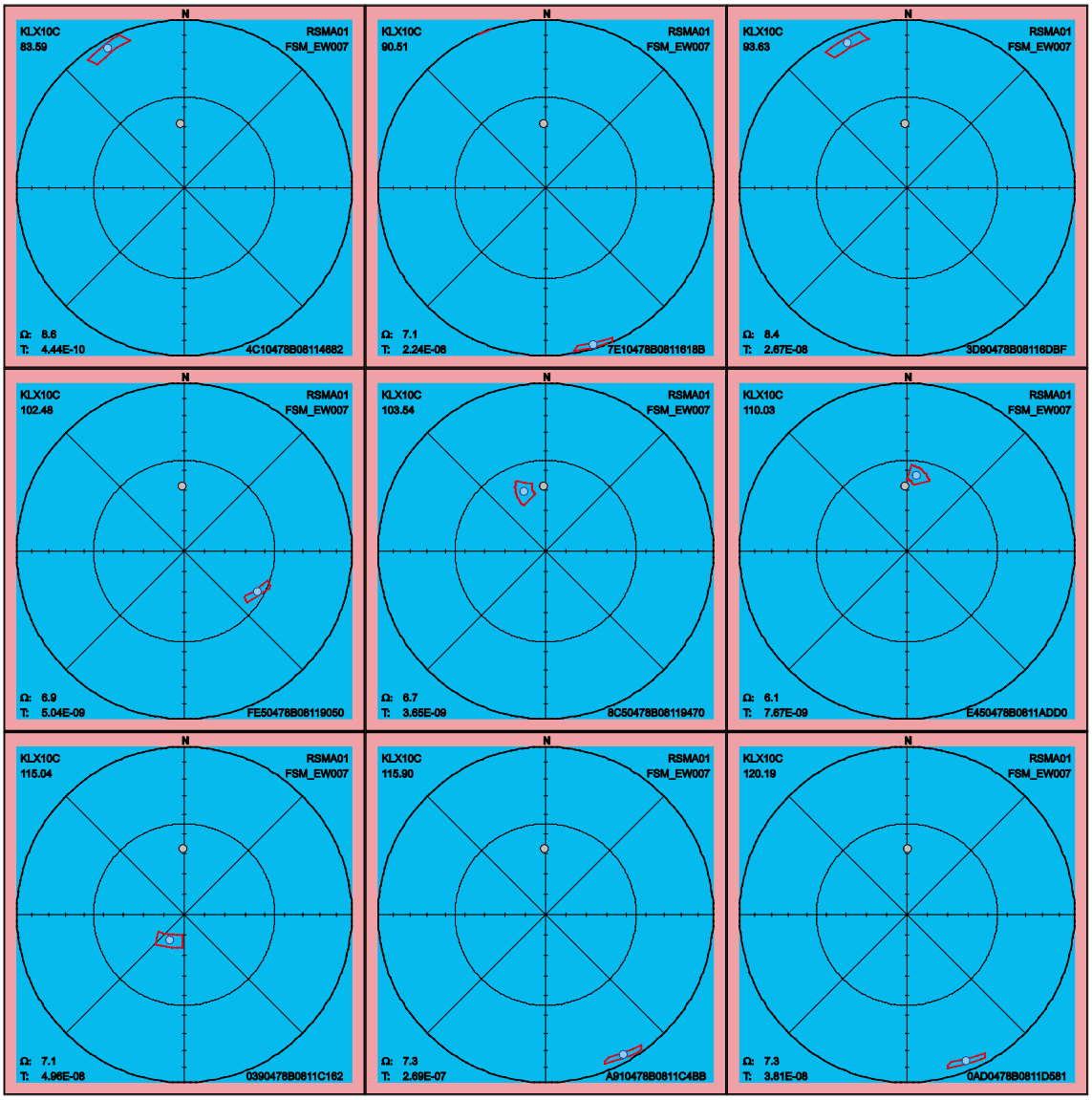

2.3.18 KLX11A

Below follow the 90th percentile sample space of uncertainty for the 49 PFL fractures in KLX11A. Attention should be paid to the three fractures listed in Table 2-16. These fractures have a maximum uncertainty, on the 90th percentile, larger than 30° and hence can have an alternative interpretation of orientation compared to the best estimate orientation that is found in the table p_fract_core in / Sicada 2008/.

Table 2-16. Fractures in KLX11A with uncertainty, Ω, larger than 30°.

FeatureId	PFL-f no	Adjusted Secup	Ω
D211478B0A11E388	8	123.61	55.5
4B91478B0A1800A9	48	524.35	72.6
5C91478B0A1AD343	64	709.84	49.1

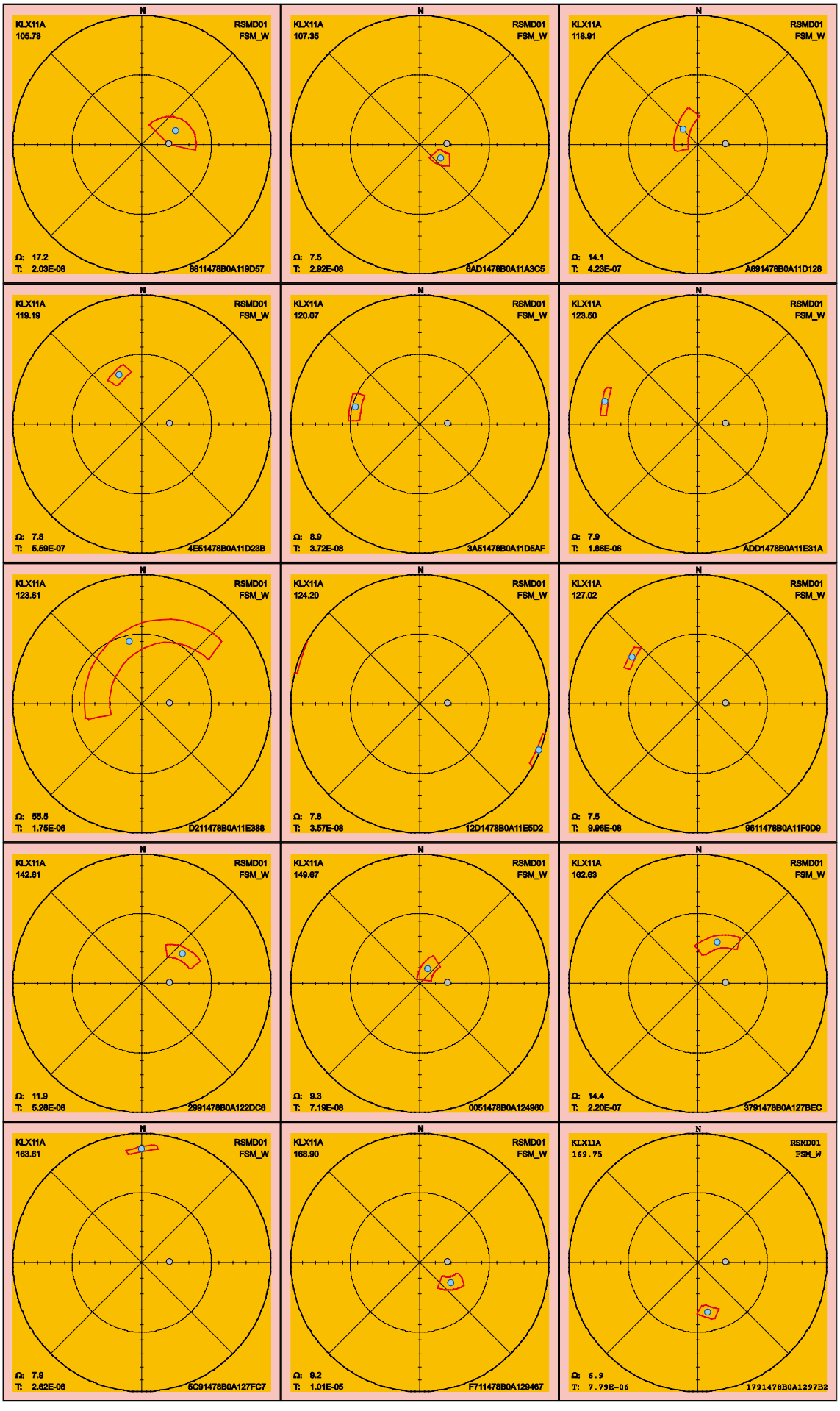
KLX11A
105.73
RSMD01
FSM_W
N
Ω: 17.2
T: 2.03E-08
8811478B0A119D57
KLX11A
107.35
RSMD01
FSM_W
N
Ω: 7.5
T: 2.92E-08
6AD1478B0A11A3C5
KLX11A
118.91
RSMD01
FSM_W
N
Ω: 14.1
T: 4.23E-07
A891478B0A11D128
KLX11A
119.19
RSMD01
FSM_W
N
Ω: 7.8
T: 5.59E-07
4E51478B0A11D23B
KLX11A
120.07
RSMD01
FSM_W
N
Ω: 8.9
T: 3.72E-08
3A51478B0A11D5AF
KLX11A
123.50
RSMD01
FSM_W
N
Ω: 7.9
T: 1.86E-06
ADD1478B0A11E31A
KLX11A
123.61
RSMD01
FSM_W
N
Ω: 55.5
T: 1.75E-06
D211478B0A11E388
KLX11A
124.20
RSMD01
FSM_W
N
Ω: 7.8
T: 3.57E-08
12D1478B0A11E5D2
KLX11A
127.02
RSMD01
FSM_W
N
Ω: 7.5
T: 9.96E-08
9611478B0A11F0D9
KLX11A
142.61
RSMD01
FSM_W
N
Ω: 11.9
T: 5.28E-08
2991478B0A122DC8
KLX11A
149.67
RSMD01
FSM_W
N
Ω: 9.3
T: 7.19E-08
0051478B0A124960
KLX11A
162.63
RSMD01
FSM_W
N
Ω: 14.4
T: 2.20E-07
3791478B0A127BEC
KLX11A
163.61
RSMD01
FSM_W
N
Ω: 7.9
T: 2.62E-08
5C91478B0A127FC7
KLX11A
168.90
RSMD01
FSM_W
N
Ω: 9.2
T: 1.01E-05
F711478B0A129467
KLX11A
169.75
RSMD01
FSM_W
N
Ω: 6.9
T: 7.79E-06
1791478B0A1297B2

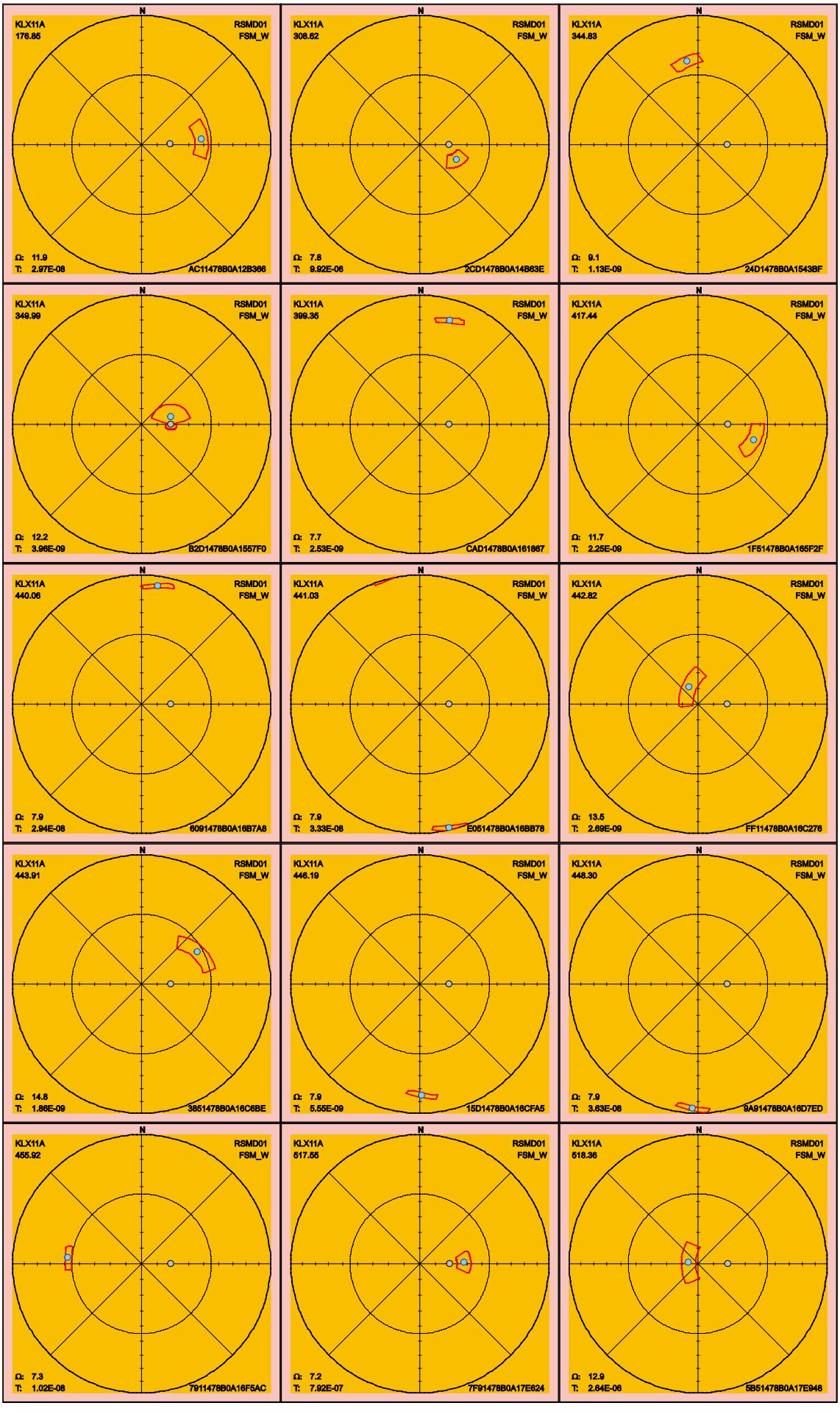
KLX11A
176.85
RSMD01
FSM_W
Ω: 11.9
T: 2.97E-08
AC11478B0A12B366
KLX11A
308.62
RSMD01
FSM_W
Ω: 7.8
T: 9.92E-06
2CD1478B0A14B63E
KLX11A
344.83
RSMD01
FSM_W
Ω: 9.1
T: 1.13E-09
24D1478B0A1543BF
KLX11A
349.99
RSMD01
FSM_W
Ω: 12.2
T: 3.96E-09
B2D1478B0A1557F0
KLX11A
399.35
RSMD01
FSM_W
Ω: 7.7
T: 2.53E-09
CAD1478B0A161867
KLX11A
417.44
RSMD01
FSM_W
Ω: 11.7
T: 2.25E-09
1F51478B0A165F2F
KLX11A
440.06
RSMD01
FSM_W
Ω: 7.9
T: 2.94E-08
6091478B0A16B7A8
KLX11A
441.03
RSMD01
FSM_W
Ω: 7.9
T: 3.33E-08
E051478B0A16BB78
KLX11A
442.82
RSMD01
FSM_W
Ω: 13.5
T: 2.69E-09
FF11478B0A16C276
KLX11A
443.91
RSMD01
FSM_W
Ω: 14.8
T: 1.86E-09
3851478B0A16C8BE
KLX11A
446.19
RSMD01
FSM_W
Ω: 7.9
T: 5.55E-09
15D1478B0A16CFA5
KLX11A
448.30
RSMD01
FSM_W
Ω: 7.9
T: 3.63E-08
9A91478B0A16D7ED
KLX11A
455.92
RSMD01
FSM_W
Ω: 7.3
T: 1.02E-08
7911478B0A16F5AC
KLX11A
517.55
RSMD01
FSM_W
Ω: 7.2
T: 7.92E-07
7F91478B0A17E624
KLX11A
518.36
RSMD01
FSM_W
Ω: 12.9
T: 2.64E-06
5B51478B0A17E948

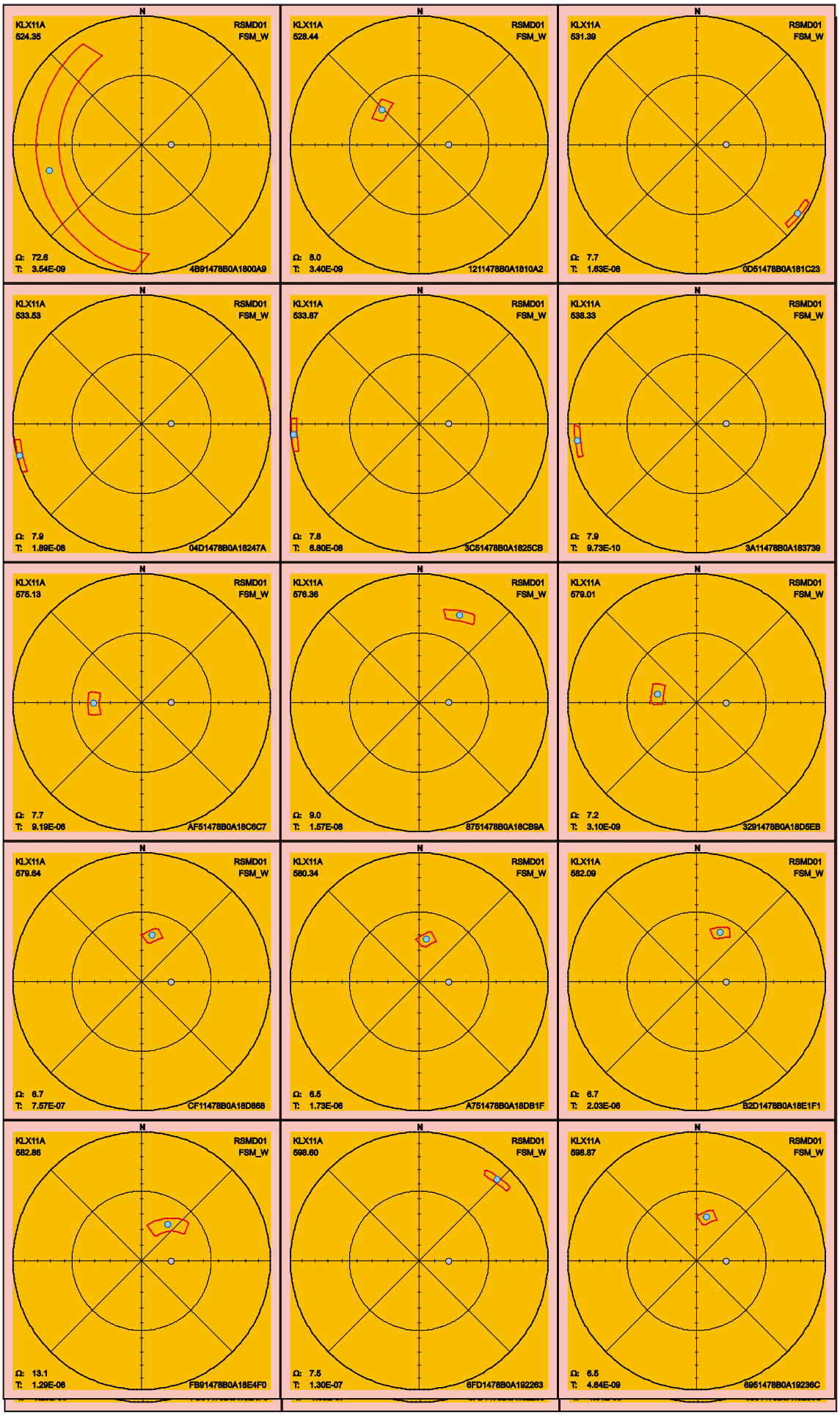
KLX11A
524.35
RSMD01
FSM_W
Ω: 72.6
T: 3.54E-09
4B91478B0A1800A9
KLX11A
528.44
RSMD01
FSM_W
Ω: 8.0
T: 3.40E-09
1211478B0A1810A2
KLX11A
531.39
RSMD01
FSM_W
Ω: 7.7
T: 1.83E-08
0D51478B0A181C23
KLX11A
533.53
RSMD01
FSM_W
Ω: 7.9
T: 1.89E-08
04D1478B0A18247A
KLX11A
533.87
RSMD01
FSM_W
Ω: 7.8
T: 6.80E-08
3C51478B0A1825CB
KLX11A
538.33
RSMD01
FSM_W
Ω: 7.9
T: 9.73E-10
3A11478B0A183739
KLX11A
575.13
RSMD01
FSM_W
Ω: 7.7
T: 9.19E-06
AF51478B0A18C6C7
KLX11A
576.36
RSMD01
FSM_W
Ω: 9.0
T: 1.57E-08
8751478B0A18CB9A
KLX11A
579.01
RSMD01
FSM_W
Ω: 7.2
T: 3.10E-09
3291478B0A18D5EB
KLX11A
579.64
RSMD01
FSM_W
Ω: 6.7
T: 7.57E-07
CF11478B0A18D868
KLX11A
580.34
RSMD01
FSM_W
Ω: 6.5
T: 1.73E-06
A751478B0A18DB1F
KLX11A
582.09
RSMD01
FSM_W
Ω: 6.7
T: 2.03E-06
B2D1478B0A18E1F1
KLX11A
582.86
RSMD01
FSM_W
Ω: 13.1
T: 1.29E-06
FB91478B0A18E4F0
KLX11A
598.60
RSMD01
FSM_W
Ω: 7.5
T: 1.30E-07
6FD1478B0A192263
KLX11A
598.87
RSMD01
FSM_W
Ω: 6.5
T: 4.64E-09
6951478B0A19236C

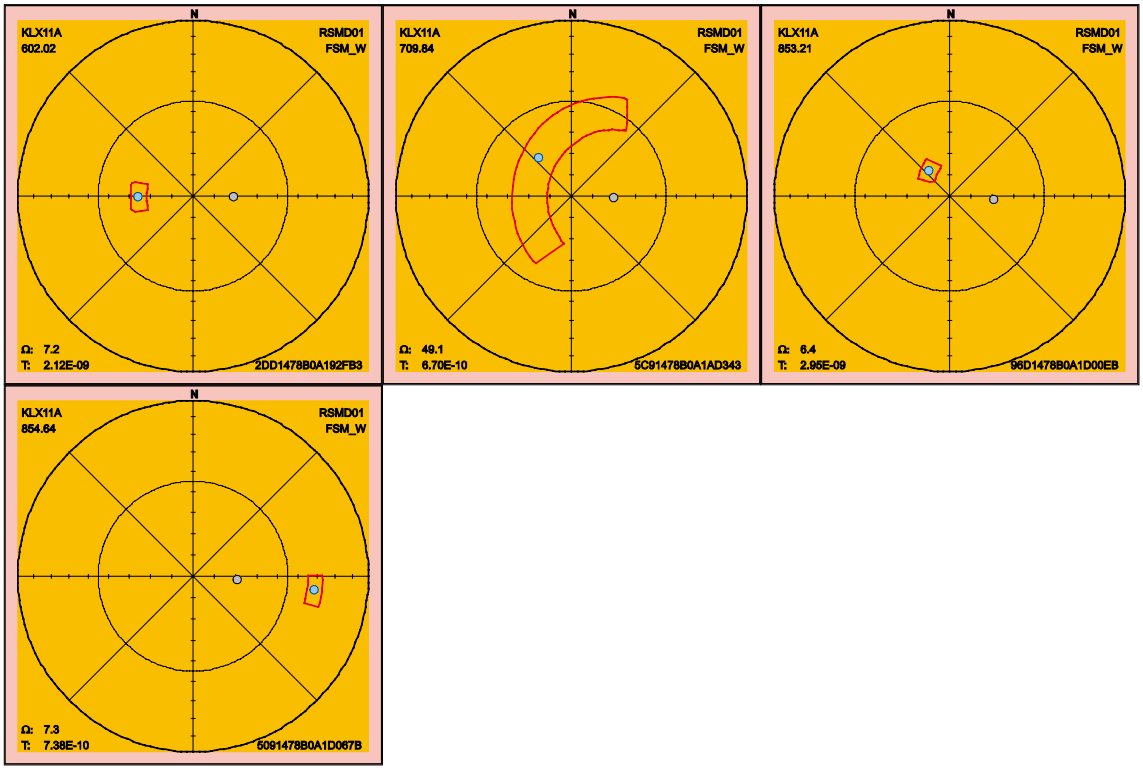

2.3.19 KLX11B

Below follow the 90th percentile sample space of uncertainty for the 37 PFL fractures in KLX11B. There are six fractures listed in Table 2-17 that have maximum uncertainty, on the 90th percentile, larger than 30°. These fractures can have an alternative interpretation of orientation compared to the best estimate orientation that is found in the table p_fract_core in /Sicada 2008/.

Table 2-17. Fractures in KLX11B with uncertainty, Ω, larger than 30°.

FeatureId	PFL-f no	Adjusted Secup	Ω
2091478B09107313	10	29.53	37.0
A091478B0910895B	14	35.25	86.7
C091478B0910C294	21	49.94	33.1
E091478B09111107	29	70.09	44.3
E091478B09112922	34	76.28	37.4
A091478B09114B18	35	85.01	88.8

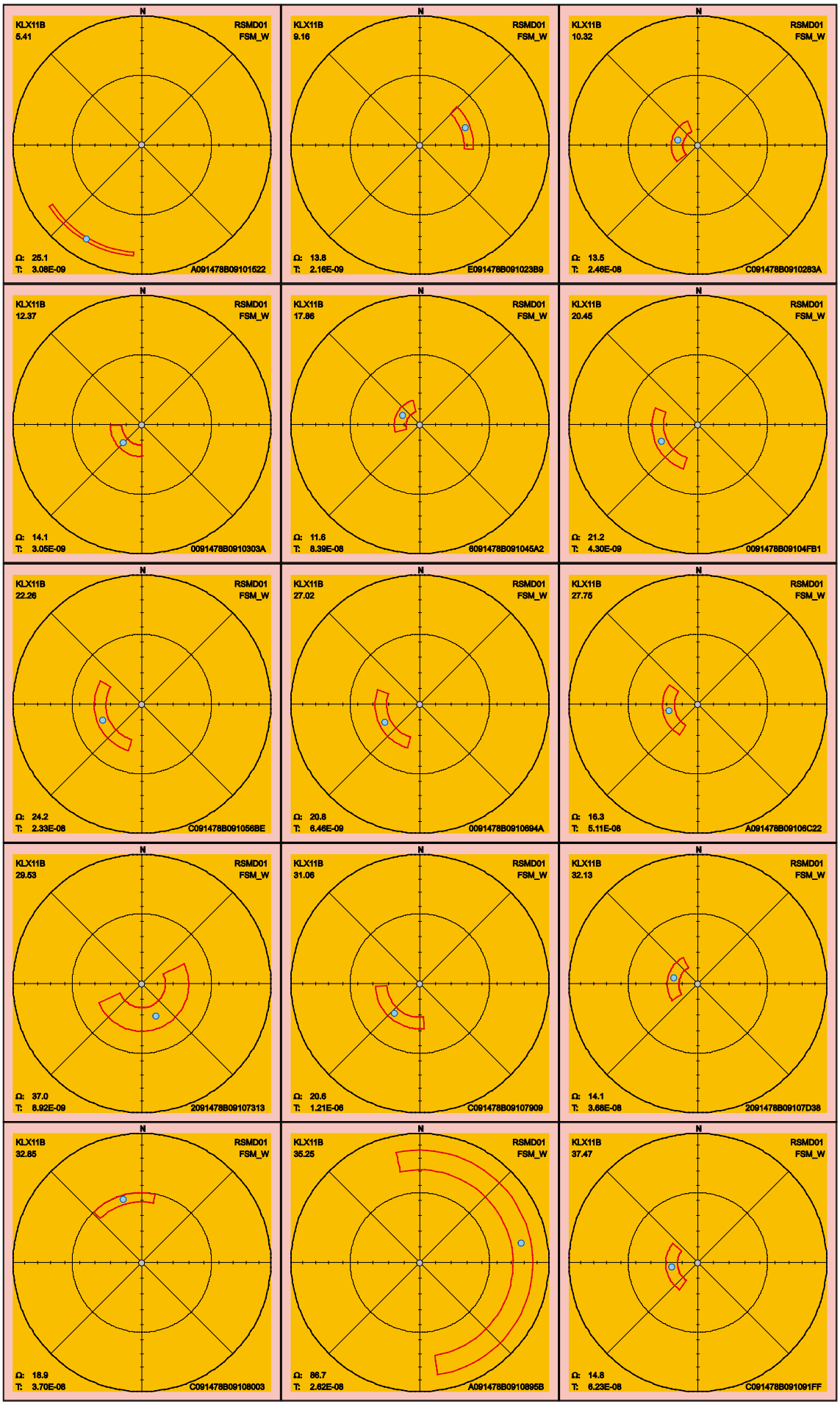
KLX11B
5.41
RSMD01
FSM_W
N
Ω: 25.1
T: 3.08E-09
A091478B09101522
KLX11B
9.16
RSMD01
FSM_W
N
Ω: 13.8
T: 2.16E-09
E091478B091023B9
KLX11B
10.32
RSMD01
FSM_W
N
Ω: 13.5
T: 2.46E-08
C091478B0910283A
KLX11B
12.37
RSMD01
FSM_W
N
Ω: 14.1
T: 3.05E-09
0091478B0910303A
KLX11B
17.86
RSMD01
FSM_W
N
Ω: 11.6
T: 8.39E-08
6091478B091045A2
KLX11B
20.45
RSMD01
FSM_W
N
Ω: 21.2
T: 4.30E-09
0091478B09104FB1
KLX11B
22.26
RSMD01
FSM_W
N
Ω: 24.2
T: 2.33E-08
C091478B091056BE
KLX11B
27.02
RSMD01
FSM_W
N
Ω: 20.8
T: 6.46E-09
0091478B0910694A
KLX11B
27.75
RSMD01
FSM_W
N
Ω: 16.3
T: 5.11E-08
A091478B09106C22
KLX11B
29.53
RSMD01
FSM_W
N
Ω: 37.0
T: 8.92E-09
2091478B09107313
KLX11B
31.06
RSMD01
FSM_W
N
Ω: 20.6
T: 1.21E-08
C091478B09107909
KLX11B
32.13
RSMD01
FSM_W
N
Ω: 14.1
T: 3.68E-08
2091478B09107D38
KLX11B
32.85
RSMD01
FSM_W
N
Ω: 18.9
T: 3.70E-08
C091478B09108003
KLX11B
35.25
RSMD01
FSM_W
N
Ω: 86.7
T: 2.62E-08
A091478B0910895B
KLX11B
37.47
RSMD01
FSM_W
N
Ω: 14.8
T: 6.23E-08
C091478B091091FF

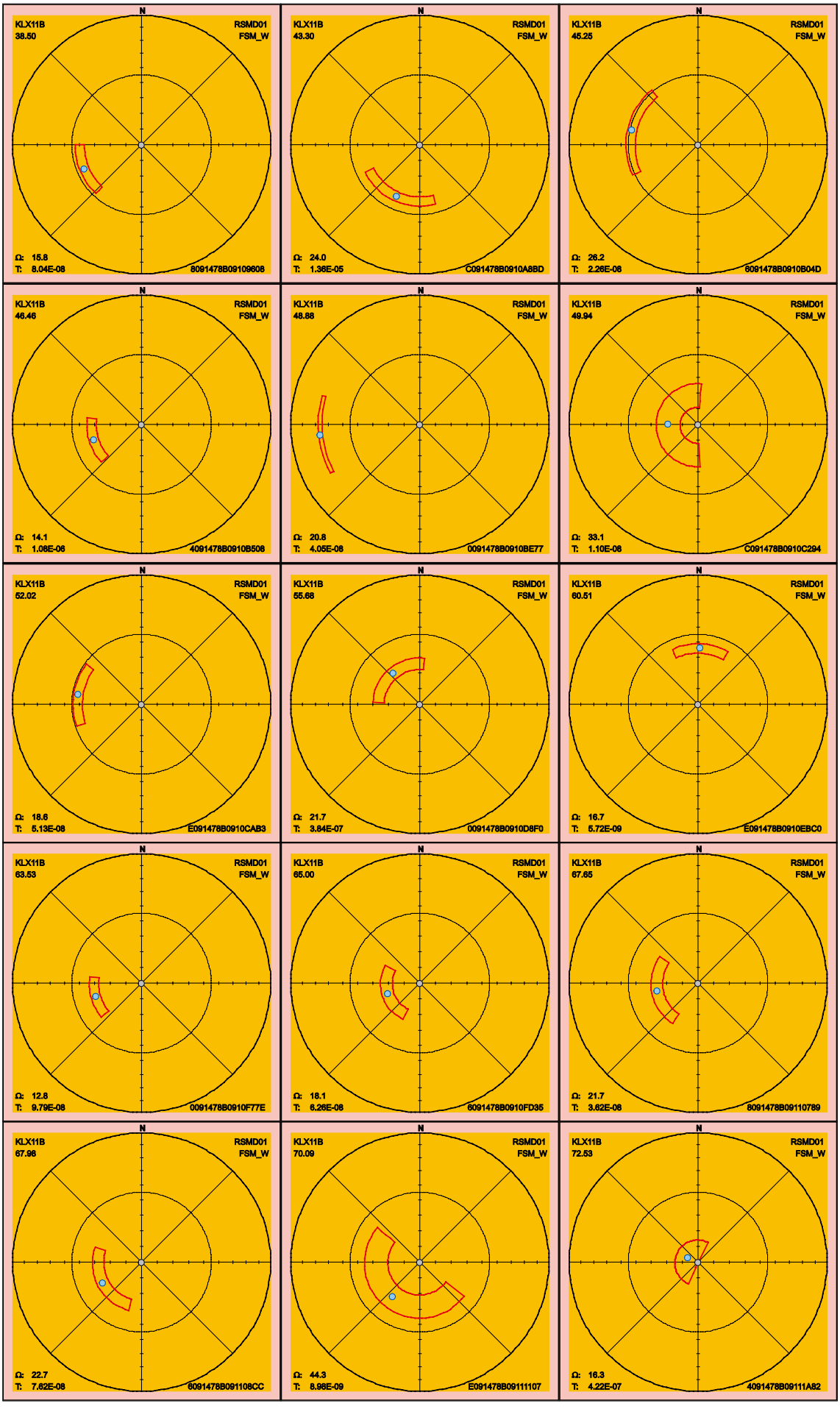
KLX11B
38.50
RSMD01
FSM_W
N
Ω: 15.8
T: 8.04E-08
8091478B09109608
KLX11B
43.30
RSMD01
FSM_W
N
Ω: 24.0
T: 1.36E-05
C091478B0910A8BD
KLX11B
45.25
RSMD01
FSM_W
N
Ω: 26.2
T: 2.26E-08
6091478B0910B04D
KLX11B
46.46
RSMD01
FSM_W
N
Ω: 14.1
T: 1.08E-06
4091478B0910B508
KLX11B
48.88
RSMD01
FSM_W
N
Ω: 20.8
T: 4.05E-08
0091478B0910BE77
KLX11B
49.94
RSMD01
FSM_W
N
Ω: 33.1
T: 1.10E-08
C091478B0910C294
KLX11B
52.02
RSMD01
FSM_W
N
Ω: 18.6
T: 5.13E-08
E091478B0910CAB3
KLX11B
55.68
RSMD01
FSM_W
N
Ω: 21.7
T: 3.84E-07
0091478B0910D8F0
KLX11B
60.51
RSMD01
FSM_W
N
Ω: 16.7
T: 5.72E-09
E091478B0910EBC0
KLX11B
63.53
RSMD01
FSM_W
N
Ω: 12.8
T: 9.79E-08
0091478B0910F77E
KLX11B
65.00
RSMD01
FSM_W
N
Ω: 18.1
T: 6.26E-08
6091478B0910FD35
KLX11B
67.65
RSMD01
FSM_W
N
Ω: 21.7
T: 3.62E-08
8091478B09110789
KLX11B
67.98
RSMD01
FSM_W
N
Ω: 22.7
T: 7.62E-08
6091478B091108CC
KLX11B
70.09
RSMD01
FSM_W
N
Ω: 44.3
T: 8.98E-09
E091478B09111107
KLX11B
72.53
RSMD01
FSM_W
N
Ω: 16.3
T: 4.22E-07
4091478B09111A82

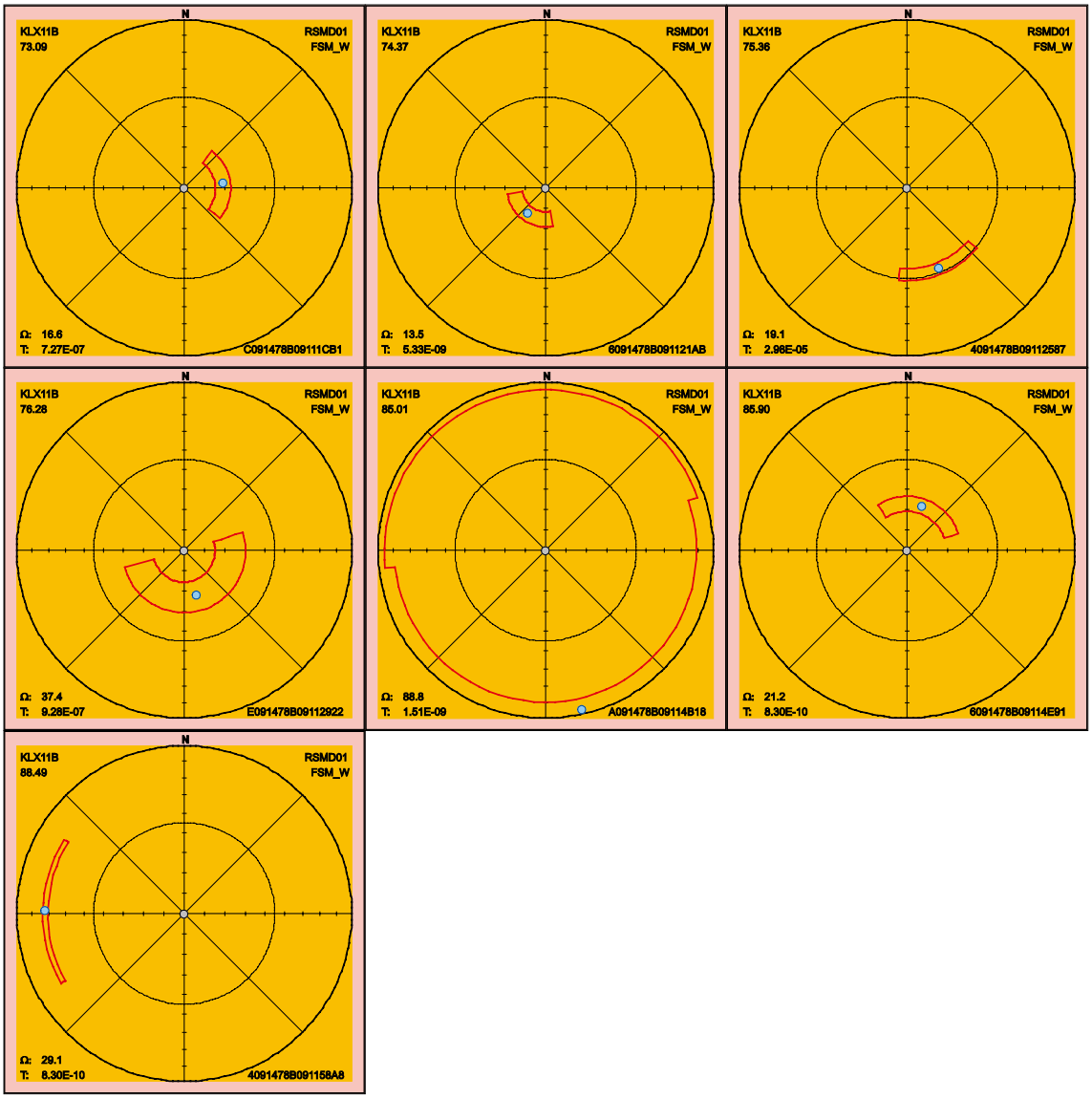
KLX11B
73.09
RSMD01
FSM_W
N
Ω: 16.6
T: 7.27E-07
C091478B09111CB1
KLX11B
74.37
RSMD01
FSM_W
N
Ω: 13.5
T: 5.33E-09
6091478B091121AB
KLX11B
75.36
RSMD01
FSM_W
N
Ω: 19.1
T: 2.98E-05
4091478B09112587
KLX11B
76.28
RSMD01
FSM_W
N
Ω: 37.4
T: 9.28E-07
E091478B09112922
KLX11B
85.01
RSMD01
FSM_W
N
Ω: 88.8
T: 1.51E-09
A091478B09114B18
KLX11B
85.90
RSMD01
FSM_W
N
Ω: 21.2
T: 8.30E-10
6091478B09114E91
KLX11B
88.49
RSMD01
FSM_W
N
Ω: 29.1
T: 8.30E-10
4091478B091158A8

2.3.20 KLX11C

There are 41 PFL fractures in KLX11C of which six have maximum uncertainty larger than 30°, see Table 2-18. These fractures can have an alternative interpretation of orientation compared to the best estimate orientation that is found in the table p_fract_core in /Sicada 2008/. Below follow the 90th percentile sample space of uncertainty for the PFL fractures in KLX11C.

Table 2-18. Fractures in KLX11C with uncertainty, Ω, larger than 30°.

FeatureId	PFL-f no	Adjusted Secup	Ω
C091478B0810799F	14	31.13	60.3
2091478B081080D7	15	32.98	67.4
E091478B08108665	16	34.40	41.9
2091478B0810CE05	24	52.73	53.1
4091478B0810FB33	27	64.28	40.4
E091478B081125E4	34	75.19	43.8

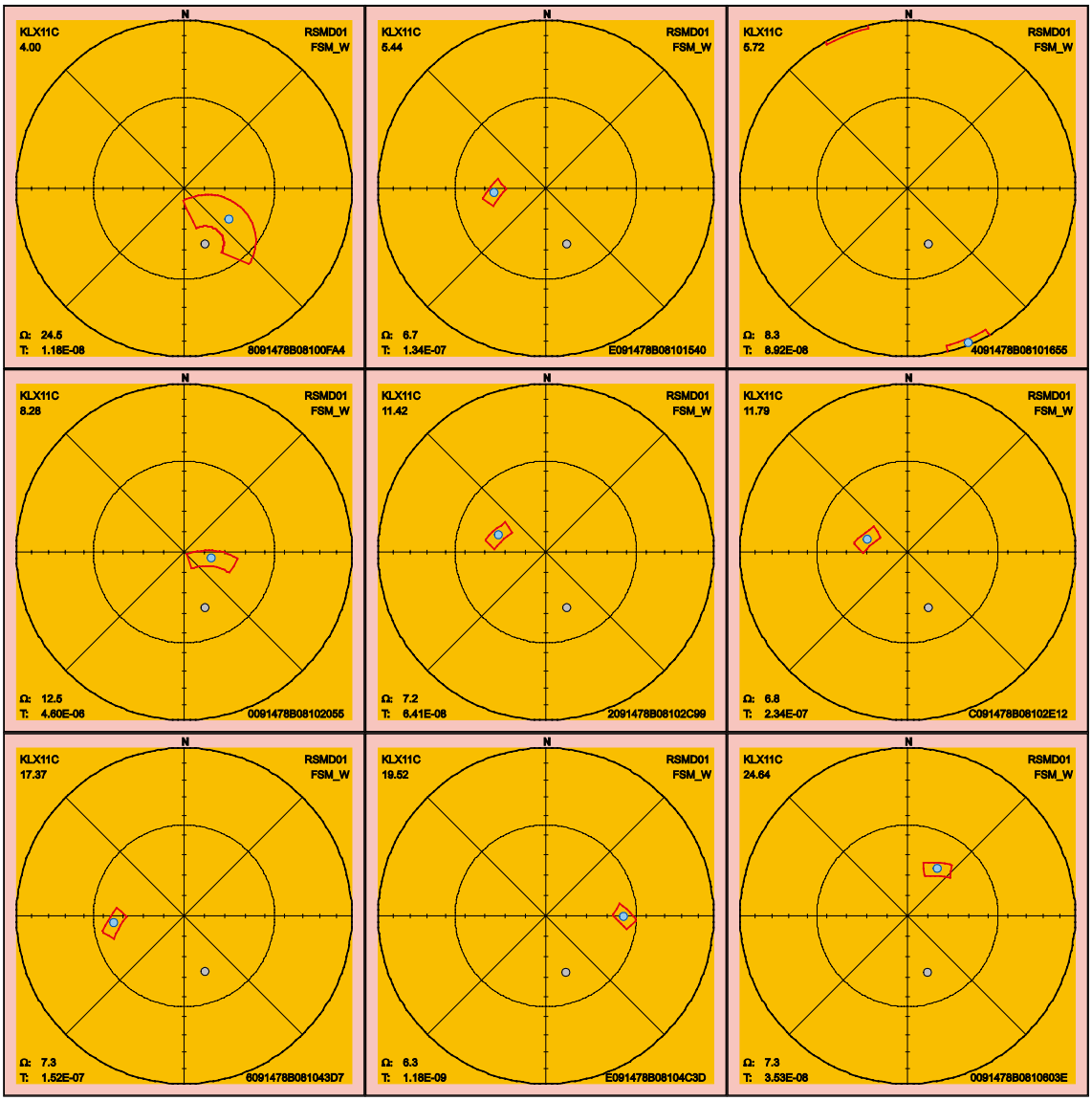

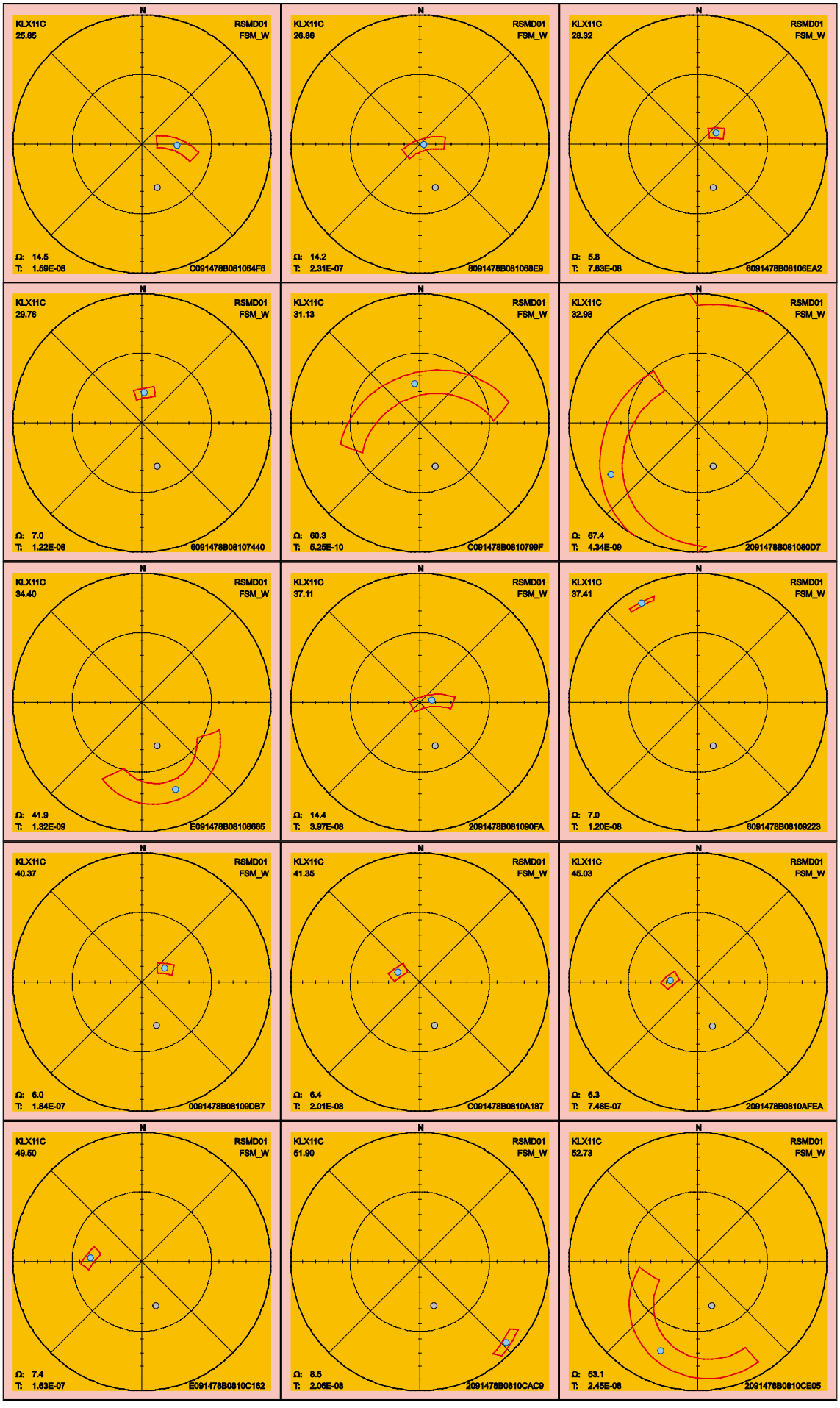
KLX11C
25.85
RSMD01
FSM_W
N
Ω: 14.5
T: 1.59E-08
C091478B081064F6
KLX11C
26.86
RSMD01
FSM_W
N
Ω: 14.2
T: 2.31E-07
8091478B081068E9
KLX11C
28.32
RSMD01
FSM_W
N
Ω: 5.8
T: 7.83E-08
6091478B08106EA2
KLX11C
29.76
RSMD01
FSM_W
N
Ω: 7.0
T: 1.22E-08
6091478B08107440
KLX11C
31.13
RSMD01
FSM_W
N
Ω: 60.3
T: 5.25E-10
C091478B0810799F
KLX11C
32.98
RSMD01
FSM_W
N
Ω: 67.4
T: 4.34E-09
2091478B081080D7
KLX11C
34.40
RSMD01
FSM_W
N
Ω: 41.9
T: 1.32E-09
E091478B08108665
KLX11C
37.11
RSMD01
FSM_W
N
Ω: 14.4
T: 3.97E-08
2091478B081090FA
KLX11C
37.41
RSMD01
FSM_W
N
Ω: 7.0
T: 1.20E-08
6091478B08109223
KLX11C
40.37
RSMD01
FSM_W
N
Ω: 6.0
T: 1.84E-07
0091478B08109DB7
KLX11C
41.35
RSMD01
FSM_W
N
Ω: 6.4
T: 2.01E-08
C091478B0810A187
KLX11C
45.03
RSMD01
FSM_W
N
Ω: 6.3
T: 7.46E-07
2091478B0810AFEA
KLX11C
49.50
RSMD01
FSM_W
N
Ω: 7.4
T: 1.63E-07
E091478B0810C162
KLX11C
51.90
RSMD01
FSM_W
N
Ω: 8.5
T: 2.06E-08
2091478B0810CAC9
KLX11C
52.73
RSMD01
FSM_W
N
Ω: 53.1
T: 2.45E-08
2091478B0810CE05

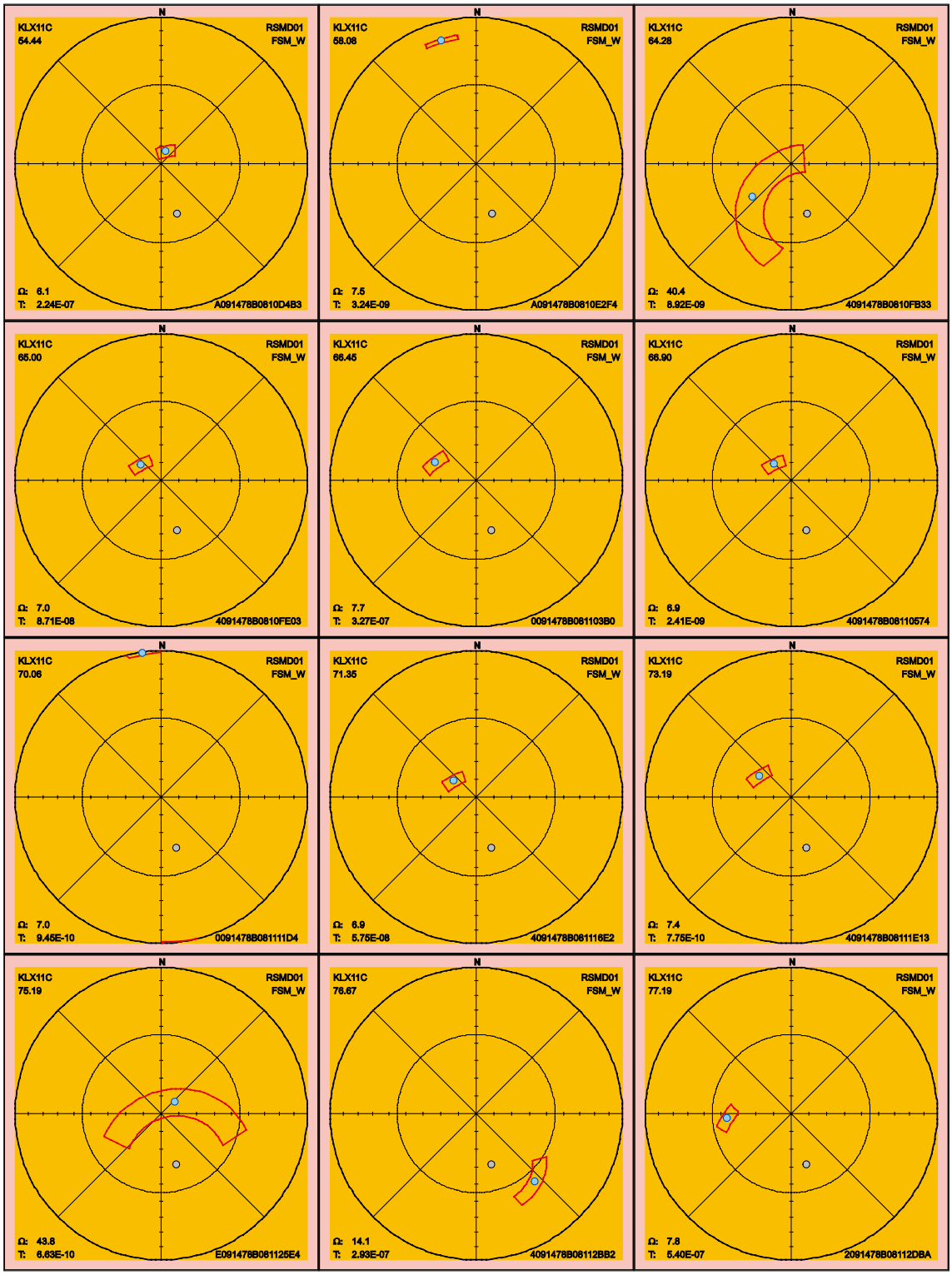
KLX11C
54.44
RSMD01
FSM_W
N
Ω: 6.1
T: 2.24E-07
A091478B0810D4B3
KLX11C
58.08
RSMD01
FSM_W
N
Ω: 7.5
T: 3.24E-09
A091478B0810E2F4
KLX11C
64.28
RSMD01
FSM_W
N
Ω: 40.4
T: 8.92E-09
4091478B0810FB33
KLX11C
65.00
RSMD01
FSM_W
N
Ω: 7.0
T: 8.71E-08
4091478B0810FE03
KLX11C
66.45
RSMD01
FSM_W
N
Ω: 7.7
T: 3.27E-07
0091478B081103B0
KLX11C
66.90
RSMD01
FSM_W
N
Ω: 6.9
T: 2.41E-09
4091478B08110574
KLX11C
70.06
RSMD01
FSM_W
N
Ω: 7.0
T: 9.45E-10
0091478B081111D4
KLX11C
71.35
RSMD01
FSM_W
N
Ω: 6.9
T: 5.75E-08
4091478B081116E2
KLX11C
73.19
RSMD01
FSM_W
N
Ω: 7.4
T: 7.75E-10
4091478B08111E13
KLX11C
75.19
RSMD01
FSM_W
N
Ω: 43.8
T: 6.63E-10
E091478B081125E4
KLX11C
76.67
RSMD01
FSM_W
N
Ω: 14.1
T: 2.93E-07
4091478B08112BB2
KLX11C
77.19
RSMD01
FSM_W
N
Ω: 7.8
T: 5.40E-07
2091478B08112DBA

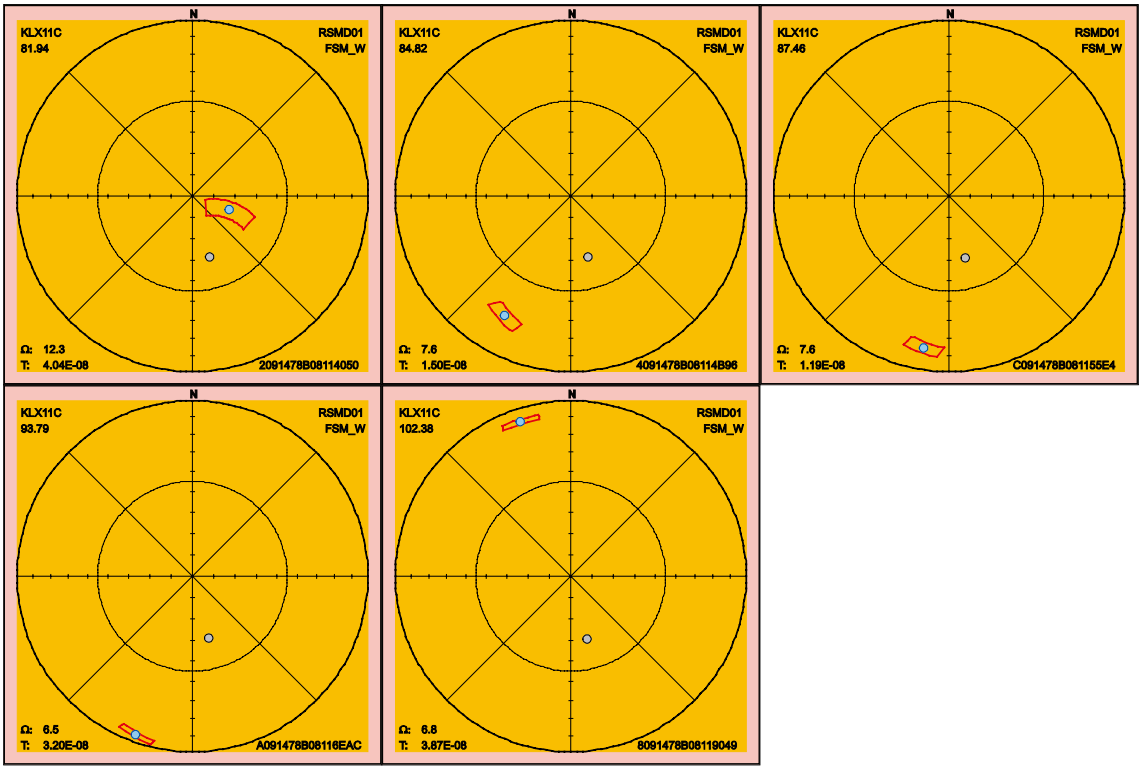

2.3.21 KLX11D

Below follow the 90th percentile sample space of uncertainty for the 49 PFL fractures in KLX11D. There are two fractures, listed in Table 2-19, that have maximum uncertainty larger than 30° and thus can have an alternative interpretation of orientation compared to the best estimate orientation that is found in the table p_fract_core in /Sicada 2008/.

Table 2-19. Fractures in KLX11D with uncertainty, Ω, larger than 30°.

FeatureId	PFL-f no	Adjusted Secup	Ω
4091478B0F10AEDA	17	44.65	55.8
4091478B0F10E9DD	26	59.75	41.1

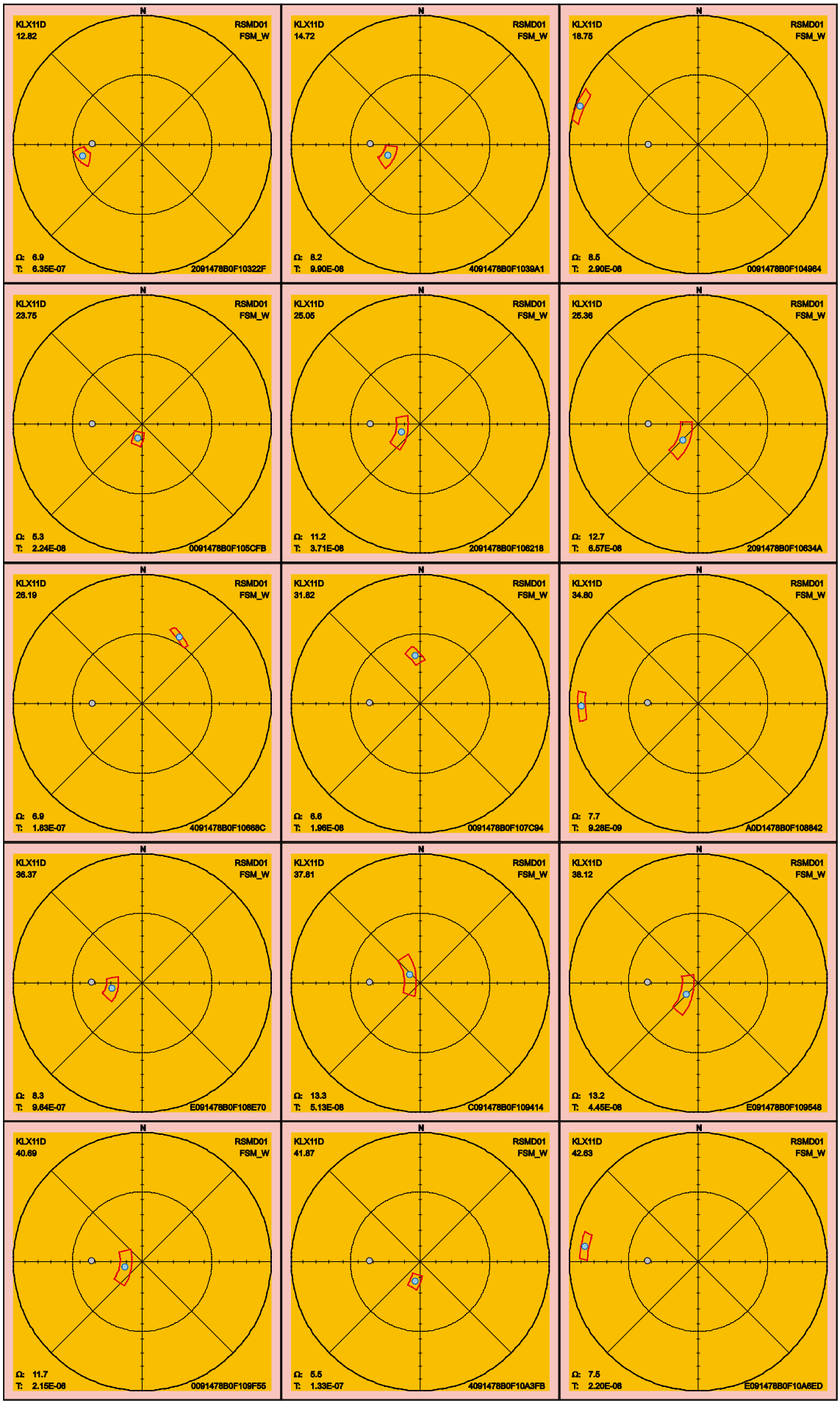
KLX11D
12.82
RSMD01
FSM_W
Ω: 6.9
T: 6.35E-07
2091478B0F10322F
KLX11D
14.72
RSMD01
FSM_W
Ω: 8.2
T: 9.90E-08
4091478B0F1039A1
KLX11D
18.75
RSMD01
FSM_W
Ω: 8.5
T: 2.90E-08
0091478B0F104964
KLX11D
23.75
RSMD01
FSM_W
Ω: 5.3
T: 2.24E-08
0091478B0F105CFB
KLX11D
25.05
RSMD01
FSM_W
Ω: 11.2
T: 3.71E-08
2091478B0F106218
KLX11D
25.36
RSMD01
FSM_W
Ω: 12.7
T: 6.57E-08
2091478B0F10634A
KLX11D
26.19
RSMD01
FSM_W
Ω: 6.9
T: 1.83E-07
4091478B0F10668C
KLX11D
31.82
RSMD01
FSM_W
Ω: 6.6
T: 1.96E-08
0091478B0F107C94
KLX11D
34.80
RSMD01
FSM_W
Ω: 7.7
T: 9.28E-09
A0D1478B0F108842
KLX11D
36.37
RSMD01
FSM_W
Ω: 8.3
T: 9.64E-07
E091478B0F108E70
KLX11D
37.81
RSMD01
FSM_W
Ω: 13.3
T: 5.13E-08
C091478B0F109414
KLX11D
38.12
RSMD01
FSM_W
Ω: 13.2
T: 4.45E-08
E091478B0F109548
KLX11D
40.69
RSMD01
FSM_W
Ω: 11.7
T: 2.15E-08
0091478B0F109F55
KLX11D
41.87
RSMD01
FSM_W
Ω: 5.5
T: 1.33E-07
4091478B0F10A3FB
KLX11D
42.63
RSMD01
FSM_W
Ω: 7.5
T: 2.20E-08
E091478B0F10A6ED

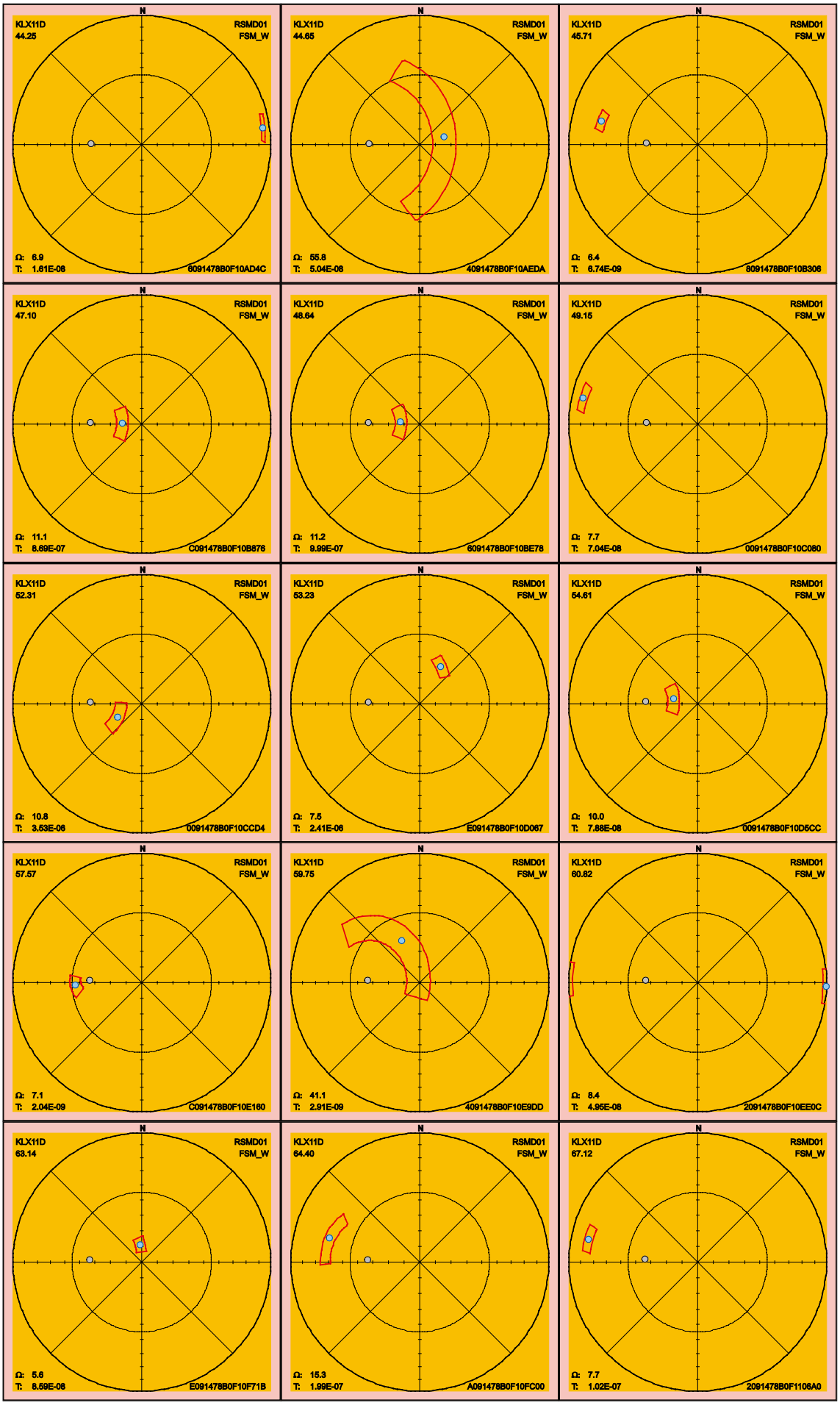
KLX11D
44.25
RSMD01
FSM_W
N
Ω: 6.9
T: 1.61E-08
6091478B0F10AD4C
KLX11D
44.65
RSMD01
FSM_W
N
Ω: 55.8
T: 5.04E-08
4091478B0F10AEDA
KLX11D
45.71
RSMD01
FSM_W
N
Ω: 6.4
T: 6.74E-09
8091478B0F10B308
KLX11D
47.10
RSMD01
FSM_W
N
Ω: 11.1
T: 8.69E-07
C091478B0F10B876
KLX11D
48.64
RSMD01
FSM_W
N
Ω: 11.2
T: 9.99E-07
6091478B0F10BE78
KLX11D
49.15
RSMD01
FSM_W
N
Ω: 7.7
T: 7.04E-08
0091478B0F10C080
KLX11D
52.31
RSMD01
FSM_W
N
Ω: 10.8
T: 3.53E-06
0091478B0F10CCD4
KLX11D
53.23
RSMD01
FSM_W
N
Ω: 7.5
T: 2.41E-06
E091478B0F10D067
KLX11D
54.61
RSMD01
FSM_W
N
Ω: 10.0
T: 7.88E-08
0091478B0F10D6CC
KLX11D
57.57
RSMD01
FSM_W
N
Ω: 7.1
T: 2.04E-09
C091478B0F10E160
KLX11D
59.75
RSMD01
FSM_W
N
Ω: 41.1
T: 2.91E-09
4091478B0F10E9DD
KLX11D
60.82
RSMD01
FSM_W
N
Ω: 8.4
T: 4.95E-08
2091478B0F10EE0C
KLX11D
63.14
RSMD01
FSM_W
N
Ω: 5.6
T: 8.59E-08
E091478B0F10F71B
KLX11D
64.40
RSMD01
FSM_W
N
Ω: 15.3
T: 1.99E-07
A091478B0F10FC00
KLX11D
67.12
RSMD01
FSM_W
N
Ω: 7.7
T: 1.02E-07
2091478B0F1106A0

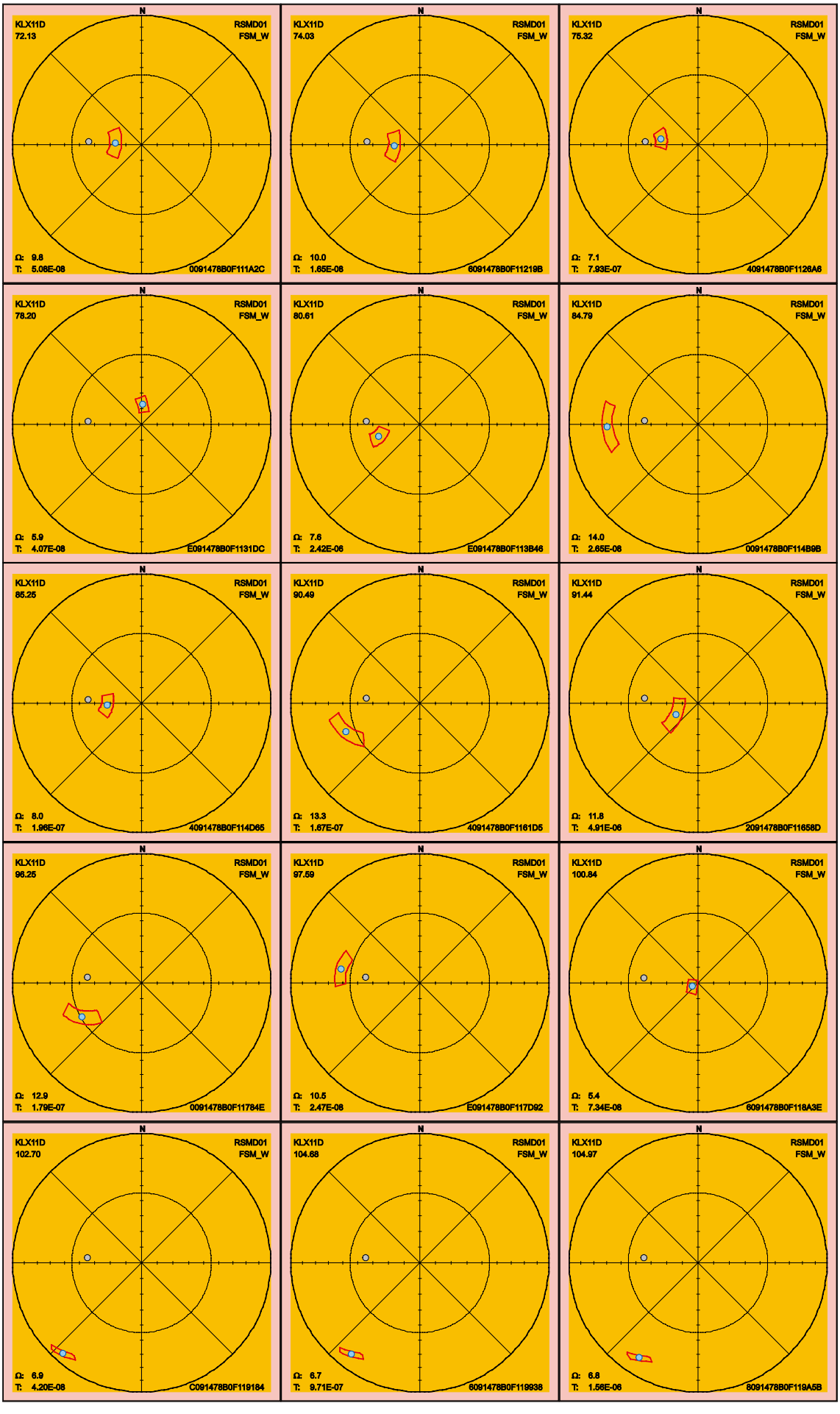
KLX11D
72.13
RSMD01
FSM_W
Ω: 9.8
T: 5.08E-08
0091478B0F111A2C
KLX11D
74.03
RSMD01
FSM_W
Ω: 10.0
T: 1.65E-08
6091478B0F11219B
KLX11D
76.32
RSMD01
FSM_W
Ω: 7.1
T: 7.93E-07
4091478B0F1126A6
KLX11D
78.20
RSMD01
FSM_W
Ω: 5.9
T: 4.07E-08
E091478B0F1131DC
KLX11D
80.61
RSMD01
FSM_W
Ω: 7.6
T: 2.42E-06
E091478B0F113B46
KLX11D
84.79
RSMD01
FSM_W
Ω: 14.0
T: 2.65E-08
0091478B0F114B9B
KLX11D
85.25
RSMD01
FSM_W
Ω: 8.0
T: 1.96E-07
4091478B0F114D65
KLX11D
90.49
RSMD01
FSM_W
Ω: 13.3
T: 1.67E-07
4091478B0F1161D5
KLX11D
91.44
RSMD01
FSM_W
Ω: 11.8
T: 4.91E-06
2091478B0F11658D
KLX11D
96.25
RSMD01
FSM_W
Ω: 12.9
T: 1.79E-07
0091478B0F11784E
KLX11D
97.59
RSMD01
FSM_W
Ω: 10.5
T: 2.47E-08
E091478B0F117D92
KLX11D
100.84
RSMD01
FSM_W
Ω: 5.4
T: 7.34E-08
6091478B0F118A3E
KLX11D
102.70
RSMD01
FSM_W
Ω: 6.9
T: 4.20E-08
C091478B0F119184
KLX11D
104.68
RSMD01
FSM_W
Ω: 6.7
T: 9.71E-07
6091478B0F119938
KLX11D
104.97
RSMD01
FSM_W
Ω: 6.8
T: 1.56E-06
8091478B0F119A5B

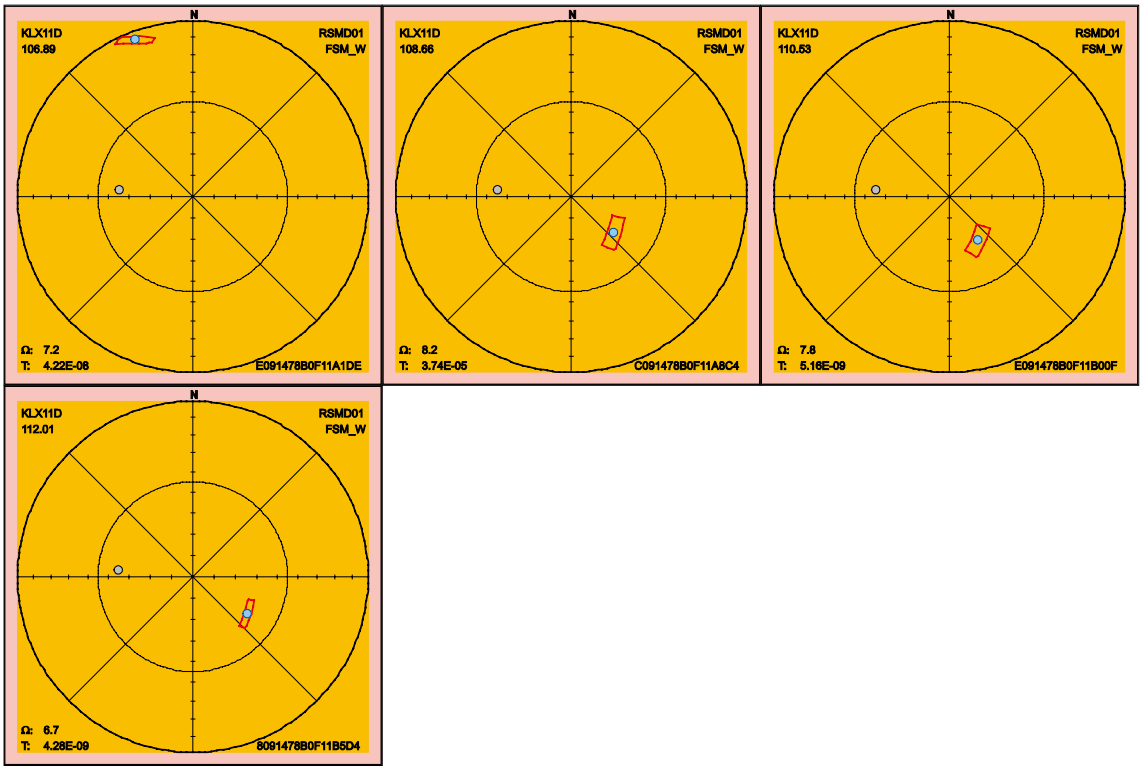

2.3.22 KLX11E

There are 37 PFL fractures in KLX11E of which two have maximum uncertainty larger than 30°, see Table 2-20. These fractures can have an alternative interpretation of orientation compared to the best estimate orientation that is found in the table p_fract_core in /Sicada 2008/. Below follow the 90th percentile sample space of uncertainty for the PFL fractures in KLX11E.

Table 2-20. Fractures in KLX11E with uncertainty, Ω, larger than 30°.

FeatureId	PFL-f no	Adjusted Secup	Ω
0091478B0E10BA7B	16	47.90	49.5
6091478B0E111005	26	69.68	53.3

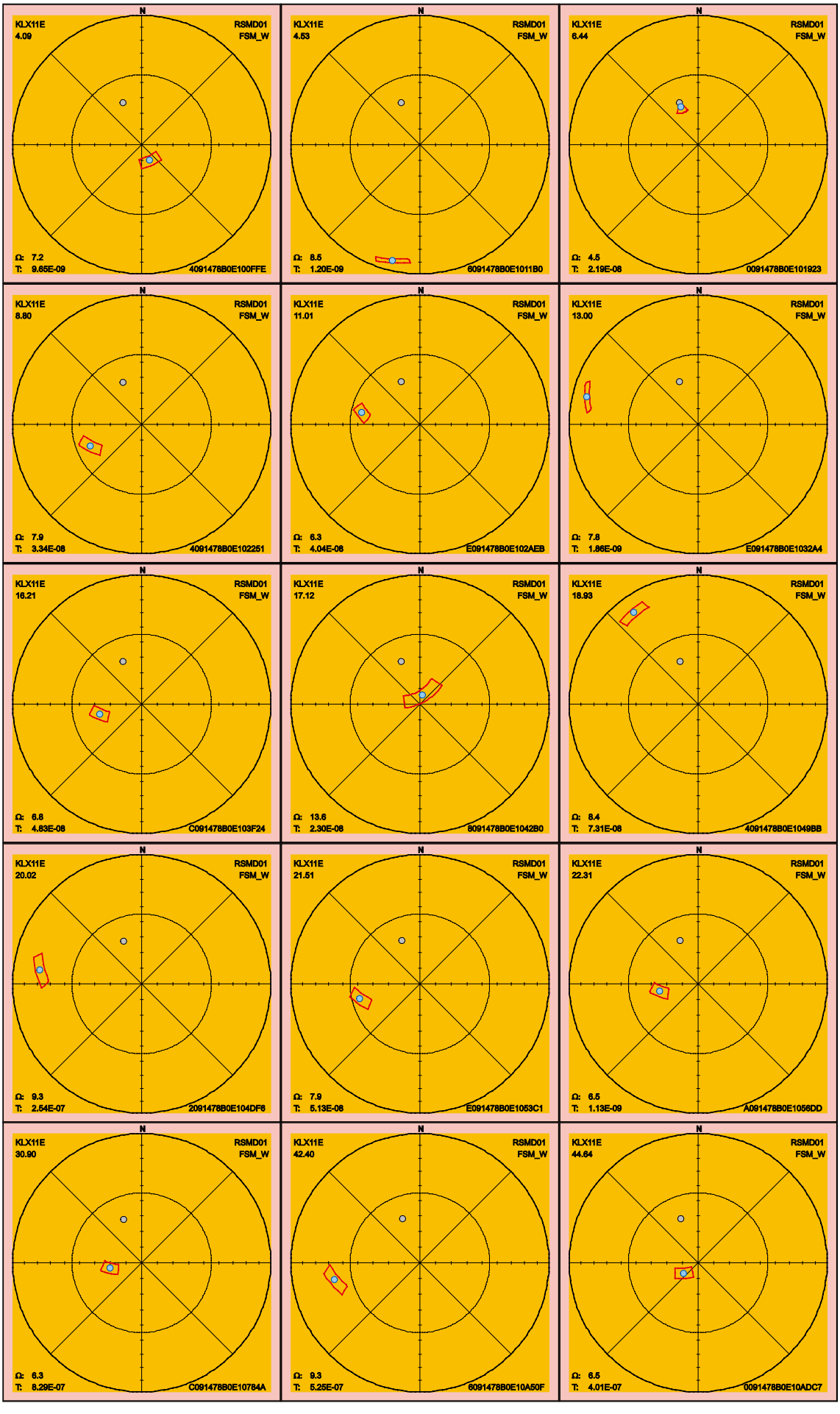
KLX11E
4.09
RSMD01
FSM_W
Ω: 7.2
T: 9.65E-09
4091478B0E100FFE
KLX11E
4.53
RSMD01
FSM_W
Ω: 8.5
T: 1.20E-09
6091478B0E1011B0
KLX11E
6.44
RSMD01
FSM_W
Ω: 4.5
T: 2.19E-08
0091478B0E101923
KLX11E
8.80
RSMD01
FSM_W
Ω: 7.9
T: 3.34E-08
4091478B0E102251
KLX11E
11.01
RSMD01
FSM_W
Ω: 6.3
T: 4.04E-08
E091478B0E102AEB
KLX11E
13.00
RSMD01
FSM_W
Ω: 7.9
T: 1.86E-09
E091478B0E1032A4
KLX11E
16.21
RSMD01
FSM_W
Ω: 6.8
T: 4.83E-08
C091478B0E103F24
KLX11E
17.12
RSMD01
FSM_W
Ω: 13.6
T: 2.30E-08
8091478B0E1042B0
KLX11E
18.93
RSMD01
FSM_W
Ω: 8.4
T: 7.31E-08
4091478B0E1049BB
KLX11E
20.02
RSMD01
FSM_W
Ω: 9.3
T: 2.54E-07
2091478B0E104DF8
KLX11E
21.51
RSMD01
FSM_W
Ω: 7.9
T: 5.13E-08
E091478B0E1053C1
KLX11E
22.31
RSMD01
FSM_W
Ω: 6.5
T: 1.13E-09
A091478B0E1056DD
KLX11E
30.90
RSMD01
FSM_W
Ω: 6.3
T: 8.29E-07
C091478B0E10784A
KLX11E
42.40
RSMD01
FSM_W
Ω: 9.3
T: 5.25E-07
6091478B0E10A50F
KLX11E
44.64
RSMD01
FSM_W
Ω: 6.5
T: 4.01E-07
0091478B0E10ADC7

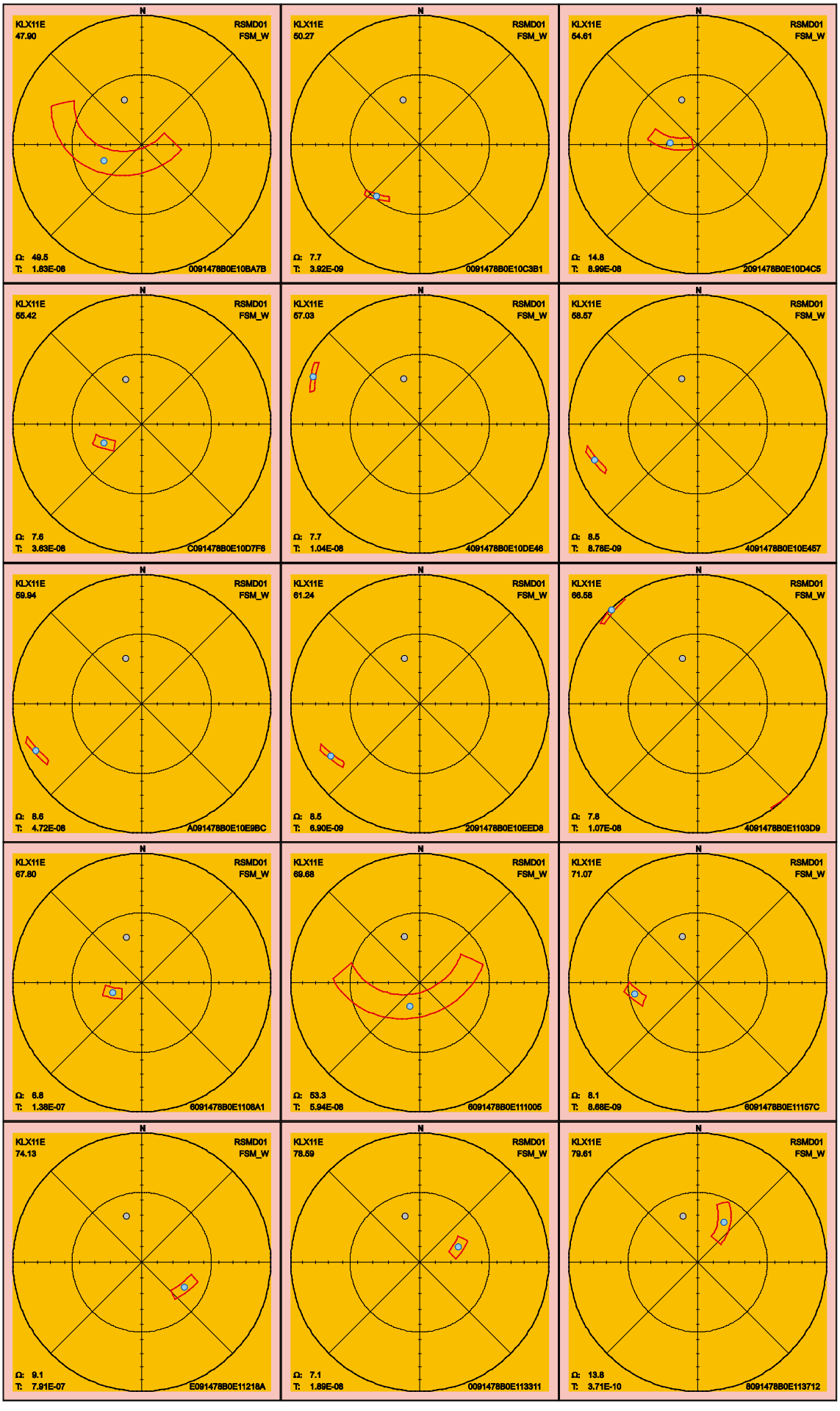
KLX11E
47.90
RSMD01
FSM_W
N
Ω: 49.5
T: 1.83E-06
0091478B0E10BA7B
KLX11E
50.27
RSMD01
FSM_W
N
Ω: 7.7
T: 3.92E-09
0091478B0E10C3B1
KLX11E
54.61
RSMD01
FSM_W
N
Ω: 14.8
T: 8.99E-08
2091478B0E10D4C5
KLX11E
55.42
RSMD01
FSM_W
N
Ω: 7.6
T: 3.63E-06
C091478B0E10D7F6
KLX11E
57.03
RSMD01
FSM_W
N
Ω: 7.7
T: 1.04E-06
4091478B0E10DE46
KLX11E
58.57
RSMD01
FSM_W
N
Ω: 8.5
T: 8.78E-09
4091478B0E10E457
KLX11E
59.94
RSMD01
FSM_W
N
Ω: 8.6
T: 4.72E-06
A091478B0E10E9BC
KLX11E
61.24
RSMD01
FSM_W
N
Ω: 8.5
T: 6.90E-09
2091478B0E10EED8
KLX11E
66.58
RSMD01
FSM_W
N
Ω: 7.8
T: 1.07E-06
4091478B0E1103D9
KLX11E
67.80
RSMD01
FSM_W
N
Ω: 6.8
T: 1.38E-07
6091478B0E1108A1
KLX11E
69.68
RSMD01
FSM_W
N
Ω: 53.3
T: 5.94E-08
6091478B0E111005
KLX11E
71.07
RSMD01
FSM_W
N
Ω: 8.1
T: 8.68E-09
6091478B0E11157C
KLX11E
74.13
RSMD01
FSM_W
N
Ω: 9.1
T: 7.91E-07
E091478B0E11218A
KLX11E
78.59
RSMD01
FSM_W
N
Ω: 7.1
T: 1.89E-06
0091478B0E113311
KLX11E
79.61
RSMD01
FSM_W
N
Ω: 13.8
T: 3.71E-10
8091478B0E113712

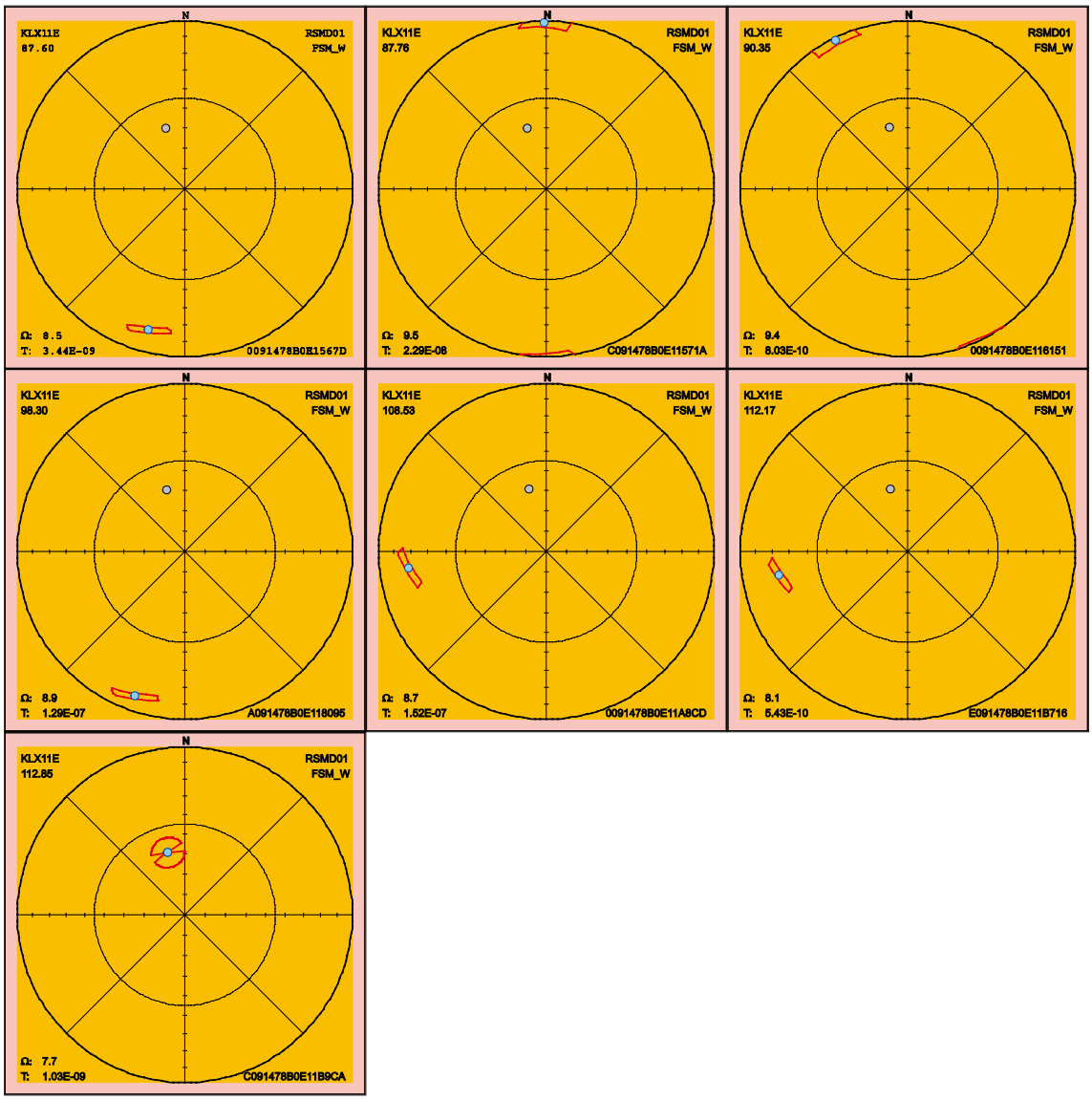
KLX11E
87.60
RSMD01
FSM_W
N
Ω: 8.5
T: 3.44E-09
0091478B0E1567D
KLX11E
87.76
RSMD01
FSM_W
N
Ω: 9.5
T: 2.29E-08
C091478B0E11571A
KLX11E
90.35
RSMD01
FSM_W
N
Ω: 9.4
T: 8.03E-10
0091478B0E116151
KLX11E
98.30
RSMD01
FSM_W
N
Ω: 8.9
T: 1.29E-07
A091478B0E118095
KLX11E
108.53
RSMD01
FSM_W
N
Ω: 8.7
T: 1.52E-07
0091478B0E11A8CD
KLX11E
112.17
RSMD01
FSM_W
N
Ω: 8.1
T: 5.43E-10
E091478B0E11B716
KLX11E
112.85
RSMD01
FSM_W
N
Ω: 7.7
T: 1.03E-09
C091478B0E11B9CA

2.3.23 KLX11F

There is no PFL fracture in KLX11F with orientation uncertainty larger than 30°. Below follow the 90th percentile sample space of uncertainty for the 21 PFL fractures.

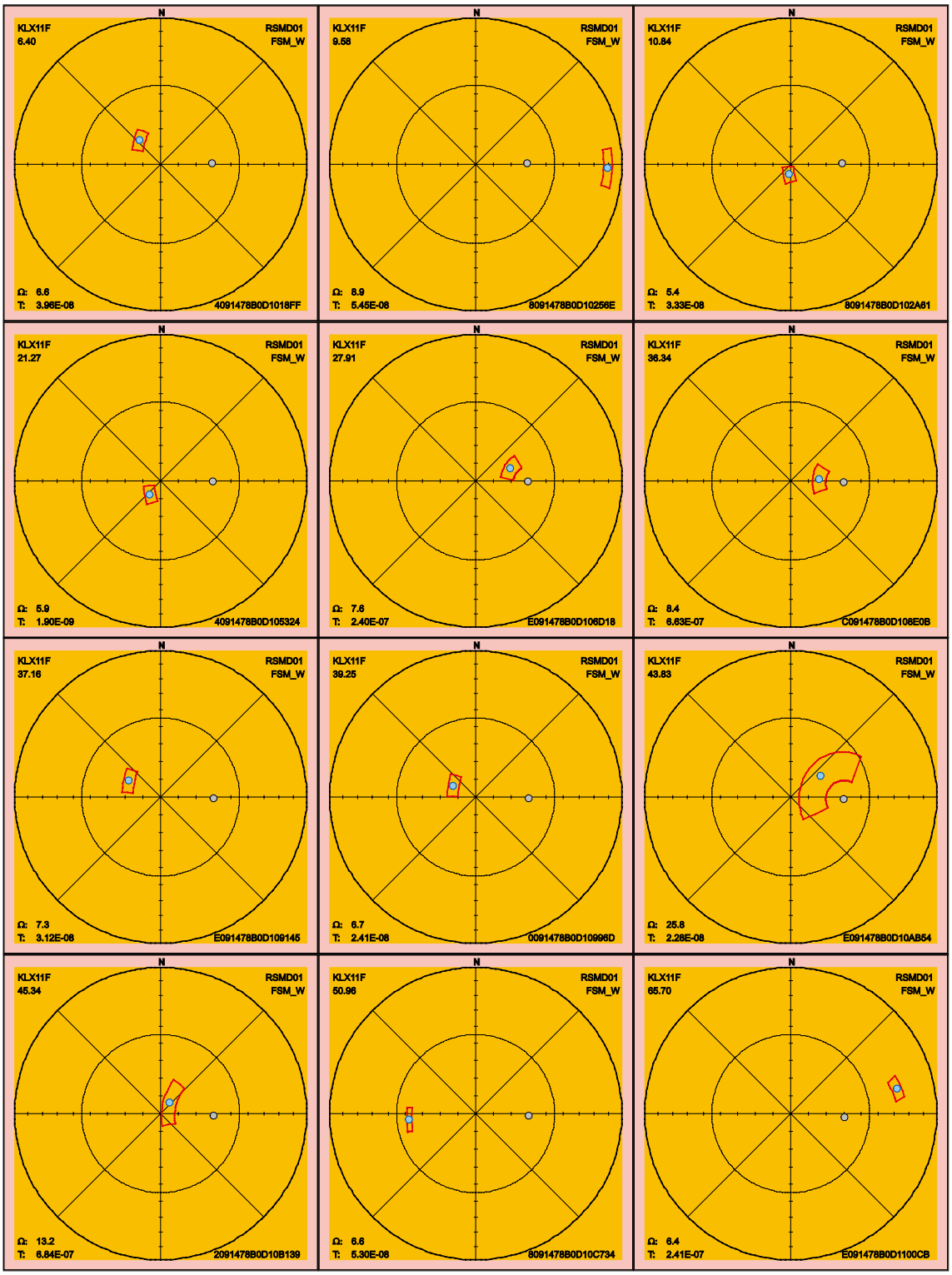

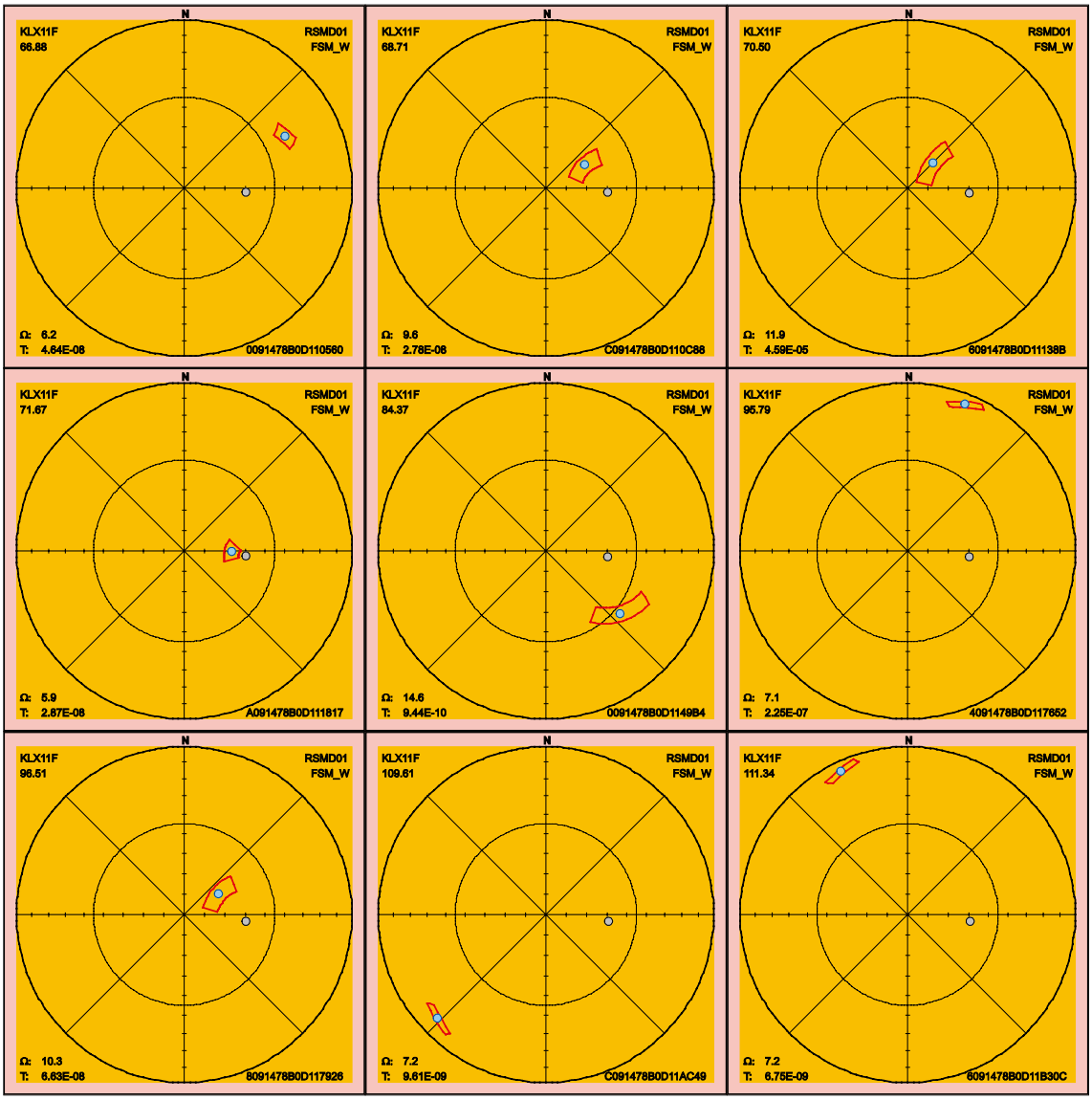

2.3.24 KLX12A

Below follow the 90th percentile sample space of uncertainty for the 73 PFL fractures in KLX12A. There are ten fractures listed in Table 2-22 that can, due to large uncertainty, have an alternative interpretation of orientation compared to the best estimate orientation that is found in the table p_fract_core in /Sicada 2008/.

Table 2-21. Fractures in KLX12A with uncertainty, Ω, larger than 30°.

FeatureId	PFL-f no	Adjusted Secup	Ω
9DD2478B0A11935E	3	103.28	74.7
A052478B0A11D925	18	121.25	30.8
D312478B0A11E32D	21	123.83	35.1
B292478B0A11ED06	23	126.35	39.6
A952478B0A11F47D	24	128.27	45.4
CB92478B0A12C8DD	48	182.82	30.3
6392478B0A139959	53	236.38	50.4
F8D2478B0A1608CE	67	396.60	46.5
7992478B0A1633D1	71	407.67	64.2
E1D2478B0A184269	76	542.91	67.2

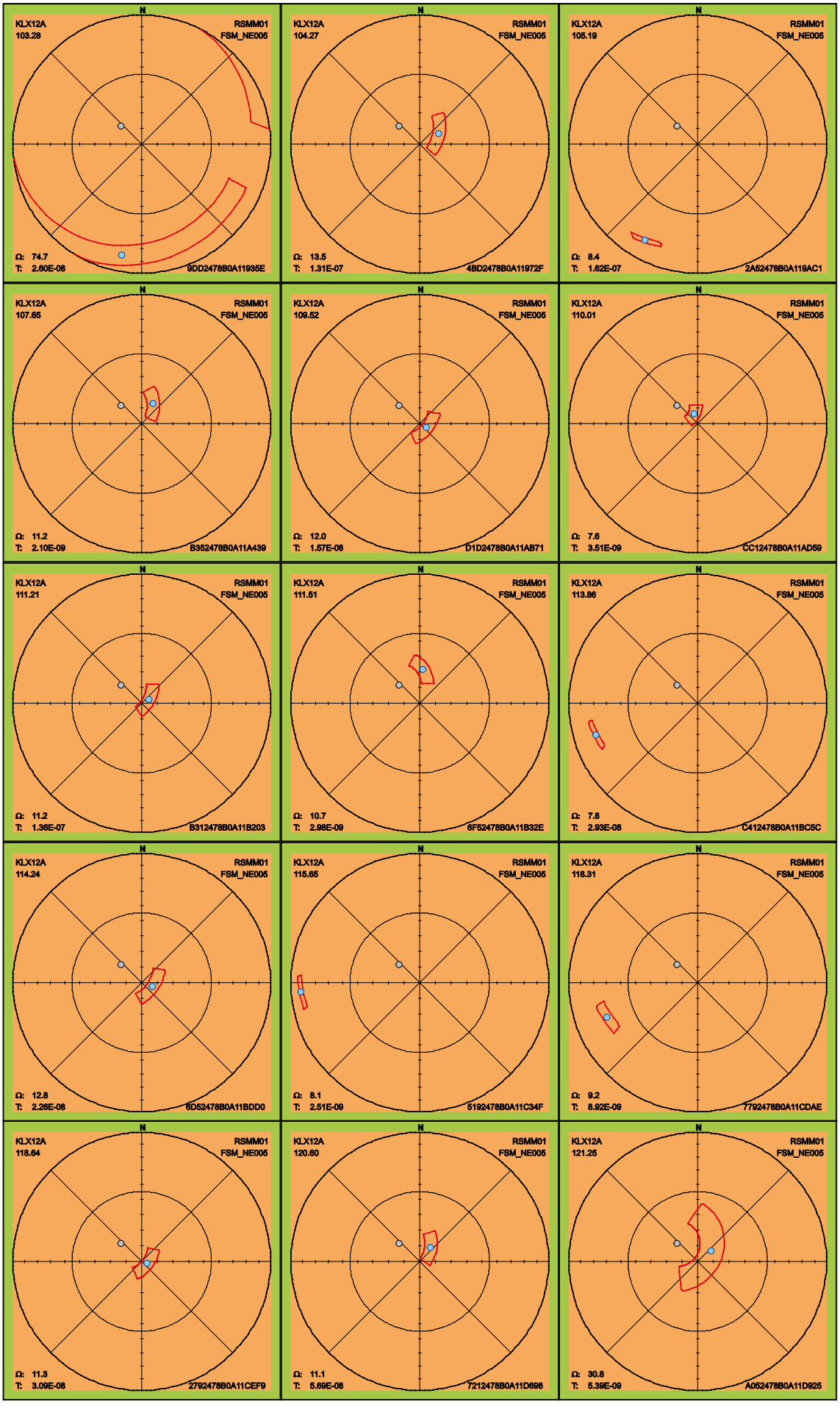
KLX12A
103.28
RSMM01
FSM_NE005
N
Ω: 74.7
T: 2.60E-08
9DD2478B0A11935E
KLX12A
104.27
RSMM01
FSM_NE005
N
Ω: 13.5
T: 1.31E-07
4BD2478B0A11972F
KLX12A
105.19
RSMM01
FSM_NE005
N
Ω: 8.4
T: 1.62E-07
2A52478B0A119AC1
KLX12A
107.65
RSMM01
FSM_NE005
N
Ω: 11.2
T: 2.10E-09
B352478B0A11A439
KLX12A
109.52
RSMM01
FSM_NE005
N
Ω: 12.0
T: 1.57E-08
D1D2478B0A11AB71
KLX12A
110.01
RSMM01
FSM_NE005
N
Ω: 7.6
T: 3.51E-09
CC12478B0A11AD59
KLX12A
111.21
RSMM01
FSM_NE005
N
Ω: 11.2
T: 1.36E-07
B312478B0A11B203
KLX12A
111.51
RSMM01
FSM_NE005
N
Ω: 10.7
T: 2.98E-09
6F52478B0A11B32E
KLX12A
113.86
RSMM01
FSM_NE005
N
Ω: 7.8
T: 2.93E-08
C412478B0A11BC5C
KLX12A
114.24
RSMM01
FSM_NE005
N
Ω: 12.8
T: 2.26E-08
6D52478B0A11BDD0
KLX12A
115.65
RSMM01
FSM_NE005
N
Ω: 8.1
T: 2.51E-09
5192478B0A11C34F
KLX12A
118.31
RSMM01
FSM_NE005
N
Ω: 9.2
T: 8.92E-09
7792478B0A11CDAE
KLX12A
118.64
RSMM01
FSM_NE005
N
Ω: 11.3
T: 3.09E-08
2792478B0A11CEF9
KLX12A
120.60
RSMM01
FSM_NE005
N
Ω: 11.1
T: 5.69E-08
7212478B0A11D698
KLX12A
121.25
RSMM01
FSM_NE005
N
Ω: 30.8
T: 5.39E-09
A052478B0A11D925

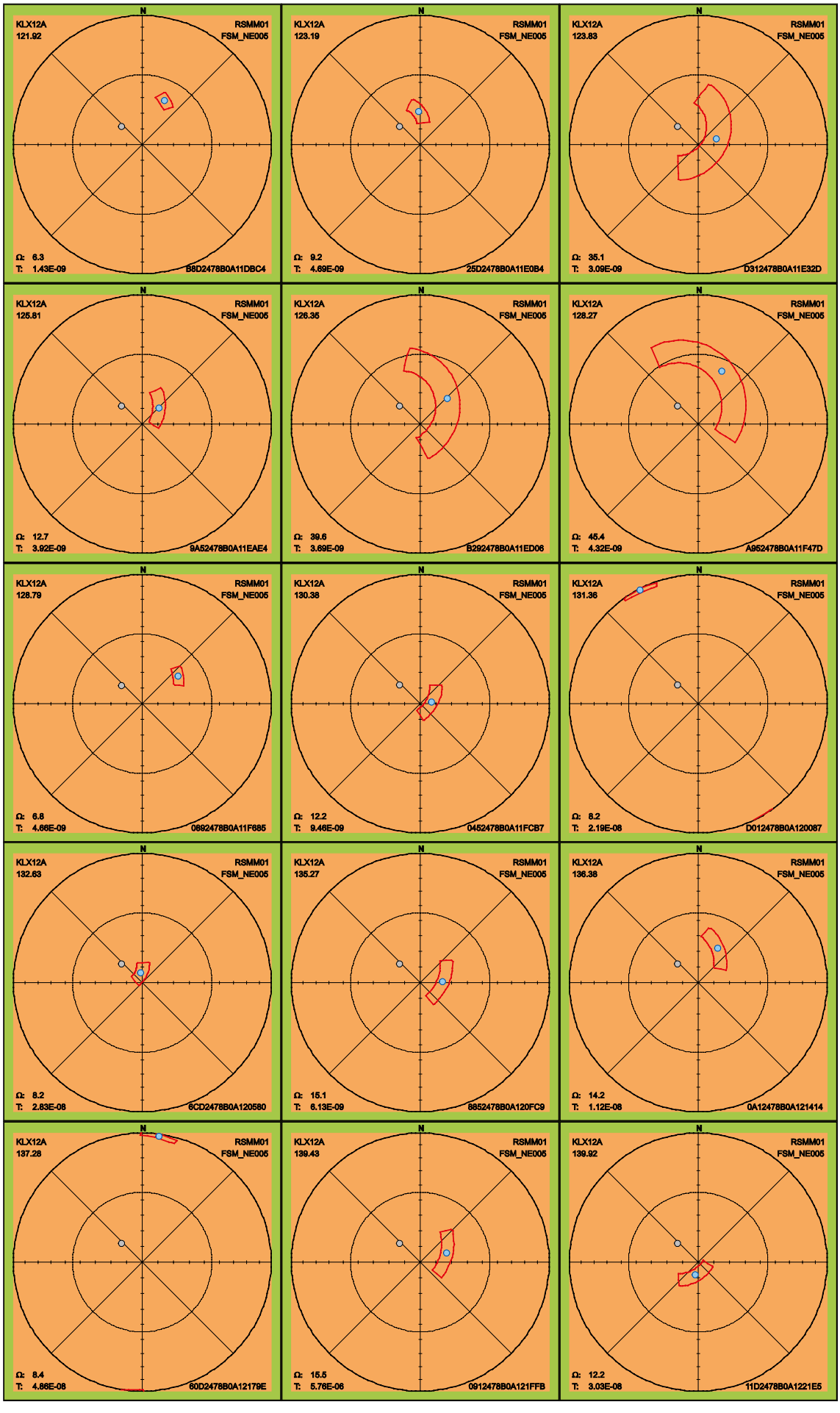
KLX12A
121.92
RSMM01
FSM_NE005
Ω: 6.3
T: 1.43E-09
B8D2478B0A11DBC4
KLX12A
123.19
RSMM01
FSM_NE005
Ω: 9.2
T: 4.69E-09
25D2478B0A11E0B4
KLX12A
123.83
RSMM01
FSM_NE005
Ω: 35.1
T: 3.09E-09
D312478B0A11E32D
KLX12A
125.81
RSMM01
FSM_NE005
Ω: 12.7
T: 3.92E-09
9A52478B0A11EAE4
KLX12A
126.35
RSMM01
FSM_NE005
Ω: 39.6
T: 3.69E-09
B292478B0A11ED06
KLX12A
128.27
RSMM01
FSM_NE005
Ω: 45.4
T: 4.32E-09
A952478B0A11F47D
KLX12A
128.79
RSMM01
FSM_NE005
Ω: 6.8
T: 4.66E-09
0892478B0A11F685
KLX12A
130.38
RSMM01
FSM_NE005
Ω: 12.2
T: 9.46E-09
0452478B0A11FCB7
KLX12A
131.36
RSMM01
FSM_NE005
Ω: 8.2
T: 2.19E-08
D012478B0A120087
KLX12A
132.63
RSMM01
FSM_NE005
Ω: 8.2
T: 2.83E-08
8CD2478B0A120580
KLX12A
135.27
RSMM01
FSM_NE005
Ω: 15.1
T: 6.13E-09
8852478B0A120FC9
KLX12A
136.38
RSMM01
FSM_NE005
Ω: 14.2
T: 1.12E-08
0A12478B0A121414
KLX12A
137.28
RSMM01
FSM_NE005
Ω: 8.4
T: 4.86E-08
80D2478B0A12179E
KLX12A
139.43
RSMM01
FSM_NE005
Ω: 15.5
T: 5.76E-06
0912478B0A121FFB
KLX12A
139.92
RSMM01
FSM_NE005
Ω: 12.2
T: 3.03E-08
11D2478B0A1221E5

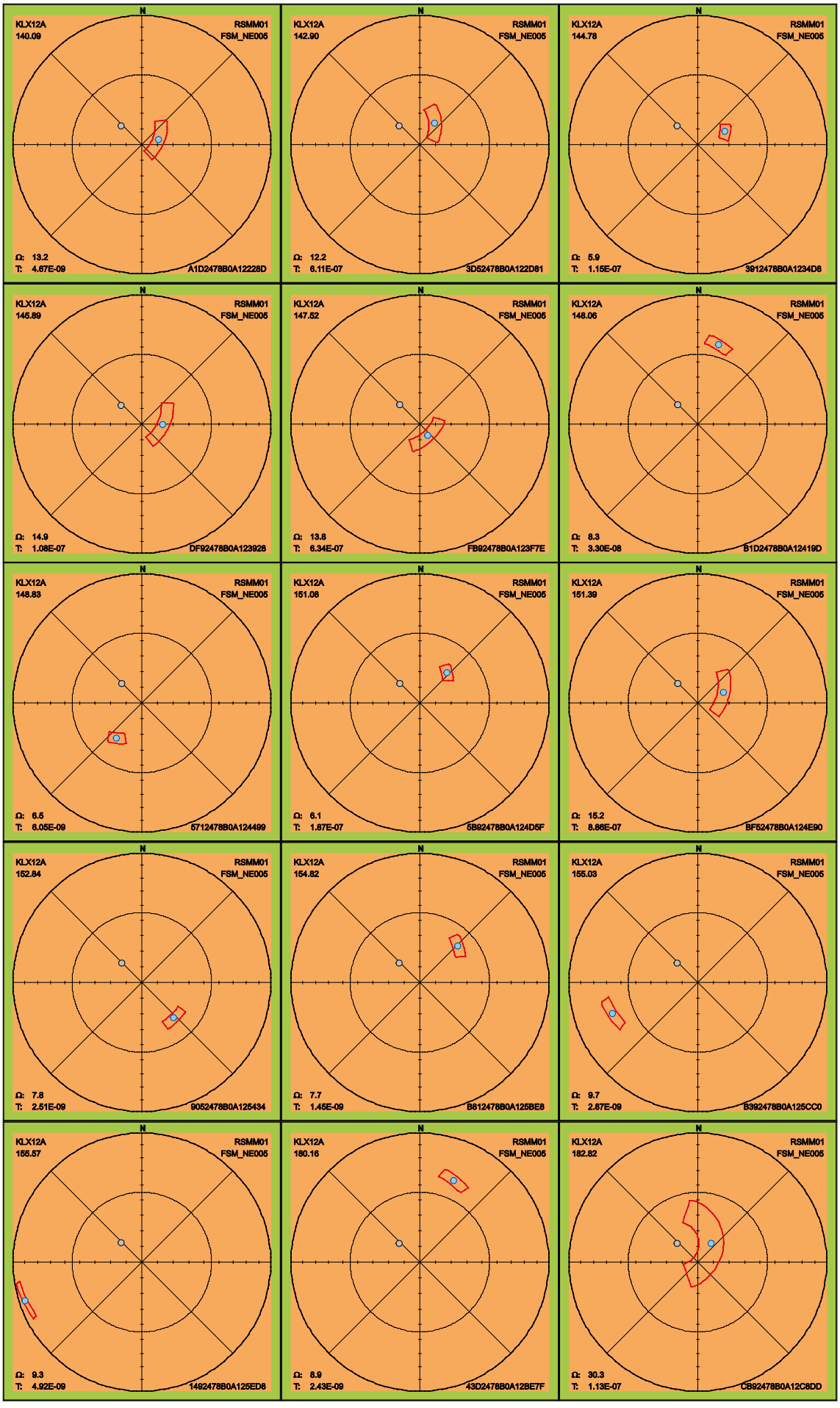
KLX12A
140.09
RSMM01
FSM_NE005
N
Ω: 13.2
T: 4.67E-09
A1D2478B0A12228D
KLX12A
142.90
RSMM01
FSM_NE005
N
Ω: 12.2
T: 6.11E-07
3D52478B0A122D81
KLX12A
144.78
RSMM01
FSM_NE005
N
Ω: 5.9
T: 1.15E-07
3912478B0A1234D8
KLX12A
145.89
RSMM01
FSM_NE005
N
Ω: 14.9
T: 1.08E-07
DF92478B0A123928
KLX12A
147.52
RSMM01
FSM_NE005
N
Ω: 13.8
T: 6.34E-07
FB92478B0A123F7E
KLX12A
148.06
RSMM01
FSM_NE005
N
Ω: 8.3
T: 3.30E-08
B1D2478B0A12419D
KLX12A
148.83
RSMM01
FSM_NE005
N
Ω: 6.5
T: 6.05E-09
5712478B0A124499
KLX12A
151.08
RSMM01
FSM_NE005
N
Ω: 6.1
T: 1.87E-07
5B92478B0A124D5F
KLX12A
151.39
RSMM01
FSM_NE005
N
Ω: 15.2
T: 8.86E-07
BF52478B0A124E90
KLX12A
152.84
RSMM01
FSM_NE005
N
Ω: 7.8
T: 2.51E-09
9052478B0A125434
KLX12A
154.82
RSMM01
FSM_NE005
N
Ω: 7.7
T: 1.45E-09
B812478B0A125BE8
KLX12A
155.03
RSMM01
FSM_NE005
N
Ω: 9.7
T: 2.87E-09
B392478B0A125CC0
KLX12A
155.57
RSMM01
FSM_NE005
N
Ω: 9.3
T: 4.92E-09
1492478B0A125ED8
KLX12A
180.16
RSMM01
FSM_NE005
N
Ω: 8.9
T: 2.43E-09
43D2478B0A12BE7F
KLX12A
182.82
RSMM01
FSM_NE005
N
Ω: 30.3
T: 1.13E-07
CB92478B0A12C8DD

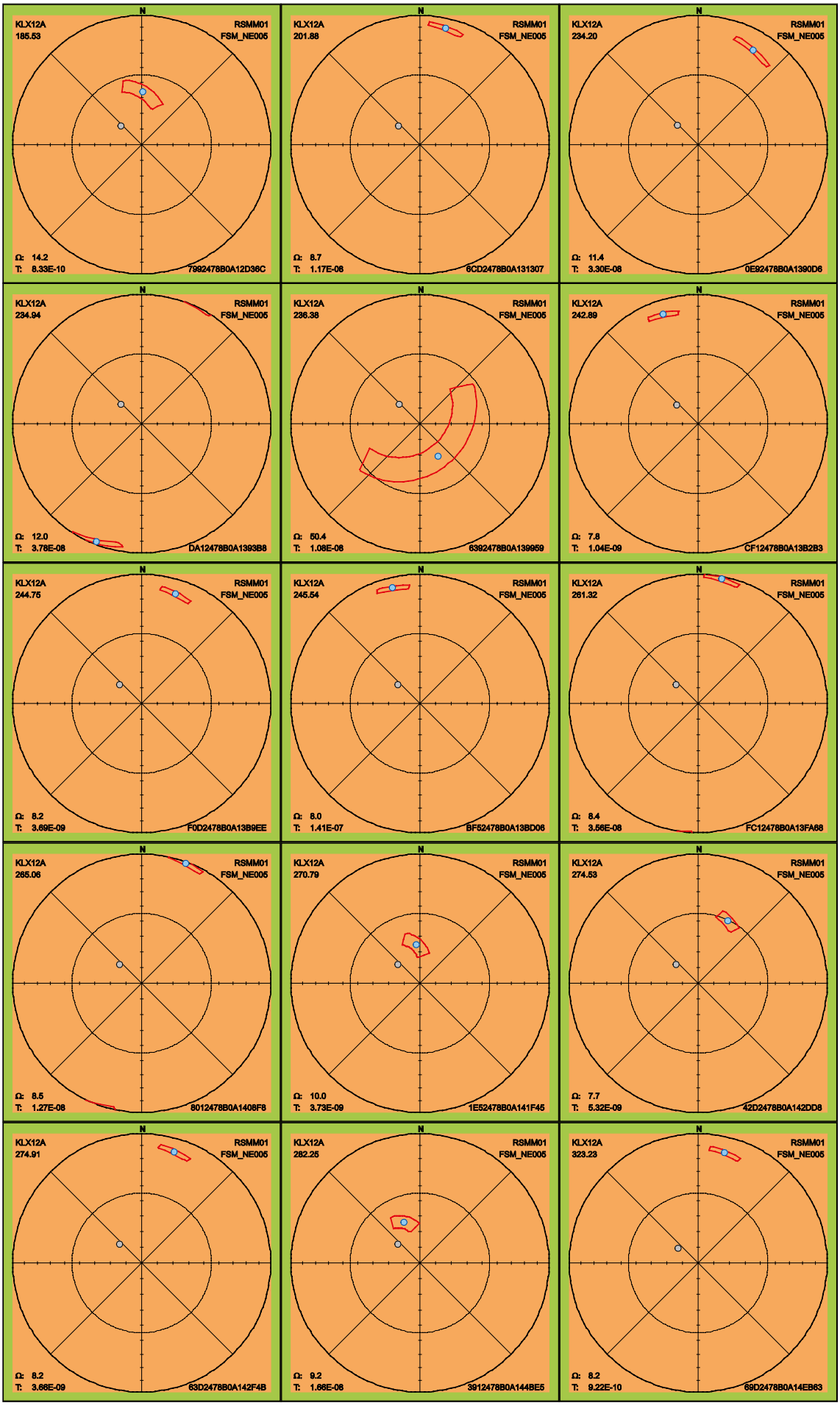
KLX12A
185.53
RSMM01
FSM_NE005
Ω: 14.2
T: 8.33E-10
7992478B0A12D36C
KLX12A
201.88
RSMM01
FSM_NE005
Ω: 8.7
T: 1.17E-08
6CD2478B0A131307
KLX12A
234.20
RSMM01
FSM_NE005
Ω: 11.4
T: 3.30E-08
0E92478B0A1390D6
KLX12A
234.94
RSMM01
FSM_NE005
Ω: 12.0
T: 3.78E-08
DA12478B0A1393B8
KLX12A
236.38
RSMM01
FSM_NE005
Ω: 50.4
T: 1.08E-08
6392478B0A139959
KLX12A
242.89
RSMM01
FSM_NE005
Ω: 7.8
T: 1.04E-09
CF12478B0A13B2B3
KLX12A
244.75
RSMM01
FSM_NE005
Ω: 8.2
T: 3.69E-09
F0D2478B0A13B9EE
KLX12A
245.54
RSMM01
FSM_NE005
Ω: 8.0
T: 1.41E-07
BF52478B0A13BD06
KLX12A
261.32
RSMM01
FSM_NE005
Ω: 8.4
T: 3.56E-08
FC12478B0A13FA68
KLX12A
265.06
RSMM01
FSM_NE005
Ω: 8.5
T: 1.27E-08
8012478B0A1408F8
KLX12A
270.79
RSMM01
FSM_NE005
Ω: 10.0
T: 3.73E-09
1E52478B0A141F45
KLX12A
274.53
RSMM01
FSM_NE005
Ω: 7.7
T: 5.32E-09
42D2478B0A142DD8
KLX12A
274.91
RSMM01
FSM_NE005
Ω: 8.2
T: 3.66E-09
63D2478B0A142F4B
KLX12A
282.25
RSMM01
FSM_NE005
Ω: 9.2
T: 1.66E-08
3912478B0A144BE5
KLX12A
323.23
RSMM01
FSM_NE005
Ω: 8.2
T: 9.22E-10
69D2478B0A14EB63

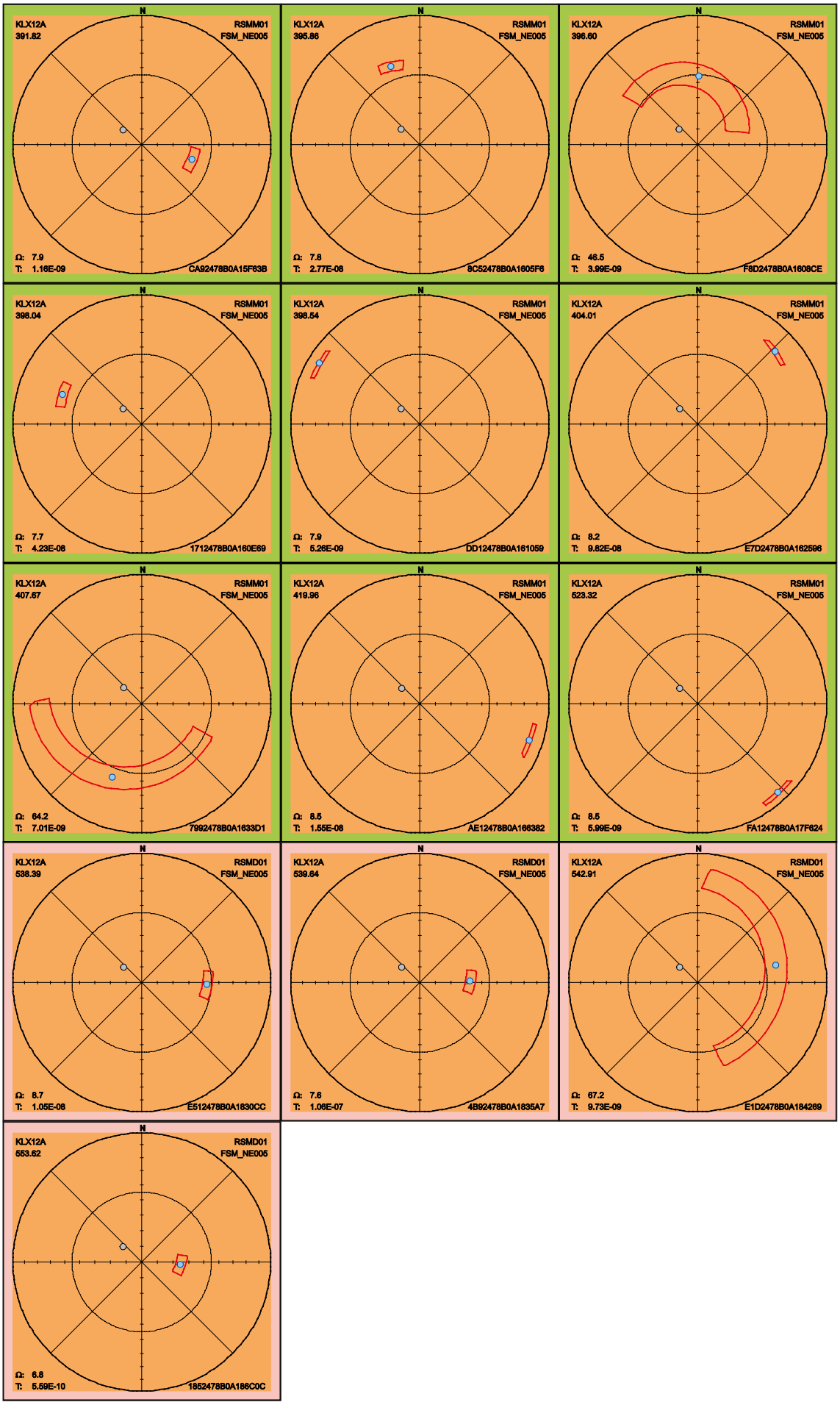
KLX12A
391.82
RSMM01
FSM_NE005
N
Ω: 7.9
T: 1.16E-09
CA92478B0A15F63B
KLX12A
395.86
RSMM01
FSM_NE005
N
Ω: 7.8
T: 2.77E-08
8C52478B0A1605F6
KLX12A
396.60
RSMM01
FSM_NE005
N
Ω: 46.5
T: 3.99E-09
F8D2478B0A1608CE
KLX12A
398.04
RSMM01
FSM_NE005
N
Ω: 7.7
T: 4.23E-08
1712478B0A160E69
KLX12A
398.54
RSMM01
FSM_NE005
N
Ω: 7.9
T: 5.26E-09
DD12478B0A161059
KLX12A
404.01
RSMM01
FSM_NE005
N
Ω: 8.2
T: 9.82E-08
E7D2478B0A162596
KLX12A
407.67
RSMM01
FSM_NE005
N
Ω: 64.2
T: 7.01E-09
7992478B0A1633D1
KLX12A
419.96
RSMM01
FSM_NE005
N
Ω: 8.5
T: 1.55E-08
AE12478B0A166382
KLX12A
523.32
RSMM01
FSM_NE005
N
Ω: 8.5
T: 5.99E-09
FA12478B0A17F624
KLX12A
538.39
RSMD01
FSM_NE005
N
Ω: 8.7
T: 1.05E-08
E512478B0A1830CC
KLX12A
539.64
RSMD01
FSM_NE005
N
Ω: 7.6
T: 1.06E-07
4B92478B0A1835A7
KLX12A
542.91
RSMD01
FSM_NE005
N
Ω: 67.2
T: 9.73E-09
E1D2478B0A184269
KLX12A
553.62
RSMD01
FSM_NE005
N
Ω: 6.8
T: 5.59E-10
1852478B0A186C0C

2.3.25 KLX13A

There are 113 PFL fractures in KLX13A of which six have maximum uncertainty larger than 30°, see Table 2-22. These fractures can have an alternative interpretation of orientation compared to the best estimate orientation that is found in the table p_fract_core in /Sicada 2008/. Below follow the 90th percentile sample space of uncertainty for the PFL fractures in KLX11E.

Table 2-22. Fractures in KLX13A with uncertainty, Ω, larger than 30°.

FeatureId	PFL-f no	Adjusted Secup	Ω
A093478B0A1190AE	1	102.52	32.2
2093478B0A12A889	13	173.26	65.9
8093478B0A133A80	20	210.63	46.3
2093478B0A13DBB8	35	251.98	54.4
A093478B0A15BBBB	58	374.75	70.0
4093478B0A175336	111	479.07	75.1

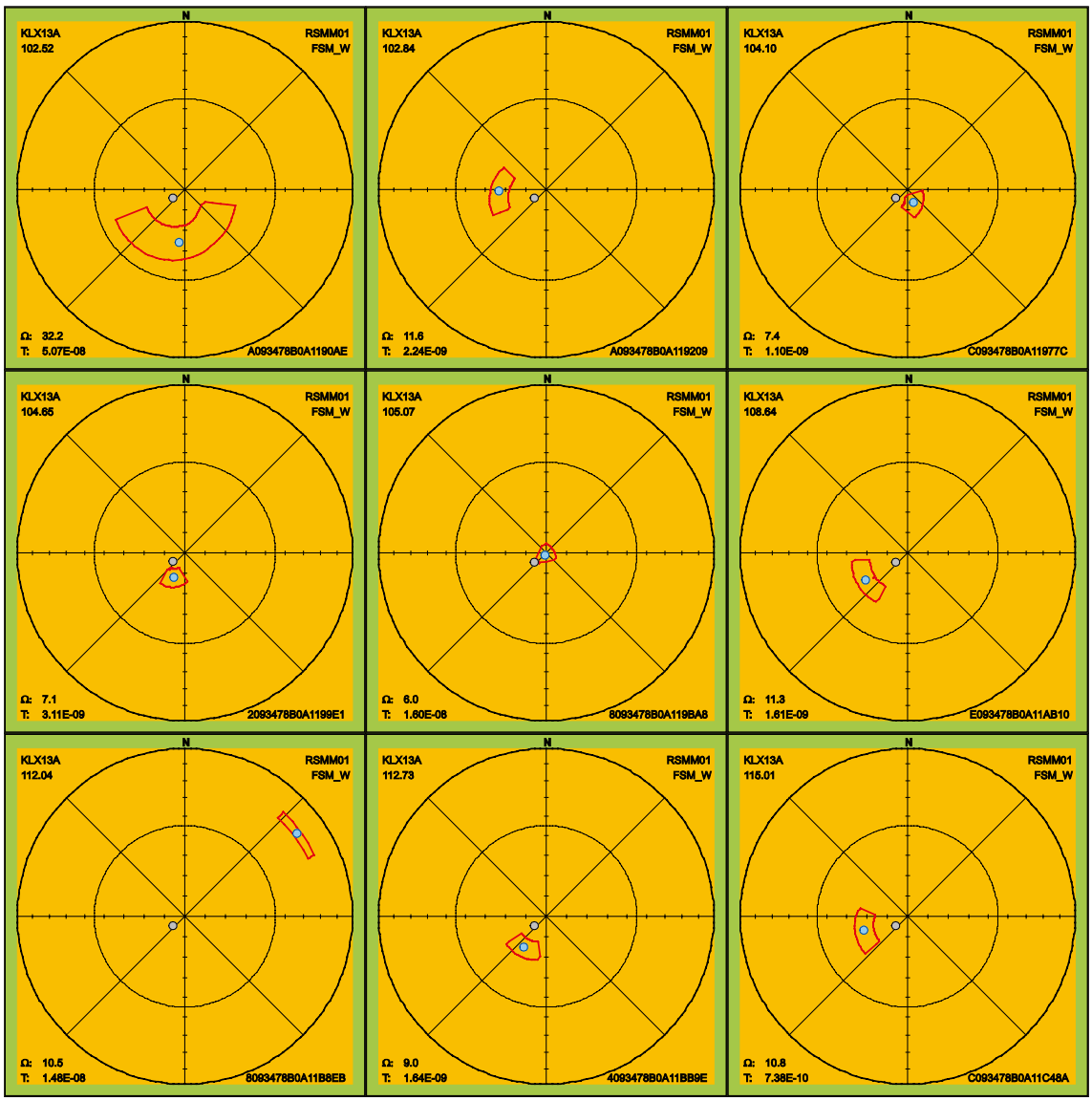

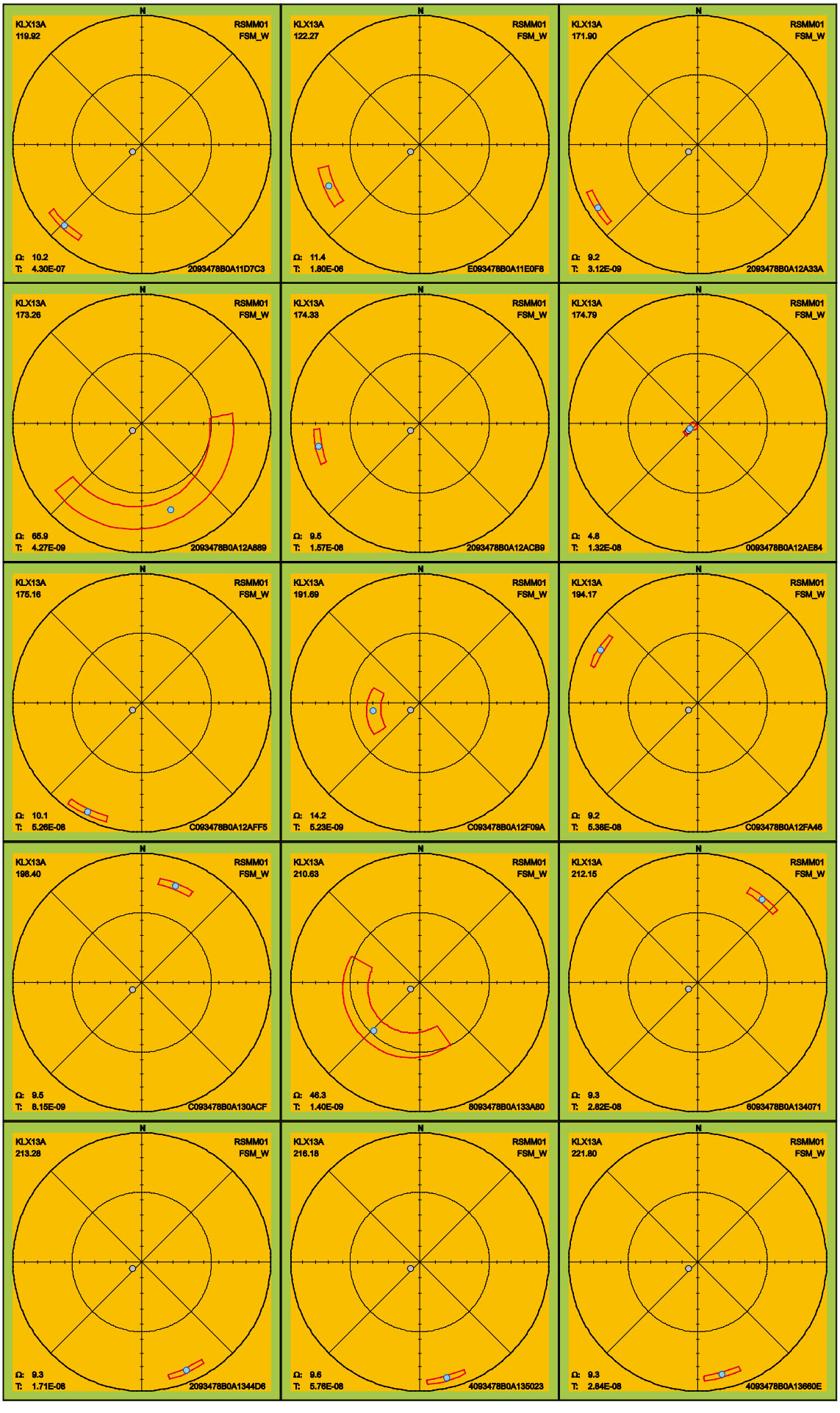
KLX13A
119.92
RSMM01
FSM_W
Ω: 10.2
T: 4.30E-07
2093478B0A11D7C3
KLX13A
122.27
RSMM01
FSM_W
Ω: 11.4
T: 1.80E-06
E093478B0A11E0F8
KLX13A
171.90
RSMM01
FSM_W
Ω: 9.2
T: 3.12E-09
2093478B0A12A33A
KLX13A
173.26
RSMM01
FSM_W
Ω: 65.9
T: 4.27E-09
2093478B0A12A889
KLX13A
174.33
RSMM01
FSM_W
Ω: 9.5
T: 1.57E-06
2093478B0A12ACB9
KLX13A
174.79
RSMM01
FSM_W
Ω: 4.8
T: 1.32E-08
0093478B0A12AE84
KLX13A
175.16
RSMM01
FSM_W
Ω: 10.1
T: 5.26E-08
C093478B0A12AFF5
KLX13A
191.69
RSMM01
FSM_W
Ω: 14.2
T: 5.23E-09
C093478B0A12F09A
KLX13A
194.17
RSMM01
FSM_W
Ω: 9.2
T: 5.38E-08
C093478B0A12FA46
KLX13A
198.40
RSMM01
FSM_W
Ω: 9.5
T: 8.15E-09
C093478B0A130ACF
KLX13A
210.63
RSMM01
FSM_W
Ω: 46.3
T: 1.40E-09
8093478B0A133A80
KLX13A
212.15
RSMM01
FSM_W
Ω: 9.3
T: 2.82E-08
6093478B0A134071
KLX13A
213.28
RSMM01
FSM_W
Ω: 9.3
T: 1.71E-08
2093478B0A1344D6
KLX13A
216.18
RSMM01
FSM_W
Ω: 9.6
T: 5.76E-08
4093478B0A135023
KLX13A
221.80
RSMM01
FSM_W
Ω: 9.3
T: 2.84E-08
4093478B0A13660E

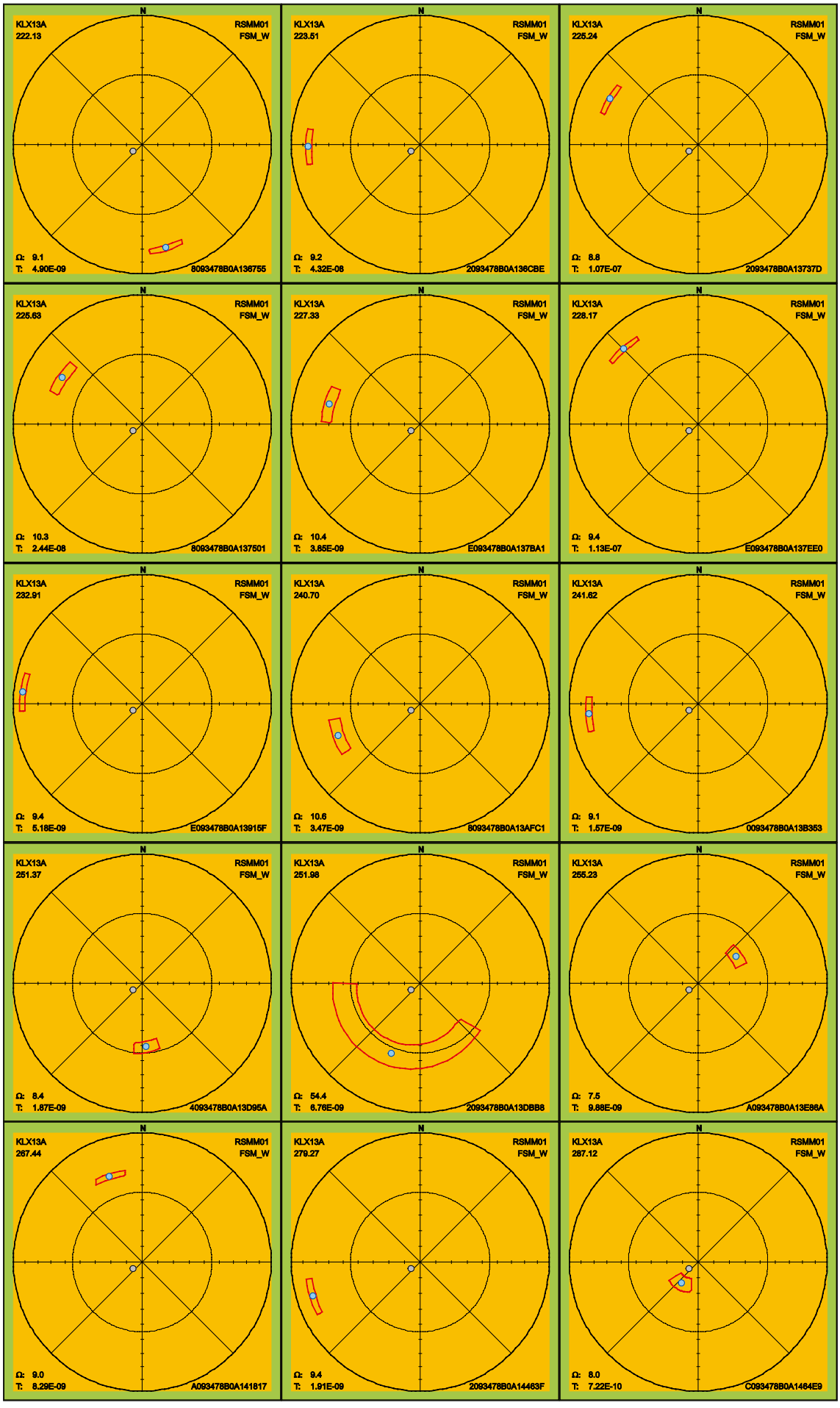
KLX13A
222.13
RSMM01
FSM_W
Ω: 9.1
T: 4.90E-09
8093478B0A136755
KLX13A
223.51
RSMM01
FSM_W
Ω: 9.2
T: 4.32E-08
2093478B0A136CBE
KLX13A
225.24
RSMM01
FSM_W
Ω: 8.8
T: 1.07E-07
2093478B0A13737D
KLX13A
225.63
RSMM01
FSM_W
Ω: 10.3
T: 2.44E-08
8093478B0A137501
KLX13A
227.33
RSMM01
FSM_W
Ω: 10.4
T: 3.85E-09
E093478B0A137BA1
KLX13A
228.17
RSMM01
FSM_W
Ω: 9.4
T: 1.13E-07
E093478B0A137EE0
KLX13A
232.91
RSMM01
FSM_W
Ω: 9.4
T: 5.18E-09
E093478B0A13915F
KLX13A
240.70
RSMM01
FSM_W
Ω: 10.6
T: 3.47E-09
8093478B0A13AFC1
KLX13A
241.62
RSMM01
FSM_W
Ω: 9.1
T: 1.57E-09
0093478B0A13B353
KLX13A
251.37
RSMM01
FSM_W
Ω: 8.4
T: 1.87E-09
4093478B0A13D95A
KLX13A
251.98
RSMM01
FSM_W
Ω: 54.4
T: 6.76E-09
2093478B0A13DBB8
KLX13A
255.23
RSMM01
FSM_W
Ω: 7.5
T: 9.88E-09
A093478B0A13E86A
KLX13A
267.44
RSMM01
FSM_W
Ω: 9.0
T: 8.29E-09
A093478B0A141817
KLX13A
279.27
RSMM01
FSM_W
Ω: 9.4
T: 1.91E-09
2093478B0A14463F
KLX13A
287.12
RSMM01
FSM_W
Ω: 8.0
T: 7.22E-10
C093478B0A1464E9

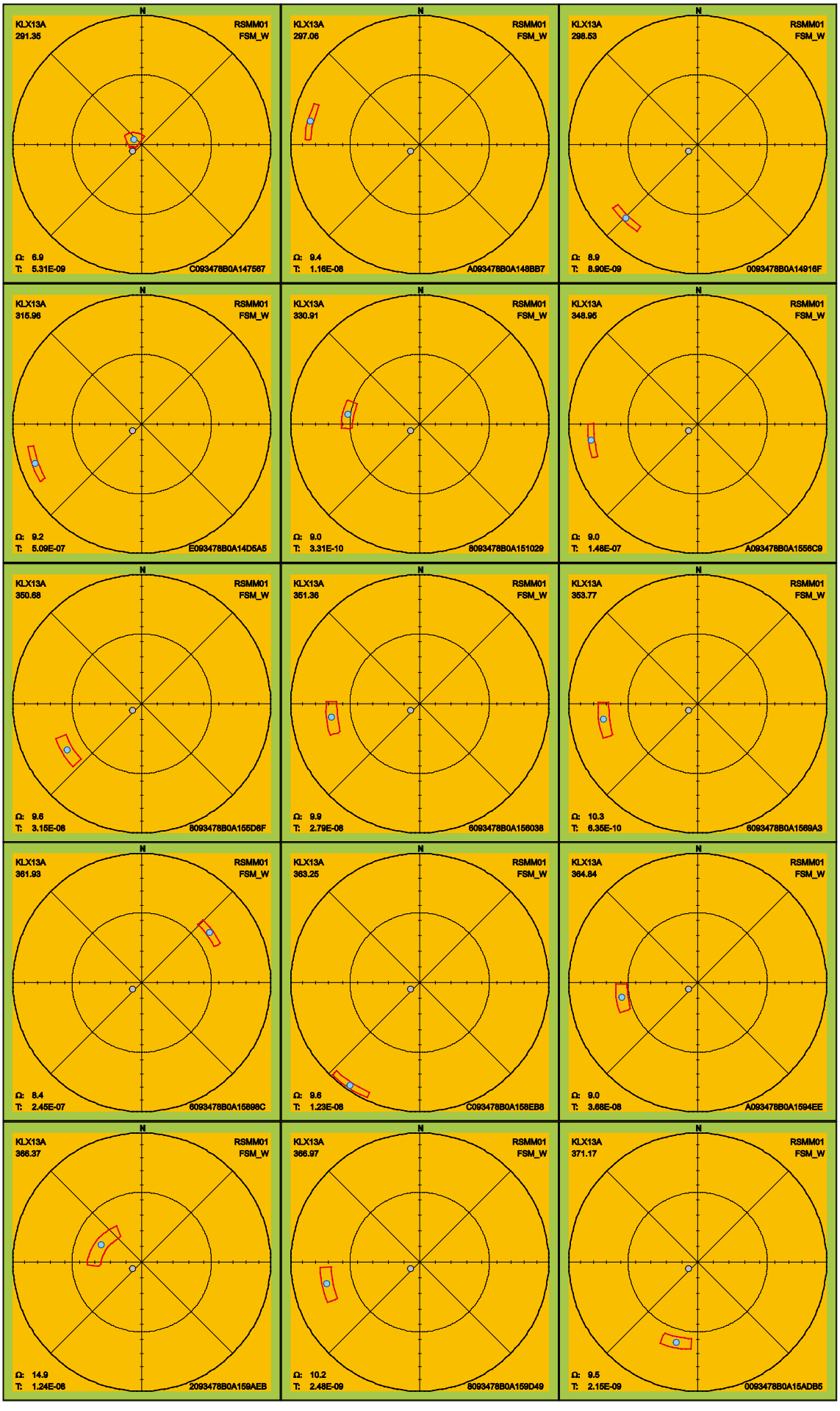
KLX13A
291.35
RSMM01
FSM_W
N
Ω: 6.9
T: 5.31E-09
C093478B0A147567
KLX13A
297.06
RSMM01
FSM_W
N
Ω: 9.4
T: 1.16E-08
A093478B0A148BB7
KLX13A
298.53
RSMM01
FSM_W
N
Ω: 8.9
T: 8.90E-09
0093478B0A14916F
KLX13A
315.96
RSMM01
FSM_W
N
Ω: 9.2
T: 5.09E-07
E093478B0A14D5A5
KLX13A
330.91
RSMM01
FSM_W
N
Ω: 9.0
T: 3.31E-10
8093478B0A151029
KLX13A
348.95
RSMM01
FSM_W
N
Ω: 9.0
T: 1.48E-07
A093478B0A1556C9
KLX13A
350.68
RSMM01
FSM_W
N
Ω: 9.6
T: 3.15E-08
8093478B0A155D6F
KLX13A
351.36
RSMM01
FSM_W
N
Ω: 9.9
T: 2.79E-08
6093478B0A156038
KLX13A
353.77
RSMM01
FSM_W
N
Ω: 10.3
T: 6.35E-10
6093478B0A1569A3
KLX13A
361.93
RSMM01
FSM_W
N
Ω: 8.4
T: 2.45E-07
6093478B0A15898C
KLX13A
363.25
RSMM01
FSM_W
N
Ω: 9.6
T: 1.23E-08
C093478B0A158EB8
KLX13A
364.84
RSMM01
FSM_W
N
Ω: 9.0
T: 3.68E-08
A093478B0A1594EE
KLX13A
366.37
RSMM01
FSM_W
N
Ω: 14.9
T: 1.24E-08
2093478B0A159AEB
KLX13A
366.97
RSMM01
FSM_W
N
Ω: 10.2
T: 2.48E-09
8093478B0A159D49
KLX13A
371.17
RSMM01
FSM_W
N
Ω: 9.5
T: 2.15E-09
0093478B0A15ADB5

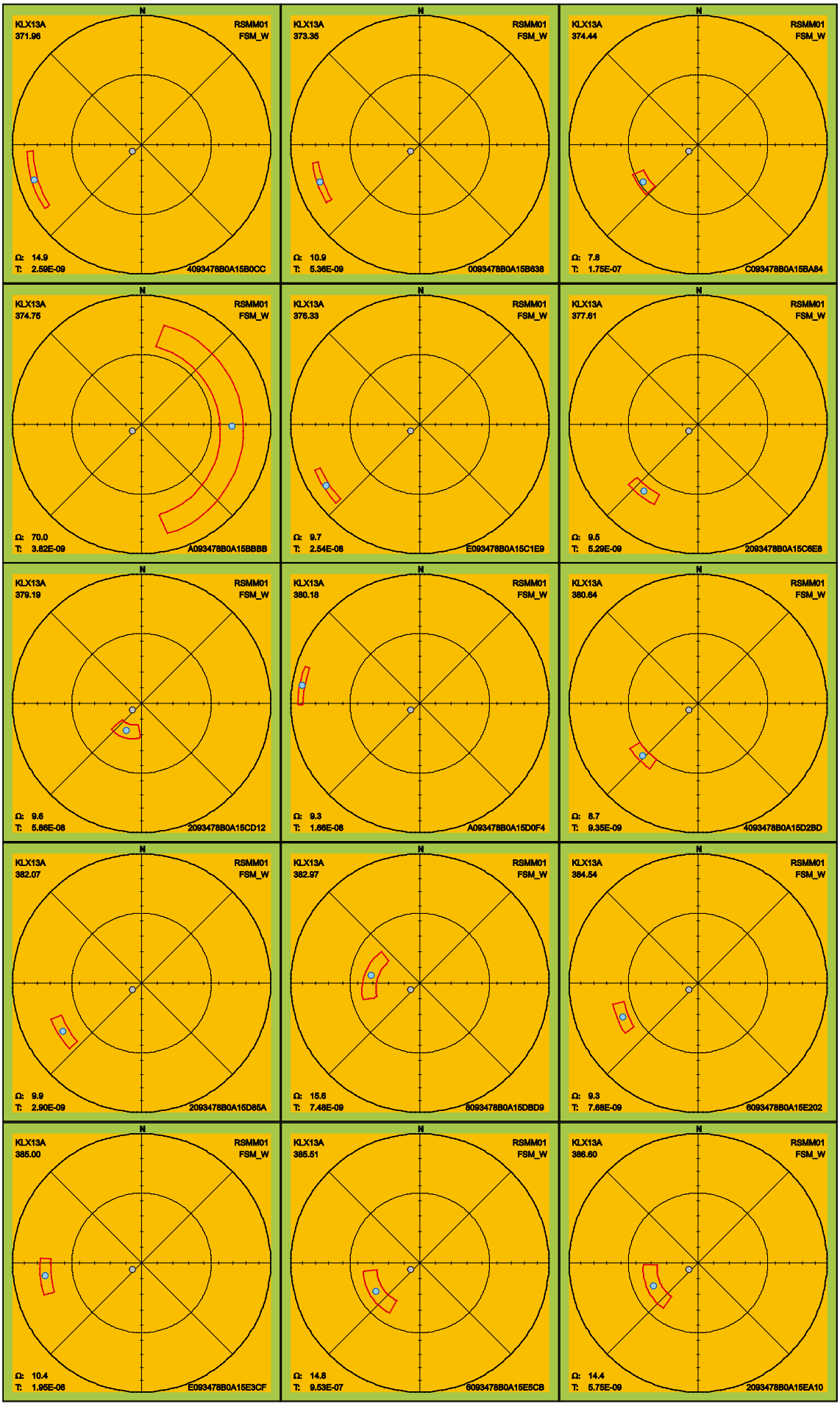
KLX13A
371.96
RSMM01
FSM_W
N
Ω: 14.9
T: 2.59E-09
4093478B0A15B0CC
KLX13A
373.35
RSMM01
FSM_W
N
Ω: 10.9
T: 5.36E-09
0093478B0A15B638
KLX13A
374.44
RSMM01
FSM_W
N
Ω: 7.8
T: 1.75E-07
C093478B0A15BA84
KLX13A
374.75
RSMM01
FSM_W
N
Ω: 70.0
T: 3.82E-09
A093478B0A15BBBB
KLX13A
376.33
RSMM01
FSM_W
N
Ω: 9.7
T: 2.54E-08
E093478B0A15C1E9
KLX13A
377.61
RSMM01
FSM_W
N
Ω: 9.5
T: 5.29E-09
2093478B0A15C6E8
KLX13A
379.19
RSMM01
FSM_W
N
Ω: 9.6
T: 5.86E-08
2093478B0A15CD12
KLX13A
380.18
RSMM01
FSM_W
N
Ω: 9.3
T: 1.66E-08
A093478B0A15D0F4
KLX13A
380.64
RSMM01
FSM_W
N
Ω: 8.7
T: 9.35E-09
4093478B0A15D2BD
KLX13A
382.07
RSMM01
FSM_W
N
Ω: 9.9
T: 2.90E-09
2093478B0A15D85A
KLX13A
382.97
RSMM01
FSM_W
N
Ω: 15.6
T: 7.48E-09
8093478B0A15DBD9
KLX13A
384.54
RSMM01
FSM_W
N
Ω: 9.3
T: 7.68E-09
6093478B0A15E202
KLX13A
385.00
RSMM01
FSM_W
N
Ω: 10.4
T: 1.95E-08
E093478B0A15E3CF
KLX13A
385.51
RSMM01
FSM_W
N
Ω: 14.8
T: 9.53E-07
6093478B0A15E5CB
KLX13A
386.60
RSMM01
FSM_W
N
Ω: 14.4
T: 5.75E-09
2093478B0A15EA10

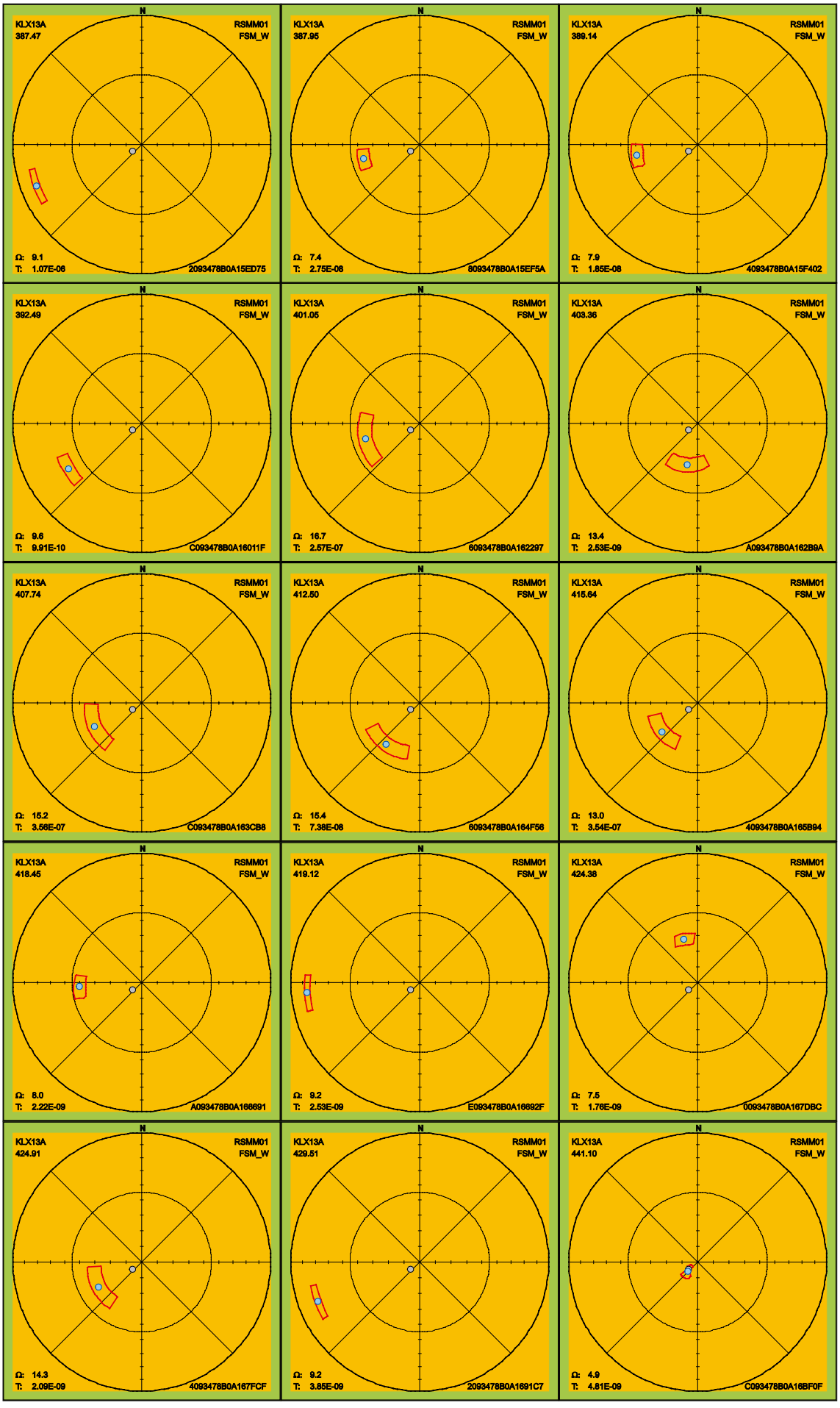
KLX13A
387.47
RSMM01
FSM_W
N
Ω: 9.1
T: 1.07E-06
2093478B0A15ED75
KLX13A
387.95
RSMM01
FSM_W
N
Ω: 7.4
T: 2.75E-06
6093478B0A15EF5A
KLX13A
389.14
RSMM01
FSM_W
N
Ω: 7.9
T: 1.85E-06
4093478B0A15F402
KLX13A
392.49
RSMM01
FSM_W
N
Ω: 9.6
T: 9.91E-10
C093478B0A16011F
KLX13A
401.05
RSMM01
FSM_W
N
Ω: 16.7
T: 2.57E-07
6093478B0A162297
KLX13A
403.36
RSMM01
FSM_W
N
Ω: 13.4
T: 2.53E-09
A093478B0A162B9A
KLX13A
407.74
RSMM01
FSM_W
N
Ω: 15.2
T: 3.56E-07
C093478B0A163CB8
KLX13A
412.50
RSMM01
FSM_W
N
Ω: 15.4
T: 7.38E-08
6093478B0A164F56
KLX13A
415.64
RSMM01
FSM_W
N
Ω: 13.0
T: 3.54E-07
4093478B0A165B94
KLX13A
418.45
RSMM01
FSM_W
N
Ω: 8.0
T: 2.22E-09
A093478B0A166691
KLX13A
419.12
RSMM01
FSM_W
N
Ω: 9.2
T: 2.53E-09
E093478B0A16692F
KLX13A
424.38
RSMM01
FSM_W
N
Ω: 7.5
T: 1.76E-09
0093478B0A167DBC
KLX13A
424.91
RSMM01
FSM_W
N
Ω: 14.3
T: 2.09E-09
4093478B0A167FCF
KLX13A
429.51
RSMM01
FSM_W
N
Ω: 9.2
T: 3.85E-09
2093478B0A1691C7
KLX13A
441.10
RSMM01
FSM_W
N
Ω: 4.9
T: 4.81E-09
C093478B0A16BF0F

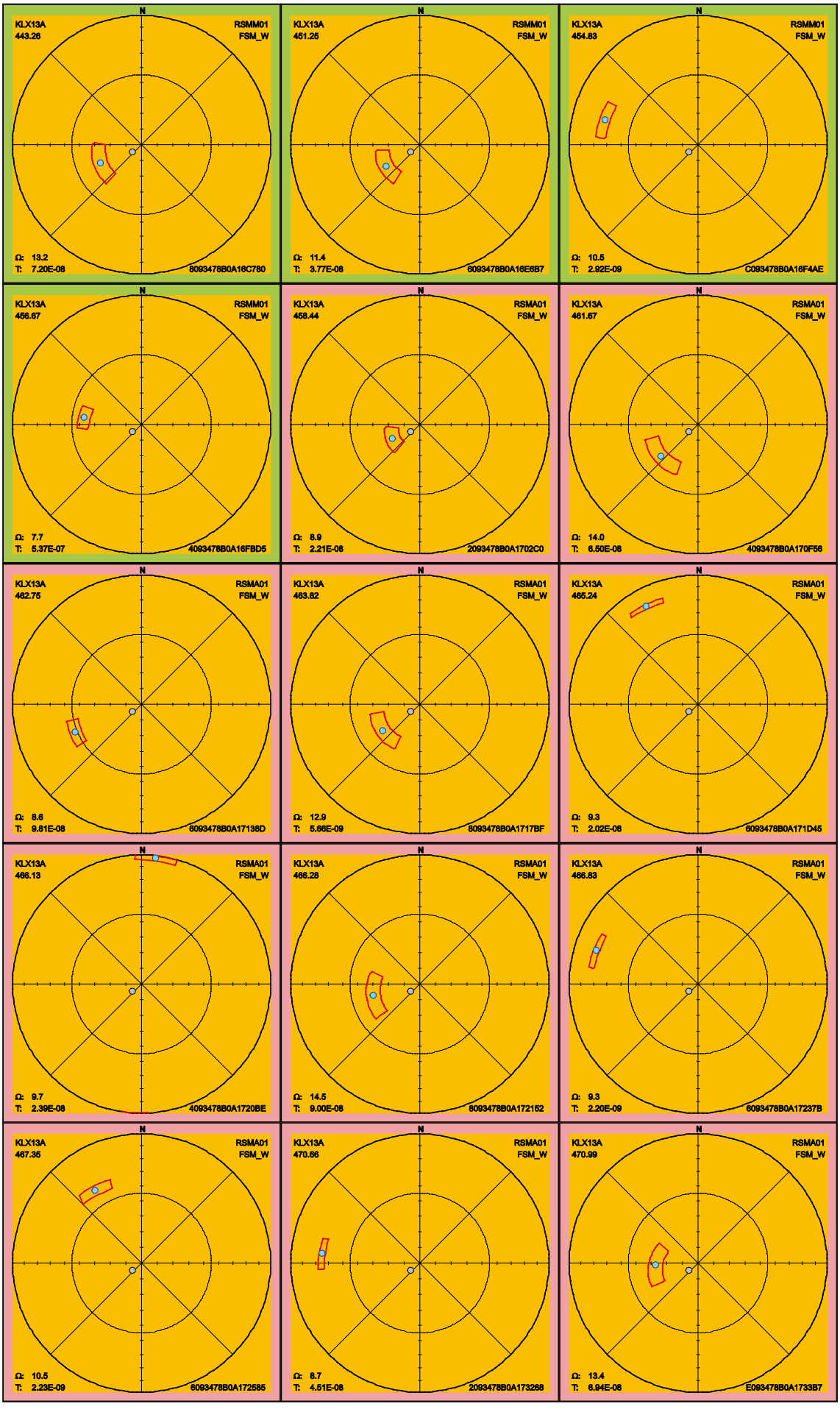
KLX13A
443.26
RSMM01
FSM_W
Ω: 13.2
T: 7.20E-08
8093478B0A16C780
KLX13A
451.25
RSMM01
FSM_W
Ω: 11.4
T: 3.77E-08
8093478B0A16E6B7
KLX13A
454.83
RSMM01
FSM_W
Ω: 10.5
T: 2.92E-09
C093478B0A16F4AE
KLX13A
456.67
RSMM01
FSM_W
Ω: 7.7
T: 5.37E-07
4093478B0A16FBD5
KLX13A
458.44
RSMA01
FSM_W
Ω: 8.9
T: 2.21E-08
2093478B0A1702C0
KLX13A
461.67
RSMA01
FSM_W
Ω: 14.0
T: 6.50E-08
4093478B0A170F56
KLX13A
462.75
RSMA01
FSM_W
Ω: 8.6
T: 9.81E-08
6093478B0A17138D
KLX13A
463.82
RSMA01
FSM_W
Ω: 12.9
T: 5.66E-09
8093478B0A1717BF
KLX13A
465.24
RSMA01
FSM_W
Ω: 9.3
T: 2.02E-08
6093478B0A171D45
KLX13A
466.13
RSMA01
FSM_W
Ω: 9.7
T: 2.39E-08
4093478B0A1720BE
KLX13A
466.28
RSMA01
FSM_W
Ω: 14.5
T: 9.00E-08
8093478B0A172152
KLX13A
466.83
RSMA01
FSM_W
Ω: 9.3
T: 2.20E-09
6093478B0A17237B
KLX13A
467.35
RSMA01
FSM_W
Ω: 10.5
T: 2.23E-09
6093478B0A172585
KLX13A
470.66
RSMA01
FSM_W
Ω: 8.7
T: 4.51E-08
2093478B0A173268
KLX13A
470.99
RSMA01
FSM_W
Ω: 13.4
T: 6.94E-08
E093478B0A1733B7

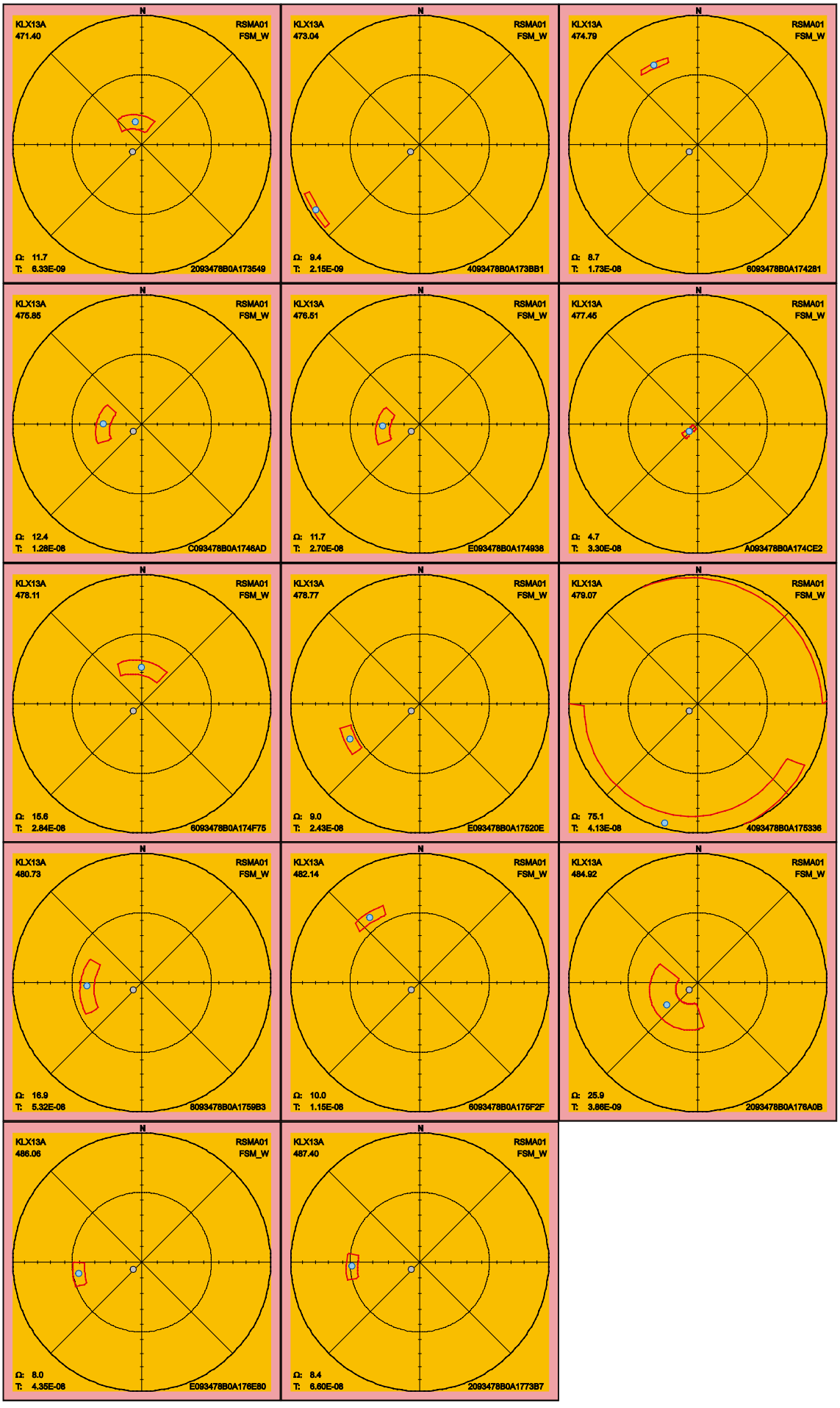
KLX13A
471.40
RSMA01
FSM_W
N
Ω: 11.7
T: 6.33E-09
2093478B0A173549
KLX13A
473.04
RSMA01
FSM_W
N
Ω: 9.4
T: 2.15E-09
4093478B0A173BB1
KLX13A
474.79
RSMA01
FSM_W
N
Ω: 8.7
T: 1.73E-08
6093478B0A174281
KLX13A
476.85
RSMA01
FSM_W
N
Ω: 12.4
T: 1.28E-08
C093478B0A1746AD
KLX13A
476.51
RSMA01
FSM_W
N
Ω: 11.7
T: 2.70E-08
E093478B0A174938
KLX13A
477.45
RSMA01
FSM_W
N
Ω: 4.7
T: 3.30E-08
A093478B0A174CE2
KLX13A
478.11
RSMA01
FSM_W
N
Ω: 15.6
T: 2.84E-08
6093478B0A174F75
KLX13A
478.77
RSMA01
FSM_W
N
Ω: 9.0
T: 2.43E-08
E093478B0A17520E
KLX13A
479.07
RSMA01
FSM_W
N
Ω: 75.1
T: 4.13E-08
4093478B0A175336
KLX13A
480.73
RSMA01
FSM_W
N
Ω: 16.9
T: 5.32E-08
8093478B0A1759B3
KLX13A
482.14
RSMA01
FSM_W
N
Ω: 10.0
T: 1.15E-08
6093478B0A175F2F
KLX13A
484.92
RSMA01
FSM_W
N
Ω: 25.9
T: 3.86E-09
2093478B0A176A0B
KLX13A
486.06
RSMA01
FSM_W
N
Ω: 8.0
T: 4.35E-08
E093478B0A176E80
KLX13A
487.40
RSMA01
FSM_W
N
Ω: 8.4
T: 6.60E-08
2093478B0A1773B7

2.3.26 KLX14A

There is one PFL fracture in KLX14A missing orientation information and thus is excluded from this section. The sample spaces of the maximum uncertainty, on the 90th percentile, for each of the 32 fractures are shown below. One fracture, see Table 2-23, has maximum uncertainty larger than 30° and can, thus, have an alternative interpretation of orientation compared to the best estimate orientation that is found in the table p_fract_core in /Sicada 2008/.

Table 2-23. Fractures in KLX14A with uncertainty, Ω, larger than 30°.

FeatureId	PFL-f no	Adjusted Secup	Ω
C0D4478B0A10AB07	9	43.96	72.7

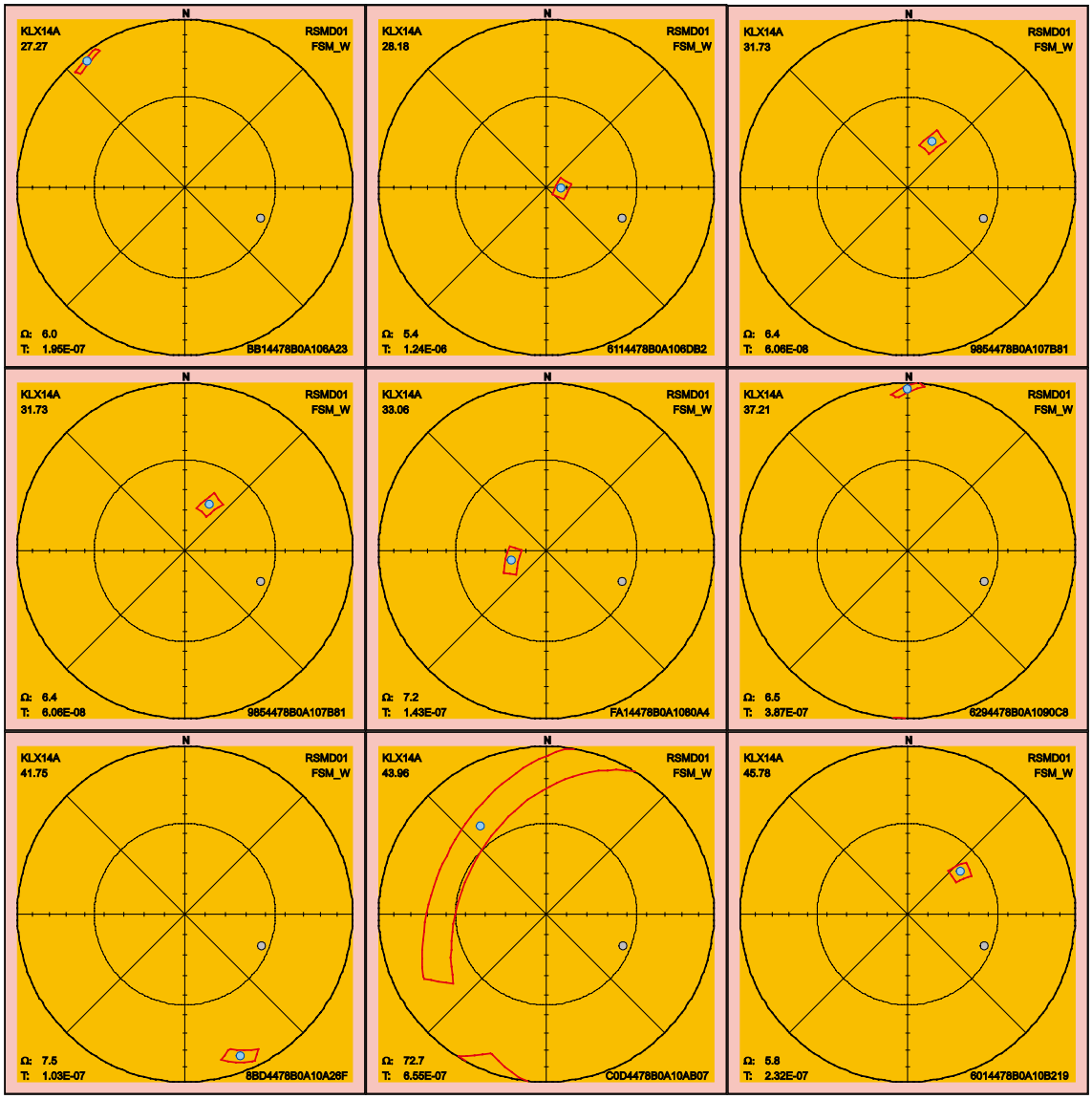

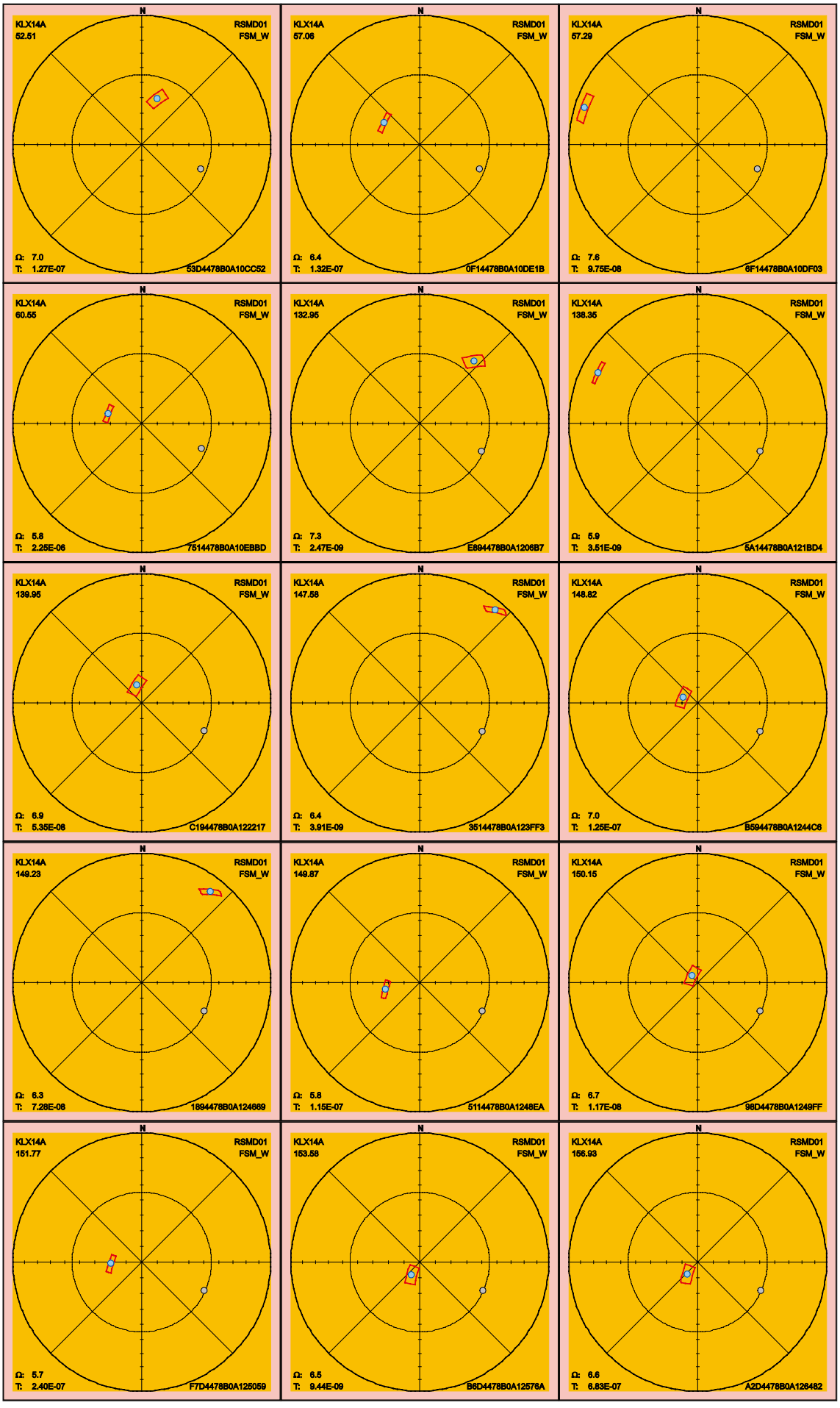
KLX14A
52.51
RSMD01
FSM_W
N
Ω: 7.0
T: 1.27E-07
53D4478B0A10CC52
KLX14A
57.06
RSMD01
FSM_W
N
Ω: 6.4
T: 1.32E-07
0F14478B0A10DE1B
KLX14A
57.29
RSMD01
FSM_W
N
Ω: 7.6
T: 9.75E-08
6F14478B0A10DF03
KLX14A
60.55
RSMD01
FSM_W
N
Ω: 5.8
T: 2.25E-06
7514478B0A10EBBD
KLX14A
132.95
RSMD01
FSM_W
N
Ω: 7.3
T: 2.47E-09
E894478B0A1206B7
KLX14A
138.35
RSMD01
FSM_W
N
Ω: 5.9
T: 3.51E-09
5A14478B0A121BD4
KLX14A
139.95
RSMD01
FSM_W
N
Ω: 6.9
T: 5.35E-08
C194478B0A122217
KLX14A
147.58
RSMD01
FSM_W
N
Ω: 6.4
T: 3.91E-09
3514478B0A123FF3
KLX14A
148.82
RSMD01
FSM_W
N
Ω: 7.0
T: 1.25E-07
B594478B0A1244C6
KLX14A
149.23
RSMD01
FSM_W
N
Ω: 6.3
T: 7.28E-08
1894478B0A124669
KLX14A
149.87
RSMD01
FSM_W
N
Ω: 5.8
T: 1.15E-07
5114478B0A1248EA
KLX14A
150.15
RSMD01
FSM_W
N
Ω: 6.7
T: 1.17E-08
98D4478B0A1249FF
KLX14A
151.77
RSMD01
FSM_W
N
Ω: 5.7
T: 2.40E-07
F7D4478B0A125059
KLX14A
153.58
RSMD01
FSM_W
N
Ω: 6.5
T: 9.44E-09
B6D4478B0A12576A
KLX14A
156.93
RSMD01
FSM_W
N
Ω: 6.6
T: 6.83E-07
A2D4478B0A126482

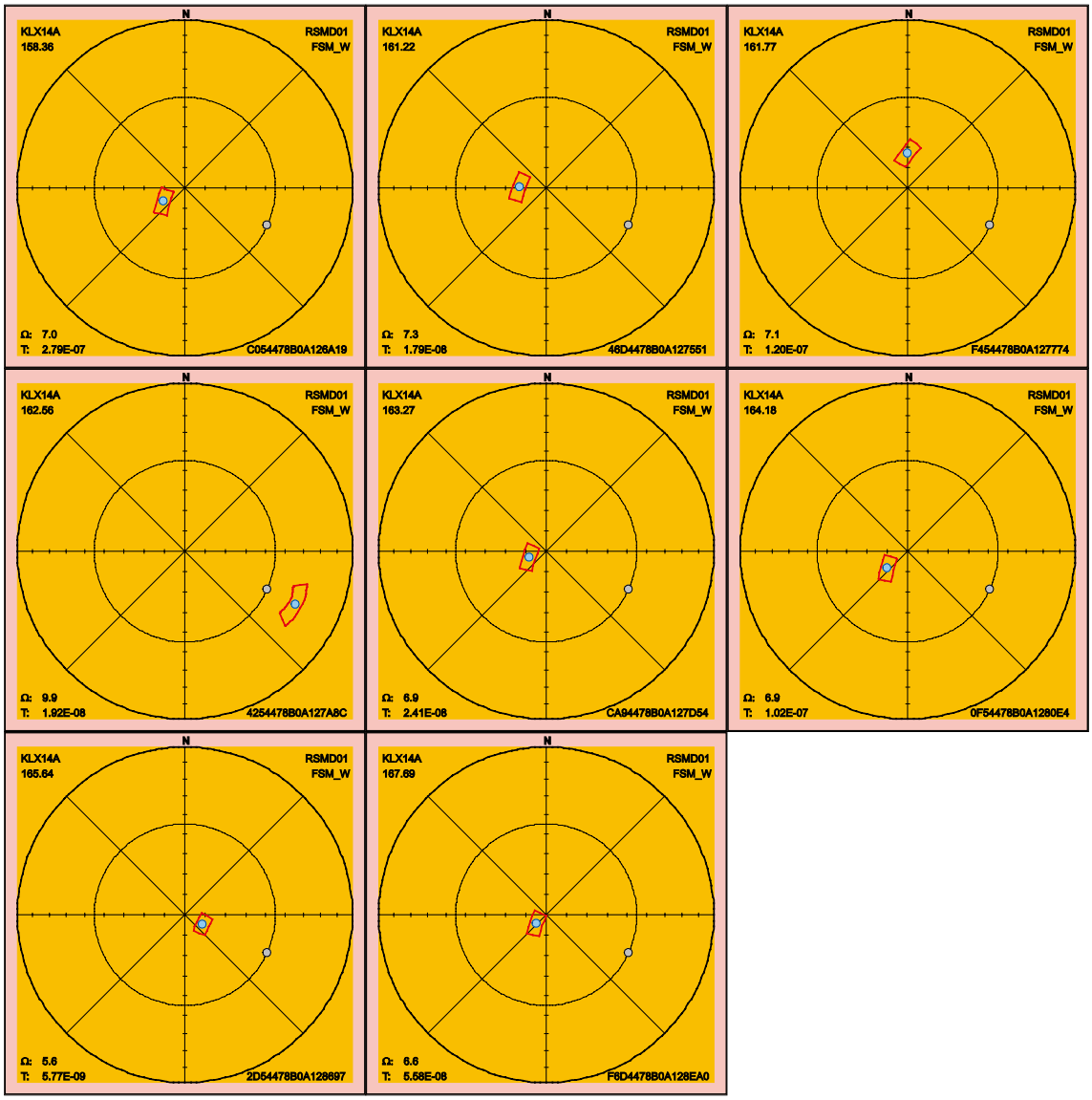

2.3.27 KLX15A

Below follow the 90th percentile sample space of uncertainty for the 75 PFL fractures in KLX15A. There are 3 fractures, listed in Table 2-24 that have a maximum uncertainty, on the 90th percentile, larger than 30° and consequently can have an alternative interpretation of orientation compared to the best estimate orientation that is found in the table p_fract_core in /Sicada 2008/.

Table 2-24. Fractures in KLX15A with uncertainty, Ω, larger than 30°.

FeatureId	PFL-f no	Adjusted Secup	Ω
BDD5478B0A130515	43	198.14	57.6
C095478B0A15E87F	59	387.75	31.2
F895478B0A15EE3E	61	389.23	39.0

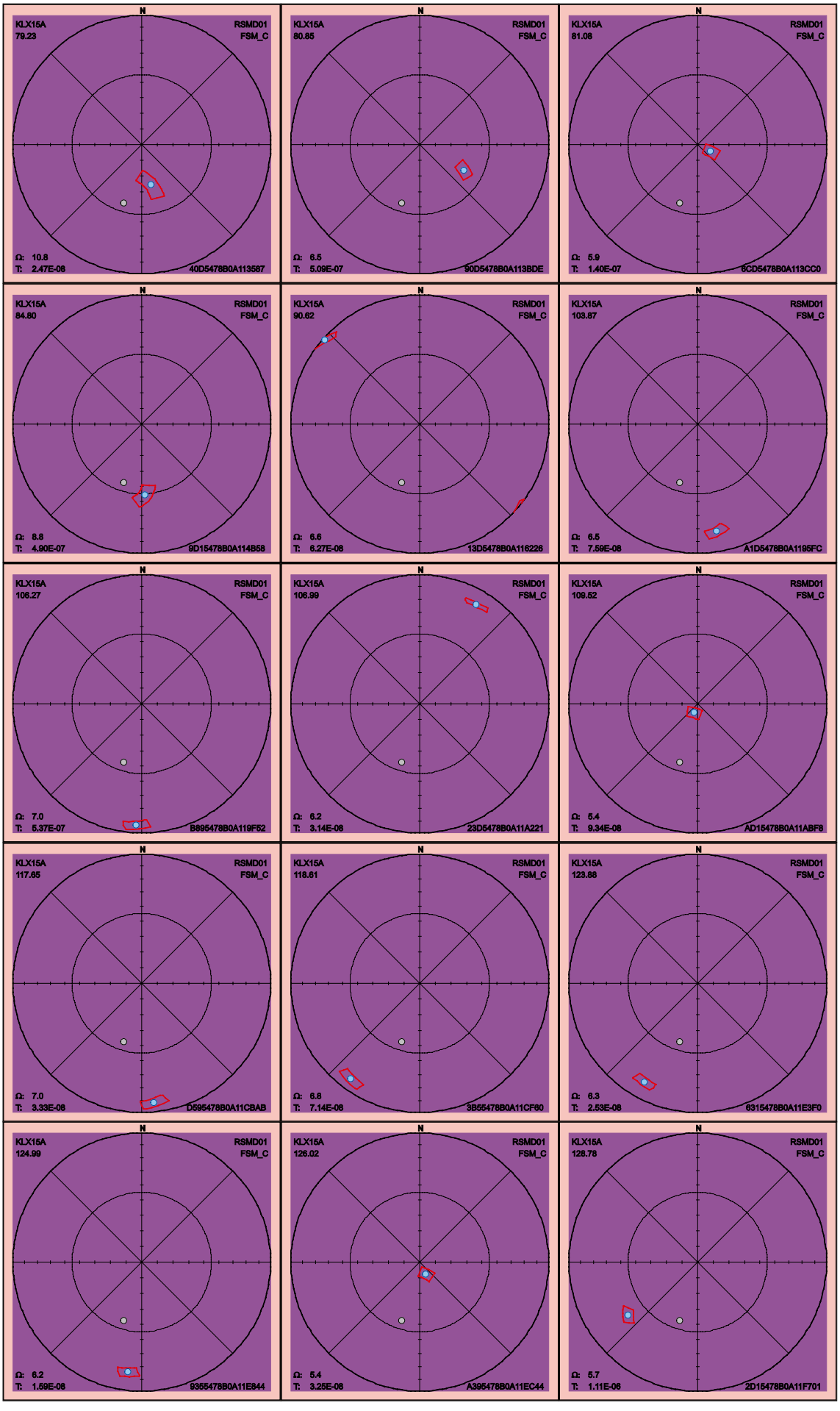
KLX15A
79.23
RSMD01
FSM_C
N
Ω: 10.8
T: 2.47E-08
40D5478B0A113587
KLX15A
80.85
RSMD01
FSM_C
N
Ω: 6.5
T: 5.09E-07
90D5478B0A113BDE
KLX15A
81.08
RSMD01
FSM_C
N
Ω: 5.9
T: 1.40E-07
8CD5478B0A113CC0
KLX15A
84.80
RSMD01
FSM_C
N
Ω: 8.8
T: 4.90E-07
9D15478B0A114B58
KLX15A
90.62
RSMD01
FSM_C
N
Ω: 6.6
T: 6.27E-08
13D5478B0A116228
KLX15A
103.87
RSMD01
FSM_C
N
Ω: 6.5
T: 7.59E-08
A1D5478B0A1195FC
KLX15A
106.27
RSMD01
FSM_C
N
Ω: 7.0
T: 5.37E-07
B895478B0A119F52
KLX15A
106.99
RSMD01
FSM_C
N
Ω: 6.2
T: 3.14E-08
23D5478B0A11A221
KLX15A
109.52
RSMD01
FSM_C
N
Ω: 5.4
T: 9.34E-08
AD15478B0A11ABF8
KLX15A
117.65
RSMD01
FSM_C
N
Ω: 7.0
T: 3.33E-08
D595478B0A11CBAB
KLX15A
118.61
RSMD01
FSM_C
N
Ω: 6.8
T: 7.14E-08
3B55478B0A11CF60
KLX15A
123.88
RSMD01
FSM_C
N
Ω: 6.3
T: 2.53E-08
6315478B0A11E3F0
KLX15A
124.99
RSMD01
FSM_C
N
Ω: 6.2
T: 1.59E-08
9355478B0A11E844
KLX15A
126.02
RSMD01
FSM_C
N
Ω: 5.4
T: 3.25E-08
A395478B0A11EC44
KLX15A
128.78
RSMD01
FSM_C
N
Ω: 5.7
T: 1.11E-08
2D15478B0A11F701

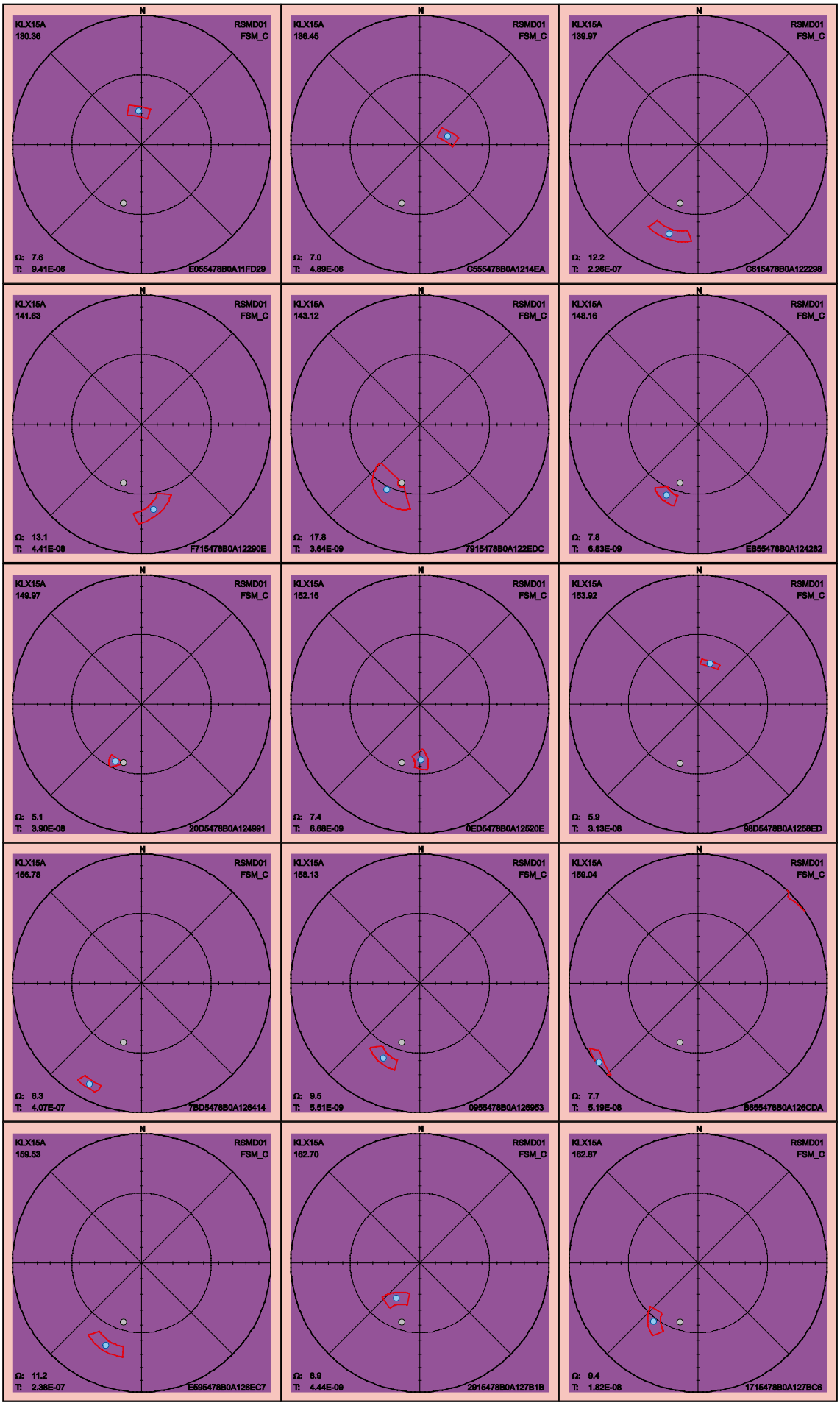
KLX15A
130.36
RSMD01
FSM_C
N
Ω: 7.6
T: 9.41E-08
E055478B0A11FD29
KLX15A
136.45
RSMD01
FSM_C
N
Ω: 7.0
T: 4.89E-08
C555478B0A1214EA
KLX15A
139.97
RSMD01
FSM_C
N
Ω: 12.2
T: 2.26E-07
C815478B0A122298
KLX15A
141.63
RSMD01
FSM_C
N
Ω: 13.1
T: 4.41E-08
F715478B0A12290E
KLX15A
143.12
RSMD01
FSM_C
N
Ω: 17.8
T: 3.64E-09
7915478B0A122EDC
KLX15A
148.16
RSMD01
FSM_C
N
Ω: 7.8
T: 6.83E-09
EB55478B0A124282
KLX15A
149.97
RSMD01
FSM_C
N
Ω: 5.1
T: 3.90E-08
20D5478B0A124991
KLX15A
152.15
RSMD01
FSM_C
N
Ω: 7.4
T: 6.68E-09
0ED5478B0A12520E
KLX15A
153.92
RSMD01
FSM_C
N
Ω: 5.9
T: 3.13E-08
98D5478B0A1258ED
KLX15A
156.78
RSMD01
FSM_C
N
Ω: 6.3
T: 4.07E-07
7BD5478B0A128414
KLX15A
158.13
RSMD01
FSM_C
N
Ω: 9.5
T: 5.51E-09
0955478B0A128953
KLX15A
159.04
RSMD01
FSM_C
N
Ω: 7.7
T: 5.19E-08
B655478B0A126CDA
KLX15A
159.53
RSMD01
FSM_C
N
Ω: 11.2
T: 2.38E-07
E595478B0A126EC7
KLX15A
162.70
RSMD01
FSM_C
N
Ω: 8.9
T: 4.44E-09
2915478B0A127B1B
KLX15A
162.87
RSMD01
FSM_C
N
Ω: 9.4
T: 1.82E-08
1715478B0A127BC6

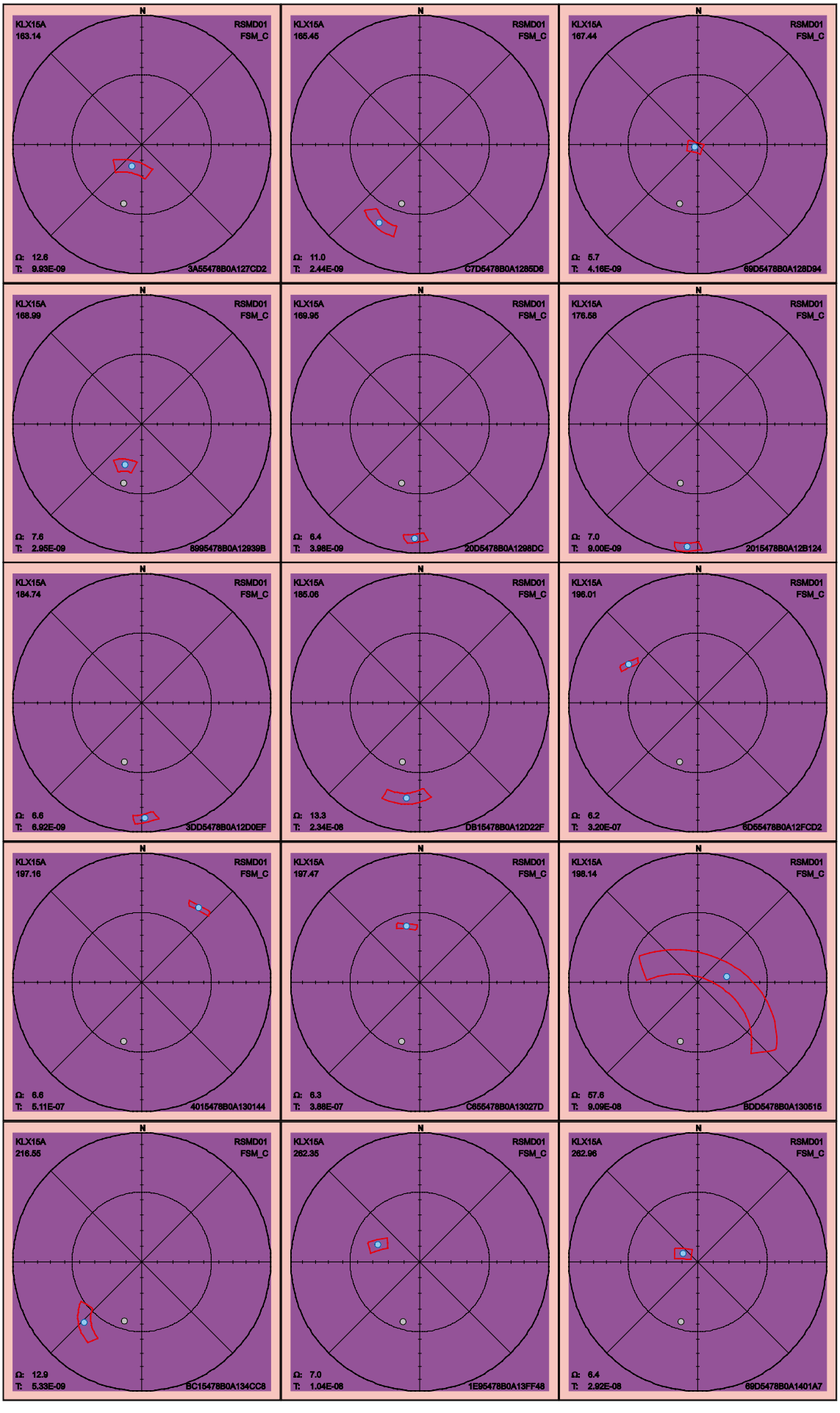
KLX15A
163.14
RSMD01
FSM_C
N
Ω: 12.6
T: 9.93E-09
3A55478B0A127CD2
KLX15A
165.45
RSMD01
FSM_C
N
Ω: 11.0
T: 2.44E-09
C7D5478B0A1285D6
KLX15A
167.44
RSMD01
FSM_C
N
Ω: 5.7
T: 4.16E-09
69D5478B0A128D94
KLX15A
168.99
RSMD01
FSM_C
N
Ω: 7.6
T: 2.95E-09
8995478B0A12939B
KLX15A
169.95
RSMD01
FSM_C
N
Ω: 6.4
T: 3.98E-09
20D5478B0A1298DC
KLX15A
176.58
RSMD01
FSM_C
N
Ω: 7.0
T: 9.00E-09
2015478B0A12B124
KLX15A
184.74
RSMD01
FSM_C
N
Ω: 6.6
T: 6.92E-09
3DD5478B0A12D0EF
KLX15A
185.06
RSMD01
FSM_C
N
Ω: 13.3
T: 2.34E-08
DB15478B0A12D22F
KLX15A
196.01
RSMD01
FSM_C
N
Ω: 6.2
T: 3.20E-07
6D55478B0A12FCD2
KLX15A
197.16
RSMD01
FSM_C
N
Ω: 6.6
T: 5.11E-07
4015478B0A130144
KLX15A
197.47
RSMD01
FSM_C
N
Ω: 6.3
T: 3.88E-07
C655478B0A13027D
KLX15A
198.14
RSMD01
FSM_C
N
Ω: 57.6
T: 9.09E-08
BDD5478B0A130515
KLX15A
216.55
RSMD01
FSM_C
N
Ω: 12.9
T: 5.33E-09
BC15478B0A134CC8
KLX15A
262.35
RSMD01
FSM_C
N
Ω: 7.0
T: 1.04E-08
1E95478B0A13FF48
KLX15A
262.96
RSMD01
FSM_C
N
Ω: 6.4
T: 2.92E-08
69D5478B0A1401A7

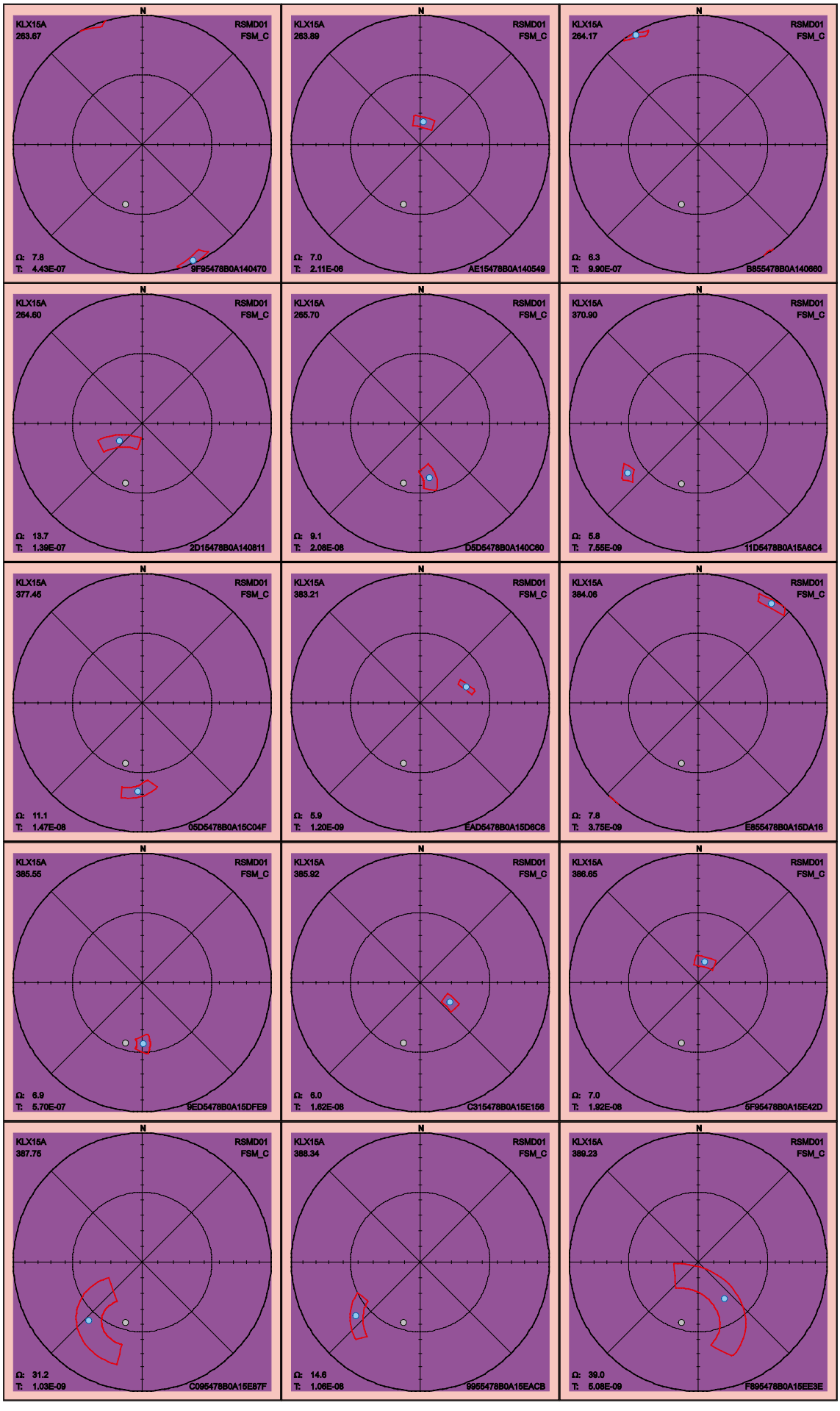
KLX15A
263.67
RSMD01
FSM_C
Ω: 7.8
T: 4.43E-07
9F95478B0A140470
KLX15A
263.89
RSMD01
FSM_C
Ω: 7.0
T: 2.11E-06
AE15478B0A140549
KLX15A
264.17
RSMD01
FSM_C
Ω: 6.3
T: 9.90E-07
B855478B0A140660
KLX15A
264.60
RSMD01
FSM_C
Ω: 13.7
T: 1.39E-07
2D15478B0A140811
KLX15A
265.70
RSMD01
FSM_C
Ω: 9.1
T: 2.08E-08
D5D5478B0A140C60
KLX15A
370.90
RSMD01
FSM_C
Ω: 5.8
T: 7.55E-09
11D5478B0A15A8C4
KLX15A
377.45
RSMD01
FSM_C
Ω: 11.1
T: 1.47E-08
05D5478B0A15C04F
KLX15A
383.21
RSMD01
FSM_C
Ω: 5.9
T: 1.20E-09
EAD5478B0A15D6C6
KLX15A
384.06
RSMD01
FSM_C
Ω: 7.8
T: 3.75E-09
E855478B0A15DA16
KLX15A
385.55
RSMD01
FSM_C
Ω: 6.9
T: 5.70E-07
9ED5478B0A15DFE9
KLX15A
385.92
RSMD01
FSM_C
Ω: 6.0
T: 1.62E-08
C315478B0A15E156
KLX15A
386.65
RSMD01
FSM_C
Ω: 7.0
T: 1.92E-08
5F95478B0A15E42D
KLX15A
387.75
RSMD01
FSM_C
Ω: 31.2
T: 1.03E-09
C095478B0A15E87F
KLX15A
388.34
RSMD01
FSM_C
Ω: 14.6
T: 1.06E-08
9955478B0A15EACB
KLX15A
389.23
RSMD01
FSM_C
Ω: 39.0
T: 5.08E-09
F895478B0A15EE3E

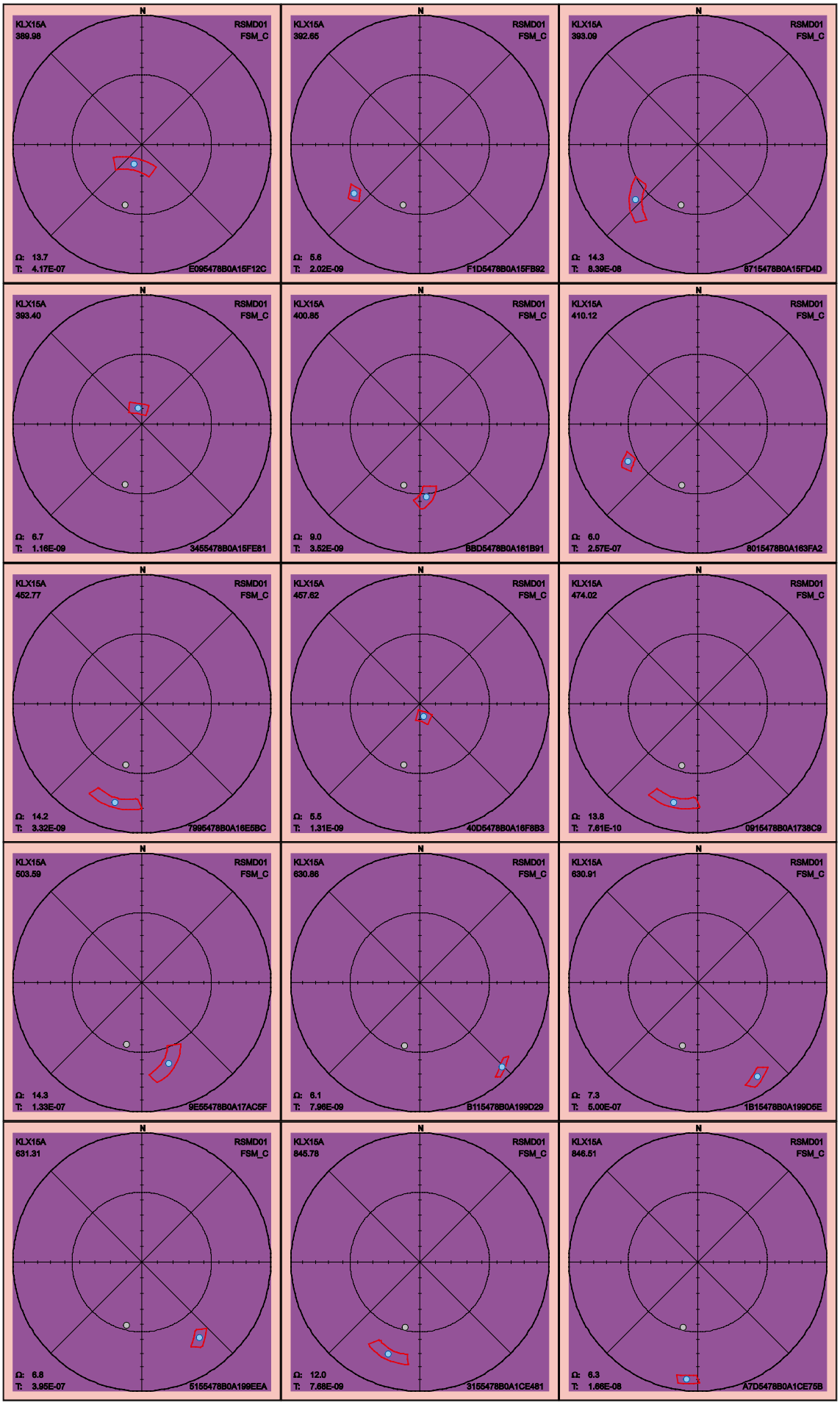
KLX15A
389.98
RSMD01
FSM_C
N
Ω: 13.7
T: 4.17E-07
E095478B0A15F12C
KLX15A
392.65
RSMD01
FSM_C
N
Ω: 5.6
T: 2.02E-09
F1D5478B0A15FB92
KLX15A
393.09
RSMD01
FSM_C
N
Ω: 14.3
T: 8.39E-08
8715478B0A15FD4D
KLX15A
393.40
RSMD01
FSM_C
N
Ω: 6.7
T: 1.16E-09
3455478B0A15FE81
KLX15A
400.85
RSMD01
FSM_C
N
Ω: 9.0
T: 3.52E-09
BBD5478B0A161B91
KLX15A
410.12
RSMD01
FSM_C
N
Ω: 6.0
T: 2.57E-07
8015478B0A163FA2
KLX15A
452.77
RSMD01
FSM_C
N
Ω: 14.2
T: 3.32E-09
7995478B0A16E5BC
KLX15A
457.62
RSMD01
FSM_C
N
Ω: 5.5
T: 1.31E-09
40D5478B0A16F8B3
KLX15A
474.02
RSMD01
FSM_C
N
Ω: 13.8
T: 7.61E-10
0915478B0A1738C9
KLX15A
503.59
RSMD01
FSM_C
N
Ω: 14.3
T: 1.33E-07
9E55478B0A17AC5F
KLX15A
630.86
RSMD01
FSM_C
N
Ω: 6.1
T: 7.96E-09
B115478B0A199D29
KLX15A
630.91
RSMD01
FSM_C
N
Ω: 7.3
T: 5.00E-07
1B15478B0A199D5E
KLX15A
631.31
RSMD01
FSM_C
N
Ω: 6.8
T: 3.95E-07
5155478B0A199EEA
KLX15A
845.78
RSMD01
FSM_C
N
Ω: 12.0
T: 7.68E-09
3155478B0A1CE481
KLX15A
846.51
RSMD01
FSM_C
N
Ω: 6.3
T: 1.66E-08
A7D5478B0A1CE75B

2.3.28 KLX16A

Below follow the 90th percentile sample space of uncertainty for the 46 PFL fractures in KLX16A. One fracture has maximum uncertainty larger than 30°, see Table 2-25, and thus can have an alternative interpretation of orientation compared to the best estimate orientation that is found in the table p_fract_core in /Sicada 2008/.

Table 2-25. Fractures in KLX16A with uncertainty, Ω, larger than 30°.

FeatureId	PFL-f no	Adjusted Secup	Ω
E8D6478B0A23A756	41	239.94	73.7

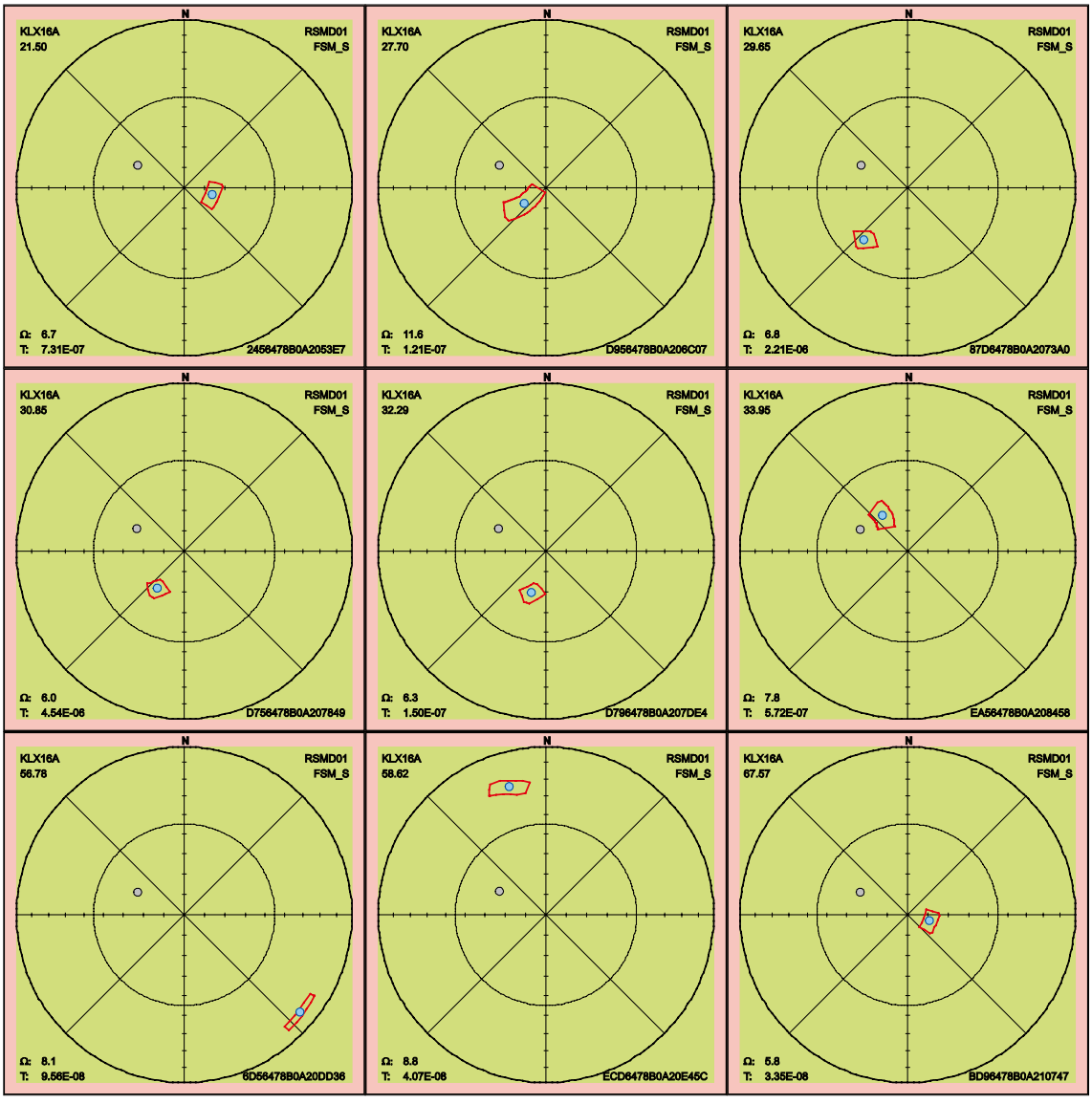

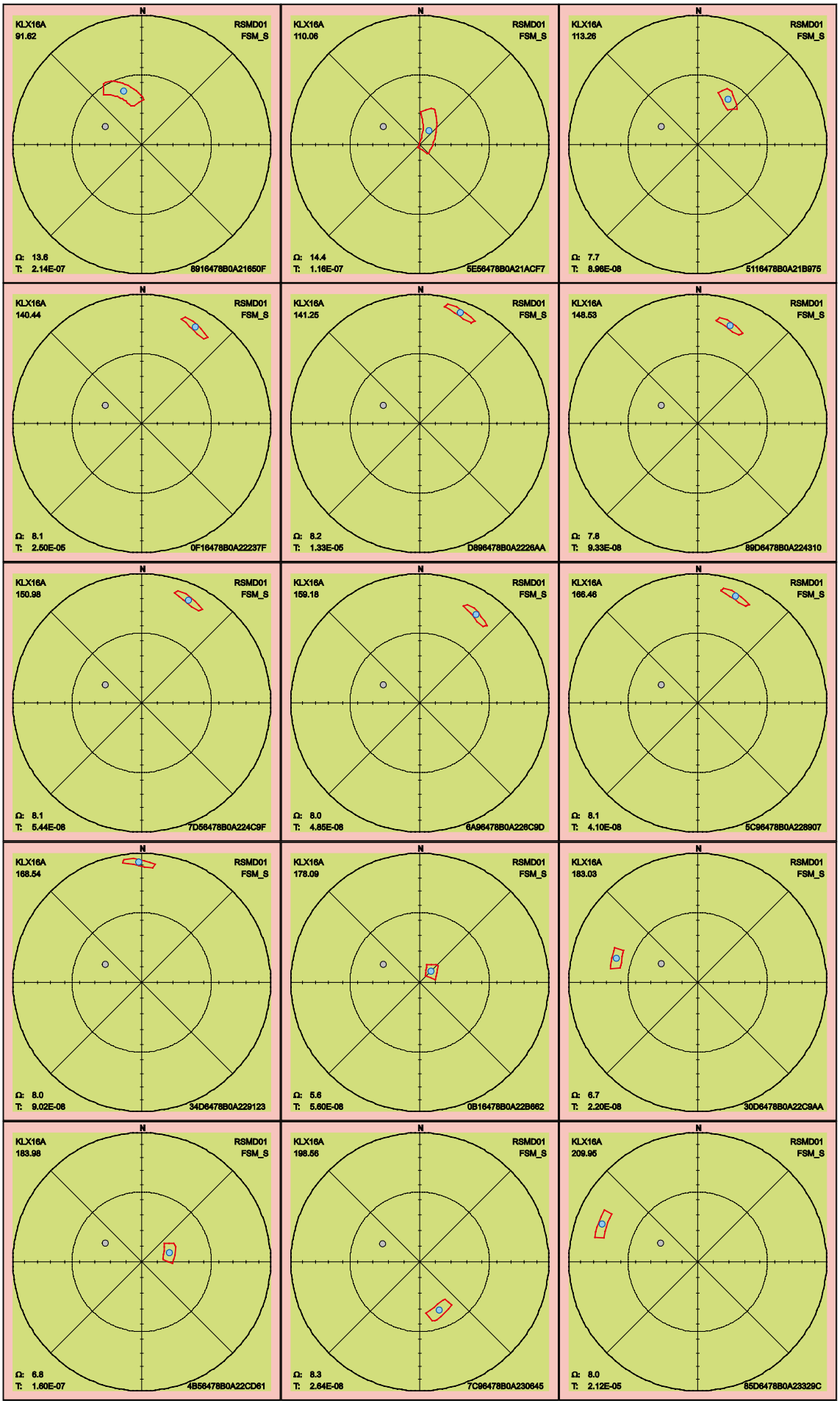
KLX16A
91.62
RSMD01
FSM_S
N
Ω: 13.6
T: 2.14E-07
8916478B0A21650F
KLX16A
110.06
RSMD01
FSM_S
N
Ω: 14.4
T: 1.16E-07
5E56478B0A21ACF7
KLX16A
113.26
RSMD01
FSM_S
N
Ω: 7.7
T: 8.98E-08
5116478B0A21B975
KLX16A
140.44
RSMD01
FSM_S
N
Ω: 8.1
T: 2.50E-05
0F16478B0A22237F
KLX16A
141.25
RSMD01
FSM_S
N
Ω: 8.2
T: 1.33E-05
D896478B0A2226AA
KLX16A
148.53
RSMD01
FSM_S
N
Ω: 7.8
T: 9.33E-08
89D6478B0A224310
KLX16A
150.98
RSMD01
FSM_S
N
Ω: 8.1
T: 5.44E-08
7D56478B0A224C9F
KLX16A
159.18
RSMD01
FSM_S
N
Ω: 8.0
T: 4.85E-08
6A96478B0A226C9D
KLX16A
166.46
RSMD01
FSM_S
N
Ω: 8.1
T: 4.10E-08
5C96478B0A228907
KLX16A
168.54
RSMD01
FSM_S
N
Ω: 8.0
T: 9.02E-08
34D6478B0A229123
KLX16A
178.09
RSMD01
FSM_S
N
Ω: 5.6
T: 5.60E-08
0B16478B0A22B662
KLX16A
183.03
RSMD01
FSM_S
N
Ω: 6.7
T: 2.20E-08
30D6478B0A22C9AA
KLX16A
183.98
RSMD01
FSM_S
N
Ω: 6.8
T: 1.60E-07
4B56478B0A22CD61
KLX16A
198.56
RSMD01
FSM_S
N
Ω: 8.3
T: 2.64E-08
7C96478B0A230645
KLX16A
209.95
RSMD01
FSM_S
N
Ω: 8.0
T: 2.12E-05
85D6478B0A23329C

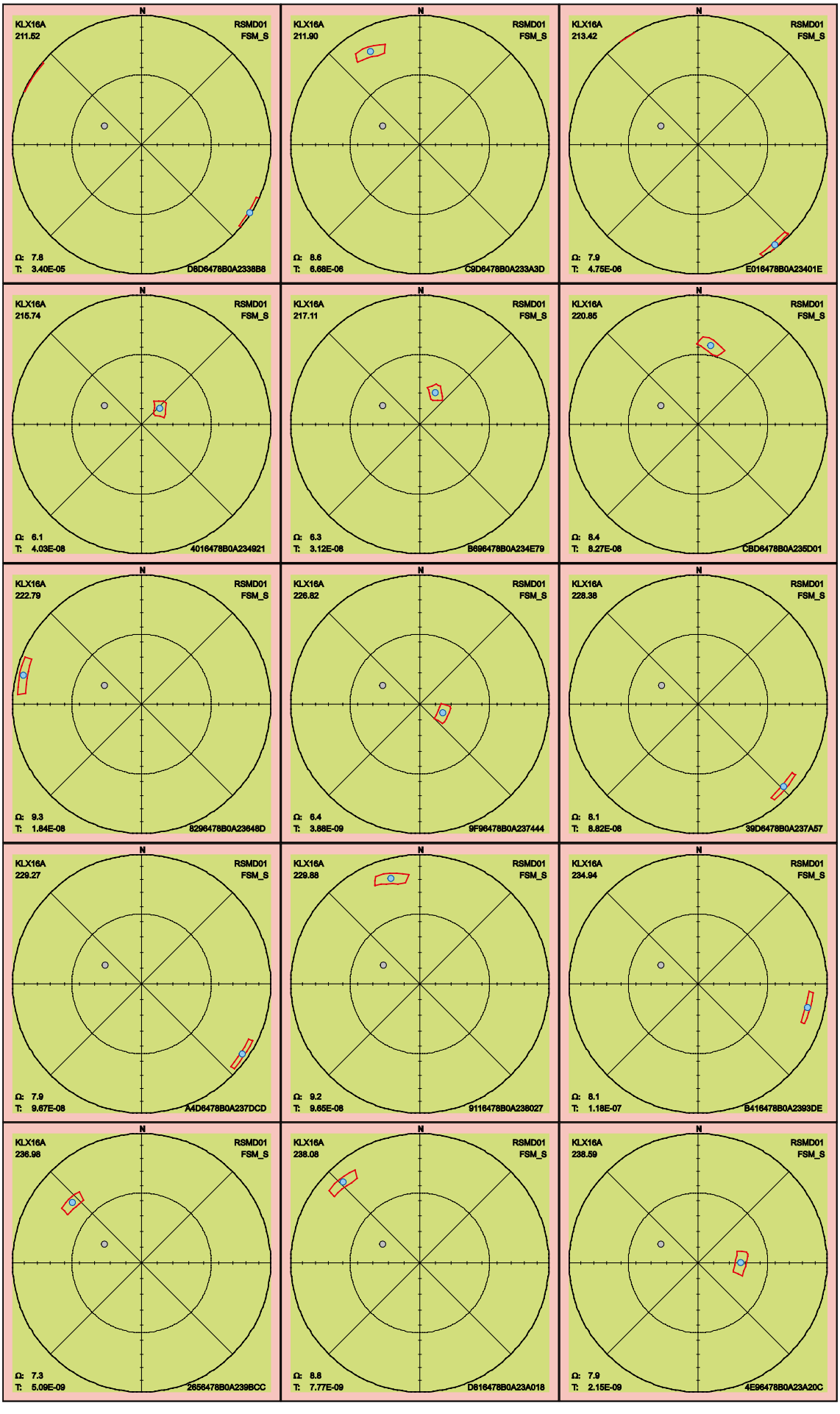
KLX16A
211.52
RSMD01
FSM_S
Ω: 7.8
T: 3.40E-05
D8D6478B0A2338B8
KLX16A
211.90
RSMD01
FSM_S
Ω: 8.6
T: 6.68E-06
C9D6478B0A233A3D
KLX16A
213.42
RSMD01
FSM_S
Ω: 7.9
T: 4.75E-06
E016478B0A23401E
KLX16A
215.74
RSMD01
FSM_S
Ω: 6.1
T: 4.03E-08
4016478B0A234921
KLX16A
217.11
RSMD01
FSM_S
Ω: 6.3
T: 3.12E-08
B696478B0A234E79
KLX16A
220.85
RSMD01
FSM_S
Ω: 8.4
T: 8.27E-08
CBD6478B0A235D01
KLX16A
222.79
RSMD01
FSM_S
Ω: 9.3
T: 1.84E-08
8296478B0A23648D
KLX16A
226.82
RSMD01
FSM_S
Ω: 6.4
T: 3.88E-09
9F96478B0A237444
KLX16A
228.38
RSMD01
FSM_S
Ω: 8.1
T: 8.82E-08
39D6478B0A237A57
KLX16A
229.27
RSMD01
FSM_S
Ω: 7.9
T: 9.67E-08
A4D6478B0A237DCD
KLX16A
229.88
RSMD01
FSM_S
Ω: 9.2
T: 9.65E-08
9116478B0A238027
KLX16A
234.94
RSMD01
FSM_S
Ω: 8.1
T: 1.18E-07
B416478B0A2393DE
KLX16A
236.98
RSMD01
FSM_S
Ω: 7.3
T: 5.09E-09
2656478B0A239BCC
KLX16A
238.08
RSMD01
FSM_S
Ω: 8.8
T: 7.77E-09
D816478B0A23A018
KLX16A
238.59
RSMD01
FSM_S
Ω: 7.9
T: 2.15E-09
4E96478B0A23A20C

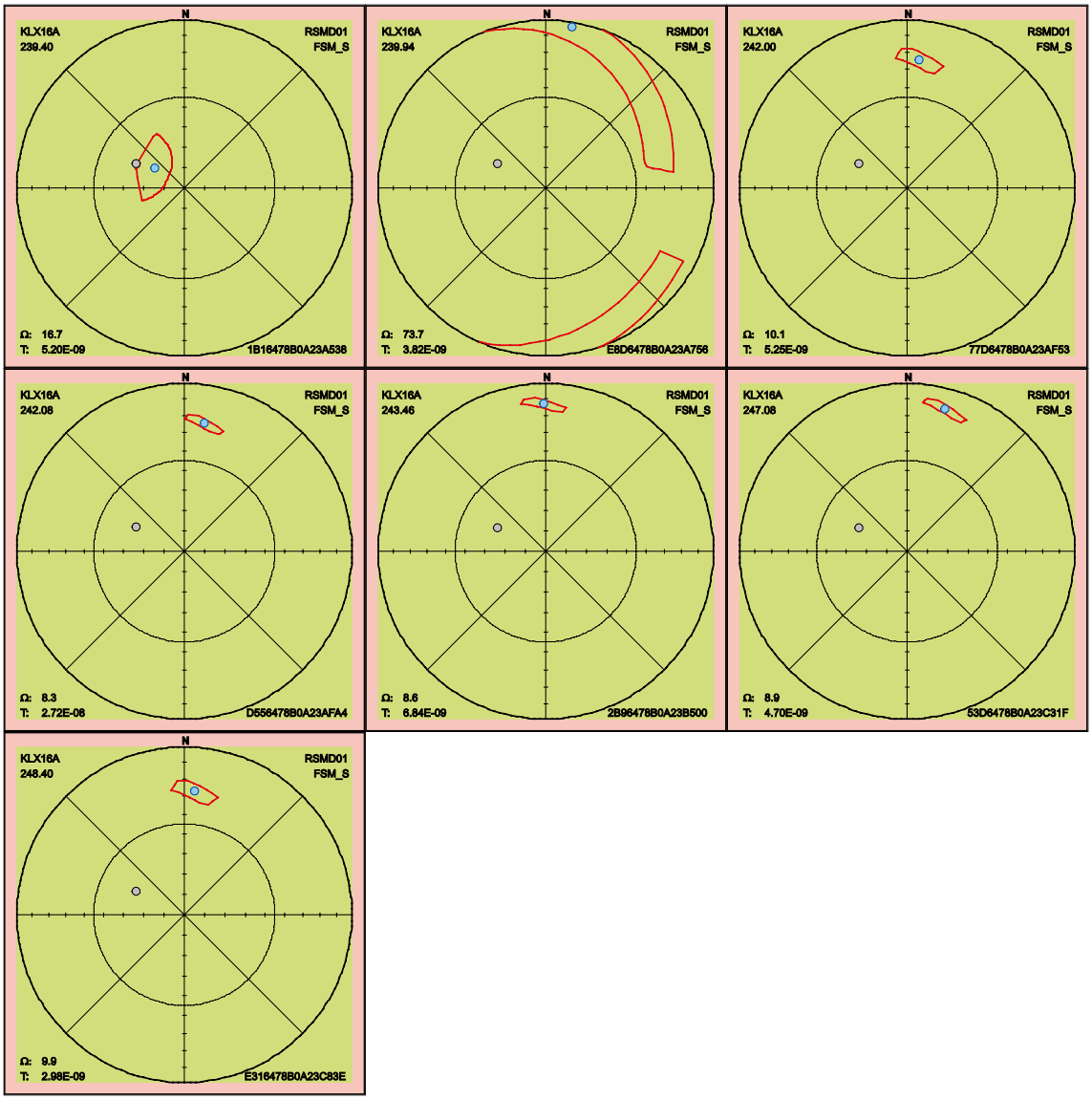

2.3.29 KLX17A

There are 29 PFL fractures in KLX13A of which two have maximum uncertainty larger than 30°, see Table 2-26. These fractures can have an alternative interpretation of orientation compared to the best estimate orientation that is found in the table p_fract_core in /Sicada 2008/. Below follow the 90th percentile sample space of uncertainty for the PFL fractures in KLX17A.

Table 2-26. Fractures in KLX17A with uncertainty, Ω, larger than 30°.

FeatureId	PFL-f no	Adjusted Secup	Ω
BBD7478B0A33BFB4	28	245.98	68.0
EE17478B0A367F28	42	425.94	47.6

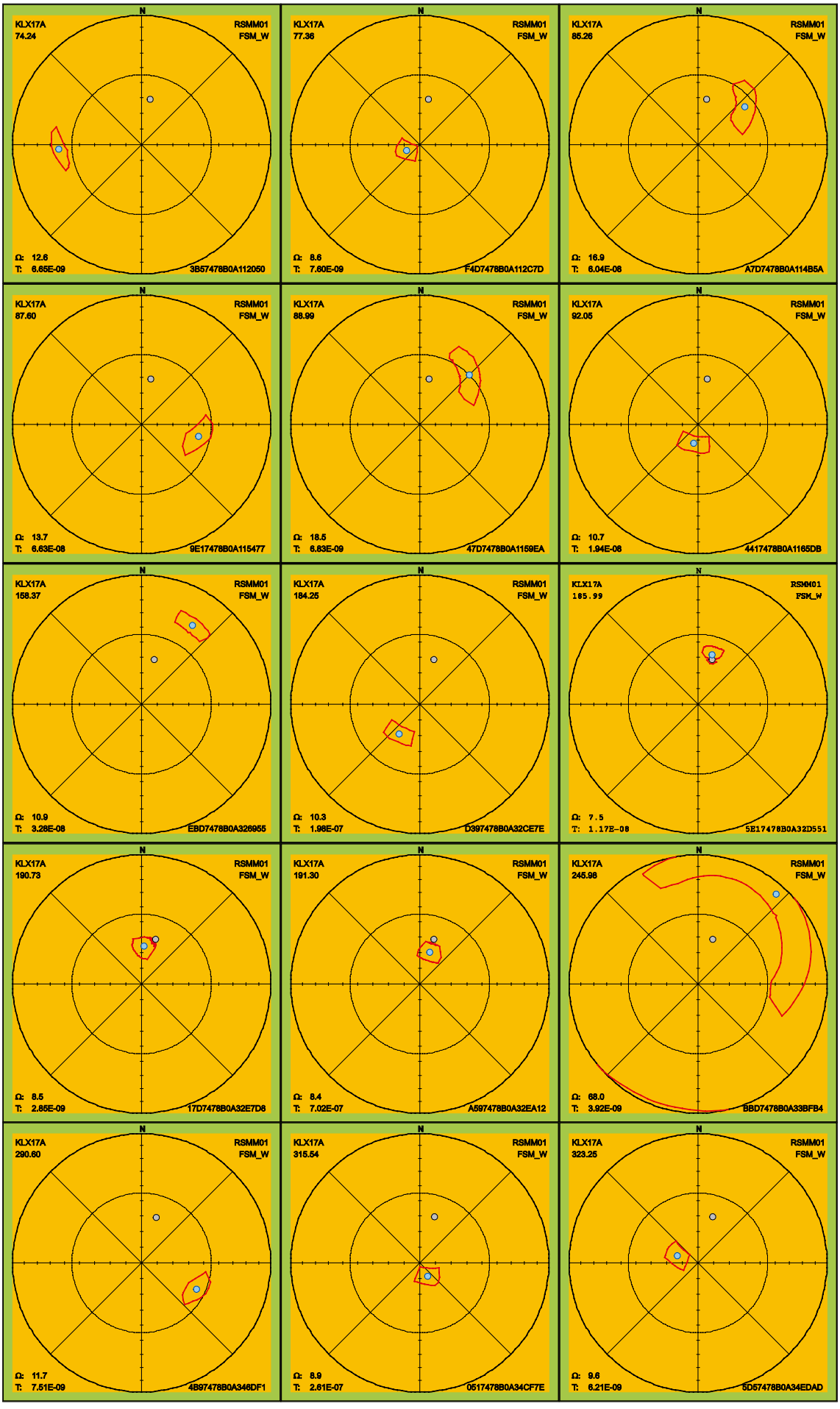
KLX17A
74.24
RSMM01
FSM_W
N
Ω: 12.6
T: 6.65E-09
3B57478B0A112050
KLX17A
77.36
RSMM01
FSM_W
N
Ω: 8.6
T: 7.60E-09
F4D7478B0A112C7D
KLX17A
85.26
RSMM01
FSM_W
N
Ω: 16.9
T: 6.04E-08
A7D7478B0A114B5A
KLX17A
87.60
RSMM01
FSM_W
N
Ω: 13.7
T: 6.63E-08
9E17478B0A115477
KLX17A
88.99
RSMM01
FSM_W
N
Ω: 18.5
T: 6.83E-09
47D7478B0A1159EA
KLX17A
92.05
RSMM01
FSM_W
N
Ω: 10.7
T: 1.94E-08
4417478B0A1165DB
KLX17A
158.37
RSMM01
FSM_W
N
Ω: 10.9
T: 3.28E-08
EBD7478B0A326955
KLX17A
184.25
RSMM01
FSM_W
N
Ω: 10.3
T: 1.98E-07
D397478B0A32CE7E
KLX17A
185.99
RSMM01
FSM_W
N
Ω: 7.5
T: 1.17E-08
5E17478B0A32D551
KLX17A
190.73
RSMM01
FSM_W
N
Ω: 8.5
T: 2.85E-09
17D7478B0A32E7D8
KLX17A
191.30
RSMM01
FSM_W
N
Ω: 8.4
T: 7.02E-07
A597478B0A32EA12
KLX17A
245.98
RSMM01
FSM_W
N
Ω: 68.0
T: 3.92E-09
BBD7478B0A33BFB4
KLX17A
290.60
RSMM01
FSM_W
N
Ω: 11.7
T: 7.51E-09
4B97478B0A346DF1
KLX17A
315.54
RSMM01
FSM_W
N
Ω: 8.9
T: 2.61E-07
0517478B0A34CF7E
KLX17A
323.25
RSMM01
FSM_W
N
Ω: 9.6
T: 6.21E-09
5D57478B0A34EDAD

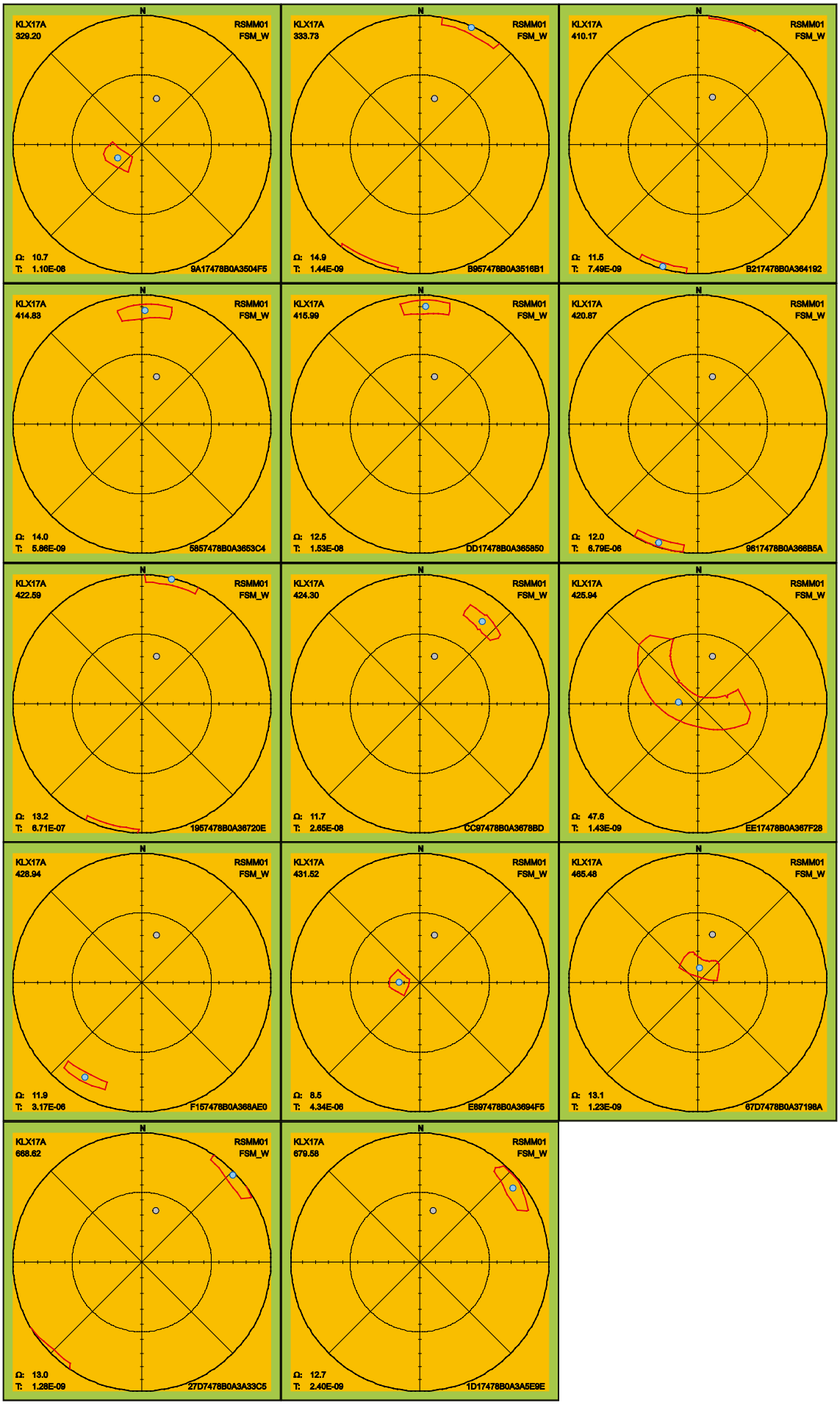
KLX17A
329.20
RSMM01
FSM_W
N
Ω: 10.7
T: 1.10E-06
9A17478B0A3504F5
KLX17A
333.73
RSMM01
FSM_W
N
Ω: 14.9
T: 1.44E-09
B957478B0A3516B1
KLX17A
410.17
RSMM01
FSM_W
N
Ω: 11.5
T: 7.49E-09
B217478B0A364192
KLX17A
414.83
RSMM01
FSM_W
N
Ω: 14.0
T: 5.86E-09
5857478B0A3653C4
KLX17A
415.99
RSMM01
FSM_W
N
Ω: 12.5
T: 1.53E-08
DD17478B0A365850
KLX17A
420.87
RSMM01
FSM_W
N
Ω: 12.0
T: 6.79E-06
9617478B0A366B5A
KLX17A
422.59
RSMM01
FSM_W
N
Ω: 13.2
T: 6.71E-07
1957478B0A36720E
KLX17A
424.30
RSMM01
FSM_W
N
Ω: 11.7
T: 2.65E-08
CC97478B0A3678BD
KLX17A
425.94
RSMM01
FSM_W
N
Ω: 47.6
T: 1.43E-09
EE17478B0A367F28
KLX17A
428.94
RSMM01
FSM_W
N
Ω: 11.9
T: 3.17E-06
F157478B0A368AE0
KLX17A
431.52
RSMM01
FSM_W
N
Ω: 8.5
T: 4.34E-06
E897478B0A3694F5
KLX17A
465.48
RSMM01
FSM_W
N
Ω: 13.1
T: 1.23E-09
67D7478B0A37198A
KLX17A
668.62
RSMM01
FSM_W
N
Ω: 13.0
T: 1.28E-09
27D7478B0A3A33C5
KLX17A
679.58
RSMM01
FSM_W
N
Ω: 12.7
T: 2.40E-09
1D17478B0A3A5E9E

2.3.30 KLX18A

Below follow the 90th percentile sample space of uncertainty for the 140 PFL fractures in KLX18A. Attention should be paid to the 12 fractures listed in Table 2-27 because these fractures have a maximum uncertainty, on the 90th percentile, larger than 30° and hence can have an alternative interpretation of orientation compared to the best estimate orientation that is found in the table p_fract_core in /Sicada 2008/.

Table 2-27. Fractures in KLX18A with uncertainty, Ω, larger than 30°.

FeatureId	PFL-f no	Adjusted Secup	Ω
E098478B0A11B1EB	10	111.09	58.9
A098478B0A1229B0	26	141.82	31.3
2098478B0A123B2C	28	146.31	39.9
A098478B0A154B54	59	347.65	53.8
6098478B0A154EB2	61	348.51	73.5
C098478B0A1554BC	62	350.06	63.5
2098478B0A15B6DC	71	375.29	68.2
6098478B0A15C5D6	76	379.14	73.7
4098478B0A1620B2	86	402.51	47.7
C098478B0A1691EE	106	431.62	57.8
6098478B0A17032C	114	460.71	69.6
C098478B0A18301A	134	538.01	69.9

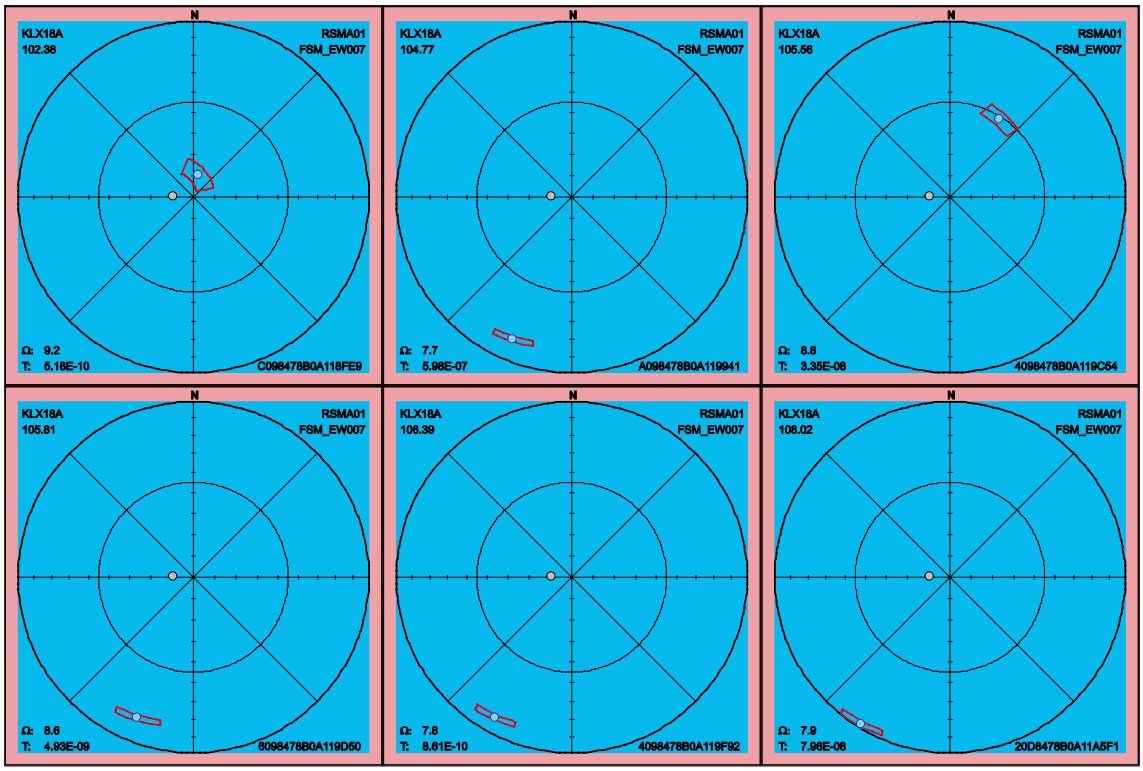

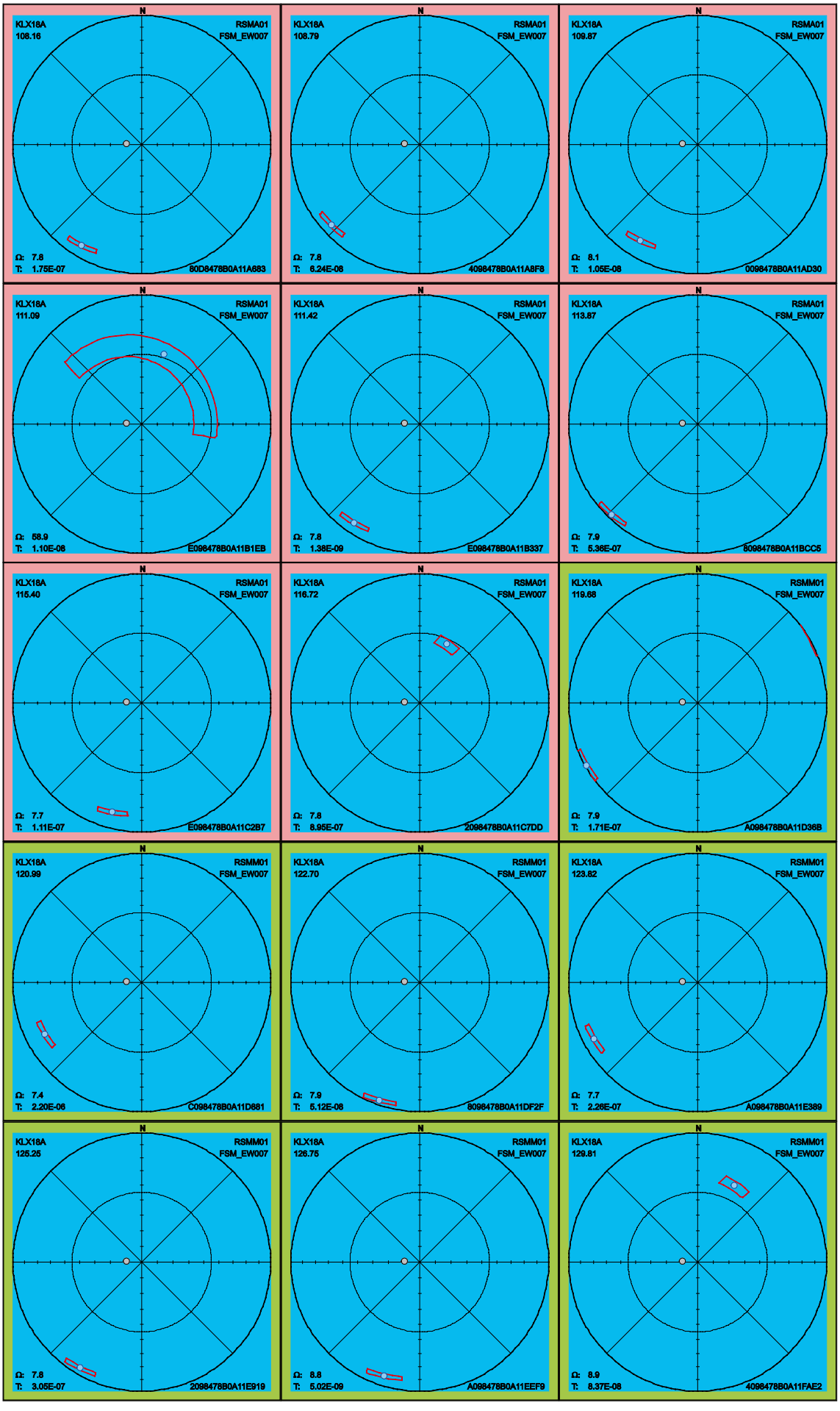
KLX18A
108.16
RSMA01
FSM_EW007
Ω: 7.8
T: 1.75E-07
80D8478B0A11A683
KLX18A
108.79
RSMA01
FSM_EW007
Ω: 7.8
T: 6.24E-08
4098478B0A11A8F8
KLX18A
109.87
RSMA01
FSM_EW007
Ω: 8.1
T: 1.05E-08
0098478B0A11AD30
KLX18A
111.09
RSMA01
FSM_EW007
Ω: 58.9
T: 1.10E-06
E098478B0A11B1EB
KLX18A
111.42
RSMA01
FSM_EW007
Ω: 7.8
T: 1.38E-09
E098478B0A11B337
KLX18A
113.87
RSMA01
FSM_EW007
Ω: 7.9
T: 5.36E-07
8098478B0A11BCC5
KLX18A
115.40
RSMA01
FSM_EW007
Ω: 7.7
T: 1.11E-07
E098478B0A11C2B7
KLX18A
116.72
RSMA01
FSM_EW007
Ω: 7.8
T: 8.95E-07
2098478B0A11C7DD
KLX18A
119.68
RSMM01
FSM_EW007
Ω: 7.9
T: 1.71E-07
A098478B0A11D36B
KLX18A
120.99
RSMM01
FSM_EW007
Ω: 7.4
T: 2.20E-06
C098478B0A11D881
KLX18A
122.70
RSMM01
FSM_EW007
Ω: 7.9
T: 5.12E-08
8098478B0A11DF2F
KLX18A
123.82
RSMM01
FSM_EW007
Ω: 7.7
T: 2.26E-07
A098478B0A11E389
KLX18A
125.25
RSMM01
FSM_EW007
Ω: 7.8
T: 3.05E-07
2098478B0A11E919
KLX18A
126.75
RSMM01
FSM_EW007
Ω: 8.8
T: 5.02E-09
A098478B0A11EEF9
KLX18A
129.81
RSMM01
FSM_EW007
Ω: 8.9
T: 8.37E-08
4098478B0A11FAE2

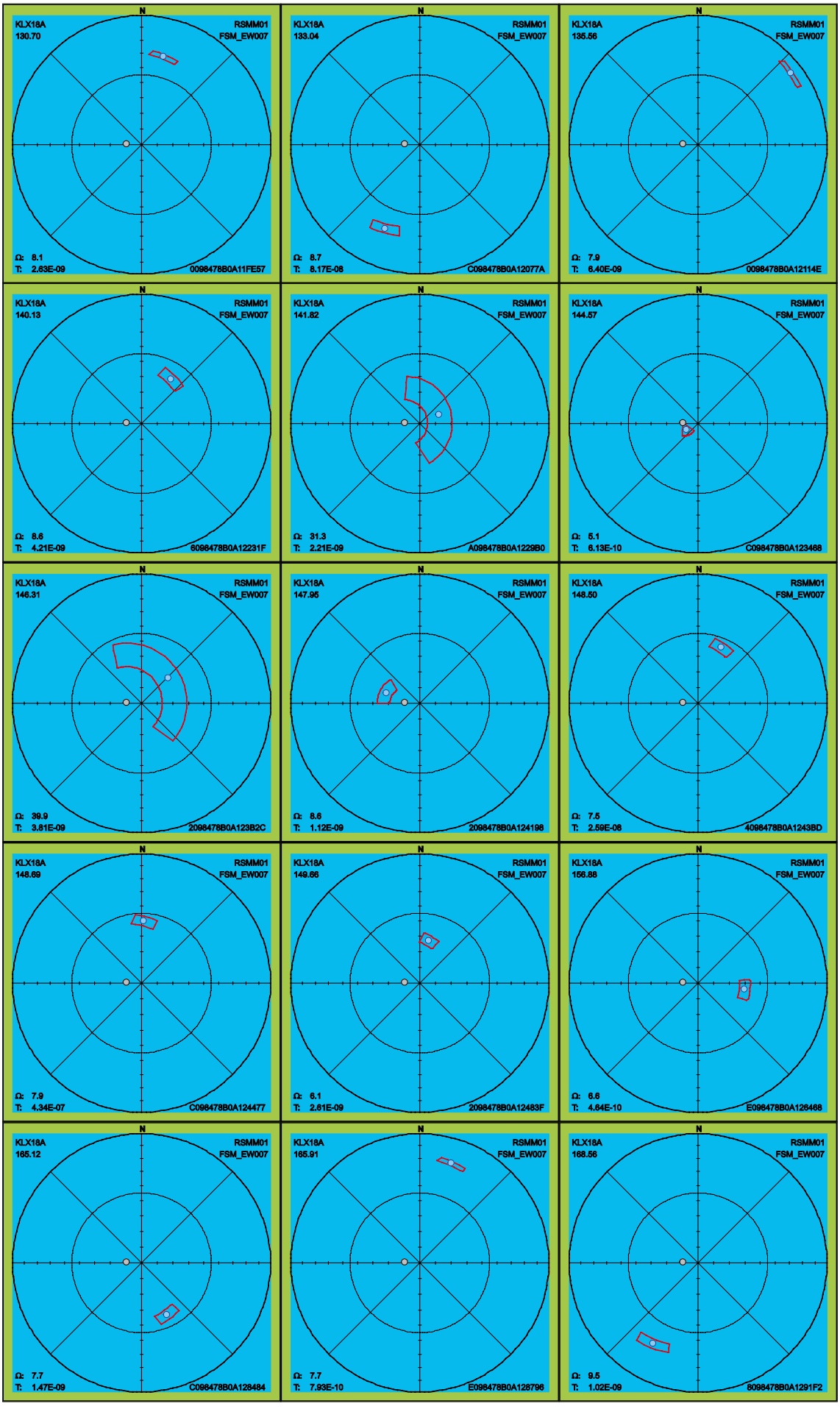
KLX18A
130.70
RSMM01
FSM_EW007
N
Ω: 8.1
T: 2.63E-09
0098478B0A11FE57
KLX18A
133.04
RSMM01
FSM_EW007
N
Ω: 8.7
T: 8.17E-08
C098478B0A12077A
KLX18A
135.56
RSMM01
FSM_EW007
N
Ω: 7.9
T: 6.40E-09
0098478B0A12114E
KLX18A
140.13
RSMM01
FSM_EW007
N
Ω: 8.6
T: 4.21E-09
8098478B0A12231F
KLX18A
141.82
RSMM01
FSM_EW007
N
Ω: 31.3
T: 2.21E-09
A098478B0A1229B0
KLX18A
144.57
RSMM01
FSM_EW007
N
Ω: 5.1
T: 6.13E-10
C098478B0A123468
KLX18A
146.31
RSMM01
FSM_EW007
N
Ω: 39.9
T: 3.81E-09
2098478B0A123B2C
KLX18A
147.95
RSMM01
FSM_EW007
N
Ω: 8.6
T: 1.12E-09
2098478B0A124198
KLX18A
148.50
RSMM01
FSM_EW007
N
Ω: 7.5
T: 2.59E-08
4098478B0A1243BD
KLX18A
148.69
RSMM01
FSM_EW007
N
Ω: 7.9
T: 4.34E-07
C098478B0A124477
KLX18A
149.66
RSMM01
FSM_EW007
N
Ω: 6.1
T: 2.61E-09
2098478B0A12483F
KLX18A
156.88
RSMM01
FSM_EW007
N
Ω: 6.6
T: 4.64E-10
E098478B0A128468
KLX18A
165.12
RSMM01
FSM_EW007
N
Ω: 7.7
T: 1.47E-09
C098478B0A128484
KLX18A
165.91
RSMM01
FSM_EW007
N
Ω: 7.7
T: 7.93E-10
E098478B0A128796
KLX18A
168.56
RSMM01
FSM_EW007
N
Ω: 9.5
T: 1.02E-09
8098478B0A1291F2

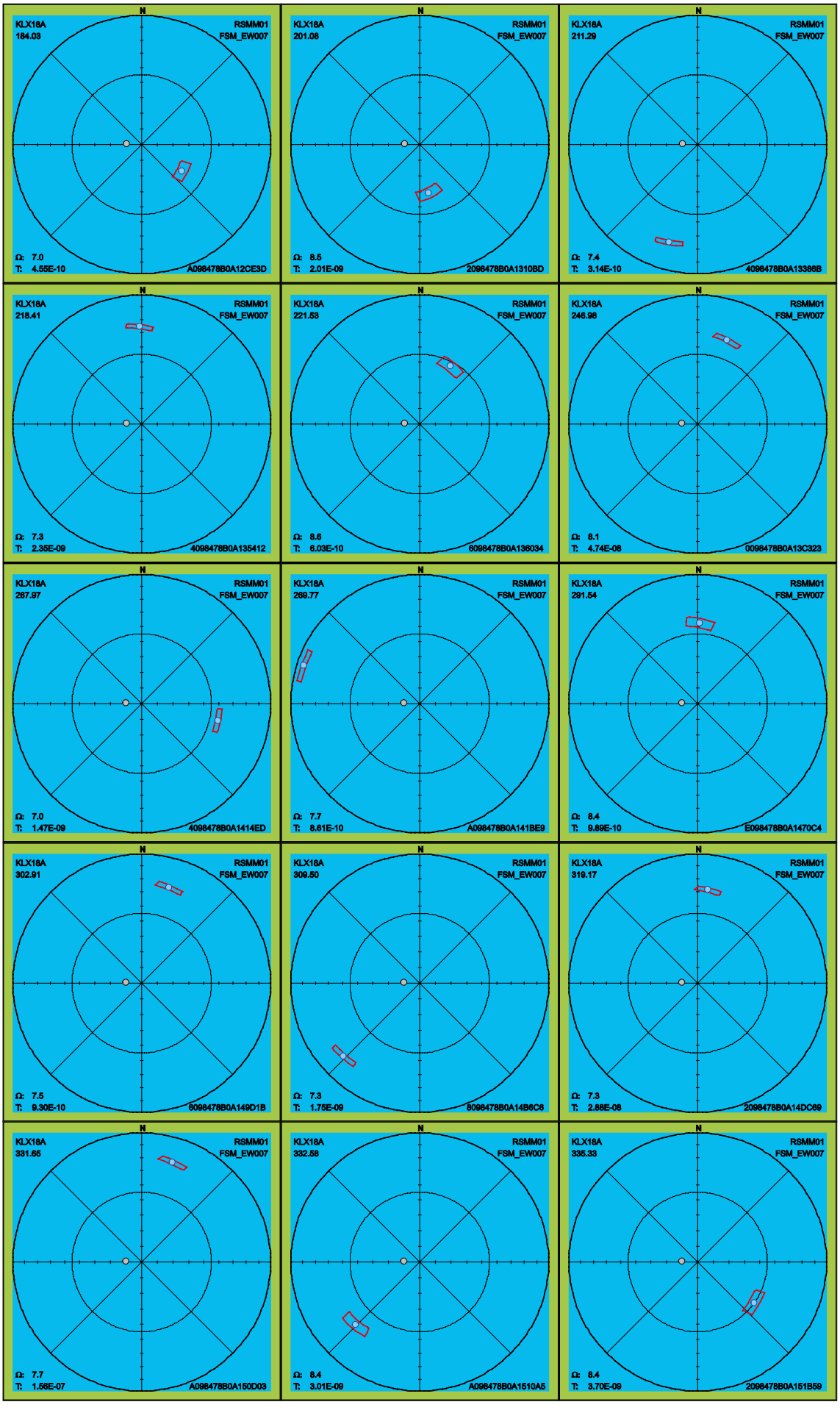
KLX18A
184.03
RSMM01
FSM_EW007
N
Ω: 7.0
T: 4.55E-10
A098478B0A12CE3D
KLX18A
201.08
RSMM01
FSM_EW007
N
Ω: 8.5
T: 2.01E-09
2098478B0A1310BD
KLX18A
211.29
RSMM01
FSM_EW007
N
Ω: 7.4
T: 3.14E-10
4098478B0A13386B
KLX18A
218.41
RSMM01
FSM_EW007
N
Ω: 7.3
T: 2.35E-09
4098478B0A135412
KLX18A
221.53
RSMM01
FSM_EW007
N
Ω: 8.6
T: 6.03E-10
6098478B0A136034
KLX18A
246.98
RSMM01
FSM_EW007
N
Ω: 8.1
T: 4.74E-08
0098478B0A13C323
KLX18A
267.97
RSMM01
FSM_EW007
N
Ω: 7.0
T: 1.47E-09
4098478B0A1414ED
KLX18A
269.77
RSMM01
FSM_EW007
N
Ω: 7.7
T: 8.61E-10
A098478B0A141BE9
KLX18A
291.54
RSMM01
FSM_EW007
N
Ω: 8.4
T: 9.89E-10
E098478B0A1470C4
KLX18A
302.91
RSMM01
FSM_EW007
N
Ω: 7.5
T: 9.30E-10
6098478B0A149D1B
KLX18A
309.50
RSMM01
FSM_EW007
N
Ω: 7.3
T: 1.75E-09
8098478B0A14B6C6
KLX18A
319.17
RSMM01
FSM_EW007
N
Ω: 7.3
T: 2.88E-08
2098478B0A14DC89
KLX18A
331.65
RSMM01
FSM_EW007
N
Ω: 7.7
T: 1.56E-07
A098478B0A150D03
KLX18A
332.58
RSMM01
FSM_EW007
N
Ω: 8.4
T: 3.01E-09
A098478B0A1510A5
KLX18A
335.33
RSMM01
FSM_EW007
N
Ω: 8.4
T: 3.70E-09
2098478B0A151B59

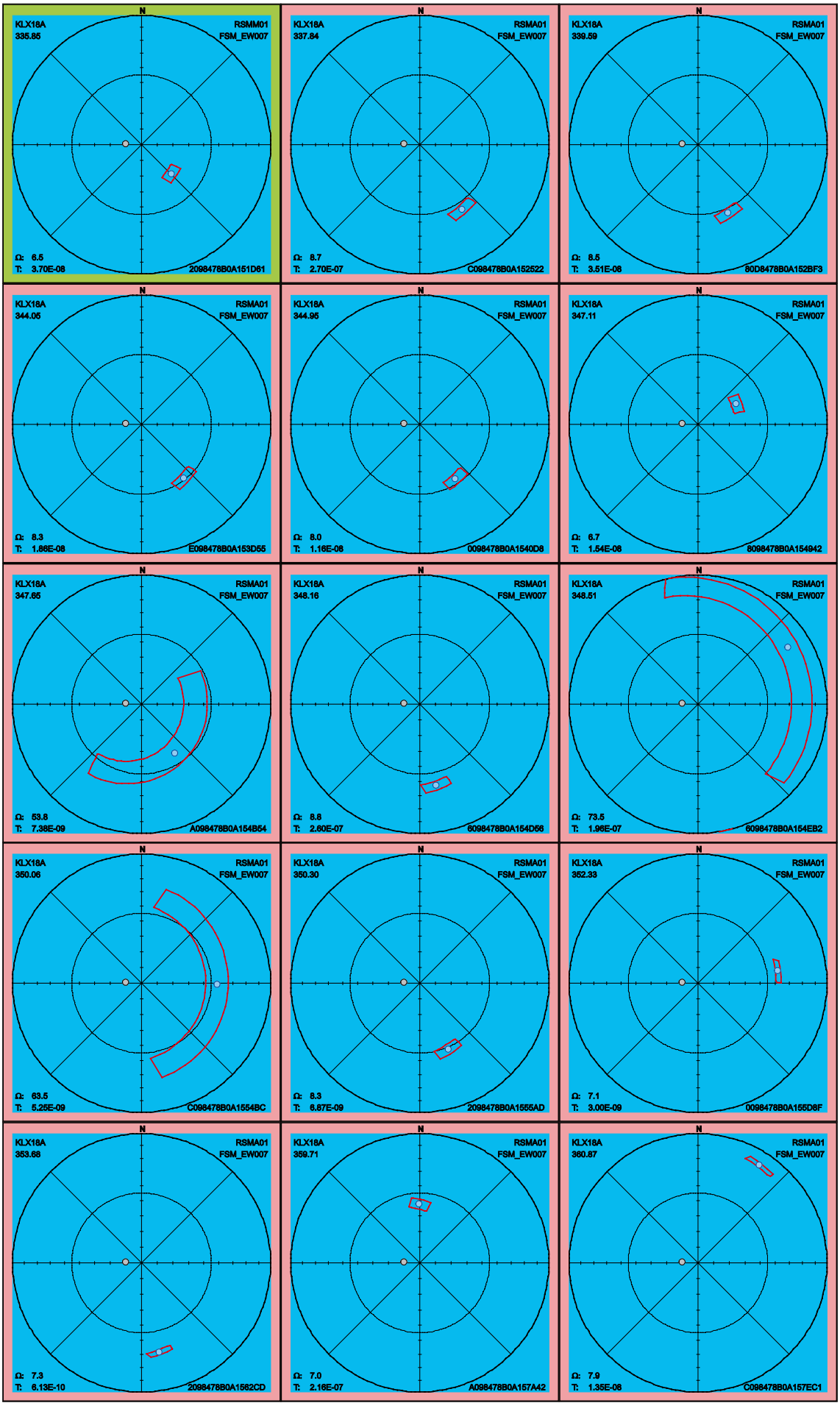
KLX18A
335.85
RSMM01
FSM_EW007
Ω: 6.5
T: 3.70E-08
2098478B0A151D61
KLX18A
337.84
RSMA01
FSM_EW007
Ω: 8.7
T: 2.70E-07
C098478B0A152522
KLX18A
339.59
RSMA01
FSM_EW007
Ω: 8.5
T: 3.51E-08
80D8478B0A152BF3
KLX18A
344.05
RSMA01
FSM_EW007
Ω: 8.3
T: 1.86E-08
E098478B0A153D55
KLX18A
344.95
RSMA01
FSM_EW007
Ω: 8.0
T: 1.16E-08
0098478B0A1540D8
KLX18A
347.11
RSMA01
FSM_EW007
Ω: 6.7
T: 1.54E-08
8098478B0A154942
KLX18A
347.65
RSMA01
FSM_EW007
Ω: 53.8
T: 7.38E-09
A098478B0A154B54
KLX18A
348.16
RSMA01
FSM_EW007
Ω: 8.8
T: 2.60E-07
6098478B0A154D66
KLX18A
348.51
RSMA01
FSM_EW007
Ω: 73.5
T: 1.98E-07
6098478B0A154EB2
KLX18A
350.06
RSMA01
FSM_EW007
Ω: 63.5
T: 5.25E-09
C098478B0A1554BC
KLX18A
350.30
RSMA01
FSM_EW007
Ω: 8.3
T: 6.87E-09
2098478B0A1555AD
KLX18A
352.33
RSMA01
FSM_EW007
Ω: 7.1
T: 3.00E-09
0098478B0A155D8F
KLX18A
353.68
RSMA01
FSM_EW007
Ω: 7.3
T: 6.13E-10
2098478B0A1562CD
KLX18A
359.71
RSMA01
FSM_EW007
Ω: 7.0
T: 2.16E-07
A098478B0A157A42
KLX18A
360.87
RSMA01
FSM_EW007
Ω: 7.9
T: 1.35E-08
C098478B0A157EC1

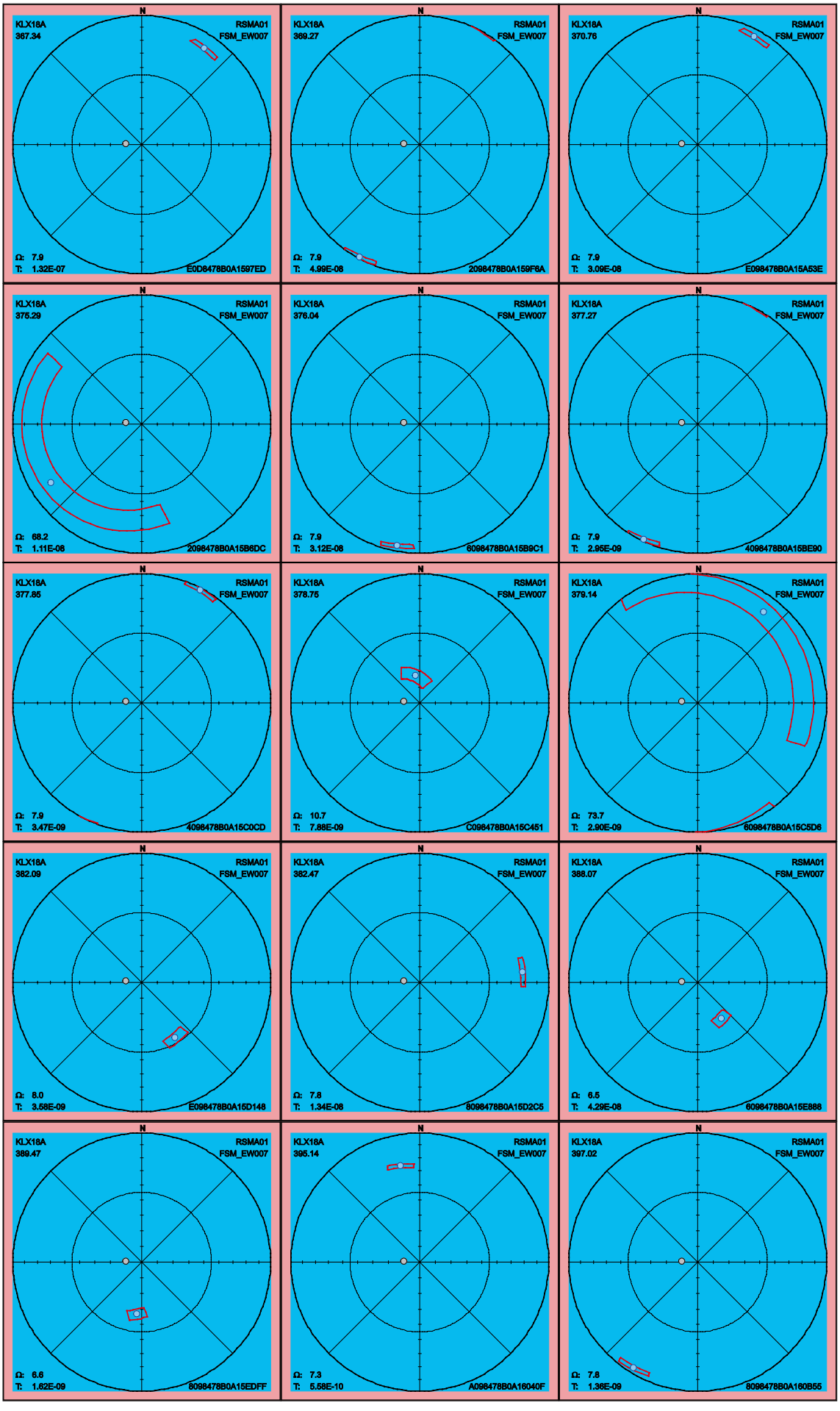
KLX18A
367.34
RSMA01
FSM_EW007
Ω: 7.9
T: 1.32E-07
E0D6478B0A1597ED
KLX18A
369.27
RSMA01
FSM_EW007
Ω: 7.9
T: 4.99E-08
2098478B0A159F8A
KLX18A
370.76
RSMA01
FSM_EW007
Ω: 7.9
T: 3.09E-08
E098478B0A15A53E
KLX18A
375.29
RSMA01
FSM_EW007
Ω: 68.2
T: 1.11E-06
2098478B0A15B6DC
KLX18A
376.04
RSMA01
FSM_EW007
Ω: 7.9
T: 3.12E-08
6098478B0A15B9C1
KLX18A
377.27
RSMA01
FSM_EW007
Ω: 7.9
T: 2.95E-09
4098478B0A15BE90
KLX18A
377.85
RSMA01
FSM_EW007
Ω: 7.9
T: 3.47E-09
4098478B0A15C0CD
KLX18A
378.75
RSMA01
FSM_EW007
Ω: 10.7
T: 7.88E-09
C098478B0A15C451
KLX18A
379.14
RSMA01
FSM_EW007
Ω: 73.7
T: 2.90E-09
6098478B0A15C5D6
KLX18A
382.09
RSMA01
FSM_EW007
Ω: 8.0
T: 3.58E-09
E098478B0A15D148
KLX18A
382.47
RSMA01
FSM_EW007
Ω: 7.8
T: 1.34E-08
8098478B0A15D2C5
KLX18A
388.07
RSMA01
FSM_EW007
Ω: 6.5
T: 4.29E-08
6098478B0A15E888
KLX18A
389.47
RSMA01
FSM_EW007
Ω: 6.6
T: 1.62E-09
8098478B0A15EDFF
KLX18A
395.14
RSMA01
FSM_EW007
Ω: 7.3
T: 5.58E-10
A098478B0A16040F
KLX18A
397.02
RSMA01
FSM_EW007
Ω: 7.8
T: 1.36E-09
8098478B0A160B55

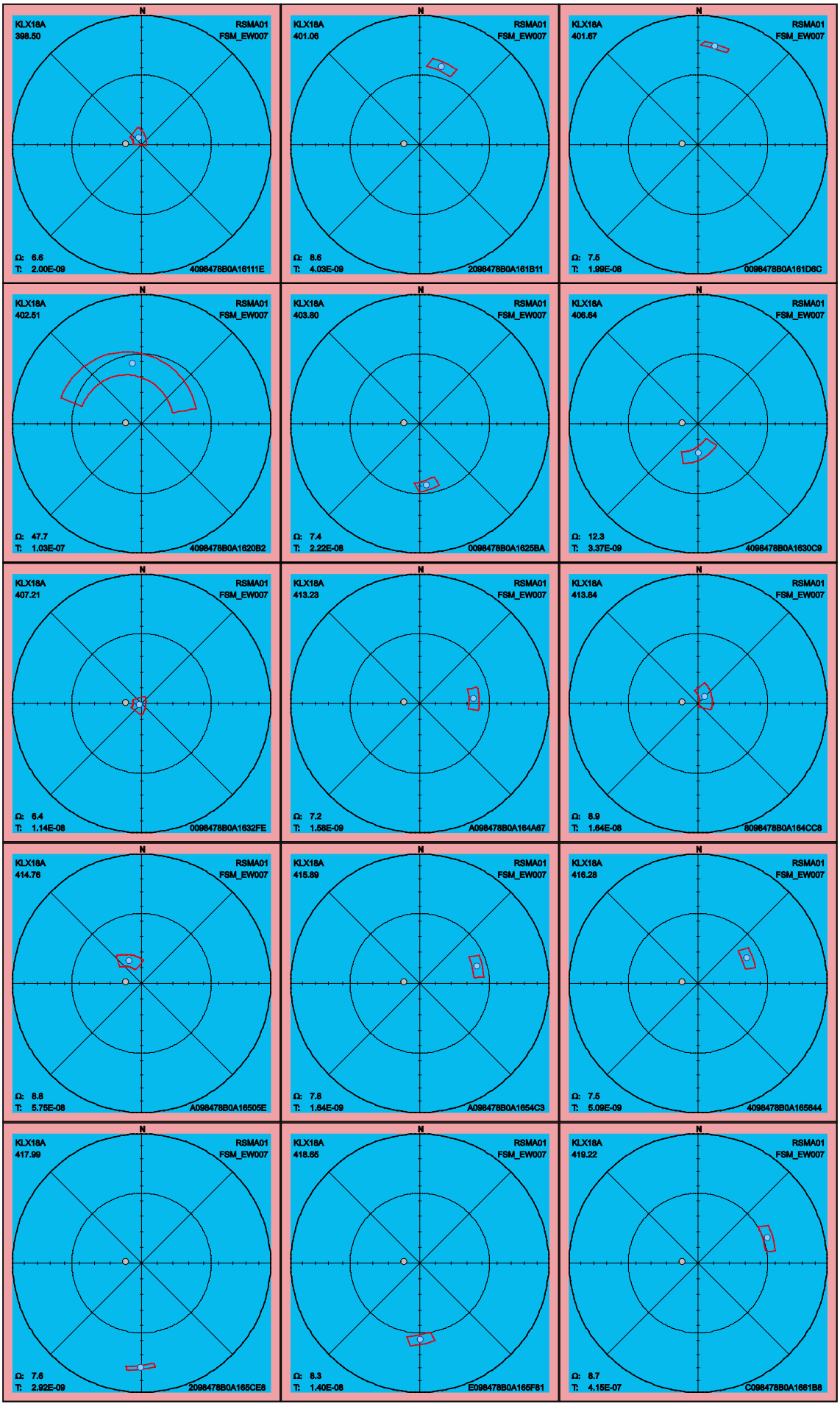
KLX18A
398.50
RSMA01
FSM_EW007
Ω: 6.6
T: 2.00E-09
4098478B0A16111E
KLX18A
401.06
RSMA01
FSM_EW007
Ω: 8.6
T: 4.03E-09
2098478B0A161B11
KLX18A
401.67
RSMA01
FSM_EW007
Ω: 7.5
T: 1.99E-08
0098478B0A161D6C
KLX18A
402.51
RSMA01
FSM_EW007
Ω: 47.7
T: 1.03E-07
4098478B0A1620B2
KLX18A
403.80
RSMA01
FSM_EW007
Ω: 7.4
T: 2.22E-08
0098478B0A1625BA
KLX18A
406.64
RSMA01
FSM_EW007
Ω: 12.3
T: 3.37E-09
4098478B0A1630C9
KLX18A
407.21
RSMA01
FSM_EW007
Ω: 6.4
T: 1.14E-08
0098478B0A1632FE
KLX18A
413.23
RSMA01
FSM_EW007
Ω: 7.2
T: 1.58E-09
A098478B0A164A67
KLX18A
413.84
RSMA01
FSM_EW007
Ω: 8.9
T: 1.64E-06
8098478B0A164CC8
KLX18A
414.76
RSMA01
FSM_EW007
Ω: 8.8
T: 5.75E-08
A098478B0A16505E
KLX18A
415.89
RSMA01
FSM_EW007
Ω: 7.8
T: 1.64E-09
A098478B0A1654C3
KLX18A
416.28
RSMA01
FSM_EW007
Ω: 7.5
T: 5.09E-09
4098478B0A165644
KLX18A
417.99
RSMA01
FSM_EW007
Ω: 7.6
T: 2.92E-09
2098478B0A165CE8
KLX18A
418.65
RSMA01
FSM_EW007
Ω: 8.3
T: 1.40E-08
E098478B0A165F81
KLX18A
419.22
RSMA01
FSM_EW007
Ω: 8.7
T: 4.15E-07
C098478B0A1661B8

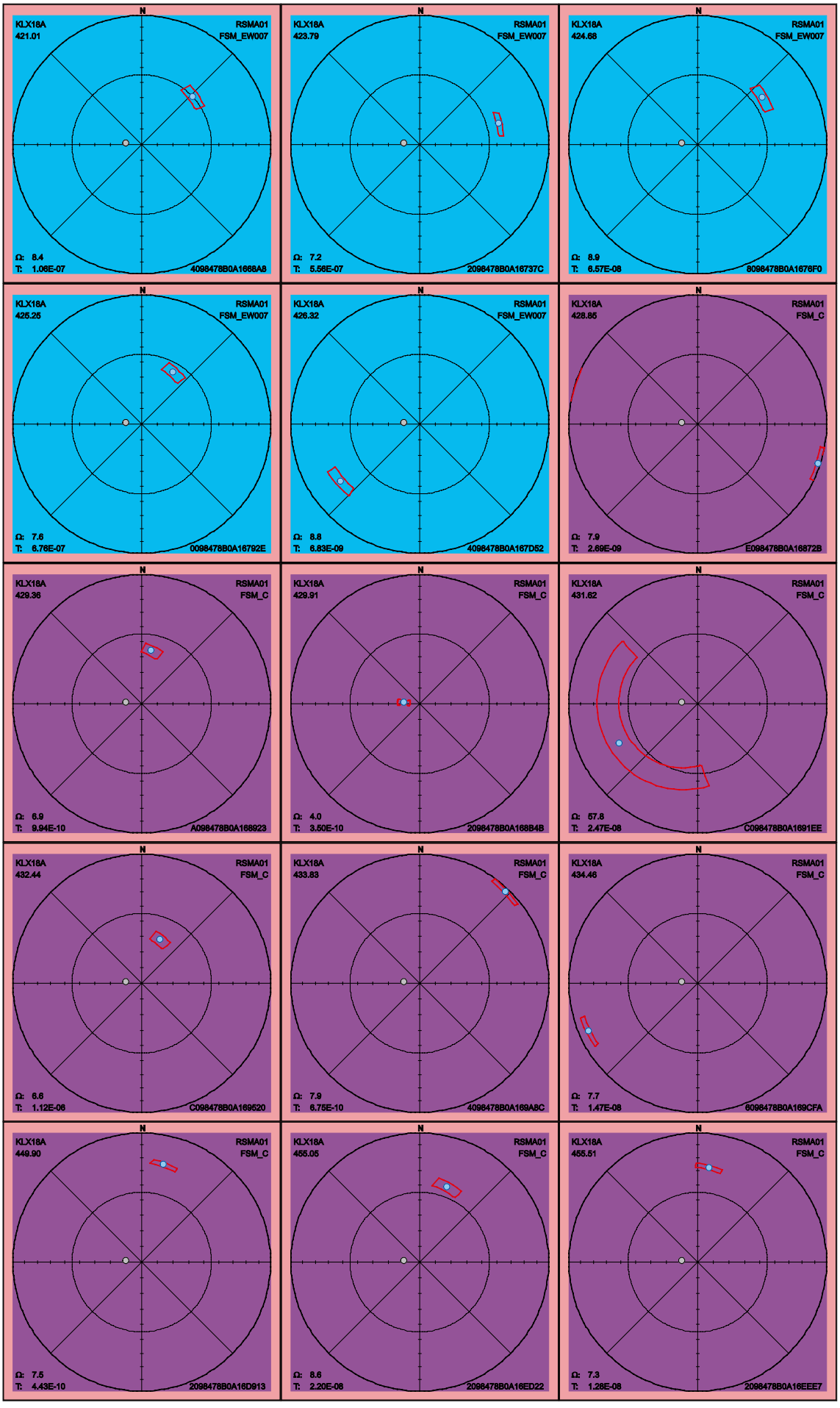
KLX18A
421.01
RSMA01
FSM_EW007
Ω: 8.4
T: 1.08E-07
4098478B0A1668A8
KLX18A
423.79
RSMA01
FSM_EW007
Ω: 7.2
T: 5.56E-07
2098478B0A16737C
KLX18A
424.68
RSMA01
FSM_EW007
Ω: 8.9
T: 6.57E-08
8098478B0A1676F0
KLX18A
425.25
RSMA01
FSM_EW007
Ω: 7.6
T: 6.76E-07
0098478B0A16792E
KLX18A
426.32
RSMA01
FSM_EW007
Ω: 8.8
T: 6.83E-09
4098478B0A167D52
KLX18A
428.85
RSMA01
FSM_C
Ω: 7.9
T: 2.69E-09
E098478B0A16872B
KLX18A
429.36
RSMA01
FSM_C
Ω: 6.9
T: 9.94E-10
A098478B0A168923
KLX18A
429.91
RSMA01
FSM_C
Ω: 4.0
T: 3.50E-10
2098478B0A168B4B
KLX18A
431.62
RSMA01
FSM_C
Ω: 57.8
T: 2.47E-08
C098478B0A1691EE
KLX18A
432.44
RSMA01
FSM_C
Ω: 6.6
T: 1.12E-06
C098478B0A169520
KLX18A
433.83
RSMA01
FSM_C
Ω: 7.9
T: 6.75E-10
4098478B0A169A8C
KLX18A
434.46
RSMA01
FSM_C
Ω: 7.7
T: 1.47E-08
8098478B0A169CFA
KLX18A
449.90
RSMA01
FSM_C
Ω: 7.5
T: 4.43E-10
2098478B0A16D913
KLX18A
455.05
RSMA01
FSM_C
Ω: 8.6
T: 2.20E-08
2098478B0A16ED22
KLX18A
455.51
RSMA01
FSM_C
Ω: 7.3
T: 1.26E-08
2098478B0A16EEE7

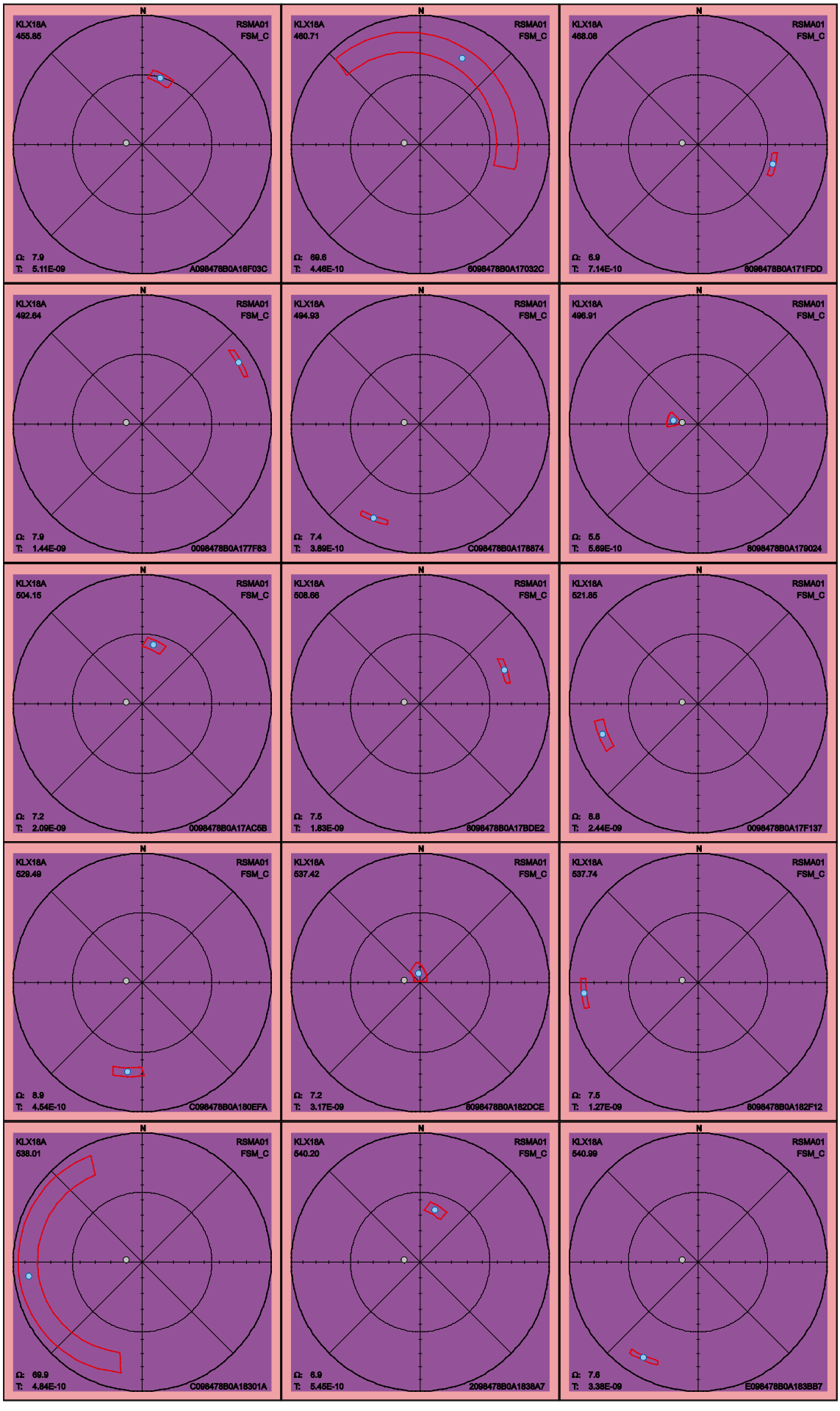
KLX18A
455.85
RSMA01
FSM_C
Ω: 7.9
T: 5.11E-09
A098478B0A16F03C
KLX18A
460.71
RSMA01
FSM_C
Ω: 69.6
T: 4.46E-10
8098478B0A17032C
KLX18A
468.08
RSMA01
FSM_C
Ω: 6.9
T: 7.14E-10
8098478B0A171FDD
KLX18A
492.64
RSMA01
FSM_C
Ω: 7.9
T: 1.44E-09
0098478B0A177F83
KLX18A
494.93
RSMA01
FSM_C
Ω: 7.4
T: 3.89E-10
C098478B0A178874
KLX18A
496.91
RSMA01
FSM_C
Ω: 5.5
T: 5.69E-10
8098478B0A179024
KLX18A
504.15
RSMA01
FSM_C
Ω: 7.2
T: 2.09E-09
0098478B0A17AC5B
KLX18A
508.66
RSMA01
FSM_C
Ω: 7.5
T: 1.83E-09
8098478B0A17BDE2
KLX18A
521.85
RSMA01
FSM_C
Ω: 8.8
T: 2.44E-09
0098478B0A17F137
KLX18A
529.49
RSMA01
FSM_C
Ω: 8.9
T: 4.54E-10
C098478B0A180EFA
KLX18A
537.42
RSMA01
FSM_C
Ω: 7.2
T: 3.17E-09
8098478B0A182DCE
KLX18A
537.74
RSMA01
FSM_C
Ω: 7.5
T: 1.27E-09
8098478B0A182F12
KLX18A
538.01
RSMA01
FSM_C
Ω: 69.9
T: 4.84E-10
C098478B0A18301A
KLX18A
540.20
RSMA01
FSM_C
Ω: 6.9
T: 5.45E-10
2098478B0A1838A7
KLX18A
540.99
RSMA01
FSM_C
Ω: 7.6
T: 3.38E-09
E098478B0A183BB7

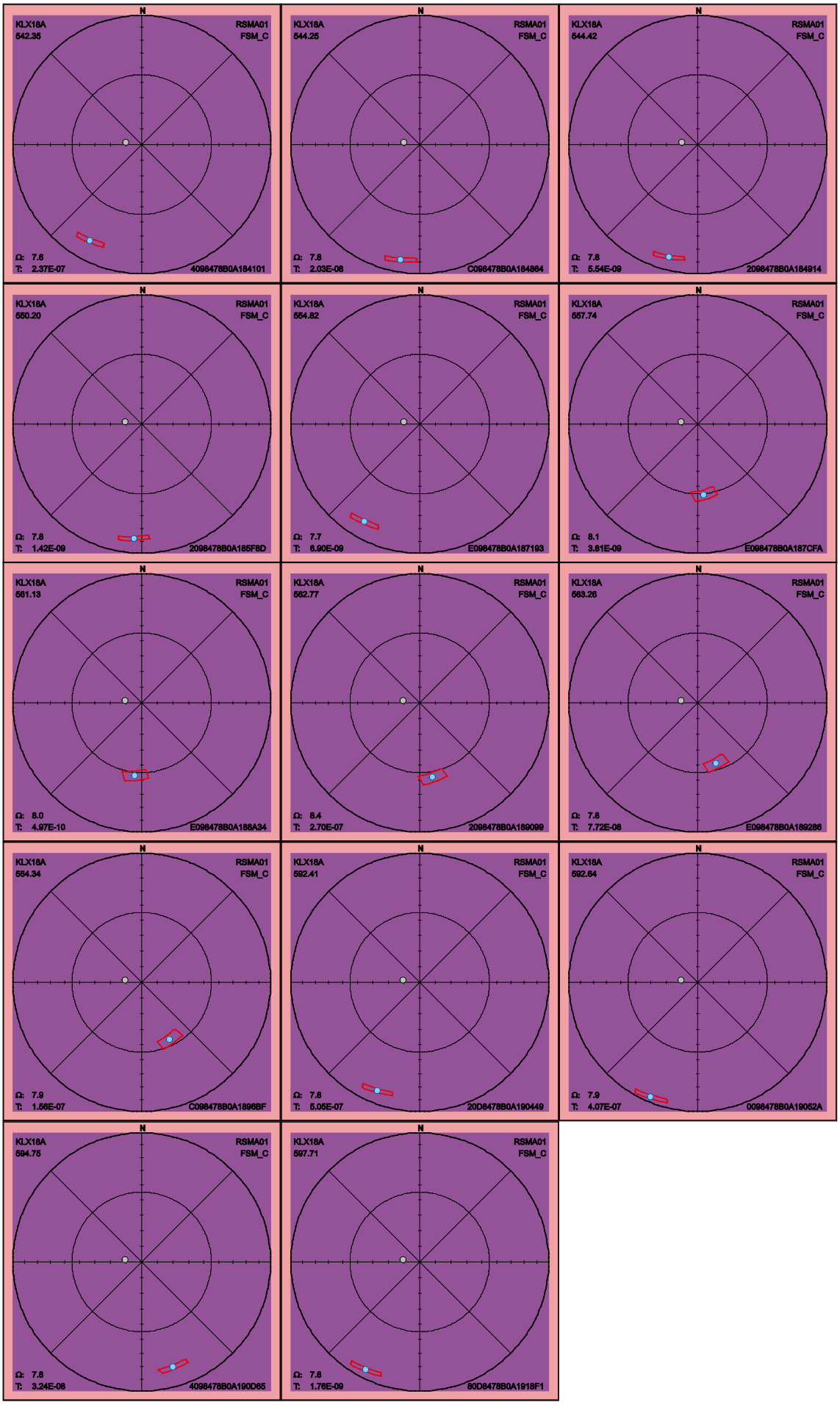
KLX18A
542.35
RSMA01
FSM_C
N
Ω: 7.6
T: 2.37E-07
4098478B0A184101
KLX18A
544.25
RSMA01
FSM_C
N
Ω: 7.8
T: 2.03E-08
C098478B0A184864
KLX18A
544.42
RSMA01
FSM_C
N
Ω: 7.8
T: 5.54E-09
2098478B0A184914
KLX18A
550.20
RSMA01
FSM_C
N
Ω: 7.8
T: 1.42E-09
2098478B0A185F8D
KLX18A
554.82
RSMA01
FSM_C
N
Ω: 7.7
T: 6.90E-09
E098478B0A187193
KLX18A
557.74
RSMA01
FSM_C
N
Ω: 8.1
T: 3.81E-09
E098478B0A187CFA
KLX18A
561.13
RSMA01
FSM_C
N
Ω: 8.0
T: 4.97E-10
E098478B0A188A34
KLX18A
562.77
RSMA01
FSM_C
N
Ω: 8.4
T: 2.70E-07
2098478B0A189099
KLX18A
563.26
RSMA01
FSM_C
N
Ω: 7.8
T: 7.72E-08
E098478B0A189286
KLX18A
564.34
RSMA01
FSM_C
N
Ω: 7.9
T: 1.56E-07
C098478B0A1896BF
KLX18A
592.41
RSMA01
FSM_C
N
Ω: 7.8
T: 5.05E-07
20D8478B0A190449
KLX18A
592.64
RSMA01
FSM_C
N
Ω: 7.9
T: 4.07E-07
0098478B0A19052A
KLX18A
594.75
RSMA01
FSM_C
N
Ω: 7.8
T: 3.24E-08
4098478B0A190D65
KLX18A
597.71
RSMA01
FSM_C
N
Ω: 7.8
T: 1.76E-09
80D8478B0A1918F1

2.3.31 KLX19A

There is one PFL fracture that lacks information about orientation in KLX19A and thus is excluded from this section. The sample space of the remaining 36 fractures is shown below. There are five fractures listed in Table 2-28 that have maximum uncertainty on the 90th percentile level larger than 30° and consequently can have an alternative interpretation of orientation compared to the best estimate orientation that is found in the table p_fract_core in /Sicada 2008/.

Table 2-28. Fractures in KLX19A with uncertainty, Ω, larger than 30°.

FeatureId	PFL-f no	Adjusted Secup	Ω
0099478B0A119244	3	102.92	51.5
6099478B0A11979B	4	104.25	61.0
2099478B0A123FBC	19	147.25	57.5
0099478B0A1A2F1C	53	668.18	38.2
4099478B0A1A3230	54	668.96	52.1

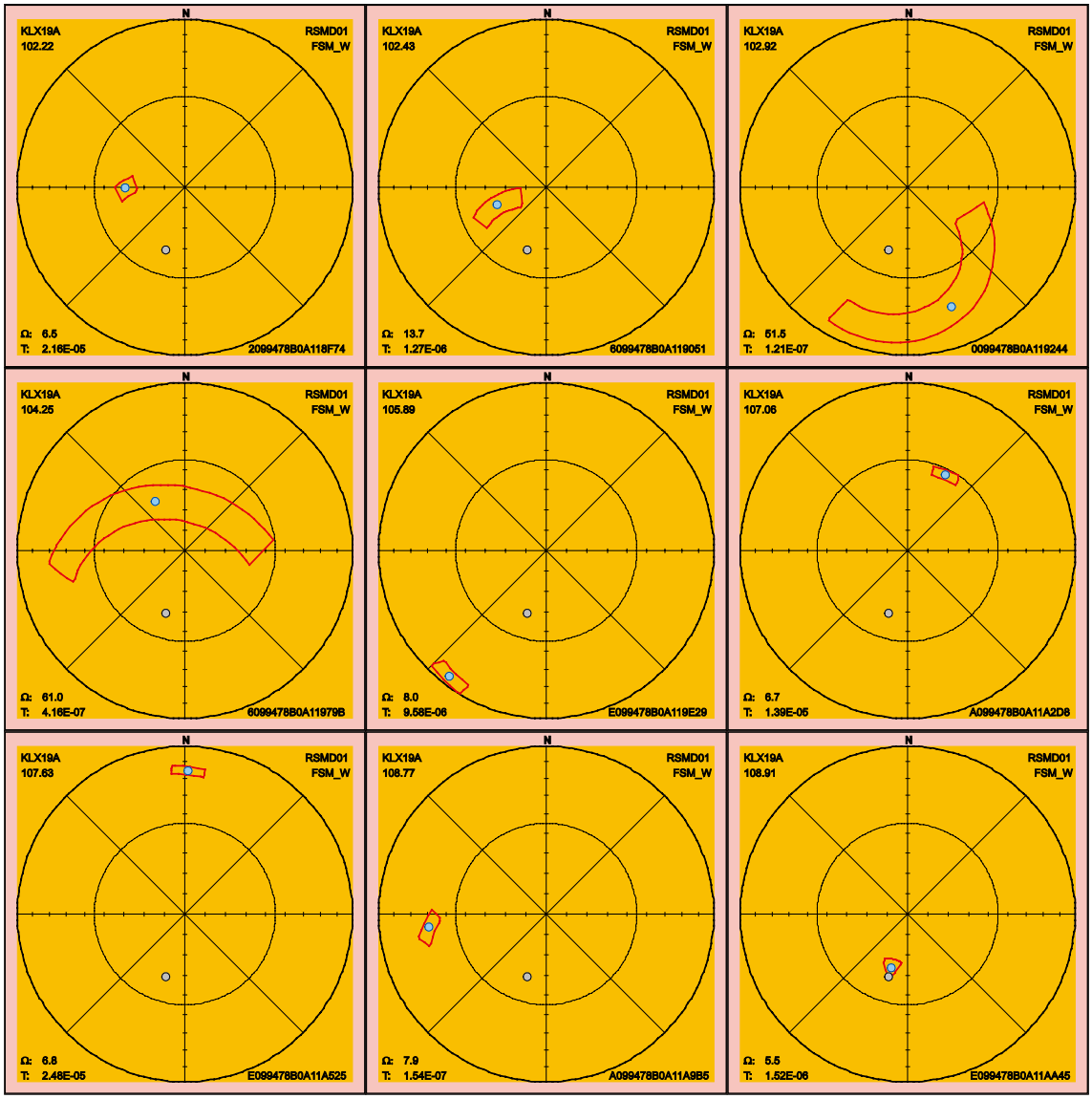

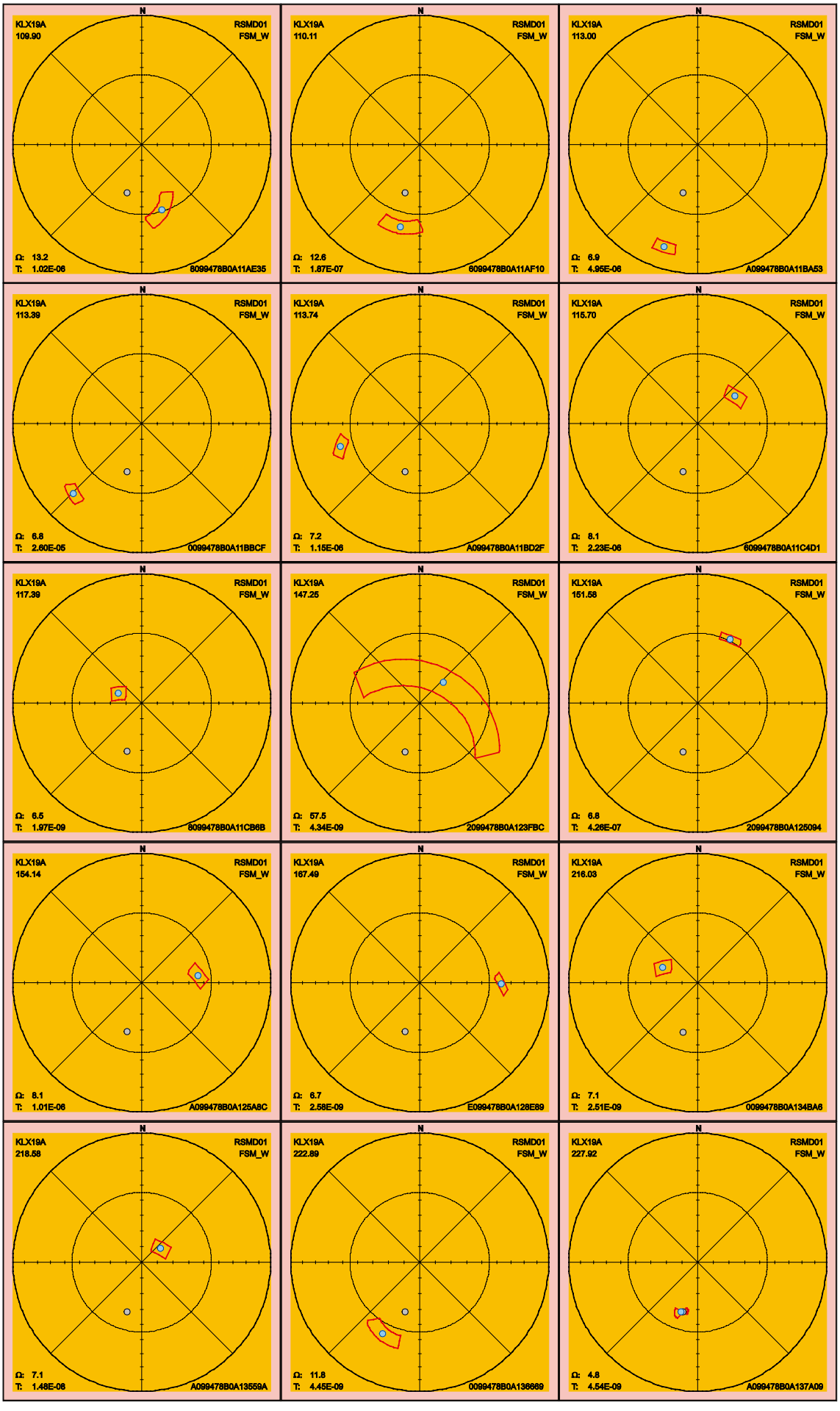
KLX19A
109.90
RSMD01
FSM_W
N
Ω: 13.2
T: 1.02E-06
8099478B0A11AE35
KLX19A
110.11
RSMD01
FSM_W
N
Ω: 12.6
T: 1.87E-07
6099478B0A11AF10
KLX19A
113.00
RSMD01
FSM_W
N
Ω: 6.9
T: 4.95E-06
A099478B0A11BA53
KLX19A
113.39
RSMD01
FSM_W
N
Ω: 6.8
T: 2.60E-05
0099478B0A11BBCF
KLX19A
113.74
RSMD01
FSM_W
N
Ω: 7.2
T: 1.15E-06
A099478B0A11BD2F
KLX19A
115.70
RSMD01
FSM_W
N
Ω: 8.1
T: 2.23E-06
6099478B0A11C4D1
KLX19A
117.39
RSMD01
FSM_W
N
Ω: 6.5
T: 1.97E-09
8099478B0A11CB6B
KLX19A
147.25
RSMD01
FSM_W
N
Ω: 57.5
T: 4.34E-09
2099478B0A123FBC
KLX19A
151.58
RSMD01
FSM_W
N
Ω: 6.8
T: 4.26E-07
2099478B0A125094
KLX19A
154.14
RSMD01
FSM_W
N
Ω: 8.1
T: 1.01E-06
A099478B0A125A8C
KLX19A
167.49
RSMD01
FSM_W
N
Ω: 6.7
T: 2.58E-09
E099478B0A128E89
KLX19A
216.03
RSMD01
FSM_W
N
Ω: 7.1
T: 2.51E-09
0099478B0A134BA6
KLX19A
218.58
RSMD01
FSM_W
N
Ω: 7.1
T: 1.48E-08
A099478B0A13559A
KLX19A
222.89
RSMD01
FSM_W
N
Ω: 11.8
T: 4.45E-09
0099478B0A136689
KLX19A
227.92
RSMD01
FSM_W
N
Ω: 4.8
T: 4.54E-09
A099478B0A137A09

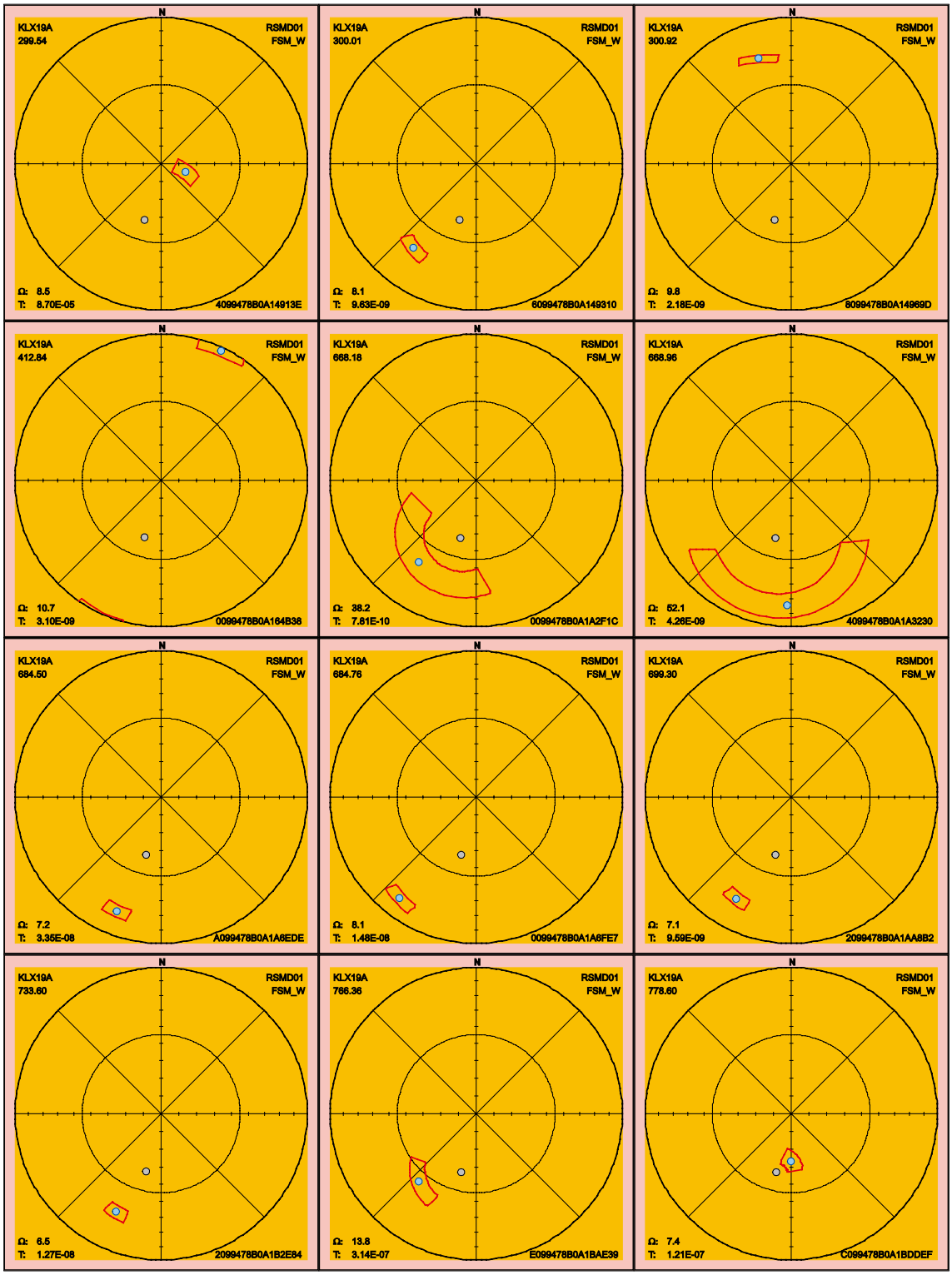
KLX19A
299.54
RSMD01
FSM_W
N
Ω: 8.5
T: 8.70E-05
4099478B0A14913E
KLX19A
300.01
RSMD01
FSM_W
N
Ω: 8.1
T: 9.63E-09
8099478B0A149310
KLX19A
300.92
RSMD01
FSM_W
N
Ω: 9.8
T: 2.18E-09
8099478B0A14969D
KLX19A
412.84
RSMD01
FSM_W
N
Ω: 10.7
T: 3.10E-09
0099478B0A164B38
KLX19A
668.18
RSMD01
FSM_W
N
Ω: 38.2
T: 7.81E-10
0099478B0A1A2F1C
KLX19A
668.96
RSMD01
FSM_W
N
Ω: 52.1
T: 4.26E-09
4099478B0A1A3230
KLX19A
684.50
RSMD01
FSM_W
N
Ω: 7.2
T: 3.35E-08
A099478B0A1A6EDE
KLX19A
684.76
RSMD01
FSM_W
N
Ω: 8.1
T: 1.48E-08
0099478B0A1A6FE7
KLX19A
699.30
RSMD01
FSM_W
N
Ω: 7.1
T: 9.59E-09
2099478B0A1AA8B2
KLX19A
733.60
RSMD01
FSM_W
N
Ω: 6.5
T: 1.27E-08
2099478B0A1B2E84
KLX19A
766.36
RSMD01
FSM_W
N
Ω: 13.8
T: 3.14E-07
E099478B0A1BAE39
KLX19A
778.60
RSMD01
FSM_W
N
Ω: 7.4
T: 1.21E-07
C099478B0A1BDDEF

2.3.32 KLX20A

There is one PFL fracture missing orientation information in KLX20A and thus omitted from this section. The 90th percentile sample space of uncertainty for the remaining 49 PFL fractures is shown below. There are eight fractures, listed in Table 2-29, that have maximum uncertainty larger than 30° and hence can be interpreted having different orientation compared to the best estimate orientation in the table p_fract_core in /Sicada 2008/.

Table 2-29. Fractures in KLX20A with uncertainty, Ω, larger than 30°.

FeatureId	PFL-f no	Adjusted Secup	Ω
A0904B8B0A11A169	4	106.94	44.0
40904B8B0A11AD40	5	110.02	58.8
80904B8B0A11EAEB	12	125.84	54.0
80904B8B0A11F27A	15	127.77	58.9
80904B8B0A128593	29	165.54	62.6
00904B8B0A128DC1	30	167.64	51.6
A0904B8B0A143B7A	47	278.01	37.1
00904B8B0A1444E7	49	280.44	30.0

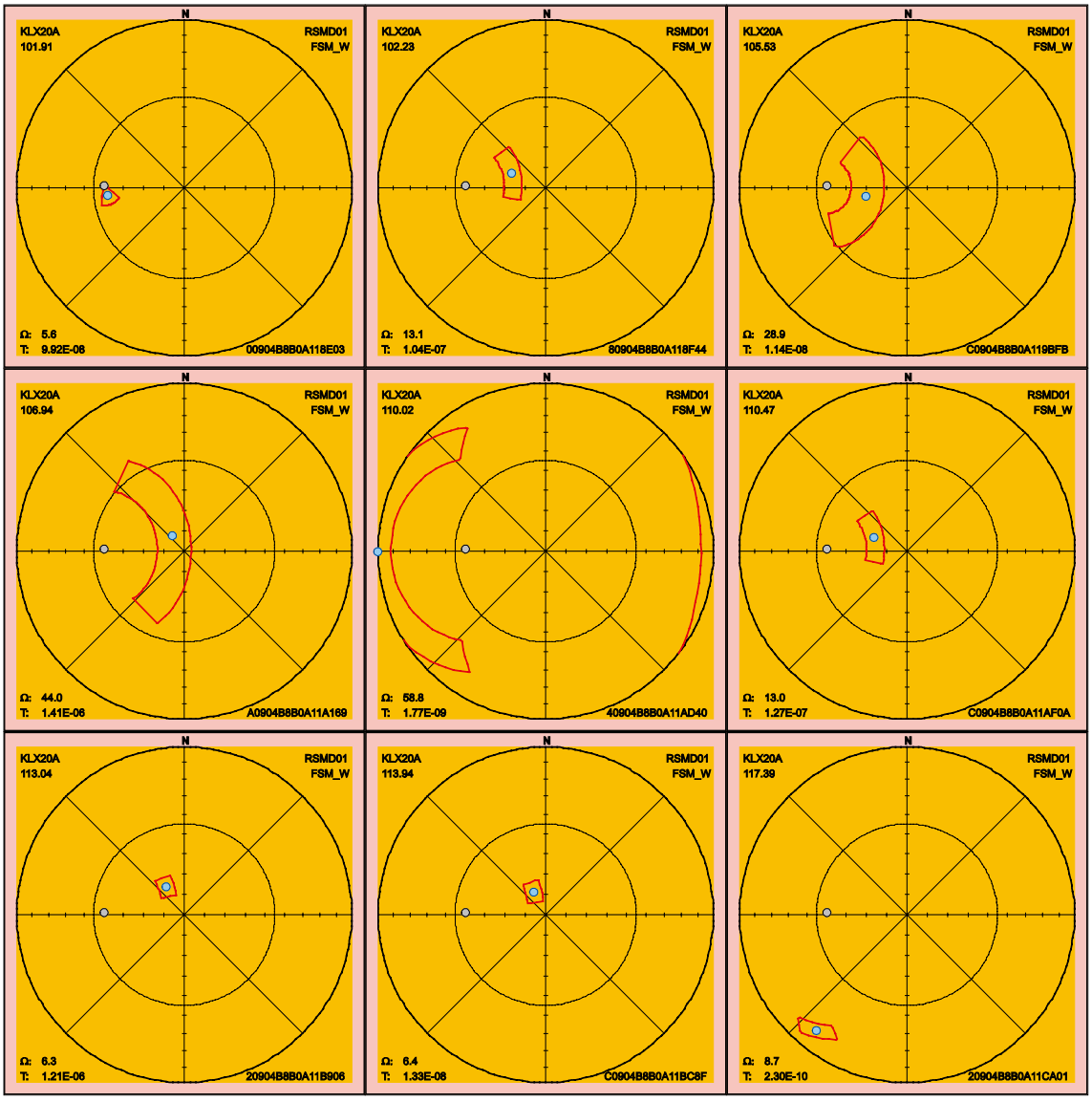

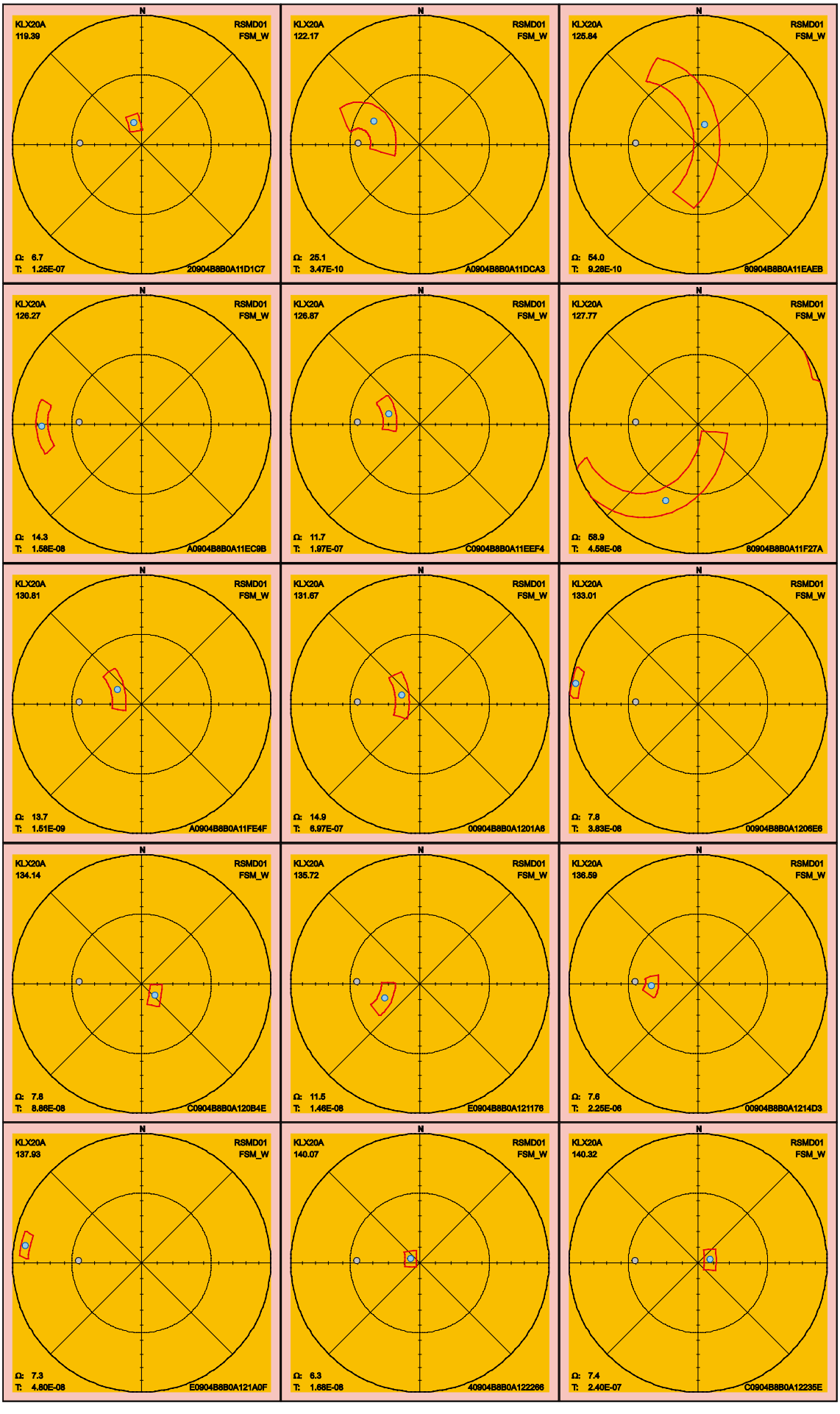
KLX20A
119.39
RSMD01
FSM_W
Ω: 6.7
T: 1.25E-07
20904B8B0A11D1C7
KLX20A
122.17
RSMD01
FSM_W
Ω: 25.1
T: 3.47E-10
A0904B8B0A11DCA3
KLX20A
125.84
RSMD01
FSM_W
Ω: 54.0
T: 9.28E-10
60904B8B0A11EAEB
KLX20A
126.27
RSMD01
FSM_W
Ω: 14.3
T: 1.58E-08
A0904B8B0A11EC9B
KLX20A
126.87
RSMD01
FSM_W
Ω: 11.7
T: 1.97E-07
C0904B8B0A11EEF4
KLX20A
127.77
RSMD01
FSM_W
Ω: 58.9
T: 4.58E-08
80904B8B0A11F27A
KLX20A
130.81
RSMD01
FSM_W
Ω: 13.7
T: 1.51E-09
A0904B8B0A11FE4F
KLX20A
131.67
RSMD01
FSM_W
Ω: 14.9
T: 6.97E-07
00904B8B0A1201A6
KLX20A
133.01
RSMD01
FSM_W
Ω: 7.8
T: 3.83E-08
00904B8B0A1206E6
KLX20A
134.14
RSMD01
FSM_W
Ω: 7.8
T: 8.86E-08
C0904B8B0A120B4E
KLX20A
135.72
RSMD01
FSM_W
Ω: 11.5
T: 1.46E-08
E0904B8B0A121176
KLX20A
136.59
RSMD01
FSM_W
Ω: 7.6
T: 2.25E-06
00904B8B0A1214D3
KLX20A
137.93
RSMD01
FSM_W
Ω: 7.3
T: 4.80E-08
E0904B8B0A121A0F
KLX20A
140.07
RSMD01
FSM_W
Ω: 6.3
T: 1.68E-08
40904B8B0A122266
KLX20A
140.32
RSMD01
FSM_W
Ω: 7.4
T: 2.40E-07
C0904B8B0A12235E

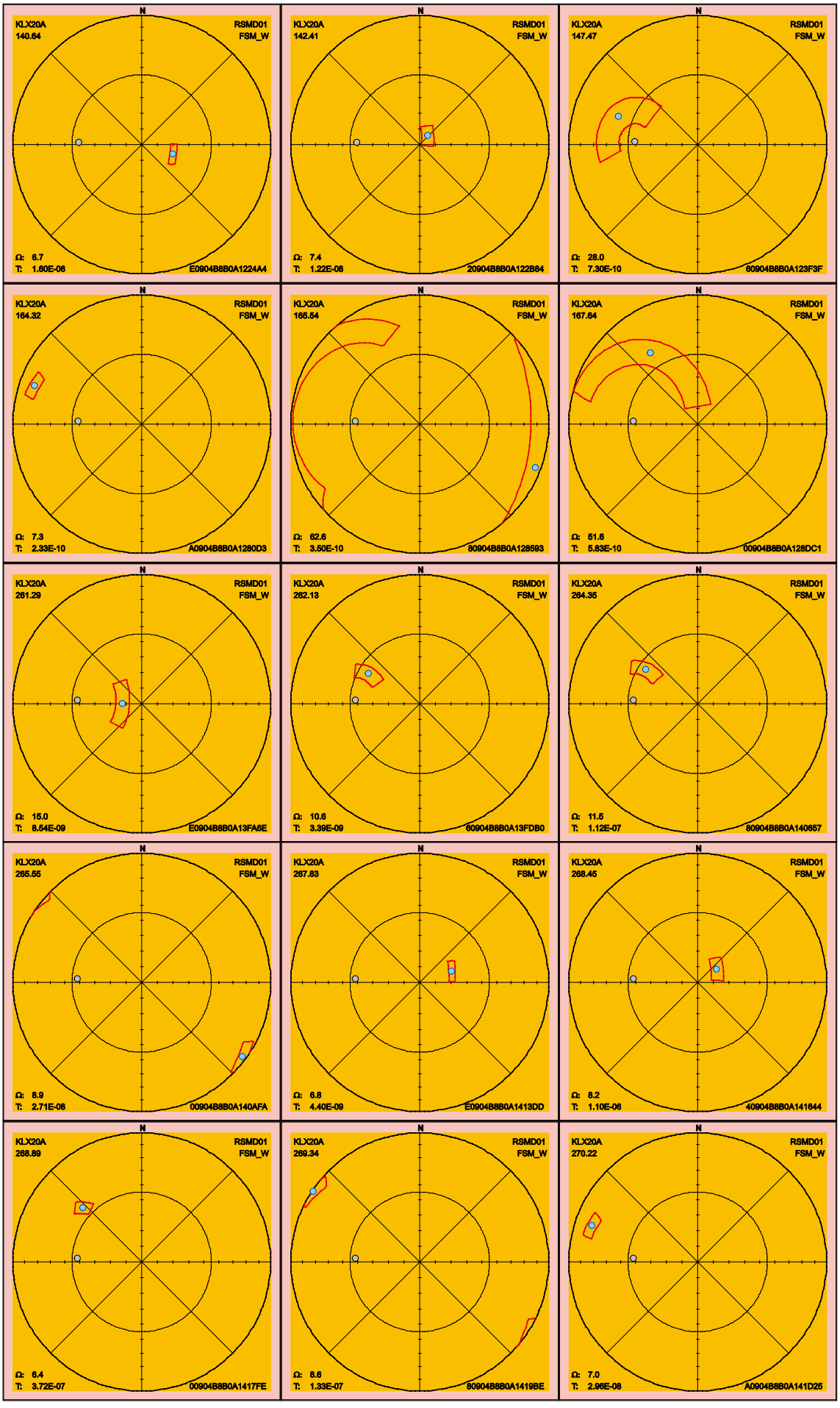
KLX20A
140.64
RSMD01
FSM_W
N
Ω: 6.7
T: 1.60E-06
E0904B8B0A1224A4
KLX20A
142.41
RSMD01
FSM_W
N
Ω: 7.4
T: 1.22E-06
20904B8B0A122B84
KLX20A
147.47
RSMD01
FSM_W
N
Ω: 28.0
T: 7.30E-10
60904B8B0A123F3F
KLX20A
164.32
RSMD01
FSM_W
N
Ω: 7.3
T: 2.33E-10
A0904B8B0A1280D3
KLX20A
165.54
RSMD01
FSM_W
N
Ω: 62.6
T: 3.50E-10
80904B8B0A128593
KLX20A
167.64
RSMD01
FSM_W
N
Ω: 51.6
T: 5.83E-10
00904B8B0A128DC1
KLX20A
261.29
RSMD01
FSM_W
N
Ω: 15.0
T: 8.54E-09
E0904B8B0A13FA8E
KLX20A
262.13
RSMD01
FSM_W
N
Ω: 10.6
T: 3.39E-09
60904B8B0A13FDB0
KLX20A
264.35
RSMD01
FSM_W
N
Ω: 11.5
T: 1.12E-07
80904B8B0A140657
KLX20A
265.55
RSMD01
FSM_W
N
Ω: 8.9
T: 2.71E-08
00904B8B0A140AFA
KLX20A
267.83
RSMD01
FSM_W
N
Ω: 6.8
T: 4.40E-09
E0904B8B0A1413DD
KLX20A
268.45
RSMD01
FSM_W
N
Ω: 8.2
T: 1.10E-06
40904B8B0A141644
KLX20A
268.89
RSMD01
FSM_W
N
Ω: 6.4
T: 3.72E-07
00904B8B0A1417FE
KLX20A
269.34
RSMD01
FSM_W
N
Ω: 8.6
T: 1.33E-07
80904B8B0A1419BE
KLX20A
270.22
RSMD01
FSM_W
N
Ω: 7.0
T: 2.96E-08
A0904B8B0A141D25

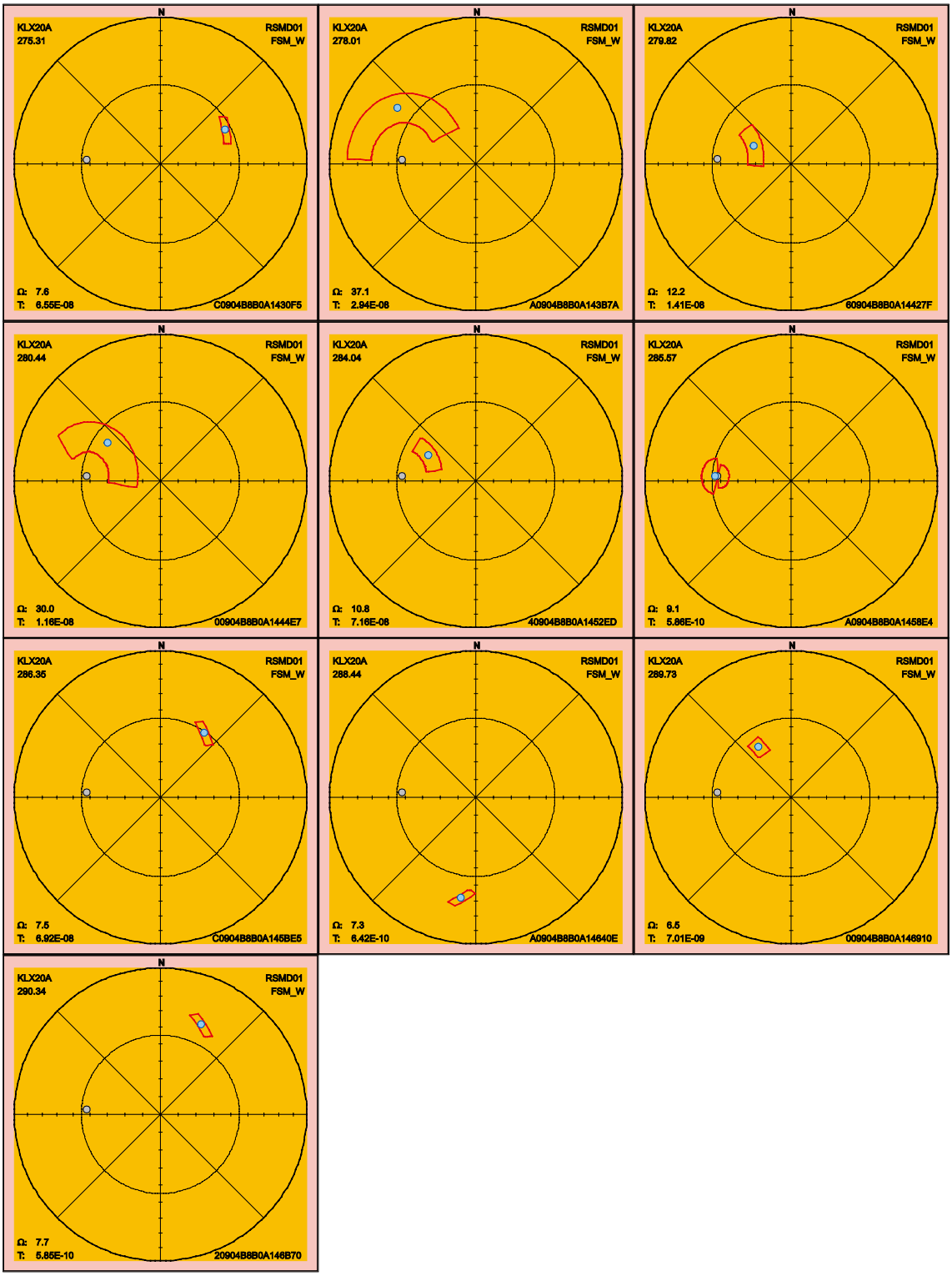
KLX20A
275.31
RSMD01
FSM_W
Ω: 7.6
T: 6.55E-08
C0904B8B0A1430F5
KLX20A
278.01
RSMD01
FSM_W
Ω: 37.1
T: 2.94E-08
A0904B8B0A143B7A
KLX20A
279.82
RSMD01
FSM_W
Ω: 12.2
T: 1.41E-08
60904B8B0A14427F
KLX20A
280.44
RSMD01
FSM_W
Ω: 30.0
T: 1.16E-08
00904B8B0A1444E7
KLX20A
284.04
RSMD01
FSM_W
Ω: 10.8
T: 7.16E-08
40904B8B0A1452ED
KLX20A
285.57
RSMD01
FSM_W
Ω: 9.1
T: 5.86E-10
A0904B8B0A1458E4
KLX20A
286.35
RSMD01
FSM_W
Ω: 7.5
T: 6.92E-08
C0904B8B0A145BE5
KLX20A
288.44
RSMD01
FSM_W
Ω: 7.3
T: 6.42E-10
A0904B8B0A14640E
KLX20A
289.73
RSMD01
FSM_W
Ω: 6.5
T: 7.01E-09
00904B8B0A146910
KLX20A
290.34
RSMD01
FSM_W
Ω: 7.7
T: 5.85E-10
20904B8B0A146B70

2.3.33 KLX21B

There is no fracture of the 39 PFL fracture in KL21B that have maximum uncertainty larger than 30°. The sample space of uncertainty, on the 90th percentile, is shown below.

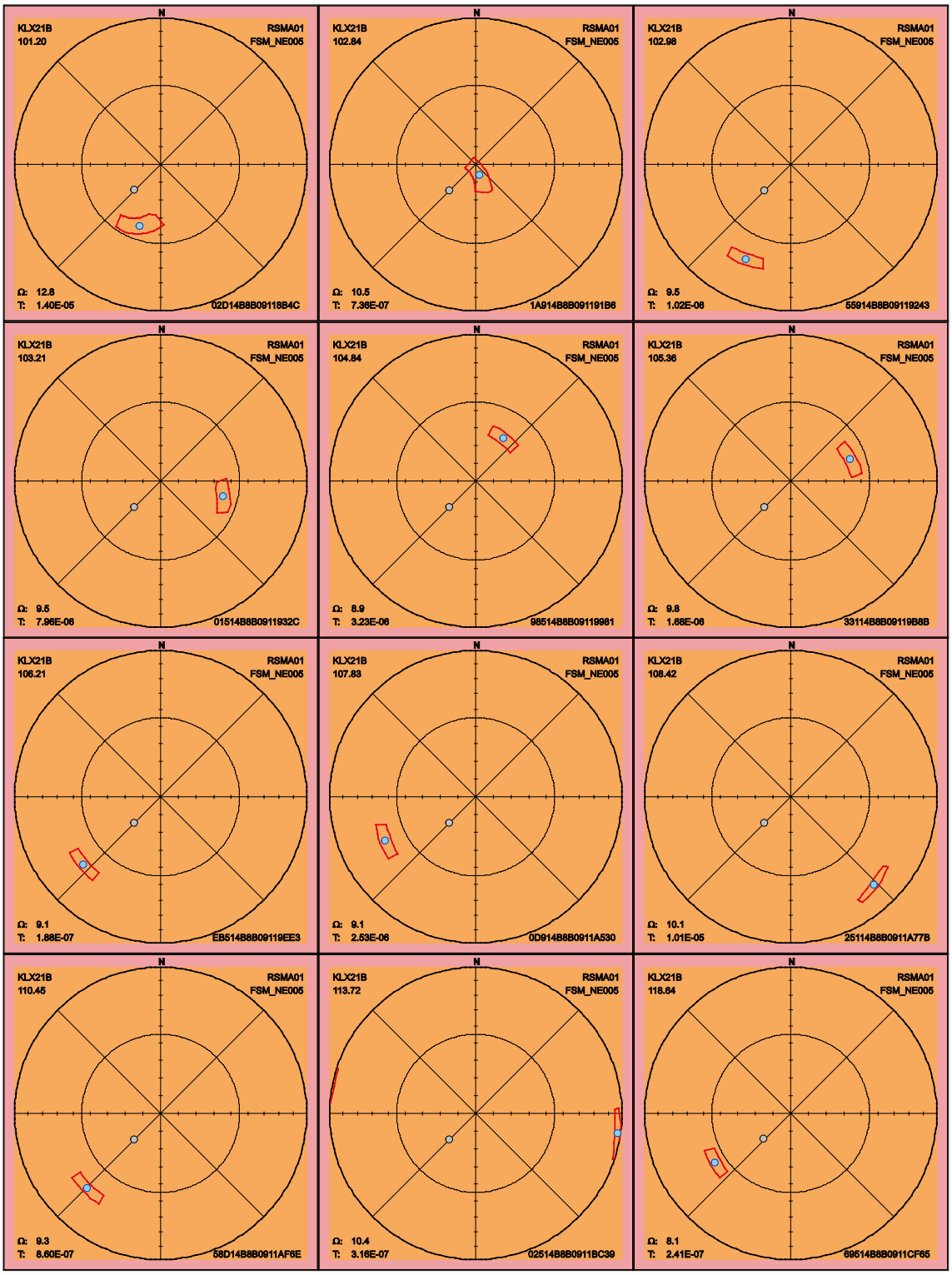

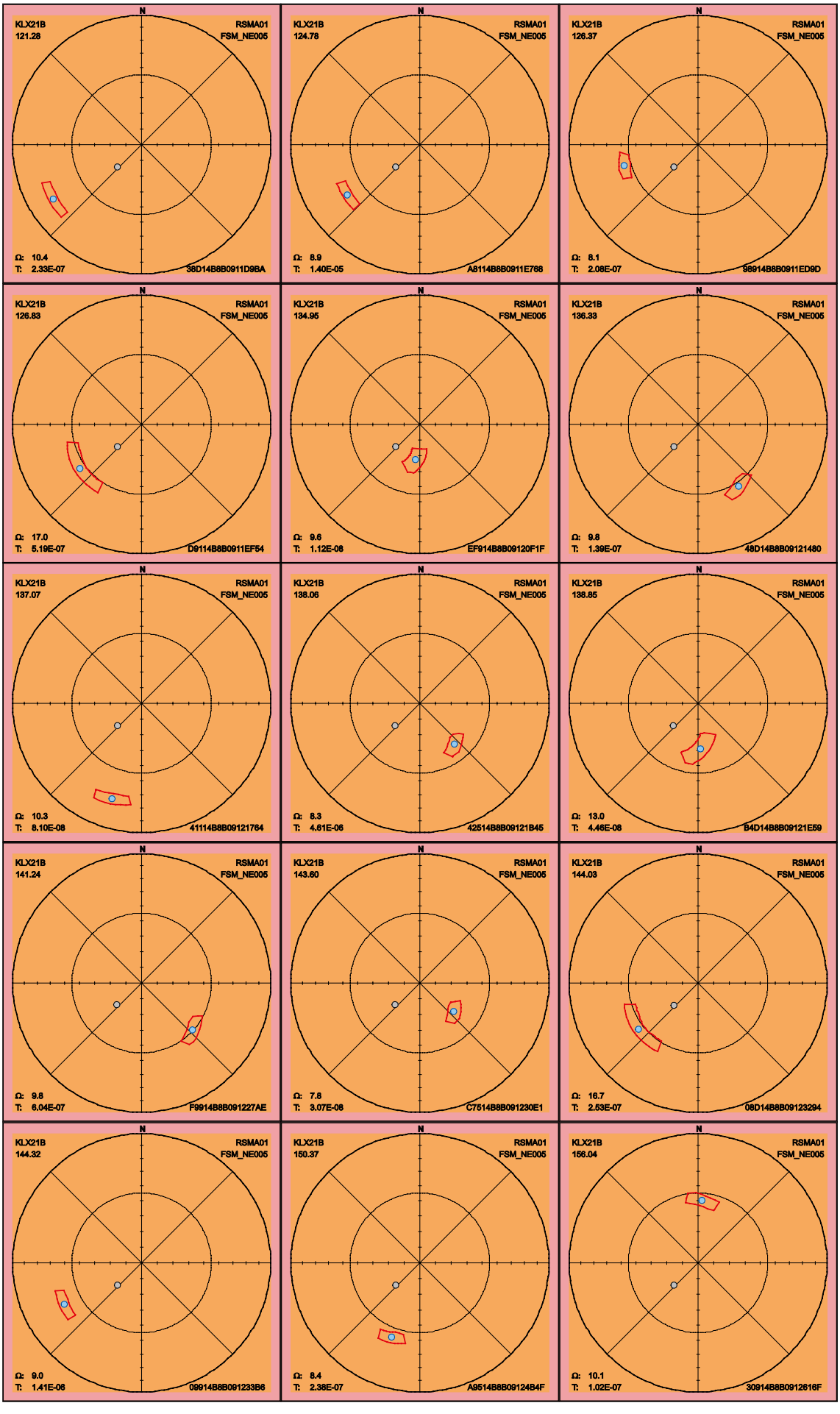
KLX21B
121.28
RSMA01
FSM_NE005
Ω: 10.4
T: 2.33E-07
38D14B8B0911D9BA
KLX21B
124.78
RSMA01
FSM_NE005
Ω: 8.9
T: 1.40E-05
A8114B8B0911E768
KLX21B
126.37
RSMA01
FSM_NE005
Ω: 8.1
T: 2.08E-07
98914B8B0911ED9D
KLX21B
126.83
RSMA01
FSM_NE005
Ω: 17.0
T: 5.19E-07
D9114B8B0911EF54
KLX21B
134.95
RSMA01
FSM_NE005
Ω: 9.6
T: 1.12E-08
EF914B8B09120F1F
KLX21B
136.33
RSMA01
FSM_NE005
Ω: 9.8
T: 1.39E-07
48D14B8B09121480
KLX21B
137.07
RSMA01
FSM_NE005
Ω: 10.3
T: 8.10E-08
41114B8B09121764
KLX21B
138.06
RSMA01
FSM_NE005
Ω: 8.3
T: 4.61E-06
42514B8B09121B45
KLX21B
138.85
RSMA01
FSM_NE005
Ω: 13.0
T: 4.46E-06
B4D14B8B09121E59
KLX21B
141.24
RSMA01
FSM_NE005
Ω: 9.8
T: 6.04E-07
F9914B8B091227AE
KLX21B
143.60
RSMA01
FSM_NE005
Ω: 7.8
T: 3.07E-08
C7514B8B091230E1
KLX21B
144.03
RSMA01
FSM_NE005
Ω: 16.7
T: 2.53E-07
08D14B8B09123294
KLX21B
144.32
RSMA01
FSM_NE005
Ω: 9.0
T: 1.41E-08
09914B8B091233B6
KLX21B
150.37
RSMA01
FSM_NE005
Ω: 8.4
T: 2.38E-07
A9514B8B09124B4F
KLX21B
156.04
RSMA01
FSM_NE005
Ω: 10.1
T: 1.02E-07
30914B8B0912616F

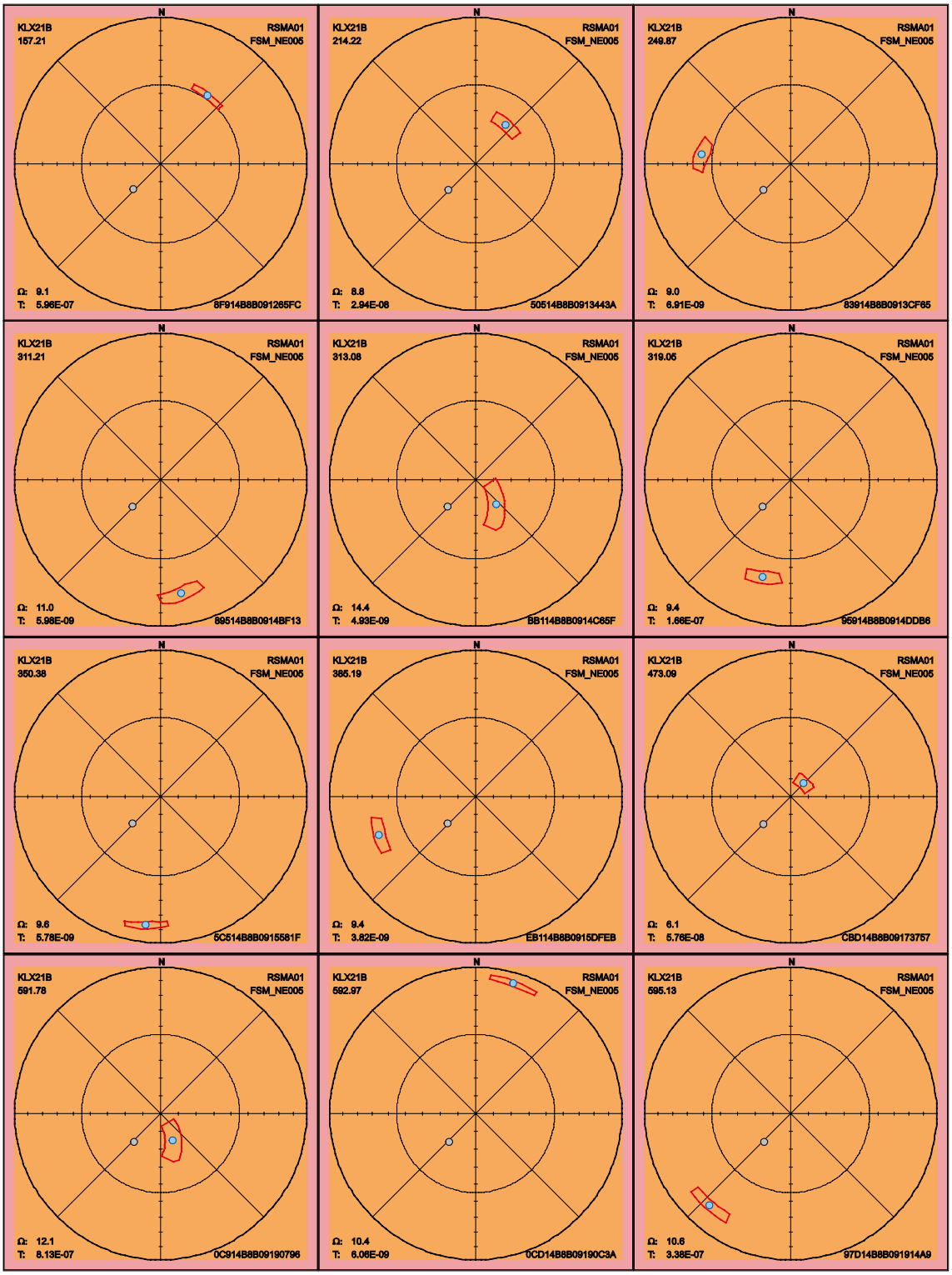

2.3.34 KLX22A

There is no PFL fracture in KLX22A with orientation uncertainty larger than 30°. Below follow the 90th percentile sample space of uncertainty for the 43 PFL fractures.

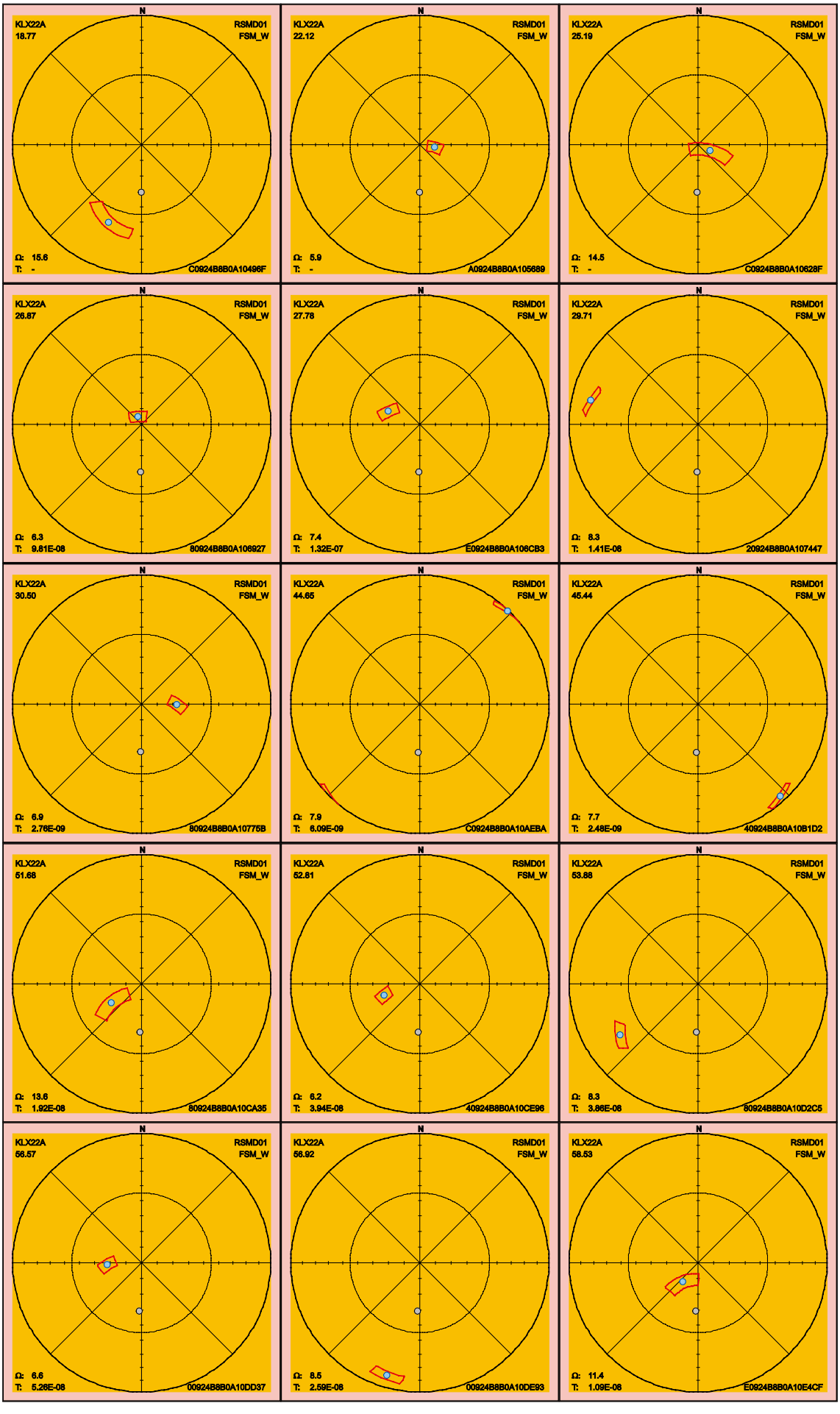
KLX22A
18.77
RSMD01
FSM_W
Ω: 15.6
T: -
C0924B8B0A10496F
KLX22A
22.12
RSMD01
FSM_W
Ω: 5.9
T: -
A0924B8B0A105689
KLX22A
25.19
RSMD01
FSM_W
Ω: 14.5
T: -
C0924B8B0A10628F
KLX22A
26.87
RSMD01
FSM_W
Ω: 6.3
T: 9.81E-08
80924B8B0A106927
KLX22A
27.78
RSMD01
FSM_W
Ω: 7.4
T: 1.32E-07
E0924B8B0A106CB3
KLX22A
29.71
RSMD01
FSM_W
Ω: 8.3
T: 1.41E-08
20924B8B0A107447
KLX22A
30.50
RSMD01
FSM_W
Ω: 6.9
T: 2.76E-09
80924B8B0A10775B
KLX22A
44.65
RSMD01
FSM_W
Ω: 7.9
T: 6.09E-09
C0924B8B0A10AEBA
KLX22A
45.44
RSMD01
FSM_W
Ω: 7.7
T: 2.48E-09
40924B8B0A10B1D2
KLX22A
51.68
RSMD01
FSM_W
Ω: 13.6
T: 1.92E-08
80924B8B0A10CA35
KLX22A
52.81
RSMD01
FSM_W
Ω: 6.2
T: 3.94E-08
40924B8B0A10CE96
KLX22A
53.88
RSMD01
FSM_W
Ω: 8.3
T: 3.86E-08
80924B8B0A10D2C5
KLX22A
56.57
RSMD01
FSM_W
Ω: 6.6
T: 5.26E-08
00924B8B0A10DD37
KLX22A
56.92
RSMD01
FSM_W
Ω: 8.5
T: 2.59E-08
00924B8B0A10DE93
KLX22A
58.53
RSMD01
FSM_W
Ω: 11.4
T: 1.09E-08
E0924B8B0A10E4CF

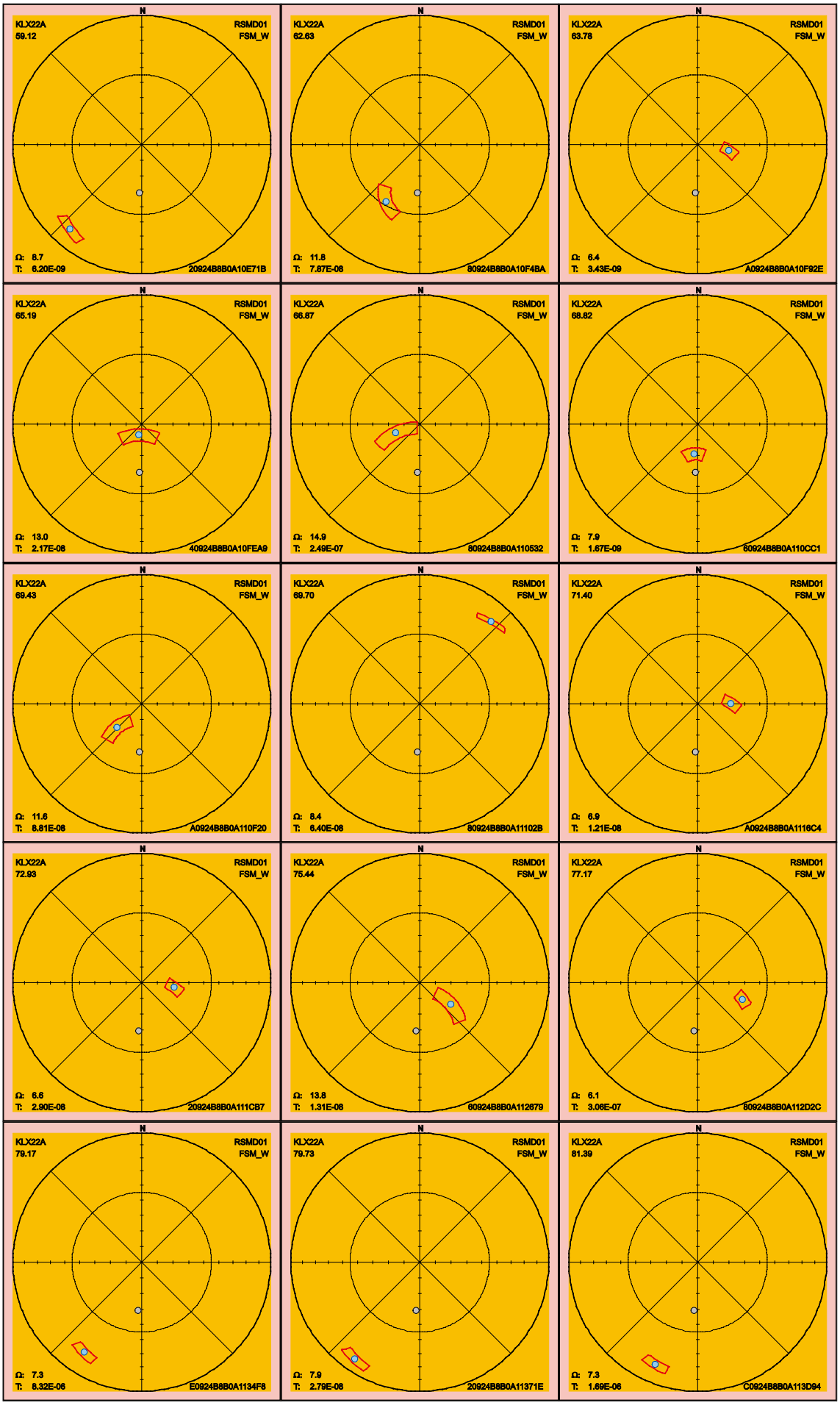
KLX22A
59.12
RSMD01
FSM_W
Ω: 8.7
T: 6.20E-09
20924B8B0A10E71B
KLX22A
62.63
RSMD01
FSM_W
Ω: 11.8
T: 7.67E-08
80924B8B0A10F4BA
KLX22A
63.78
RSMD01
FSM_W
Ω: 6.4
T: 3.43E-09
A0924B8B0A10F92E
KLX22A
65.19
RSMD01
FSM_W
Ω: 13.0
T: 2.17E-08
40924B8B0A10FEA9
KLX22A
66.87
RSMD01
FSM_W
Ω: 14.9
T: 2.49E-07
80924B8B0A110532
KLX22A
68.82
RSMD01
FSM_W
Ω: 7.9
T: 1.67E-09
80924B8B0A110CC1
KLX22A
69.43
RSMD01
FSM_W
Ω: 11.6
T: 8.81E-08
A0924B8B0A110F20
KLX22A
69.70
RSMD01
FSM_W
Ω: 8.4
T: 6.40E-08
80924B8B0A11102B
KLX22A
71.40
RSMD01
FSM_W
Ω: 6.9
T: 1.21E-08
A0924B8B0A1116C4
KLX22A
72.93
RSMD01
FSM_W
Ω: 6.6
T: 2.90E-08
20924B8B0A111CB7
KLX22A
75.44
RSMD01
FSM_W
Ω: 13.8
T: 1.31E-08
80924B8B0A112679
KLX22A
77.17
RSMD01
FSM_W
Ω: 6.1
T: 3.06E-07
80924B8B0A112D2C
KLX22A
79.17
RSMD01
FSM_W
Ω: 7.3
T: 8.32E-08
E0924B8B0A1134F8
KLX22A
79.73
RSMD01
FSM_W
Ω: 7.9
T: 2.79E-08
20924B8B0A11371E
KLX22A
81.39
RSMD01
FSM_W
Ω: 7.3
T: 1.69E-08
C0924B8B0A113D94

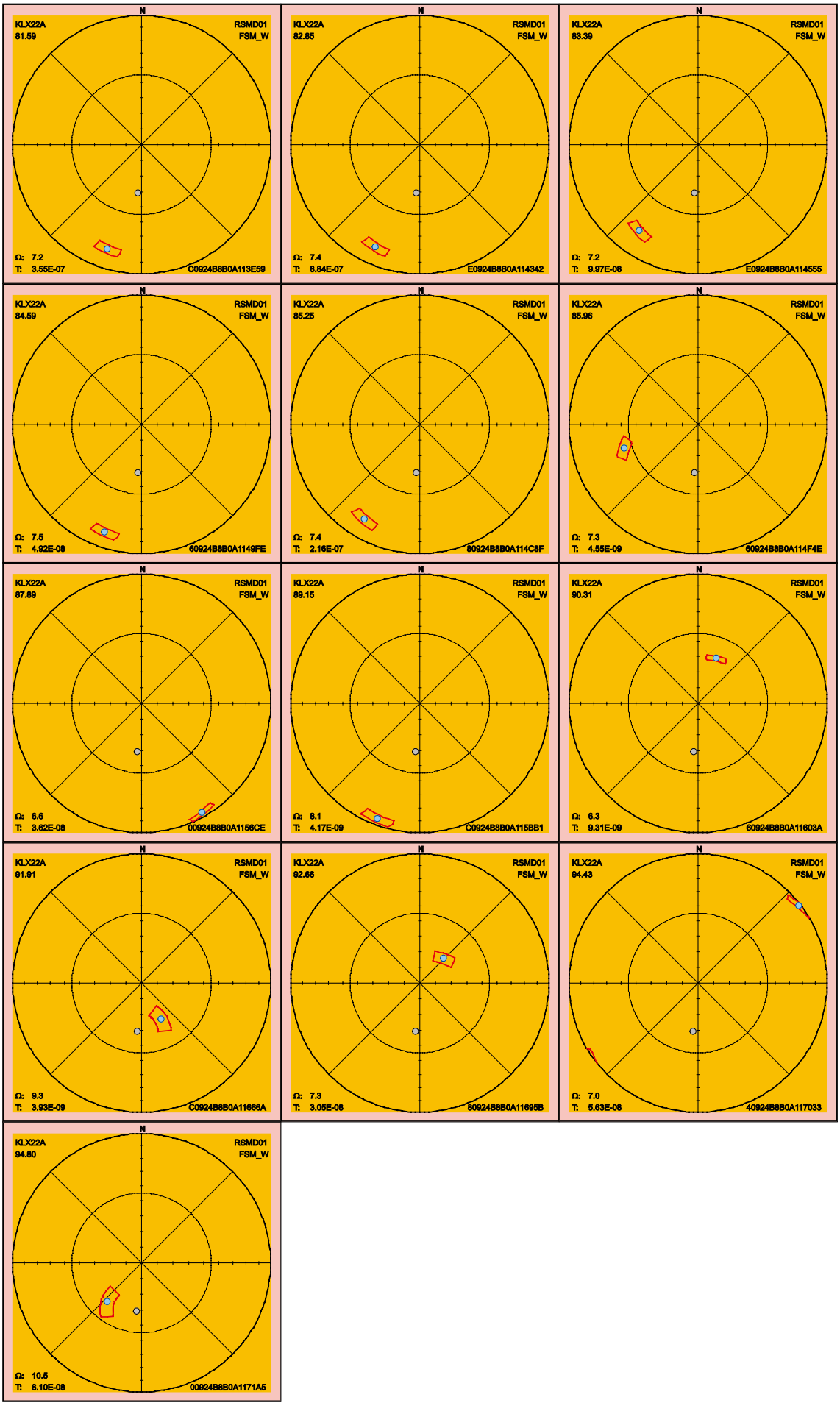
KLX22A
81.59
RSMD01
FSM_W
N
Ω: 7.2
T: 3.55E-07
C0924B8B0A113E59
KLX22A
82.85
RSMD01
FSM_W
N
Ω: 7.4
T: 8.84E-07
E0924B8B0A114342
KLX22A
83.39
RSMD01
FSM_W
N
Ω: 7.2
T: 9.97E-08
E0924B8B0A114555
KLX22A
84.59
RSMD01
FSM_W
N
Ω: 7.5
T: 4.92E-08
60924B8B0A1149FE
KLX22A
85.25
RSMD01
FSM_W
N
Ω: 7.4
T: 2.16E-07
60924B8B0A114C8F
KLX22A
85.96
RSMD01
FSM_W
N
Ω: 7.3
T: 4.55E-09
60924B8B0A114F4E
KLX22A
87.89
RSMD01
FSM_W
N
Ω: 6.6
T: 3.62E-08
00924B8B0A1156CE
KLX22A
89.15
RSMD01
FSM_W
N
Ω: 8.1
T: 4.17E-09
C0924B8B0A115BB1
KLX22A
90.31
RSMD01
FSM_W
N
Ω: 6.3
T: 9.31E-09
60924B8B0A11603A
KLX22A
91.91
RSMD01
FSM_W
N
Ω: 9.3
T: 3.93E-09
C0924B8B0A11666A
KLX22A
92.66
RSMD01
FSM_W
N
Ω: 7.3
T: 3.05E-08
80924B8B0A11695B
KLX22A
94.43
RSMD01
FSM_W
N
Ω: 7.0
T: 5.63E-08
40924B8B0A117033
KLX22A
94.80
RSMD01
FSM_W
N
Ω: 10.5
T: 6.10E-08
00924B8B0A1171A5

2.3.35 KLX22B

Below follow the 90th percentile sample space of uncertainty for the 27 PFL fractures in KLX22B. There are two fractures, listed in Table 2-30, that have maximum uncertainty, on the 90th percentile, larger than 30° and thus can have an alternative interpretation of orientation compared to the best estimate orientation that is found in the table p_fract_core in /Sicada 2008/.

Table 2-30. Fractures in KLX22B with uncertainty, Ω, larger than 30°.

FeatureId	PFL-f no	Adjusted Secup	Ω
C0924B8B0910781F	9	30.82	74.1
00924B8B09109F3B	14	40.86	55.9

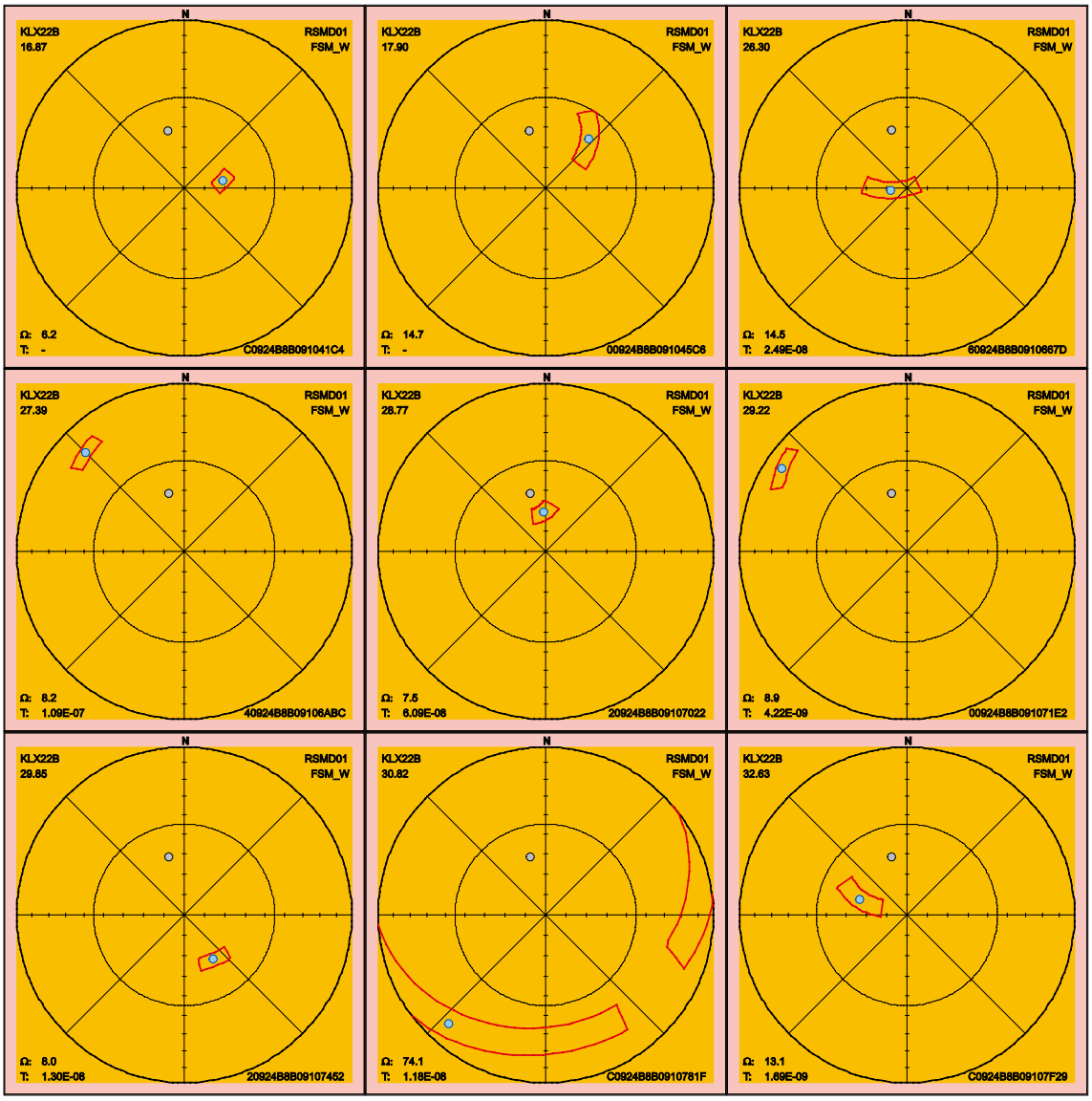

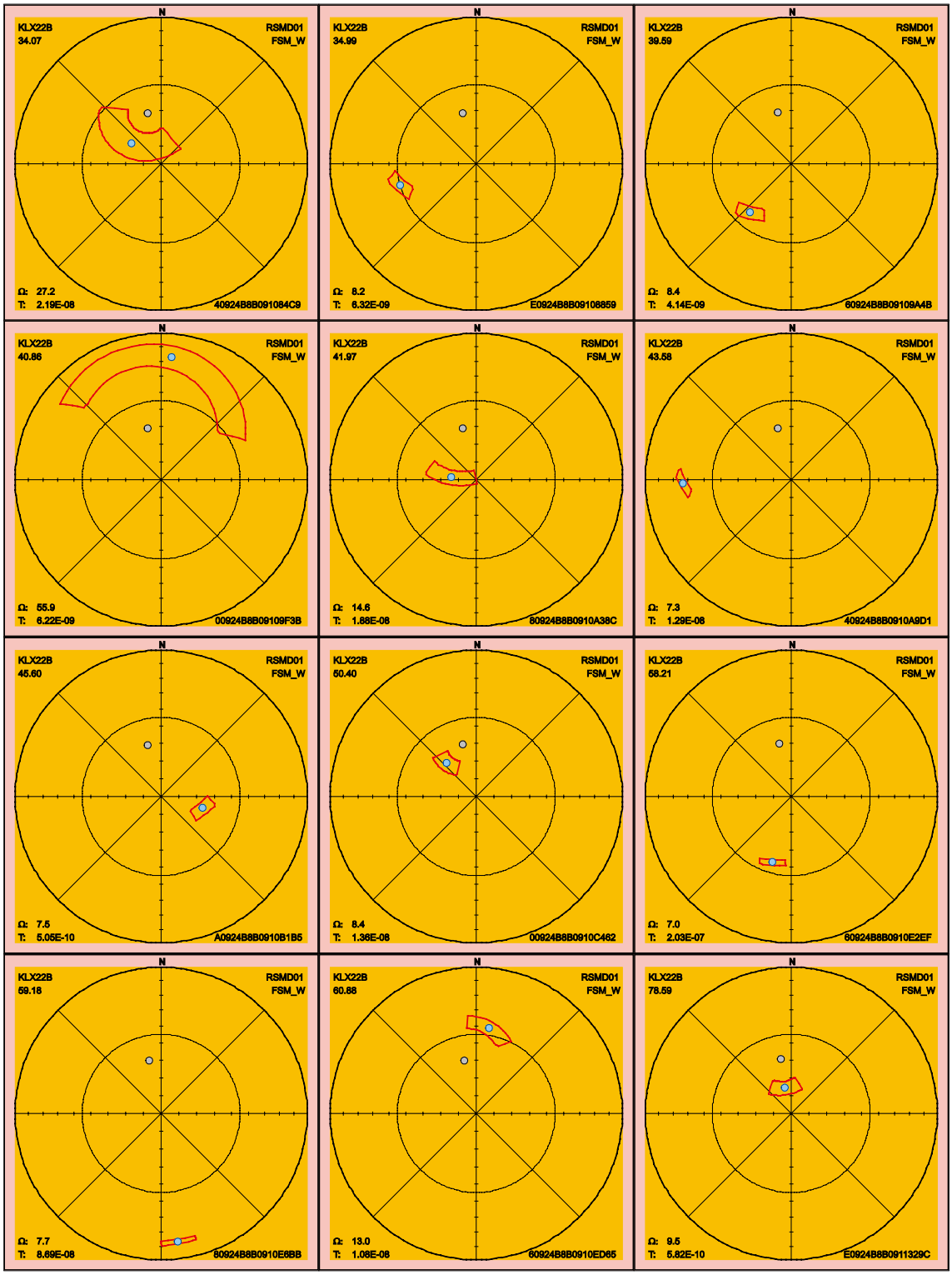
KLX22B
34.07
RSMD01
FSM_W
N
Ω: 27.2
T: 2.19E-08
40924B8B091084C9
KLX22B
34.99
RSMD01
FSM_W
N
Ω: 8.2
T: 6.32E-09
E0924B8B09108859
KLX22B
39.59
RSMD01
FSM_W
N
Ω: 8.4
T: 4.14E-09
80924B8B09109A4B
KLX22B
40.86
RSMD01
FSM_W
N
Ω: 55.9
T: 6.22E-09
00924B8B09109F3B
KLX22B
41.97
RSMD01
FSM_W
N
Ω: 14.6
T: 1.88E-08
80924B8B0910A38C
KLX22B
43.58
RSMD01
FSM_W
N
Ω: 7.3
T: 1.29E-08
40924B8B0910A9D1
KLX22B
45.60
RSMD01
FSM_W
N
Ω: 7.5
T: 5.05E-10
A0924B8B0910B1B5
KLX22B
50.40
RSMD01
FSM_W
N
Ω: 8.4
T: 1.36E-08
00924B8B0910C462
KLX22B
58.21
RSMD01
FSM_W
N
Ω: 7.0
T: 2.03E-07
80924B8B0910E2EF
KLX22B
59.18
RSMD01
FSM_W
N
Ω: 7.7
T: 8.69E-08
80924B8B0910E6BB
KLX22B
60.88
RSMD01
FSM_W
N
Ω: 13.0
T: 1.08E-08
60924B8B0910ED65
KLX22B
78.59
RSMD01
FSM_W
N
Ω: 9.5
T: 5.82E-10
E0924B8B0911329C

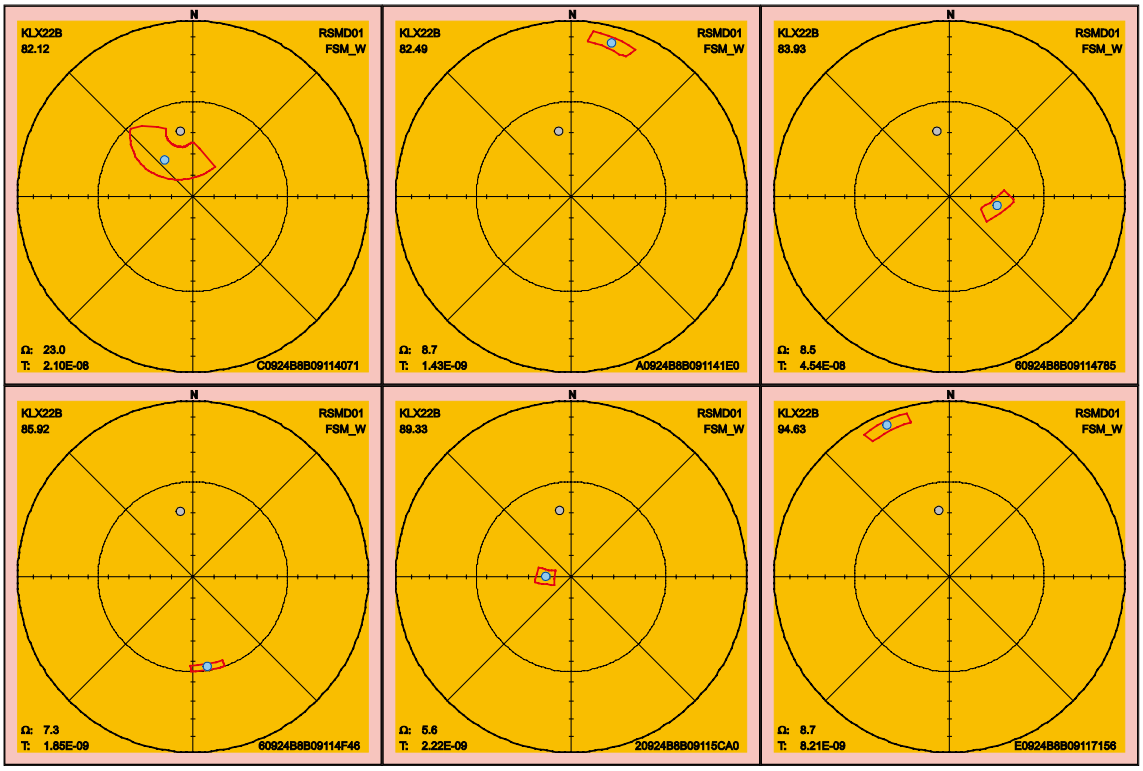

2.3.36 KLX23A

There is one fracture missing information about orientation in KLX23A and consequently is excluded from this section. Of the remaining 16 fractures one has maximum uncertainty larger than 30°, see Table 2-31. Fractures having large uncertainty can have an alternative interpretation of orientation compared to the best estimate orientation that is found in the table p_fract_core in /Sicada 2008/. Below follow the 90th percentile sample space of uncertainty for the PFL fractures in KLX23A.

Table 2-31. Fractures in KLX23A with uncertainty, Ω, larger than 30°.

FeatureId	PFL-f no	Adjusted Secup	Ω
A0D34B8B0A216B13	16	93.10	34.4

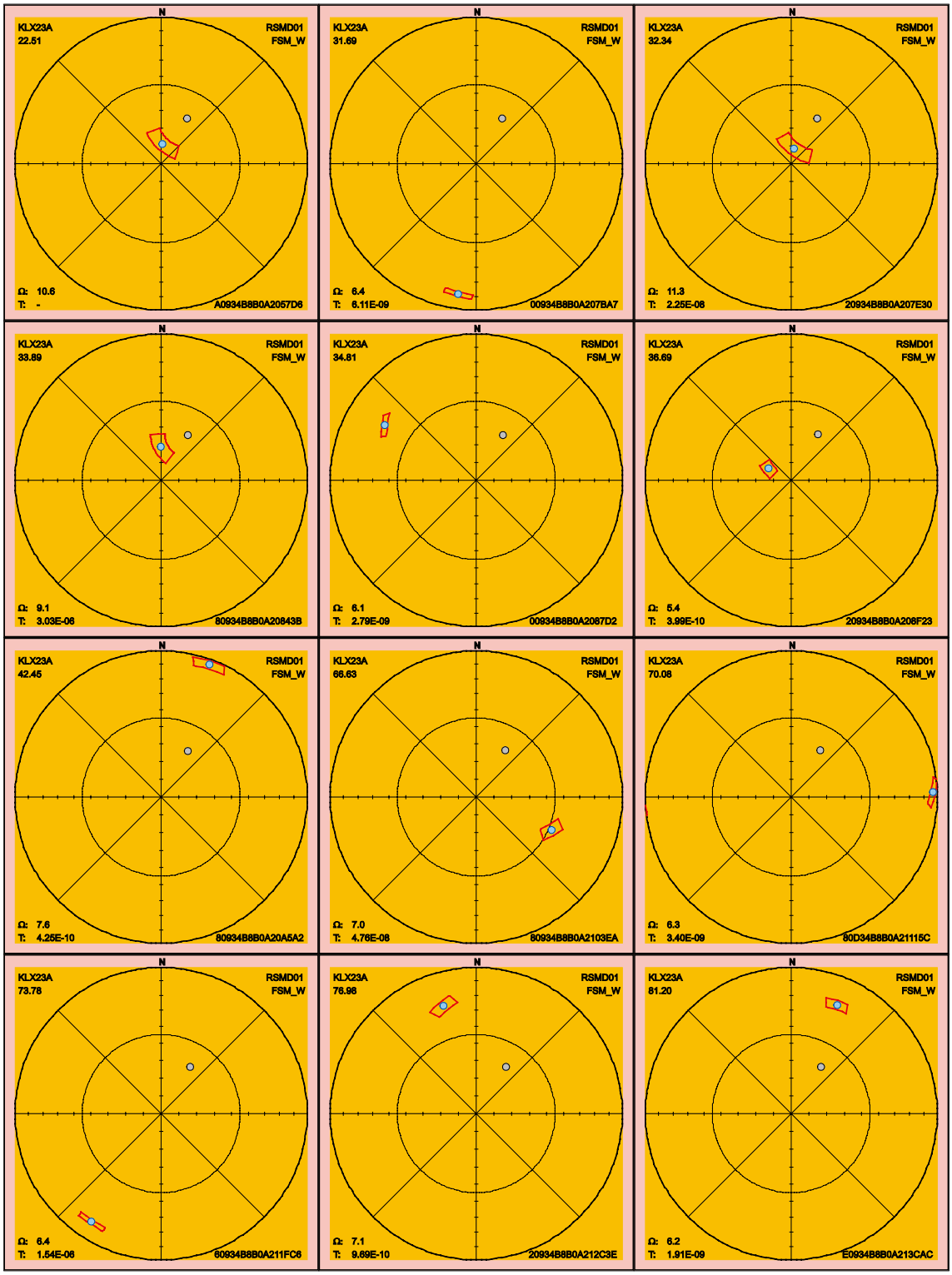
KLX23A
22.51
RSMD01
FSM_W
Ω: 10.6
T: -
A0934B8B0A2057D6
KLX23A
31.69
RSMD01
FSM_W
Ω: 6.4
T: 6.11E-09
00934B8B0A207BA7
KLX23A
32.34
RSMD01
FSM_W
Ω: 11.3
T: 2.25E-08
20934B8B0A207E30
KLX23A
33.89
RSMD01
FSM_W
Ω: 9.1
T: 3.03E-08
80934B8B0A20843B
KLX23A
34.81
RSMD01
FSM_W
Ω: 6.1
T: 2.79E-09
00934B8B0A2067D2
KLX23A
36.69
RSMD01
FSM_W
Ω: 5.4
T: 3.99E-10
20934B8B0A208F23
KLX23A
42.45
RSMD01
FSM_W
Ω: 7.6
T: 4.25E-10
80934B8B0A20A5A2
KLX23A
66.63
RSMD01
FSM_W
Ω: 7.0
T: 4.76E-08
80934B8B0A2103EA
KLX23A
70.08
RSMD01
FSM_W
Ω: 6.3
T: 3.40E-09
80D34B8B0A21115C
KLX23A
73.78
RSMD01
FSM_W
Ω: 6.4
T: 1.54E-08
80934B8B0A211FC6
KLX23A
76.98
RSMD01
FSM_W
Ω: 7.1
T: 9.69E-10
20934B8B0A212C3E
KLX23A
81.20
RSMD01
FSM_W
Ω: 6.2
T: 1.91E-09
E0934B8B0A213CAC

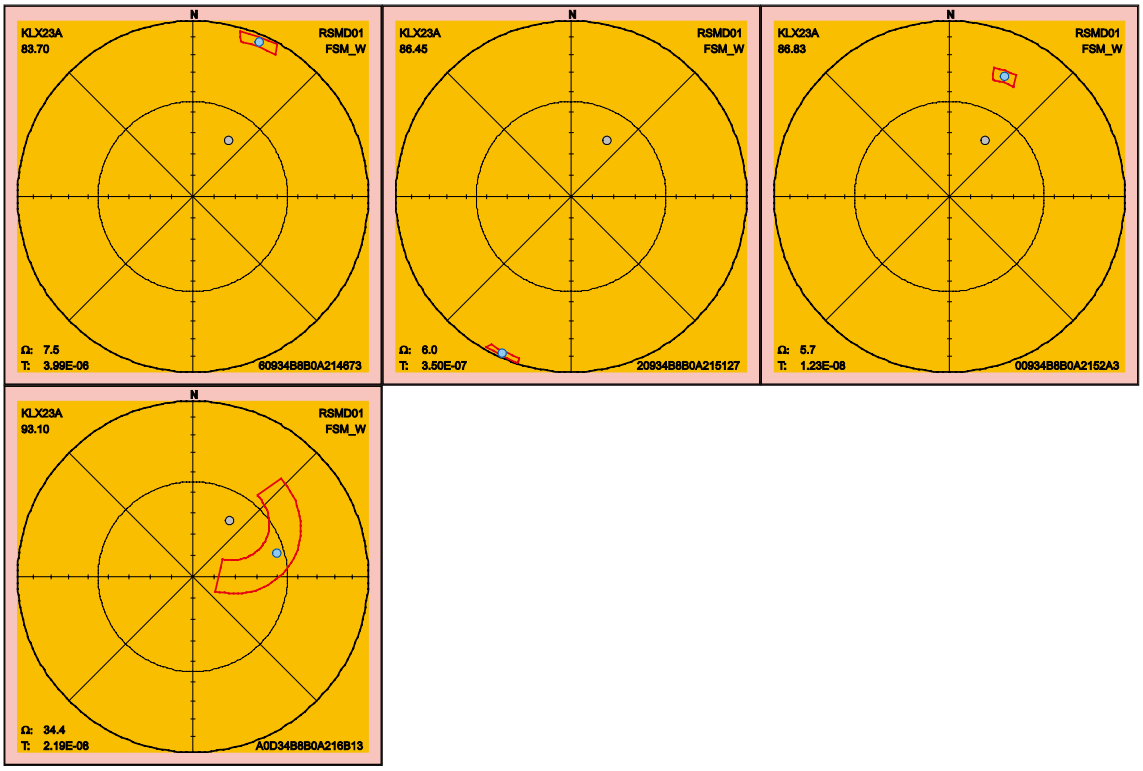

2.3.37 KLX23B

Below follow the 90th percentile sample space of uncertainty for the four PFL fractures in KLX23B. There is one fracture, see Table 2-32, that has maximum uncertainty, on the 90th percentile, larger than 30°.

Table 2-32. Fractures in KLX23B with uncertainty, Ω, larger than 30°.

FeatureId	PFL-f no	Adjusted Secup	Ω
80934B8B09204923	1	18.80	41.41

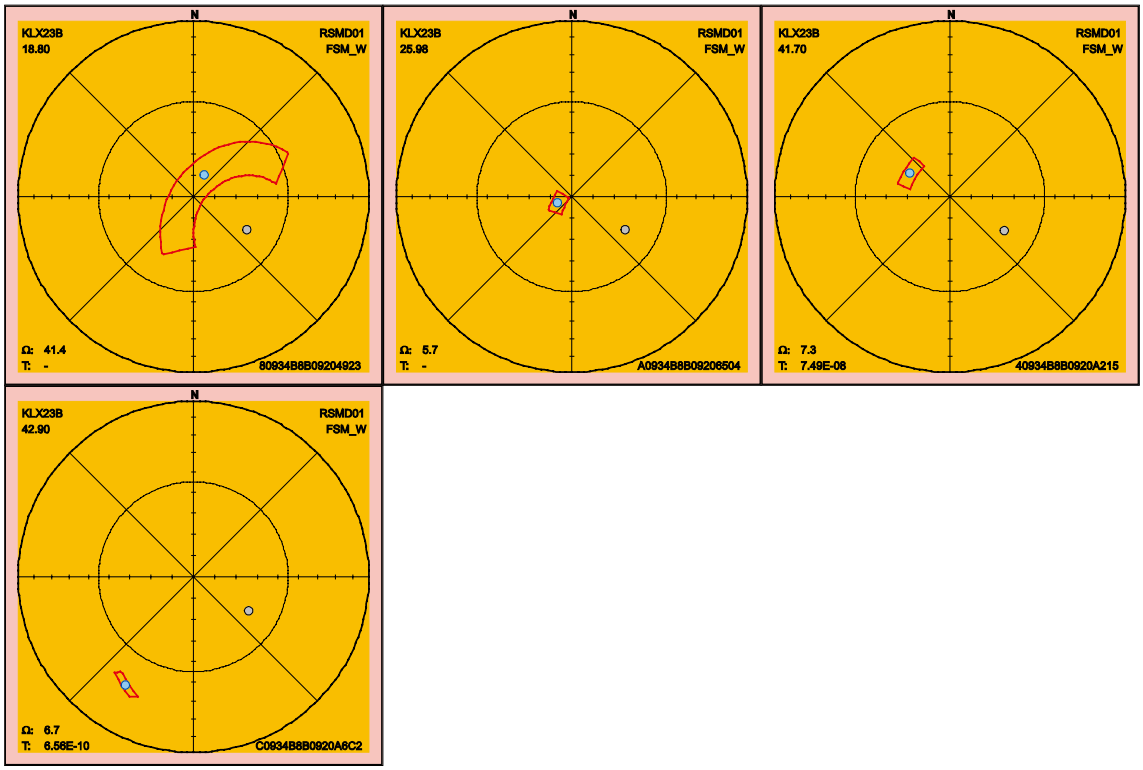

2.3.38 KLX24A

There are 41 PFL fractures in KLX24A of which one has maximum uncertainty larger than 30°, see Table 2-33. A fracture can have an alternative interpretation of orientation compared to the best estimate orientation in the table p_fract_core in /Sicada 2008/ if the uncertainty is large. Below follow the 90th percentile sample space of uncertainty for the PFL fractures in KLX24A.

Table 2-33. Fractures in KLX24A with uncertainty, Ω, larger than 30°.

FeatureId	PFL-f no	Adjusted Secup	Ω
00944B8B0A107BC2	4	31.72	55.5

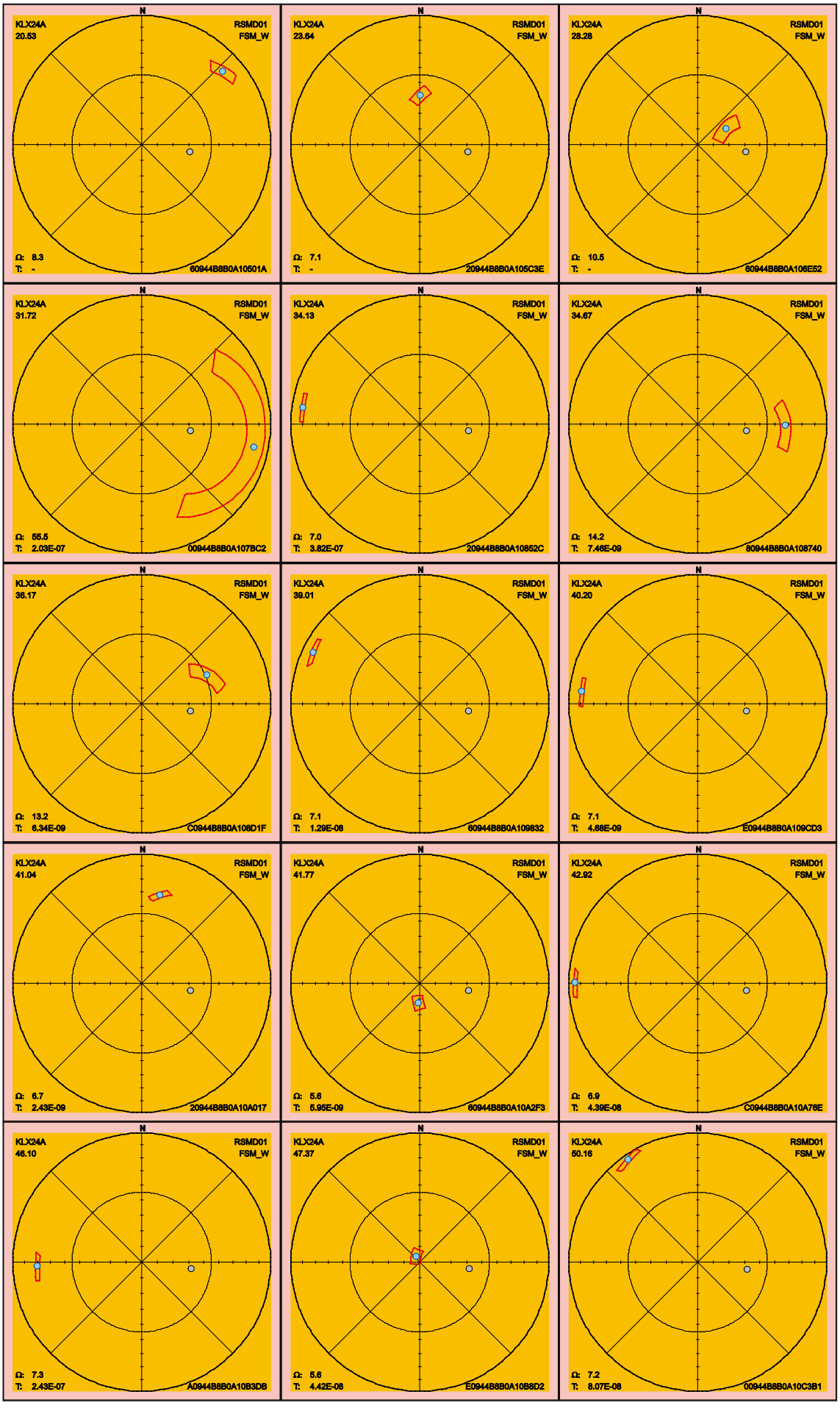
KLX24A
20.53
RSMD01
FSM_W
N
Ω: 8.3
T: -
60944B8B0A10501A
KLX24A
23.64
RSMD01
FSM_W
N
Ω: 7.1
T: -
20944B8B0A105C3E
KLX24A
28.28
RSMD01
FSM_W
N
Ω: 10.5
T: -
60944B8B0A106E52
KLX24A
31.72
RSMD01
FSM_W
N
Ω: 55.5
T: 2.03E-07
00944B8B0A107BC2
KLX24A
34.13
RSMD01
FSM_W
N
Ω: 7.0
T: 3.82E-07
20944B8B0A10852C
KLX24A
34.67
RSMD01
FSM_W
N
Ω: 14.2
T: 7.46E-09
80944B8B0A108740
KLX24A
36.17
RSMD01
FSM_W
N
Ω: 13.2
T: 6.34E-09
C0944B8B0A108D1F
KLX24A
39.01
RSMD01
FSM_W
N
Ω: 7.1
T: 1.29E-08
60944B8B0A109832
KLX24A
40.20
RSMD01
FSM_W
N
Ω: 7.1
T: 4.68E-09
E0944B8B0A109CD3
KLX24A
41.04
RSMD01
FSM_W
N
Ω: 6.7
T: 2.43E-09
20944B8B0A10A017
KLX24A
41.77
RSMD01
FSM_W
N
Ω: 5.6
T: 5.95E-09
60944B8B0A10A2F3
KLX24A
42.92
RSMD01
FSM_W
N
Ω: 6.9
T: 4.39E-08
C0944B8B0A10A76E
KLX24A
46.10
RSMD01
FSM_W
N
Ω: 7.3
T: 2.43E-07
A0944B8B0A10B3DB
KLX24A
47.37
RSMD01
FSM_W
N
Ω: 5.6
T: 4.42E-08
E0944B8B0A10B8D2
KLX24A
50.16
RSMD01
FSM_W
N
Ω: 7.2
T: 8.07E-08
00944B8B0A10C3B1

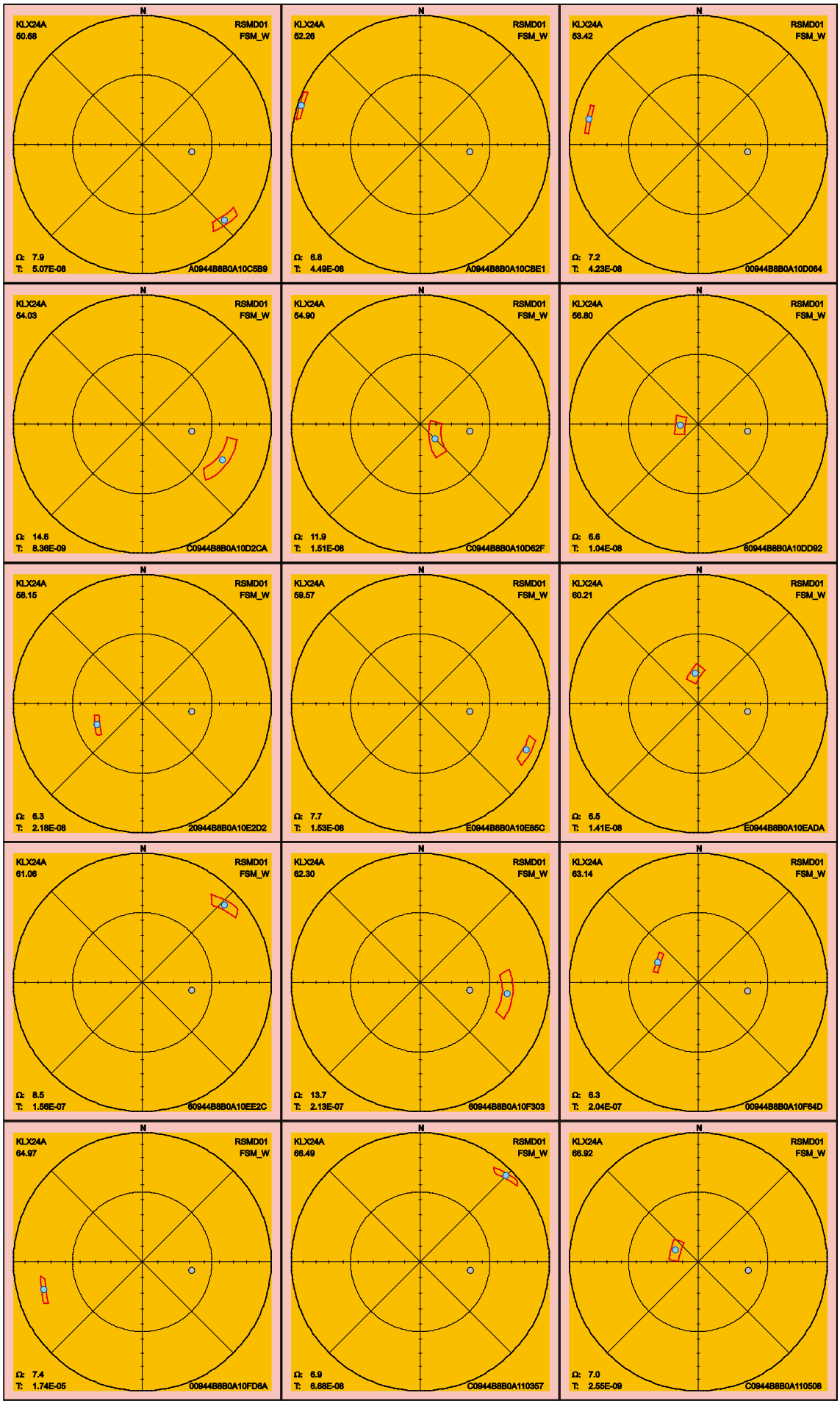
KLX24A
60.68
RSMD01
FSM_W
Ω: 7.9
T: 5.07E-08
A0944B8B0A10C5B9
KLX24A
62.26
RSMD01
FSM_W
Ω: 6.8
T: 4.49E-08
A0944B8B0A10CBE1
KLX24A
63.42
RSMD01
FSM_W
Ω: 7.2
T: 4.23E-08
00944B8B0A10D064
KLX24A
54.03
RSMD01
FSM_W
Ω: 14.6
T: 8.36E-09
C0944B8B0A10D2CA
KLX24A
54.90
RSMD01
FSM_W
Ω: 11.9
T: 1.51E-08
C0944B8B0A10D62F
KLX24A
56.80
RSMD01
FSM_W
Ω: 6.6
T: 1.04E-08
60944B8B0A10DD92
KLX24A
58.15
RSMD01
FSM_W
Ω: 6.3
T: 2.18E-08
20944B8B0A10E2D2
KLX24A
59.57
RSMD01
FSM_W
Ω: 7.7
T: 1.53E-08
E0944B8B0A10E85C
KLX24A
60.21
RSMD01
FSM_W
Ω: 6.5
T: 1.41E-08
E0944B8B0A10EADA
KLX24A
61.06
RSMD01
FSM_W
Ω: 8.5
T: 1.56E-07
60944B8B0A10EE2C
KLX24A
62.30
RSMD01
FSM_W
Ω: 13.7
T: 2.13E-07
60944B8B0A10F303
KLX24A
63.14
RSMD01
FSM_W
Ω: 6.3
T: 2.04E-07
00944B8B0A10F64D
KLX24A
64.97
RSMD01
FSM_W
Ω: 7.4
T: 1.74E-05
00944B8B0A10FD6A
KLX24A
66.49
RSMD01
FSM_W
Ω: 6.9
T: 6.68E-08
C0944B8B0A110357
KLX24A
66.92
RSMD01
FSM_W
Ω: 7.0
T: 2.55E-09
C0944B8B0A110508

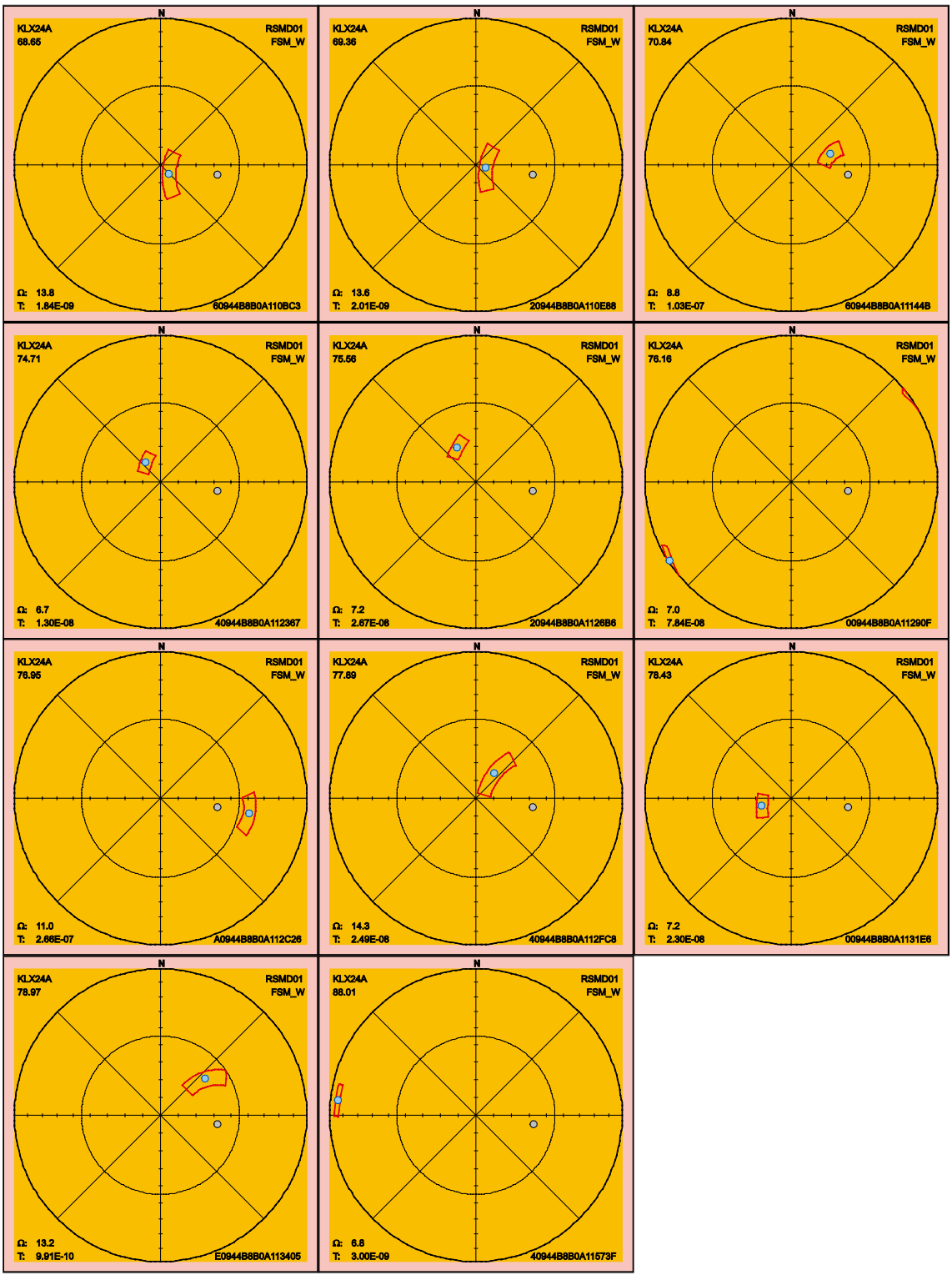
KLX24A
68.65
RSMD01
FSM_W
N
Ω: 13.8
T: 1.84E-09
60944B8B0A110BC3
KLX24A
69.36
RSMD01
FSM_W
N
Ω: 13.6
T: 2.01E-09
20944B8B0A110E88
KLX24A
70.84
RSMD01
FSM_W
N
Ω: 8.8
T: 1.03E-07
60944B8B0A11144B
KLX24A
74.71
RSMD01
FSM_W
N
Ω: 6.7
T: 1.30E-08
40944B8B0A112367
KLX24A
75.56
RSMD01
FSM_W
N
Ω: 7.2
T: 2.67E-08
20944B8B0A1126B6
KLX24A
76.16
RSMD01
FSM_W
N
Ω: 7.0
T: 7.84E-08
00944B8B0A11290F
KLX24A
76.95
RSMD01
FSM_W
N
Ω: 11.0
T: 2.66E-07
A0944B8B0A112C26
KLX24A
77.89
RSMD01
FSM_W
N
Ω: 14.3
T: 2.49E-08
40944B8B0A112FC8
KLX24A
78.43
RSMD01
FSM_W
N
Ω: 7.2
T: 2.30E-08
00944B8B0A1131E6
KLX24A
78.97
RSMD01
FSM_W
N
Ω: 13.2
T: 9.91E-10
E0944B8B0A113405
KLX24A
88.01
RSMD01
FSM_W
N
Ω: 6.8
T: 3.00E-09
40944B8B0A11573F

2.3.39 KLX25A

Below follow the 90th percentile sample space of uncertainty for the eight PFL fractures in KLX25A. There is only one fracture, see Table 2-34, that has maximum uncertainty on the 90th percentile larger than 30° and hence might have an alternative interpretation of orientation compared to the best estimate orientation that is found in the table p_fract_core in /Sicada 2008/.

Table 2-34. Fractures in KLX25A with uncertainty, Ω, larger than 30°.

FeatureId	PFL-f no	Adjusted Secup	Ω
20954B8B0A10840C	6	33.97	50.4

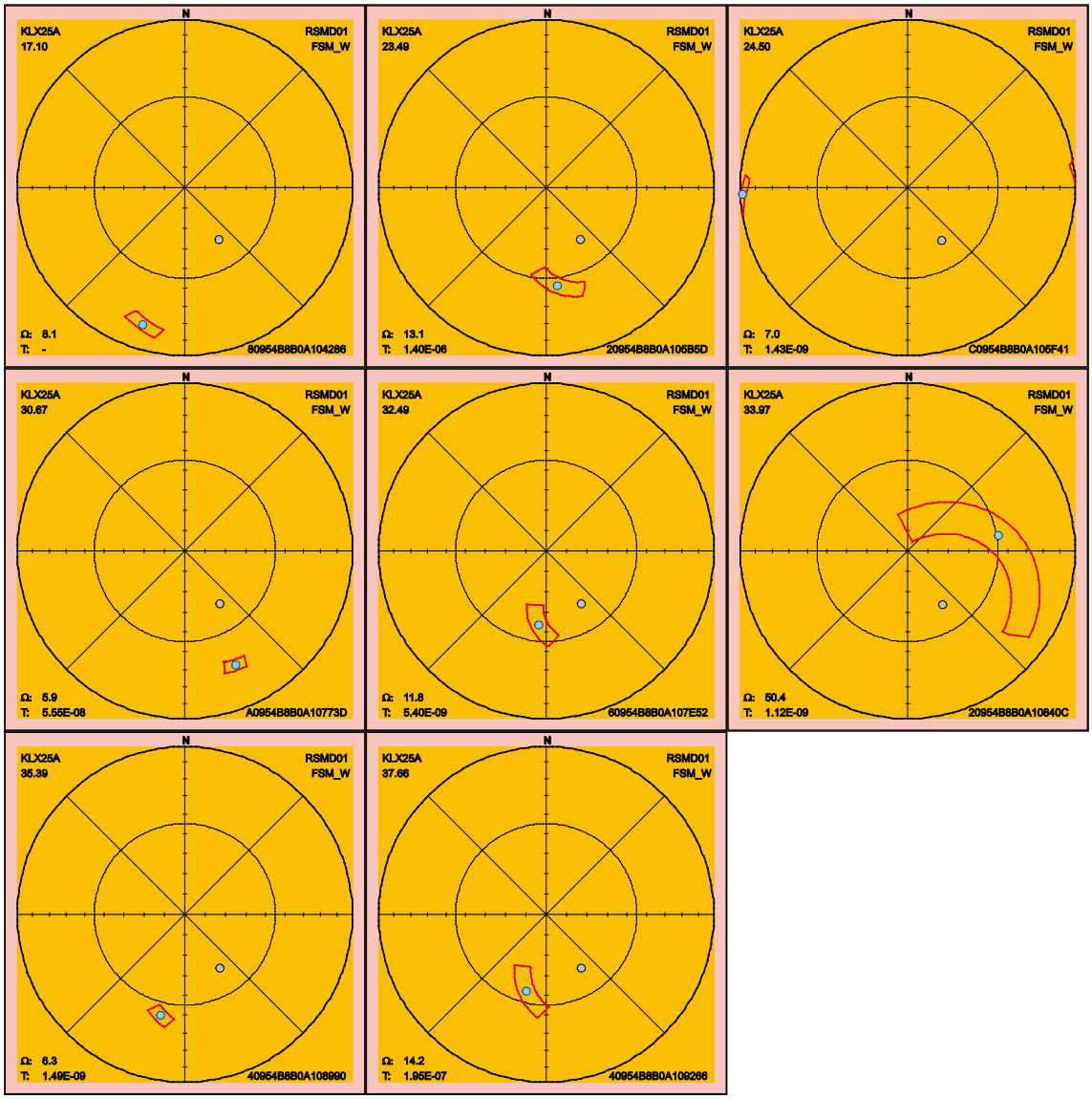

2.3.40 KLX26A

There are 23 PFL fractures in KLX26A of which one has maximum uncertainty larger than 30°, see Table 2-35. A fracture with large uncertainty can have a different interpretation of the orientation compared to the table p_fract_core in /Sicada 2008/. Below follow the 90th percentile sample space of uncertainty for all the PFL fractures.

Table 2-35. Fractures in KLX26A with uncertainty, Ω, larger than 30°.

FeatureId	PFL-f no	Adjusted Secup	Ω
C0964B8B0A1096D9	15	38.63	56.4

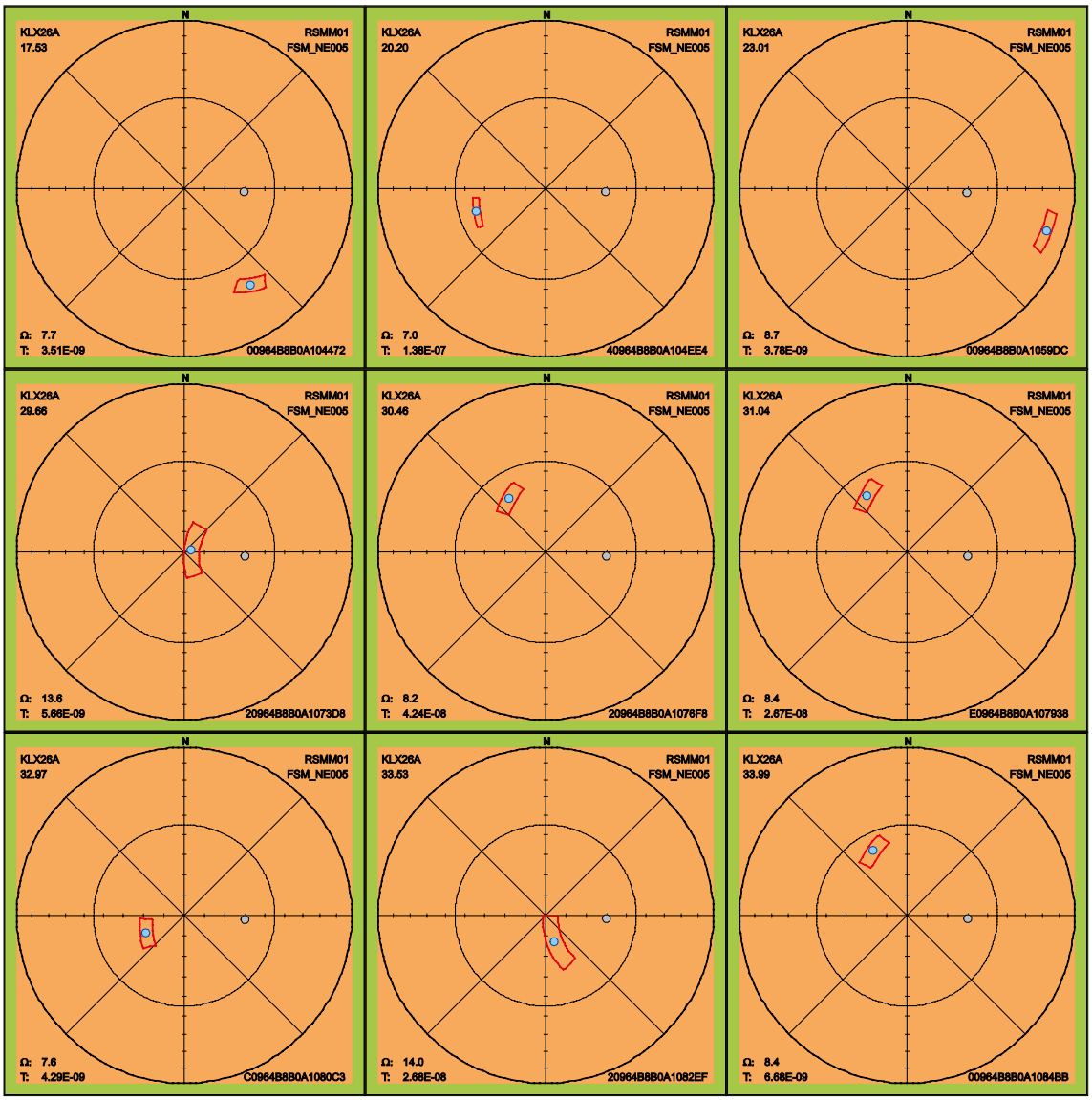

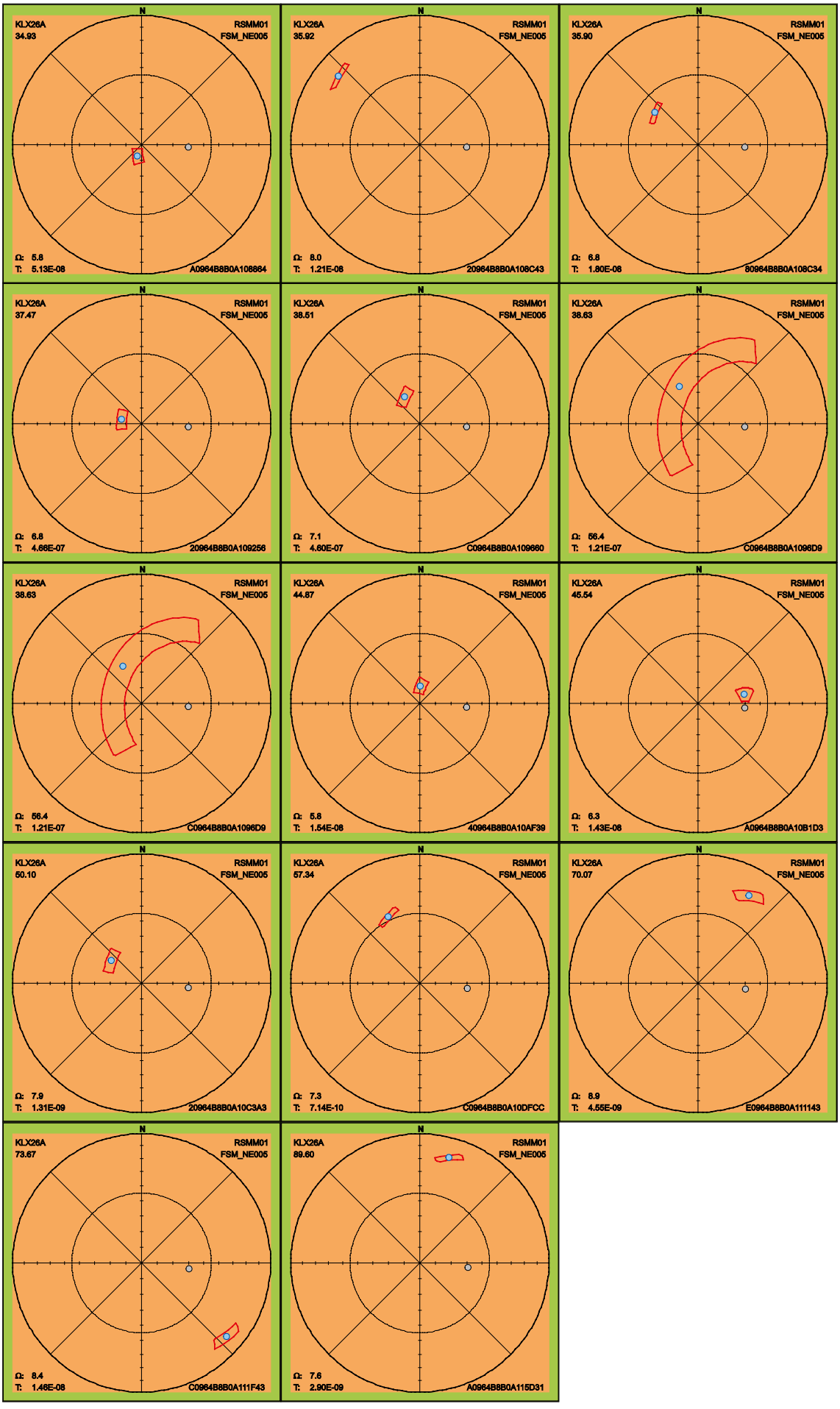
KLX26A
34.93
RSMM01
FSM_NE005
Ω: 5.8
T: 5.13E-08
A0964B8B0A108864
KLX26A
35.92
RSMM01
FSM_NE005
Ω: 8.0
T: 1.21E-08
20964B8B0A108C43
KLX26A
35.90
RSMM01
FSM_NE005
Ω: 6.8
T: 1.80E-08
80964B8B0A108C34
KLX26A
37.47
RSMM01
FSM_NE005
Ω: 6.8
T: 4.66E-07
20964B8B0A109256
KLX26A
38.51
RSMM01
FSM_NE005
Ω: 7.1
T: 4.60E-07
C0964B8B0A109660
KLX26A
38.63
RSMM01
FSM_NE005
Ω: 56.4
T: 1.21E-07
C0964B8B0A1096D9
KLX26A
38.63
RSMM01
FSM_NE005
Ω: 56.4
T: 1.21E-07
C0964B8B0A1096D9
KLX26A
44.87
RSMM01
FSM_NE005
Ω: 5.8
T: 1.54E-08
40964B8B0A10AF39
KLX26A
45.54
RSMM01
FSM_NE005
Ω: 6.3
T: 1.43E-08
A0964B8B0A10B1D3
KLX26A
50.10
RSMM01
FSM_NE005
Ω: 7.9
T: 1.31E-09
20964B8B0A10C3A3
KLX26A
57.34
RSMM01
FSM_NE005
Ω: 7.3
T: 7.14E-10
C0964B8B0A10DFCC
KLX26A
70.07
RSMM01
FSM_NE005
Ω: 8.9
T: 4.55E-09
E0964B8B0A111143
KLX26A
73.67
RSMM01
FSM_NE005
Ω: 8.4
T: 1.46E-08
C0964B8B0A111F43
KLX26A
89.60
RSMM01
FSM_NE005
Ω: 7.6
T: 2.90E-09
A0964B8B0A115D31

2.3.41 KLX26B

There is no PFL fracture with maximum uncertainty larger than 30° in KLX26B. The sample space of the maximum uncertainty, on the 90th percentile, is shown below for all 17 fractures.

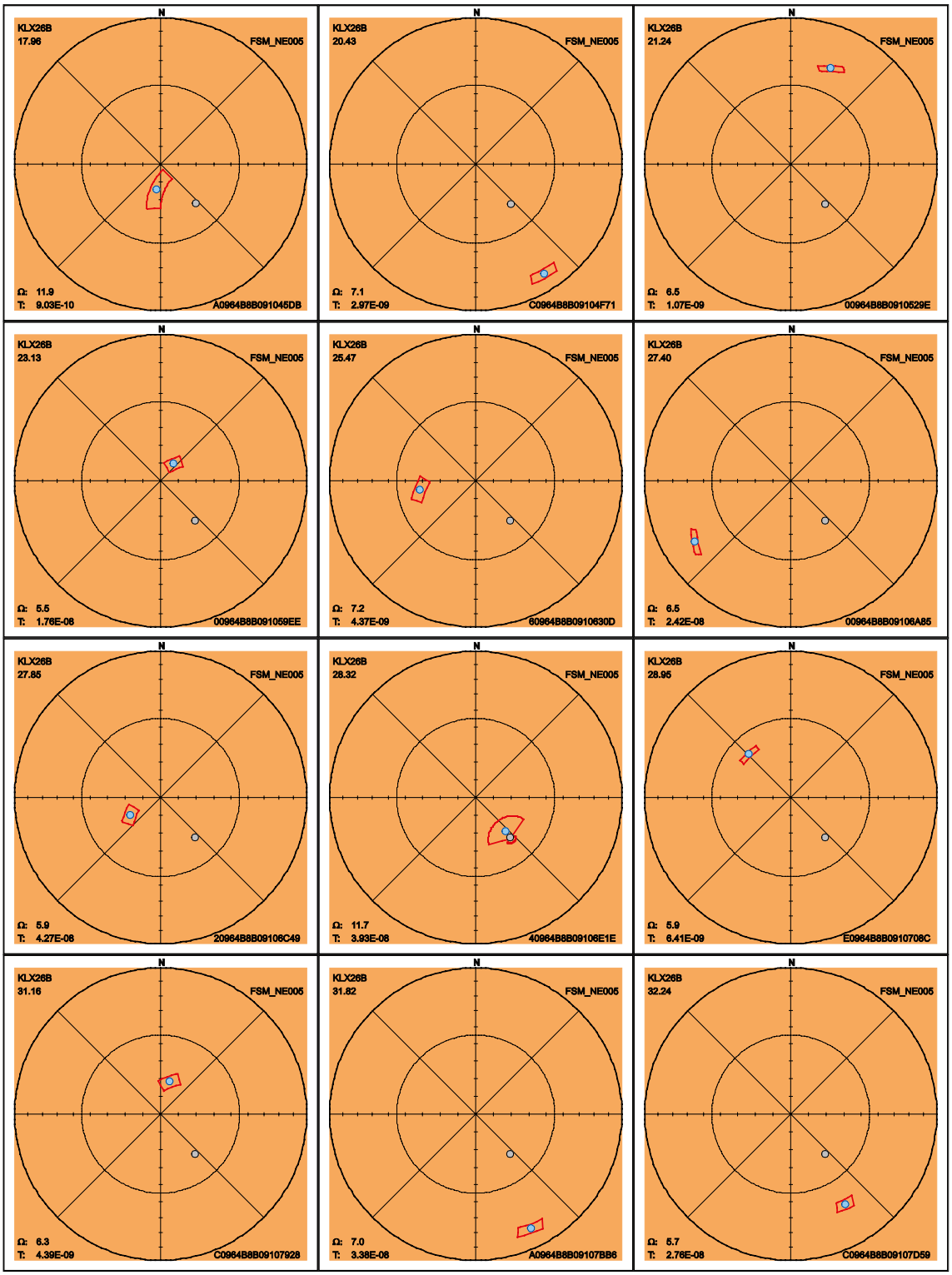

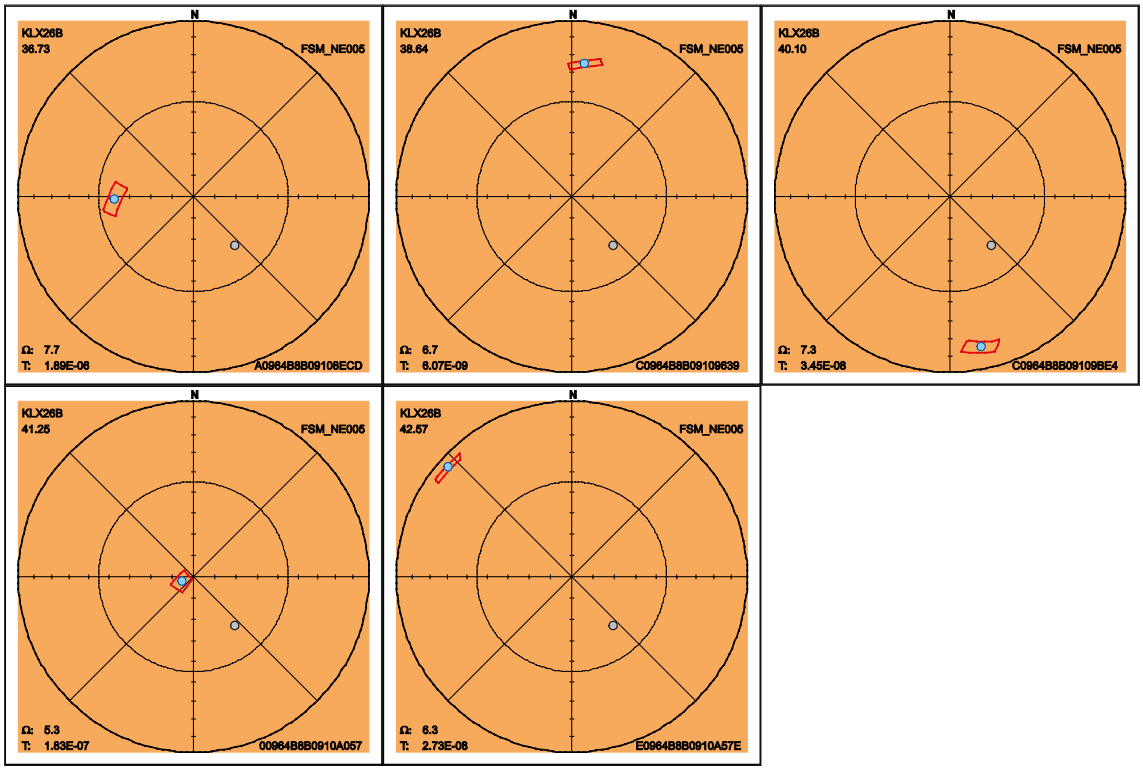

2.3.42 KLX28A

In KLX28A there is no PFL fracture with maximum uncertainty larger than 30°. Below follow the 90th percentile sample space of uncertainty for the 24 PFL fractures.

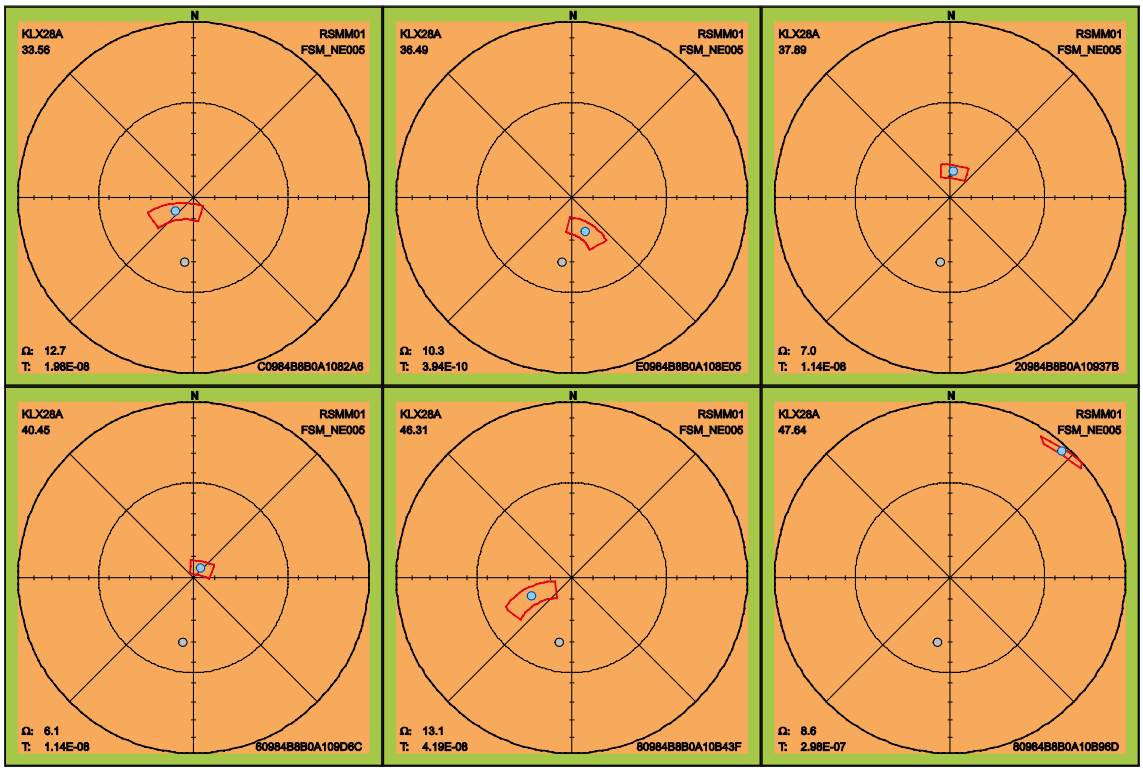

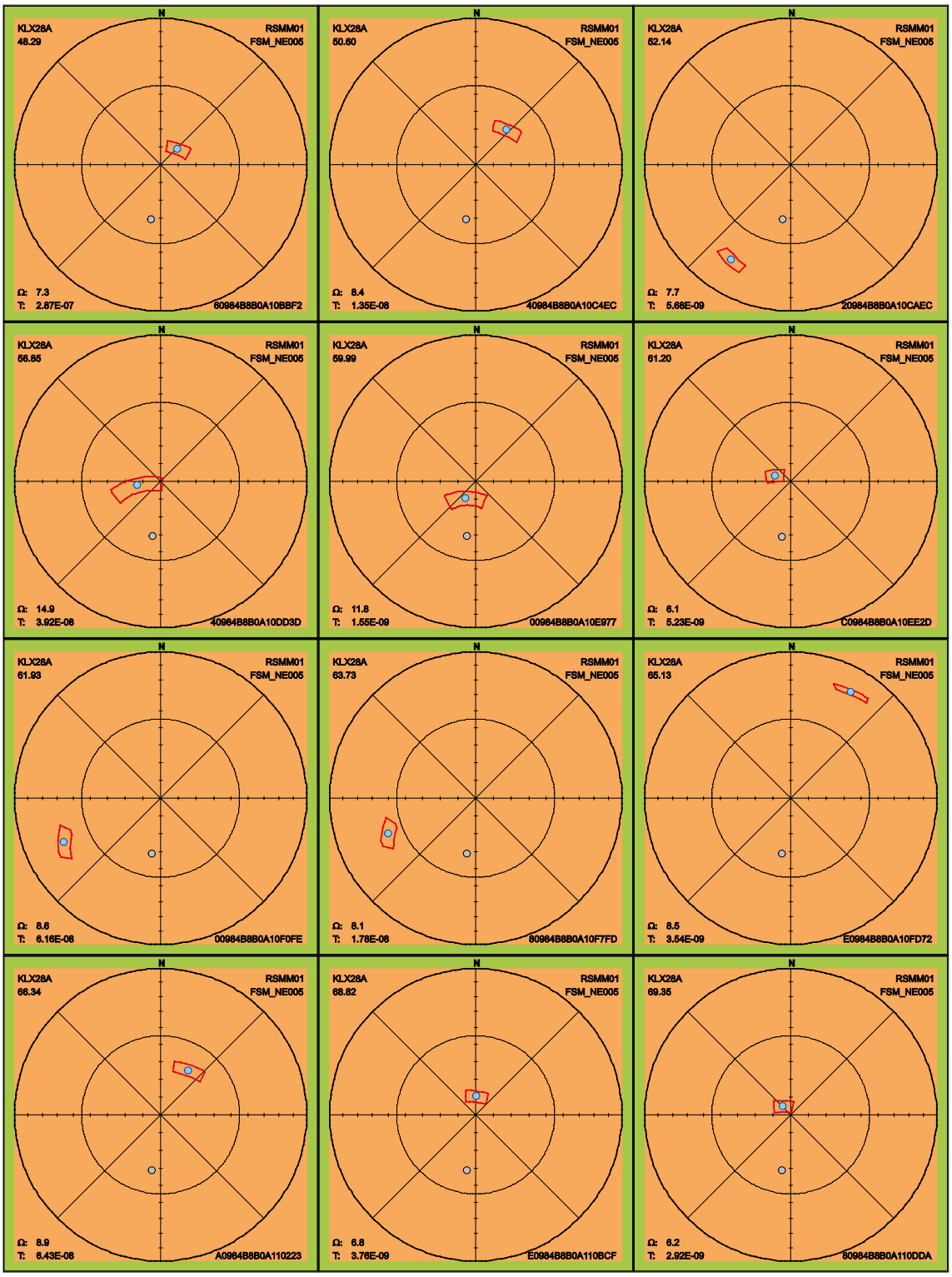
KLX28A
48.29
RSMM01
FSM_NE005
N
Ω: 7.3
T: 2.67E-07
60984B8B0A10BBF2
KLX28A
50.60
RSMM01
FSM_NE005
N
Ω: 8.4
T: 1.35E-08
40984B8B0A10C4EC
KLX28A
52.14
RSMM01
FSM_NE005
N
Ω: 7.7
T: 5.68E-09
20984B8B0A10CAEC
KLX28A
56.85
RSMM01
FSM_NE005
N
Ω: 14.9
T: 3.92E-08
40984B8B0A10DD3D
KLX28A
59.99
RSMM01
FSM_NE005
N
Ω: 11.8
T: 1.55E-09
00984B8B0A10E977
KLX28A
61.20
RSMM01
FSM_NE005
N
Ω: 6.1
T: 5.23E-09
C0984B8B0A10EE2D
KLX28A
61.93
RSMM01
FSM_NE005
N
Ω: 8.6
T: 6.16E-08
00984B8B0A10F0FE
KLX28A
63.73
RSMM01
FSM_NE005
N
Ω: 8.1
T: 1.78E-08
80984B8B0A10F7FD
KLX28A
65.13
RSMM01
FSM_NE005
N
Ω: 8.5
T: 3.54E-09
E0984B8B0A10FD72
KLX28A
66.34
RSMM01
FSM_NE005
N
Ω: 8.9
T: 6.43E-08
A0984B8B0A110223
KLX28A
68.82
RSMM01
FSM_NE005
N
Ω: 6.8
T: 3.76E-09
E0984B8B0A110BCF
KLX28A
69.35
RSMM01
FSM_NE005
N
Ω: 6.2
T: 2.92E-09
80984B8B0A110DDA

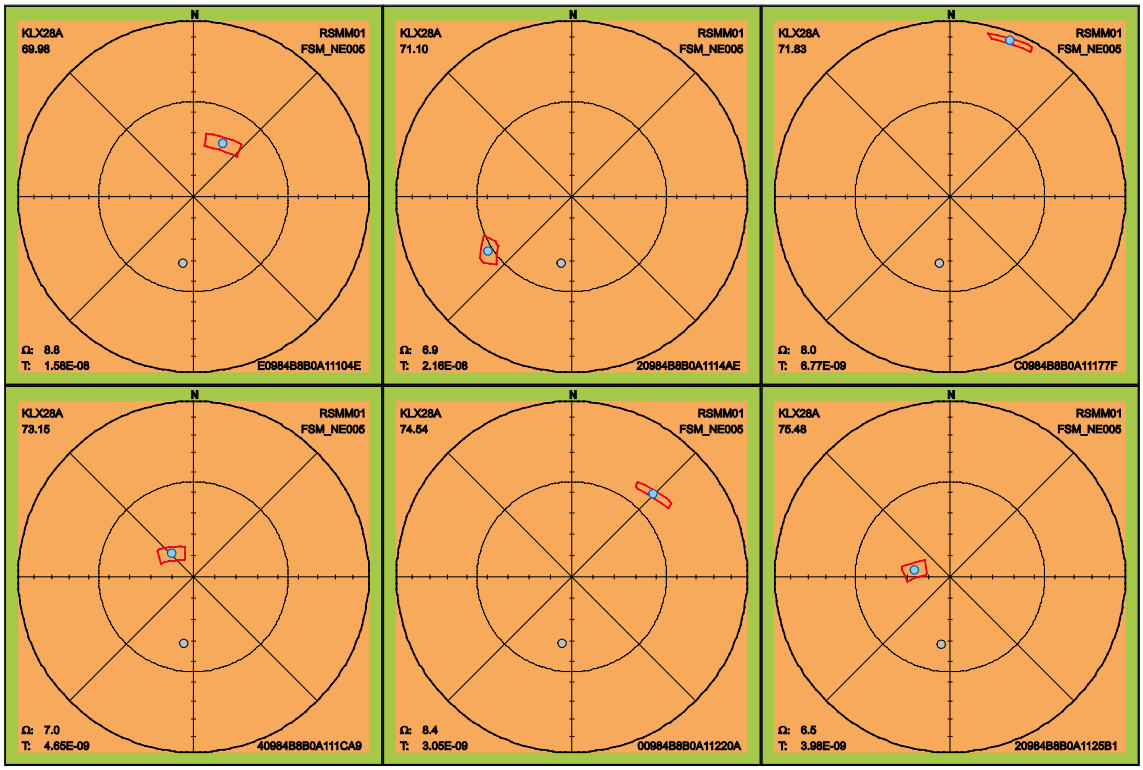

2.3.43 KLX29A

There is no PFL fracture in KLX29A with orientation uncertainty larger than 30°. Below follow the 90th percentile sample space of uncertainty for the 27 PFL fractures.

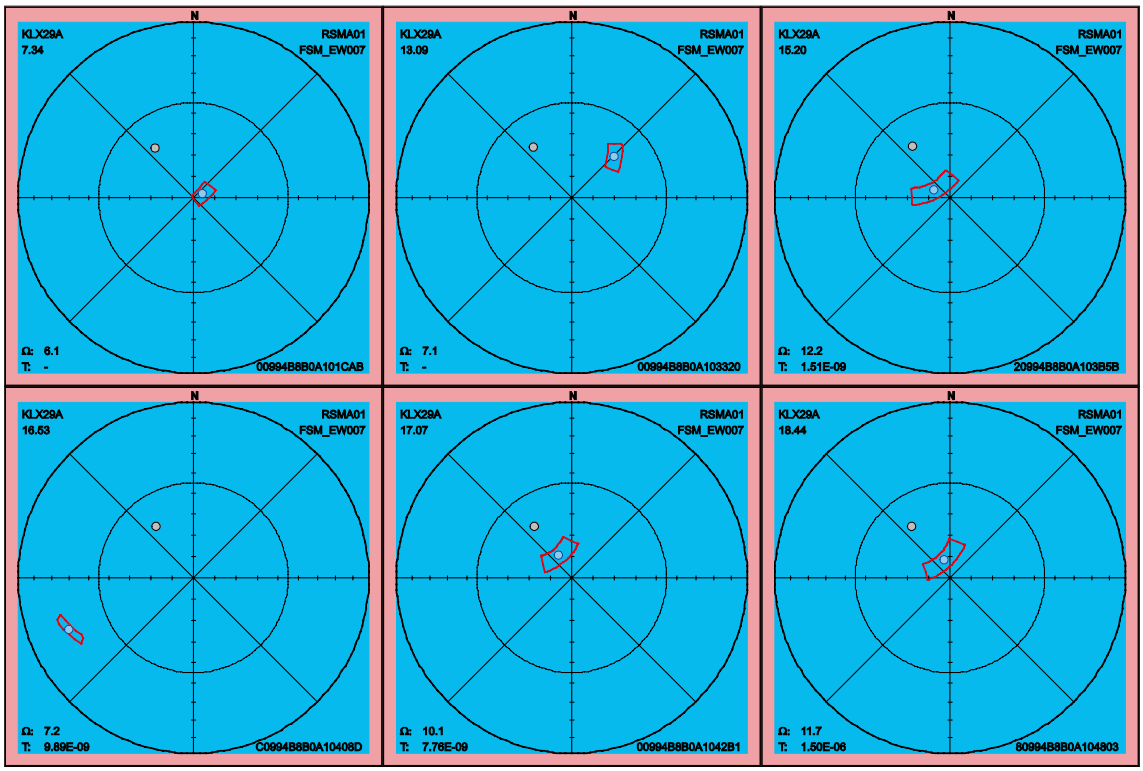

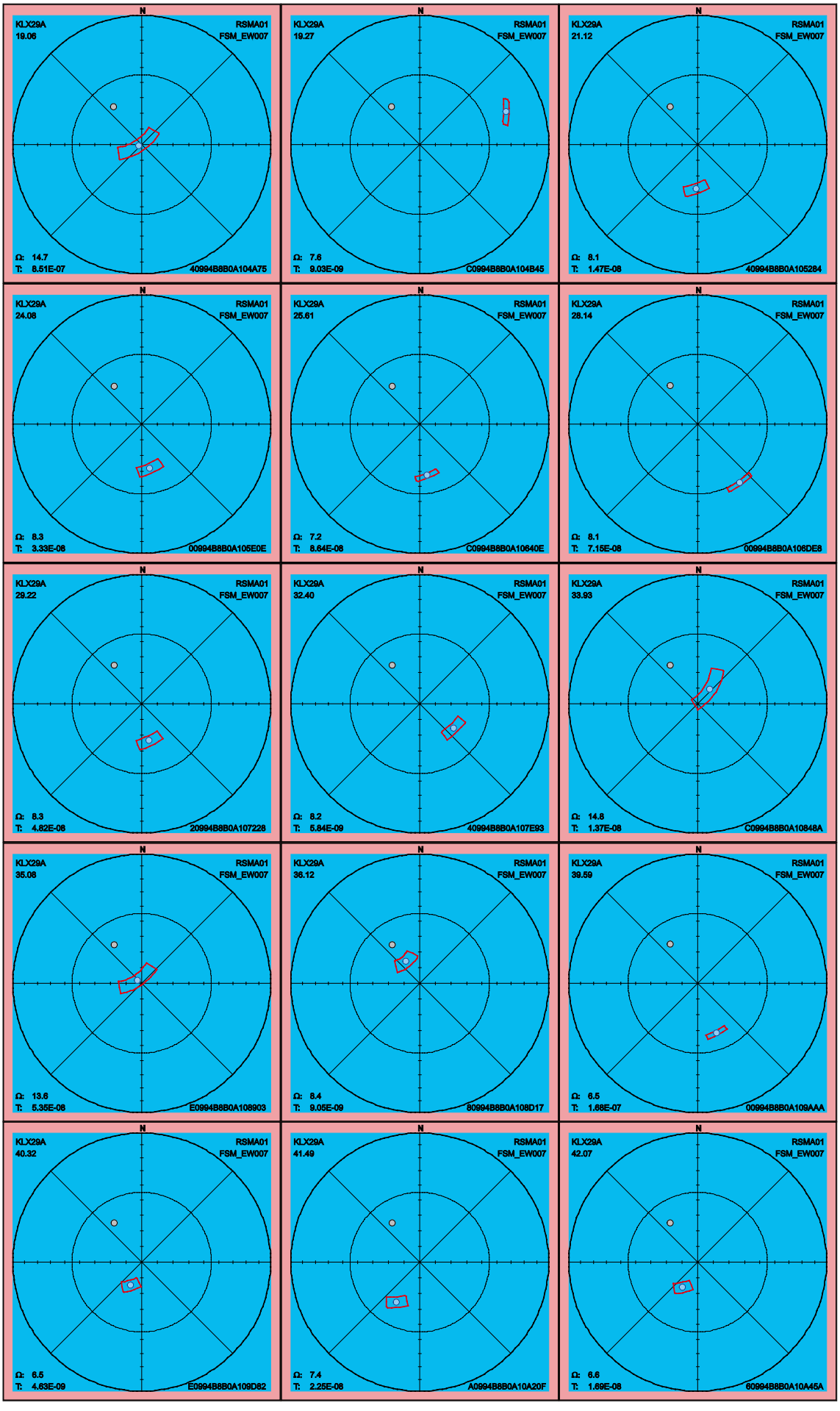
KLX29A
19.06
RSMA01
FSM_EW007
N
Ω: 14.7
T: 8.51E-07
40994B8B0A104A75
KLX29A
19.27
RSMA01
FSM_EW007
N
Ω: 7.6
T: 9.03E-09
C0994B8B0A104B45
KLX29A
21.12
RSMA01
FSM_EW007
N
Ω: 8.1
T: 1.47E-08
40994B8B0A105284
KLX29A
24.08
RSMA01
FSM_EW007
N
Ω: 8.3
T: 3.33E-06
00994B8B0A105E0E
KLX29A
25.61
RSMA01
FSM_EW007
N
Ω: 7.2
T: 8.64E-08
C0994B8B0A10640E
KLX29A
28.14
RSMA01
FSM_EW007
N
Ω: 8.1
T: 7.15E-08
00994B8B0A106DE8
KLX29A
29.22
RSMA01
FSM_EW007
N
Ω: 8.3
T: 4.82E-08
20994B8B0A107228
KLX29A
32.40
RSMA01
FSM_EW007
N
Ω: 8.2
T: 5.84E-09
40994B8B0A107E93
KLX29A
33.93
RSMA01
FSM_EW007
N
Ω: 14.8
T: 1.37E-08
C0994B8B0A10848A
KLX29A
35.08
RSMA01
FSM_EW007
N
Ω: 13.6
T: 5.35E-08
E0994B8B0A108903
KLX29A
36.12
RSMA01
FSM_EW007
N
Ω: 8.4
T: 9.05E-09
80994B8B0A108D17
KLX29A
39.59
RSMA01
FSM_EW007
N
Ω: 6.5
T: 1.68E-07
00994B8B0A109AAA
KLX29A
40.32
RSMA01
FSM_EW007
N
Ω: 6.5
T: 4.63E-09
E0994B8B0A109D82
KLX29A
41.49
RSMA01
FSM_EW007
N
Ω: 7.4
T: 2.25E-08
A0994B8B0A10A20F
KLX29A
42.07
RSMA01
FSM_EW007
N
Ω: 6.6
T: 1.69E-08
60994B8B0A10A45A

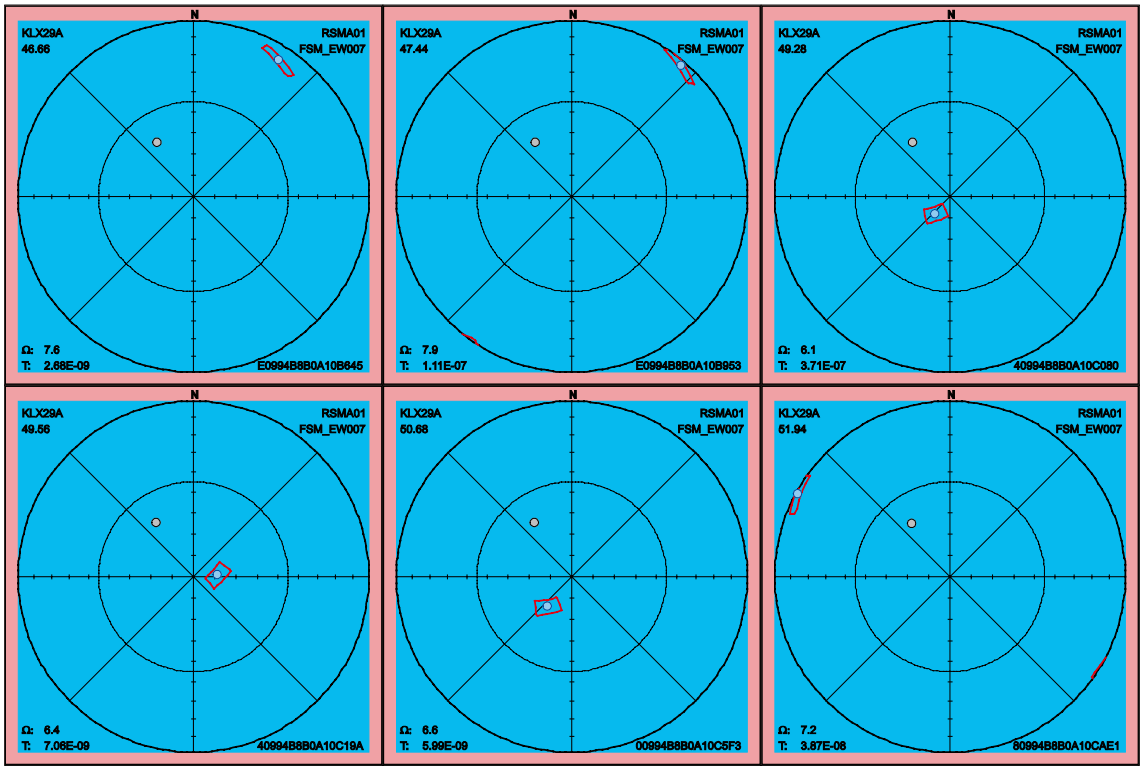
N
KLX29A
46.66
RSMA01
FSM_EW007
Ω: 7.6
T: 2.68E-09
E0994B8B0A10B645
N
KLX29A
47.44
RSMA01
FSM_EW007
Ω: 7.9
T: 1.11E-07
E0994B8B0A10B953
N
KLX29A
49.28
RSMA01
FSM_EW007
Ω: 6.1
T: 3.71E-07
40994B8B0A10C080
N
KLX29A
49.56
RSMA01
FSM_EW007
Ω: 6.4
T: 7.06E-09
40994B8B0A10C19A
N
KLX29A
50.68
RSMA01
FSM_EW007
Ω: 6.6
T: 5.99E-09
00994B8B0A10C5F3
N
KLX29A
51.94
RSMA01
FSM_EW007
Ω: 7.2
T: 3.87E-08
80994B8B0A10CAE1

3 Summary of uncertainty of orientation per rock domain and fracture domain

For convenience the data have been split on the different rock domains, RSM, and fracture domains, FSM, and a coarse compilation of the results is given in this chapter.

3.1 Maximum uncertainty, Ω

This section shows two graphs of the cumulative density function of the maximum uncertainty, one when data are split on rock domains, RSM, and one where data are split on fracture domains, FSM. Figure 3-1 shows that, as expected, there are only minor differences in the orientation uncertainty between the different rock domains. There are slightly more fractures with uncertainty larger than 30° in RSMA01 than the other two rock domains which is due to KLX09B residing in this domain. In Table 3-1 the median, x_{50}, the average, $\overline{\mathbf{x}}$, and the standard deviation, σ, are shown for the maximum orientation uncertainty for the different rock domains.

When dividing the data to the different fracture domains, FSM, there appear to be a difference between FSM_S, having the lowest uncertainty and FSM_N having the largest, which is not expected. One reason could be that there are few data in FSM_S, only 46, that makes the data less reliable and more sensitive to lack of a few high values. The reason for FSM_N to have larger orientation uncertainty is that borehole KLX09B resides in this fracture domain and thereby increase the orientation uncertainty.

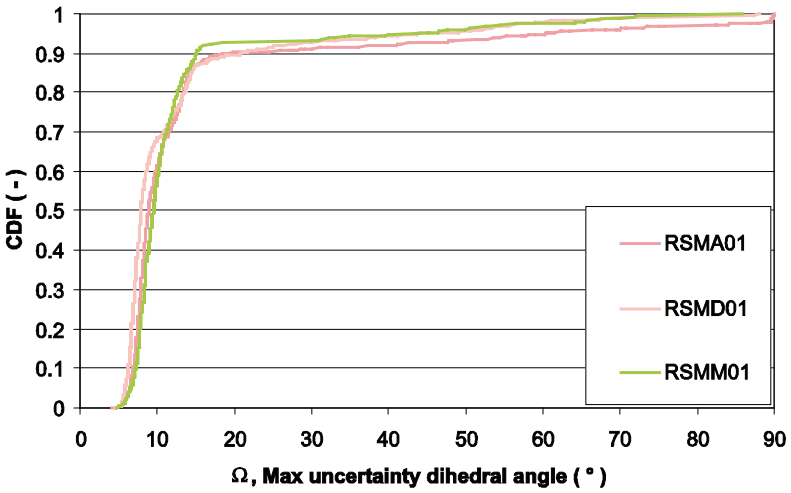

Figure 3-1. *The cumulative density function of the largest orientation uncertainties of PFL fractures in the different rock domains.*

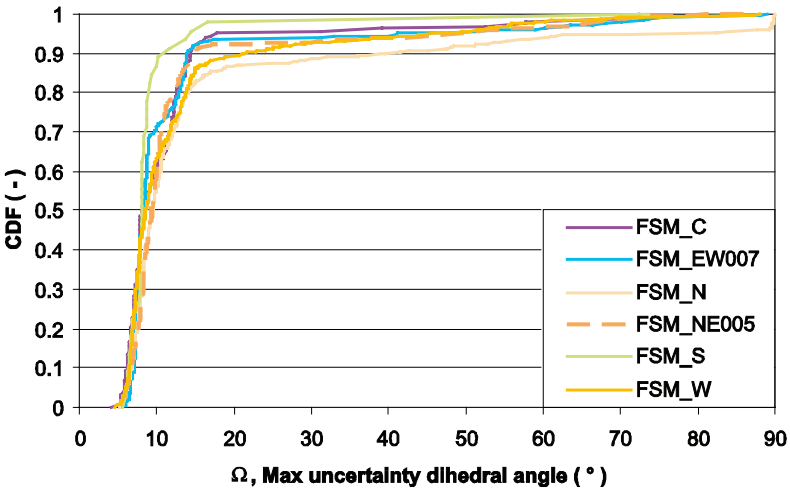

Figure 3-2. The cumulative density function of the largest orientation uncertainties of PFL fractures in the different fracture domains.

3.2 Maximum uncertainty versus transmissivity

This section shows one cross plot of uncertainty versus transmissivity of each rock and fracture domain to get a grasp picture the PFL fractures in each domain.

By visual inspection there is no major difference between the graphs of the different rock domains, see Figure 3-3 to Figure 3-5. The only difference notable is that the transmissivity values in RSMM01 seem to be lower than for the other two domains, which is also seen in Table 3-1.

By visual inspection there is no major difference between the graphs of the different rock domains FSM_C (Figure 3-6), FSM_EW007 (Figure 3-7), FSM_NE005 (Figure 3-9) and FSM_W (Figure 3-11) more than the number of fractures in each domain. The pattern in FSM_N (Figure 3-8) and FSM_S (Figure 3-10) is however different. There are more fractures with large uncertainty in FSM_N, due to KLX09B and there is only one PFL fracture with large orientation uncertainty in FSM_S. According to Table 3-1 the fracture domains FSM_N and FSM_S seem to have a little bit higher transmissivity values than the remaining four fracture domains.

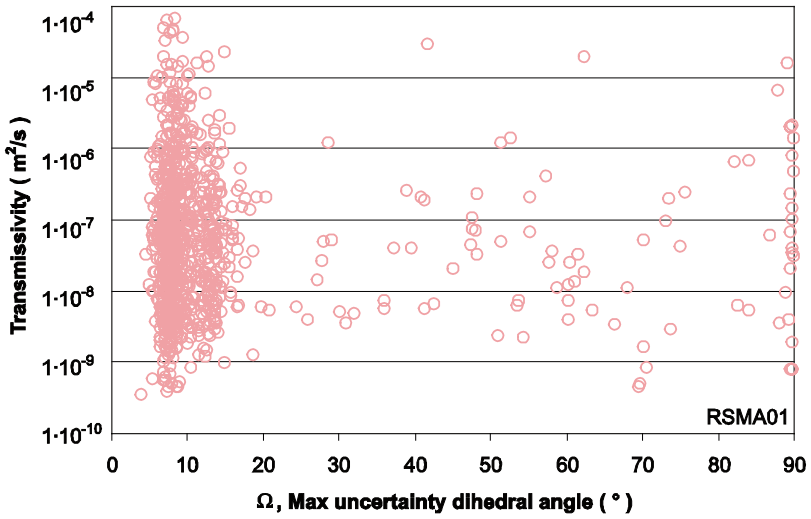

Figure 3-3. The transmissivity versus the uncertainty of the PFL fractures in RSMA01.

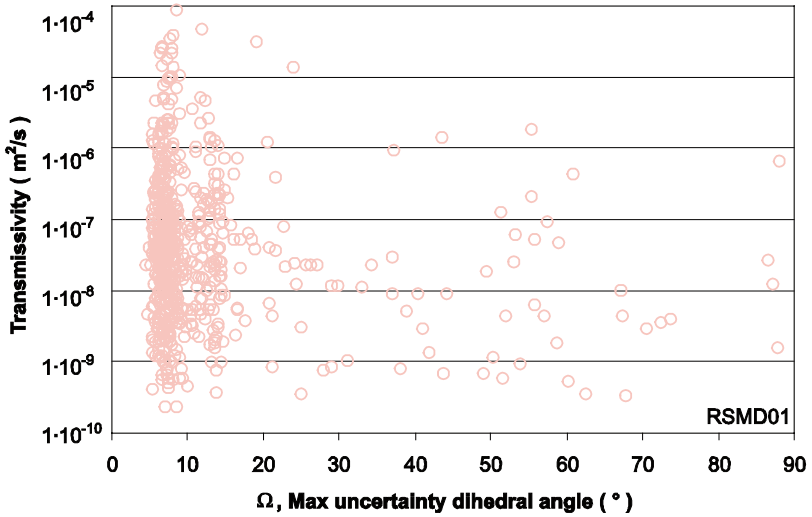

Figure 3-4. The transmissivity versus the uncertainty of the PFL fractures in RSMD01.

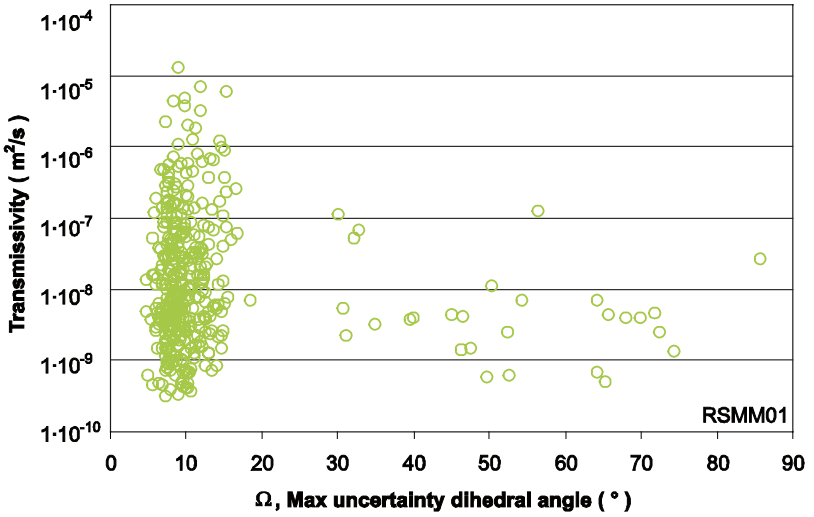

Figure 3-5. The transmissivity versus the uncertainty of the PFL fractures in RSMM01.

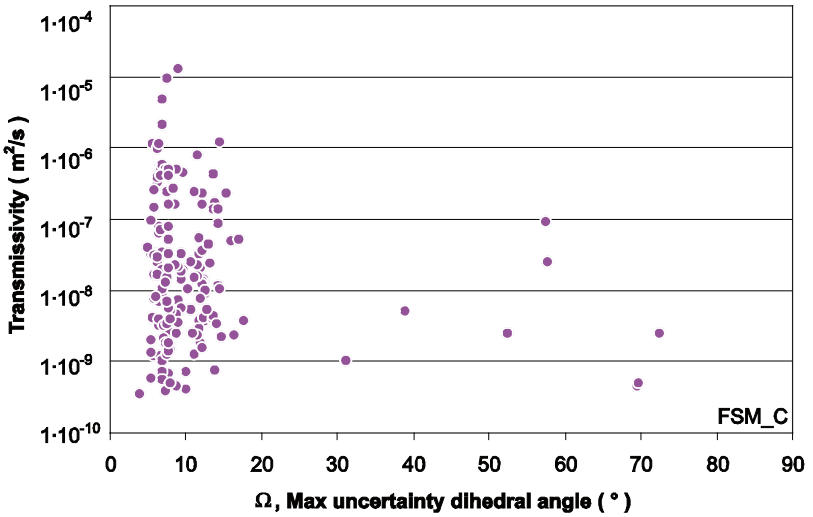

Figure 3-6. The transmissivity versus the uncertainty of the PFL fractures in FSM_C.

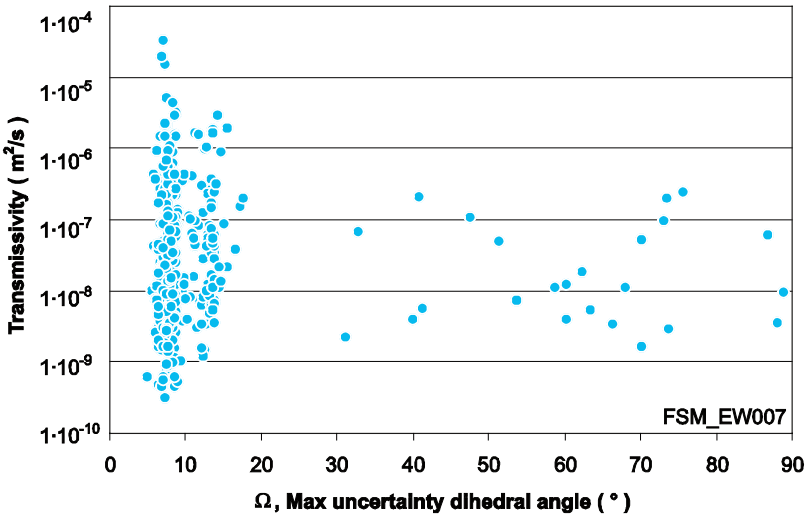

Figure 3-7. *The transmissivity versus the uncertainty of the PFL fractures in FSM_EW007.*

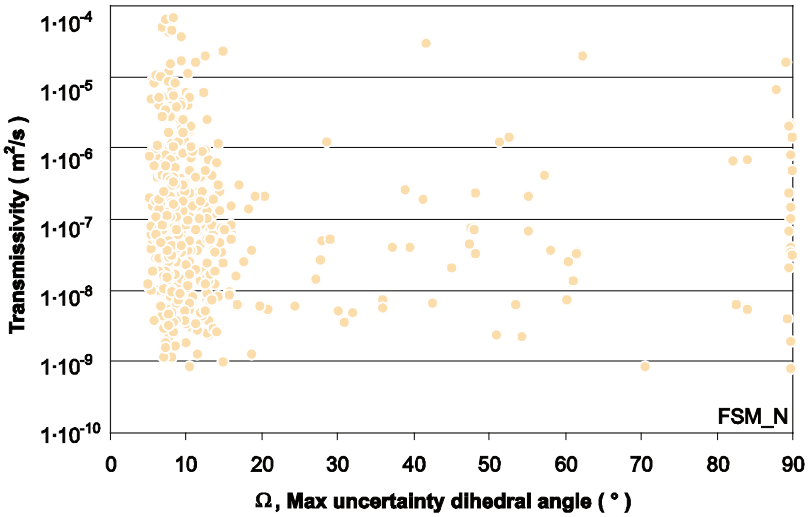

Figure 3-8. *The transmissivity versus the uncertainty of the PFL fractures in FSM_N.*

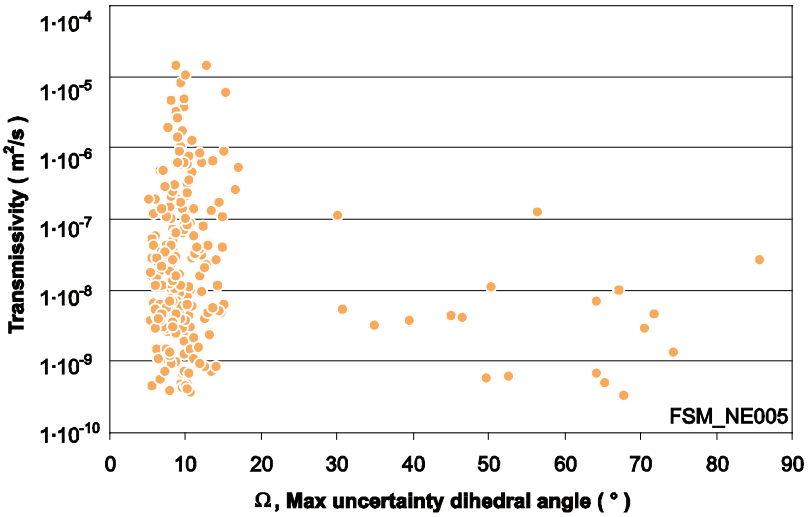

Figure 3-9. *The transmissivity versus the uncertainty of the PFL fractures in FSM_NE005.*

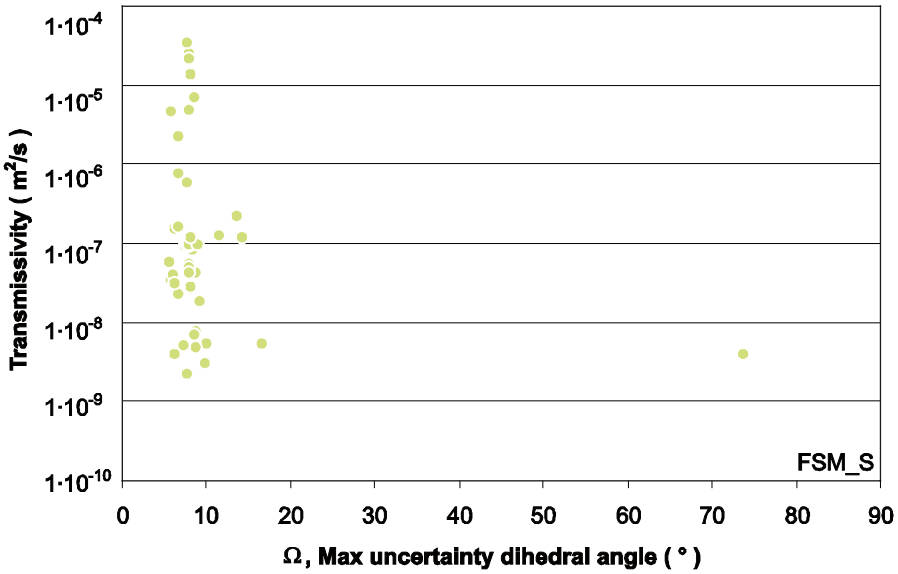

Figure 3-10. *The transmissivity versus the uncertainty of the PFL fractures in FSM_S.*

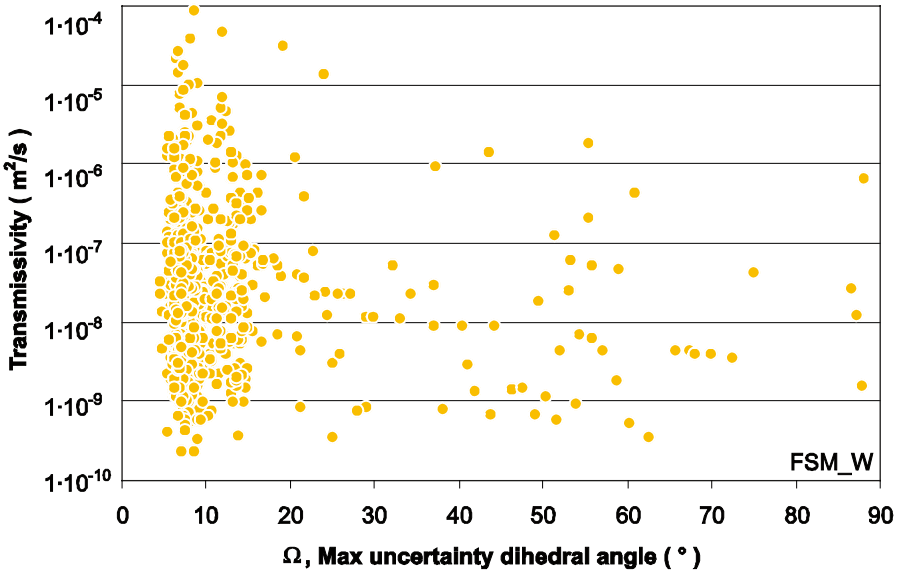

Figure 3-11. *The transmissivity versus the uncertainty of the PFL fractures in FSM_W.*

Table 3-1 shows that there does not seem to be any major differences in transmissivity or orientation uncertainty between the different fracture and rock domains. RSMM01 seem to have somewhat lower transmissivity and a little bit higher orientation uncertainty than the other rock domains. Regarding the fracture domains; FSM_N and FSM_S seem to have lower transmissivity values than the other fractures domains together with a higher orientation uncertainty in FSM_N, and lower orientation uncertainty in FSM_S, than the other domains.

Table 3-1. Statistics of transmissivity and maximum orientation uncertainty subdivided according to rock domains and fracture domains.

RSM/FSM	# of data	Transmissivity (m^2/s)			Log (T)			Orientation uncertainty (°)		
		X_{50}	$\bar{x}$	σ	X_{50}	$\bar{x}$	σ	X_{50}	$\bar{x}$	σ
RSMA01	923	$4.8 \cdot 10^{-8}$	$1.1 \cdot 10^{-6}$	$5.0 \cdot 10^{-6}$	–7.32	–7.26	1.01	8.9	14.6	17.3
RSMD01	618	$3.3 \cdot 10^{-8}$	$1.0 \cdot 10^{-6}$	$5.3 \cdot 10^{-6}$	–7.48	–7.41	1.05	7.9	12.5	13.0
RSMM01	384	$7.6 \cdot 10^{-9}$	$1.9 \cdot 10^{-7}$	$9.0 \cdot 10^{-7}$	–8.12	–7.92	0.92	9.5	12.8	12.2
FSM_C	164	$1.3 \cdot 10^{-8}$	$2.8 \cdot 10^{-7}$	$1.3 \cdot 10^{-6}$	–7.88	–7.77	0.99	8.2	11.6	11.0
FSM_EW007	378	$2.4 \cdot 10^{-8}$	$3.8 \cdot 10^{-7}$	$2.1 \cdot 10^{-6}$	–7.61	–7.53	0.92	8.3	12.4	13.7
FSM_N	488	$7.2 \cdot 10^{-8}$	$1.6 \cdot 10^{-6}$	$6.5 \cdot 10^{-6}$	–7.14	–7.06	1.02	9.5	16.4	19.8
FSM_NE005	247	$1.1 \cdot 10^{-8}$	$3.8 \cdot 10^{-7}$	$1.6 \cdot 10^{-6}$	–7.96	–7.76	1.03	9.4	13.0	13.4
FSM_S	46	$8.6 \cdot 10^{-8}$	$2.5 \cdot 10^{-6}$	$7.0 \cdot 10^{-6}$	–7.07	–7.02	1.11	8.1	9.8	9.9
FSM_W	620	$2.7 \cdot 10^{-8}$	$8.3 \cdot 10^{-7}$	$4.9 \cdot 10^{-6}$	–7.57	–7.50	1.02	8.5	13.0	13.0

4 References

Forsmark T, Wikström M, Forssman I, Rhén I, 2007. Oskarshamn site investigation. Correlation of Posiva Flow Log anomalies to core mapped features in KLX17A, KLX18A, KLX19A, KLX20A, KLX21B. SKB P-07-215, Svensk Kärnbränslehantering AB.

Kristiansson S, Pöllänen J, Väisäsvaara J, Kyllönen H, 2006. Difference flow logging of boreholes KLX22A, KLX22B, KLX23A, KLX23B, KLX24A and KLX25A. Subarea Laxemar. Oskarshamn site investigation. SKB P-06-246, Svensk Kärnbränslehantering AB.

La Pointe P, Fox A, Hermanson J, Öhman J, 2008. Site Descriptive Modeling Laxemar, Stage Site, Geological discrete fracture network model for the Laxemar site, version Site. SKB R-08-55, Svensk Kärnbränslehantering AB.

Munier R, Stigsson M, 2007. *in prep* Implementation of Uncertainties in borehole geometries and geological orientation data in SICADA. SKB R-07-19, Svensk Kärnbränslehantering AB.

Pöllänen J, 2007. Difference flow logging of boreholes KLX28A and KLX29A Subarea Laxemar. Oskarshamn site investigation. SKB P-07-17, Svensk Kärnbränslehantering AB

Sicada, 2008. Sicada_08_040

SKB, 2008. *in prep* Site descriptive modelling, SDM-Site Laxemar, Geology. SKB R-08-54, Svensk Kärnbränslehantering AB.

Teurneau B, Forsmark T, Forssman I, Rhén I, 2007. Oskarshamn site investigation. Correlation of Posiva Flow Log anomalies to core mapped features in KLX05, KLX06, KLX07A-B and KLX08. SKB P-07-212, Svensk Kärnbränslehantering AB.

Wikström M, Forsmark T, Teurneau B, Forssman I, Rhén I, 2007a. Oskarshamn site investigation. Correlation of Posiva Flow Log anomalies to core mapped features in KLX09, KLX09B-G. KLX10, KLX10B-C and KLX11A-F. SKB P-07-213, Svensk Kärnbränslehantering AB.

Wikström M, Forsmark T, Zetterlund M, Forssman I, Rhén I, 2007b. Oskarshamn site investigation. Correlation of Posiva Flow Log anomalies to core mapped features in KLX12A, KLX13A, KLX14A, KLX15A and KLX16A. SKB P-07-214, Svensk Kärnbränslehantering AB.

Wikström M, Forsmark T, Forssman I, Rhén I, 2007c. Oskarshamn site investigation. Correlation of Posiva Flow Log anomalies to core mapped features in KLX22A-B, KLX23A-B, KLX24A, KLX25A, KLX26A-B, KLX27A, KLX28A and KLX29A. SKB P-07-216, Svensk Kärnbränslehantering AB

Appendix A

Manually changed beta uncertainty.

During the work of this report an error was reported from Sicada, that the beta uncertainty values were calculated erroneous in Boremap. Instead of waiting for a new data delivery and thereby delaying the report, the author made the necessary calculations in p_fract_core_eshi /Sicada 2008/ to get the right beta uncertainty values.

The formula used was

$$\beta_{\text{uncertainty, NEW}} = \frac{\beta_{\text{uncertainty, OLD}} - A}{2} + A$$

Where

$$A = \begin{cases} 4 & 0 \le \alpha \le 30 \\ 5.6 & 30 < \alpha \le 60 \\ 25 & 60 < \alpha \le 90 \\ 70 & 0 \le \alpha \le 90 \end{cases} \; \textit{if} \; \begin{matrix} \text{and fracture} \\ \text{and fracture} \\ \text{and fracture} \\ \text{Non} - \textit{visible} \end{matrix} \; \begin{matrix} \text{Visible} \\ \text{Visible} \\ \text{Visible} \\ \end{matrix} \; \text{in BIPS}$$

Appendix B

Alternative couplings of PFL to fracture

For two of the PFL-f features that were concatenated as one, see Table 1-3, there are alternative interpretations. PFL no 52 in KLX07A might be coupled to the fracture with feature Id E417438B0A13141C and PFL no 27 in KLX19A might be coupled to 0099478B0A1490FB.

Below is shown the sample space, on 90th percentile, of the maximum uncertainty of the two alternative fractures.

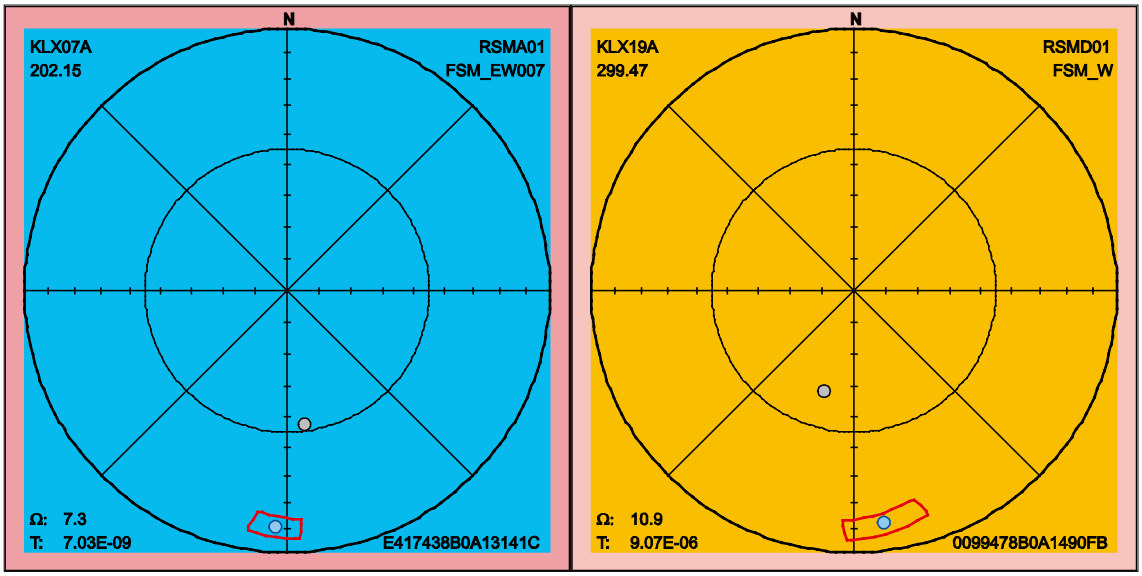

Appendix C

Microsoft Excel VBA code

```
Option Explicit

'*******************************************************************************
'*******************************************************************************
'*******************************************************************************
'***                                                                          ***
'*** Routines that was used in calculating the orientation uncertainty and   ***
'*** producing the sample spaces for the 0.9 percentile of the uncertainty    ***
'***                                                                          ***
'*******************************************************************************
'***                                                                          ***
'*** Input is:                                                               ***
'*** The current work book with the following data:                          ***
'***    Column A: IDCODE, i.e. borehole name                                  ***
'***    Column B: PFL anomaly number                                          ***
'***    Column C: Transmissivity                                              ***
'***    Column D: Feature ID                                                  ***
'***    Column E: Rock domain                                                 ***
'***    Column F: Fracture domain                                             ***
'***    Column G: arbitrary                                                   ***
'*** p_fract_core with columns containing the following                      ***
'***    Column F: Adjusted secup                                              ***
'***    Column AD: strike                                                     ***
'***    Column AE: dip                                                        ***
'***    Column AF: alpha                                                      ***
'***    Column AG: uncert alpha                                               ***
'***    Column AH: beta                                                       ***
'***    Column AI: uncert beta                                                ***
'*** p_object_location with columns containing the following                ***
'***    column H: length                                                      ***
'***    column O: Inclination                                                 ***
'***    column P: Bearing                                                     ***
'***    column Q: inclination uncertainty                                     ***
'***    column R: bearing uncertainty                                         ***
'***                                                                          ***
'*** Intermediate saved data in the current workbook                         ***
'***    column H: adjusted secup                                              ***
'***    Column I: strike                                                      ***
'***    Column J: dip                                                         ***
'***    Column K: alpha                                                       ***
'***    Column L: uncert alpha                                                ***
'***    Column M: beta                                                        ***
'***    Column N: uncert beta                                                 ***
'***    column O: Inclination                                                 ***
'***    column P: Bearing                                                     ***
'***    column Q: inclination uncertainty                                     ***
'***    column R: bearing uncertainty                                         ***
'***                                                                          ***
'*******************************************************************************
'***                                                                          ***
'*** A workbook called "template_uncertainty_plots.xls" is needed where the  ***
'*** template for the sample space stereograms is stored, and all data is     ***
'*** written and stored in different copies of the temlpate.                  ***
'***                                                                          ***
'*** The workbook have to containt the sheets:                               ***
'***    - above_30                                                            ***
'***    - omega_vs_T                                                          ***
'***    - max_uncert                                                          ***
'***    - template_uncert                                                     ***
'***                                                                          ***
'*******************************************************************************
'*******************************************************************************
'*******************************************************************************

Sub main()

Dim currentWorkbook As String
```

```
    currentWorkbook = ActiveWorkbook.Name


    Call get_data_from_p_fract_core(currentWorkbook, "p_fract_core_eshi_001.xls")
    Call get_data_from_p_fract_core(currentWorkbook, "p_fract_core_eshi_002.xls")
    Call get_data_from_p_fract_core(currentWorkbook, "p_fract_core_eshi_003.xls")

    Call get_data_from_object_location(currentWorkbook, "object_location.xls")

    Call check_written_data(currentWorkbook)

    Call make_uncertainty_plots(currentWorkbook)


End Sub
```

```
'*****************************************************************************
'*** Extract the needed information from p_fract_core_eshi and write to the  ***
'*** current workbook                                                        ***
'*****************************************************************************
Sub get_data_from_p_fract_core(currentWorkbook, fileName)

Dim currentFeatureID As String

Dim i As Long
Dim j As Long
Dim k As Long
Dim nofPFL As Integer
Dim nofFoundFrax As Integer

Dim featIDMatrix(1 To 2000) As String
Dim dataMatrix(1 To 2000, 1 To 7) As String

Dim PFLnumber(1 To 2000) As Integer


   Sheets("extract_from_IR_xl").Select
   Range("A1").Select

   'Save all Feature ID in a matrix
   i = 1
   While ActiveCell.Offset(i + 1, 0) <> ""
      featIDMatrix(i) = ActiveCell.Offset(i + 1, 3)
      i = i + 1
   Wend
   nofPFL = i - 1

   'Find data in p_fract_core
   Windows(fileName).Activate
   Range("A1").Select

   i = 1
   k = 1
   While ActiveCell.Offset(i, 0) <> ""
      currentFeatureID = ActiveCell.Offset(i, 59)
      For j = 1 To nofPFL
         If currentFeatureID = featIDMatrix(j) Then
            dataMatrix(k, 1) = ActiveCell.Offset(i, 5)   'Adjusted secup
            dataMatrix(k, 2) = ActiveCell.Offset(i, 29) 'strike
            dataMatrix(k, 3) = ActiveCell.Offset(i, 30) 'dip
            dataMatrix(k, 4) = ActiveCell.Offset(i, 31) 'alpha
            dataMatrix(k, 5) = ActiveCell.Offset(i, 32) 'uncert_alpha
            dataMatrix(k, 6) = ActiveCell.Offset(i, 33) 'beta
            dataMatrix(k, 7) = ActiveCell.Offset(i, 34) 'uncert_beta
            PFLnumber(k) = j
            k = k + 1
         End If
      Next j
      i = i + 1
   Wend
   nofFoundFrax = k - 1

   'write the saved data to the current workbook
   Windows(currentWorkbook).Activate
   Range("A1").Select

   For i = 1 To nofFoundFrax
      ActiveCell.Offset(PFLnumber(i) + 1, 7) = dataMatrix(i, 1)
      ActiveCell.Offset(PFLnumber(i) + 1, 8) = dataMatrix(i, 2)
      ActiveCell.Offset(PFLnumber(i) + 1, 9) = dataMatrix(i, 3)
      ActiveCell.Offset(PFLnumber(i) + 1, 10) = dataMatrix(i, 4)
      ActiveCell.Offset(PFLnumber(i) + 1, 11) = dataMatrix(i, 5)
      ActiveCell.Offset(PFLnumber(i) + 1, 12) = dataMatrix(i, 6)
      ActiveCell.Offset(PFLnumber(i) + 1, 13) = dataMatrix(i, 7)
   Next i
End Sub
```

```
'*****************************************************************************
'*** Save the orientation data of the boreholes and calculate the            ***
'*** orientation of the hole at each PFL fracture                            ***
'*****************************************************************************
Sub get_data_from_object_location(currentWorkbook, fileName)

Dim holeName As String

Dim i As Integer
Dim j As Integer

Dim adjSecUp As Single
Dim bearing As Single

Dim IDCODEmatrix(1 To 10000) As String
Dim dataMatrix(1 To 10000, 1 To 5) As Single


   'Save data from object_location
   Windows(fileName).Activate
   Range("A1").Select

   i = 1
   While ActiveCell.Offset(i + 1, 0) <> ""
      IDCODEmatrix(i) = ActiveCell.Offset(i + 1, 0)
      dataMatrix(i, 1) = ActiveCell.Offset(i + 1, 7)  'Length
      dataMatrix(i, 2) = ActiveCell.Offset(i + 1, 14) 'Inclination
      dataMatrix(i, 3) = ActiveCell.Offset(i + 1, 15) 'bearing
      dataMatrix(i, 4) = ActiveCell.Offset(i + 1, 16) 'inclination_uncert
      dataMatrix(i, 5) = ActiveCell.Offset(i + 1, 17) 'bearing_uncert

      i = i + 1
   Wend

   'Calculate the orientation at the current fracture
   'and write the data to the current workbook
   Windows(currentWorkbook).Activate
   Range("A1").Select

   i = 2
   While ActiveCell.Offset(i, 0) <> ""
      holeName = ActiveCell.Offset(i, 0)
      adjSecUp = ActiveCell.Offset(i, 7)

      'Skip all data untill the right Borehole name is found
      j = 1
      While IDCODEmatrix(j) <> holeName
         j = j + 1
      Wend

      'Find the current depth
      While adjSecUp > dataMatrix(j, 1)
         j = j + 1
      Wend

      'Calculate the bearing at current depth
      If Abs(dataMatrix(j, 3) - dataMatrix(j - 1, 3)) > 180 Then
         bearing = (dataMatrix(j, 3) + dataMatrix(j - 1, 3) + 360) / 2
         If bearing > 360 Then bearing = bearing - 360
      Else
         bearing = (dataMatrix(j, 3) + dataMatrix(j - 1, 3)) / 2
      End If

      'write the borehole data at the current depth to the workbook
      ActiveCell.Offset(i, 14) = (dataMatrix(j, 2) + dataMatrix(j - 1, 2)) / 2
      ActiveCell.Offset(i, 15) = bearing
      ActiveCell.Offset(i, 16) = dataMatrix(j, 4)
      ActiveCell.Offset(i, 17) = dataMatrix(j, 5)

      i = i + 1

   Wend

End Sub
```

```
'*****************************************************************************
'*** Calculate Strike and dip from alpha, beta, inclination and bearing and  ***
'*** compare with the values from p_fract_core_eshi                          ***
'*****************************************************************************
Sub check_written_data(currentWorkbook)

Dim i As Integer

Dim pi As Double
Dim pi_over180 As Double

Dim alpha180 As Double
Dim beta180 As Double
Dim bear180 As Double
Dim incl180 As Double
Dim strike180 As Double
Dim dip180 As Double

Dim alpha As Double
Dim beta As Double
Dim bear As Double
Dim incl As Double
Dim strike As Double
Dim dip As Double

Dim nx As Double
Dim ny As Double
Dim nz As Double
Dim xynx As Double
Dim xyny As Double

Dim cosAngle As Double
Dim sinAngle As Double

   pi = 4 * Atn(1)
   pi_over180 = Atn(1) / 45


   Windows(currentWorkbook).Activate
   Sheets("extract_from_IR_xl").Select
   Range("A1").Select

   i = 1
   While ActiveCell.Offset(i + 1, 0) <> ""
      alpha180 = ActiveCell.Offset(i + 1, 10)
      beta180 = ActiveCell.Offset(i + 1, 12)
      bear180 = ActiveCell.Offset(i + 1, 15)
      incl180 = ActiveCell.Offset(i + 1, 14)

      alpha = alpha180 * pi_over180
      beta = beta180 * pi_over180
      bear = bear180 * pi_over180
      incl = incl180 * pi_over180


      nx = Cos(pi / 2 - bear) * Sin(-incl) * Cos(-beta) * Cos(alpha) - Sin(pi / 2 -
bear) * Sin(-beta) * Cos(alpha) - Cos(pi / 2 - bear) * Cos(-incl) * Sin(alpha)
      ny = Sin(pi / 2 - bear) * Sin(-incl) * Cos(-beta) * Cos(alpha) + Cos(pi / 2 -
bear) * Sin(-beta) * Cos(alpha) - Sin(pi / 2 - bear) * Cos(-incl) * Sin(alpha)
      nz = Cos(-incl) * Cos(-beta) * Cos(alpha) + Sin(-incl) * Sin(alpha)


      strike180 = nx ^ 2 + ny ^ 2 + nz ^ 2

      If nz > 0 Then
         nz = -nz
         xynx = -nx / (nx ^ 2 + ny ^ 2) ^ 0.5
         xyny = -ny / (nx ^ 2 + ny ^ 2) ^ 0.5
      Else
         xynx = nx / (nx ^ 2 + ny ^ 2) ^ 0.5
         xyny = ny / (nx ^ 2 + ny ^ 2) ^ 0.5
      End If
```

```
        'Arcsin(x) = Atn(x / Sqr(-x * x + 1))
        'Arccos(x) = Atn(-x / Sqr(-x * x + 1)) + 2 * Atn(1)
        dip180 = 90 + Atn(nz / Sqr(-nz * nz + 1)) / pi_over180

        cosAngle = (Atn(-xynx / Sqr(-xynx * xynx + 1)) + 2 * Atn(1)) / pi_over180
        sinAngle = Atn(xyny / Sqr(-xyny * xyny + 1)) / pi_over180


        If sinAngle >= 0 Then
           strike180 = 180 - cosAngle
        Else
           strike180 = 180 + cosAngle
        End If

        ActiveCell.Offset(i + 1, 18) = strike180
        ActiveCell.Offset(i + 1, 19) = dip180
        i = i + 1
    Wend

End Sub
```

```
'*****************************************************************************
'*** Make all the uncertainty plots from the intermediate storede data in    ***
'*** this workbook                                                           ***
'*****************************************************************************
Sub make_uncertainty_plots(currentWorkbook)

Dim holeName As String
Dim transmissivity As String
Dim featureID As String
Dim RSM As String
Dim FSM As String
Dim length As String
Dim PFLnumber As String

Dim i As Integer
Dim nofData As Integer

Dim alpha As Double
Dim alphaUnc As Double
Dim beta As Double
Dim betaUnc As Double

Dim bear As Double
Dim bearUnc As Double
Dim incl As Double
Dim inclUnc As Double

Dim strike As Double
Dim dip As Double

Dim omega As Double

Dim boundingStrikeDip(1 To 300, 1 To 2) As Double

   Windows(currentWorkbook).Activate
   Sheets("extract_from_IR_xl").Select
   Range("A1").Select

   i = 2
   holeName = ActiveCell.Offset(1, 0)

   'Run through all lines of data
   While ActiveCell.Offset(i, 0) <> ""

      'If a new borehole starts;
      '   - sort the uncertainty data
      '   - Close the workbook
      '   - Create a new workbook for the new borehole
      If holeName <> ActiveCell.Offset(i, 0) Then
         If i <> 2 Then 'The first time there is no workbook to close
            Call SortUncertdata(holeName)
            Call CloseUncertWorkbook(holeName)
         End If
         holeName = ActiveCell.Offset(i, 0)
         Call MakeUncertWorkbook(holeName)
      End If

      'Read current data
      Windows(currentWorkbook).Activate
      Sheets("extract_from_IR_xl").Select
      Range("A1").Select

      alpha = ActiveCell.Offset(i, 10)
      alphaUnc = ActiveCell.Offset(i, 11)
      beta = ActiveCell.Offset(i, 12)
      betaUnc = ActiveCell.Offset(i, 13)

      bear = ActiveCell.Offset(i, 15)
      bearUnc = ActiveCell.Offset(i, 17)
      incl = ActiveCell.Offset(i, 14)
      inclUnc = ActiveCell.Offset(i, 16)
```

```
        transmissivity = Format(ActiveCell.Offset(i, 2), "0.00E-00")
        If ActiveCell.Offset(i, 2) = "" Then transmissivity = ""

        PFLnumber = ActiveCell.Offset(i, 1)
        featureID = ActiveCell.Offset(i, 3)
        RSM = ActiveCell.Offset(i, 4)
        FSM = ActiveCell.Offset(i, 5)
        length = ActiveCell.Offset(i, 7)

        strike = ActiveCell.Offset(i, 8)
        dip = ActiveCell.Offset(i, 9)

        'Calculate and save the current sample space
        Call Calculate_samplespace_surface(currentWorkbook, alpha, alphaUnc, beta,
betaUnc, bear, bearUnc, incl, inclUnc, boundingStrikeDip, nofData, omega)
        'Create new sheet and printi
        Call create_new_uncert_sheet(holeName, featureID, transmissivity, RSM, FSM,
length, strike, dip, bear, incl, omega, PFLnumber)
        Call print_data_sheet(boundingStrikeDip, nofData)
        Call print_omega_on_Max_uncert_sheet(omega, featureID, holeName)
        Call print_omega_vs_T_on_sheet(omega, transmissivity, featureID, holeName,
PFLnumber, length, RSM, FSM)

        Windows(currentWorkbook).Activate
        Sheets("extract_from_IR_xl").Select
        Range("A1").Select

        i = i + 1
    Wend

    'Sort and close the last borehole data
    Call SortUncertdata(holeName)
    Call CloseUncertWorkbook(holeName)

End Sub
```

```
'*****************************************************************************
'*** Printing the data on the sheet omega_vs_T and the values if omega is    ***
'*** greater than 30 degres, on the above_30 sheet                           ***
'*****************************************************************************
Sub print_omega_vs_T_on_sheet(omega, transmissivity, featID, BHName, PFLno, adjSecUp,
RSM, FSM)

Dim i As Integer

   Sheets("omega_vs_T").Select
   Range("A1").Select

   'Find next empty row
   i = 0
   While ActiveCell.Offset(i, 0) <> ""
      i = i + 1
   Wend

   'Write data
   If transmissivity <> "" Then
      ActiveCell.Offset(i, 0) = BHName
      ActiveCell.Offset(i, 1) = PFLno
      ActiveCell.Offset(i, 2) = adjSecUp
      ActiveCell.Offset(i, 3) = featID
      ActiveCell.Offset(i, 4) = omega
      ActiveCell.Offset(i, 5) = transmissivity
      ActiveCell.Offset(i, 6) = RSM
      ActiveCell.Offset(i, 7) = FSM
   End If

   'If Omega is larger than 30 degrees save the fracture on the above_30 sheet
   If omega > 30 Then
      Sheets("above_30").Select
      Range("A1").Select

      'Find next empty row
      i = 0
      While ActiveCell.Offset(i, 0) <> ""
         i = i + 1
      Wend

      'Write data
      ActiveCell.Offset(i, 0) = featID
      ActiveCell.Offset(i, 1) = PFLno
      ActiveCell.Offset(i, 2) = adjSecUp
      ActiveCell.Offset(i, 3) = omega
   End If


End Sub
```

```
'*****************************************************************************
'*** Printing the data on the sheet Max_uncert                             ***
'*****************************************************************************
Sub print_omega_on_Max_uncert_sheet(maxDihedral, featID, BHName)

Dim i As Integer
   Sheets("max_uncert").Select
   Range("A1").Select

   ActiveCell.Offset(0, 3) = BHName

   'Find the next empty row
   i = 0
   While ActiveCell.Offset(i, 0) <> ""
      i = i + 1
   Wend

   ActiveCell.Offset(i, 0) = featID
   ActiveCell.Offset(i, 1) = maxDihedral

End Sub


'*****************************************************************************
'*** Sort the data and calculate the cumulative denstity function numbers   ***
'*****************************************************************************
Sub SortUncertdata(holeName)
Dim i As Integer
Dim nofData As Integer

   Windows(holeName & "_uncert_plots.xls").Activate
   Sheets("max_uncert").Select

   'Sort the data
   Columns("A:B").Select
   Selection.Sort Key1:=Range("B1"), Order1:=xlDescending, Header:=xlGuess, _
      OrderCustom:=1, MatchCase:=False, Orientation:=xlTopToBottom, _
      DataOption1:=xlSortNormal
   Range("A1").Select

   'Find the number of data
   i = 0
   While ActiveCell.Offset(i, 0) <> ""
      i = i + 1
   Wend
   nofData = i

   'Write the CDF numbers from 1 to 0
   For i = 1 To nofData
      ActiveCell.Offset(i - 1, 2) = 1 - (i - 1) / (nofData - 1)
   Next

End Sub


'*****************************************************************************
'*** Save and Close the workbook                                           ***
'*****************************************************************************
Sub CloseUncertWorkbook(holeName)

   Windows(holeName & "_uncert_plots.xls").Activate

   ActiveWorkbook.Save

   Windows(holeName & "_uncert_plots.xls").Close

End Sub
```

```
'*****************************************************************************
'*** Create a new uncertainty sheet, write data (except the samplespace) and ***
'*** colour the stereogram based on FSM and RSM                              ***
'*****************************************************************************
Sub create_new_uncert_sheet(holeName, featID, transmissivity, RSM, FSM, length, strike,
dip, bear, incl, omega, PFLno)

Dim pi As Double

   pi = Atn(1) * 4

   'Copy the template and rename
   Windows(holeName & "_uncert_plots.xls").Activate
   Sheets("Template_uncert").Select
   Sheets("Template_uncert").Copy Before:=Sheets("Template_uncert")
   Sheets("Template_uncert (2)").Select
   Sheets("Template_uncert (2)").Name = holeName & "_" & featID & "_PFL_" & PFLno
   Range("A1").Select

   'write Data
   ActiveCell.Offset(6, 1) = bear
   ActiveCell.Offset(6, 2) = incl
   ActiveCell.Offset(6, 3) = Cos((90 - bear) * pi / 180) * 2 ^ 0.5 * Sin((90 + incl) / 2
* pi / 180)
   ActiveCell.Offset(6, 4) = Sin((90 - bear) * pi / 180) * 2 ^ 0.5 * Sin((90 + incl) / 2
* pi / 180)

   ActiveCell.Offset(8, 1) = strike
   ActiveCell.Offset(8, 2) = dip
   ActiveCell.Offset(8, 3) = Cos((180 - strike) * pi / 180) * 2 ^ 0.5 * Sin(dip / 2 * pi
/ 180)
   ActiveCell.Offset(8, 4) = Sin((180 - strike) * pi / 180) * 2 ^ 0.5 * Sin(dip / 2 * pi
/ 180)

   ActiveCell.Offset(11, 7) = holeName
   ActiveCell.Offset(12, 7) = length
   ActiveCell.Offset(13, 7) = RSM
   ActiveCell.Offset(14, 7) = FSM
   ActiveCell.Offset(15, 7) = omega
   ActiveCell.Offset(15, 7) = FormatNumber(omega, 1)
   If transmissivity <> "" Then
      ActiveCell.Offset(16, 7) = transmissivity
   Else
      ActiveCell.Offset(16, 7) = "-"
   End If
   ActiveCell.Offset(17, 7) = featID

   'Colour the Stereogram interior based on Fracture domain
   ActiveSheet.ChartObjects("Chart 1").Activate
   ActiveChart.PlotArea.Select

   Select Case FSM
      Case "FSM_C"
         With Selection.Interior
            .ColorIndex = 38
         End With
      Case "FSM_EW007"
         With Selection.Interior
            .ColorIndex = 40
         End With
      Case "FSM_N"
         With Selection.Interior
            .ColorIndex = 36
         End With
      Case "FSM_NE005"
         With Selection.Interior
            .ColorIndex = 35
         End With
      Case "FSM_S"
         With Selection.Interior
            .ColorIndex = 34
         End With
      Case "FSM_W"
```

```
            With Selection.Interior
               .ColorIndex = 37
            End With
         Case Else
            With Selection.Interior
               .ColorIndex = 2
            End With
       End Select


      'Colour the Stereogram frame based on rock domain
      ActiveChart.ChartArea.Select
      Select Case RSM
         Case "RSMA01"
            With Selection.Interior
               .ColorIndex = 7
            End With
         Case "RSMD01"
            With Selection.Interior
               .ColorIndex = 44
            End With
         Case "RSMM01"
            With Selection.Interior
               .ColorIndex = 6
            End With
         Case Else
            With Selection.Interior
               .ColorIndex = 2
            End With
      End Select

      Range("A1").Select

End sub
```

```
'*****************************************************************************
'*** Print the sample space data to the stereonet using equal area lower     ***
'*** hemisphere                                                              ***
'*****************************************************************************
Sub print_data_sheet(boundingStrikeDip, nofData)

Dim i As Integer
Dim p As Integer

Dim dist As Double
Dim strikeAngle As Double
Dim pi As Double

   pi = Atn(1) * 4

   ActiveCell.Offset(10, 1) = boundingStrikeDip(1, 1)
   ActiveCell.Offset(10, 2) = boundingStrikeDip(1, 2)
   ActiveCell.Offset(10, 3) = Cos((180 - boundingStrikeDip(1, 1)) * pi / 180) * 2 ^ 0.5
* Sin(boundingStrikeDip(1, 2) / 2 * pi / 180)
   ActiveCell.Offset(10, 4) = Sin((180 - boundingStrikeDip(1, 1)) * pi / 180) * 2 ^ 0.5
* Sin(boundingStrikeDip(1, 2) / 2 * pi / 180)

   p = 2

   'If the data is on oposite sides of the stereonet then calculate the
   'intersection to the border and make a blank row to break the line
   For i = 2 To nofData
      dist = ((Cos((180 - boundingStrikeDip(i, 1)) * pi / 180) * 2 ^ 0.5 *
Sin(boundingStrikeDip(i, 2) / 2 * pi / 180) _
            - Cos((180 - boundingStrikeDip(i - 1, 1)) * pi / 180) * 2 ^ 0.5 *
Sin(boundingStrikeDip(i - 1, 2) / 2 * pi / 180)) ^ 2 _
           + (Sin((180 - boundingStrikeDip(i, 1)) * pi / 180) * 2 ^ 0.5 *
Sin(boundingStrikeDip(i, 2) / 2 * pi / 180) _
            - Sin((180 - boundingStrikeDip(i - 1, 1)) * pi / 180) * 2 ^ 0.5 *
Sin(boundingStrikeDip(i - 1, 2) / 2 * pi / 180)) ^ 2) ^ 0.5

      If dist > 1 Then
         strikeAngle = boundingStrikeDip(i, 1) + 180
         ActiveCell.Offset(p + 9, 1) = strikeAngle
         ActiveCell.Offset(p + 9, 2) = 90
         ActiveCell.Offset(p + 9, 3) = Cos((180 - strikeAngle) * pi / 180)
         ActiveCell.Offset(p + 9, 4) = Sin((180 - strikeAngle) * pi / 180)

         p = p + 2
         strikeAngle = boundingStrikeDip(i - 1, 1) + 180
         ActiveCell.Offset(p + 9, 1) = strikeAngle
         ActiveCell.Offset(p + 9, 2) = 90
         ActiveCell.Offset(p + 9, 3) = Cos((180 - strikeAngle) * pi / 180)
         ActiveCell.Offset(p + 9, 4) = Sin((180 - strikeAngle) * pi / 180)
         p = p + 1

      End If

      ActiveCell.Offset(p + 9, 1) = boundingStrikeDip(i, 1)
      ActiveCell.Offset(p + 9, 2) = boundingStrikeDip(i, 2)
      ActiveCell.Offset(p + 9, 3) = Cos((180 - boundingStrikeDip(i, 1)) * pi / 180) * 2
^ 0.5 * Sin(boundingStrikeDip(i, 2) / 2 * pi / 180)
      ActiveCell.Offset(p + 9, 4) = Sin((180 - boundingStrikeDip(i, 1)) * pi / 180) * 2
^ 0.5 * Sin(boundingStrikeDip(i, 2) / 2 * pi / 180)
      p = p + 1
   Next i

End Sub
```

```
'*****************************************************************************
'***  calculate the sample space using the uncertainties from the fracture   ***
'***  and borehole                                                           ***
'*****************************************************************************
Sub Calculate_samplespace_surface(currentWorkbook, alpha, alphaUnc, beta, betaUnc, bear,
bearUnc, incl, inclUnc, boundingStrikeDip, nofData, omega)

Dim more2Find As Boolean
Dim larger As Boolean
Dim smaller As Boolean

Dim i As Integer
Dim j As Integer
Dim k As Integer
Dim m As Integer
Dim n As Integer
Dim p As Integer

Dim nofBIpairs As Integer
Dim nofBetaStep As Integer
Dim nofAlphaStep As Integer
Dim nofAlphaStepMinBetaCouple As Integer
Dim nofAlphaStepMaxBetaCouple As Integer
Dim dataToSave As Integer
Dim nofAlphaUnc As Double
Dim nofBetaUnc As Double
Dim nofBearUncert As Double
Dim nofInclUncert As Double

Dim fracStrike As Double
Dim fracDip As Double

Dim strike180 As Double
Dim dip180 As Double
Dim alpha180 As Double
Dim beta180 As Double

Dim tempBear As Double
Dim tempIncl As Double

Dim maxBeta As Double
Dim minBeta As Double
Dim maxAlpha As Double
Dim minAlpha As Double

Dim betaStepLength As Double
Dim alphaStepLength As Double
Dim inclStepLength As Double
Dim bearStepLength As Double

Dim dist As Double
Dim minDist As Double

Dim tempOmega As Double

Dim usable(1 To 300) As Boolean

Dim alphaBetaMatrix(1 To 120, 1 To 2, 1 To 101) As Double
Dim tempMaxAlphaCouple(1 To 200, 1 To 2) As Double
Dim tempMinAlphaCouple(1 To 200, 1 To 2) As Double
Dim tempMaxBetaCouple(1 To 200, 1 To 2) As Double
Dim tempMinBetaCouple(1 To 200, 1 To 2) As Double
Dim MaxBetaCouple(1 To 200, 1 To 2) As Double
Dim MinBetaCouple(1 To 200, 1 To 2) As Double

Dim tempBoundingAlphaBeta(1 To 300, 1 To 2) As Double
Dim boundingAlphaBeta(1 To 300, 1 To 2) As Double

   'Decide number of parts to divide the uncertainties in
   nofAlphaUnc = Int(alphaUnc / 2) + 1
   nofBetaUnc = Int(betaUnc / 2) + 1
   nofBearUncert = Int(bearUnc / 2) + 1
   nofInclUncert = Int(inclUnc / 2) + 1
```

```
   'At least 2 parts...
   If nofAlphaUnc < 2 Then nofAlphaUnc = 2
   If nofBetaUnc < 2 Then nofBetaUnc = 2
   If nofBearUncert < 2 Then nofBearUncert = 2
   If nofInclUncert < 2 Then nofInclUncert = 2
   '...and not more than 30 for the a/b uncertainty together with 10 for B/I uncertainty
   If nofAlphaUnc > 30 Then nofAlphaUnc = 30
   If nofBetaUnc > 50 Then nofBetaUnc = 50
   If nofBearUncert > 30 Then nofBearUncert = 30
   If nofInclUncert > 10 Then nofInclUncert = 10

   'calculate the length of the incremental steps in alpha and beta space
   betaStepLength = 2 * betaUnc / nofBetaUnc
   alphaStepLength = 2 * alphaUnc / nofAlphaUnc

   nofData = (nofAlphaUnc + 1) * 2 + (nofBetaUnc + 1) * 2

   'make the matrix with the circumferense alpha beta values
   k = 1
   For j = 0 To nofAlphaUnc
      alphaBetaMatrix(k, 1, 1) = alpha - alphaUnc + j * alphaStepLength
      alphaBetaMatrix(k, 2, 1) = beta - betaUnc
      k = k + 1
   Next j
   For j = 0 To nofBetaUnc
      alphaBetaMatrix(k, 1, 1) = alpha + alphaUnc
      alphaBetaMatrix(k, 2, 1) = beta - betaUnc + j * betaStepLength
      k = k + 1
   Next j
   For j = nofAlphaUnc To 0 Step -1
      alphaBetaMatrix(k, 1, 1) = alpha - alphaUnc + j * alphaStepLength
      alphaBetaMatrix(k, 2, 1) = beta + betaUnc
      k = k + 1
   Next j

   For j = nofBetaUnc To 0 Step -1
      alphaBetaMatrix(k, 1, 1) = alpha - alphaUnc
      alphaBetaMatrix(k, 2, 1) = beta - betaUnc + j * betaStepLength
      k = k + 1
   Next j

   p = 2 'on first layer the best alpha and beta circumferense for the mid bear/incl is
stored
   inclStepLength = 2 * inclUnc / nofInclUncert
   bearStepLength = 2 * bearUnc / nofBearUncert

   'Calculate the strike and dip using the bearing+-uncertainty and inclination+-uncert
   'then calculate which alpha/beta values this corresponds to using the best estimated
bearing and inclination, i.e. variables bear and incl read from object_location
   For m = 0 To nofInclUncert
      For n = 0 To nofBearUncert

         For j = 1 To nofData
            tempBear = bear - bearUnc + n * bearStepLength
            tempIncl = incl - inclUnc + m * inclStepLength
            'If the inclination pass through vertical then the bearing need to be
adjusted as well
            If tempIncl < -90 Then tempBear = tempBear + 180
            If tempBear > 360 Then tempBear = tempBear - 360

            If alphaBetaMatrix(j, 1, 1) > 90 Then
               Call calc_strike_dip(180 - alphaBetaMatrix(j, 1, 1), alphaBetaMatrix(j,
2, 1) + 180, tempBear, tempIncl, strike180, dip180)
               Call calc_alpha_beta(strike180, dip180, bear, incl, alpha180, beta180)

               alphaBetaMatrix(j, 1, p) = 180 - alpha180
               alphaBetaMatrix(j, 2, p) = beta180 + 180
               If alphaBetaMatrix(j, 2, p) > 360 Then alphaBetaMatrix(j, 2, p) =
alphaBetaMatrix(j, 2, p) - 360

            ElseIf alphaBetaMatrix(j, 1, 1) < 0 Then
               Call calc_strike_dip(-alphaBetaMatrix(j, 1, 1), alphaBetaMatrix(j, 2, 1)
+ 180, tempBear, tempIncl, strike180, dip180)
```

```
                Call calc_alpha_beta(strike180, dip180, bear, incl, alpha180, beta180)

                alphaBetaMatrix(j, 1, p) = -alpha180
                alphaBetaMatrix(j, 2, p) = beta180 + 180
                If alphaBetaMatrix(j, 2, p) > 360 Then alphaBetaMatrix(j, 2, p) =
alphaBetaMatrix(j, 2, p) - 360

            Else
                Call calc_strike_dip(alphaBetaMatrix(j, 1, 1), alphaBetaMatrix(j, 2, 1),
tempBear, tempIncl, strike180, dip180)
                Call calc_alpha_beta(strike180, dip180, bear, incl, alpha180, beta180)

                alphaBetaMatrix(j, 1, p) = alpha180
                alphaBetaMatrix(j, 2, p) = beta180

            End If

         Next j
         p = p + 1
      Next n
   Next m


   'calculate number of surfaces due to the division of Bearing and inclination
   nofBIpairs = (nofInclUncert + 1) * (nofBearUncert + 1)


   'Make all beta-values to be within the same 360° range
   For m = 2 To nofBIpairs + 1 'on layer 1 the circumference of alpha/beta values are
stored,
                               'and the ones corresponding to uncertainties in the
borehole direction
                               'is hence stored on layer 2 to number of combinations+1
      For j = 1 To nofData
         If Abs(alphaBetaMatrix(j, 2, m) - alphaBetaMatrix(j, 2, 1)) > 180 Then
            If alphaBetaMatrix(j, 2, m) > alphaBetaMatrix(j, 2, 1) Then
               alphaBetaMatrix(j, 2, m) = alphaBetaMatrix(j, 2, m) - 360
            Else
               alphaBetaMatrix(j, 2, m) = alphaBetaMatrix(j, 2, m) + 360
            End If
         End If
      Next j
   Next m

   'Find maximum and minimum alpha and beta values
   maxBeta = -720
   minBeta = 720
   maxAlpha = -90
   minAlpha = 90

   For m = 1 To nofBIpairs + 1
      For j = 1 To nofData
         If alphaBetaMatrix(j, 1, m) < minAlpha Then minAlpha = alphaBetaMatrix(j, 1, m)
         If alphaBetaMatrix(j, 1, m) > maxAlpha Then maxAlpha = alphaBetaMatrix(j, 1, m)
         If alphaBetaMatrix(j, 2, m) < minBeta Then minBeta = alphaBetaMatrix(j, 2, m)
         If alphaBetaMatrix(j, 2, m) > maxBeta Then maxBeta = alphaBetaMatrix(j, 2, m)
      Next
   Next

   'calculate new steps including the whole span of values
   nofBetaStep = Int((maxBeta - minBeta) / betaStepLength)
   nofAlphaStep = Int((maxAlpha - minAlpha) / alphaStepLength)
   betaStepLength = (maxBeta - minBeta) / nofBetaStep
   alphaStepLength = (maxAlpha - minAlpha) / nofAlphaStep

   'Initiate matrices containing the extreme values
   For k = 1 To 200
      tempMaxAlphaCouple(k, 1) = -90
      tempMinAlphaCouple(k, 1) = 90
      tempMaxBetaCouple(k, 2) = -720
      tempMinBetaCouple(k, 2) = 720
   Next k
```

```
   'Find the largest and smallest Alpha values
   For k = 0 To nofBetaStep
      For m = 1 To nofBIpairs + 1
         For j = 1 To nofData
            If alphaBetaMatrix(j, 2, m) <= minBeta + k * betaStepLength + betaStepLength
/ 2 Then    'if beta value is less than upper bound
               If alphaBetaMatrix(j, 2, m) >= minBeta + k * betaStepLength -
betaStepLength / 2 Then 'if beta value is larger than lower bound
                  If alphaBetaMatrix(j, 1, m) > tempMaxAlphaCouple(k + 1, 1) Then
                     tempMaxAlphaCouple(k + 1, 1) = alphaBetaMatrix(j, 1, m)
                     tempMaxAlphaCouple(k + 1, 2) = alphaBetaMatrix(j, 2, m)
                  End If
                  If alphaBetaMatrix(j, 1, m) < tempMinAlphaCouple(k + 1, 1) Then
                     tempMinAlphaCouple(k + 1, 1) = alphaBetaMatrix(j, 1, m)
                     tempMinAlphaCouple(k + 1, 2) = alphaBetaMatrix(j, 2, m)
                  End If
               End If
            End If

         Next j
      Next m
   Next k

   'Find the largest and smallest beta values
   For k = 0 To nofAlphaStep
      For m = 1 To nofBIpairs + 1
         For j = 1 To nofData
            If alphaBetaMatrix(j, 1, m) < minAlpha + k * alphaStepLength +
alphaStepLength / 2 Then
               If alphaBetaMatrix(j, 1, m) > minAlpha + k * alphaStepLength -
alphaStepLength / 2 Then
                  If alphaBetaMatrix(j, 2, m) > tempMaxBetaCouple(k + 1, 2) Then
                     tempMaxBetaCouple(k + 1, 1) = alphaBetaMatrix(j, 1, m)
                     tempMaxBetaCouple(k + 1, 2) = alphaBetaMatrix(j, 2, m)
                  End If
                  If alphaBetaMatrix(j, 2, m) < tempMinBetaCouple(k + 1, 2) Then
                     tempMinBetaCouple(k + 1, 1) = alphaBetaMatrix(j, 1, m)
                     tempMinBetaCouple(k + 1, 2) = alphaBetaMatrix(j, 2, m)
                  End If
               End If
            End If

         Next j
      Next m
   Next k

   'Erase numbers larger than smallest alfa edge and smaller than largest alfa edge on
the max and min beta edges
   m = 0
   For k = 1 To nofAlphaStep + 1
      larger = False
      If tempMinBetaCouple(k, 2) >= tempMaxAlphaCouple(1, 2) Then larger = True
      If tempMinBetaCouple(k, 2) >= tempMinAlphaCouple(nofBetaStep + 1, 2) Then larger =
True
      If larger = False Then
         m = m + 1
         MinBetaCouple(m, 1) = tempMinBetaCouple(k, 1)
         MinBetaCouple(m, 2) = tempMinBetaCouple(k, 2)
      End If
   Next k
   nofAlphaStepMinBetaCouple = m

   m = 0
   For k = 1 To nofAlphaStep + 1
      smaller = False
      If tempMaxBetaCouple(k, 2) <= tempMaxAlphaCouple(nofBetaStep + 1, 2) Then smaller
= True
      If tempMaxBetaCouple(k, 2) <= tempMinAlphaCouple(1, 2) Then smaller = True
      If smaller = False Then
         m = m + 1
         MaxBetaCouple(m, 1) = tempMaxBetaCouple(k, 1)
         MaxBetaCouple(m, 2) = tempMaxBetaCouple(k, 2)
      End If
```

```
   Next k
   nofAlphaStepMaxBetaCouple = m


   'Concatenate the bounding lines to one circumference
   m = 1
   For k = 1 To nofAlphaStepMinBetaCouple
      tempBoundingAlphaBeta(m, 1) = MinBetaCouple(k, 1)
      tempBoundingAlphaBeta(m, 2) = MinBetaCouple(k, 2)
      m = m + 1
   Next k
   For k = 1 To nofBetaStep + 1
      tempBoundingAlphaBeta(m, 1) = tempMaxAlphaCouple(k, 1)
      tempBoundingAlphaBeta(m, 2) = tempMaxAlphaCouple(k, 2)
      m = m + 1
   Next k
   For k = nofAlphaStepMaxBetaCouple To 1 Step -1
      tempBoundingAlphaBeta(m, 1) = MaxBetaCouple(k, 1)
      tempBoundingAlphaBeta(m, 2) = MaxBetaCouple(k, 2)
      m = m + 1
   Next k
   For k = nofBetaStep + 1 To 1 Step -1
      tempBoundingAlphaBeta(m, 1) = tempMinAlphaCouple(k, 1)
      tempBoundingAlphaBeta(m, 2) = tempMinAlphaCouple(k, 2)
      m = m + 1
   Next k
   nofData = m
   tempBoundingAlphaBeta(m, 1) = tempBoundingAlphaBeta(1, 1)
   tempBoundingAlphaBeta(m, 2) = tempBoundingAlphaBeta(1, 2)


   'Calculate the orientations in strike/dip space
   For k = 1 To nofData
      Call calc_strike_dip(tempBoundingAlphaBeta(k, 1), tempBoundingAlphaBeta(k, 2),
bear, incl, strike180, dip180)
      boundingStrikeDip(k, 1) = strike180
      boundingStrikeDip(k, 2) = dip180
   Next k

   'Calculate maximum omega
   omega = 0
   Call calc_strike_dip(alpha, beta, bear, incl, fracStrike, fracDip)
   For k = 1 To nofData
      tempOmega = dihedral(boundingStrikeDip(k, 1), boundingStrikeDip(k, 2), fracStrike,
fracDip)
      If tempOmega > omega Then omega = tempOmega
   Next k

End Sub
```

```
'*****************************************************************************
'*** Save the uncertainty template to the name of the current borehole       ***
'*****************************************************************************
Sub MakeUncertWorkbook(holeName)

    Workbooks.Open fileName:= _
        "template_uncertainty_plots.xls"

    ActiveWorkbook.SaveAs fileName:= _
        holeName & "_uncert_plots.xls", _
        FileFormat:=xlNormal, Password:="", WriteResPassword:="", _
        ReadOnlyRecommended:=False, CreateBackup:=False

End Sub
```

```
'*****************************************************************************
'*** Calculate strike an dip from Alpha, beta, bearing and inclination       ***
'*****************************************************************************
Sub calc_strike_dip(alpha180, beta180, bear180, incl180, strike180, dip180)

Dim pi As Double
Dim pi_over180 As Double
Dim alpha As Double
Dim beta As Double
Dim bear As Double
Dim incl As Double
Dim strike As Double
Dim dip As Double

Dim nx As Double
Dim ny As Double
Dim nz As Double
Dim xynx As Double
Dim xyny As Double

Dim cosAngle As Double
Dim sinAngle As Double

   pi = 4 * Atn(1)
   pi_over180 = Atn(1) / 45

   alpha = alpha180 * pi_over180
   beta = beta180 * pi_over180
   bear = bear180 * pi_over180
 incl = incl180 * pi_over180


   nx = Cos(pi / 2 - bear) * Sin(-incl) * Cos(-beta) * Cos(alpha) - Sin(pi / 2 - bear) *
Sin(-beta) * Cos(alpha) - Cos(pi / 2 - bear) * Cos(-incl) * Sin(alpha)
   ny = Sin(pi / 2 - bear) * Sin(-incl) * Cos(-beta) * Cos(alpha) + Cos(pi / 2 - bear) *
Sin(-beta) * Cos(alpha) - Sin(pi / 2 - bear) * Cos(-incl) * Sin(alpha)
   nz = Cos(-incl) * Cos(-beta) * Cos(alpha) + Sin(-incl) * Sin(alpha)

   If nz > 0 Then
      nz = -nz
      xynx = -nx / (nx ^ 2 + ny ^ 2) ^ 0.5
      xyny = -ny / (nx ^ 2 + ny ^ 2) ^ 0.5
   Else
      xynx = nx / (nx ^ 2 + ny ^ 2) ^ 0.5
      xyny = ny / (nx ^ 2 + ny ^ 2) ^ 0.5
   End If

   'Arcsin(x) = Atn(x / Sqr(-x * x + 1))
   'Arccos(x) = Atn(-x / Sqr(-x * x + 1)) + 2 * Atn(1)
   dip180 = 90 + Atn(nz / Sqr(-nz * nz + 1)) / pi_over180

   If Abs(xynx) < 1 Then
      cosAngle = (Atn(-xynx / Sqr(-xynx * xynx + 1)) + 2 * Atn(1)) / pi_over180
   ElseIf xynx >= 1 Then
      cosAngle = 0
   Else
      cosAngle = 180
   End If

   If Abs(xyny) < 1 Then
      sinAngle = Atn(xyny / Sqr(-xyny * xyny + 1)) / pi_over180
   ElseIf xyny >= 1 Then
      sinAngle = 90
   Else
      sinAngle = -90
   End If

   If sinAngle >= 0 Then
      strike180 = 180 - cosAngle
   Else
      strike180 = 180 + cosAngle
   End If

End Sub
```

```
'*****************************************************************************
'*** Calculate Alpha and beta from strike, dip bearing and inclination       ***
'*****************************************************************************
Sub calc_alpha_beta(strike180, dip180, bear180, incl180, alpha180, beta180)

Dim strike As Double
Dim dip As Double
Dim bear As Double
Dim incl As Double
Dim alpha As Double
Dim beta As Double

Dim Vx As Double
Dim Vy As Double
Dim Vz As Double

Dim betaVx As Double
Dim betaVy As Double

Dim cosAngle As Double
Dim sinAngle As Double

Dim pi As Double
Dim pi_over180 As Double

   pi = 4 * Atn(1)
   pi_over180 = Atn(1) / 45

   strike = strike180 * pi_over180
   dip = dip180 * pi_over180
   bear = bear180 * pi_over180
   incl = incl180 * pi_over180

   'Vector expressed in local Borehole coordinate system
   Vx = Sin(-incl) * Cos(pi / 2 - bear) * Cos(-strike) * Sin(dip) + Sin(-incl) * Sin(pi
/ 2 - bear) * Sin(-strike) * Sin(dip) + Cos(-incl) * Cos(dip)
   Vy = -Sin(pi / 2 - bear) * Cos(-strike) * Sin(dip) + Cos(pi / 2 - bear) * Sin(-
strike) * Sin(dip)
   Vz = -Cos(-incl) * Cos(pi / 2 - bear) * Cos(-strike) * Sin(dip) - Cos(-incl) * Sin(pi
/ 2 - bear) * Sin(-strike) * Sin(dip) + Sin(-incl) * Cos(dip)

   If Vz < 0 Then
      Vx = -Vx
      Vy = -Vy
      Vz = -Vz
   End If

   If Abs(Vz) < 1 Then
      'Arcsin(x) = Atn(x / Sqr(-x * x + 1))
      alpha180 = Atn(Vz / Sqr(-Vz * Vz + 1)) / pi_over180
   Else
      alpha180 = 90
   End If

   betaVx = Vx / (Vx ^ 2 + Vy ^ 2) ^ 0.5
   betaVy = Vy / (Vx ^ 2 + Vy ^ 2) ^ 0.5

   If Abs(betaVx) < 1 Then
      cosAngle = (Atn(-betaVx / Sqr(-betaVx * betaVx + 1)) + 2 * Atn(1)) / pi_over180
   ElseIf betaVx >= 1 Then
      cosAngle = 0
   Else
      cosAngle = 180
   End If


   If Abs(betaVy) < 1 Then
      sinAngle = Atn(betaVy / Sqr(-betaVy * betaVy + 1)) / pi_over180
   ElseIf betaVy >= 1 Then
      sinAngle = 90
   Else
      sinAngle = -90
   End If

   If sinAngle < 0 Then
      beta180 = cosAngle
   Else
      beta180 = 360 - cosAngle
   End If

End Sub
```

```
'*****************************************************************************
'*** Calculate dihedral angle between 2 vectors expressed as strike and dip  ***
'*****************************************************************************
Function dihedral(strike1, dip1, strike2, dip2)

Dim alfa1 As Double
Dim beta1 As Double
Dim gamma1 As Double

Dim alfa2 As Double
Dim beta2 As Double
Dim gamma2 As Double

Dim a As Double

   alfa1 = Cos(-strike1 * Atn(1) / 45) * Sin(dip1 * Atn(1) / 45)
   alfa2 = Cos(-strike2 * Atn(1) / 45) * Sin(dip2 * Atn(1) / 45)

   beta1 = Sin(-strike1 * Atn(1) / 45) * Sin(dip1 * Atn(1) / 45)
   beta2 = Sin(-strike2 * Atn(1) / 45) * Sin(dip2 * Atn(1) / 45)

   gamma1 = Cos(dip1 * Atn(1) / 45)
   gamma2 = Cos(dip2 * Atn(1) / 45)

   a = Abs(alfa1 * alfa2 + beta1 * beta2 + gamma1 * gamma2)
   'Arccos(x) = Atn(-x / Sqr(-x * x + 1)) + 2 * Atn(1)
   If a < 1 Then
      dihedral = (Atn(-a / Sqr(-a * a + 1)) + 2 * Atn(1)) * 45 / Atn(1)
   Else
      dihedral = 0
   End If

End Function
```